INTERNATIONAL EARTH SCEINCES COLLOQUIUM ON THE AEGEAN REGIONS
4–7 October 2005

PROCEEDINGS

Dokuz Eylül University
Engineering Faculty
Department of Geology
İzmir 羊 TURKEY
October 2007

ORGANIZING AND EXECUTIVE COMMITTEE

President
Prof. Dr. M. Eran NAKOMAN

Honorary President
Prof. Dr. Emin ALICI

Vice Presidents
Prof. Dr. Faruk ÇALAPKULU Prof. Dr. Özkan PİŞKİN Prof. Dr. Necdet Türk

Secretariat
Assoc. Prof. Dr. Mümtaz Çolak
Prof. Dr. Hülya İNANER
Res. Assist. Dr. Cem KINCAL
Science Specialist Belgin KOÇER
Assist. Prof. Dr. Ersin KORALAY
Res. Assist. Dr. A. Melis SOMAY
Prof. Dr. Gültekin TARCAN

Members
Res. Assist. Mehmet AKBULUT
Prof. Dr. Zafer AKÇIĞ
Dr. Hasan BAYKAL
İsmet CENGİZ, M.Sc.
Assoc. Prof. Dr. Ünsal GEMİCİ
Prof. Dr. Cüneyt GÜZELİŞ
Res. Assist. Dr. Hülya KAÇMAZ
Res. Assist. Ülkü KARAKURT
Prof. Dr. Mevlüt KEMAL
Prof. Dr. Yalçın KOCA
Prof. Dr. Halil KÖSE
Assist. Prof. Dr. Tolga OYMAN
Prof. Dr. Sacit ÖZER
Prof. Dr. Coşkun SARI
Prof. Dr. Müjgan ŞALK
Res. Assist. Dr. Murat TOKÇAER
Sabri YILDIRIM, M.Sc.
Res. Assist. Dr. Yeşim Yücel ÖZTÜRK

SCIENTIFIC COMMITTEE

Prof. Dr. F. AKGÜN	TURKEY
Prof. Dr. S. ALEXANDER	USA
Prof. Dr. S. ARAI	JAPAN
Prof. Dr. Ö. AYDAN	JAPAN
Prof. Dr. R. BİRSOY	TURKEY
Prof. Dr. Y. K. BİRSOY	TURKEY
Prof. Dr. O. CANDAN	TURKEY
Prof. Dr. R. CHESSEX	SWITZERLAND
Prof. Dr. K. CHRISTANIS	GREECE
Prof. Dr. M. DELALOYE	SWITZERLAND
Prof. Dr. Y. DİLEK	USA
Prof. Dr. C. DOGLIONI	ITALY
Assoc. Prof. Dr. T. EMRE	TURKEY
Prof. Dr. B. ERDOĞAN	TURKEY
Prof. Dr. O. EROSKAY	TURKEY
Prof. Dr. C. GÖNCÜOĞLU	TURKEY
Prof. Dr. C. HELVACI	TURKEY
Prof. Dr. U. İNCİ	TURKEY
Prof. Dr. F. INNOCENTI	ITALY
Prof. Dr. D. IVANOV	BULGARIA
Prof. Dr. A. İ. KARAYİĞİT	TURKEY
Prof. Dr. E. KASAPOĞLU	TURKEY
Prof. Dr. G. KELLING	UK
Dr. N. KONAK	TURKEY
Prof. Dr. Z. KVACEK	CZECH REPUBLIC
Prof. Dr. L. LAZZARINI	ITALY
Prof. Dr. Y. MART	ISRAEL
Prof. Dr. E. MERİÇ	TURKEY
Prof. Dr. R. OBERHANSLI	GERMANY
Prof. Dr. A. OKAY	TURKEY
Prof. Dr. M. OKRUSCH	GERMANY
Prof. Dr. G. ÖNAL	TURKEY
Prof. Dr. İ. ÖZGENÇ	TURKEY
Prof. Dr. İ. ÖZPEKER	TURKEY
Prof. Dr. D. PAPANIKOLAOU	GREECE
Prof. Dr. C. W. PASSCHIER	GERMANY
Prof. Dr. A. PEKDEĞER	GERMANY
Prof. Dr. A. H. F. ROBERTSON	UK
Prof. Dr. Y. SAVAŞÇIN	TURKEY
Prof. Dr. S. A. SHELTON	USA
Prof. Dr. J. P. SUC	FRANCE
Prof. Dr. Ş. ŞİMŞEK	TURKEY
Prof. Dr. O. TATAR	TURKEY
Prof. Dr. T. TAYMAZ	TURKEY
Prof. Dr. T. TODOROV	BULGARIA
Prof. Dr. N. M. TOKSÖZ	USA
Prof. Dr. J. M. WOODSIDE	THE NETHERLANDS
Prof. Dr. W. A. P. WIMBLEDON	UK
Prof. Dr. H. YILMAZ	TURKEY
Prof. Dr. Y. YILMAZ	TURKEY
Prof. Dr. E. YÜZER	TURKEY
Prof. Dr. B. ZHENG	CHINA

PREFACE

First of all, we would like to thank you for your patience and apologize for the delay in the publishing of *IESCA-2005 Proceedings*, which was caused by factors out of our control like reviewers not returning the manuscripts in time or authors not making the corrections promptly enough, and our concerns for accompolishing this task with the least possible number of errors. We would also like to thank all the authors who contributed the 39 papers in this *Proceedings* book, which we hope will contribute to the understanding and solving of the newly appearing geological problems of the Aegean region.

The 10th International Earth Sciences Colloquium on the Geology of the Aegean Regions (IESCA-2005) was held between 4-7 October 2005 in İzmir, Turkey with over 200 participating scientists, and is organized every 5 years by the Geological Engineering Department of Dokuz Eylül University, İzmir, Turkey. 162 oral and 90 poster presentations in total took place in 7 sessions with 82 oral and 47 poster in General Geology, 16 oral in Mineral Deposits, 14 oral and 5 poster in Energy Resources, 8 oral in Industrial-Raw Materials, 16 oral and 17 poster in Engineering and Environmental Geology, 17 oral in Geological Risks, and 9 oral and 21 poster in Geophysics.

There were 450 abstracts submitted to the Colloquium by scientists from 35 different countries on various topics in earth sciences. Althought the submitted abstracts were published under the general subject titles such as General Geology, Mineral Deposits, Energy Resources, Industrial-Raw Materials, Engineering and Environmental Geology, Geological Risks and Geophysics as submitted by the authors, the presentations published in *IESCA-2005 Proceedings* appear in the alphabetical order of the first author's surname.

We are grateful to all the scientists who reviewed the papers for their efforts and time they spent on improving the original manuscripts. We would also like to thank those scientists who contributed as additional reviewers.

Before they were published, some of the manuscripts have been edited to improve their English with particular emphasis on not deviating from the scientific point the author was attempting to make. Therefore, scientific ideas expressed in these presentations belong solely to their authors.

Acknowledgements are due to TUBITAK (The Scientific and Technological Research Council of Turkey) for their financial support, without which it would not be possible to publish this *Proceedings* volume, and to Prof. Dr. Hülya İnaner and Lecturer Nuri Uğurkan Tanyer for the meticulous and unwavering efforts they put into editing the papers and preparing them for publication.

Cordially

Prof. Dr. M. Eran NAKOMAN
President of the Organizing and Executive Committee

Additional Reviewers:

Prof. Dr. M. ERGÜN	TURKEY
Assoc. Prof. Dr. Ü. GEMİCİ	TURKEY
Prof. Dr. H. İNANER	TURKEY
Prof. Dr. T. KAYA	TURKEY
Prof. Dr. Y. KOCA	TURKEY
Prof. Dr. Ö. PİŞKİN	TURKEY
Prof. Dr. C. SARI	TURKEY
Prof. Dr. G. TARCAN	TURKEY
Prof. Dr. N. TÜRK	TURKEY

TABLE OF CONTENTS

Akbulut M., Pişkin Ö. and Karayiğit A. İ.; PETROGRAPHY AND ORE MICROSCOPY OF THE SILICA CARBONATE METASOMATITES KNOWN AS LISTVENITES IN THE MİHALIÇÇIK REGION, ESKİŞEHİR-TURKEY **1**

Akyol N., Zhu L., Mitchell B. J., Sözbilir H. and Danışman M. A.; NEW INSIGHTS ON WESTERN ANATOLIAN (TURKEY) STRUCTURE AND TECTONICS FROM THE 2002-2003 SEISMIC EXPERIMENT **9**

Aydan Ö., Kumsar H. and Türk N.; FAULTING AND SHAKING CHARACTERISTICS OF EARTHQUAKES IN İZMİR AND ITS CLOSE VICINITY **15**

Baysal G., Tecim V. and Kıncal C.; AN APPLICATION OF MULTI-CRITERIA DECISION ANALYSIS IN THE HARMANDALI (IZMIR) WASTE DISPOSAL SITE USING GEOGRAPHICAL INFORMATION SYSTEMS (GIS) **31**

Butuzova L.F., Zubkova V.V., Bulyga O. S., Isayeva L.N. and Turchanina O.N.; INFLUENCE OF THE SULPHUR OF COALS ON COKING AND SEMI-COKING PROCESSES **43**

Caldarola F., Grippo A., Guario I. M., Laviano R., Milella M. and Scandale E.; THE RUPESTRAL CHURCHES OF LAMA D'ANTICO, SAN GIOVANNI AND SAN LORENZO AND EUPLO IN FASANO (ITALY): SOME DECAY PATTERNS **51**

Ceylan S. and Özer N.; FRACTAL ANALYSIS OF AFTERSHOCKS OF EARTHQUAKES IN AKSEHIR-AFYON AND GOKOVA GRABENS, TURKEY **59**

Çoban F. and Kocabaş C.; THE MINERALOGICAL AND GEOCHEMICAL CHARACTERISTICS OF PHOSPHATE OCCURRENCES IN MIOCENE TUFFS (AYVACIK-ÇANAKKALE) **65**

Diamantopoulos A.; A CARDINAL PROBLEM OF THE KINEMATIC PATH OF THE INTERNAL HELLENIDES (PELAGONIAN CORDILLIERA, NORTHERN-CENTRAL GREECE): NATURE AND DETERMINATION OF DEFORMATION-CONTACT ZONES **71**

Diamantopoulos A.; SEMI-BRITTLE ASYMMETRIC SHEAR PLANES CONTROLLING THE CENOZOIC KINEMATICS OF INTERNAL HELLENIDES (NORTHERN GREECE): FIELD EVIDENCES FROM ASKION AND EASTERN VERNON MOUNTAIN RANGES **81**

Ercan A. Ö. and Tabatabaee S.H.; DIRECT DETECTION OF OIL AT GACHSARAN PROVEN FIELD; CASE HISTORY FROM IRAN **91**

Galant Y.; MANTLE-DERIVED OIL AND GAS OF THEKURA RIFT (AZERBAIJAN) **111**

İnaner H., Coşar Y.Z. and Nakoman E.; RESOURCES, QUALITY AND ECONOMIC IMPORTANCE OF SOLID FOSSIL FUELS AND PEAT DEPOSITS IN TURKEY **117**

İnaner H.; GEOLOGICAL HERITAGE, GEOPARKS, GEOTOURISM AND TURKEY **125**

Küçükuysal (İpekgil) C. and Lünel A. T.; BEYPAZARI-OYMAAĞAÇ GRANITOID: ITS GEOLOGY, PETROGRAPHY, GEOCHEMISTRY AND TECTONIC SIGNIFICANCE **137**

Khalaji A. A., , Esmaeily D. and Valizadeh M.V.; GEOCHEMICAL CONSTRAINTS ON THE SOURCE CHARACTERISTICS AND ATTENDANT TECTONICS OF THE BOROUJERD GRANITOID MASS, SANANDAJ- SIRJAN ZONE, WESTERN IRAN **143**

Khalaji A. A., Esmaeily D. and Valizadeh M.V.; PETROLOGY AND GEOCHEMISTRY OF THE BOROUJERD GRANITOID ROCKS SANANDAJ - SIRJAN ZONE, WESTERN IRAN **153**

Kıncal C. and Koca M. Y.; GIS-BASED ENGINEERING GEOLOGICAL MAPPING IN THE INNER BAY OF IZMIR (TURKEY) **163**

Kıncal C. and Koca M. Y.; LIQUEFACTION ANALYSIS APPLIED TO THE INNER BAY SOILS OF BORNOVA PLAIN, IZMIR/TURKEY **173**

Kıncal C. and Çakıcı S.; ENGINEERING GEOLOGICAL MAP PREPARATION IN ALLUVIAL FIELDS : CASE STUDY, BORNOVA PLAIN (IZMIR-TURKEY) **181**

Kıncal C., Özyalın Ş. and Zarif H.; SEISMIC RISK DETERMINATION OF BORNOVA PLAIN SOILS IN IZMIR (TURKEY) USING S-WAVE AND P-WAVE VELOCITY MEASUREMENTS **193**

Kırdım Ö., Karayiğit A. İ., Querol X.; CHARACTERIZATION OF FEED COAL, FLY ASH AND BOTTOM ASH FROM SEYITOMER POWER PLANT, KUTAHYA, TURKEY **205**

Kocabaş C. and Çoban F.; THE MINERALOGY AND GEOCHEMISTRY OF A BENTONITE DEPOSIT BETWEEN YENİKÖY AND AKÇAKERTİL (BİGADİÇ) **213**

Kozłowska A.; CEMENT CHARACTERISTICS OF THE CARBONIFEROUS SANDSTONES OF CENTRAL POLAND **221**

Kumsar H. and Aydan Ö.; FAULTING AND SHAKING CHARACTERISTICS OF EARTHQUAKES IN DENİZLİ PROVINCE (TURKEY) **231**

Kuruoğlu M. and Özden G.; SEISMIC RISK OF QUATERNARY SOIL DEPOSITS FOR LONG DISTANCE EARTHQUAKES IN İZMİR METROPOLITAN AREA **243**

Melinte M. C.; CRETACEOUS CALCAREOUS NANNOPLANKTON BIOSTRATIGRAPHY OF THE SOUTHERN ROMANIAN BLACK SEA REGION **251**

Menlikli G. F. and Baykal A.; MINERALOGY, GEOCHEMISTRY AND UTILITY OF TRIAS SEDIMENTS IN SIZMA - YÜKSELEN (KONYA) **261**

Özçelik M., Şener E. and Ertunç A.; A STRIPE METHOD FOR PRODUCING ENGINEERING GEOLOGICAL MAP OF BURDUR (TURKEY) URBAN AREA **273**

Özer N., Altınok Y., Ceylan S., Kurt H. and Kolçak D.; AFTERSHOCK BEHAVIOURS OF THE EARTHQUAKES IN AKŞEHİR-AFYON AND GÖKOVA GRABENS, TURKEY **283**

Seyman F. and Karagüzel R.; GROUNDWATER POTENTIAL OF SENİRKENT-ULUBORLU (ISPARTA) BASIN **289**

Siavalas G., Kalaitzidis S., Chatziapostolou A. and Christanis K.; ASSESSMENT OF LIGNITE-DERIVED CONTAMINATION DEGREE OF ALFEIOS RIVER SEDIMENTS, CENTRAL PELOPONNESE, GREECE **295**

Şener (Tay) Ş. , Karagüzel R. and Mutlutürk M.; DOMESTIC SOLID WASTE LANDFILL SITE SELECTION IN SENİRKENT-ULUBORLU (ISPARTA) BASIN **305**

Şimşek C.; THE HYDROGEOLOGICAL AND GEOLOGICAL ASSESSMENTS OF THE TORBALI AND SELÇUK WASTE SITES AND ITS ENVIRONMENTAL EFFECTS **317**

Tombros S. F., St. Seymour K., Spry P. G., Williams-Jones A. E. and Zouzias D.; PANORMOS BAY AU-AG-TE EPITHERMAL MINERALIZATION, TINOS ISLAND, HELLAS: MULTIPLE MECHANISMS OF DEPOSITION FOR AN UNUSUAL CALC-ALKALINE GRANITE RELATED SYSTEM **325**

Turchanina O.N., Butuzova L.F., Bechtel A., Safin V.A., Isaeva L.N. and Butuzov G.N.; NEW INDEXES FOR COAL GENETIC TYPE DETERMINATION **335**

Üşenmez K., Kıncal C., Koca M.Y.; SOME CEMENT BASED GROUT MIX APPLICATIONS IN TERRACE UNITS PLACED THROUGH DALAMAN RIVER **343**

Yücel K. T., Gülmez S. and Eroğlu Ö.; EVALUATION OF PHYSICAL PROPERTIES OF MORTAR MATERIALS USED IN PSIDIA ANTIOCHEIA AT ANATOLIA **357**

Zouzias D. and St. Seymour K.; REVIVING THE DREAM: A PILOT PROJECT ON THE SUSTAINABLE DEVELOPMENT OF NISYROS VOLCANO **363**

PETROGRAPHY AND ORE MICROSCOPY OF THE SILICA CARBONATE METASOMATITES KNOWN AS LISTVENITES IN THE MİHALIÇÇIK REGION, ESKİŞEHİR-TURKEY

Akbulut M.[1], Pişkin Ö.[1] and Karayiğit A. İ.[2]

[1]Dokuz Eylül University, Department of Geological Engineering, 35160 Buca-İzmir, Turkey
makbulut@deu.edu.tr,. ozkan.piskin@deu.edu.tr
[2]Hacettepe University, Department of Geological Engineering, 06532 Beytepe-Ankara, Turkey
aik@hacettepe.edu.tr

Abstract: The silica-carbonate metasomatites of the Mihalıççık region (Eskişehir) formerly named as listvenites are hosted by serpentinized ultramafics which tectonically overlay the Mihalıççık metamorphic assemblages. The metasomatites are mainly in three basic types: carbonate rocks, silica-carbonate rocks and birbirites. The carbonate rocks are mainly made of fine to medium grained rhombohedric dolomites and contain accessory goethite and limonite. Silica-carbonate rocks, on the contrary, are made of silica and dolomite, showing primary carbonatization and secondary silicification. Rare opaque minerals such as chromite, magnetite, pyrite, marcasite, hematite, and goethite may be observed in polished sections of silica-carbonate rocks. The third metasomatite in the Mihalıççık region is birbirite, which looks like a brown coloured compact quartzite. These assemblages show brecciated and mylonitized texture and include only microcrystalline quartz, coarse quartz veinlets cutting the latter, radial opals and opaque phases. The opaque phases of this type are magnetites transformed from chromites, arsenopyrite, glaucodot, bravoite (NiS-nickeliferous pyrite), gersdorffite, skutterudite , marcasite, hematite and goethite. Euhedral pyrite crystals are also present. When discussed on the basis of strict description of listvenite, it may clearly be seen that chromium-mica (fuchsite), which is an important component of the listvenite, is absent in the metasomatites of the study area. In conclusion, the alteration assemblages of Mihalıççık region are not proper listvenites but might be regarded as members of the listvenitic series.

Keywords: listvenite; silica-carbonate alteration; ore-microscopy; Mihalıççık

1. INTRODUCTION

The term “listvenite” refers to structure controlled low temperature hydrothermal alteration products in ophiolitic terrains. These metasomatic/hydrothermal products are generally found in shear contacts of ophiolitic serpentinites and show rocky morphology. Listvenites are composed of carbonate (ankerite or magnesite), quartz, fuchsite (greenish coloured Cr-mica), and accessory minerals, such as various sulphide phases (e.g. pyrite, bravoite, gersdorffite, skutterudite). Relict chromites of the serpentinite protolith mostly accompany this paragenesis. Listvenite research is practically important because of their spatial relation with low temperature precious metal deposits.

There are two major ophiolitic belts in Turkey which are remnants of the closure of Neo-Tethyan Ocean. In past years, many of the listvenite studies are focused along the Northern Ophiolitic Belt.

Present study aims to present the petrography and ore microscopy of the alteration assemblages in Mihalıççık (Eskişehir) region, which were previously named as “listvenites”.

2. MATERIALS AND METHODS

Petrography and ore paragenesis of the metasomatites in Mihalıççık region is studied by combined usage of polarising microscope and conventional air and oil immersion techniques in reflected light microscopy.

3. GEOLOGICAL SETTING

Study area is located in the south of İzmir-Ankara Suture, which is regarded as one of the border zones between fragments remaining from the closure of Neo-Tethys. During Campanian, the

Anatolide-Tauride block had subducted under the Sakarya continent, resulting in blueschist metamorphism (Okay et al., 2001; Akbulut et al., 2006). Subsequently, the accretionary mélange and/or ophiolites are thrust over this blueschist basement (Figure 1a) and are later intruded by several Eocene intrusions.

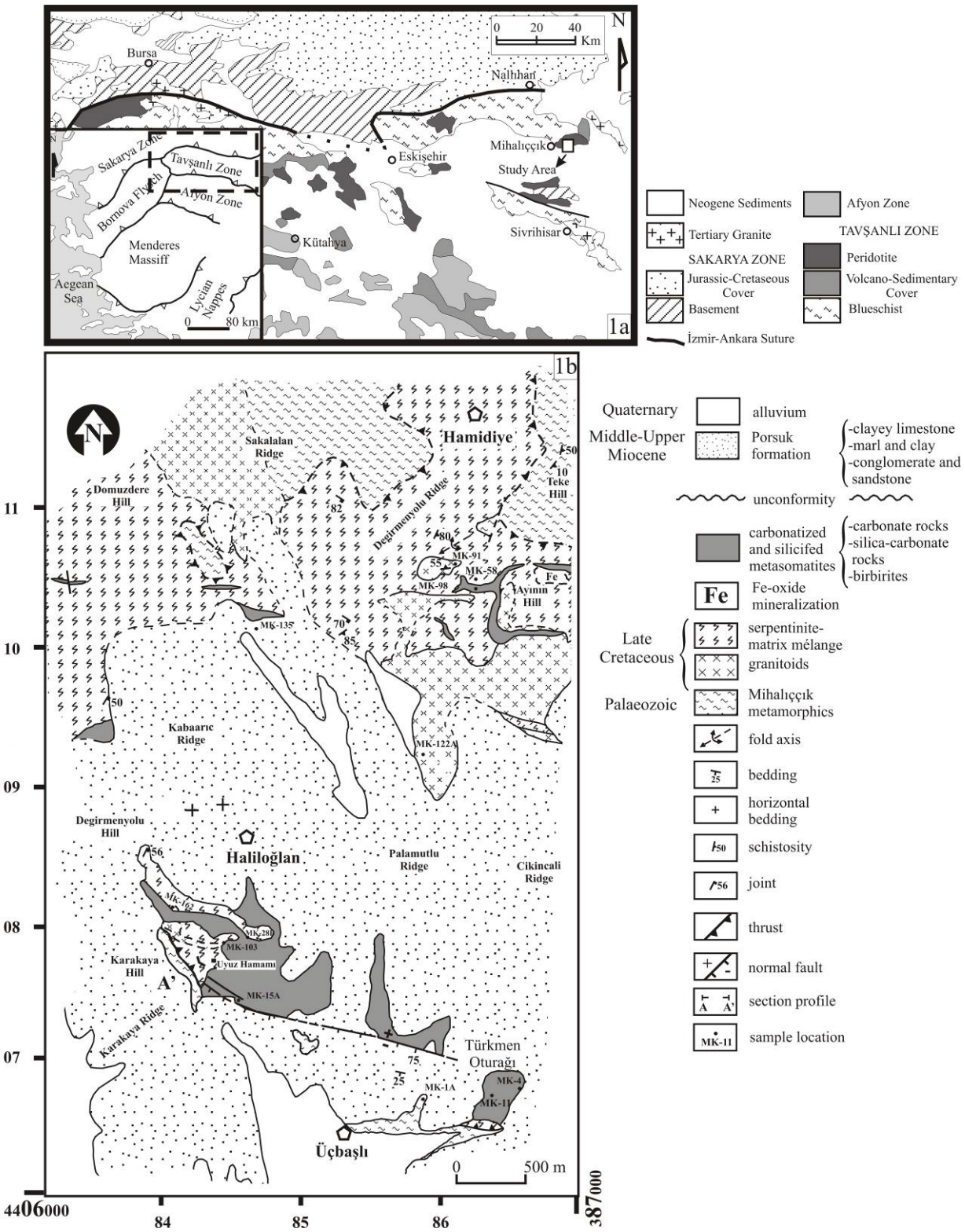

Figure 1. (a) Regional geology and location of the study area (from Okay et al., 1998); (b) Geological map of the study area (Akbulut et al., 2006).

The Upper Cretaceous serpentinite-matrix mélange including the silica-carbonate metasomatites in Mihalıççık region rest on the Mihalıççık Metamorphics comprising graphite schists, chlorite-actinolite schists, glaucophane schists and quartzites (Figure. 1b).

The serpentinite-matrix mélange include mainly serpentinites, cherts, mudstones and recrystallized limestone blocks and is uncomformably overlain by the Porsuk Formation of Middle-Upper Miocene. The serpentinites of the mélange are greenish coloured and have brittle lithology with many joints and fractures. Their mineralogy consists mainly of chrysotile, antigorite, lizardite, bastite, pyroxene, chromite, chrome-spinels and talc.

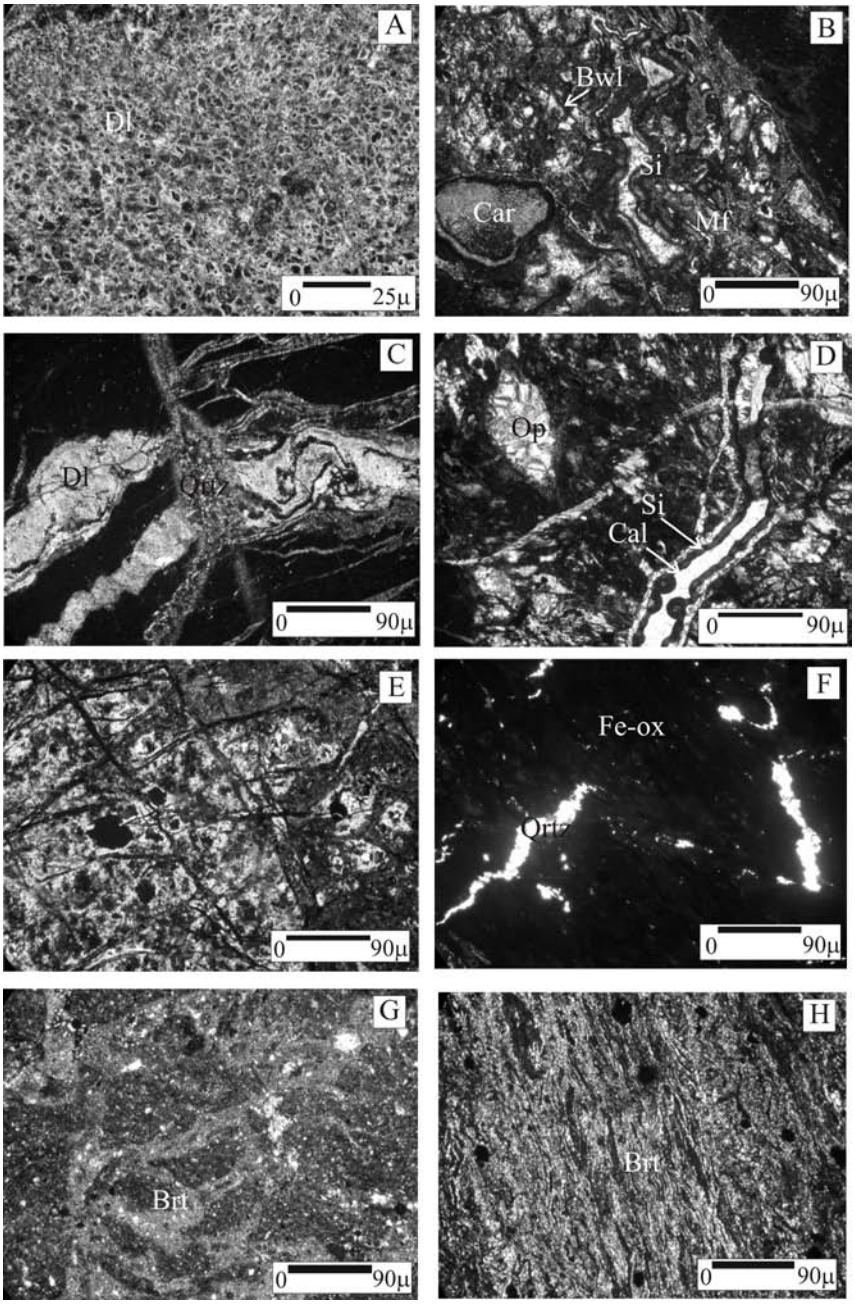

Figure 2. Photomicrographs of the silica-carbonate metasomatites of the Mihalıççık region under polarized light (+N) (from Akbulut et al., 2006). (A) carbonate rock; (B), (C), (D), (E) and (F) silica-carbonate rock; (G) and (H) birbirites. Dl: dolomite , Car: carbonate, Mf: mafic mineral, Bwl: bowlingite, Qrtz: quartz, Op: opal, Cal: calcite, Si: silica, Fe-ox: iron oxides, Brt: birbirite

Due to the tectonic contact relations and lack of thermal metamorphism at their contacts, the granitoids in the study area are regarded as fragments of a former intrusion that is sliced and tectonically included into the obducting mélange (Akbulut et al., 2006).

The Mihalıççık silica-carbonate metasomatites are hosted by the serpentinites of the mélange forming dyke or pod-like alteration bodies and presenting rocky morphologies. The alteration bodies show the former fracture zones along the host rock. The metasomatites are mainly in three basic types: carbonate rocks, silica-carbonate rocks and birbirites.

4. PETROGRAPHY OF THE SILICA-CARBONATE METASOMATITES

The first type of metasomatites in the area is carbonate rocks. These rocks comprise fine to medium grained rhombohedric dolomites (Figure 2a). The texture of the original lithology is not preserved.

The second type is the silica-carbonate rocks. They are completely made of silica and dolomite and rare bowlingite as remnants of primary ultrabasic lithology. In this type, primary stage of carbonatization and secondary stage of silicification can be traced via primarily carbonatized mafic minerals and bowlingite which are surrounded by colloform and radial silica (Figure 2b) and/or microcrystalline silica that cross-cuts the primary carbonates (Figure 2c). The secondary carbonates (e.g. calcite) located inwards the secondary silica veins are precipitates of a much later stage (Fig. 2d). In some of the specimens of this type, a stockwork-like texture formed by carbonates, silica and bowlingite can be observed (Figure 2e), whereas in some parts, a silica-rich and carbonate-free mineralogy is observed with only fine-grained quartz crystals and iron-oxides (Figure 2f).

The third metasomatite type in the Mihalıççık region is birbirite. This assemblage resembles a brown coloured compact quartzite in hand specimens. This type shows brecciated (Figure 2g) and mylonitized (Figure 2h) texture and lacks any carbonate minerals. Brecciation of the rock can hardly be observed as a ghost texture due to the intense silicification. Silica is in form of microcrystalline quartz, coarse quartz veinlets and radial opals. Fractures of the rock are filled with iron-oxides and colloform quartz.

4.1. Ore Microscopy

Although the silica-carbonate metasomatites of Mihalıççık bear accessory amounts of opaque phases, they show an interesting spectrum of paragenesis ranging from orthomagmatic stage to low temperature hydrothermal stage.

The original rock of the metasomatites, the serpentinites include chromites (Figure 3a), chromium-spinel, magnetite (formed by replacement of chromite along the rims and cracks, Figure 3b) and some very fine-grained heazlewoodite, together with minor electrum and two generations of pyrite. Pyrite I is observed as small relict grains which are replaced by limonite, hematite and goethite (Figure 3c), whereas pyrite II is observed as a hipidiomorphic phase along fibres of serpentinite (Figure 3a).

General paragenesis of the metasomatites include chromite (largely replaced by magnetite), pyrite, gersdorffite [(Ni,Co,Fe)AsS], skutterudite [(Co,Ni, Fe)As_{3-x}](?), glaucodot [(Co,Fe)AsS], arsenopyrite, marcasite, bravoite (NiS-nickeliferous pyrite), hematite and goethite. The distribution of opaque phases is not homogeneous in metasomatites; some types are very poor in ore minerals, whereas some are relatively rich.

For example, the carbonate rocks of the metasomatic assemblage are very poor in opaque phases. This type contains only accessory goethite and limonite. Even the

primary oxides and sulphides of the serpentinite protolith are absent in this type.

On the contrary, the opaque minerals paragenesis of silica-carbonate rocks is a little more interesting. In silica-carbonate rocks, the transition from orthomagmatic to hydrothermal stage is apparent. The chromites are generally found as totally replaced by magnetite (Figure 3d). These minerals preserve their euhedral structure. Magnetites are accompanied by marcasites of hydrothermal stage which are found as partly transformed into colloidal goethite (Figure 3e). This rock also includes euhedral pyrites which are totally replaced by hematite and goethite while preserving their euhedral structure (Figure 3f).

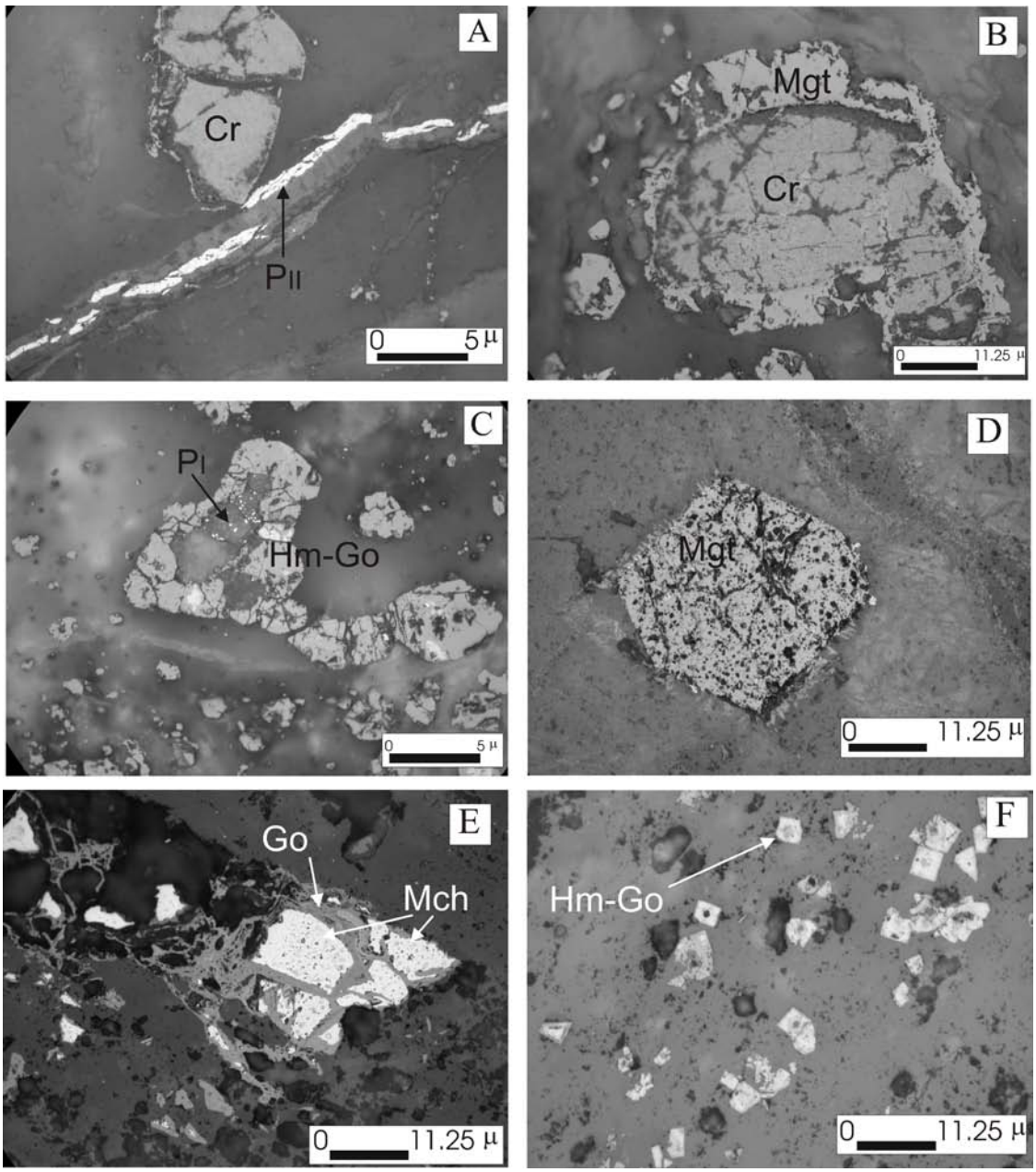

Figure 3. Photomicrographs of opaque phases in serpentinites and silica-carbonate metasomatites (all photos are in // N and in air). (A), (B) and (C) show some of the opaque phases in serpentinites. (D) euhedral chromite which is replaced by magnetite in silica-carbonate rock; (E) marcasite partially replaced by colloidal goethite along its rims in silica-carbonate rock; (F) euhedral pyrite grains replaced into hematite and goethite in silica-carbonate rock (Cr: Chromite; Mgt: magnetite; PI: pyrite I; PII: pyrite II; Go: goethite; Hm-Go: hematite-goethite).

The third metasomatite type (birbirite) is relatively richer in opaque mineral assemblages than the silica-carbonate rocks. Birbirites include euhedral magnetites which are transformed from chromites. These magnetites are generally transformed into hematite and goethite along their fractures and rims (Figure 4a). Rhombohedral arsenopyrite (Figure 4b) of the hydrothermal stage accompanies this paragenesis with minor glaucodot which is hardly identified by its much yellowish colour than the arsenopyrite. Bravoite (NiS-nickeliferous pyrite) is generally found as small grains in the rock (Figure 4b). However, it is also observed that small grains gather to form larger bravoite crystals. Characteristic zoned structure of bravoite can only be observed by HNO_3 etching (Figure 4b) of the polished sections. As a low temperature phase, bravoite replaces the rhombohedral arsenopyrite of higher temperature (Figure 4c). Accessory gersdorffite (Figure 4d) and very fine grained skutterudite accompany the paragenesis with marcasite (Figure 4e), which is observed in fractures of birbirites together with supergene products of hematite and goethite. Euhedral pyrite crystals are also present in this type.

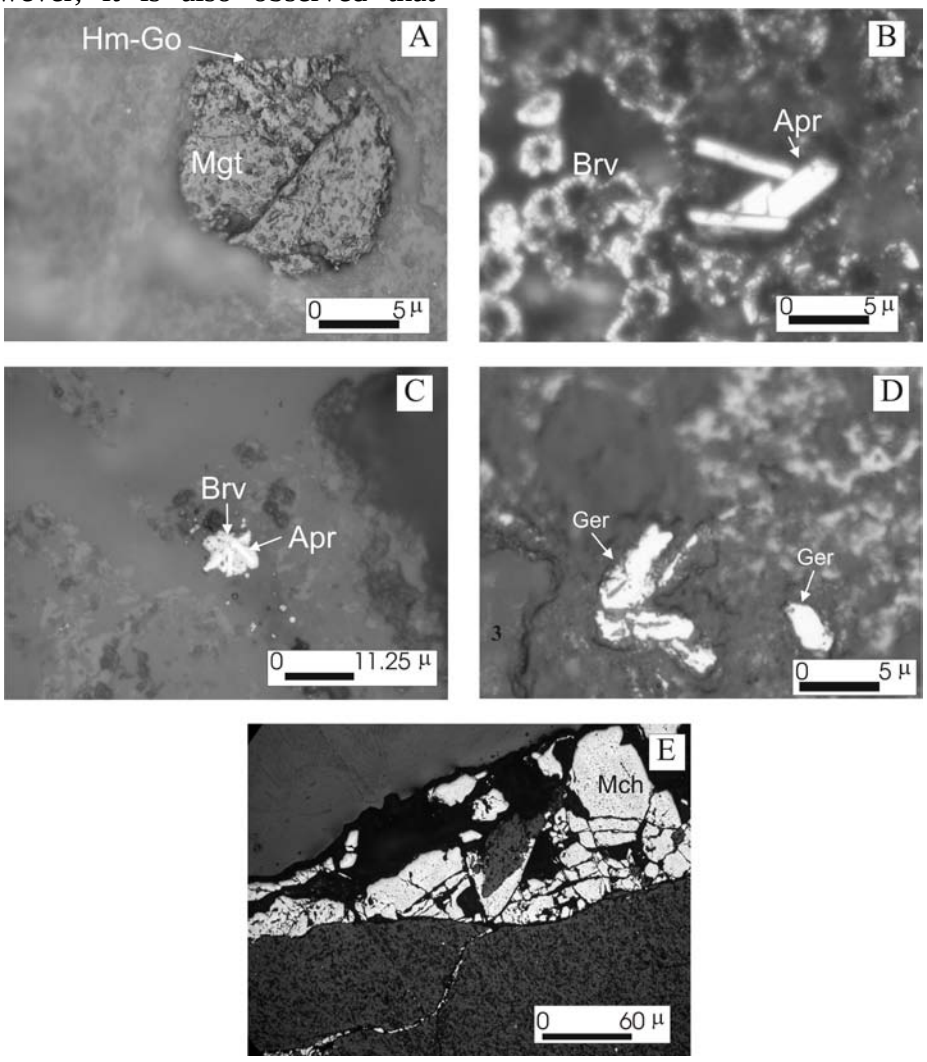

Figure 4. Photomicrographs of polished sections of birbirite assemblages. (A) euhedral magnetite that is transformed from chromite. Note the hematite and goethite transformations along rims (// N, air); (B) rhombohedric arsenopyrite (Apr) and bravoite (Brv). Note the zoned structure of bravoite after HNO3 etching (// N, oil); (C) bravoite (Brv) replacing the arsenopyrite (Apr) (// N, air); (D) accessory gersdorfite (Ger) (// N, oil); (E) marcasite (Mch) along fractures of the birbirite assemblages (// N, air).

5. CONCLUDING REMARKS

The metasomatic assemblages of Mihalıççık region are products of metasomatism between low temperature hydrothermal fluids and serpentinite host rock. The mineralogy of the metasomatites consists of variations of silica and carbonates. Three basic types of metasomatites were identified; carbonate rocks, silica-carbonate rocks and birbirites. It is obvious by the microscopic observations that carbonatization is the first stage of metasomatism, which is followed by silicification. Thus, carbonate rocks are the first product of metasomatism followed by silica-carbonate rock formation. The intensity of the silicification increases in later stages forming birbirite assemblages. Microscopic observations also indicate that opaque phases are in accessory amounts in all of the metasomatites and these occurrences are economically not important. The poorest metasomatic assemblages are carbonate rocks with minor hematite and goethite. A relative increase is clearly seen in sulfide phases with progressing silicification (e.g. marcasite in silica-carbonate rocks and arsenopyrite, bravoite in birbirites). During carbonate rock generation, the primary sulfides seem to be dissolved by the hydrothermal/metasomatic fluid. With the silicification stage, new sulfide phases precipitate. Replacement of arsenopyrite by bravoite indicates a decrease in temperature during progressing alteration.

When discussed on the basis of original listvenite description given by Rose (1837, 1842), which is also lately discussed by Halls and Zhao (1995), it is seen that fuchsite, which is an important component of the listvenite is absent in the metasomatites of the study area. Hence, the alteration assemblages of Mihalıççık region are not proper listvenites but might be regarded as members of the listvenitic series.

REFERENCES

Akbulut M., Pişkin Ö., Karayiğit A.İ., 2006. The genesis of the carbonatized and silicified ultramafics known as listvenites: a case study from the Mihalıççık region (Eskişehir), NW Turkey. *Geological Journal*, 41: 557-580.

Halls C., Zhao R., 1995. Listvenite and related rocks: perspectives on terminology and mineralogy with reference to an occurrence at Cregganbaum, Co. Mayo, Republic of Ireland. *Mineralium Deposita*, 30: 303-313.

Okay A.İ., Tansel İ., Tüysüz O., 2001. Obduction, subduction and collision as reflected in the Upper Cretaceous-Lower Eocene sedimentary record of western Turkey. *Geological Magazine*, 138: 117–142.

Okay, A.İ., Harris, N.B.W., Kelley, S.P., 1998. Exhumation of blueschists along a Tethyan suture in northwest Turkey. *Tectonophysics*, 285: 275-299.

Rose G., 1837. Mineralogisch-geognostiche Reise nach dem Ural, dem Altai und dem Kaspischen Meere. Volume 1: Reise nach dem nördlichen Ural und dem Altai. C.W. Eichhoff (Verlag der Sanderschen Buchhandlung): Berlin.

Rose G., 1842. Mineralogisch-geognostiche Reise nach dem Ural, dem Altai und dem Kaspischen Meere. Volume 2: Reise nach dem sudlichen Ural und dem Kaspischen Meere, Uebersicht der Mineralien und Gebirgsarten des Ural. G.E. Reimer (Verlag der Sanderschen Buchhandlung): Berlin.

(This page is left blank intentionally.)

NEW INSIGHTS ON WESTERN ANATOLIAN (TURKEY) STRUCTURE AND TECTONICS FROM THE 2002-2003 SEISMIC EXPERIMENT

Akyol N.[1], Zhu L.[2], Mitchell B. J.[2], Sözbilir H.[3] and Danışman M. A.[1]

[1] Department of Geophysics, Engineering Faculty, Dokuz Eylül University, İzmir, Turkey
nihal.akyol@deu.edu.tr, ali.danisman@deu.edu.tr
[2] Department of Earth & Atmospheric Sciences, Saint Louis University, MO, USA.
lupei@eas.slu.edu, mitchbj@eas.slu.edu
[3] Department of Geology, Engineering Faculty, Dokuz Eylül University, İzmir, Turkey.
hasan.sozbilir@deu.edu.tr

Abstract: Western Turkey is one of the most seismically active continental regions in the world and much of it has been undergoing ~NS-directed extensional deformation. Between November, 2002 and October, 2003, seismologists from Saint Louis University and Dokuz Eylül University in İzmir, Turkey, deployed 50 seismic stations in western Turkey, in the framework of a cooperative project. The project supported by NSF (National Science Foundation) and TÜBİTAK (Technical Research Council of Turkey) has been entitled "Integrated Seismological Studies of Crust/Upper Mantle Structure and Anisotropy in Western Anatolia". We installed five broadband and 45 short-period temporary seismic stations, distributed partly as a dense, 100-km-long, N-S linear array and partly as a regional network, throughout the Menderes Massif of western Turkey in order to better understand crust/mantle structure/anisotropy and seismic activity in Western Anatolia. Different methods were applied to the data collected by this network and additional data, from GEOForschungsNetz, IRIS/USGS Network and KOERI Network, in the Aegean Region.

Key words: Western Anatolia (Turkey), Crustal Thickness Variation, Seismicity, Seismotectonics, Shear-wave Splitting, Crust/Upper Mantle Structure/Anisotropy.

1. DATA

We used 5 STS-2 broadband and 24 Mark L-22 short-period (2 Hz) three-component sensors. The IRIS/PASSCAL instrument center provided 24 L22 sensors and Reftek 72A recorders with peak sensitivity at 2 Hz and Saint Louis University (SLU) provided five sets of broadband STS-2 sensors and Reftek 72A recorders. 20 of the short-period instruments were first deployed for six months along a 50-km-long N-S line between Salihli and Ödemiş in the central Menderes Massif. They were redeployed in May, 2003 to extend the line southward an additional 50 km from Ödemiş to Dalama. This design provided a 100-km-long N-S profile with a station spacing of 3 to 4 km. The profile traversed two prominent E-W trending grabens in western Turkey: the Büyük Menderes Graben (BMG) and the Küçük Menderes Graben (KMG). The remaining four short-period and five broadband instruments were installed to form a regional network over a 150×150 km^2 area surrounding the linear array (Figure 1). All stations recorded 24-bit data continuously at 40 sps (samples per second). This digitization rate provides a sampling resolution that permits accurate event locations. Accurate timing of recordings were ensured by frequently synchronizing recorder's internal clock with the GPS time. Time drifts were recorded and were used to make time corrections to waveform data. In most cases, the corrections were less than 10 ms. The stations were visited every one or two months for maintenance and data download. The data were converted to SEED format and organized in a database managed with PASSCAL software. In total, we collected more than 120 GB of compressed waveform data, which is 93% of the amount of data that should have been collected with no down time for any station. The data set has been permanently archived at the IRIS data management center (Zhu et al., 2006a).

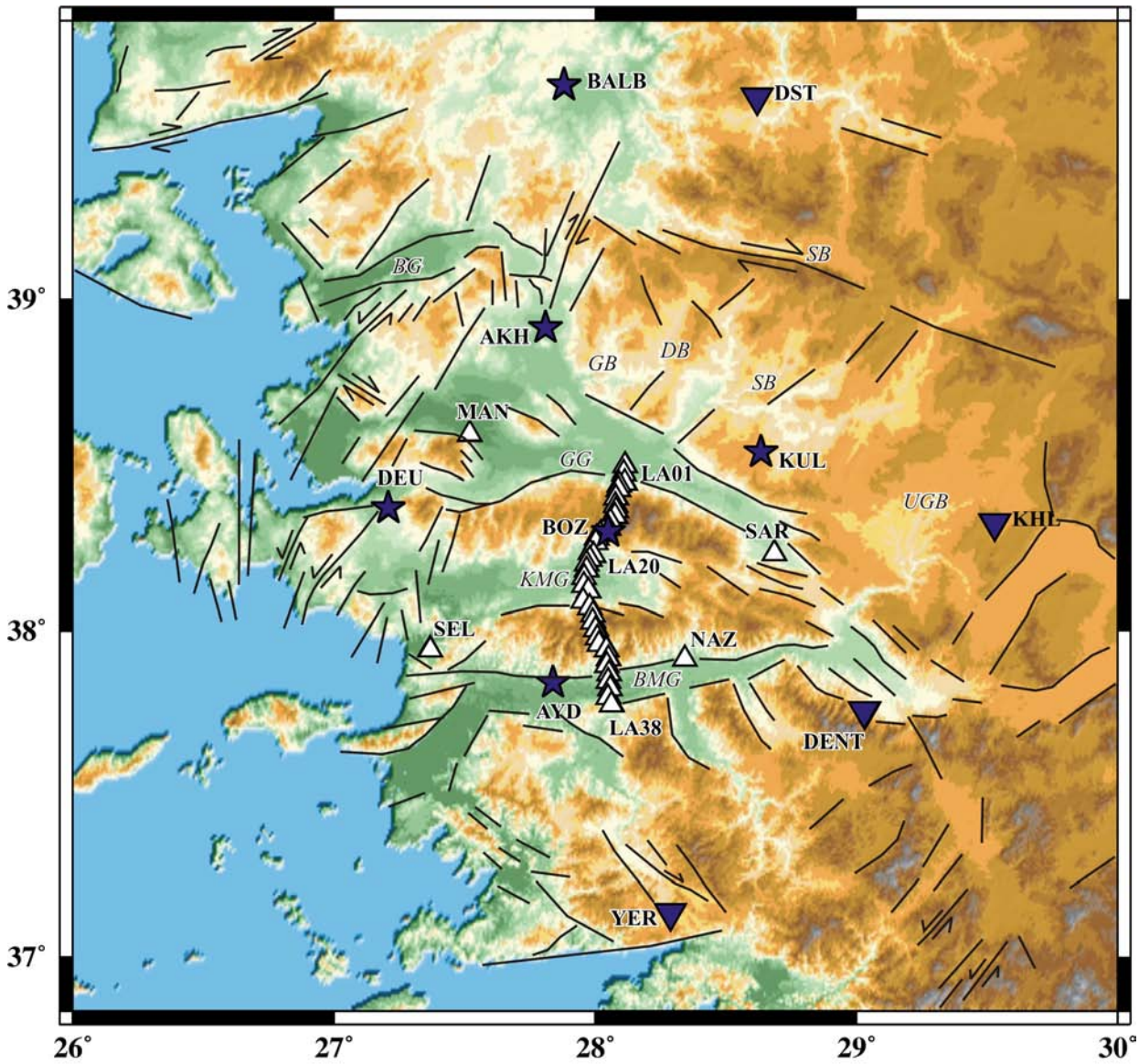

Figure 1. Map showing station coverage of western Anatolia 2002-2003 seismic recording experiment (modified from Akyol et al., 2006). Tectonic features were modified from Şengör et al. (1985), Şengör (1987), Konak & Şenel (2002), Şaroğlu et al. (1992) and Bozkurt(2000). GG: Gediz Graben, KMG: Kucuk Menderes Graben, BBG: Buyuk Menderes Graben, BG: Bakırcay Graben, SB: Simav Basin, GB: Gördes Basin, DB: Demirci Basin, UGB: Uşak-Gürle Basin. Gray paralel lines with arrows represent strike slip movements. White triangles and stars represent short-period and broadband instruments of Western Anatolia Seismic Recording Experiment, respectively. BALB is broadband and DST, KHL, DENT, YER are short-period stations operated by KOERI.

2. METHODS

The best 1-D P-wave velocity model, earthquake locations and station corrections were obtained simultaneously from the joint-inversion process (VELEST algorithm; Kissling et al. 1994; Kissling et al. 1995) by using the data from our network and 5 permanent seismic stations operated by KOERI (Kandilli Observatory and Earthquake Research Institute). Our velocity model is characterized by crustal velocities that are significantly lower than average continental values (Akyol et al., 2006).

We combined teleseismic waveform data from our seismic network and permanent seismic stations in the Aegean region to determine crustal thickness variation using receiver function analysis method. Two different receiver function

analysis applications (H-κ stacking method; Zhu, 1993; Zandt et al., 1995 and CCP stacking method; Kosarev et al.,1999;Zhu, 2000) show that Moho increases in depth by 4 to 8 km over a lateral distance of less than 100 km from the metamorphic core complexes to the upper plates, in the Aegean region (Zhu et al., 2006a).

By using, a relative relocation algorithm (HypoDD program of Waldhauser and Ellsworth, 2000), we relocated local earthquakes, original catalog locations reported by KOERI. After relocations, earthquakes are highly concentrated in three main clusters, including moderate-sized events and their aftershock activities, and reveal linear features in seismicity. The movements from the original catalog locations are as large as 20 km (Zhu et al., 2006b). We obtained moment tensors and focal depths of 71 earthquakes (CAP method; Zhu and Helmberger,1996).

Shear wave spillitting parameters (fast polarization direction and delay time) were determined using data from 5 broadband stations of our temporary network. Splitting measurements provide excellent lateral resolution but poor vertical resolution of polarization anisotropy. Shear wave splitting parameters were found by a grid search over the parameter space by minimizing energy in the tangential component (Silver and Chan, 1991) and checked by analyzing the particle motion of each phase used in this application.

3. CONCLUSIONS

The joint-inversion application has revealed that crustal velocities are significantly lower than average continental values. The lower crustal velocities are associated with fluids at high pore pressure and high level of fractionation rather than presence of partial melt in the region. The lower crust is more homogenous than the upper crust. Our results show that seismic activity in western Turkey is higher than previously reported and recent seismicity is related to active seismogenic zones in the region. The hypocentral distribution of the events indicates that dominant seismogenic depth for the region is about 9-10 km (Akyol et al., 2006).

Receiver function analysis results show a general trend of westward crustal thinning from 36 km in central Anatolia, to 28-30 km in western Turkey, to 25 km in the Aegean Sea. Significant crustal thinning has taken place beneath the Central Menderes Massif (28 to 30 km) and the Cyladic Massif (25 to 26 km) Metamorphic Core Complexes. Outside these metamorphic belts in western Turkey and the Aegean Sea, the crust is 32-34 km thick. The long-lived elevated Moho under the metamorphic core complexes suggests that the lower crust in the Aegean region is at least three times stronger than that in the Basin & Range Province, where the Moho is much flatter (Zhu et al., 2006a).

High resolution earthquake relocations and moment tensor determinations (Figure 2) has revealed that the left-lateral strike-slip (Derbent) fault near Buldan connects the Gediz graben in the north and the eastern end of the Büyük Menderes graben in the south. The right-lateral strike-slip (Beyler) fault south of İzmir, has an ENE-WSW strike. It is interesting to note that these two faults have opposite senses of motion (left-lateral vs. right-lateral) and nearly perpendicular strikes. The fault near Sındırgı, is a southdipping normal (Hisarköy) fault with a left-lateral strike-slip component. Our results suggest that a small portion of the overall N-S extension occurring in western Turkey is accommodated by slip on conjugate strike-slip faults. This means that, in addition to crustal thinning by normal faulting, some E-W shortening occurred during the N-S extension (Zhu et al., 2006b). The results suggest that “pure shear model” could explain present-day crustal deformation in the region (Figure 2d).

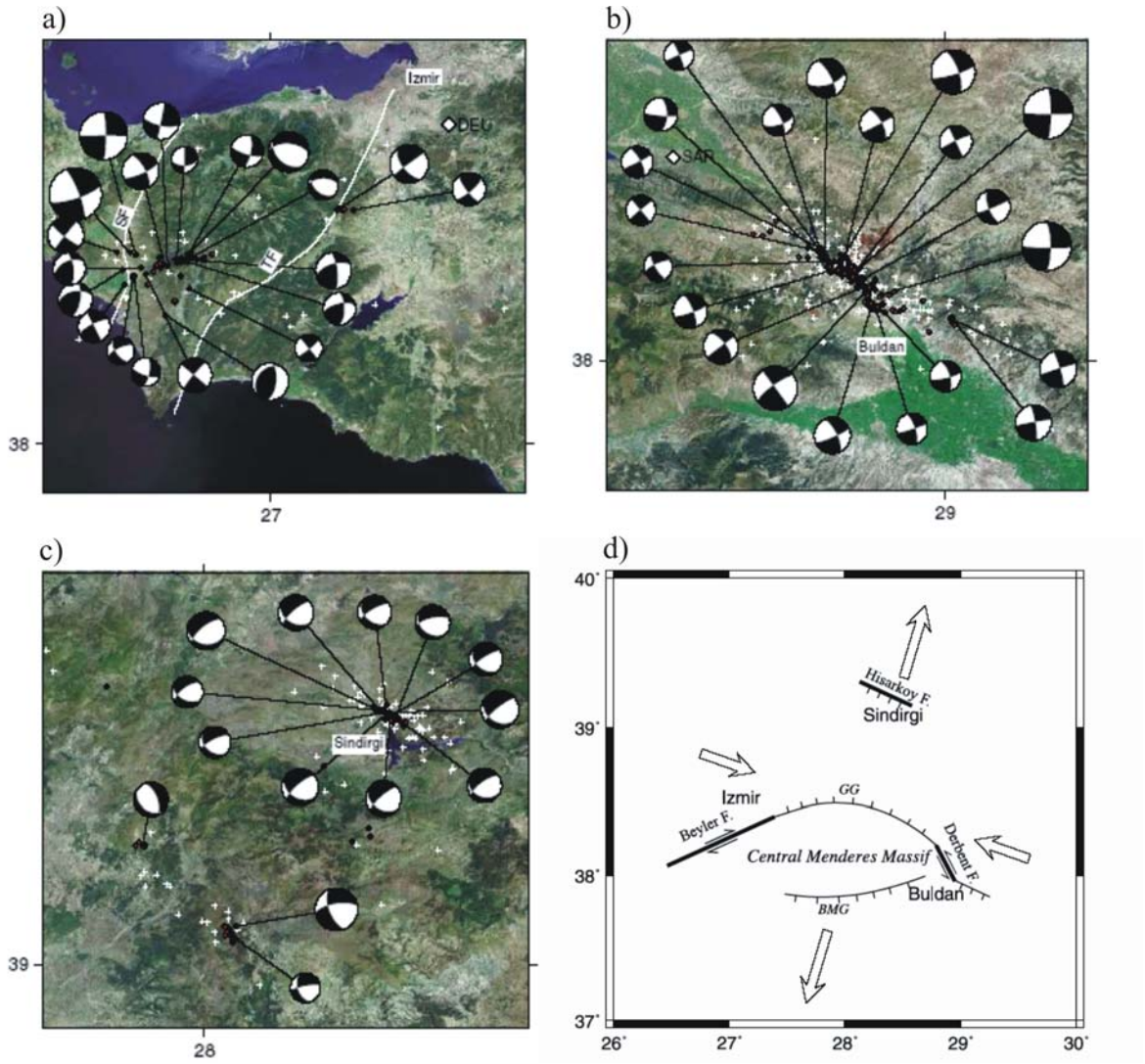

Figure 2. High resolution earthquake relocations and moment tensor determinations for three clustered events (modified from Zhu et al., 2006b). a) İzmir, b)Buldan and c) Sındırgı clusters. Relocated events (red dots) and the lowerhemisphere projections of focal mechanisms from waveform inversion on the top of high-resolution satellite image. Their original KOERI locations are shown as white-crosses. White colored lines represent two mapped faults, the Tuzla Fault (TF) and the Seferihisar Fault (SF), near the İzmir cluster. d) A pure-shear model explaining orientations and slip directions of the three identified active faults (thickened lines) in western Turkey. Arrows show the extensional and compressional directions inferred from averaging all fault plane solutions.

The results of shear-wave spliting measurements implies that anisotropy orientation is consistent with the direction of major vertical shear plain or the resistance corresponding compressional acceleration of the southwestward motion of Anatolian block in the region. Present-day active mechanism in the depth may suggest that the region is under the infulence of a couple of shear-zone trigerred by compression.

ACKNOWLEDGEMENTS

We thank Mike Fort of IRIS/PASSCAL, Oğuz Demir, Zülfikar Erhan, Adem Sömer and Emre Timur for their dedicated efforts in installing and maintaining all of the seismic stations during the course of this study. Our work benefited greatly from the cooperation and support of village officials and many residents of towns and villages throughout western Anatolia. We are also grateful to K. Kekovalı of KOERI for providing us

waveform data of several permanent seismic stations and İbrahim Çemen for his geological comments. This project was supported by the National Science Foundation (NSF), Office of International Science and Engineering, under Grant INT-0217493 and by the Scientific and Technical Research Council of Turkey (TÜBİTAK), the Research Grant Committee of Marine, Terrestrial and Atmospheric Sciences, under Grant YDABAG-102Y015.

REFERENCES

Akyol, N., L. Zhu, B. J. Mitchell, H. Sözbilir, and K. Kekovalı, 2006. Crustal structure and local seismicity in western Anatolia, *Geophys. J. Int.*, doi: 10.1111/j.1365-246X.2006.03053.x, in press.

Bozkurt, E., 2000. Timing of Extension on the Buyuk Menderes Graben, Western Turkey, and Its Tectonic Implications, in Tectonics and Magmatism in Turkey and the Surrounding Area, pp. 385-403, eds: Bozkurt, E., Winchester J.-A. & Piper, J.D.A., *Geol. Soc. London Special Publication*, 173.

Kissling, E., Ellsworth, W.-L., Eberhart-Phillips, D., and Kradolfer, U., 1994. Initial Reference Models in Local Earthquake Tomography, *J. Geophys*. Res., 99(B10), 19,635-19,646.

Kissling, E., Kradolfer, U., and Maurer, H., 1995. Program Velest User's Guide, *Institute of Geophysics, ETH* Zuerich.

Konak, N., and Şenel, M., 2002. Geological Map of Turkey at 1:500000 scale. *General Directorate of Mineral and Research Exploration of Turkey Publication*.

Kosarev, G., Kind, R., Sobolev, S., Yuan, X., Hanka, W., and Oreshin, S., 1999. Seismic evidence for a detached Indian lithospheric mantle beneath Tibet, *Science*, 283 (5406), 1306–1309,

Şaroğlu, F., Emre, Ö., and Kuşçu, İ., 1992. Active fault map of Turkey. *General Directorate of Mineral and Research Exploration of Turkey Publication*.

Şengör, A.-M.-C., Görür, N., and Şaroğlu F., 1985. Strike-slip Faulting and Related Basin Formations in Zones of Tectonic Escape: Turkey as a Case Study, in Strike-slip Faulting and Basin Formation, pp. 227-264, eds: Biddle K.-T. & Christie-Blick N., *Soc. Econ. Paleontol. Mineral. Special Publication*.

Şengör, A.-M.-C., 1987. Cross-Faults and Differential Stretching of Hanging Walls in Regions of Low-Angle Normal Faulting: Examples from Western Turkey, in Continental Extensional Tectonics, pp.575-589, eds: Coward, M.-P, Dewey J.-F. & Hancock, P.-L., *Geol. Soc. London Publication*.

Waldhauser, F., and Ellsworth, W., 2000. A double-difference earthquake location algorithm: Method and application to the northern Hayward fault, CA, *Bull. Seismol. Soc. Am.*, 90, 1353–1368.

Zandt, G., Myers, S. C., and Wallace, T. C., 1995. Crust and mantle structure across the Basin and Range-Colorado Plateau boundary at 37oN latitude and implications for Cenozoic extensional mechanism, *J. Geophys. Res.*, 100, 10,529–10,548.

Zhu, L., 1993. Estimation of crustal thickness and Vp/Vs ratio beneath the Tibetan Plateau from teleseismic converted waves, Eos Trans. AGU, 74(16), *Spring Meet. Suppl.*, 202.

Zhu, L., 2000. Crustal structure across the San Andreas Fault, southern California from teleseismic converted waves, *Earth Planet. Sci. Lett.*, 179, 183–190.

Zhu, L., and Helmberger, D. V., 1996. Advancement in source estimation

techniques using broadband regional seismograms, *Bull. Seismol. Soc. Am.*, 86, 1634–1641.

Zhu, L., Mitchell, B. J., Akyol, N., Cemen, I., and Kekovali, K., 2006a. Crustal thickness variations in the Aegean region and its implications for the extension of continental crust, *J. Geophys. Res.*, 111, B01,301,doi:10.1029/2005JB003,770.

Zhu, L., Akyol, N., Mitchell, B. J., and Sözbilir, H., 2006b. Seismotectonics of Western Turkey from High Resolution Earthquake Relocations and Moment Tensor Determinations, *Geoph. Res. Lett.*, 33, L07316, doi:10.1029/2006GL025842.

FAULTING AND SHAKING CHARACTERISTICS OF EARTHQUAKES IN İZMİR AND ITS CLOSE VICINITY

Aydan Ö.[1], Kumsar H.[2] and Türk N.[3]

[1]Tokai University, Dept. of Marine Civil Eng, Orido 3-20-1, Shimizu-ku, Shizuoka, Japan
aydan@scc.u-tokai.ac.jp
[2]Pamukkale University, Department of Geological Engineering, Kınıklı Campus, Denizli, Turkey
hkumsar@pamukkale.edu.tr
[3]Dokuz Eylül University, Department of Geological Engineering, Bornova, İzmir, Turkey

Abstract: İzmir with a population of more than 2 million people is the third largest city in Turkey. It suffered from very large earthquakes in the past and one of the most devastating events occurred in 1929. The geotechnical conditions vary from very soft sediments to hard rocks. Some areas are particularly prone to severe ground liquefaction. This study is concerned with the possible faulting mechanism and characteristics of future earthquakes in İzmir and its close vicinity on the basis of past earthquakes and past and present regional seismicity. The first part of the study is concerned with the faulting mechanism, recurrence and fundamental characteristics of possible earthquakes. In the second half, characteristics of strong ground motions recorded in İzmir and its close vicinity are presented and their possible implications are discussed. The faulting mechanism of regional earthquakes indicated that the classical horst-graben concept is not sufficient to explain the earthquake mechanism in İzmir and its close vicinity. The magnitude of earthquakes inferred may range between 6.3 and 7.2. The highest disturbing stress and mean stress concentration with a compressive character occurs in İzmir, which may be interpreted such that an earthquake due to strike-slip faulting with or without vertical component is likely.

Key words: İzmir, earthquake, liquefaction, characteristics, design spectra

1. INTRODUCTION

İzmir is the third largest city in Turkey with a population of more than 2 milllion. It suffered from very large earthquakes in the past. The most destructive recent event occurred in 1929, the epicenter of which was about 50 km away from İzmir. The geotechnical conditions varies from very soft sediments to hard rocks. However, a large populated part of the city is situated on soft sediments, which may either liquefy or prolong the period of shaking. As a result, a very large earthquake may ruin the entire city. Recent evaluations of crustal straining from the use of GPS measurements indicated that very large concentrations of crustal strains occur in the northern part of İzmir Bay (Aydan, 2000; Aydan et al., 2000a, 2000b). The amplitude of the concentration is much larger than other regions of Turkey. İzmir municipality initiated a project called RADIUS to assess the seismic vulnerability of İzmir and its close vicinity. Although it was the first study of its kind in Turkey, the scenarios are very optimistic in view of the past seismic history of İzmir.

This study is concerned with the possible faulting mechanism and characteristics of future earthquakes on the basis of past earthquakes and past and present seismicity of the region. The first part of the study is concerned with the faulting mechanism, recurrence and fundamental characteristics of possible earthquakes. In the second half, characteristics of strong ground motions recorded in İzmir and its close vicinity and crustal straining are presented and their possible implications are discussed.

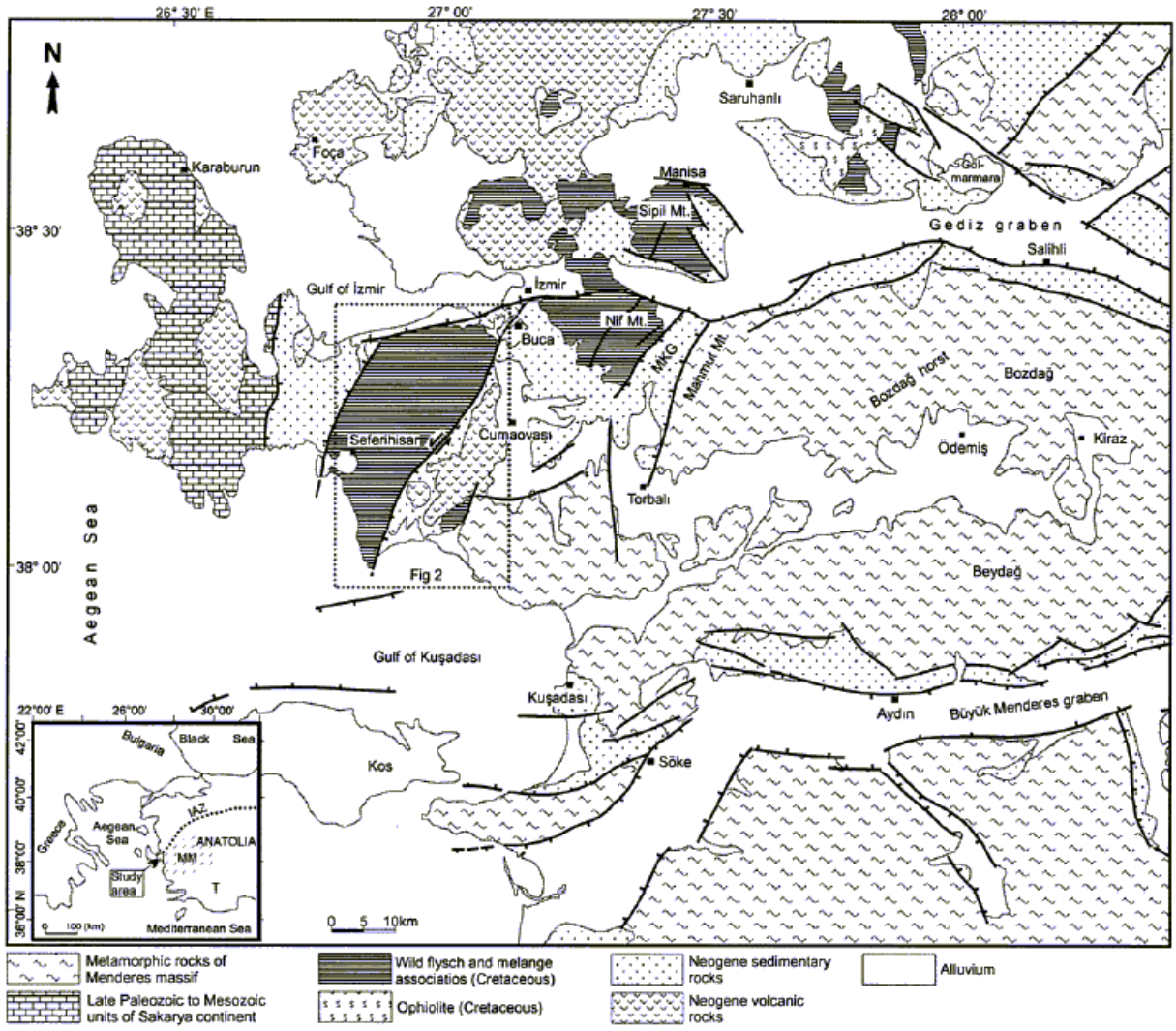

Figure 1. Geological features of İzmir and its close vicinity (after Genç et al., 2001)

2. GEOLOGY AND TECTONICS

The regional geology is shown in Figure 1. The city of İzmir and its close vicinity is situated over İzmir-Ankara-Erzincan Sture Zone (IAEZSZ). Its eastern part consists of metamorphic rocks of Menderes massif, while the western part of the units of Sakarya Continent. The strike of the IAEZSZ is N30E. The area was volcanically very active till Holocene (Genç et al., 2001). This volcanic activity is associated with the back-arc mechanism resulting from the subduction of African plate beneath plates of Aegean and Anadolu. As a result, the northern part of the region is covered with volcanic rocks. Volcanic rocks of andesitic type outcrop along southern (Kadifekale, Susuzdede) and northern side (Yamanlar) of İzmir Bay. The basement rock beneath the volcanic rocks is flysch. Alluvial sedimentary deposits cover river beds and shores of the Bay. These sedimentary deposits become very thick, particularly in the northern side (Çiğli, Karşıyaka) of the Bay and Bornova. These sedimentary deposits are mainly due to Gediz river, whose outlet to the sea was diverted to the north of the Bay in 1900s. The other thick sedimentary alluvial deposits are found along K. Menderes, Gediz and Bakırçay Rivers.

The initial phase of the regional tectonics probably involves N-S contraction associated with the closure of Tethys Ocean. The resulting Anadolu plate is sandwiched between the stationary Euro-Asian plate and the nortward moving African plate and it has been still

uplifted due to the subduction of the African plate beneath the Anadolu plate. The uplifting results in the stretching of the upper most part of the crust, which is the major driving mechanism for the development of horst-graben systems in Western Turkey (i.e. K. Menderes, B. Menderes, Gediz, Bakırçay Ovası), and the rotation of the Anadolu plate due to Coriolis force associated with the rotation of the earth causes lateral strike-slip movements within the deformable Anadolu plate (Aydan, 1997) (Figure 2).

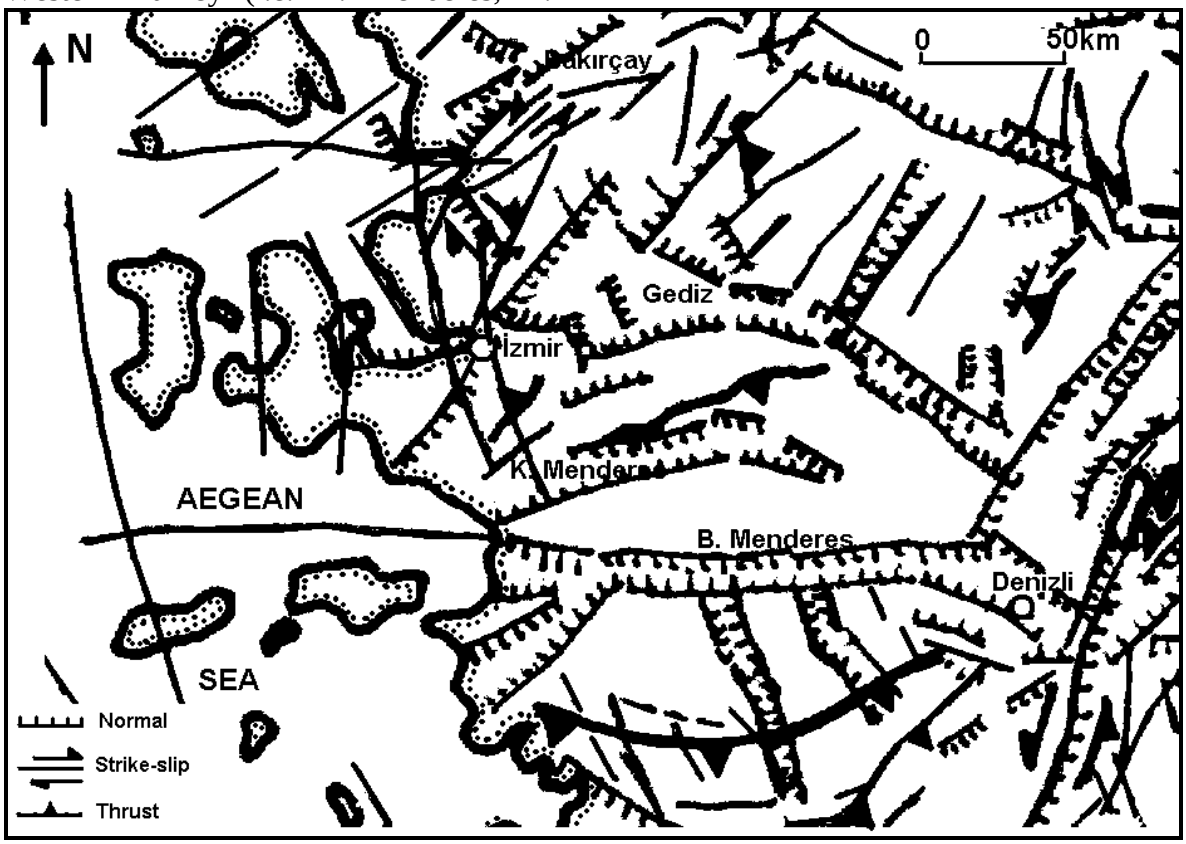

Figure 2. Major faults of İzmir and its close vicinity (after Aydan et al., 1998)

The faults can be grouped into three groups, namely, E-W normal faults and NW-SE and NE-SW lateral strike slip faults. Although NW-SE faults have generally the sinistral sense of relative movements, Doğanbey fault, which runs almost sub-parallel to the East Anadolu Suture Zone IAESZ, is said to be dextral lateral strike-slip fault. However, Genç et al., (2001) recently claimed that it could be a sinistral fault. The major tectonic features may be summarised as Urla-Orhaneli suture fault, Doğanbey sture fault, Gediz, K. Menderes, Bakırçay basin faults, Agamemnon II sinistral fault, Tire-Gördes fault, Torbalı-Akhisar fault. Agamemnon-I normal fault, Karaburun-Ayvacık fault bounds morphologically İzmir Bay and Karaburun Peninsula (Figure 3). The fault associated with the Bakırçay basin fault extends into the Aegean Sea just the north of Aliağa and passes the northern tip of Karaburun peninsula. This is also one of the major active lateral strike-slip fault in the close vicinity of İzmir.

Figure 3. Views of some faults in İzmir and its close vicinity

3. GEOTECHNICAL CONDITIONS

The geotechnical conditions in İzmir and its close vicinity varies from very soft ground to hard rocks. The heavily populated areas and business quarters of İzmir are all located on soft grounds. Figure 4 shows a regional and close-up geotechnical conditions. Borings at Konak and Basmane associated with İzmir metro project indicated that the weathered bed rocks are found to be at about 20m below the ground surface. The soil between the ground surface and weathered bed rock consists of clay, gravelly sand, clayey silt, sand and artificial fill. The total thickness of liquefiable sand layers ranges between 2m to 5m. Borings at Çiğli, Karşıyaka and Bostanlı districts in the northern side of İzmir Bay indicated that ground consisted of loose sand, silty sand, soft silty clay layers.

Andesitic rocks at the northern and southern sides of the bay area are generally jointed and subjected to a certain degree of weathering. The jointing near ground surface is intense. Limestone outcrops in the southern side of the bay and extends from Belkahve to Doğanbey Burnu. They may contain carstic cavities. Flysh rocks are generally observed in the southern side of the bay. It is a heavily foliated rock formation and it is easily weathered soon after the excavation.

4. SEISMICITY AND RECURRENCE

Historical earthquakes before 1900 are well documented in several earthquake catalogues prepared by ITU (Ergin et al., 1967 ; Eyidoğan et al., 1991), Kandilli Observatory (Ayhan et al., 1981), Earthquake Engineering Department of Turkey (Gençoğlu et al., 1990), TEDBASE (Aydan et al., 1996; Aydan,

1997), Istanbul University (Soysal et al. 1981). However, the conversion of the non-instrumental seismicity data is always a subjective issue. The seismicity of the region is divided into two broad groups, namely, historical seismicity and instrumented seismicity.

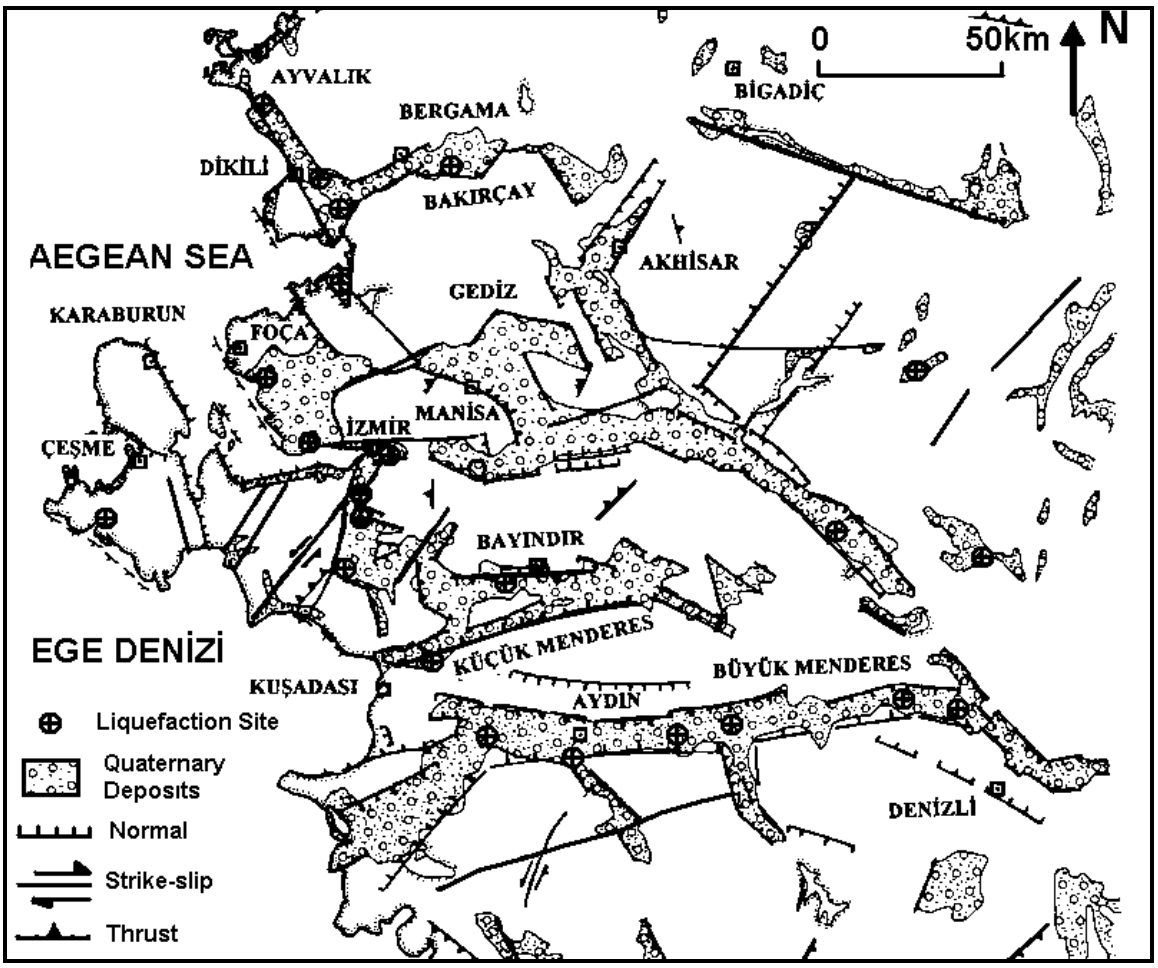

Figure 4. Regional and close-up geotechnical conditions and historical liquefaction sites

4.1. Historical Seismicity

The antique cities such as old İzmir (presently Bayraklı district), Efes, Milet, Bergama and Sart in the region were affected by strong earthquakes in the past. The strong historical earthquakes are summarized in Table 1. Magnitudes were inferred from the empirical relation suggested by Ergin et al. (1967). As can be noted from this table, earthquakes of Magnitude 7 class do occur in the region. The region is also affected by 7.5 class earthquakes in neighboring provinces.

Figure 5 shows the plot of historical earthquakes for about 1900 years. Large earthquakes with a magnitude greater than 6.4 occur every 300 year.

4.2. Instrumental Seismicity

The magnitudes of the earthquakes that occurred between 1900-2004 were not greater than 6.4 (Figure 6 and Figure 7). Figure 6 shows the cumulative magnitude and the magnitude of earthquakes as a function of time between 1900 and 2005. Figure 7 shows the seismicity of the region between 1973 and 2005 before the recent seismic activity in Sığacık Bay. The tendency of the cumulative magnitude has been increasing at an alarming rate. If there is no problem with the recording of the seismic activity before 1990, the energy release is quite high between 1990 and 2005. The shape of the curve resembles the tertiary phase of creep tests of geo-materials. It seems

that the region has entered one of its high seismic activity periods.

Table 1. List of historical earthquakes in İzmir and its close vicinity

Day	Mon	Year	Io	M	Lat	Lon	Dead	Location
1	1	17	10	7.5	38.63	27.59	0	İzmir, Efes, Sart, Aydın, Manisa
1	1	44	8	6.4	38.2	27.4	0	Manisa-Efes
1	1	105	8	6.4	38.9	27	0	Aliağa
1	1	178	8	6.5	38.3	27.1	0	İzmir
1	1	688	9	6.5	38.41	27.3	20000	İzmir
1	1	1039	8	6.8	38.4	27.3	0	İzmir
20	3	1389	8	6.7	38.4	26.3	0	Sakız
1	1	1546	7	6.3	38.2	25.9	0	Sakız
20	5	1654	8	6.4	38.5	27.1	0	İzmir
23	1	1674	7	6.2	38.4	26.3	0	Sakız
14	2	1680	7	6.2	38.4	27.2	0	İzmir
10	7	1688	10	6.8	38.3	26.2	15000	İzmir
13	1	1690	7	6.4	38.6	27.4	0	İzmir
1	9	1723	8	6.4	38.4	27	500	İzmir
4	4	1739	8	6.8	38.5	26.9	80	İzmir Bay, Foça
24	11	1772	8	6.4	38.8	26.7	0	Foça
3	7	1778	9	6.4	38.4	26.8	200	İzmir
1	1	1801	10	6.8	38.3	26.2	0	İzmir
19	11	1852	8	6.3	38.4	26.1	0	İzmir
3	11	1862	10	6.9	38.5	27.9	280	Turgutlu
16	8	1863	8	6.2	38.3	26.1	0	Sakız
2	2	1866	8	6.4	38.4	26	0	Sakız
1	3	1880	9	6.8	38.4	26.1	4000	Sakız
29	7	1880	9	6.7	38.6	27.1	30	Menemen
3	4	1881	9	6.5	38.3	26.2	50	Sakız, Tsunami
15	10	1883	9	6.8	38.3	26.6	15000	Çeşme
14	12	1890	8	6.2	37.85	27.25	0	Efes

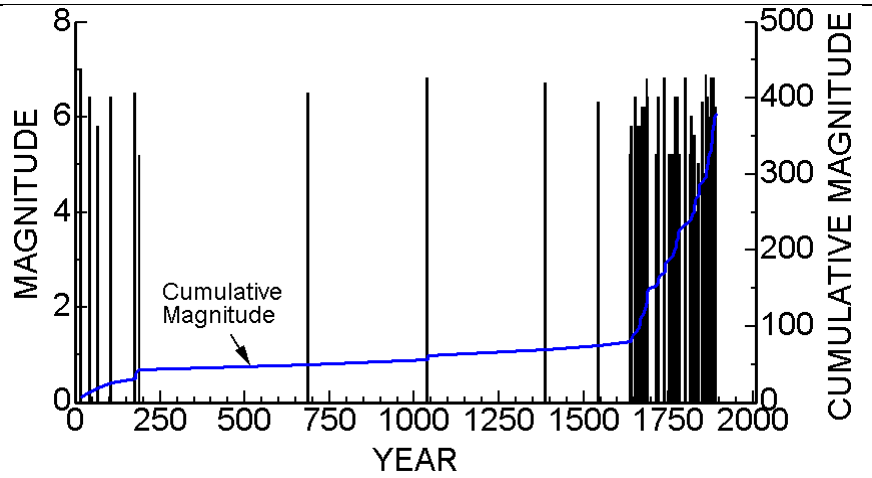

Figure 5. The cumulative magnitude and the magnitude of earthquakes as a function of time for the last 1900 years

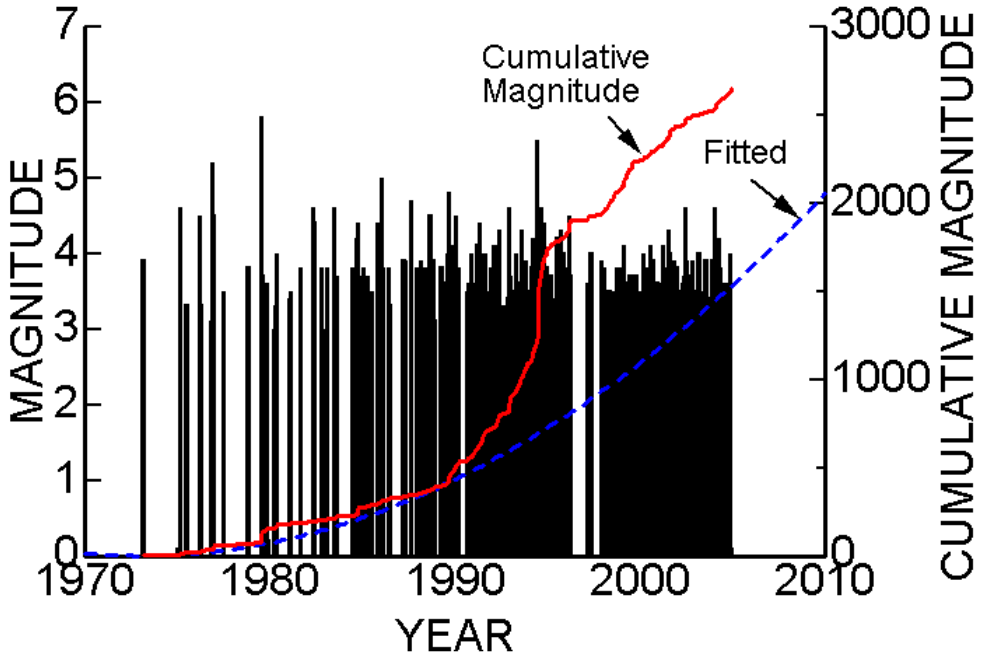

Figure 6. The seismicity of the region between 1973 and 2005 before the recent seismic activity in Sığacık Bay

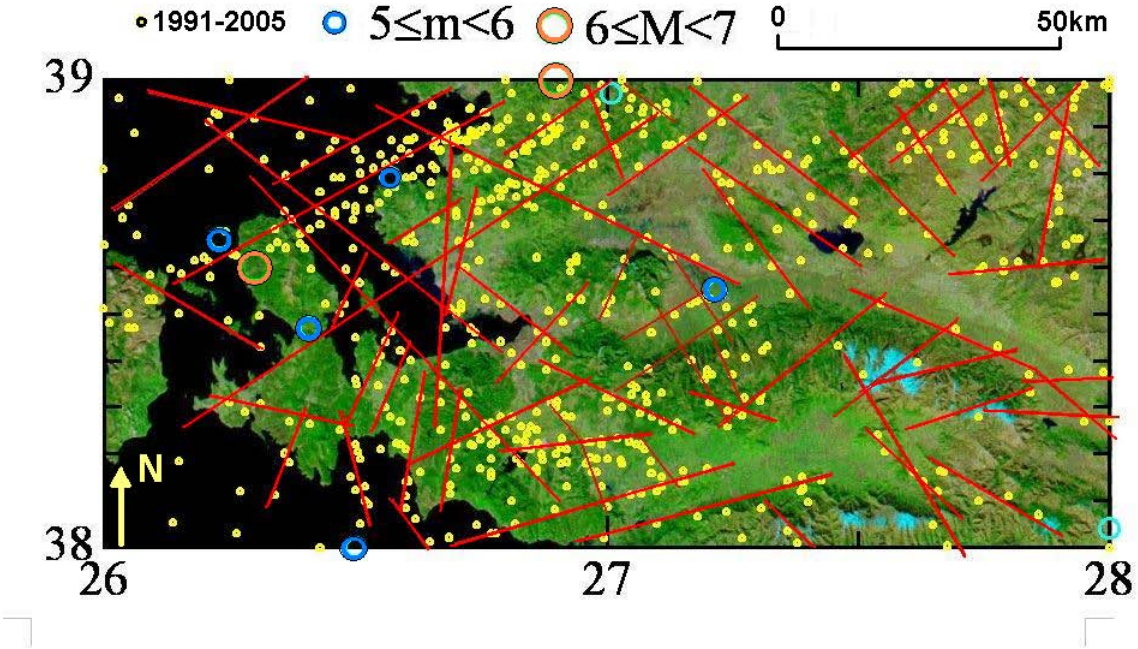

Figure 7. The epicenters of the recent seismicity of the region between 1991 and 2005 before the recent seismic activity in Sığacık Bay and inferred faults

4.3. Earthquake Occurrence Frequencies and Magnitude Relation

The seismicity of the region bounded between latitudes 36.67-38.83N and longitudes 27.16-31.08E was also studied by Gençoğlu et al. (1990) for a period between 1900 and 1986. The empirical relation of Gutenberg-Richter (1942) of the following form is used

$$\log N = a - bM \qquad (1)$$

Coefficients obtained by Gençoğlu et al., (1990) and by Aydan et al. (2002) together with observed data are shown in Figure 8. The maximum magnitudes of earthquakes inferred from these relations range between 6.43 and 6.53 for the given period of time. The inferred b coefficients

in the relation are very similar to each other and it is close to the b coefficient of the global seismicity. Furthermore, the computed results indicate that M 7-7.5 class earthquakes may occur at time intervals ranging between 400 to 800 years.

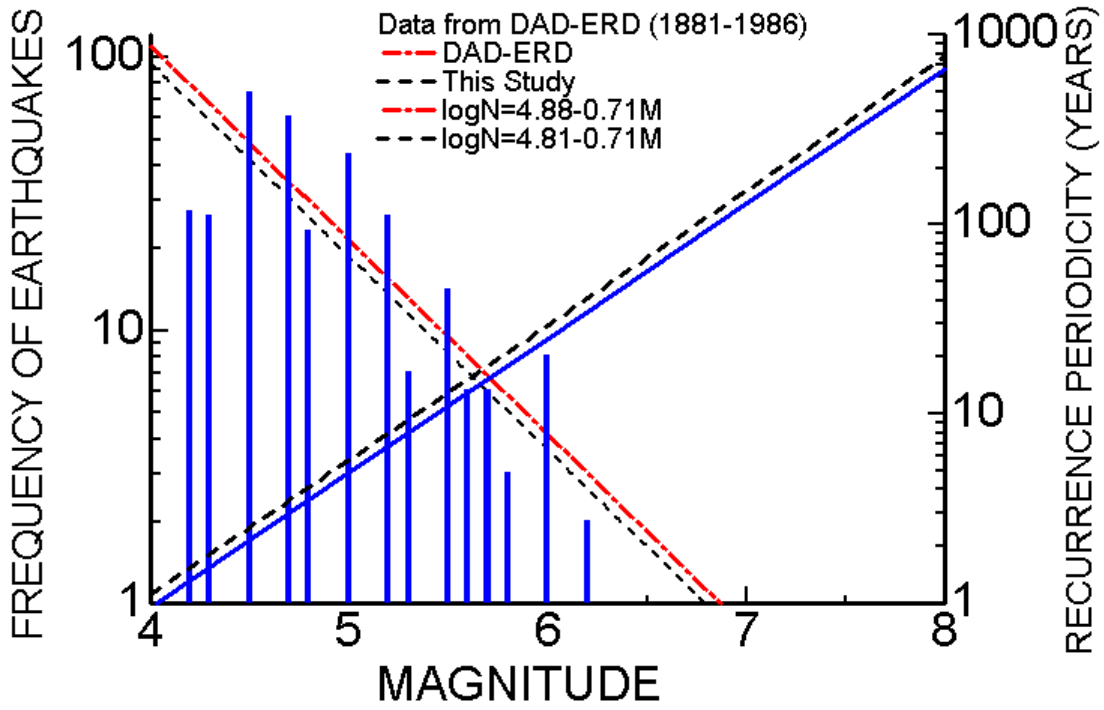

Figure 8. The frequency, magnitude and recurrence relations for the last century

5. CHARACTERISTICS OF EXISTING FAULTS AND EARTHQUAKES

5.1. Inference of Characteristics of Possible Earthquakes from Existing Faults

The striations and internal structure of the faults are just evidences of stress state that caused them, and they may also indicate the type of earthquake they produced. Therefore, the data for the faults for a given region may be used to infer the possible mechanism and characteristics of earthquakes. For such a study, the young faults must be given priority. The methodology for the inference of the possible mechanism of the faults require data on dip, dip direction and striation orientation (Aydan, 2000). A large scale map of the active faults of Turkey is prepared by MTA. The only active faults in the region around İzmir are Doğanbey fault, faults of Gediz Valley and strike-slip faults in the vicinity of Aliağa and Çandarlı Bay (Figure 9). In other words no active faults are mapped along İzmir Bay in-spite of many earthquakes around the Bay. The authors have been investigating the faults in the region. The strike of faults in the region can be grouped as NW-SE, E-W and NE-SW. Figure 10 also shows the inferred faulting mechanisms using the measurements done by the authors and the method proposed by Aydan et al. (2002). The faulting mechanism must be in the form of normal faulting with a small amount of sinistral or dextral slip for the region. Furthermore, the inferred faulting mechanisms are quite similar to those of recent earthquakes in the region.

Aydan and his co-workers (Aydan et al., 1996; Aydan, 1997; Aydan and Hasgür, 1997; Aydan and Kumsar, 1997; Aydan et al., 2002) proposed various empirical relations among several parameters of the earthquakes based on Turkish earthquake data only. The methodology proposed by Aydan et al. (2002) is the determination of characteristics of earthquakes through the

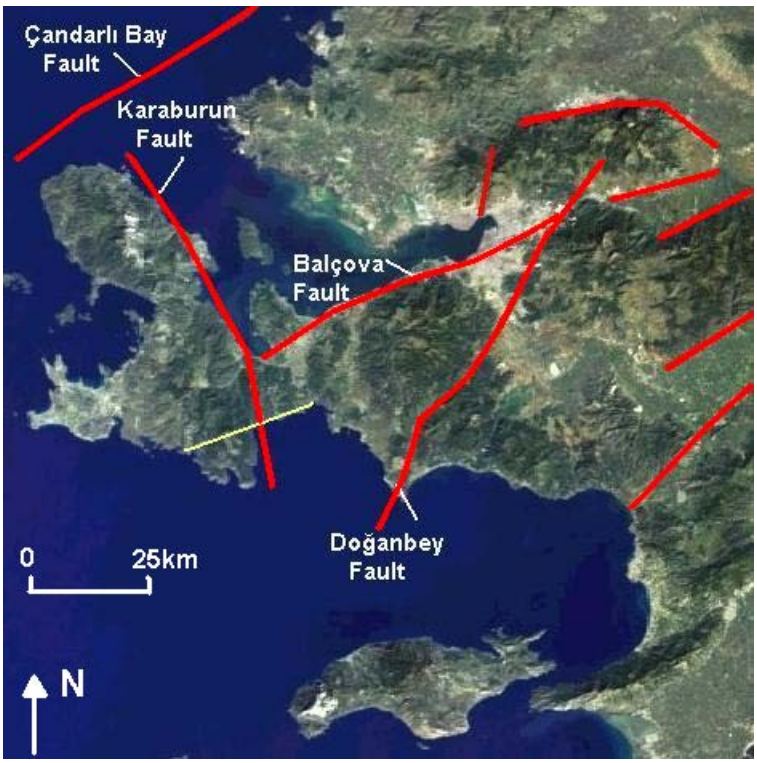

Figure 9. Major faults in İzmir and its close vicinity

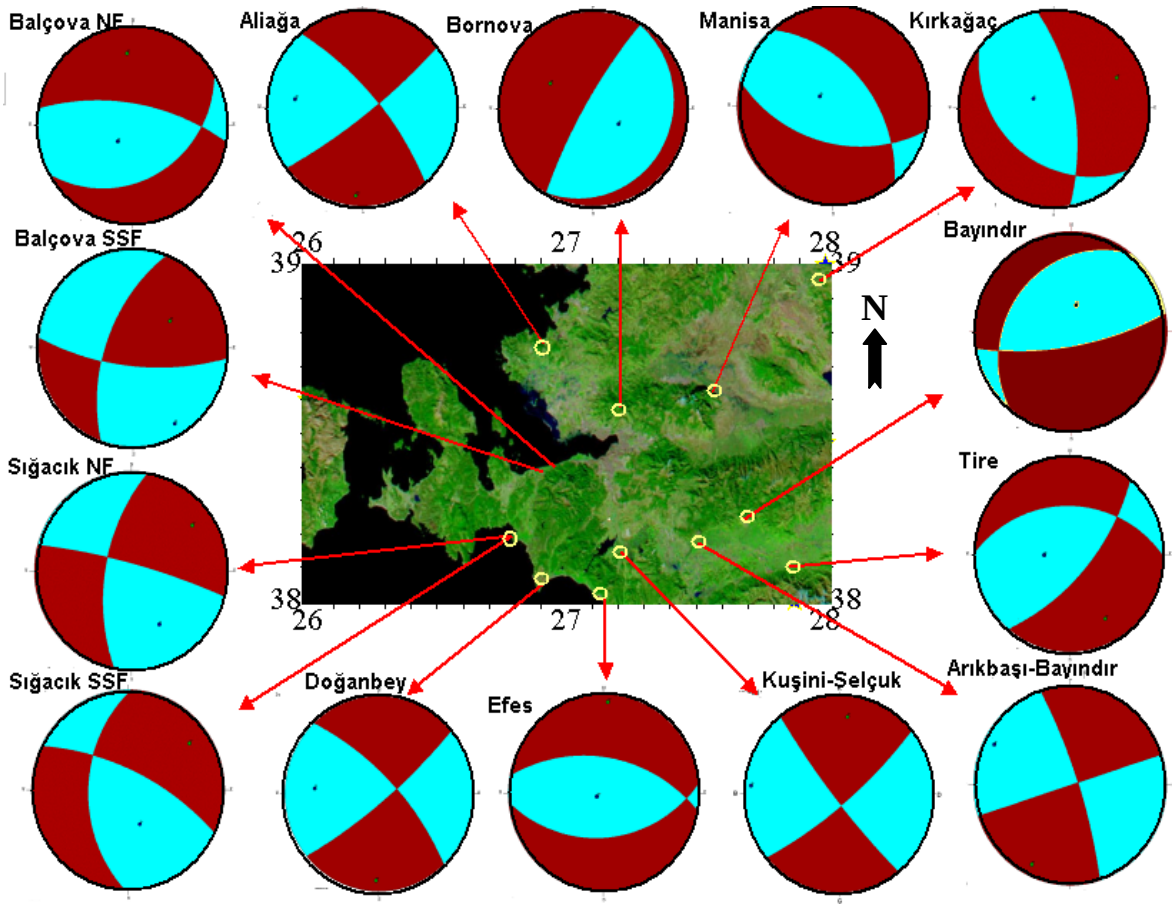

Figure 10. Inferred focal plane solutions from existing faults in İzmir and its close vicinity

utilization of the surface trace length of the fault. Although the actual length of faults may be longer than their surface trace length, it may be useful for determining the earthquake characteristics. First the magnitude of earthquake is either obtained graphically or non-linear back analysis of the empirical relations of Aydan (1997). Once the magnitude of the earthquake is determined, then the other characteristics of the expected earthquakes can be obtained from other empirical relations.

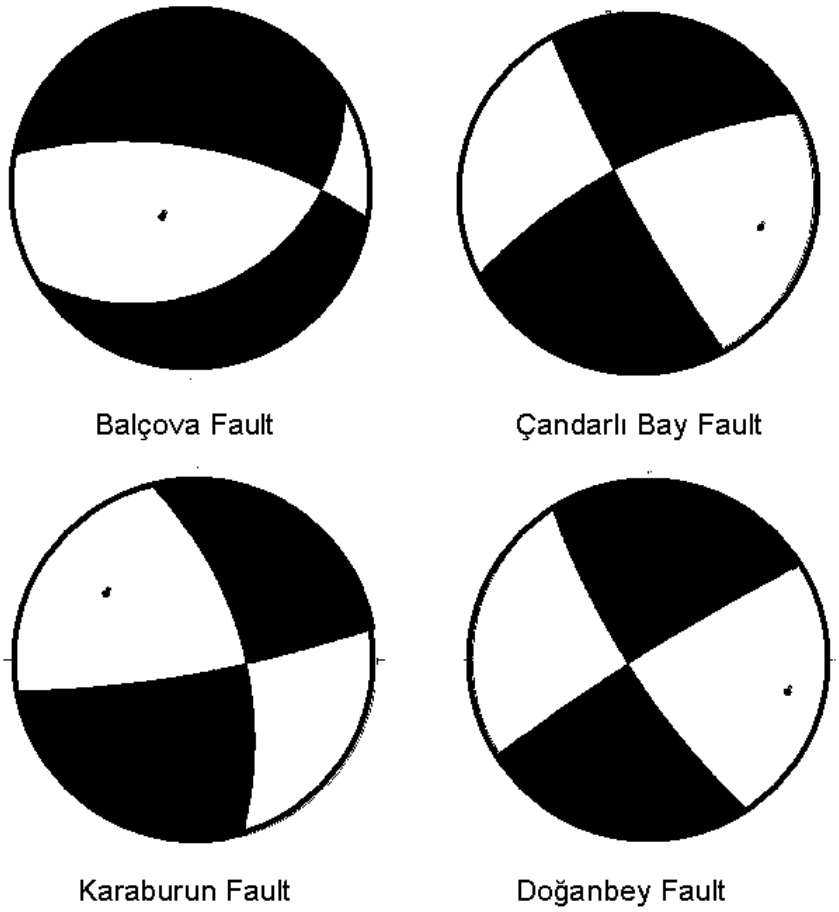

Figure 11. Inferred focal mechanism solutions for major faults in İzmir and its close vicinity

The most prominent faults in the region are Doğanbey, Balçova, Karaburun and Çandarlı faults (Figure 9). The inferred characteristics of possible earthquakes and their focal plane solutions to be produced by the faults are given in Table 2 and Figure 11. The surface magnitude of the earthquakes may range between 6.3 and 6.9 while moment magnitude may range between 6.6 and 7.2. The maximum ground acceleration may range between 430 to 744 gals in soft ground, which may be very critical for inducing both structural failure and ground liquefactions. Furthermore, relative fault slips may range between 35 to 84 cm.

Table 2. Inferred characteristics of the earthquakes for İzmir region

Fault		Magnitude		Depth (km)	Amax (Gal) (R=25km)	RVHA	UMAX (cm)
Name	Length (km)	M_s	M_w				
Balçova	35	6.30	6.57	19.96	432	0.51	35.0
Çandarlı Bay	50	6.54	6.83	21.71	538	0.52	50.0
Doğanbey	85	6.90	7.21	24.45	744	0.53	84.0
Karaburun	60	6.67	6.96	22.89	605	0.52	60.0

5.2. Faulting Mechanisms and Shaking Characteristics of Past Earthquakes

Faulting mechanisms of earthquakes that have occurred within the region bounded by Latitudes 37-39 and Longitudes 26-28 are obtained by several researchers and institutes, specifically Canıtez ve Üçer (1967), Kalafat (1998), Eyidoğan and Jackson (1995), ETHZ for earthquakes between 2000-2003 and Harvard and USGS for earthquakes between 1986 and 2003 and they are shown in Figure 12. The dominant faulting mechanism is either normal faulting with the lateral strike slip components or lateral strike-slip faulting with normal component. The faulting mechanism of 2005 earthquakes in Sığacık Bay is quite similar to those of 2003 Seferihisar earthquakes.

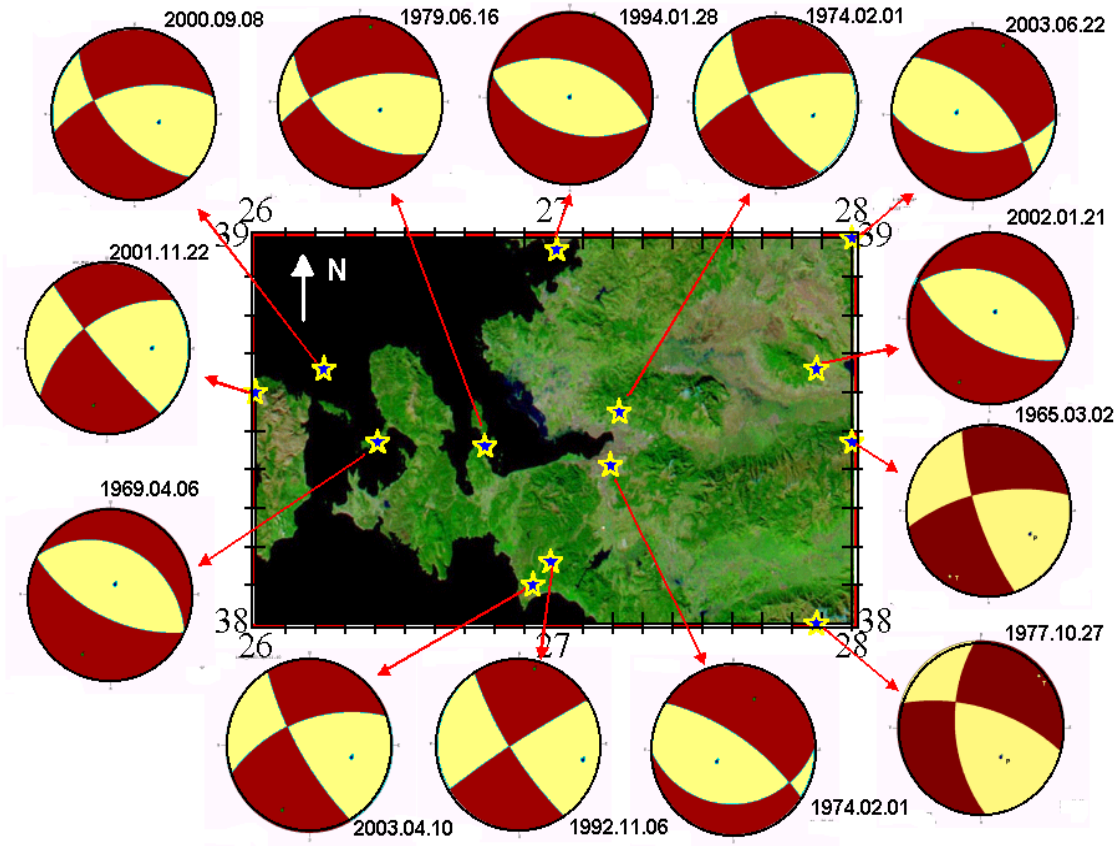

Figure 12. Focal mechanism of earthquakes in İzmir and its close vicinity

One of the earliest strong motions records was taken during the earthquake of December 16, 1977 with a magnitude of 5.3. This earthquake was very close to the İzmir city center (24km) and it was probably associated with either Balçova or Doğanbey faults where they intersect each other. The NS component of this earthquake was 391gal and it is yet the largest strong motion record in İzmir. Figure 13 shows acceleration response spectra of three components of several earthquakes including the 1977 earthquake and recent Sığacık Bay earthquakes. The relative acceleration response spectra exceed the designated relative acceleration of Turkish Seismic Design Code. The results also indicate that if the ground accelerations are similar to those of the 1977 earthquake, RC buildings having a story number more than 4 may be severely affected by the earthquakes.

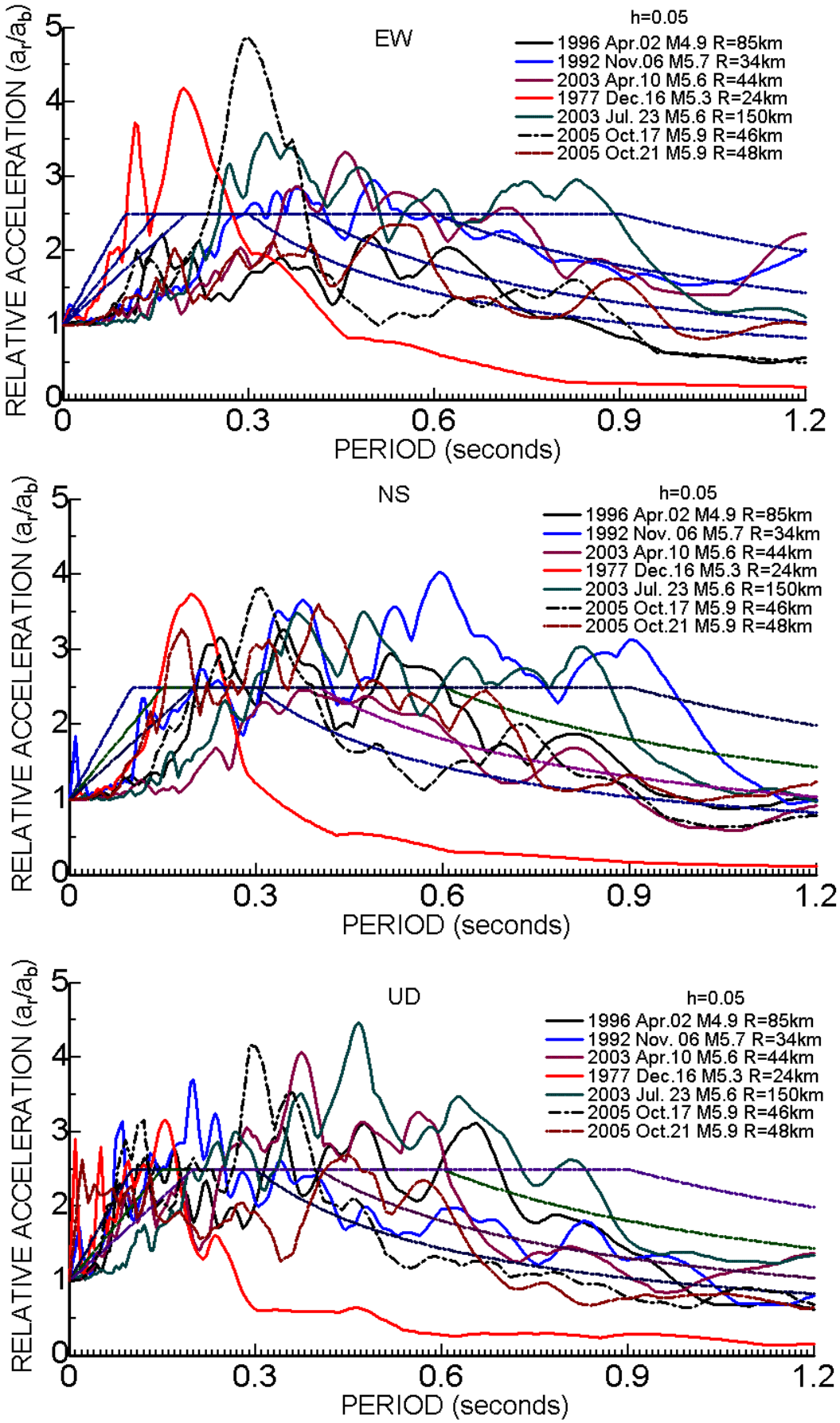

Figure 13. Response spectra of selected strong motion records of earthquakes taken at Bornova

6. CURRENT CRUSTAL STRAINING IN THE VICINITY OF İZMİR

From the crustal deformation measurements by GPS (Reilinger et al., 1997) and computations of mean stress variations, it is clarified that the region is undergoing a stretching strain regime (Aydan, 2000a, 2003; Aydan et al., 2000). Figure 14 shows the deformation rates and disturbing stress rate distribution in Western Turkey, in which the highest stress rate concentration occurs in İzmir. The concentration of the disturbing stress rate nearby İzmir is particularly of great concern since such a stress field should result in strike-slip faulting at the location where Balçova or Doğanbey faults intersect each other.

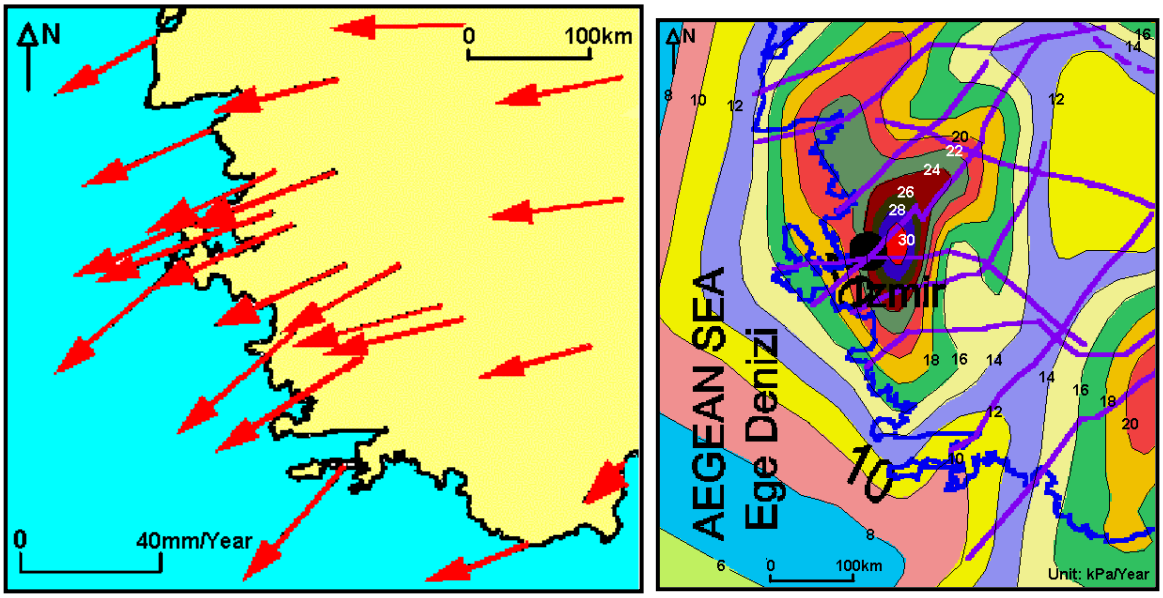

Figure 14. Motion and disturbing stress rate in Western Anadolu

7. CONCLUSIONS

Several aspects such as geology, tectonics, faulting and shaking characteristics and current crustal straining of the İzmir region are presented. The conclusions from this study may be summarised as follows:

The faulting mechanism of regional earthquakes indicated that the classical horst-graben concept is not sufficient to explain the earthquake mechanism in İzmir and its close vicinity.

Although the dominant faulting mechanism is normal faulting, the lateral strike slip faulting is also observed.

The magnitude of earthquakes inferred from fault traces may range between 6.3 and 7.2.

The relative acceleration response spectra of past earthquakes of İzmir exceed the designated relative acceleration of Turkish Seismic Design Code.

From the crustal deformation measurements by GPS and computations of mean stress variations, the highest disturbing stress and mean stress concentration with a compressive character occurs in the İzmir, which may be interpreted such that an earthquake due to strike-slip faulting with or without vertical component is likely in the near future. Therefore, real-time monitoring of regional straining is of great importance for the region.

REFERENCES

Aydan, Ö., 1997. Seismic characteristics of Turkish earthquakes," *Turkish Earthquake Foundation*, TDV/TR 97-007.

Aydan, Ö., 2000. A stress inference method based on GPS measurements for the directions and rate of stresses in the earth's crust and their variation with time, *Yerbilimleri*, 22, 21-32.

Aydan, Ö. (2003): The earthquake prediction and earthquake risk in Turkey and the applicability of Global Positioning System (GPS) for these purposes. *Turkish Earthquake Foundation*, TDV/KT 024-87, 1-73 (in Turkish).

Aydan, Ö. and Hasgür, Z., 1997. Acceleration characteristics of Turkish earthquakes. *The 4th National Earthquake Engineering Conference*, 30-37.

Aydan, Ö. and Kumsar, H., 1997. A site investigation of Oct. 1, 1995 Dinar Earthquake," *Turkish Earthquake Foundation*, TDV/DR 97-003, 116.

Aydan, Ö., Sezaki, M. and Yarar, R., 1996. The seismic characteristics of Turkish Earthquakes, *The 11th World Conf. on Earthquake Eng.*, CD-2, Paper No:1270.

Aydan, Ö., Kumsar, H. and Ulusay, R., 2000a. The implications of crustal strain-stress rate variations computed from GPS measurements on the earthquake potential of Turkey. *Int. Conf. of GIS on Earth Science and Applications*. ICGEAS 2000, Menemen.

Aydan, Ö., Ulusay, R. and Kumsar H., 2000b. An approach for earthquake occurrences in Western Anatolia through GPS measurements, *The Symp. on Earthquake Potential of Western Anatolia*, 279-292.

Aydan, Ö, Kumsar, H., and Ulusay, R., 2002. How to infer the possible mechanism and characteristics of earthquakes from the strations and ground surface traces of existing faults. *JSCE, Earthquake and Structural Engineering Division*, Vol. 19, No.2, 199-208.

Ayhan, E., Alsan, E., Sancaklı, N. and Üçer, S.B., 1981. A catalog of earthquakes for Turkey and surrounding area (1881-1980). *Boğaziçi University* (in Turkish).

Canıtez, N. and S.B. Üçer, 1967. Computer determinations for the fault plane solutions in and near Anatolia, *Tectonophysics*, 4(3), 235-244.

Ergin, K., Güçlü, U. and Uz, Z., 1967. A catalog of earthquakes for Turkey and surrounding area. *ITU, Faculty of Mining Engineering*, No. 24.

ETHZ. Automatic Moment Tensor Solutions. http://www.seismo.ethz.ch/mt/

Eyidoğan, H., Güçlü, U., Utku, Z., Değirmenci E., 1991. *Türkiye Büyük Depremleri Makro-sismik Rehberi* (1900-1988). ITU, Maden Fakültesi, 198p.

Eyidoğan, H. and J. Jackson, 1995. A seismological study of normal faulting in the Demirci, Alaşehir and Gediz earthquakes of 1969-1970 in the Western Turkey. Implications for the nature and geometry of deformation in the continental crust. *Geophys. J. R. Astr. Soc.*, 81, 569-607

Genç, C.Ş., Altunkaynak, Ş., Karacık, Z., Yazman, M. Ve Yılmaz, Y. 2001. The Çubukdağ graben, South of İzmir: its tectonic significance in the Neogene geological evolution of the western Anatolia, *Geodinamica Acta*, 14, pp 45-55.

Gençoğlu, S., İnan, I. and Güler, H., 1990. Türkiyenin Deprem Tehlikesi. (Earthquake danger of Turkey) *Pub. of the Chamber of Geophysical Engineers of Turkey, Ankara*.

Gutenberg, B. and Richter, C.F., 1942. Earthquake magnitude, intensity, energy and acceleration. *Bulletin of Seismological Society of America*, 32, 163-191.

Harvard University Seismology: http://www.seismology.harvard.edu

İzmir Municipality, 1999: Radius Project.

Kalafat, D., 1998. An investigation of fault plane solutions of tectonic structures of Anadolu, *Deprem Araştırma Bülteni*, Ankara, Yıl 25, Sayı 77, 1-217.

Reilinger, R.E, S.C. McClusky, M.B., Oral, R.W., King, M., Toksöz, N., Barka, A.A., Kınık, I., Lenk, O. and Şanlı I., 1997. Global positioning system measurements of present-day crustal movements in the Arabia-Africa-Euroasia plate collision zone, *J. Geophysical Research*, 102(B5), 9983-9999.

Soysal, H., Sipahioğlu, S., Kolçak, D. and Altınok, Y., 1981. A catalog of earthquakes for Turkey and surrounding area (BC 2100-AD1900). *Istanbul University, Earth Science Faculty*, TUBITAK, Proje No. TBAG 341(in Turkish).

USGS. Moment Tensor & Broadband Source Parameter Search http://earthquake.usgs.gov/

(This page is left blank intentionally.)

AN APPLICATION OF MULTI-CRITERIA DECISION ANALYSIS IN THE HARMANDALI (IZMIR) WASTE DISPOSAL SITE USING GEOGRAPHICAL INFORMATION SYSTEMS (GIS)

Baysal G.[1], Tecim V.[1] and Kıncal C.[2]

[1]Dokuz Eylul Univ., Faculty of Economics and Administrative Sciences, Dept. of Econometrics, 35160, Buca-Izmir/Turkiye

[2]Dokuz Eylul Univ., Engineering Faculty, Geological Engineering Dept., 35100, Bornova- Izmir/Turkiye

Abstract: In various aspects of our lives, we all come face to face with different decision problems everyday. Decision problems have different importance levels. They can be deliberated in a wide screen from daily simple decision situations to important strategic decisions. Both of them have common features. They contain two components; criteria and alternatives. Criteria are factors for evaluating the decision problem. Alternatives are determined according to the criteria. Decision problems need techniques to solve the structure which have multiple criteria.

Multi-Criteria Decision Analysis (MCDA) had been developed to solve decision problems which have multiple structures. MCDA methods contain different ways for different problem structures (Triantaphyllou, E., 2000). ELECTRE (Elimination and Choice Translating Reality; English translation from the French original, Triantaphyllou, 2000), TOPSIS (the Technique for Order Preference by Similarity to Ideal Solution) and AHP (Analytic Hierarchy Process) are the methods which are well known and used very often. These methods provide a matrix form to evaluate all criteria and all alternatives which belong to the decision problem at the same time.

Spatial data are used in real life applications of decision problems. These spatial data are important for the problems. Geographical Information Systems (GIS) are used to analyse these data and prepare maps. Spatial data and non-spatial data are connected together in GIS and they are used for supporting the decision making process.

In this study, Harmandali (Izmir) waste disposal site is examined using MCDA with the help of GIS. The aim of this study is to analyse Harmandali (Izmir) waste disposal site for suitability. TOPSIS and ELECTRE methods were used to analyse this site.

1. INTRODUCTION

Decision problems are met in every aspect of life. We solve a lot of decision problems in our daily lives. They can be in different importance levels from simple problems to strategic decisions. Decision problems have multiple criteria in real life applications. Criteria are factors for evaluating the decision problems. It's important to satisfy these criteria for solving decision problems.

Multi-Criteria Decision Analysis (MCDA) had been developed to analyse these criteria and to solve decision problems (Belton and Stewart, 2002). MCDA can be evaluated in two different classes: Multiattribute Decision Making (MADM) and Multiobjective Decision Making (MODM). MADM includes a selection of the best alternative in a set of alternatives which have already been decribed. MODM hasn't got any alterrnatives. Decision makers design a best alternative in MODM. They use mathematical functions. Criterion includes both the concepts of attribute and objective (Malczewski, 1999). In this study the best alternative had been selected in a set of alternatives. The selection was made by using TOPSIS method.

TOPSIS method provides the evaluation of criteria and alternative in a matrix structure at the same time. Harmandali Waste Disposal Site borehole data were examined by using TOPSIS and ELECTRE methods. The results of ELECTRE method didn't support two criteria. But the result of TOPSIS method provided a suitable solution. So, only the TOPSIS method application is explained

in this study. The results of the ELECTRE method are expressed at the end of the study.

Geographical Information Systems (GIS) are used to analyse these data and prepare intelligent maps (Tecim, 2001). GIS maps are called “intelligent maps”, because these maps provide the use of statistical and spatial data together (Malczewski, 1999).

Borehole data for Harmandali Waste Disposal Site (Figure 1) have been used in this study. TOPSIS method is applied on these data and GIS suitability maps have been prepared by using these data. The results of two analyses were evaluated together, and commented on. The aim of the study is to select the most suitable area for the waste disposal site in Harmandali.

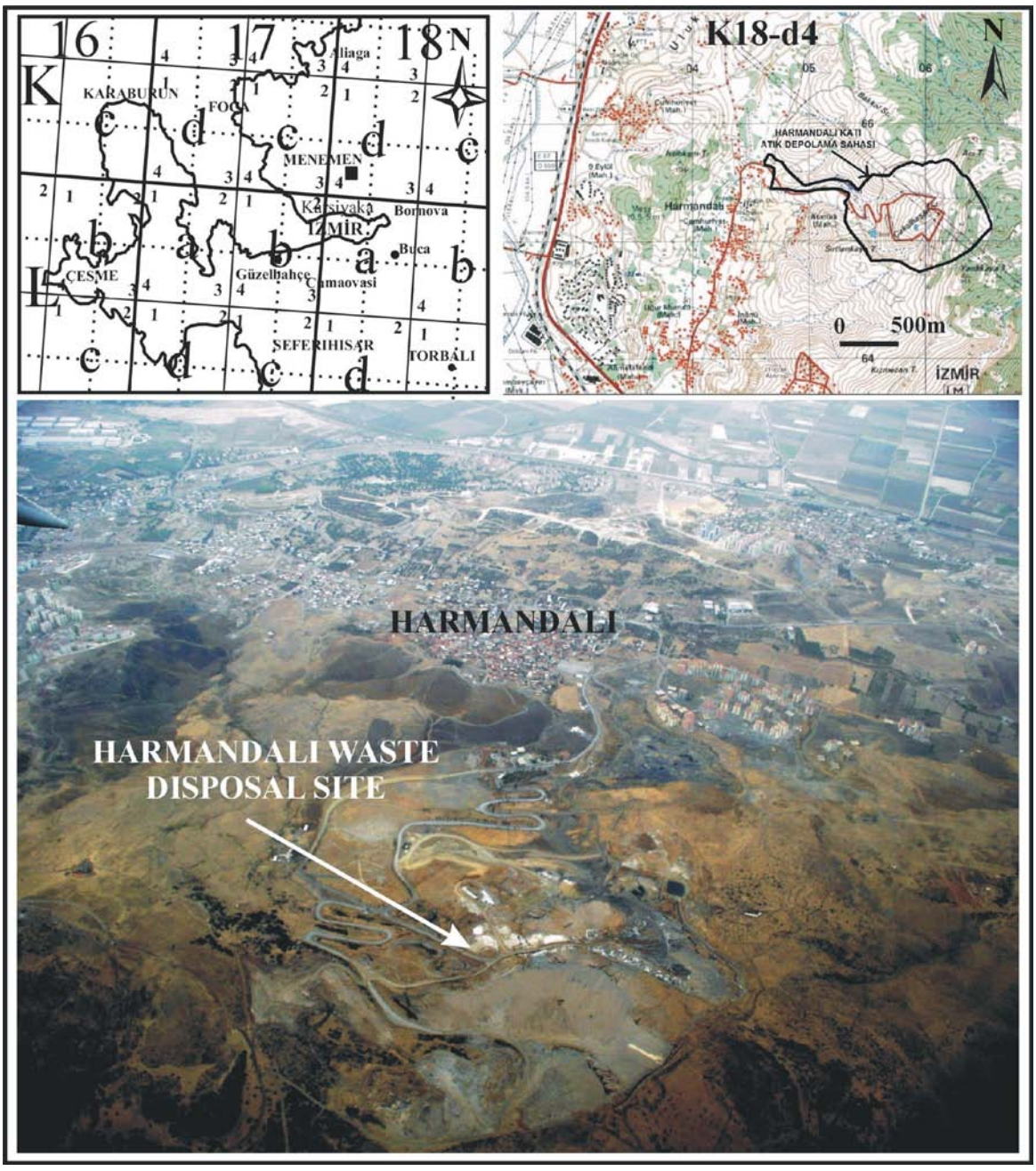

Figure 1. Harmandali Waste Disposal Site Location Map

2. GEOLOGICAL SETTING

1/5000 scale geological map and the tectonic map were prepared by Hacettepe University International Karst Water Resources Application and Research Center (UKAM, 1990). Figure 2b shows the Upper Cretaceous Bornova melange, the Neogene pyroclastic rocks and the slopewash.

2.1 Bornova Flysch Formation

Bornova Flysch formation covers nearly half of the study area. Quartz bands and sandstone-mudstone intercalations can be seen in the Bornova Flysch formation, which is exposed between 30-200 meter elevations in the study area (Dubertret ve Kalafatçıoğlu, 1973). Mudstones do not represent bedding plains but thin laminations can be seen. Sandstones have thin or moderate thickness of bedding planes and dip to northwestern.

2.2 Pyroclastic Formations

Pyroclastic rocks seen commonly in the study area unconformably overlie Bornova Flysch formation. Volcanic breccia, agglomerate and andesitic tuffs are exposed as Pyroclastic rocks in the study area. Pyroclastic rocks are composed of deterioration products of the andesites. Joint sets can be seen in andesites in and around the study area (UKAM, 1990).

2.3 Slopewash

Slopewash was formed by pyroclastic cover rocks, outcrops along the Şarlak Stream, which is in the west of the study area. Also sandstone gravels and clay and mill-size particles can be seen in the slopewash. The thickness of the slopewash was determined as 19 meters in the SK-1 titled borehole.

2.4 Borings

24 soil borings (360 m) and 4 observation borings were conducted in the Harmandalı (Izmir) area to observe the soil suitability for storing solid waste disposals by Izmir municipality (Figure 2a).

To analyze geotechnical and engineering properties of the existing soils in the study area, disturbed and undisturbed soil and rock samples were taken from the boreholes. Also, in-situ Standard Penetration Test (SPT), Lugeon Tests were conducted in the field. RQD(%) values were calculated using core samples which were taken from borings.

Except the soil borings, also in 4 locations, observation boreholes with 30 meters depth were cut in the existing soils to find out if solid waste disposals affect the groundwater table or not. So, observation borings were conducted perpendicularly to the flow direction of the ground water to analyze the effect of the solid waste storage on ground water.

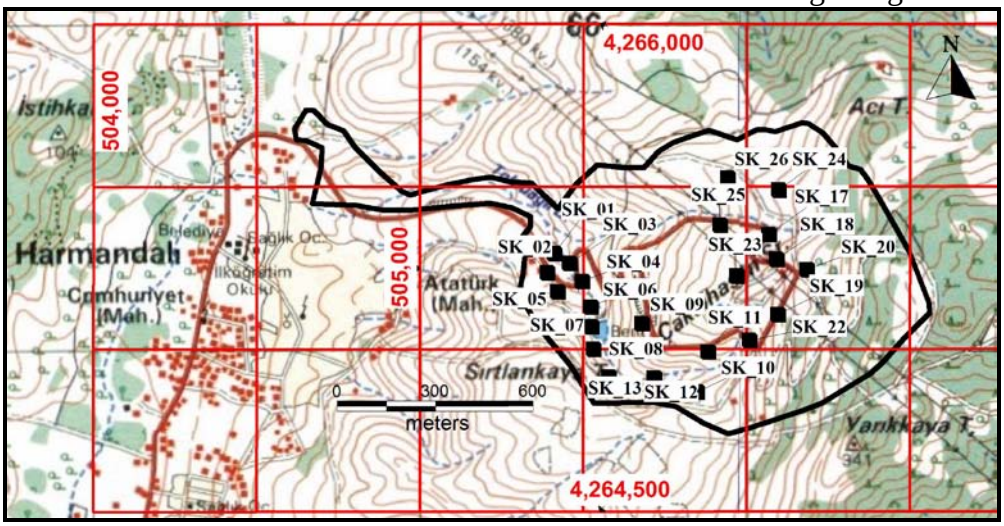

(a)

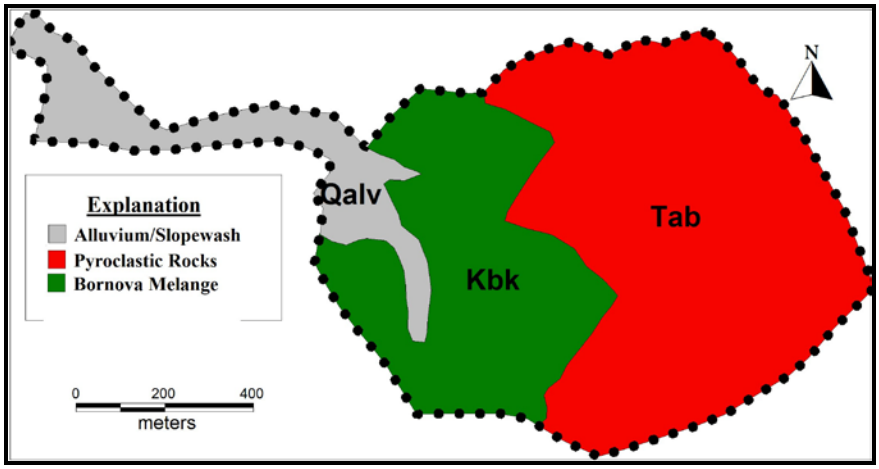

(b)

Figure 2. (a) Location map of the boreholes, (b) Geological map of the study area (modified from UKAM (1990).

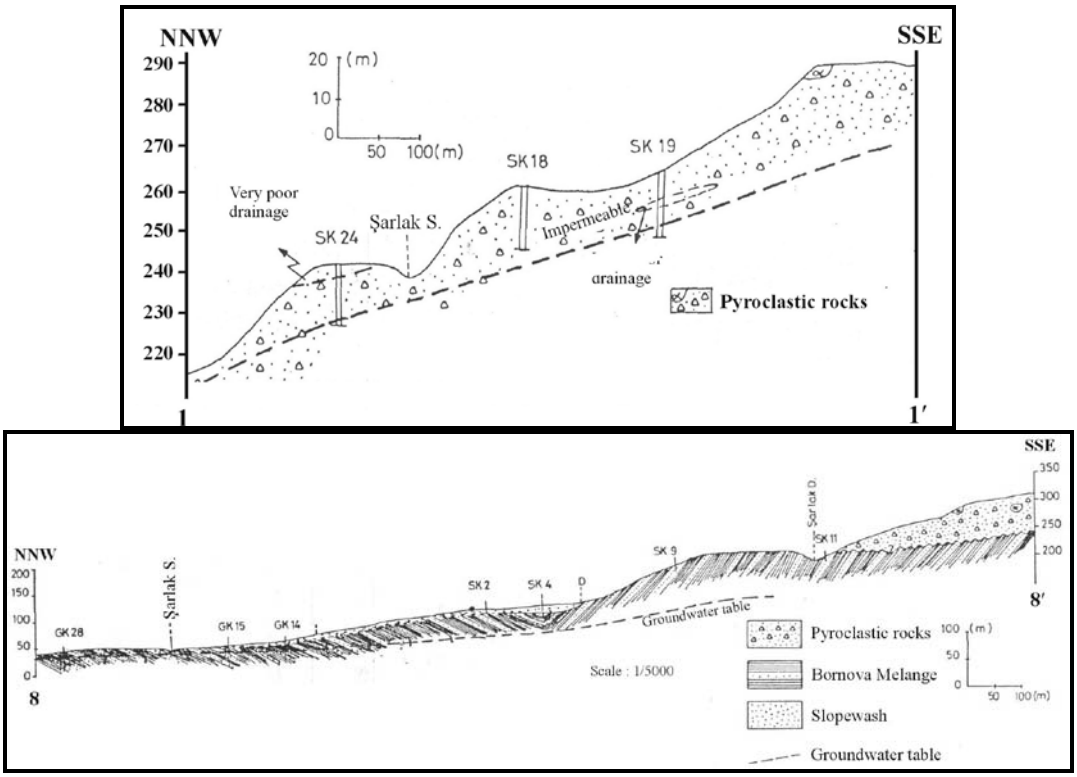

Figure 3. Cross-sections showing the relationship between the contacts of the formations

2.5 Cross-Sections

Cross-sections were taken to present continuity of the geological formations under the ground surface. Soil borehole data were used during the preparetion of the cross-sections (Figure 3).

Criteria for TOPSIS method were based on the Medical Waste Control Regulations (1993). In the regulations, there are some rules to choose the suitable land for medical waste disposal. Five criteria are determined according to the regulations. These criteria are given below:

- ***Criterion 1:*** *The Solid Waste Disposal Area must be at least 5 km away from an airport.*
- ***Criterion 2:*** *The Solid Waste Disposal Area must be at lest 3 km away from the nearest settlement.*
- ***Criterion 3:*** *The soil thickness of The Solid Waste Disposal Area must be more than 3 m.*

- ***Criterion 4:*** *The desposal area floor must be at least 2 m away from groundwater table.*
- ***Criterion 5:*** *The soil permeability value must be bigger than 10-9.*

The TOPSIS method provides an outranking relation for the alternatives. This method helps to select the best alternative. Before starting with the steps of the TOPSIS method, expressing the GIS maps for Harmandali is useful for understanding the criteria. Firstly, the map for each criterion had been prepared. Latitude and longitude values of boreholes had been used for these maps. 5 maps for 5 criteria were prepared with MapInfo Professional 7.5. They are shown below:

For Criterion-1 (Figure 4), 5000 meter-buffer zone was constituted. Although the nearest airport must be at least 5000 meters away from the waste disposal site according to Medical Waste Control Regulations (2005), Cigli Airport is in the buffer zone. This area isn't suitable for Criterion 1.

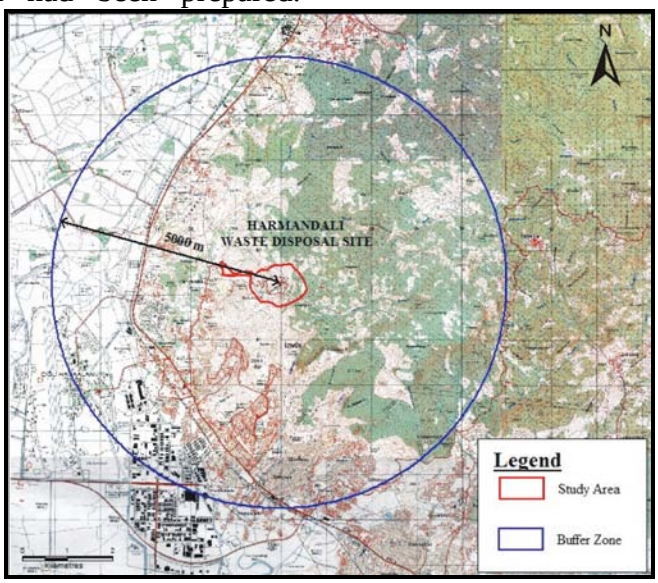

Figure 4. The Distance Between The Waste Disposal Site and The Nearest Airport (Criterion-1)

According to Criterion-2 (Figure 5), the nearest settlement must be at least 3000 meters away from the waste disposal site according to the Medical Waste Control Regulations (2005). But Harmandali, Cigli, Ulukent districts are placed in this buffer zone. Harmandali Waste Disposal Site also violates Criterion-2.

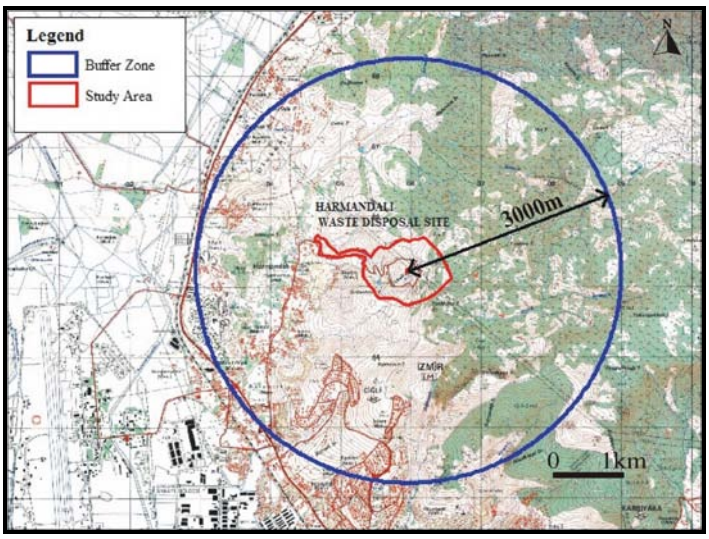

Figure 5. The Distance Between The Waste Disposal Site and The Nearest Settlement (Criterion-2)

Soil thickness map was prepared by using soil thickness values in the borehole logs (UKAM, 1990) (Table 1 and Figure 6). The soil thickness value must not be less than 3 meters according to the Medical Waste Control Regulations (2005). The suitable areas are shown in green and yellow in this map.

The groundwater depths in all boreholes have been measured by Hacettepe University International Karst Water Resources Application and Research Center members. The distance of groundwater table from the floor of waste disposal site must not be less than 2 meters. Whole site is suitable for this criterion (Figure 7) as the minimum distance for groundwater table from the floor is more than 2 meters and it is shown in red.

Table 1. Soil Thicknesses obtained from soil borings (UKAM, 1990).

Borehole Number	X (m)	Y (m)	Soil Thickness (m)	Borehole Number	X (m)	Y (m)	Soil Thickness (m)
SK_01	505410	4265295	4.00	SK_12	505717	4264911	2.50
SK_02	505390	4265235	4.00	SK_13	505578	4264915	4.50
SK_03	505458	4265265	3.00	SK_17	506068	4265353	1.00
SK_04	505496	4265209	3.00	SK_18	506091	4265277	1.00
SK_05	505421	4265178	2.00	SK_19	506096	4265106	1.50
SK_06	505523	4265131	3.00	SK_20	506185	4265244	3.50
SK_07	505524	4265070	5.00	SK_22	506008	4265028	3.00
SK_08	505531	4265000	5.00	SK_23	505969	4265226	1.50
SK_09	505680	4265079	1.00	SK_25	505918	4265382	4.00
SK_10	505847	4264868	2.00	SK_26	505941	4265527	1.00
SK_11	505882	4264991	0.50				

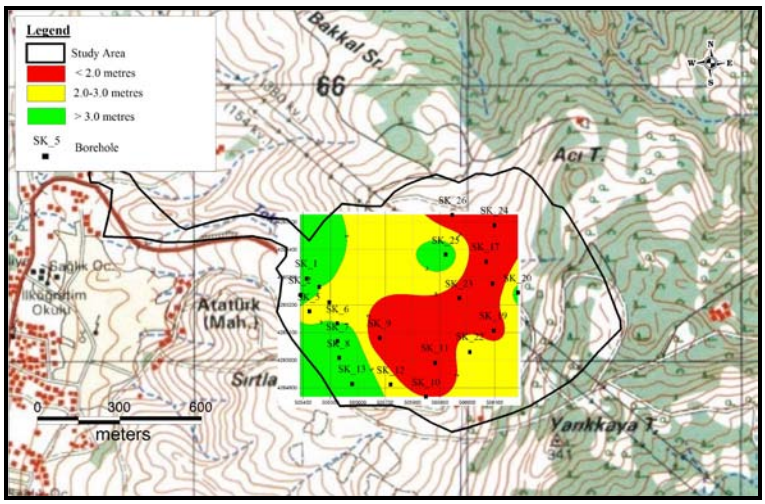

Figure 6. The Relation Between Waste Disposal Site and Soil Thickness (Criterion-3)

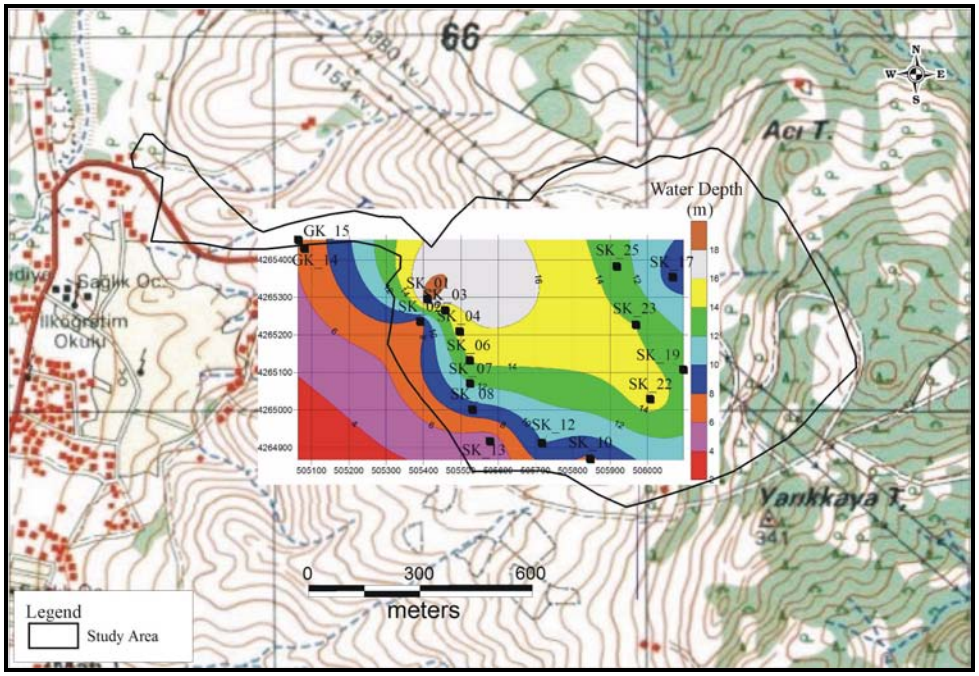

Figure 7. The Relation Between Location of the Waste Disposal Site and Groundwater Table Map (Criterion-4)

Table 2. Permeability Values Obtained from Borehole Lugeon Tests

Borehole Number	Permeability (K)	Borehole Number	Permeability (K)
SK_1	0,0000000430	SK_12	0,0000007100
SK_2	0,0000000460	SK_13	0,0000000640
SK_3	0,0000000760	SK_17	0,0000001300
SK_4	0,0000001200	SK_18	0,0000000001
SK_5	0,0000007100	SK_19	0,0000000001
SK_6	0,0000001100	SK_20	0,0000001300
SK_7	0,0000000016	SK_22	0,0000000001
SK_8	0,0000000140	SK_23	0,0000000001
SK_9	0,0000001100	SK_25	0,0000000920
SK_10	0,0000000001	SK_26	0,0000000001
SK_11	0,0000000130		

Permeability zoning map was prepared using unconfined water test data obtained from boreholes (Table 2). Suitable non-permeable areas are shown in red in the Permeability map (Figure 8), all other regions of the waste disposal site being permeable. In permeable areas, the leakage water can infiltrate to inner layer of the soil. If the waste disposal site is chosen in the area which is shown green, a non-permeable layer must be used on the soil and the permeability must be prevented.

The steps of the TOPSIS method are shown below (Yaralioglu, 2004):

Step 1: Decision Matrix (A)

Criteria and alternatives are shown together in a matrix structure. Rows of the matrix are the alternatives and columns are the criteria. This matrix is called "Decision Matrix" (Table 3). Decision Matrix (A) is shown below:

There are three c5 values in Table 3. The values of column (2) point out the real permeability values. The values of column (1) were used to prepare the GIS map. The suitable permeability values are shown by "0" and the non-suitable permeability values are shown by "1". The values of column (3) were appointed for TOPSIS method. The most suitable permeability values were appointed by "20". The other values were sorted from the best to the worst with five-interval point. SK_1, SK_2, ..., SK_26 are the names of the boreholes. The values of soil thickness, the depth of the groundwater table and permeability values (2) have been taken from the boring logs. The airport distance and the nearest settlement from the waste disposal site were measured using the GIS map. They are the horizontal distance values.

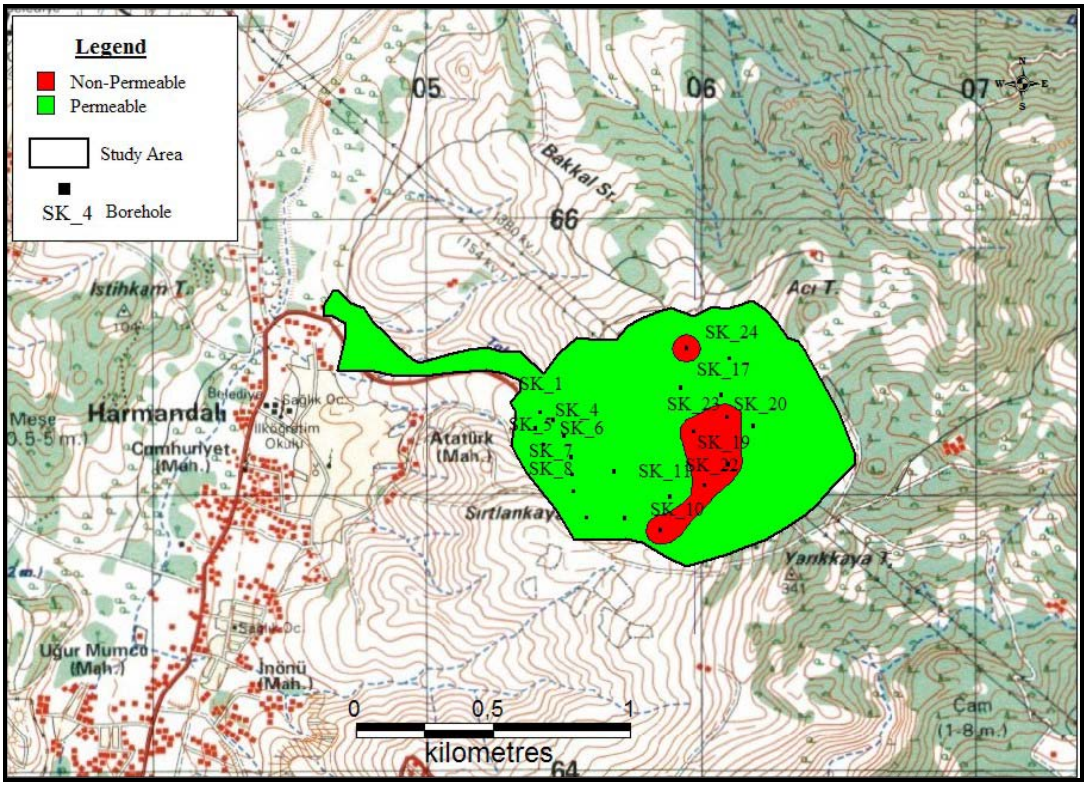

Figure 8. The Relation Between Waste Disposal Site and Permeability Values (Criterion-5)

Table 3. Decision Matrix (A)

Criteria	c1	c2	c3	c4	c5	c5	c5
Alternatives	Airport distance (m)	The nearest settlement (m)	Soil thickness (m)	The depth of the underground water (m)	Permeability (suitable:0, non-suitable:1) (1)	Permeability (2)	(3)
SK_1	4815	1091	4	19	1	0,0000000430	10
SK_2	4769	1054	4	7	1	0,0000000460	10
SK_3	4839	1145	3	14,5	1	0,0000000760	10
SK_4	4828	1168	3	15	1	0,0000001200	5
SK_5	4748	1170	2	9	1	0,0000007100	5
SK_6	4819	1253	3	14	1	0,0000001100	5
SK_7	4787	1248	5	12	1	0,0000000016	15
SK_8	4769	1249	5	9	1	0,0000000140	10
SK_9	4934	1403	1	13	1	0,0000001100	5
SK_10	4994	1567	2	7,5	0	0,0000000001	20
SK_11	5074	1598	0,5	12,5	1	0,0000000130	10
SK_12	4896	1440	2,5	10	1	0,0000007100	5
SK_13	4767	1298	4,5	4,5	1	0,0000000640	10
SK_17	5407	1829	1	9	1	0,0000001300	5
SK_18	5387	1833	1	11	0	0,0000000001	20
SK_19	5318	1818	1,5	13	0	0,0000000001	20
SK_20	5459	1923	3,5	10	1	0,0000001300	5
SK_22	5206	1727	3	15	0	0,0000000001	20
SK_23	5260	1710	1,5	14	0	0,0000000001	20
SK_25	5284	1688	4	13	1	0,0000000920	10
SK_26	5374	1754	1	12	0	0,0000000001	20

Weights of criteria were determined according to importance of criteria. The most important criterion is permeability (c5), because the leakage water infiltrates under the layer of soil. This situation presents hazards both for nature and for humans. So the weight of this criterion is 0,30. The second important criterion is soil thickness value (c39). If the soil has a suitable thickness, the waste and the waste water can't diffuse into the inner layers of the ground. The weight of the soil thickness was determined as 0,25. And other criteria were sorted according to importance levels. Weights are shown below (Table 4):

Table 4. Weights of Criteria

Criteria	Weights
c1	0,15
c2	0,1
c3	0,25
c4	0,2
c5	0,3

Step 2: Standard Decision Matrix (R)

The formula shown below is applied to all elements of the decision matrix to constitute the standard decision matrix (R) (Table 5):

$$r_{ij} = \frac{a_{ij}}{\sqrt{\sum_{k=1}^{m} a_{kj}^2}}$$

Standard Decision Matrix (R) is shown below:

$$R = \begin{bmatrix} r_{11} & r_{12} & \cdots & r_{1n} \\ r_{21} & r_{22} & \cdots & r_{2n} \\ \vdots & & \ddots & \vdots \\ r_{m1} & r_{m2} & \cdots & r_{mn} \end{bmatrix}$$

Step 3: Weighted Standard Decision Matrix (V)

All elements of the matrix are multiplied by weights. Weights of criteria were given in Table 4. Weighted Standart Decision Matrix (Table 6) is calculated with this operation.

Step 4: Ideal (A*) and Negative Ideal (A-) Solutions

Ideal (A*) solution is the biggest number for each criterion column and negative ideal (A-) solution is the smallest number for each criterion column in a maximization problem. Ideal (A*) and negative Ideal (A-) solutions are shown below:

$$A^* = \{193{,}4926;\ 53{,}76315;\ 0{,}45402;\ 1{,}30648;\ 2{,}030983\}$$

$$A^- = \{146{,}3726;\ 16{,}15129;\ 0{,}00454;\ 0{,}073286;\ 0{,}081239\}$$

Step 5: Calculating Discrimination Measures

The discrimination measure is calculated to determine the bias of each value in the decision matrix from its own ideal (A*) and negative ideal (A-) solution value (Table 7). Formulas of discrimination measures are shown below:

$$S_i^* = \sqrt{\sum_{j=1}^{n} (v_{ij} - v_j^*)^2}$$

$$S_i^- = \sqrt{\sum_{j=1}^{n} (v_{ij} - v_j^-)^2}$$

Step 6: Calculating Relative Closeness (C_i^*) to The Ideal Solution

The formula of the relative closeness is shown below:

$$C_i^* = \frac{S_i^-}{S_i^- + S_i^*},$$

C_i^* values were calculated to determine closeness of alternatives to the ideal solution. If C_i^* value of an alternative is near to "1", the alternative will be near to the ideal solution. If C_i^* value of an alternative is near to "0", it will be near to the negative ideal solution. C_i^* values are shown in Table 8 (C_i^* values were sorted from the biggest to the smallest):

Table 5. Standart Decision Matrix (R)

Alternatives	c1	c2	c3	c4	c5
SK_1	1003,551	173,0516	1,162292	6,532399	1,692486
SK_2	984,4681	161,5129	1,162292	0,886669	1,692486
SK_3	1013,58	190,6062	0,653789	3,804534	1,692486
SK_4	1008,978	198,3407	0,653789	4,07144	0,423121
SK_5	975,8171	199,0205	0,290573	1,465718	0,423121
SK_6	1005,219	228,2592	0,653789	3,546676	0,423121
SK_7	991,9136	226,4411	1,816082	2,605721	3,808093
SK_8	984,4681	226,8041	1,816082	1,465718	1,692486
SK_9	1053,769	286,1814	0,072643	3,058104	0,270798
SK_10	1079,553	356,9966	0,290573	1,01786	6,769944
SK_11	1114,417	371,2613	0,018161	2,827389	1,692486
SK_12	1037,6	301,4749	0,45402	1,809529	0,423121
SK_13	983,6425	244,9489	1,471026	0,36643	1,692486
SK_17	1265,493	486,3551	0,072643	1,465718	0,423121
SK_18	1256,148	488,4848	0,072643	2,18953	6,769944
SK_19	1224,175	480,5226	0,163447	3,058104	6,769944
SK_20	1289,951	537,6315	0,88988	1,809529	0,423121
SK_22	1173,155	433,6215	0,653789	4,07144	6,769944
SK_23	1197,618	425,1266	0,163447	3,546676	6,769944
SK_25	1208,572	414,2581	1,162292	3,058104	1,692486
SK_26	1250,093	447,286	0,072643	2,605721	6,769944

Table 6. Weighted Standard Decision Matrix (V)

Borehole number	c1	c2	c3	c4	c5
SK_1	150,5327	17,30516	0,290573	1,30648	0,507746
SK_2	147,6702	16,15129	0,290573	0,177334	0,507746
SK_3	152,0371	19,06062	0,163447	0,760907	0,507746
SK_4	151,3466	19,83407	0,163447	0,814288	0,126936
SK_5	146,3726	19,90205	0,072643	0,293144	0,126936
SK_6	150,7829	22,82592	0,163447	0,709335	0,126936
SK_7	148,787	22,64411	0,45402	0,521144	1,142428
SK_8	147,6702	22,68041	0,45402	0,293144	0,507746
SK_9	158,0653	28,61814	0,018161	0,611621	0,081239
SK_10	161,933	35,69966	0,072643	0,203572	2,030983
SK_11	167,1626	37,12613	0,00454	0,565478	0,507746
SK_12	155,6399	30,14749	0,113505	0,361906	0,126936
SK_13	147,5464	24,49489	0,367757	0,073286	0,507746
SK_17	189,8239	48,63551	0,018161	0,293144	0,126936
SK_18	188,4223	48,84848	0,018161	0,437906	2,030983
SK_19	183,6263	48,05226	0,040862	0,611621	2,030983
SK_20	193,4926	53,76315	0,22247	0,361906	0,126936
SK_22	175,9732	43,36215	0,163447	0,814288	2,030983
SK_23	179,6428	42,51266	0,040862	0,709335	2,030983
SK_25	181,2858	41,42581	0,290573	0,611621	0,507746
SK_26	187,5139	44,7286	0,018161	0,521144	2,030983

According to this table, suitable borehole numbers for waste disposal were sorted as SK_20, SK_17, SK_18, SK_26 and SK_19 (we can deliberate that SK_25, SK_23 and SK_22 are suitable). The areas around suitable borehole locations can be

used for the waste disposal site in Harmandali (İzmir).

On the other hand, SK_1, SK_2 and SK_3 were determined as suitable boreholes according to ELECTRE method. But these areas do not support Criteria-1 and Criteria-2. Because these boreholes areas are closer to the airport and the nearest settlement than TOPSIS results require (Figure 9).

Table 7. Ideal (S*) and negative ideal (S-) discrimination measures

Alternatives	S*	S-
SK_1	56,36567	7,507707
SK_2	59,31246	7,701458
SK_3	54,08818	7,354467
SK_4	54,14259	7,358165
SK_5	58,06611	7,620112
SK_6	52,77594	7,264705
SK_7	54,48294	7,381256
SK_8	55,40016	7,443128
SK_9	43,4953	6,595097
SK_10	36,38218	6,031764
SK_11	31,19505	5,585253
SK_12	44,6672	6,683353
SK_13	54,51181	7,383212
SK_17	6,677883	2,58416
SK_18	7,127909	2,669814
SK_19	11,42856	3,380615
SK_20	2,138043	1,462205
SK_22	20,38228	4,514674
SK_23	17,85832	4,22591
SK_25	17,43691	4,175752
SK_26	10,87081	3,297091

4. RESULTS

Harmandali Waste Disposal Site is not a suitable area for waste storage. Firstly, this region does not comply with criteria 1 and 2. A lot of villages and settlement areas are placed around the waste disposal area and Cigli Airport is closer than 5000 meters. There isn't any borehole area which supports the other three criteria (Criterion-3, Criterion-4 and Criterion-5) in Harmandali Waste Disposal Site. SK_20, SK_18, SK_26, SK_19, SK_23 and SK_22 were determined as suitable according to the result of TOPSIS method. When these borehole points on the map are examined, it can be seen that they satisfy only two criteria. When the permeability value is suitable, the soil thickness value is not. When the soil thickness value is suitable, the permeability value is not. Decision makers must decide which criterion is more important. If SK_20 and SK_25 boreholes are chosen for waste disposal, a non-permeable layer must be placed on the ground, as the permeability values of SK_20 and SK_25 are not suitable. If SK_18, SK_26, SK_19, SK_23 and SK_22 are selected, the soil thickness value will be less than 3 meters. It's less than the limit value. In this case, the soil must be strengthened. SK_17 is in the second order of the relative closeness table. But in the overlay map, SK_17 does not seem to be a suitable area. So this borehole point must not be selected.

Tablo 8. Relative Closeness (C_i^*) Values

Alternative	C*
SK_20	0,970962
SK_17	0,907119
SK_18	0,90047
SK_26	0,848341
SK_19	0,841857
SK_25	0,756534
SK_23	0,75157
SK_22	0,720524
SK_11	0,577032
SK_10	0,517344
SK_9	0,415513
SK_12	0,413889
SK_13	0,310352
SK_6	0,305906
SK_7	0,295125
SK_8	0,290921
SK_4	0,274307
SK_3	0,269023
SK_5	0,255284
SK_2	0,214689
SK_1	0,074224

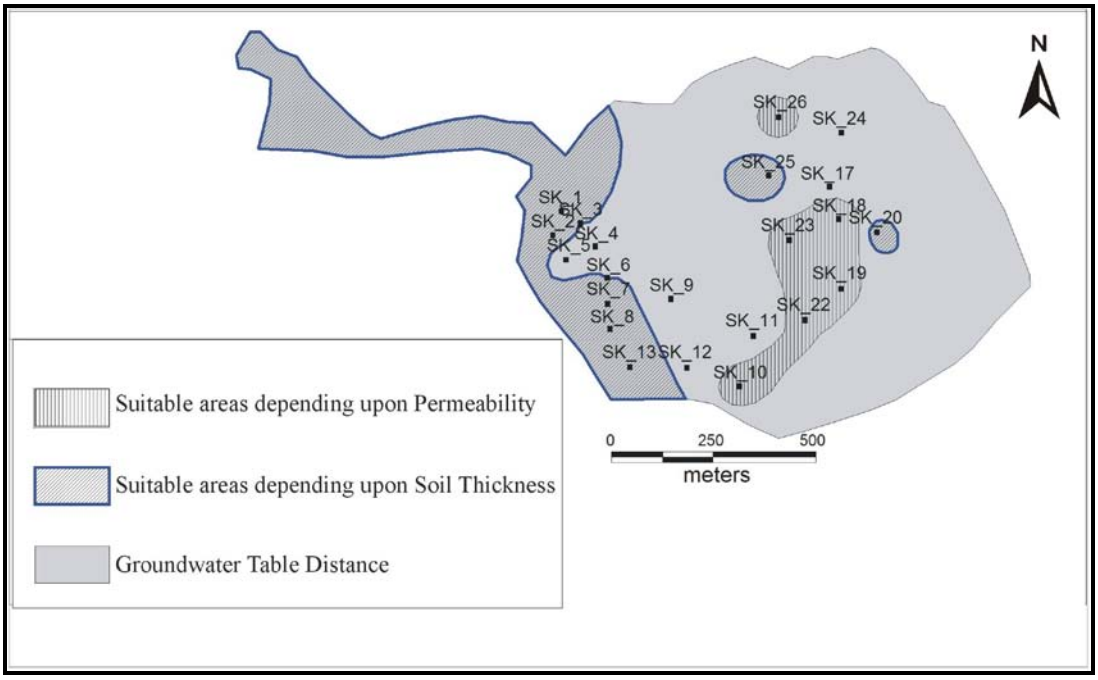

Figure 9. Overlaying of three criteria (Criterion-3, Criterion-4, Criterion-5). (The groundwater table distance is suitable for all of the waste disposal site).

In this study, MCDA and GIS were used together to find the suitable site. Both analyses helped each other to select the suitable area. Results of these analyses were compared with each other, were evaluated together and ultimate decisions were made. Decision making is a complex process that includes more situations and more disciplines. In this study, MCDA and GIS supported each other and they helped the decision maker.

5. REFERENCES

Belton, V., Stewart T. J. (2002). Multiple Criteria Decision Analysis:An Integrated Approach, *Kluwer Academic Publishers*, Massachusetts.

Malczewski, J. (1999). GIS and Multicriteria Decision Analysis, *John Wiley & Sons*, Canada.

Medical Waste Control Regulations (2005). www.istabip.org.tr/yasa/tibbiatik.html (In Turkish).

Tecim, V., (2001). Geographical Information Systems, Basic Concepts, Application Areas, *İlkem Publishing*, p. 181 (in Turkish).

Triantaphyllou, E. (2000), Multi-criteria Decision Making Methods: A Comparative Study, *Kluwer Academic Publishers*, Dordrecht.

UKAM, (1990), "Soil Investigation Report of İzmir–Harmandalı Solid Waste Disposal Site" (In Turkish), *Hacettepe University International Karst Water Resources Application and Research Center*, p.40, Ankara.

Yaralioglu, K. (2004). Decision Support Method in Application, *İlkem Publishing* (in Turkish).

INFLUENCE OF THE SULPHUR OF COALS ON COKING AND SEMI-COKING PROCESSES.

Butuzova L.F.[1], Zubkova V.V.[2], Bulyga O. S.[3], Isayeva L.N.[3] and Turchanina O.N.[1]

[1]Donetsk National Technical University, 48 Artema str.,Donetsk 83000, Ukraine,
lfb@skif.net

[2]Institute of Chemistry, Jan Kochanowski University, 5 Checinska Street, 25-020 Kielce,Poland,
Walentyna.Zubkowa@pu.kielce.pl

[3]L.M.Litvinenko Institute of Physical Organic and Coal Chemistry, National Academy of Sciences of the Ukraine, 70 R.Luxemburg str., Donetsk 83114, Ukraine

Abstract: The displacement of non-volatile mass of coal charge during carbonization has been studied using X-ray examination with contrasting elements embedded in it. The thermal behavior of the pairs of low- and high-sulphur coals was studied by differential thermal analyses and classical Fisher and Sapozhnikov methods.

It has been shown that the macrostructure of the coal plastic layer depends on the coal genetic type by reductivity. The significant differences in the origin coals, semi-cokes and cokes structure and microstructure for low-reduced and reduced samples have been estimated.

Data of optical microscopy well agree with the results of the yield of vapor-gas products during semi-coking, results of the differential thermal analysis and data of the coke's mechanical properties.

Key words: sulphur coals, quality, cokes, semi-cokes

1. INTRODUCTION

High sulfur content is the effect of a geological history of coal bed and one of the most important criterions of a fuel quality (e.g. Bechtel et al., 2002; Butuzova et al., 2005; Butuzova et al., 2001). The sulphur compounds have a negative influence upon its thermal processing (poisoning, corrosion, air pollution) and change its caking ability.

It was found in previous studies (e.g. Sklyar et al., 1986; Zubkova, 1999) that due to plasticization and swelling of grains in the heated coal charge, displacement processes occur in its non-volatile mass. Dangerous internal pressures, developed during carbonization of some coking coals, are of major importance for cokemaking because they can damage the oven's walls.

When well-caking coal is heated, the grains are swollen and form a gas-saturated foamlike mass. Due to this phenomenon, the plastic layer of a well-caking coal acquires a complicated structure since there appeare three constituent zones: swollen grains, gas-saturated zone and compressed zone. These zones have been studied using X-ray examination of a coal charge with contrasting elements embedded in it (e.g. Zubkova, 2002). The process of the movement of non-volatile mass can be characterized roughly as curves showing the relationship between the displacement and temperature dl=f(T).

It is natural to suggest that a structural peculiarity of the two types, LRC and RC, should result in distinctions in the shape of displacement curves of non-volatile mass depending on the temperature. There are no data in the scientific literature on how the coals of different genetic type by reductivity (GTR) acts on the character of shrinkage curve during coking and on the way of monolithic solid residue formation.

The objective of this paper is to find out how the coal rank and GTR influence the movement of non-volatile mass of coal charge during coking, to study the carbonization process, microstructure and properties of semi-cokes and cokes, obtained from Donets coals of LRC and RC types.

2. MATERIAL AND METHODS

The pairs of low- and high-sulphur coals (~76-88 Cdaf) formed under reduced (RC) and low-reduced (LRC) conditions during early diagenesis were investigated (Table 1). These coals are classified as petrographically homogeneous with low proportion of inertinite and high proportion of vitrinite (> 80%).

Table 1. Characteristics of initial coals, wt %

Coal mine, seam	Type	Ro,r, %	Petrographic components, vol. %			Proximate and ultimate analysis, %					
			Vt	L	I	Wa	Ad	Vdaf	Cdaf	Hdaf	Sdt
Trudovskaya, l4	LRC	0.55	86	5	9	1.0	1.6	37.3	78.4	4.95	1.05
Zasyadko, l4	LRC	1.01	89	6	5	1.4	2.6	31.6	87.8	5.16	1.09
Gagarina, m3	LRC	1.18	85	3	12	1.2	3.7	28.7	87.4	5.06	0.70
Trudovskaya, k8	RC	0.49	80	8	12	0.9	4.6	46.2	76.1	5.43	5.85
Zasyadko, k8	RC	0.96	83	3	14	0.8	2.7	31.7	87.3	5.23	2.81
Gagarina, m4o	RC	0.96	87	3	10	0.8	12.2	35.6	83.6	4.88	3.75

The proximate and ultimate analyses, semi-coking and coking (classical Fisher and Sapozhnikov methods) of the samples were carried out according to standard procedures.

The thermal behavior of coals was studied by a differential thermal analysis which was carried in a Paulic-Paulic-Erdei Q-1500D thermobalance at the heating rate of 10 0C min-1 in a closed ceramic crucible.

The displacement of non-volatile mass of coal charge during carbonization has been studied using X-ray examination with contrasting elements (a strip of copper foil) embedded in it. The method was described earlier (e.g. Zubkova, 2002). Coals were heated in the coking chamber placed in a furnace with vertical unilateral heating. Heat from the heaters was transferred to the charge through a steel plate. The heating rate was 4 K min-1 and it was controlled by a microprocessor. The final temperature of heating of the furnace was 1050 ^{0}C. In the sidewalls of the furnace and the chamber, special windows were provided for passage of X-rays. The contrasting element moved together with the surrounding coal and reflected the movement of non-volatile mass of the coal charge in the course of coking.

The determination of semi-cokes' and cokes' microstructures was performed on polished sections with the help of a LOMO MIM-8M optical microscope using reflected polarized light either in air (magnification x 300) or in immersion oil (magnification x 900) by a point-counting method (500 points).

Pore diameters and pore wall thickness were quantitatively determined with the help of "scaled" ocular. These data permit to identify five groups and to calculate the proportions of pores and walls inside these groups, a compactness parameter corresponding to the wall surface/pore surface ratio, as well as the average rate of occurrence for pores and cell walls.

Mechanical strength of cokes was assessed by impact testing. 20 g of 9 - 13 mm sized fraction of coke was spread in an even layer on the bottom of a metal barrel with a vertically installed metal tube. Then, a 1 kg load, placed at 1m above the barrel, was dropped 15 times on the sample (corresponding work: 147 J). The resulting coke fragments were screened through 5, 2.5, 1 and 0.5 mm sieves, and each fraction was weighed. From these data, a strength index (SI) was defined as being the destruction work W, needed for the formation of a unit of new surface S, i.e. SI (%) = dW / dS. A crushing resistance indicator (R %) was calculated from the amounts of blocks larger than 2.5 mm and was expressed as :

$$R = 100 (\sum ai) / G$$

where ai = respective weights of 2.5 - 5, 5 - 9 and 9 - 13 mm sized coke particles; G = weight of the coke sample. Moreover, an abrasion index (AI) was determined as the yield (%) of the 0.5 mm fraction.

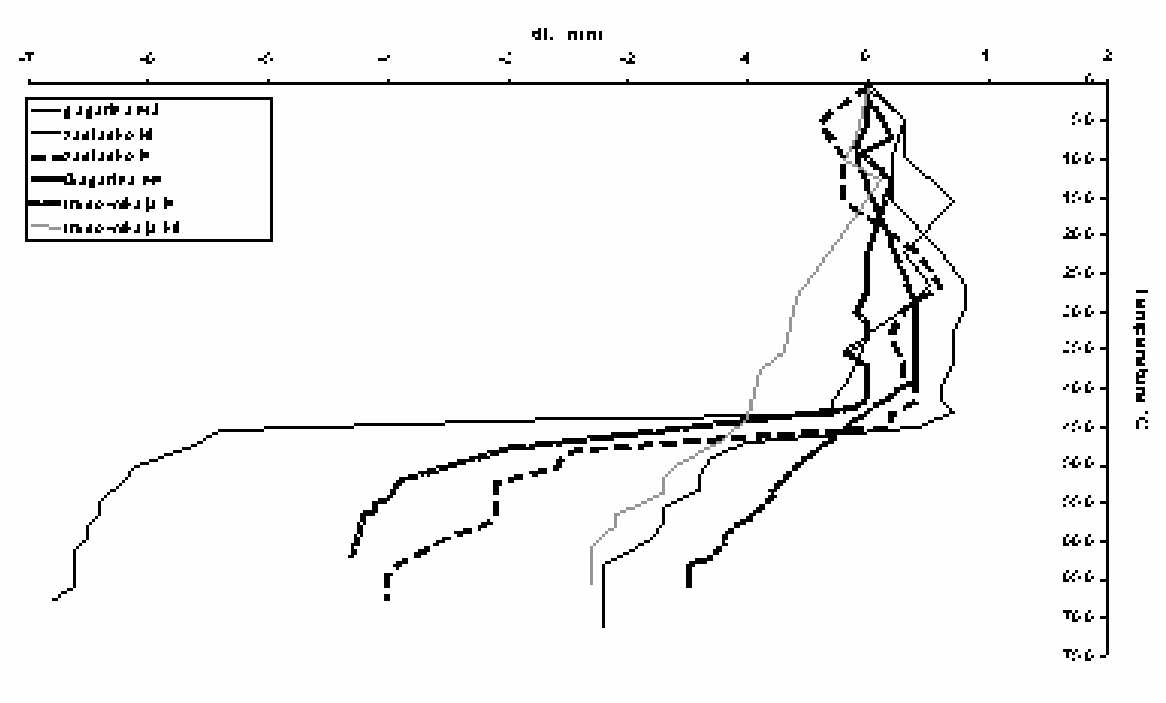

Figure 1. Schematic path taken by the contrasting element in the process of different coals carbonisation

3. RESULTS AND DISCUSSION

In Figure 1, experimentally found curves show the movement of non-volatile mass of the charge on heating pure low- and middle-rank coals of different genetic type by reductivity. The position $\Delta l=0$ corresponds to the projection of the contrasting element on the X-ray film before heating is switched on. During heating, the position of the contrasting element changes relating to the reference 0 on the X-ray film and we can observe a trajectory of its movement as a function of temperature. As can be followed in Figure 1, the corresponding trajectories are different for coals of different rank and GTR. Experimental curves for the displacement of non-volatile mass of the well-caking coals heated are shown in Figure 1 (Gagarina, Zasiadko). When an individual piece of reduced type G coal (curves: Zasyadko k8, Gagarina m4) is heated, the non-volatile mass practically does not displace at the stage of the swollen grains before the transition of coal into a viscous-fluid state (below temperature 430-440 ^{0}C). Therefore, the pressure forces of the layers of grains on each other are equal, i.e. the pressure of the swollen grains practically

counterbalances the pressure in the gas-saturated zone. In the case of G coals of low-reduced type (curves: Zasyadko l4, Gagarina m3) the forces are not equal, the non-volatile mass displaces towards to the cold side of the coking chamber and a looser residue is formed before temperature 440 ^{0}C.

When converted to a viscous-flowing state (>440 ^{0}C), the foamlike mass of the gas-saturated zone in the plastic mass moves only to the heating wall under the action of intralayer pressure and is pressed together into a compact zone on the surface of semi-coke. The foamy mass of G coals is sharply transferred to the heating wall ($\Delta l < 0$). The Δl value falls when turning from LRC to a RC samples. It means that the foamlike plastic mass of RC is pressed to form a denser compact residue on carbonization.

Displacement of the non-volatile mass when heating non-caking D coals is represented by lines (Trudowskaja) in Fig. 1 depending on temperature. These coals do not form a plastic layer but the process of displacement of non-volatile mass takes place in the coal charge due to the interaction between swollen grains during heating. Therefore, the non-caking coals would decrease the scope of displacement of the contrasting element compared to the similar process taking place during carbonization of G coals. Indeed the distance over (Δl) which a mass of coal D will be transferred (-1.5-2.3 mm) is less than the distance which the mass of coal G has moved (> -4 mm). As it follows from Figure 1, the parameter Δl additionally decreases in a temperature range of 500-650 0C. This indicates that the process of compressing the non-resolidified mass continues in the compressed zone and when the plastic mass gets resolidified.

From the comparison, it follows that for all the coals used, the curves do not coincide with each other. The greatest deviation of curves takes place in coals G. As can be seen in Figure 1, less dense, less compact residue is formed in a LRC of D grade.

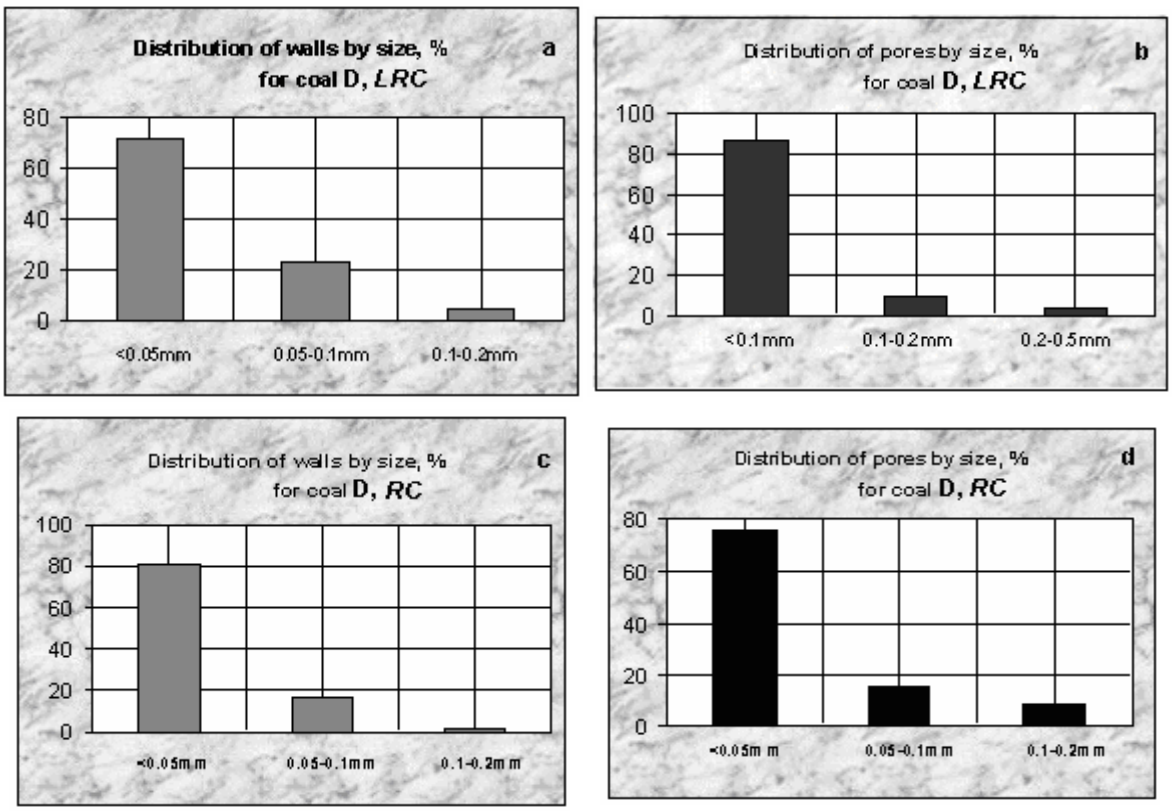

Figure 2. Quantitative indices of the macrostructure of semi-cokes obtained from coals of different genetic type

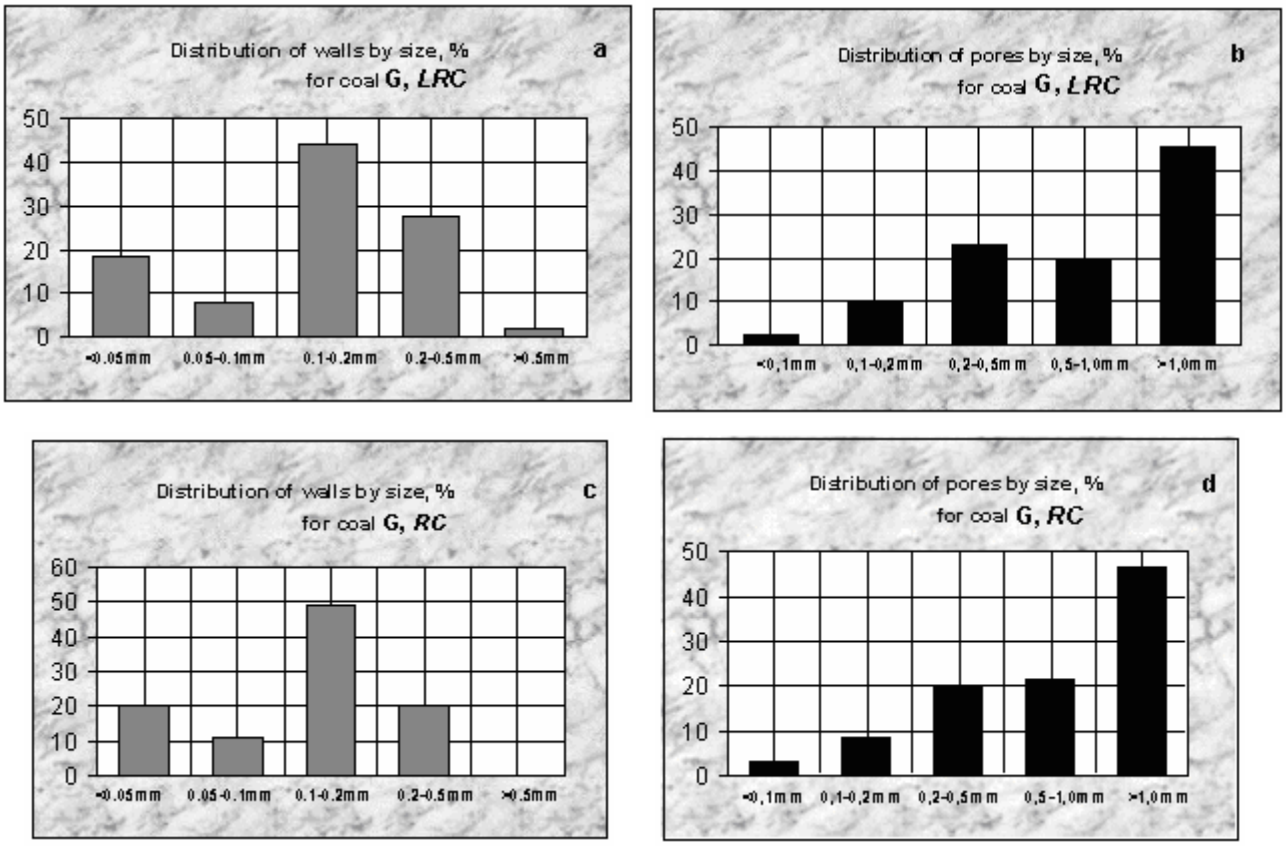

Fig 3. Quantitative indices of the macrostructure of semi-cokes obtained from coals D of different genetic type

Figures 2 and 3 show the results of the semi-coke's microstructure determination. As it can be seen in the Figures, the distribution of pores and walls into groups by size depends on the coal genetic type and coalification degree. In general, low-rank coals of RC type give less compactness (C=Z/P), semi-cokes with a higher volume of pores (P, %) and lesser relative content of walls (Z, %). This is a weak-coked material with less content of small pores compared to semi-cokes of LRC type.

Increasing of the coals coalification degree results in the increasing of the semi-coke's compactness owing to a general decrease in the pore volume. The amount of thick walls (<0.05 mm) decreases considerably in the middle-rank coals, but the content of middle walls (0.1-0.2 mm) increases. The pores with a diameter less than 0.1 mm are prevalent in the semi-cokes from D coals, and pores with a diameter greater than 1.0 mm in the case of semi-cokes from G coals.

Data of optical microscopy well agree with the results of the differential thermal analysis.

According to the non-isothermal pyrolysis technique samples were heated up to 1000 ^{0}C. The values for the mass loss at 850 ^{0}C and the effective energy of activation (E) in the process of vapour-gaseous products formation were calculated by the equation:

$$E=4.57\ T_2\ T_1(\lg K_2-\lg K_1) / (T_2-T_1)\ 1000$$

where T_1 and T_2 are equal to temperature values for two points on the portion of a straight line: $\lg[-\lg (me-m\tau)/me] - 1/T$; K1 and K2 are their corresponding values of $-\lg (m_e-m_\tau)/me$; m is mass loss at different temperatures.

Table 2. Derivatographic data for the studied coals

Coal mine, seam	Type	Coal grade	The basic decomposition period		Δma at 850°C, %	dm/dt, mg/g·min	E , kJ/mole
			T,°C	Δma,%			
Trudovskaya, l4	LRC	D	405	7,0	31,3	10	91,7
Zasyadko, l4	LRC	G	450	5,5	29,8	12	56,6
Gagarina, m3	LRC	G	450	5,4	29,9	11	57,0
Trudovskaya, k8	RC	D	390	9,1	36,9	23	112,8
Zasyadko, k8	RC	G	450	5,2	27,3	12	38,1
Gagarina, m4o	RC	G	450	4,9	28,1	12	43,9

As is seen in Table 2, the E value changes considerably with the change of coal genetic type. The maximal E value is observed for D type reduced coals which are in good agreement with a higher value for the mass loss at 850 ^{0}C. Decreasing of the E value for coals under investigation depends on the step-by-step decreasing in the mass loss value. The presence of the linear inversely proportional relation between the parameters E and the mass loss value at 850 ^{0}C has been observed (Figure 4).

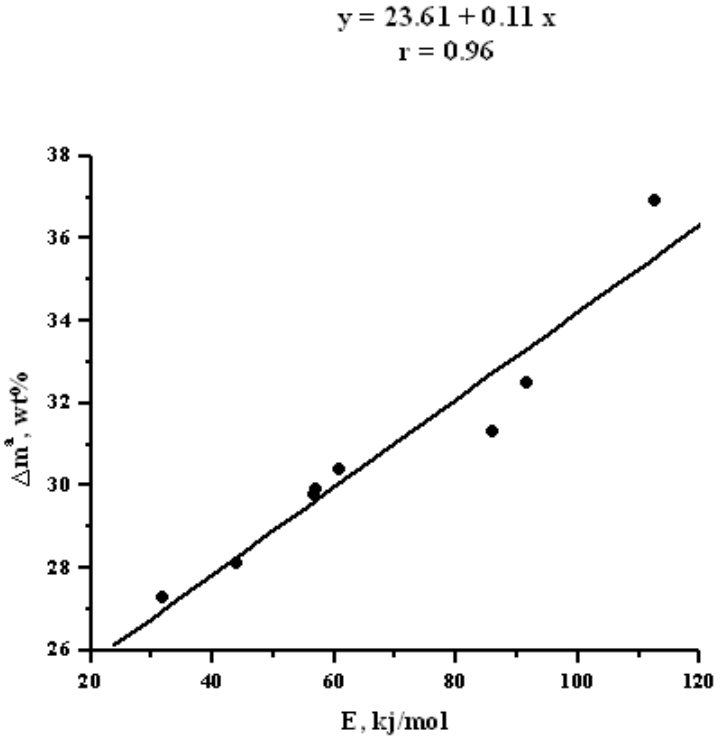

Figure 4. Dependence of mass loss variations on the effective energy of activation of the thermodestruction process for coals G and D

The results of semi-coking and coking experiments have been given in Table 3. These data show that the semi-coking of reduced coals considerably increases the yield of liquid and volatile products, conversion degree as compared to isomethamorphic low-reduced coals. The data of the mechanical properties of the resulting cokes show that RC cokes display better mechanical properties (strength index, crushing resistance and the abrasion indexes) compared to those of LRC cokes. These improvements appear to depend on the sulphur content (GTR) in original coals, and together with coal rank determine the yield of products and coke quality.

The experimental data obtained by us show that with a change of the coal type the amount of vapour-gaseous products of decomposition of coal changes, and the distribution of intralayer pressure between zones of plastic layer is disturbed.

Table 3. Yield of the semi-coking products for coals of different genetic types and coalification degree

Coal, seam	Type	Mechanical properties			Yield of pyrolysis products (wt %)				Conver-sion, wt. %
		SI, %	AI,%	R, %	Semi coke	H2O	Tars	Gas+ losses	
Trudovskaya, l4	LRC	-	-	-	64.8	17.5	9.0	8.7	35.2
Zasyadko, l4	LRC	87.6	32.4	42.4	82.5	3.0	5.5	11.5	17.5
Gagarina, m3	LRC	83.4	31.3	44.5	84.4	2.3	5.3	8.0	15.6
Trudovskaya, k8	RC	-	-	-	62.1	10.7	14.3	12.9	37.9
Zasyadko, k8	RC	91.3	27.2	48.7	78.5	1.5	6.0	14.0	21.5
Gagarina, m4o	RC	95.1	27.1	46.2	71.8	1.0	4.7	22.5	28.2

According to the theory of "Contrast method", chemical processes which occur in the plastic layer determine the fluidity of the molten phase and greatly influence the migration of the evolving volatile matter (VM). These volatile species can induce a swelling inside a viscous plastic medium and also can condense into the coal mass.

In the study reported previously (e.g. Turchanina et al., 2005) it has been shown that the destruction processes and removal of the aliphatic structures from the coal organic mass occur more intensely in RC samples which lead to the formation of the semi-cokes with a higher proportion of the “crystalline” phase in comparison with LRC. The rigid structure of RC semi-cokes offers a higher resistance to wall pressure, and the non-molten coal undergoes an increasing densification.

These hypotheses explain the influence of coal GTR on their coking ability. RC is concentrated of VM, especially by tars (Table 3). It is evident that during coking of these coals tars condense into the coal mass rather than migrate to the walls through semi-coke and coke. Therefore, the push into a compressed layer is higher for RC of different coalification degrees.

4. CONCLUSION

The results of our work demonstrate the differences in the devolatilization process, inducing condensation of tars and different ways of VM migration for RC and LRC of low- and middle- rank. It can be pointed out that the higher the rank of coal the higher the magnitude of non-VM displacement (Δl) is. The general trend is also a decrease of Δl value from RC to LRC independently of the considered coal.

It has been shown that the macrostructure of the coal plastic layer depends on the coal genetic type by reductivity. The significant differences in the original coals’, semi-cokes’ and cokes’ microstructures and properties for low-reduced and reduced samples have been estimated.

Data of optical microscopy well agree with the results of the yield of vapor-gas products of semi-coking, results of the differential thermal analysis and data of cokes’ mechanical properties.

REFERENCES

Bechtel, A., Butuzova, L., Turchanina, .O., 2002. Thermochemical and geochemical characteristics of sulphur coals. *Fuel Processing Technology*, 77-78, 45-52.

Butuzova, L., Bechtel, A., Turchanina, O., Isajeva, L., Matsenko, G., 2001. Effect of the coal genetic type on the pyrolysis products composition and structure. *Acta Universitatis Carolinae –Geologica*, 45 (2 -4), 17-22.

Butuzova, L., Bechtel, A., Turchanina, O., Safin, V., Butuzov, G., Isayeva, L.., 2005. Organic sulphur as a main index for the low-rank coal genetic type determination. *Bulletin of Geosciences*, 1, 3-9.

Sklyar, M., Vasil'ev, Yu., Valters, N., Soldatenko, E., Zubkova, V., 1986. The investigation of the process for coke massive formation. *Koks I Khimiya*, 6, 13-17.

Turchanina, O., Butuzova, L., Safin, V., Isaeva, L., 2005. The possibility of sulphur redistribution in the semi-coking products of low-reduced and reduced coals. *Bulletin of Geosciences*, 1, 99-103.

Zubkova, V., Prezhdo, V., Sklyar, M., Preobrazhenskaya, N., 1999. Influence of the technological factors on the displacement of non-volatile mass of coal charge during coking. *Uglechimicheskij Zhurnal*, 1-2, 30-32.

Zubkova, V. V:., 2002. Investigation of influence of interaction between coals in binary blends on displacement of non-volatile mass of coal charge during carbonization. *Fuel Processing Technology*, 76, 105-119.

THE RUPESTRAL CHURCHES OF LAMA D'ANTICO, SAN GIOVANNI AND SAN LORENZO AND EUPLO IN FASANO (ITALY): SOME DECAY PATTERNS

Caldarola F.[1], Grippo A.[2], Guario I. M.[3], Laviano R.[4], Milella M.[5] and Scandale E.[6]

[1]Via Ricasoli n. 67, 70056 Molfetta (Ba), Italy francesca.caldarola@virgilio.it
[2]Via Miliscola n. 133, 80072 Pozzuoli (Na), Italy - alessandragrippo@hotmail.com
[3]Via Putignani n. 251, 70122 Bari, Italy – irgua@libero.it
[4]Geomineralogical Department, University of Bari, Via Orabona n. 4, 70125 Bari, Italy.
r.laviano@geomin.uniba.it
[5]Superintendence for Apulian Cultural Heritage, Piazza Federico II di Svevia, 70125 Bari, Italy.
milella@artipuglia.it
[6]Geomineralogical Department, University of Bari, Via Orabona n. 4, 70125 Bari, Italy.
scandale@geomin.uniba.it

Abstract: All around Apulia region (South-Eastern part of Italy) rupestral settlements represent an extraordinary and fascinating discovery: house-caves and church-caves belong to the civil, religious and artistic life of this ancient land. As a matter of fact, people settled in these territories gave birth, all along a series of rifts (locally known as Lamae), to very crowded villages with paths, water rain wells, stores and shelters while the church, with its charming wall paintings, was the physical and ideal centre of the community.

Our research focuses on the hypogean churches of Lama d'Antico, San Giovanni and San Lorenzo and Euplo in order to improve the knowledge about the degradation of wall paintings on a calcarenitic substrate. The analysis have revealed incrustations made up of sulphates, nitrates, chlorides and calcium-oxalate films; the main pigments discovered are minium, carbon black, red and yellow ochre.

The diagnostic methods used are: Optical Microscopy (OM), Scanning Electron Microscopy (SEM) with Microanalysis (EDS), X-Ray Photoelectron Spectroscopy (XPS), Ion Exchange Chromatography (IC), X-Ray Diffraction on Powder (PXRD), FT-IR, RAMAN Spectroscopy.

The interaction between experts of many different doctrines has been necessary to the formulation of hypothesis of conservative treatments on rupestral settlements, which are so many but not yet sufficiently known in Apulia and in the whole Mediterranean area.

Key words: Wall painting, Hypogeum, Calcarenitic Rock, Red Ochre, Carbon Black.

1. INTRODUCTION

On the occasion of the Master "Characterization and Conservation of stone and ceramic materials" (Academic Year 2002/2003, 2003/2004), held in cooperation with the Geomineralogical Department of the University of Bari, CIASU of Fasano and the Superintendence for Apulian Cultural Heritage, under the supervision of professor Eugenio Scandale, we had the possibility to develop an innovative and multidisciplinary methodology with the aim of characterizing the decay of stone and wall paintings of the hypogeous churches of Lama d'Antico, San Giovanni and San Lorenzo and Euplo situated in the homonymous Rupestral Park in Fasano (Bari). The experimental diagnostic stage followed a preliminary cognitive investigation aimed at organizing the area not only of historical, architectonical and landscape conservation study but also of geological and static study. The samples collected have been analysed with the instrumentation available in the Geomineralogical Department and in the Department of Chemistry of the University of Bari, in cooperation with the University of Lecce. Results have partly confirmed what has been obtained from

data in literature, from preliminary studies and from on-the-spot investigations (the recognition of pictorial techniques, the pigments used, the wall paintings decay).

2. MATERIAL AND METHODS

Quality assessment of conservation state of the three hypogeous churches was preliminary to any diagnostic survey.

An accurate visual inspection has permitted the observation of wide phenomena of decay which have jeopardized most of stone and pictorial surfaces especially in the settlement of Lama d'Antico and San Giovanni.

A second stage of research dealt with the structural analysis of manufacture by a first examination of physical-mechanical characteristics of calcarenitic substrate through the drawing of samples in quarries near to the hypopogeum.

Once the above-mentioned analysis was concluded, we turned to the wall paintings sampling stage, trying to operate as less invasively as possible, choosing, at the same time, the most representative areas where we investigated the degradation phenomenon. Samples have been drawn under the shape of small fragments preferring the areas marking the boundary of gaps. Data regarding each drawing have been filed in a special register accompanied by photos, maps and information on the analysis carried out.

We took advantage of the following instrumental methodologies in order to conduct researches: Optical Microscopy (OM), Scanning Electron Microscopy (SEM) with Microanalysis (EDS) on thin sections as well as on microscopical samples; X-Ray Diffraction on Powder (PXRD); FT-IR; RAMAN Spectroscopy.

3. GEOMORFOLOGICAL CHARACTERS OF LAMA D'ANTICO RUPESTRAL SETTLEMENT

The rupestral village of Lama d'Antico, with the near churches of San Giovanni and San Lorenzo and Euplo, is situated in Lama Tamurrone along the apulian Adriatic coast edge of the land of Fasano.

Geomorfological elements typical of the area are mainly represented by a series of sea-terraces slightly degrading towards the sea and by small-sized erosive fractures, parallel between each other and perpendicular to the coast-line.

Along the Adriatic coast band erosion has removed most of the sequence of Bradanic Ditch leaving the oldest term, locally known as Calcarenite di Gravina (Ricchetti et al., 1988).

The geotectonic origin of the area and the characteristics of malleability of calcarenitic stone have affected geometry and morphology of rupestral settlements in grotta, which are widespread in the area.

The sequence of sea-terraces is cut along the entire coast band by a large network of erosive fractures, locally known as "lamae". They are transitory watercourses perpendicular to coast-line and subparallel between each other. They have a flat ground, very wide and covered by a thick blanket of red soil with calcarenitic stones allowing the cultivation of olives and vines; their walls are often steep.

4. ARCHITECTURAL STRUCTURE AND PICTORIAL DECORATION

4.1 The church of Lama d'Antico

The rupestral village of Lama d'Antico is one of the oldest examples of human settlement which is not alternative to most strictly urban settlements. It is, therefore, part of the most representative inhabitable types of medieval communities.

Church was undoubtedly the nerve-centre of life in the village: its location inside the rupestral hamlet responds to a precise urban choice. It is digged out in the central area of Lama Tammurone, in the Northern ridge, and has a stately facade with traces of frescos. It is datable between X century and 1050 and appears as a building with an extended plan (about m 6,10 wide x m 10,20 deep) divided by a

series of pillars (Laviano et al., 2003), arched into two different aisles (Figure 1).

Figure 1. Lama d'Antico: internal view of the church

These mentioned aisles were cut in their centre, near the side-entrance, by a solemn dome (at present collapsed), connected to the upper part through pendentives and likely covered by tiles. The remaining part of the ceiling has barrel vaults of different heights. It is an extremely rare type of building, to such an extent that the church of Lama d'Antico, in virtue of its peculiarity, occupies an exclusive place among Apulian rupestral churches (Dell'Aquila and Messina (1998)).

In terms of pictorial decoration, the state of negligence and decay, along with static disarrangements, high moisture related to water seepages and anthropic aggressions which threaten the integrity of the entire settlement, has jeopardised almost entirely the visibility of most of pictorial representations. Frescos of a very original version of the Déesis, Cristo Pantocratore Vergine col Bambino and San Giovanni Battista are in the upper part of the apse, whereas, a real pictorial cycle must have been represented along the walls with Santi Vescovi (Figure 2), portraying a series of small blind arches. Portraits of San Lorenzo, San Teodoro, San Biagio and SS. Cosma e Damiano are also easily recognizable.

Figure 2. Lama d'Antico: Bishops painted on the arched wall

4.2 The church of San Giovanni

The church of San Giovanni reflects the architectural typology typical of a Byzantine era place of cult divided into vestry, narthex, bema (a narrow cross-passage) and naos. It is of a smaller size compared with Lama d'Antico and it develops on a rectangular framework whose sizes are: 5.25 m wide, 7.70 m deep and 2.30 m high (Laviano et al., 2003). The naos is separated from the bema through a lithoid iconostasis which had been destroyed in the past and recently rebuilt (Figure 3). It is covered with a level vault; light and air get into the environment through the entrance room only (enclosed by a temporary door) and a small window which illuminates faintly the bema.

Figure 3. San Giovanni: view of the reconstructed lithoid iconostasis

What remains visible of the wall paintings in the inside of the church suggests the presence of a program of theological representations of wide sizes.

About twenty years ago the historian Antonio Chionna (Chionna, 1973) conferred on the church the name of San Giovanni Battista on the basis of the best preserved fresco and the presence, on the left side of the entrance, of a basin considered as a christening font.

Other present depictions are: L'ingresso di Cristo a Gerusalemme and I mesi zodiacali in the narthex; San Giorgio e il drago in the naos; San Benedetto and two medallions on which are the symbols of the Evangelists San Giovanni and San Matteo on the iconostasis; l'Annunciazione and the Dèesis in the bema.

Figure 4. San Lorenzo: external view of the church

4.3 The church of San Lorenzo

The church of San Lorenzo and Euplo fans out (6.90 m wide x 7.40 m deep) in the calcarenitic rock with an only central pillar and a double templon (Figure 4). Two small apses open on the North-Western side of the crypt, connected with the lithoid iconostasis: the first of them is of a rectangular shape, while the second is semicircular. The structural arrangement of the crypt let us suppose the current plan of the church is the result of a later spatial reorganization which has doubled the internal room with the addition, far away from the entrance, of another apse and another templon (Figure 5). The better preserved wall paintings are just in this part of the church (Figure 6); among the most representative pictures we can mention the two Santi Vescovi (1, 2 – Figure 5), in which traces of two superimposed layers of mortars are well recognisable; the portraits of San Basilio and San Benedetto (3 – Figure 5); the wall painting of Santo Stefano in the contiguous arcosolium (4 – Figure 5); the representation of Dèesis in the rectangular apse (6 – Figure 5), together with the archangels Gabriele and Raffaele (5,7 – Figure 5); the portraits of San Nicola, San Paolo and San Pietro on the wall between the two apses; (8 – Figure 5) and, finally, the picture of Sant'Euplo painted in the diaconicon (9 – Figure 5).

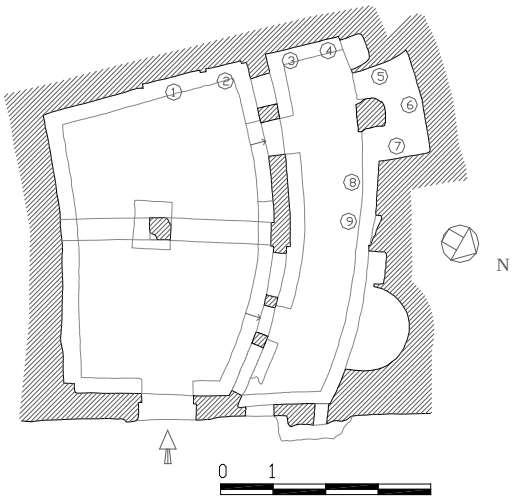

Figure 5. San Lorenzo: map of the church

Figure 6. San Lorenzo: best preserved frescos in the *bema*

5. RESULTS AND DISCUSSION

5.1 The church of Lama d'Antico

In the church-cave of Lama d'Antico, particularly humid because of the infiltration of meteoric and irrigation water coming from the fields overhanging the flat ceiling, different forms of degradation have been detected. In addition to the anthropic damage (vandalism, destruction, etc.) efflorescences, incrustations, detachments and gaps have been found mainly on the pictorial surfaces, while alveola, biological patina, ruderal and higher

plants have been discovered on the stone surfaces.

From the analysis done, it appears that the Northern, Southern and Western walls of the church have been fully hit by the formation of calcium-oxalate films.

Their composition is not constant. In addition to the calcium oxalate (in its behydrated form-weddellite - more unstable) are also other components, in varying concentrations: calcium sulphate, silicates, nitrates, organic compounds.

The most probable origin of the oxalate seems biological, because of a wide patina, made up predominantly of photosynthetic micro-organisms (algae, cyanobacteria and lichens) to which dust and mould have adhered (Caldarola et. al., 2001).

The analysis of saline efflorescences, white-coloured and filamentous, has revealed nitrates, chlorides and sulphates.

Another phenomenon of degradation found is the formation of surface incrustations, of varying thickness and dark in colour. On a first examination, such incrustations may be attributed to processes of sulphation of the carbonate matrix. It cannot be denied that a degradation from chemioautotrophs micro-organisms also occurs in this process.

A detailed analysis by SEM of a representative specimen of such phenomenon has revealed the presence of calcium sulphate geminated in clusters of plates in the characteristic appearance of desert rose or needle-shaped crystals.

In the zone of more compact texture, three layers can be discerned:

- *the upper layer, made up of a mass of calcium sulphate with fragments of calcite and quartz of Aeolian origin;*
- *the intermediate layer, made up mainly of Si and Mg in almost identical proportions;*
- *the lower layer, with the presence of C, and traces of S, Ca, Cl, Si and Mg.*

The incrustations are detaching, and cause the rising of the underlying pictorial film. As far as the latter is concerned, the analysed specimen shows that, on the stone substratum, a single thin layer of mortar is laid (about μm 100), with lime and inert matter made up of calcite, iron oxides and quartz.

As far as the nature of pigments used is concerned, it is certainly the red ochre, because of the presence of hematite (Laviano et al., 2003).

5.2 The church of San Giovanni

Observing the frescos found on the walls of the narthex, naos and bema of the hypogeum of San Giovanni, wide blackish incrustations compromising the legibility can be seen. The degradation is particularly evident on the Northern and Western walls of the narthex. The analysis of specimen taken from this zone, led by Scanning Electron Microscopy (SEM) and X-Ray Diffraction on Powder (PXRD), show the presence of calcium sulphate, chlorides and phosphates [above all $Ca_5(OH)(PO_4)_3$]. Those salts come quite certainly from the fertilizers used to improve the productivity of the overhanging fields, and have penetrated inside the hypogeum through the numerous lithoclases of the calcarenitic rock. The FT-IR analyses have shown the presence of nitrates too.

Considering the pictorial layers, specialists have tried to understand what mortars, pigments and techniques have been used, in order to find out useful data to confirm the presence of many hands inside the church. The most representative specimen is S.G.2.7., taken from the North side wall of the narthex. In such specimen, a palimpsest can be seen, with the superimposing of 3 pictorial layers (strata). The distance between the upper layer and the lower is about 1-1,5 mm.

In the lower layer, the presence of lead suggests that the pigment used is minium (Pb_3O_4).

The intermediate layer seems to be made of carbon black in the upper part and hematite in the lower one.

The upper layer of the palimpsest, on the contrary, is made up of ochre, whose colour varies from yellow to red according to the smaller or greater quantity of iron oxide and its degree of hydration (Laviano et al., 2003).

The presence of ochre has been found in other specimen.

As far as the techniques of execution of the frescos are concerned, the analysis of the thin sections has revealed differences in the preparatory layers. On the Easter wall of the bema two different layers of mortar have been found: the lower layer is coarse, with calcarenitic clusters, quartz, iron oxides and iron hydroxides, vegetable fibres and evident fractures due to the drawing of materials, while the upper layer looks refined and homogeneous.

Generally, the layers are 55 to 165 □m thick.

5.3 The church of San Lorenzo

The decoration of the North-Western and South-Eastern walls of the naos is particularly damaged because of the big stagnation of moisture; there are wide saline efflorescences (above all chlorides and nitrates), biological films (the walls are very damp, but not directly exposed to the sun light, that is why the colonizing species are algae), incrustations (mostly made up of calcium sulphate and organic substances), swellings and numerous gaps.

An illustrative image of the consistence of the incrustations is given by the SEM analysis, where crystals of halite in cubic shape add to crystals of calcium sulphate in the typical shape of desert rose (Figure 7).

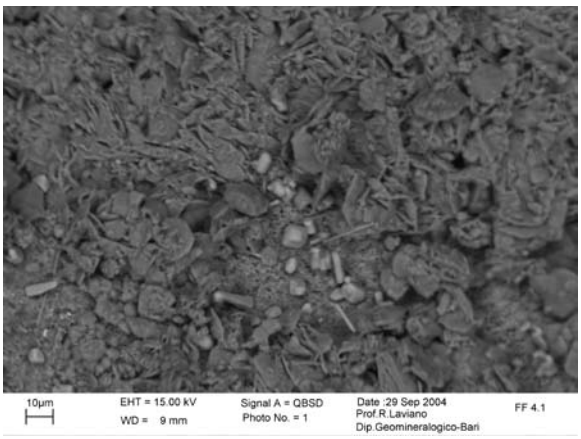

Figure 7. Lorenzo: SEM image of cubic and needle-shaped NaCl crystals

Best preserved are, however, the frescos in the North-Western zone of the bema, where the microclimate is very propitious to the preservation.

Considering the research on the nature of pigments, the use of yellow and red ochre can be found for the presence of hematite, while mortars are mainly made up of gypsum and calcite. Three layers of the pictorial film can be seen, overhung by a surface layer of sulphation:

a) *quartz and iron (iron silicates?) are inside the upper layer, precisely in those crystals which appear more compact and solid, and which are soaked in a matrix of calcium and magnesium;*

b) *the intermediate layer, lighter, does not have iron;*

c) *in the lower layer, the calcium-iron proportion is inverted compared to the upper layer .*

Interesting is also the presence of pyroxenes and olivins, which allows us to think about the use of umber as a pigment (Figure 8).

Finally, we can testify numbers of dry finishes; as a matter of fact, it is possible to notice some pictorial stratifications on the North-Western and South-Western walls of the hypogeum.

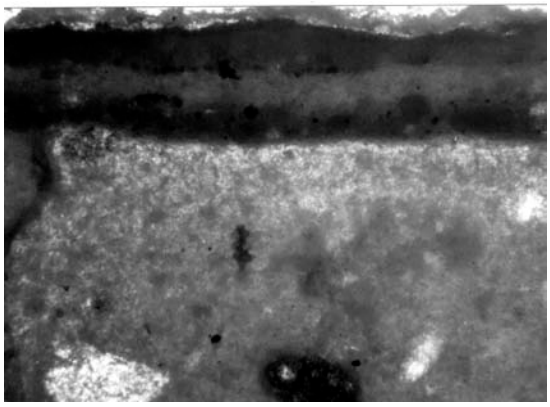

Figure 8. San Lorenzo: three different layers of the pictorial film (OM – 40X – N//)

6. CONCLUSIONS

The pieces of research carried out are among the first conducted in the Apulian region (municipality of Fasano) on medieval frescos located in rupestral settlements. They therefore represent an important step toward the knowledge of materials and pictorial techniques resulting from the constructive practice of the past and are the starting point for the creation of a precious collection of data related to forms of degradation widely spread in this immense cultural heritage (Apulia has more than 400 rupestral settlements of which 364 are frescoed). Data are also important in order to widen the extent of research until reaching possible comparisons with coeval undertakings in other areas of Apulia and Eastern Mediterranean. The exchange of information with study groups from the near churches of Lama d'Antico, San Giovanni and San Lorenzo and Euplo allows significant comparisons between the three rupestral settlements.

The study has highlighted the fact that in the three settlements the representations have been performed by means of the technique of fresco. Some palimpsests have been detected in San Giovanni, while in San Lorenzo there are numbers of dry finishes.

In Lama d'Antico and in San Giovanni mortars are exclusively of carbonate nature with the addition of inert matters such as limestone fragments, vegetable fibres, quartz and iron oxides. In San Lorenzo, on the other hand, underlying mortar has been prepared by adding calcium sulphate.

Moreover, in Lama d'Antico and in San Lorenzo a single preparatory layer has been detected, whereas in San Giovanni a better executive accuracy with the use of two superimposed mortar layers, the most superficial of which has thinner grain, has been observed.

The fact needs to be observed that, in spite of the differences in preparation of underlying mortar, the pigments used are mainly of inorganic origin in the three hypogeum: ochre (in Lama d'Antico, San Giovanni and San Lorenzo), umber (in San Lorenzo), minium (in San Giovanni), with the exception of carbon black (in San Giovanni).

The three settlements present different forms of degradation in regard to conservation.

A phenomenon of deterioration must have occurred in San Giovanni threatening wall paintings more seriously than in Lama d'Antico and San Lorenzo.

The reason for those discordances has to be found in environmental differences of the three settlements.

If the presence of sulphates, nitrates and chlorides in these settlements can be explained in a convincing way by a mechanism of combined action of atmospheric pollution, fertilizers, sea-aerosol and biodeteriorating microflora, the impact of the phenomenon strikes because of its macroscopic difference of appearance.

Patinas detected in Lama d'Antico and San Lorenzo have an earthy and powdery form and a changing colour, from green to brown. They are very likely due to the growing of lichens.

Wall paintings in the church of San Giovanni appear strongly damaged by the development of a dark patina which causes the detachment of mortar into thicker and more compact scales than

those observed in Lama d'Antico and in San Lorenzo.

Pictorial surfaces in this case seem apparently colonized by a fungus microflora prevailing on the autotrophic component (chemio as well as photoautotrophic). This leads us to interpret also the growing darkness and the detachment of mortar as something due to spread of melaminic fungus mycelium.

Such macroscopic observation could match also with the results of chemical and mineralogical analyses which have revealed the presence of calcium oxalate films only in Lama d'Antico and San Lorenzo but not in San Giovanni. This confirms the hypothesis that the chemical and physical degradation of the settlements is seriously worsened by phenomena of biodeterioration: while the lithological composition of the lower layer observed is similar (calcarenitic substrate), the microenvironment is not.

Therefore, in Lama d'Antico a biological sequence has developed, determining a degradation more similar to the decay found in external environment, while, in San Giovanni typical alterations of a confined environment such as a hypogeum have been detected.

In the light of what has been analysed so far, it has to be concluded that rupestral settlements represent the ideal research area on the evolution of rupestral pictorial techniques and of the forms of biodeterioration in order to identify effective conservation treatments.

7. ACKNOWLEDGEMENT

We warmly thank Drs. Maria Guario for the English revision of the manuscript.

8. REFERENCES

Caldarola, F., Cafaro, M. P., Fragasso, L., Grippo A., Laviano, R., Milella, M., Sabatelli, L., Scandale, E., Schirone, E., 2004. The degradation of stone and wall paintings of two rupestral churches: Lama d'Antico and San Giovanni (Fasano, Italy). *32nd International Geological Congress*, Florence, Italy.

Chionna, A., 1973. Il villaggio rupestre di Lama d'Antico, *Grafischena*, Fasano, Italy.

Dell'Aquila, F. and Messina A., 1998. Le chiese rupestri di Puglia e Basilicata, Adda, Bari, Italy.

Laviano, R., Milella, M., Sabbatini, l., Scandale, E., Caldarola, F., Colaleo, R., De Mauro, P., Moschettini, G. and Sabatelli, L., 2004. Forme di degrado negli insediamenti rupestri del territorio di Fasano: indagini sulla statica e sulle raffigurazioni pittoriche della chiesa ipogea di Lama d'Antico. Diagnostica per la tutela dei materiali e del costruito - 2003, *Sito Reale di San Leucio*, Napoli, Italy.

Laviano, R., Milella, M., Sabbatini, l., Scandale, E., Cafaro, M. P., Fragasso, L., Grippo, A. and Schirone, E., 2004. Forme di degrado degli insediamenti rupestri nel territorio di Fasano: statica e pitture murali nella chiesa ipogea di San Giovanni. Diagnostica per la tutela dei materiali e del costruito - 2003, *Sito Reale di San Leucio*, Napoli, Italy.

Ricchetti, G., Ciaranfi, N., Luperto Sinni, E., Monelli, F.and Pieri, P., 1988. Geodinamica ed evoluzione sedimentaria e tettonica dell'Avampaese Apulo. *Memorie Società Geologica Italiana*, Roma, Italy.

FRACTAL ANALYSIS OF AFTERSHOCKS OF EARTHQUAKES IN AKSEHIR-AFYON AND GOKOVA GRABENS, TURKEY

Ceylan S. and Özer N.

Istanbul University, Engineering Faculty, Geophysical Engineering Department, 34320 Avcilar, Istanbul, Turkey, (savasceylan@gmail.com, naside@istanbul.edu.tr)

Abstract: Fractal analysis is a powerful statistical tool because of its scale invariance property. Many phenomena in geophysics show multifractal properties such as frequency-size distribution of earthquakes, faults and fractures. Having fractal distribution requires that number of objects larger than a specified size has a power-law dependence on size.

In this study, The Aksehir-Afyon Graben (AAG) in west-central Turkey and the Gokova Gulf in the southwest of Turkey are selected as research areas. The earthquakes of 15 December 2000 Sultandagi-Aksehir, 03 February 2002 Cay-Eber and Cobanlar in AAG, and 04 August 2004 Gulf of Gokova, 20 December 2004 Ula and 10 January 2005 Oren earthquakes in Gokova Graben are selected for investigation.

b-value of Gutenberg-Richter relation and p-value of modified Omori's law are calculated for the selected earthquakes. Then capasity dimension (D_0) of the earthquake activity, information dimension (D_1) and correlation dimension (D_2) of the earthquake distribution for both areas are calculated, using the standard box counting method. The correlation between these dimensions, b and p values, and changes are examined for precusory events and aftershock sequences of the earthquakes in these grabens.

Key words: multifractals, b-value, p-value, fractal dimension.

1. INTRODUCTION

The analysis of time scaling properties of seismic events can give accurate and useful information about seismic events and can be used to better characterize seismic patterns. In order to find a scaling law, especially Poisson distribution, which assumes that each event from the elapsed time is independent from the previous events, has been widely used among several other distribution methods. However, it has been shown in recent studies that a time-correlation exists among seismic events, and this correlation is better characterized by power laws (Nanjo and Nagahama, 2000; Telesca et. al, 2004). Using power laws for seismic sequences is not new in geophysics. Gutenberg and Richter (1954) found out that there is a power law scaling between the magnitudes and frequencies of earthquakes.

The main reason that fractal analysis has become so popular recently is its scale invariance property, which means one dimension value can describe the dynamics of a fractured system, at any scale. Such fractal structures are named as monofractals. Since whole system dynamics is represented by one scaling exponent, such systems can be considered homogeneous. In cases that it is essential to explain the scaling properties of a system with different exponents, the structure can be a multifractal. It is possible that multifractals are composed of subsets which can be defined by different scaling exponents (Turcotte, 1997; Telesca et. al, 2004). Multifractal systems can be accepted as more heterogeneous structures and the energy that creates the dynamics of the system is not equally distributed in time scale.

In geophysical point of view, whatever the physical environment or system is, system dynamics are defined by all factors that cause an earthquake. The scaling property of an object carries the statictical analysis of all possible physical factors such as magnitude, fault length, crustal structure, etc. Therefore, it is quite possible that a good study and careful interpretation of scaling properties of

seismically active regions can give accurate results about how dynamics of the region under study change by time.

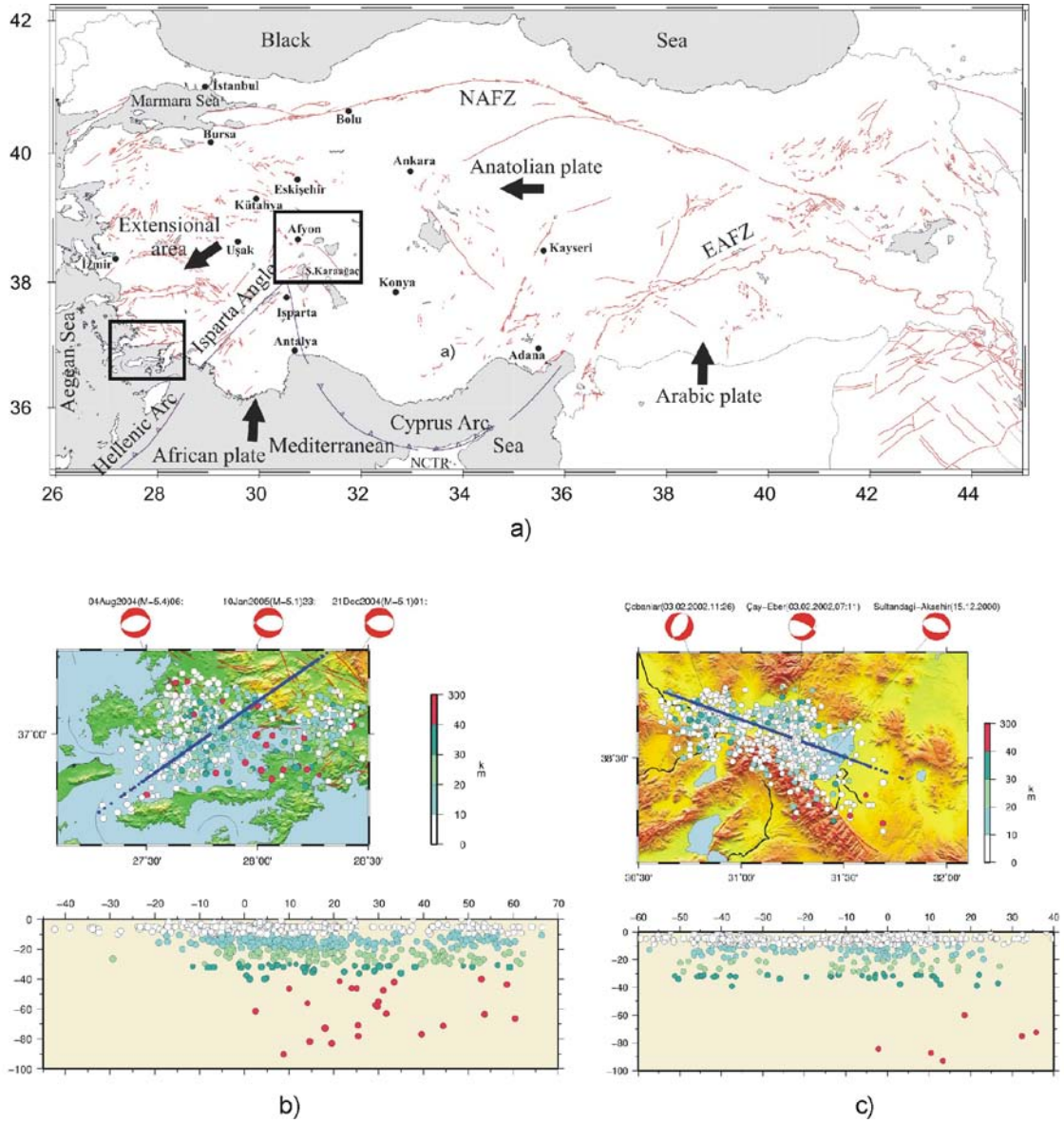

Figure 1. a) Tectonic map of Turkey and the study regions. b) Earthquakes in Gokova Graben and depth section c) Earthquakes in AAG and depth section (Ozer et al., 2005)

In this paper, two seismically active regions are selected for investigation. 1) AAG is a NW-SE trending graben and separates central Anatolia from the intersection of the Hellenic and Cyprus arcs in west-central Anatolia, namely Isparta Angle, and 2) the Gokova Gulf, which is a E-W trending graben in southeast of the Aegean Sea (Figure 1).

2. METHOD

2.1. Multifractals

The phenomena such as fractures and earthquakes are "self similar" systems at any scale and can be defined by a power law. The value of the power stands for the fractal dimension, which indicates "the degree of order" in a chaotic system. Fractals are defined as

$$N_i = \frac{C}{r_i^D} \qquad (1)$$

where N is the number of objects (earthquakes) larger than a specified size of r, C is the ratio constant and D is the fractal dimension (Turcotte, 1997).

For multifractal systems, higher order moments of the equation above (Equation 1) is used to analyse the behaviour of the events. The capasity dimension (D_0) is the same as the dimension above and indicates the probability of the existence of a datum point within a specified area. The capasity dimension does not contain the frequency or size information. The information dimension (D_1) is a special form of capasity dimension and is the measure of expectation or surprise (Baker and Gollub, 1990). The correlation dimension (D_2) is the last dimension value used, and unlike capasity dimension it includes the frequency information (Sarraille and Difalco, 1992). A system for which these three dimensions are equal is considered as monofractal and in this sense monofractals are homogeneous since they have the same scaling property (Baker and Gollub, 1990; Turcotte, 1997; Telesca et al., 2004).

All these dimensions can be derived from the same equation below (Equation 2), where N is the number of objects, C(r) is the correlation integral (Equation 3), r is the "box" size, q is the order of the moment and H(x) is the Heaviside function. For information dimension, the lim→1 form of Equation 2 is used (Nanjo and Nagahama, 2000; Mittag, 2003).

$$D_q = \frac{\log C_q(r)}{\log(r)} \qquad (2)$$

$$C_q(r) = \left\{ \frac{1}{N} \sum_{i=1}^{N} \left[\frac{1}{N} \sum_{j=1}^{N} H\left(r - \left|x_i - x_j\right|\right) \right]^{q-1} \right\}^{1/(q-1)} \qquad (3)$$

In the correlation integral (Equation 3), the Heaviside function serves a step function and is used to count the data in boxes.

As a matter of fact, geophysicists have in a way been using fractals before the term of fractal was introduced to the world by Mandelbrot (1967). The b-value of Gutenberg-Richter (1954), which is also a power law, indicates scaling properties too and its relation between fractal dimension is defined as D=2b (Aki, 1981).

2.2. Data and Calculation

Earthquake data are obtained from Kandilli Observatory. Aftershock sequences are decided according to present fault data and tectonic settings of the regions and seperated from the main data by means of defining polygons. The calculations are performed within the time interval of 1 hour (0.04167 days). The same aftershock data are also used for the capasity dimension of active faults, because earthquakes already show the active parts of the existing faults, which have the capasity to produce an earthquake. Moreover, this calculation method is prefered in order to prevent the possible errors during digitizing the fault coordinates, which are not precise enough.

The occurrence times of main shocks are accepted as the starting times. In order to follow the changes in fractal dimensions, b- and p-values by the time, all earthquakes elapsed from the occurrence time of the main shocks are included in each interval for which calculations are performed. The threshold magnitude is chosen as 0.0 not to lose any data point that capasity of existing active fault system has produced. Fractal dimensions are calculated by using the box counting method with a similar method indicated in Grassberger and Procaccia (1983) and using the algorithm of Liebovitch and Toth (1989).

3. RESULTS

For both regions, all fractal dimensions are close to the value of 1, which is the fractal dimension of a line. This might be the indication of normal faulting, since there is little spreading in two dimensional space. The differences between the fractal dimensions can provide information about the heterogenity of the region. The values calculated for AAG are closer to each other and more correlated than the values calculated for Gokova Graben (Figure 2),

which might mean that the underground structure of AAG is more homogeneous than Gokova Graben (Figure 3).

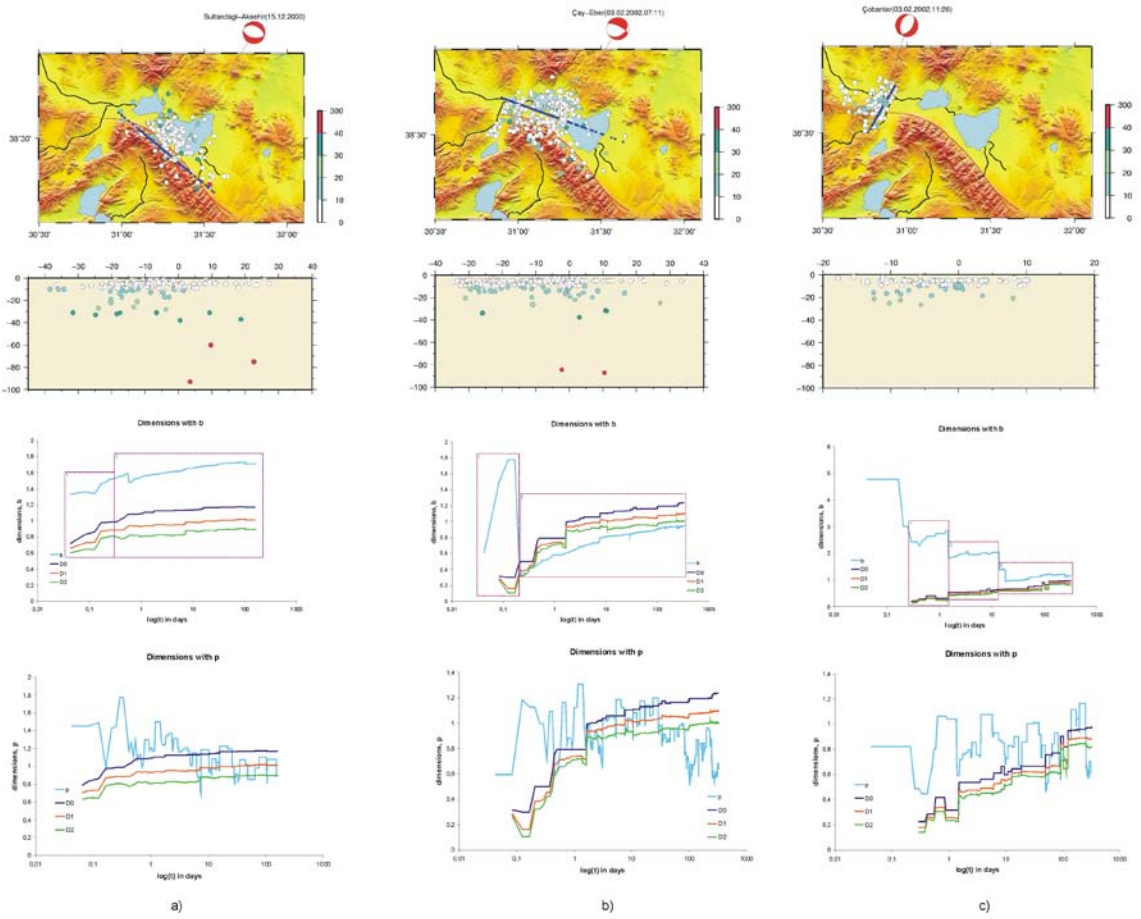

Figure 2. Aftershock locations, b-value, p-value changes with fractal dimensions in time scale a) Sultandagi-Aksehir earthquake b) Cay-Eber earthquake and c)Cobanlar earthquake in AAG

For the first hours of Cay-Eber and Cobanlar earthquakes, there is a negative correlation between b-value and fractal dimensions. Although there are earthquakes with magnitudes between 3.0 and 3.4 for Cay-Eber earthquake, the information and correlation dimensions decrease until a respectively larger aftershock occurs with the magnitude of 5.1, while capasity dimension almost stays unchanged. The same relation exists for Cobanlar earthquake too, but the decreases are in quite smaller ranges. For Sultandagi earthquake, there is a positive correlation between fractal dimensions and b-value in common, at 0.125 days. Prior to that day, there are three aftershocks with respectively larger magnitudes of 3.7-3.9. These earthquakes cause decay in b-value but raise in fractal dimensions.

For the rest of the data of these three earthquakes, Cay-Eber and Sultandagi show similar behaviours as explained above. However, in Cobanlar earthquake negative correlation exists until the end of the observation period in general, and two more subsets can be identified easily as shown in Figure 2a.

For Ula earthquake, two subsets of fractal behaviour are detected. In the first subset (the period from the beginning to nearly 7.5 days) there is a positive correlation between b-value and fractal dimensions. Within this period, magnitudes of aftershocks are higher than the second subset and there are respectively smaller earthquakes in the days of 1.3 and 6.5. These earthquakes are

well distinguished in the fractal dimensions as decays. In the second period, there is a sudden decrease in magnitudes by the time except the days of 76.083 (magnitude of 3.1), 93.958 (magnitude of 3.3) and 196.75 (magnitude of 3.4) and b-value starts to decrease as fractal dimensions increase (Figure 3a).

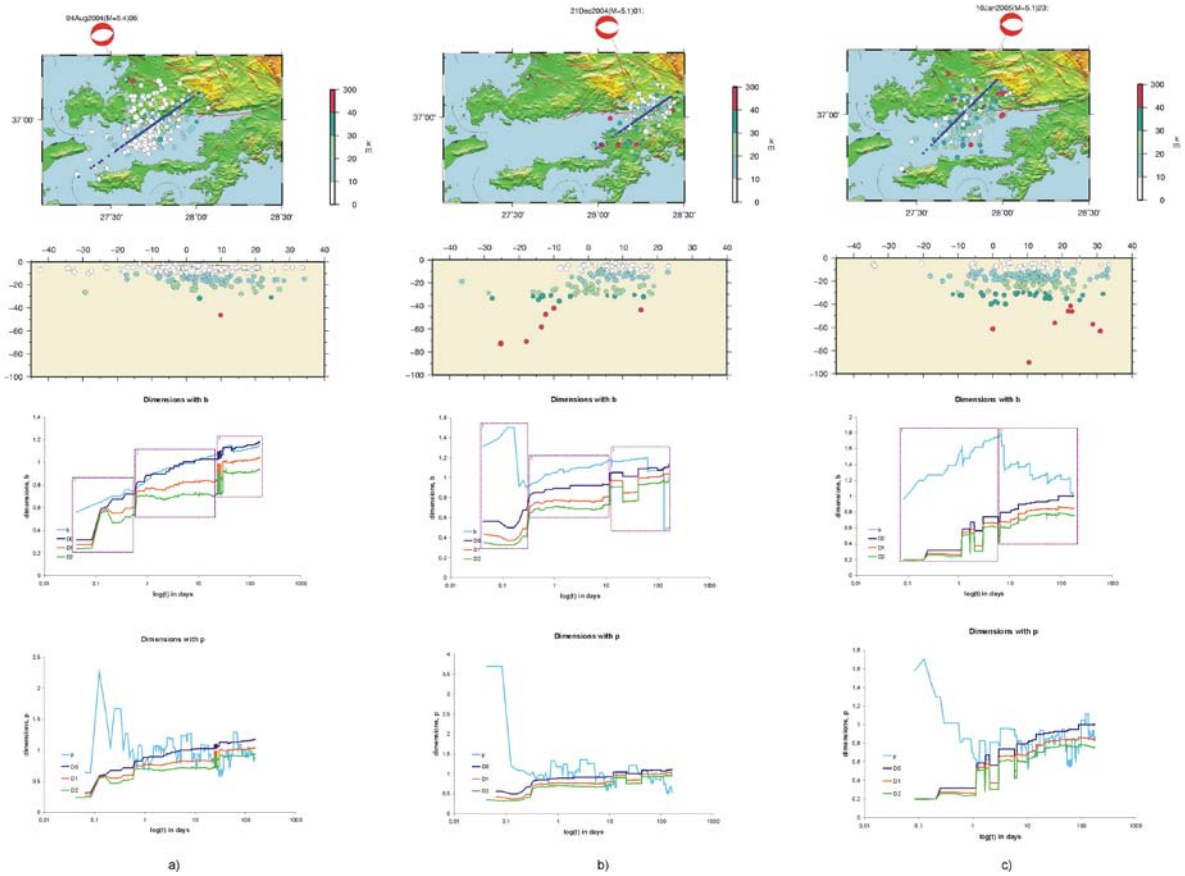

Figure 3. Aftershock locations, b-value, p-value changes with fractal dimensions in time scale a) Gokova Gulf earthquake b) Ula earthquake and c)Oren earthquake in Gokova Graben

In the second pattern of Oren earthquake (Figure 3b), fractal dimensions are almost steady. The magnitudes within this period are around 3.2. There are some aftershocks with higher magnitudes, and the small raises might be caused by these shocks. However, the fractal dimensions decrease in general tendency until the day of 9.25 then become steady. Within that period there are aftershocks with magnitudes of maximum 3.4 and on the day of 12.9 there is a larger aftershock with a magnitude of 4.1. During the whole pattern, b-value has an increasing trend and on the days with larger aftershocks mentioned above, the slope of the b-value gets higher values, as fractal dimensions becomes steady.

The similar behaviour is also seen in other earthquakes. No different behaviour is found in Gokova earthquake. There are no obvious patterns found between p-value and the fractal dimensions, except that they are negatively correlated.

4. CONCLUSION AND DISCUSSION

In this paper, two seismic regions in Turkey is investigated by means of multifractals, and patterns which can describe the scaling properties of the regions are defined. It has been observed that all sequences consist of different scaling patterns which change by time. The capasity dimension value is steady when small earthquakes occur, which might indicate the energy accumulation on the fault.

Before the occurrence of larger aftershocks, there are decays in information and correlation dimensions, as capasity dimension is steady or shows little increase. However, no certain patterns could be defined between the decay rates and dimension changes.

Although Sultandagi and Cay-Eber earthquakes are on the same fault, their scaling behaviours are different. As an interpretation of correlation between seismic parameters, it can be said that energy release was more continuous and linear in Sultandagi earthquake, while it was more sudden in Cay-Eber earthquake.

ACKOWLEDGEMENTS

The maps used in this paper are prepared by using the Generic Mapping Tools software of Wessel and Smith (1998).

REFERENCES

Aki, K., 1981. Probabilistic synthesis of precursory phenomena. In Earthquake Prediction, Simpson, D. W., Richards, P. G., (Eds.), pp. 556-74, *American Geophysical Union*, Washington, D.C.

Baker, G. L., Gollub, J. P., 1990. Chaotic dynamics an introduction, *Cambridge Unversity Press*, New York.

Grassberger, P., Procaccia, L., 1983. Measuring the strangeness of strange attractors, *Physica 9D*, 189-208.

Gutenberg, B., Richter, C., 1954. Seismicity of the earth, *Princeton Uni. Press*, New York.

Kandilli Observatory, Kandilli Rasathanesi ve Deprem Araştırma Enstitüsü, www.koeri.boun.edu.tr, August 2005.

Liebovitch, L.S., Toth, T., 1989. A fast algorithm to determine fractal dimensions by box counting, *Physics Letters A*, 141, 386-390.

Mandelbrot, B.B., 1967. How long is the coast of Britain? Statistical self-similarity and fractional dimension, *Science*, 156, 636-638.

Mittag, R. J., 2003. Fractal analysis of earthquake swarms of Vogtland/NW-Bohemia intraplate seismicity, *Journal of Geodynamics*, 35, 173-189.

Nanjo, K., Nagahama, H., 2000. Fractal properties of spatial distributions of aftershocks and active faults, *Chaos, Solitons and Fractals*, 19, 387-397.

Ozer, N., Altınok, Y., Ceylan, S., Kurt, H., Kolçak, D., 2005, Aftershock sequences in Aksehir-Afyon and Gokova grabens, Turkey, *IESCA 2005*, SSG18. 4-7 October 2005, İzmir (Poster sunu).

Telesca, L., Lapenna, V., Macchiato, M., 2004. Mono- and multi-fractal investigation of scaling properties in temporal patterns of seismic sequences, *Chaos, Solitons and Fractals*, 19, 1-15.

Turcotte, D. L., 1997. Fractals and chaos in geology and geophysics, 2nd edition Cambridge, *Cambridge Univ. Press*, New York.

Sarraille, J., Difalco, P., 1992. Computer program for estimation of fractal dimension, ftp://ftp.immt.pwr.wroc.pl/pub/fractal, August 2005.

Wessel, P. and Smith, W. H. F., 1998. New improved version of Generic Mapping Tools Released, *EOS*, 79, 579.

THE MINERALOGICAL AND GEOCHEMICAL CHARACTERISTICS OF PHOSPHATE OCCURRENCES IN MIOCENE TUFFS (AYVACIK-ÇANAKKALE)

Çoban F. and Kocabaş C.

Balikesir University, Faculty of Engineering and Architecture, Department of Geological Engineering, 10145 Çağış, Balıkesir, Turkey
fcoban@balikesir.edu.tr, cumhurkocabas@yahoo.com

Abstract: Phosphate occurrences in tuff levels of Miocene lacustrine sequence (sandstone, siltstone, bituminous shale, marl, tuff) occurred as phosphated and phosphated-carbonated concreations in Nusratlı-Arıklı (Ayvacık-Çanakkale). These concretions are on average 2-4 cm. in diameter, and they exhibit a concentric structure. Their nucleus parts were formed from carbonate, tuff and/or biogenic clasts. Phosphatic zones have two different types of mineral compositions:

Fluorapatite + analcime + montmorillonite + calcite

Carbonate-apatite + calcite + analcime + quartz.

Scanning electrone microscope (SEM) investigations indicate that phosphates are grown up with layered montmorillonite and/or calcite. Montmorillonites have a honeycomb morphology and aggregates with rough surfaces of 5 micron on average in size. Calcite is grown up as globular grains 0.1-0.2 µm in diameter.

When compared with the major element contents of typical marine phosphorites, phosphated and phosphated-carbonated concretions are enriched in SiO_2, Al_2O_3, Na_2O and K_2O. Contents of major oxides varies between; SiO_2: 23.75-42.05 %, Al_2O_3: 5.10-6.00 %, Fe_2O_3: 1.40-3.81 %, CaO: 18.53-33,01 %, K_2O: 1.00-6.49 %, Na_2O: 0.61-3.98 %, P_2O_5: 11.81-20.60 %. Geological, mineralogical and geochemical data indicate that syngenetic phosphate occurrences in tuff levels of Neogene volcano-sedimentary sequences may have a hydrothermal origin.

Key words: Tuff, hydrothermal, concreation, phosphate

1. INTRODUCTION

A great deal of study has been done about phosphate occurrences. These studies are concerned with sedimentary phosphates. Phosphates having economic potential have been studied as the most important aspects of the phosphorites (Kazanov, 1937). The other investigators followed and improved this base studies. According to Kazanov, (1937) deep marine phosphate occurrences were formed by the sea water currents involving excess carbonic acid. While they approach the shallow marine environments, they ascend and are warmed. The pH of the water increases, becomes alkaline, and dissolved phosphate is precipitated by biochemical conditions. On the other hand, the investigations about phosphate nodules indicate that the nucleus of this nodules are formed by carbonated and/or organic materials.

In this study, the phosphate occurrences in Nusratlı-Arıklı Village (Ayvacık-Çanakkale) were investigated. Phosphate occurrences were formed in Miocene tuff levels related to the lacustrine environment. They are various in size and show phosphated and phosphated-carbonated nodule shapes. The mineral assemblages were determined by X-ray diffraction and SEM (Scanning electron microscope). Some comparisons were made according to the chemical analyses. It is determined that the nucleus part of this concretions are mainly tuff, and these phosphate occurrences have an hydrothermal origin.

2. MATERIAL AND METHODS

The phosphates and related minerals in concretions were studied by X-ray diffraction (XRD). Scanning electron microscope (SEM) was used for

determining the morphologic properties of phosphate minerals and their relationship with other minerals. Major elements were determined for the comparison of phosphate occurrences with tuffs and similar occurences of the same age.

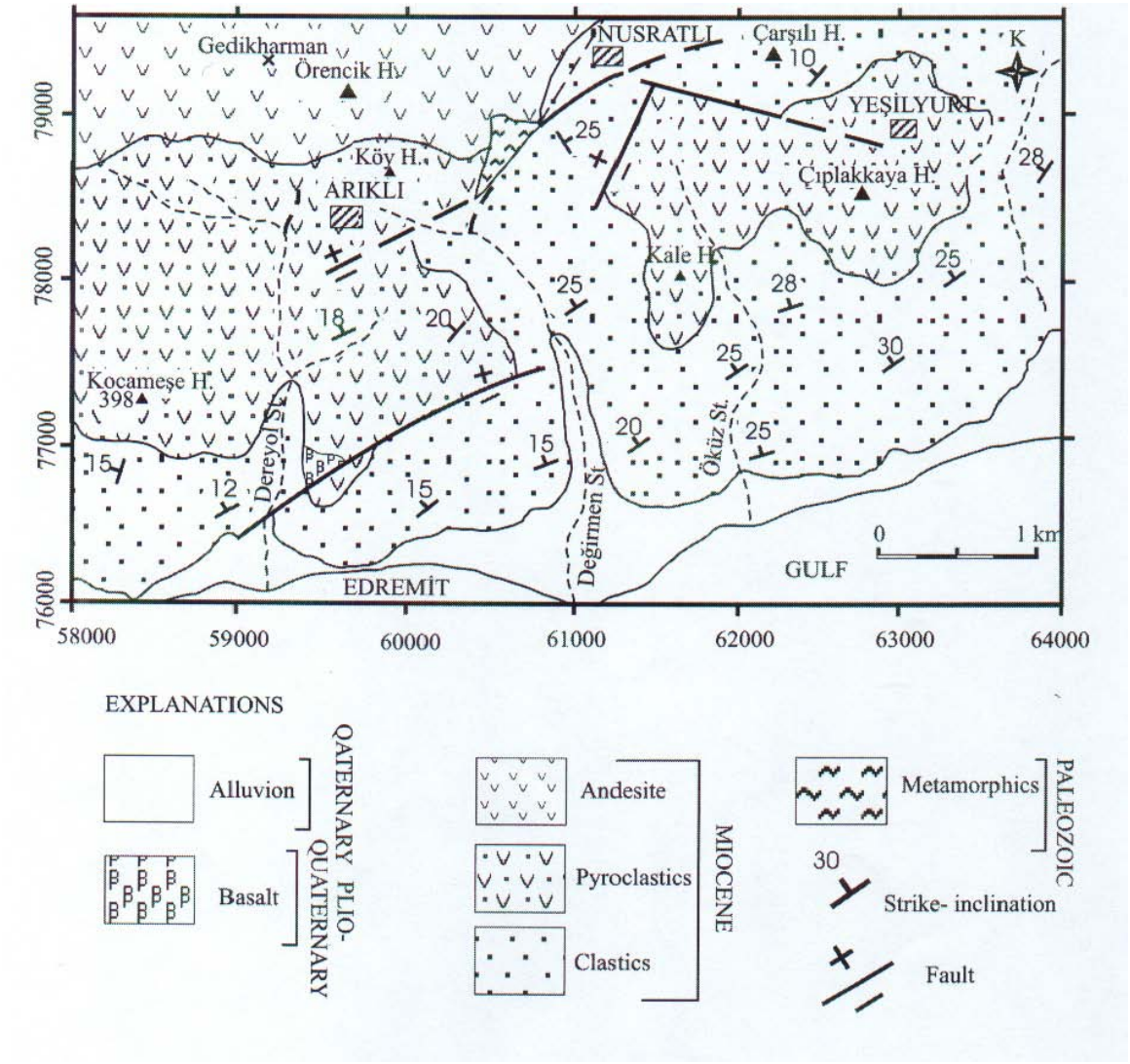

Figure 1. Geological map of the study area

X-Ray diffraction and SEM investigations were made in the laboratory of Georgia University Department of Geology (America). Major elements were determined in the laboratory of General Directorate for Mineral Research and Exploration (Turkey).

3. GEOLOGICAL SETTINGS

The main regional geological studies, including the investigation area, were carried out by Siyako et. al., (1989) and Çelik et. al., (1999). Paleozoic metamorphic rocks are the oldest rock assemblages in the study area. Miocene sequence overlies the metamorphics unconformably, and consists of (from bottom to the top) lacustrine clastics including volcanic intercalations, volcanics and pyroclastics with phosphated concreations in different levels. The basalts outcrop in restricted areas, and they are Plio-Quaternary aged (Figure 1).

Paleozoic metamorphic rocks mainly consist of phyllite, mica-schist, and calc-schist. The main subject of the study, Miocene rocks including phosphate concretions overlie the metamorphics uncomformably. These rock assemblages begin with lacustrine clastics including volcanic intercalations at the lower levels,

and they are followed by pyroclastics to the top. Andesites were determined at upper levels.

Lacustrine clastics mainly consist of shale, sandstone, siltstone, marl and tuff around Çarşılı Hill. The unit contains foldings of the same age with subsidence in small scale. The main lithology of the unit is bituminous thin bedded siltstones. Massif and thin bedded shales outcrop at Taşlıtarla Ridge. Lacustrine clastics begin with this conglomeratic levels in the study area. Medium, hard and yellowish tuff levels are observed as bands 40-50 cm thick.

Pyroclastics overlie the lacustrine clastics with a graditional contact. They are composed of tuffs in different colors. The tuffs are characterized by pyroclastics in the lower levels and clastics in the upper levels. Kaolinitization can be seen at some levels.

The tuffs in the study area include concretions in different sizes (0,5-10 cm). Some of them are phosphated. In the southwest of Yeşilyurt Village, the concretions, irregularly distributed in tuffs, are as follows; 1)Phosphated concretions, 2) Phosphated-carbonated concretions, 3)Carbonated concretions, 4)Manganese concretions, 5) Limonite concretions.

4. RESULTS AND DISCUSSION

4.1. Mineralogy

The most important mineral of phosphorus is apatite. Apatite is known both as a mineral and a mineral group. General formula as a group is $A_5(BO_4)X$. Element dispersion is A: Ca, B: P, V, As and X: Cl, F, OH respectively. The formula of this mineral group is $Ca_5(PO_4)_3$ (F, Cl, OH) (Ford, 1932). An apatite group mineral flourapatite can generally be found in magmatic and metamorphic rocks.

In the study area, 25 representative samples were collected. X-ray diffraction method is used for determining the phosphate minerals and mineral parageneses of tuffs and concretions. 15 concretions and 10 tuff samples were subjected to X-ray diffraction. It is indicated that phosphate minerals in the concretions generally consist of fluorapatite, carbonate- apatite, and hydroxyapatite.

Two different types of mineral paragenesis were determined in the parent rock (tuff) including the concretions. Concretions containing fluorapatite have the mineral assemblage of feldspar + smectite + analcime + illite + quartz. Concretions containing carbonate-apatite have the mineral assemblage of feldspar + smectite + kaolinite + quartz. Calcite can accompany these main mineral assemblages. Mineral paragenesis of tuffs is similar with nucleuses of phosphated concretions. Mineral assemblages of concretions and related tuffs are shown in Table 1.

According to SEM investigation, outer rims of the phosphated concretions have rough surfaces. Globular phosphate aggragates reach approximately up to 5 µ size.

Montmorillonite shows honeycomb and layered morphology. Some of the globular phosphate aggregate grows up in the cavities of montmorillonites, and some of it grows over them. Montmorillonites have curled edges and sheet like morphology in these samples.

4.2. Geochemistry

In the study area, 10 samples from concretions and 10 samples from related tuffs were collected for major element analyses. Major element contents were obtained for 20 representative samples. Major element contents of phosphated, phosphated-carbonated, carbonated, manganese and limonite concretions were given in Table 2.

Table 1. Mineral paragenesis of the concretions and related tuffs

MINERAL PARAGENESIS	
1. Phosphated concreation	
Nucleus	feldspar + montmorillonite + illite + quartz
Outer rim	fluorapatite + analcime + quartz + montmorillonite + calcite
2. Phosphated- carbonated concreation	
Nucleus-outer rim	calcite + quartz
Middle rim	carbonateapatite + calcite + analcime + quartz
3. Carbonated concreation	
Nucleus	calcite + dolomite ± feldspar
Rim	calcite + dolomite ± feldspar
4. Manganese concreation	
Nucleus	calcite + dolomite ± feldspar
Rim	manganese- sulphur + montmorillonite + illite + quartz + feldspar
	manganese- sulphur + feldspar + montmorillonite + hematite
5. Limonite concreation	
Nucleus	hematite-limonite + montmorillonite
Rim	hematite-limonite + montmorillonite
6. TUFF I	feldspar + montmorillonite + analcime + illite + quartz
7. TUFF	feldspar + montmorillonite + kaolinite + quartz

Table 2. Major element contents for different concreations (P_{1-2-3}: Phosphated concreations, P_{4-5}: Carbonated concreations, P_{6-7}: Phosphated-carbonated concreations, P_8: Manganese concreation, P_{9-10}: Limonate concreations).

	SiO_2	Al_2O_3	Fe_2O_3	CaO	MgO	Na_2O	K_2O	TiO_2	MnO	P_2O_5	LOI
P_1	29.49	5.10	1.40	33.01	0.22	3.10	1.00	0.10	0.43	20.60	5.48
P_2	25.10	6.00	1.45	30.52	0.33	2.51	1.80	0.20	0.90	12.03	17.78
P_3	42.05	8.50	1.81	18.53	0.50	3.79	2.33	0.20	1.59	14.01	6.26
P_4	37.54	8.49	3.81	19.50	1.49	0.61	6.49	0.33	0.12	11.81	7.56
P_5	23.75	5.28	1.62	32.73	0.98	3.98	1.26	0.11	0.83	15.98	24.26
P_6	47.50	9.88	2.13	14.31	1.12	0.20	8.81	0.32	1.22	0.30	14.00
P_7	23.10	4.59	1.50	35.03	0.51	1.78	1.80	0.11	1.20	0.10	29.29
P_8	26.59	5.34	1.54	33.42	0.79	1.78	2.68	0.21	1.54	0.04	23.87
P_9	59.09	9.16	3.19	0.75	1.61	0.40	9.34	0.32	0.01	0.06	13.38
P_{10}	58.87	10.93	3.64	0.25	1.34	0.31	10.78	0.34	0.67	0.05	28.79

Major element contents of phosphated and carbonated concretions were compared with the Australian phosphate nodules and Japanese phosphorite nodules of the same age (Figure 2). The concretions are enriched in SiO_2, $A1_2O_3$, Na_2O and K_2O. Concretions show similar values in MgO, TiO_2, MnO and CaO contents with the compared nodules. On the other hand, phosphated and carbonated concretions have low Fe_2O_3 content. P_2O_5 contents of concretions are higher than Australian phosphate nodules and lower than Japanese phosphorite nodules (Table 3).

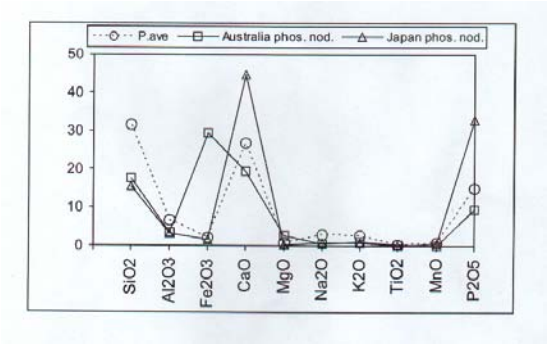

Figure 2. Comparison with the average values of studied concreations and Australia phosphate nodules (Burnett & Riggs, 1990) and Japan phosphorite nodules (Ogihara, 1999). (P. ave: Average values of 4 concreations $P_{1\text{-}2\text{-}3}$: Phosphated concreations and P_4: Phosphated-carbonated concreations).

Tuffs major element contents are as follows; SiO_2: 60.8-80.5 %, $A1_2O_3$: 10.9-17.3 %, Fe_2O_3: 0.2-4.6 %, CaO 0.1-2.1 MgO: 0.1 %, Na_2O: 0.1-0.9 %, K_2O: 1.6-13.5 %, TiO_2: 0.1-0.7 %, P_2O_5: 0.1-0.3 %. It is indicated that the tuffs have rhyodasite character, and they have a high K_2O content. In respect of this, they are rich in K. The average P_2O_5 content of tuffs is 0.13

On the other hand, tuffs and concretions in this tuffs are compared in respect of their major element contents. There is not a significant difference in Fe_2O_3, MgO, TiO_2 and MnO contents. Tuffs have higher $A1_2O_3$, SiO_2 and K_2O values than phosphated concretions. Phosphated concretions have higher CaO and P_2O_5 values than tuffs.

The phosphated zones have the average element contents of 43.85 ppm Cu, 79 ppm Pb, 262 ppm Zn, 517.95 ppm As, and 0.3 ppm Ag. The contents of Cu, Pb, Zn, As and Ag are high enough to prove the hydrothermal origin.

Table 3. Major element contents of Miocene Australia phosphate nodules (P_{AUS}.), (Burnett & Riggs, 1990) and Miocene Japan phosphorite nodules (P_{JAPAN}), (Ogihara, 1999)

	SiO_2	Al_2O_3	Fe_2O_3	MgO	CaO	MnO	TiO_2	P_2O_5	K_2O	Na_2O	F
P_{AUS}	17.6	3.46	29.5	2.59	19.6	0.06	0.26	9.6	1.04	0.6	2.0
P_{JAPAN}	15.5	3.16	1.52	0.14	44.71	0.44	0.12	32.85	0.68	0.68	1.76

5. CONCLUSIONS

The vitric-crystalline tuffs have concentric phosphate occurrences within their structure. In the centre and nucleus of this concretions, the main mineral assemblages of phosphated occurrences are fluorapatite [(CaF) Ca_4 $(PO_4)_3$], carbonate- apatite [Ca_{10} $(PO_4)_6$ $CO_3.H_2O$)] and hydroxyapatite [Ca_5 (PO_4) OH]. The nucleus of the concretions generally consists of tuff. The nucleus parts of the carbonated-phosphated concretions rarely include calcite.

If chemical compositions are compared with the marine phosphorites (Altschuler, 1980) and some phosphate nodules (Burnett and Riggs, 1990), it is indicated that studied concreations have higher SiO_2, $A1_2O_3$, Na_2O and K_2O contents. SiO_2, $A1_2O_3$, Na_2O and K_2O enrichment in phosphate nodules indicates the presence of hydrous aluminium silicates (Altschuler, 1980; Burnett and Riggs, 1990). The clay minerals (montmorillonite, illite) determined by XRD pattern and SEM observations support this conclusion. On the other hand, the high values of K_2O in tuffs leads to enrichment of K_2O in phosphated concretions.

Some of the typical phosphate nodules in the world are generally formed in marine environments. There is less terrigenous material supply. Calcite replacement occurs related to the Eh, pH, alkalinite, and supplied ions. The nucleus of these nodules consists of calcite and organic material. The main mineral was

determined as carbonate-apatite and fluorapatite in these nodules (Baturin, 1982; Ece, 1990). Phosphate nodules formed by biochemical-chemical precipitation present biogenic residues in the nucleus of this nodules. In the study area, there is not sufficient evidence of calcite replacement or biogenic/ biochemical precipitation.

It is determined that Cu, Pb, Zn, As and Ag contents in the phosphated concretions are very high. On the other hand, high values of Zn, As, Mo, Ag and Pb were determined by Çelik et. al.(1999) in phosphated zones in the studied area. The intense value of these elements indicate hydrothermal origin. The silis zone at the crack line support the hydrothermal effect in the study area.

According to the case studies and laboratuary investigations, phosphate occurences in the Miocene volcano-sedimentary sequence at tuff levels have a hydrothermal origin. The phosphore and hot solutions ascended along crack systems of NE- SW direction have formed phosphate occurrences after or before diagenesis.

ACKNOWLEDGEMENTS

We would like to thank Prof. Dr. A. Mermut (University of Saskatchewan, Canada) for obtaining the publications about phosphate deposits of the world and Prof. Dr. I. Ece for helping us about chemical analyses, electron microscope, X-ray diffraction in the laboratuary of Georgia University.

REFERENCES

Altschuler, Z.S., 1980. The Geochemistry of Trace Elements in Marine Phosphorites. Part 1

Characteristic Abudances and Enrichment. *The Society of Economic Paleontologists and Mineralogist (SEPM) Special Publication*, 29, 19-30. USA..

Baturin, N. G., 1982. Phosphorites on the sea floor (Origin, composition and distribution). *Developments in Sedimentology*, 33, 343.

Burnett, W.C. and Riggs, S.R., 1990. Phosphate Deposits of the World. Vol:3, Neogene to modern phophorites, Cambrige University Press, London.

Çelik, E., Ayok, F. & Demir, N., 1999. Mine report of Ayvacik - Küçükkuyu (City of Çanakkale) phosphate ore. General Directorate for Mineral Research and Exploration Report No. 891, Balıkesir, Turkey (unpublished).

Ece, Ö. I., 1990. Geochemistry and occurrence of authigenetic phosphate nodules from the Desmoinesian cyclic Excello epeiric sea of the mid continent, USA. *Marine and Petroleum Geology*. 7, 298- 312.

Ford, W.E., 1932. Dana's Text Book of Mineralogy". *John Wiley and Sons. Fourth Edition*, USA.

Kazakov, A.V., 1937. Chemical nature of the phosphatic substance of phosphoprites and their genesis. Tr. Nauchno-Issled. *Inst. Udobr. Insektofungits.*, 139, Moskow.

Ogihara, S.,1999. Geochemical characteristics of phosphorite and carbonate nodules from Miocene Funakawa formation, western margin of the Yokote Basin northeast Japan. *Sedimentary Geology*, 125, 69-82, Elsevier.

Siyako, M., Bürkan, K.A. and Okay, A.İ.,1989. The Tertiary Geology of Biga and Gelibolu Peninsula and hydrocarbon possibilities, *TPDJ Bülten*, 1/3, 183- 199, Ankara, Turkey.

A CARDINAL PROBLEM OF THE KINEMATIC PATH OF THE INTERNAL HELLENIDES (PELAGONIAN CORDILLIERA, NORTHERN-CENTRAL GREECE): NATURE AND DETERMINATION OF DEFORMATION-CONTACT ZONES

Diamantopoulos A.

National Technical University of Athens, School of Mining and Metallurgical Engineering, Section of Geosciences, Greece, diamantopoulos@metal.ntua.gr

Abstract: A summary of the proposed orogenic models for Pelagonian Cordillera of Internal Hellenides reveals two major aspects. On the one hand, Tertiary kinematics has been yielded in an extensional geodynamic regime. On the other hand, shortening structures towards the actual orogenic front is advocated. However, extensional and shortening structures that coexist along deformation-contact zones appear a common phenomenon. Field evidences in Northern and Central Greece corroborate this conclusion. Additionally, thrust, detachment fault and tectonic contact are used to express the concept of nappe-emplacements for identical cases. This confirmation introduces the question: What are the natural and geometrical characteristics of a deformation-contact zone for the determination of its actual character in space-time? Having in mind our field data, we connote that the role of produced structures, their spatial distribution and intensity, the anterior activations and the architecture are of primary importance, determining the physical genetic regime of deformation-contacts.

Key words: Kinematic path, Internal Hellenides, Deformation-contact zones, Attica

1. INTRODUCTION - PROBLEM IN THE KINEMATIC PATH & DEFORMATION-CONTACT ZONES

> "...since experimental data are of varying degrees of quality, and the field evidence is frequently subjective, apparent inconsistencies are frequently encountered." Chinner, (1966).

Recent studies in Alpine-type orogens of the Mediterranean notice the important role of asymmetric shear planes, arranging the architecture and rheology of the upper crust (Augier, 2004; Rossetti et al., 2005). The latter is conveyed by a network of mechanical discontinuities, defining a heterogeneous geological unit. Of particular importance is that these weakness zones determine exhumation and cause mineralogical-textural transformations of subducted crust.

In many studies thrust, detachment and tectonic contact are used to express the concept of nappe-emplacements, paradoxically for identical instances. On the one hand, where the action of detachments is advocated, primary field evidences are not sufficiently presented. In several instances, the interpretation of the observed shear planes in the field and in hanginwall- and footwall-related rocks is incompletely determined. These speculations indirectly cause the downgrading of the natural deformation and the mechanical behavior of shear planes. Field studies also connote the complexity of extensional tectonics and support its limited and ambiguous role (Wheeler and Butler, 1994; Butler and Freeman, 1996). In many cases, co-existing extensional and shortening structures combined with ductile and brittle progressive shear strain have been confirmed (Mukhopadhyay et al., 1997; Diamantopoulos, 2004; present work). These confirmations introduce a double-faced question: Is the characterization of a deformation-contact zone the theme of interpretation? What are the accurate characteristics of the latter in order to reveal its actual character in space and time? The term deformation-contact zone refers to a shear zone, which brings in contact two geological members of identical or of different tectono-stratigraphic units. The accumulated strain

as well as fault-related rocks characterize its field view.

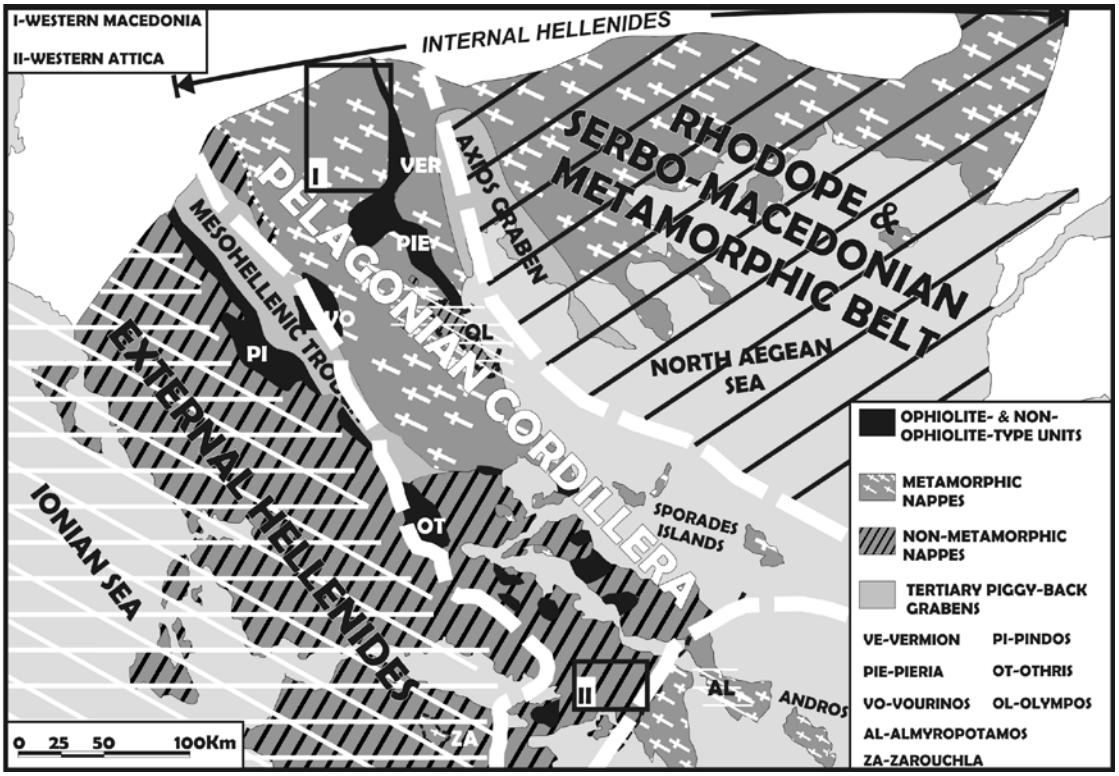

Figure 1. Pelagonian Cordillera and Serbomacedonian-Rhodope belt in Northern-Central Greece. Boxes show the investigated regions, Western Macedonia and Western Attica.

In the context of the present approach, Internal Hellenides correspond to sequences affected by Early Cretaceous orogenic phenomena, including Pelagonian Cordillera and domains of SerboMacedonian-Rhodope metamorphic belt, Figure 1. Field studies in Parnis mountain of Central Greece and in Western Macedonia of Northern Greece (Diamantopoulos, 2005) constitute our field background, Figure 1. It is the purpose of this work to show the importance of kinematic analysis, determining the actual genetic regime of deformation-contact zones. A particular analysis of Parnis mt. is presented, describing new kinematic data and conclusions regarding the geodynamics of Western Attica.

2. CENOZOIC OROGENIC PROCESSES IN INTERNAL HELLENIDES

Two fundamental models have been proposed for Cenozoic geodynamics of Internal Hellenides, including horizontal and gravity forces during mountain building. Katsikatsios et al. (1986), Mercier and Vergely (2001) and Brown and Robertson (2004) advocated the action of shortening shear zones during Tertiary. Kilias (1995), Falalakis (2004) and Diamantopoulos (2005) presented data for the activity of semi-brittle shear zones, outlining important omissions of intermediate geological members.

3. ARCHITECTURE AND KINEMATICS OF DEFORMATION-CONTACT ZONES

The term lateral escape is used below, replacing the term extension. Its concept here reveals the asymmetric stretching in horizontal direction together with vertical displacements due to gravity instabilities. The internal mechanism and the geometrical characteristics for the case of stretching and shortening shear planes is represented in Figure 2. Detailed analysis along several deformation-contact zones allow us to depict their architecture, Figure 3. Discrete shear planes of variable

orientation and co-existing extensional and shortening structures outline their internal geometry, Figures 3 and 4.

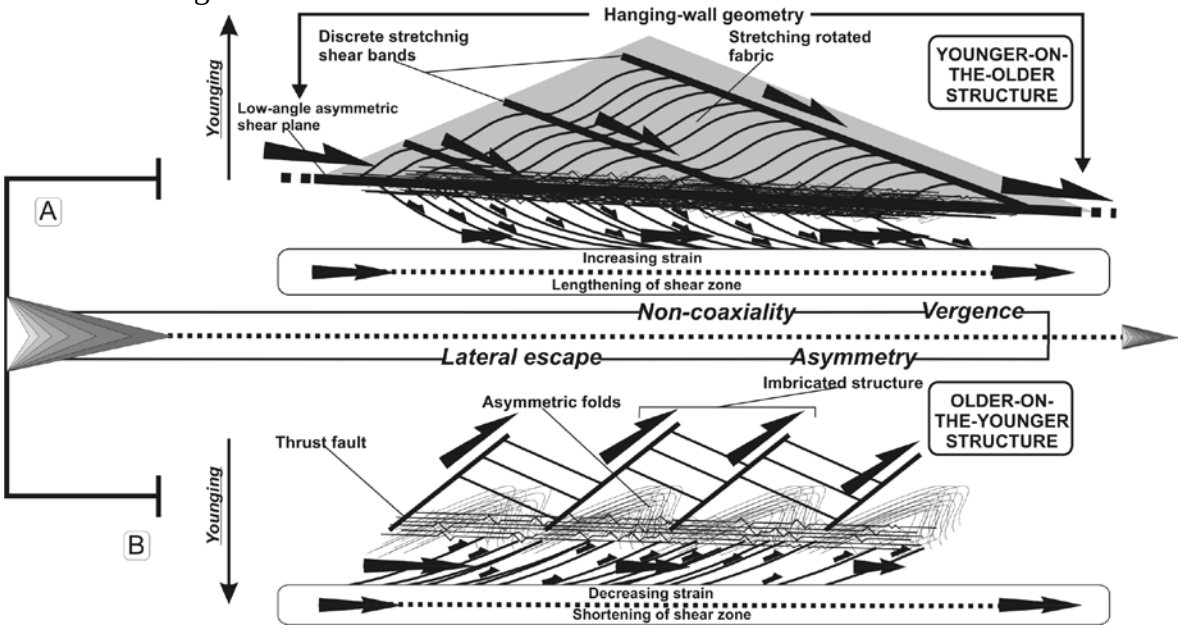

Figure 2. A) Stretching regime of shear bands. B) Shortening regime of shear bands.

4. EVIDENCES FROM WESTERN ATTICA (CENTRAL GREECE)

4.1 Structural plates of Attica & Tectonic Units of Parnis mt.

Four mountain ranges define Athens basin, Aigaleo-Parnis mts. in the west and Hymittos-Penteli mts. in the east. The first group characterizes an Upper Plate (UP), which has not experienced any regional metamorphic event. The second group constitutes the Lower metamorphic Plate (LP), outlined by a marked heterogeneous architecture, Figure 5A. A dominant Tertiary HP/LT event characterizes the LP (Altherr and Seidel 2002.). The kinematics of the sequences in Parnis mt., the geometry of deformation-contact zones and their genesis are investigated. An interaction with the metamorphic core of eastern Attica is observed.

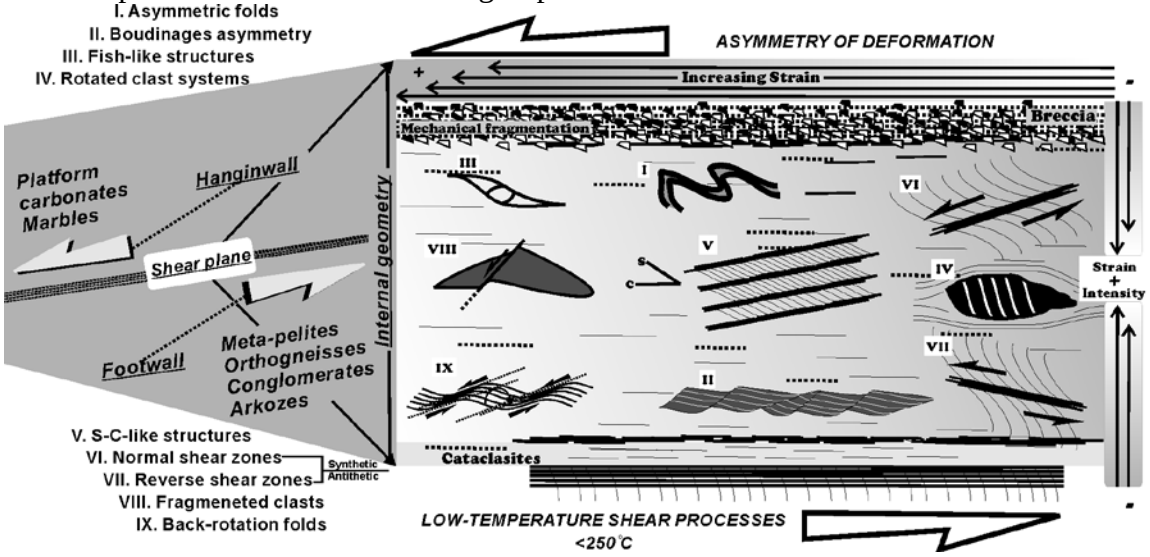

Figure 3. The architecture of semi-brittle/brittle deformation-contacts, based on our field studies (based on more than 300 field structures).

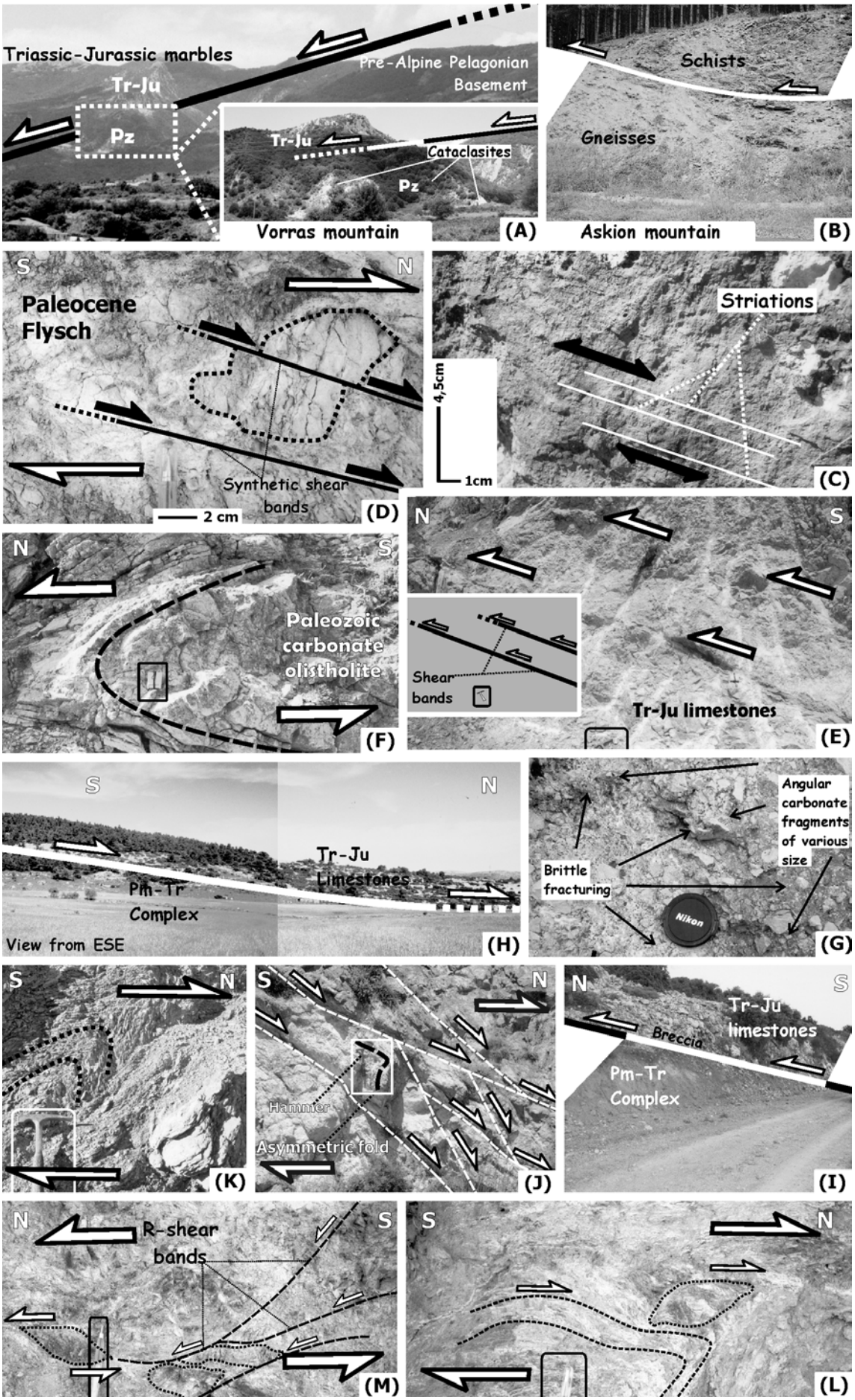
Triassic-Jurassic marbles
Tr-Ju
Pz
Pre-Alpine Pelagonian Basement
Tr-Ju
Cataclasites
Pz
Vorras mountain
(A)
Schists
Gneisses
Askion mountain
(B)
S
N
Paleocene Flysch
Synthetic shear bands
2 cm
(D)
Striations
4,5cm
1cm
(C)
N
S
Paleozoic carbonate olistholite
(F)
Shear bands
Tr-Ju limestones
(E)
S
N
Pm-Tr Complex
Tr-Ju Limestones
View from ESE
(H)
Angular carbonate fragments of various size
Brittle fracturing
Nikon
(G)
S
N
(K)
Hammer
Asymmetric fold
(J)
Breccia
Tr-Ju limestones
Pm-Tr Complex
(I)
N
S
R-shear bands
(M)
(L)

Figure 4. Field structures along deformation-contact zones. A) Triassic-Jurassic marbles overly pre-Alpine Pelagonian Basement (Vorras mt.), B) pre-Alpine Schists overly Gneisses (Askion mt.), C) Horizontal striations along contact zone (Parnis mt.), D) R-Riedle shears within flysch, (Parnis mt.), E) Shear bands within limestones (Parnis mt.), F) Isoclinal fold within Paleozoic olistholite, G) Mechanical fragmentation due cataclasis (Parnis mt.), H) Klippe of Triassic–Jurassic limestones (Parnis mt.), I) Deformation-contact zone (Parnis mt.) J) R-shear bands, (Parnis mt.), K) Asymmetric folds in Permo-Triassic rocks (Parnis mt.), L) Kinematic indicators within ultramafic-mafic cataclasites (Parnis mt.), M) Synthetic shear bands within ultramafic-mafic cataclasites (Parnis mt.)

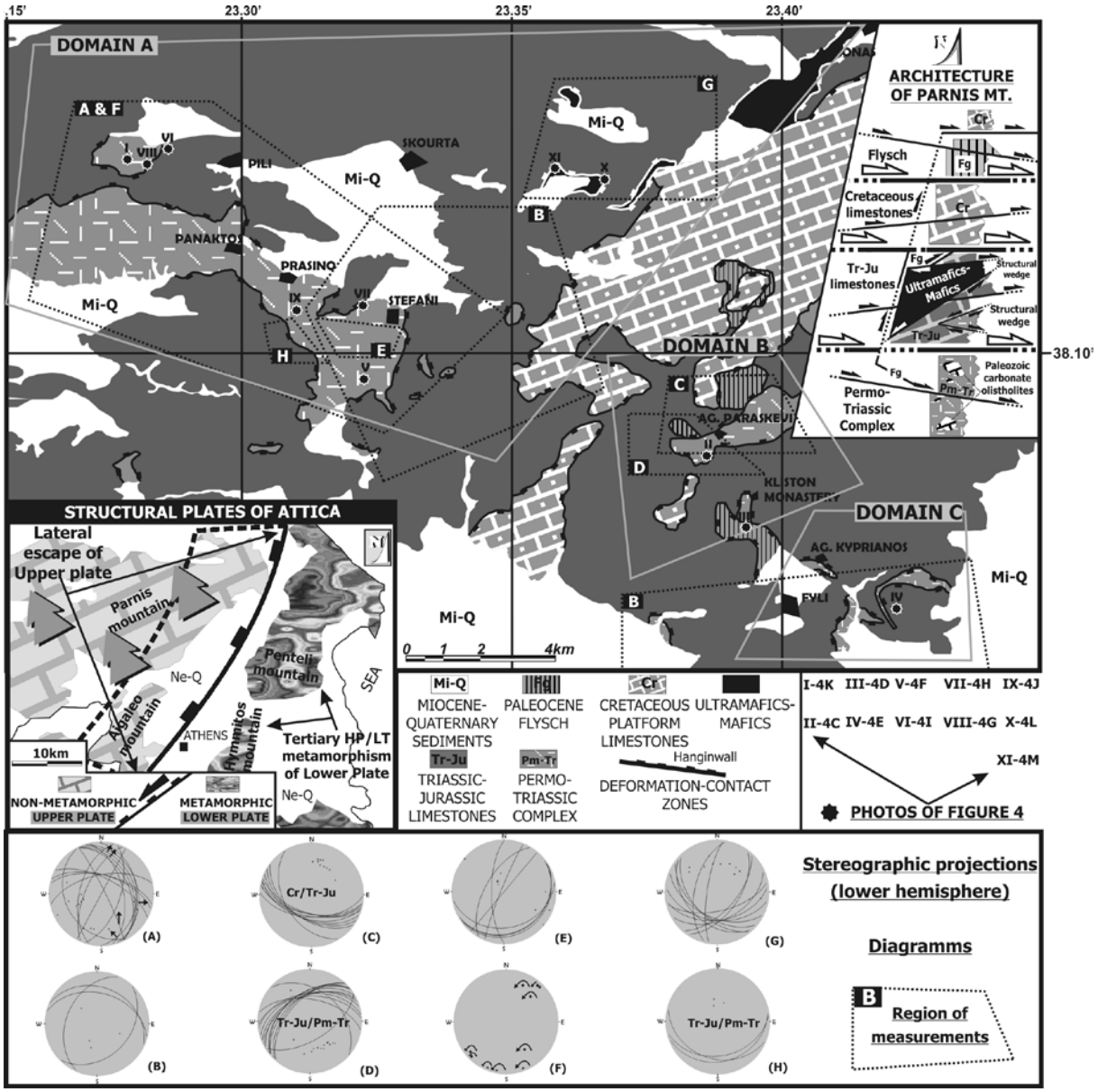

Figure 5 A. Geological map of Parnis mountain (Western Attica). In the right side, the tectono-stratigraphic column. Inset map, the UP and LP of Attica. Stereograhic projections. A) Shear bands within Permo-Triassic rocks, B) Shear bands within Triassic-Jurassic limestones, C) Geometry of deformation-contact zone, D) Geometry of deformation-contact zone, E) SS-surfaces of Paleozoic olistholite, F) Fold axes of Permo-Triassic rocks. G) Shear bands within Ultramafics-mafics, H) Geometry of deformation-contact zone.

Pre-Neogene sequences of Parnis mt. are grouped in three separated tectonic units, Figure5A (fossil findings by Katsikatsios et al., 1986). Sub-Pelagonian unit: (I) Permo-Triassic complex, containing sandstones, arkozes, volcanic rocks, conglomerates and Paleozoic carbonate olistholites that are strongly

deformed. Pyroclastic and volcanic rocks co-exist with the former members. (II) Triassic-Jurassic shallow-water platform limestones. Ultramafic-Mafic Unit: This unit mainly encloses serpentinites and harzburgitic peridotites. Their structural location is intricate, presenting as structural wedges within Triassic-Lias limestones. Their boundaries with the adjacent formations characterize asymmetric shear planes, outlined by ultramafic-mafic cataclasites, Figures 4L and 4M. Cretaceous Unit: (I) Cretaceous limestones with Rudists and (II) Paleocene flysch. Our analysis below concludes the structural allocthony of Cretaceous unit and its higher structural location.

4.2 Geometry & kinematic of deformation-contact zones

Kinematic analysis along the contacts revealed a prominent shear event, affecting the entire nappe-pile. Steep- and low-angle brittle deformation-contact zones were observed over the whole area, Figure 4. Several asymmetric geological structures and apparent striations systems of variable slip show the dominance of non-coaxial processes, Figures 4C-4D-4E-4F-4J-4K-4L-4M and 5B. Fault breccia, googe and cataclasites found along the shear planes witness nappe-emplacements in brittle conditions.

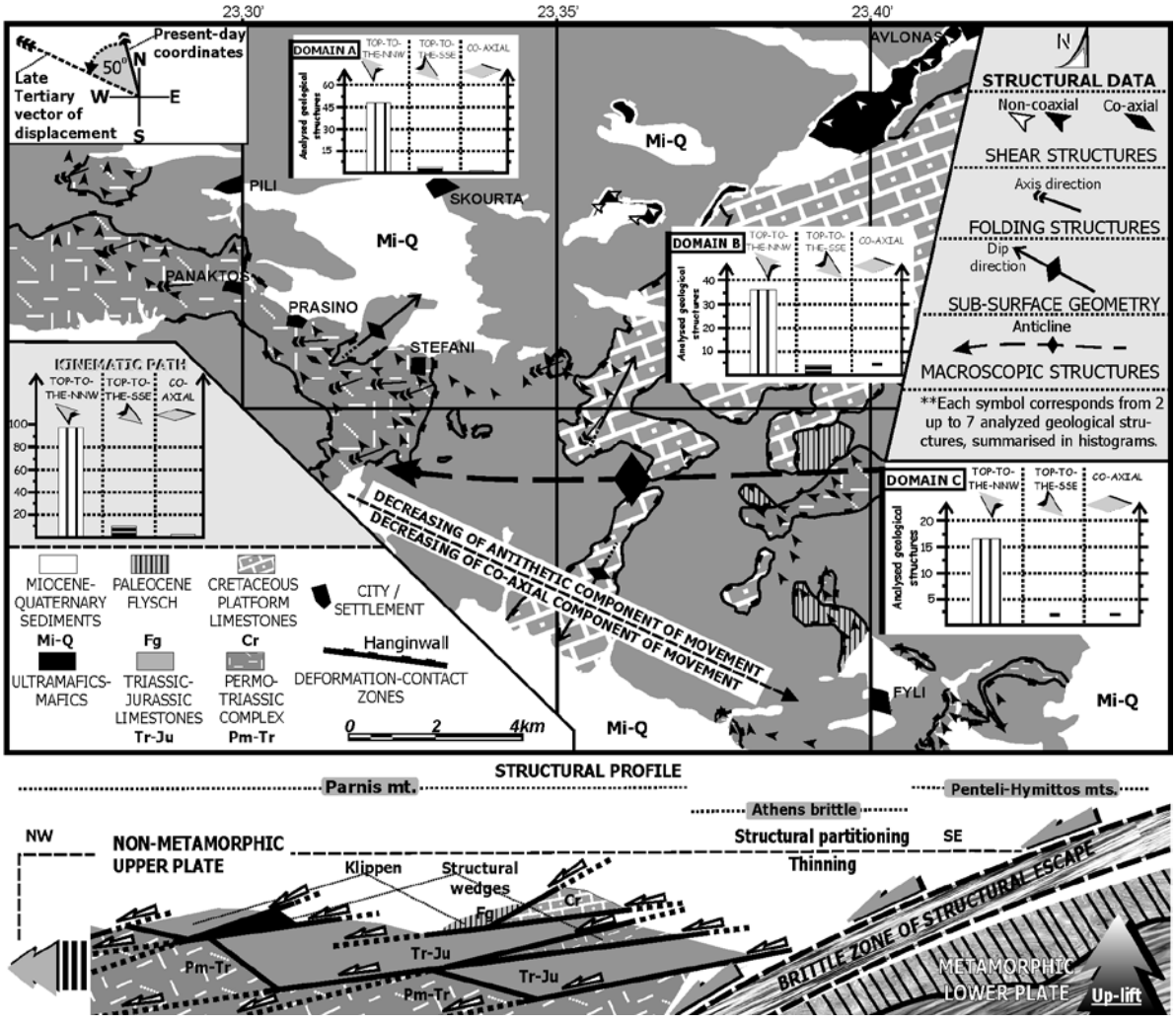

Figure 5 B. Structural map of Parnis mountain. Histogram in the left shows the summary of the analyzed structures. Three histograms give the kinematic analysis in domains A-B-C. Profile in the bottom depicts schematically the lateral escape of the UP in relation to the LP of Attica.

Cataclasites represent a heterogeneous tectonic mix of clastic, volcanic, ultramafic, mafic and carbonate lithologies. Mapping of more than 120

kinematic indicators shows a north-northwestwards lateral escape of the sequences, Figure 5B. A minimum value of antithetic sense of shear decreases towards southeast, Figure 5B. The presence of the co-axial component of movement constitutes a local phenomenon with minimum participation, Figure 5B. Co-existing extensional and shortening structures dominate along the deformation-contact zones. Internal shear planes, mainly synthetic to the dominant component of displacement of the footwall formations, constitute a characteristic structural feature. Cataclasis is also connected to Paleozoic carbonates olistholites, transposed them in breccia. In many cases, carbonate olistholites have been folded with northwards vergence, Figures 4F, 6. Flysch sequence shapes klippen, lying onto Permo-Triassic rocks and onto Triassic-Jurassic carbonates. Also, although the emplacement of the Triassic-Jurassic carbonates onto the Permo-Triassic sequence is generally observed, detailed observations revealed structural wedges of the latter within the Triassic-Jurassic carbonates. Brittle shear bands within Triassic-Jurassic limestones appear an identical kinematics near contact-zones with that of the entire area, Figures 4 and 6.

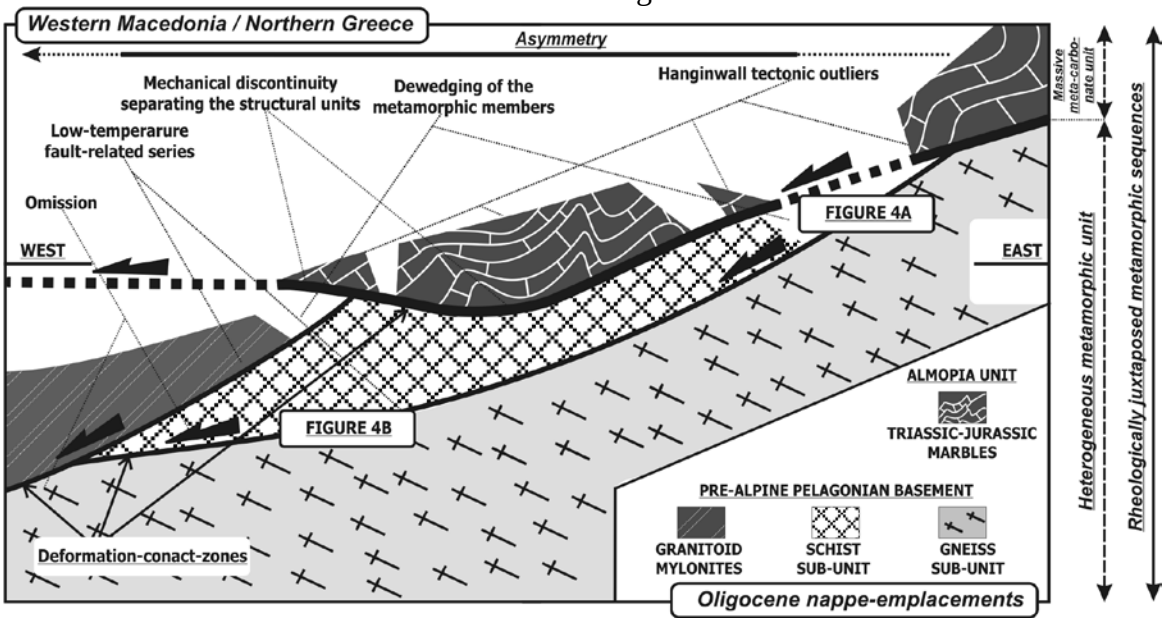

Figure 6. Schematic illustration of the nappe-emplacements in Northern Greece. Semi-brittle/brittle mechanical discontinuities convey the nappe-pile with a westward asymmetry.

4.3 Timing of shear deformation & Syn-orogenic nappe-emplacements

Intense orogenic processes are thought to be responsible for the described kinematics. The active involvement of flysch in the above structural complexity marks the Late Tertiary age of the nappe-emplacements. In this interval Pelagonian Cordillera is coincided with the orogenic front of Hellenides. Thus, a syn-orogenic lateral escape towards north-northwest is proved, which is altered in WNW direction, given the clockwise rotation of North-Western Greece in Late Cenozoic (~500 see Hinsbergen et al., (2005)). Our data also indicate the asymmetric architecture and intense thinning of Parnis mt., (I) the direct contact of Cretaceous Unit onto Sub-Pelagonian unit, eliminating ultramafics-mafics, (II) the emplacement of flysch onto Permo-Triassic Complex and Triassic-Jurassic limestones, (III) the dominance of asymmetric kinematic indicators along the contacts, causing their non-coaxial lengthening.

All of the above indicate the structural partitioning of Internal Hellenides in Western Attica. This process is probably combined with the unroofing of the

metamorphic tectonites of eastern Attica in Penteli and Hymittos mountains, Figure 5B. In Late Tertiary more than 20 kilometers (vertically) separated the structural plates of Attica. Thus, a noted differentiation mechanism from brittle fracturing in the UP to ductile tectonites of LP could be connoted.

5. EVIDENCES FROM WESTERN MACEDONIA (NORTHERN GREECE)

Field studies in Northern Greece revealed the dominance of semi-brittle asymmetric shear planes within the metamorphic nappe-pile, Figure 4A, 4B and 6. Low-temperature fault-related series and kinematic indicators showed the nappe-stretching of Internal Hellenides. A prominent asymmetry in semi-brittle conditions is concluded toward WSW during the Oligocene emplacement of Internal onto External Hellenides (Diamantopoulos, 2005).

6. NATURE OF DEFORMATION-CONTACT ZONES AND EXHUMATION PROCESSES

Our analysis outlines that fault-related rocks, the formed structures as well as the dominant deformation regime are of primary importance. The determination of the symmetry or asymmetry is also essential. In this context, the relation of shear strain vs. stress of the intervening rocks is crucial, expressing an increasing or decreasing behavior (Means 1995). Natural characteristics of deformation-contact zones are depicted in Figure 7. An intention analysis of these parameters could be considered decisive for the evolution of shear zones.

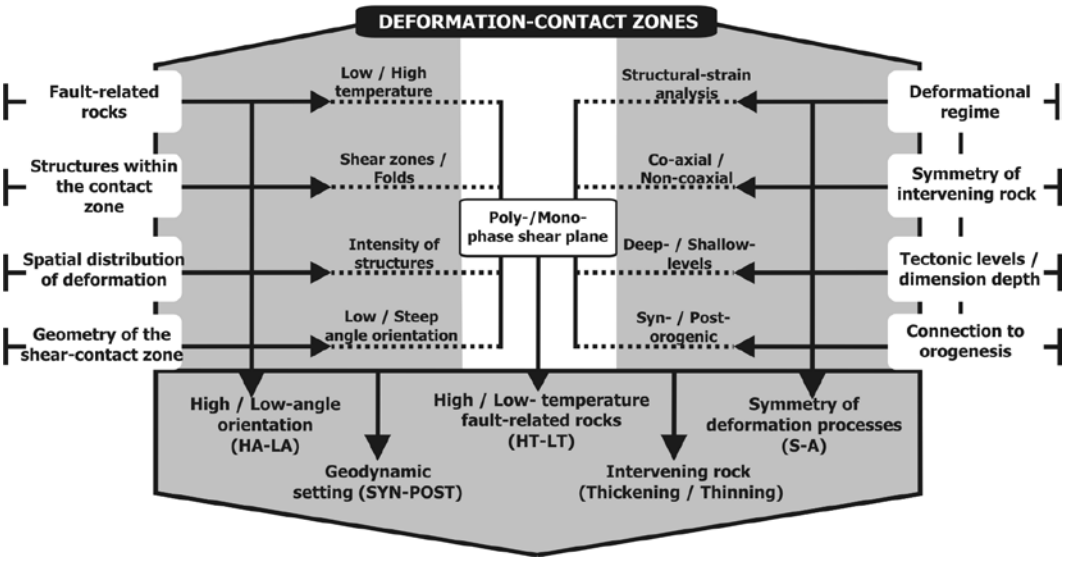

Figure 7. Natural characteristics of deformation-contact zones.

An additional parameter of the mechanical evolution of shear zones is their influence in exhumation processes. With particular emphasis in Western Macedonia, data by Kilias (1995) and Diamantopoulos (2005) prove the genesis of Tertiary inherited mechanical discontinuities in upper crust. The critical point is their evolution in pre-Cenozoic times. With reference to Western Attica, a new consideration is presented here for its Cenozoic evolution. The division of Attica in an UP and in a LP explains satisfactorily its present-day architecture, outlined by a noticeable NE-SW directed zone of NNW-ward kinematic asymmetry.

7. CONCLUSION & DISCUSSION

Our data point out the very careful usage of the terms detachment, tectonic contact and thrust. It is proposed that more accurate terms have to be inquired for the determination of the natural shear zone-related processes. The common

affirmation of co-existing extensional and shortening structures reinforces this suggestion. The term extensional shear zone is inferior in the fact that the produced structures are not exclusively extensional. Even in the emplacement of high-grade metamorphic sequences onto low-grade field studies prove the asymmetrical and stretching character of shear zones (Rossetti et al., 2005). The term detachment essentially characterizes a deformation-contact zone, in which the displaced geological members appear a primary paleo-geodynamic relation, and constitutes a secondary characteristic. Kinematic indicators depicted in Figure 3 possibly mark a satisfied field guide. Of fundamental importance is the periodicity of the action of deformation-contact zones, given that in poly-phase or mono-phase cases, the total tectonic strain differs. The above field examples reveal that the produced structures, their spatial distribution and intensity, the asymmetry of deformation and the anterior activations note precious parameters. The parameters in Figure 7 constitute a first step to this direction. Pre-existing mechanical anisotropy is also related to the newly formed structures and to the mechanical behavior of shear zones (Carreras, 1997). On the one hand, the genesis of multiple shear planes is connected to pre-existing mechanical discontinuities and weak stratigraphic horizons. On the other hand, their temporal action is determined in pure orogenic setting and also in destabilized processes of the orogens (Mallavieille, 1997; Burov et al., 2001).

In conclusion, kinematic analysis in the UP of Attica (Parnis mt.) reveals a north-northwestward lateral escape in Late Tertiary. Shortening and extensional structures dominate along semi-brittle/brittle deformation-contact zones. Our analysis remarks that the a priori adoption of a term for deformation-contact zones should be avoided due to heterogeneous natural strain. Thus, a negative answer to the first question of the Introduction is reasonable. Structural models for Cenozoic geodynamics of Internal Hellenides possibly represent in reality a structural ‘antinomy’.

ACKNOWLEDGEMENTS

Mr. Panousopoulos Anastasios is particularly thanked for important help and discussions in the field. Phd Candidate Baziotis Ioannis is also cordially thanked for fruitful discussions regarding the metamorphic evolution of eastern Attica.

REFERENCES

Augier, R., 2004. Evolution Tardi-Orogéniquès des Cordillieres Betiques (Espagne): Apports d’ une etude integree. These, *Universite de Pierre et Marie Curie*, France (unpublished).

Altherr R., Seidel W., 2002. I-type plutonism in a continental back-arc setting: Miocene granitoids and monzonites from the central Aegean Sea, Greece. *Contrib Mineral Petrol*, 143, pp. 397-415.

Brown, A. M. S., Robertson, H. F. A., 2004. Evidences for Neotethys rooted within the Vardar suture zone from the Voras Massif, northernmost Greece. *Tectonophysics* 381, 143-173.

Butler, R. W. H., Freeman, S., 1996. Can crustal extension be distinguished from thrusting in the internal parts of mountain belts? A case history of Entrelor shear zone, Western Alps. *Journal of Structural Geology*, 18, 909-923.

Burov, E., Jolivet, L., Pourhiet, L., Poliakov, A., 2001. A thermomechanical model of exhumation of high pressure (HP) and ultra-high pressure (UHP) metamorphic rocks in Alpine-type collision belts. *Tectonophysics*, 342, 113-136.

Carreras, J., 1997. Shear zones in foliated rocks: geometry and kinematics. In

Evolution of Geological structures in Micro- to Macro-scales. *Edited by S. Sengupta*. 185-201.

Chinner, A., 1966. The significance of the aluminum silicates in metamorphism. *Earth Science Reviews*, 2, 111-126.

Diamantopoulos, A., 2005. Semi-brittle asymmetric shear planes controlling the Cenozoic kinematics of Internal Hellenides (Northern Greece): Field evidences from Askion and eastern Vernon mountain ranges. *IESCA 2005*, Izmir, Turkey, *Abstracts book* 31.

Diamantopoulos A., 2004. Intra-plate deformation and sub-surface tectonic structure of the western borderline of Ptolemais-Kozani graben (Northern Greece): Evidences for back-arc compressional tectonics in the Hellenic Orogenic arc. 1st Panhellenic Congress of Young geologists, *University of Athens, Department of Geology, Proceedings book* pp. 39 (in press pp. 1-18).

Falalakis, G. 2004: Kinematic analysis and deformation in the boundary of Serbo-macedonian and Rhodope crystalline masses (Kerkini and Vrondou mountains, Macedonia). *Phd Thesis, University of Thessaloniki, Department of Geology*, Greece (unpublished).

Hinsbergen, Van D.J., Langereis, C.G., Meulenkamp, J.E. 2005. Revision of the timing, magnitude and distribution of Neogene rotations in the Western Aegean region. *Tectonophysics*, 396, 1-34.

Katsikatsios, G., Mettos, A., Vidakis, M., 1986. Athinai-Elefsis Sheet. *I.G.M.E.*

Kilias, 1995. Tectonic evolution of the Olympos-Ossa mountains: Emplacement of the blueschists unit in eastern Thessaly and exhumation of Olympus-Ossa carbonate dome as a result of Tertiary extension (Greece). *Mineral Wealth*, 96, 7-22.

Malavieille, J., 1997. Normal faulting and exhumation of metamorphic rocks in mountain belts. In *Evolution of Geological Structures in Micro- to Macroscales*, 47-57.

Means, W. D., 1995. Shear zones and rock history. *Tectonophysics*, 247, 157-160.

Mercier, J. L., Vergely, P., 2001. The Paikon Massif revisited, comments on the Late Cretaceous-Paleogene geodynamics of the Axios-Vardar Zone. How many Jurassic ophiolitic basins? (Hellenides, Macedonia, Greece). *Bull. Geo. Soc. Greece*, XXIV/6, 2099-2112.

Mukhopadhyay, D. K., Bharda, B. K., Ghosh, K., Srivastava, C., 1997. Development of compressional and extensional structures during progressive ductile shearing, Main Central Thrust Zone, Lesser Himachal Himalaya. In *Evolution of Geological Structures in Micro- to Macroscales,* 203-217.

Rossetti, F., Faccenna, C., Crespo-Blanc, A., 2005. Structural and kinematic constraints to the exhumation of the Alpujarride Complex (Central Betic Cordillera, Spain). *Journal of Structural Geology*, 27, 199-216.

Wheeler, J., Butler, R. W. H., 1994. Criteria for identifying structures related to true crustal extension in orogens. *Journal of Structural Geology*, 16, 1023-1027.

SEMI-BRITTLE ASYMMETRIC SHEAR PLANES CONTROLLING THE CENOZOIC KINEMATICS OF INTERNAL HELLENIDES (NORTHERN GREECE): FIELD EVIDENCES FROM ASKION AND EASTERN VERNON MOUNTAIN RANGES

Diamantopoulos A.

National Technical University of Athens, School of Mining and Metallurgical Engineering, Section of Geosciences, Greece, diamantopoulos@metal.ntua.gr

Abstract: Several metamorphic sub-units of Almopia Unit and of pre-alpine Pelagonian Basement of Internal Hellenides, in Askion and eastern Vernon mountains of Northern Greece, arrange a younger-on-the older architecture. Structural analysis of the contacts of the sub-units and of the footwall formations documented the following structural features. The tectonic nature of the contacts and their low-angle orientation were proven, accompanied by low-temperature fault-related series. Kinematic indicators outline an intense non-coaxial lengthening towards west-southwest. A prominent WSW non-coaxial strain in semi-brittle up to brittle conditions is also constrained in footwall. Previous data combined with isotopic ages connote the Oligocene age of the inferred shear strain, indicating that structural partitioning of Internal Hellenides occurred concurrently with their emplacement onto External Hellenides.

Key words: Semi-brittle shear zones, Oligocene geodynamics, Internal Hellenides

1. INTRODUCTION

There is growing evidence that the spatiotemporal evolution of the orogens is strictly connected to stretchi ng processes within domains of high potential energy (Malavieille, 1993; Vanderhaeghe and Teyssier, 2001). In these circumstances, kinematic analysis constitutes a powerful tool for the elucidation of nappe-emplacements during mountain building (Laubscher, 1969). Structural and geochronological studies of the Internal Hellenides reveal a complicated Alpine orogenic evolution (Most, 2003; Robertson, 2004). Their Cenozoic geodynamics is outlined by their emplacement onto the External Hellenides in Late Tertiary (Godfriaux and Ricou, 1991). This large-scale orogenic process is being responsible for the formation of window-type domes, as the Olympos mountain (Figure 1). The aim of the present study is to analyze the Cenozoic kinematics of the Askion and eastern Vernon mountains in Northern Greece (Figure 1), by presenting new kinematic data, qualitative estimation of nappe-emplacements and suggesting a dynamic model for mountain building in the Internal Hellenides.

2. GEOLOGY AND TECTONICS

2.1 Major Tectonic Units of North Pelagonian Belt

Geological studies in North-Central Pelagonian Belt show the arrangement of six major tectonic units (data by Aubouin, 1965; Mercier, 1968; Mountrakis, 1982; Papanikolaou & Stojanov, 1983; Brunn, 1990; Godfriaux and Ricou, 1991) (Figure 1), appearing from the bottom to the top: (I) Olympos Unit, consisting of Triassic-Eocene carbonates and Eocene flysch, correlated to the Gavrovo-Tripolitsa Unit of External Hellenides, (II) Eocene HP/LT metamorphic belt (Ambelakia Unit), (III) pre-Alpine Pelagonian basement, comprising pre-Permian metamorphic and igneous rocks, (IV) Almopia Unit, containing Late-Jurassic meta-sediments, Triassic-Jurassic marbles and Permo-Triassic rocks, (V) Ultramafic and mafic Unit of Mesozoic age and (VI) Cretaceous Unit, with platform limestones and flysch.

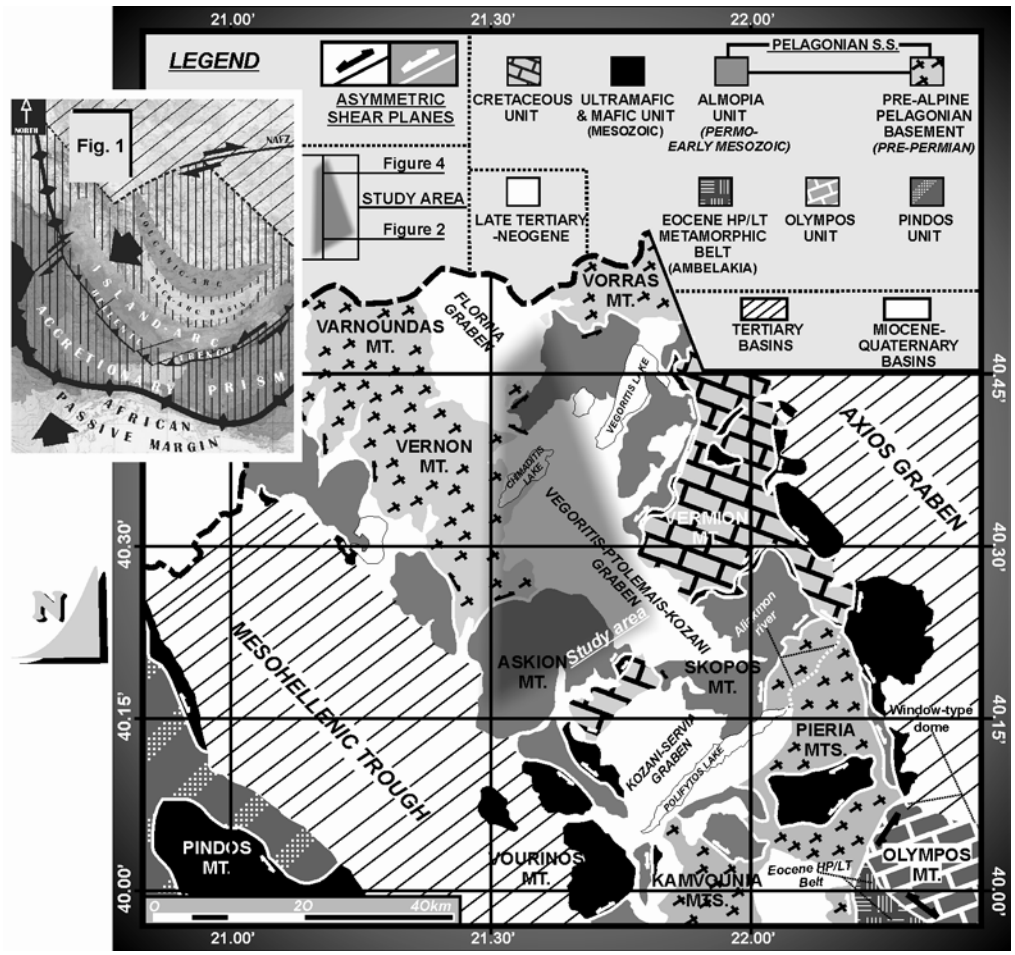

Figure 1. Geotectonic map of North-Central Pelagonian Belt (Northern Greece).

2.2 Geological setting of Askion and eastern Vernon mountains

In the study area, pre-Alpine Pelagonian basement consists of three distinctive sub-units (Figures 2 and 4). Schist sub-unit contains mica schists, amphibolites and intercalations of gneisses. Gneiss sub-unit consists of ortho-gneisses and migmatites (Figure 6C). The sub-unit of Granitoid mylonites composes strongly sheared ortho-gneisses with cm-wide fieldspars. Almopia Unit includes the Triassic-Jurassic marbles and a volcano-sedimentary series. Triassic-Jurassic marbles characterise thick-layered rocks, forming frequently in the macroscopic scale isoclinal folds. The volcano-sedimentary series contains Permian-Triassic rocks, metasandstones, metarkozes, red limestones and volcanic rocks (Figure 2).

3. MAIN MICRO- AND MESOSCOPIC FIELD STRUCTURES IN FOOTWALL-RELATED ROCKS

Structural and petrographic mapping revealed the overprinting of the low-temperature structures onto the syn-metamorphic penetrative textures in the pre-alpine and the Permo-Triassic rocks. The main Sn+1 discrete crenulation cleavage-penetrative S-texture dominates. A well defined stretching-mineral lineation Ln+1 is determined within Sn+1-planes. Isoclinal folds, with parallel axial planes to Sn+1, are developed with parallel axes to the Ln+1, outlining their syn-metamorphic character. Sn+1 strikes in NW-SE direction, following parallel the boundary of pre-Alpine rocks with the Triassic-Jurassic marbles. Several measurements of Sn+1 texture reveal ductile macrostructures with a NW-SE axis direction in Askion mt., Figures 3A

and 3B. Ln+1 strikes in a NW-SE direction with an unstable dip direction (Figure 3C).

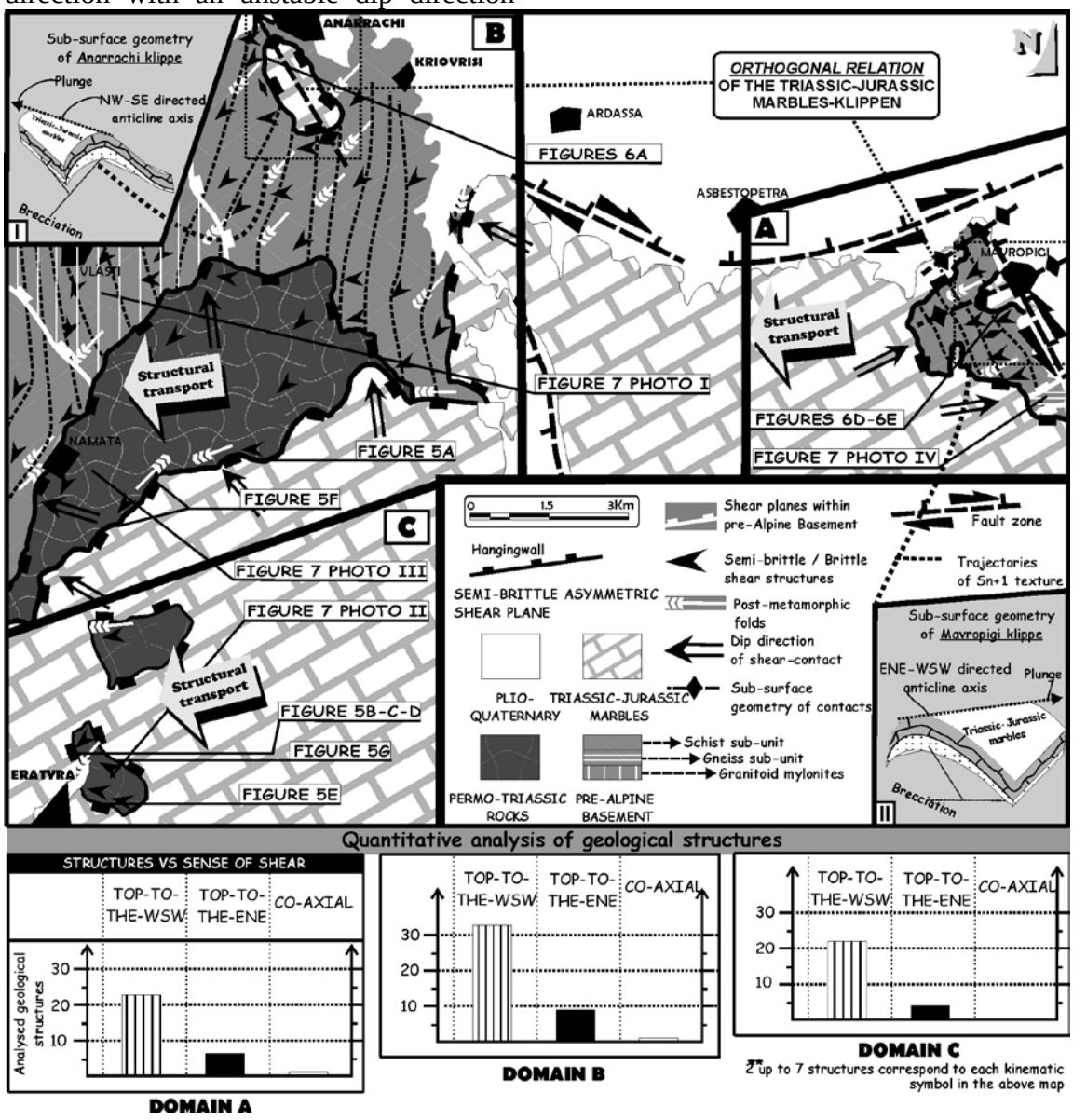

Figure 2. Structural map of Askion mt. Quantitative kinematic analysis is represented in the histograms, in three domains A, B and C. Photos of Figures 5, 6 and 7 are also illustrated.

Tight, disharmonic folds and a Sn+2 planar-shape element parallel to the axial planes of the former folds compose secondary fabric elements (Figure 3F). An Ln+2 stretching-mineral lineation is also constrained, directed NE-SW (Figure 3C). Therefore, the metamorphic sequences are dominated by Sn+1 texture, combined with the two previous linear-shape elements. The latter appear angular up to orthogonal relation. Open, chevron folds and kink bands compose another group with post-metamorphic cross-folds, appearing WSW-ward vergence (Figures 3D and 3E). Semi-brittle and brittle shear zones within ultra-cataclasites, of WSW-ward sense of shear, cross-cut the former ductile structures (Figure 6F). High-angle faults and mega-anticlines are also observed in the Plio-Quaternary sediments and in the metamorphic sequences (Diamantopoulos and Panousopoulos, 2004) (Figure 2 and 4).

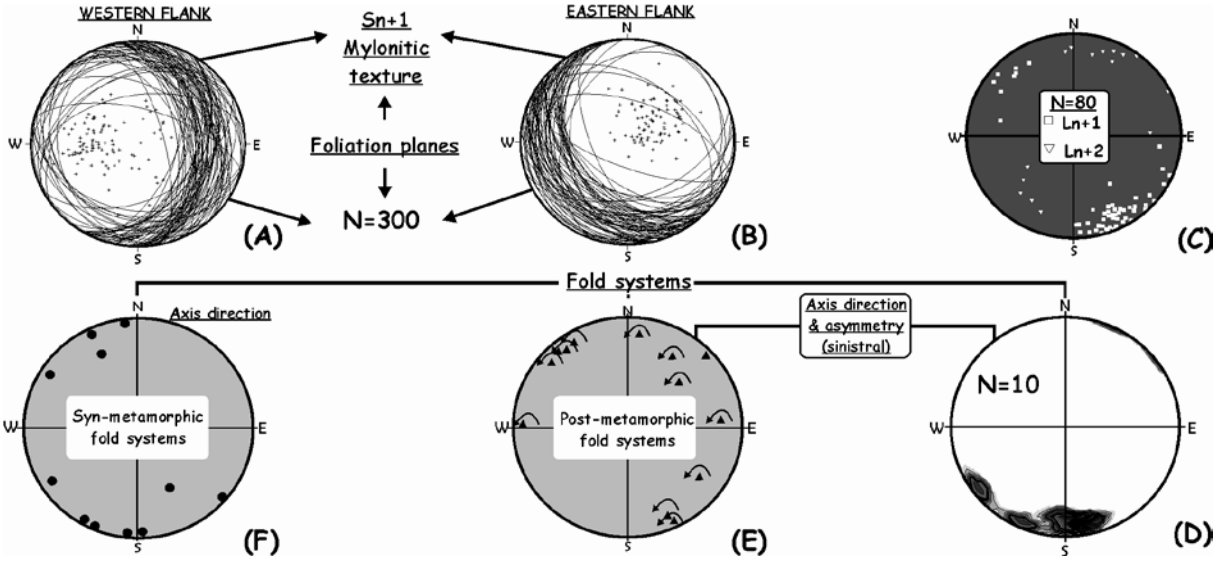

Figure 3. Stereographic projections (lower hemisphere) of the fabric elements in Askion mt. A) Sn+1 texture in western flank, B) Sn+1 texture in eastern flank, C) Linear-fabric elements, D) Folds of Permo-Triassic rocks, E) Folds of pre-alpine rocks and F) Folds of pre-alpine rocks.

4. GEOMETRY AND KINEMATICS OF THE SEMI-BRITTLE SHEAR PLANES

Spyropoulos (1992) advocated the normal transition from Permo-Triassic rocks towards Triassic-Jurassic marbles. The contact between the pre-alpine rocks with the alpine has been assumed as thrust plane (Mountrakis, 1982; Most, 2003). The nature of the latter contact is of special importance with significant paleo-geodynamic implications (Celet et al., 1976). Structures in all the scales of observation were used for kinematic analysis (Turner and Weiss, 1963; Hansen, 1971; Kornprobst, 2002; Passchier and Trouw, 2005).

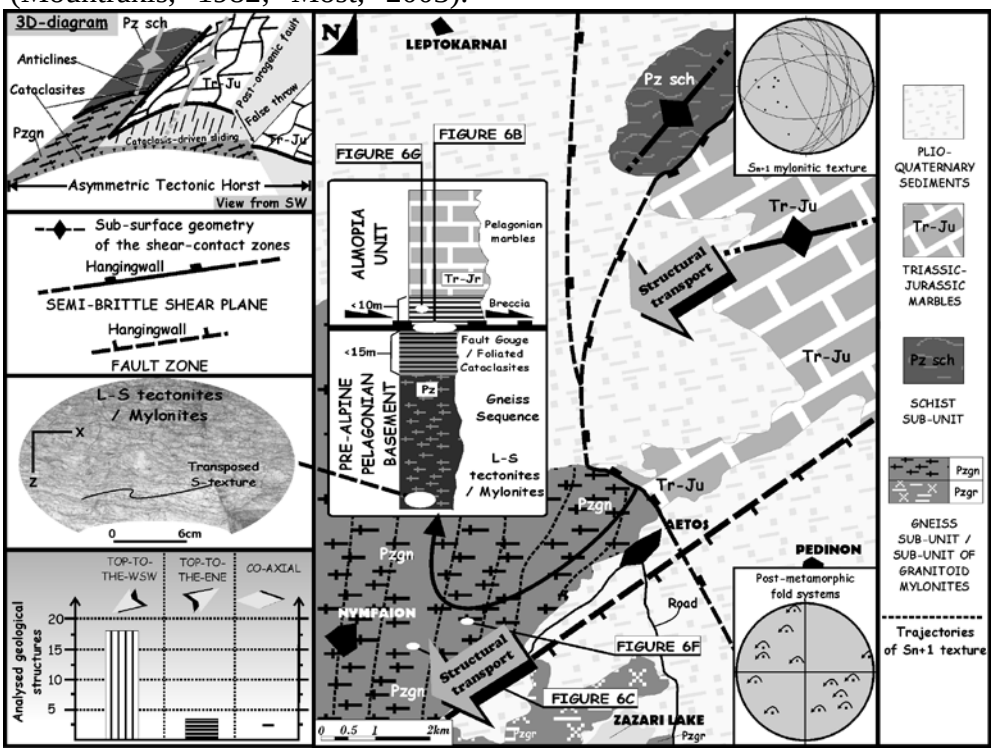

Figure 4. Structural map of eastern Vernon mt. Histogram reveals the quantitative analysis of the geological structures. Photos of Figure 6 are also represented.

4.1 Contact Zone among Permo-Triassic and Triassic-Jurassic metamorphic sequences

The contact of Permo-Triassic rocks with the overlying marbles appear knife sharp (Figure 5F). In all the cases, the existence of nappe-emplacements is apparent and fault breccia and gouge dominate in all the locations. Transitional lithologies in the upper parts of Permo-Triassic rocks, expressed by calc-schists, are locally observed in tectonic relation with the overlying marbles, Figure 5G. The lithological variety of footwalls facilitates cataclasis-driven fragmentation. The low-angle orientation of the contact is noticed in the study area (up to 350). Near and within contacts, asymmetric boudinages of quartzitic bodies and meta-clastic microlithons with a west-southwestward asymmetry dominate (Figures 2, 5D and 5B). Asymmetric folds inside a fine-grained matrix and tight folds with sub-horizontal axial planes prove the asymmetry of deformation towards WSW (Figures 5A and 5C). S-C structures – foliation fish, rotated microlithons of intact rock forming σ-/δ-type clasts also show a WSW-wards non-coaxiality (Figure 5E). High-angle NE-SW directed faults (dip>350) displace the described contact, causing slidings of hangingwalls towards WSW. Post-metamorphic cross-fold systems of Permo-Triassic rocks also mark a WSW-ward non-coaxial strain (Figure 3D).

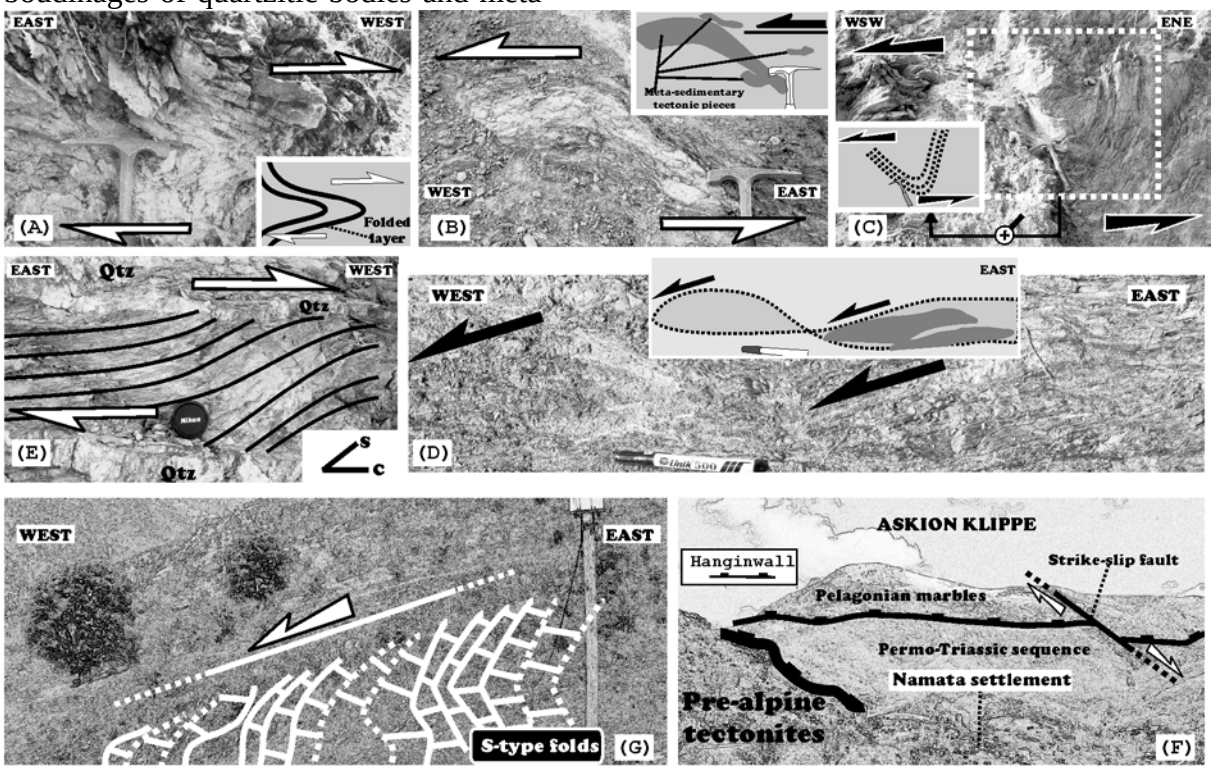

Figure 5. Contact Triassic-Jurassic marbles (Tr-Ju) – Permo-Triassic (Pm-Tr) rocks. A) Fold in calc-schists, B) Stretched pieces within the contact, C) Fold in phyllites, D) Asymmetric boudinage, E) S-C structure in phyllites, F) View of the contact, G) S-folds in calc-schists.

4.2 Contact Zone among Alpine and pre-Alpine metamorphic sequences

The klippen of Triassic-Jurassic marbles, revealing structural partitioning, in combination with the sharp character of their contact with the pre-alpine rocks reveal the tectonic nature of the contact (Figures 2, 4 and 6A). In eastern Vernon and eastern Askion, Permo-Triassic rocks are absent and Triassic-Jurassic marbles are emplaced directly onto pre-alpine rocks. Thus, Permo-Triassic rocks de-wedge towards east. In all the cases marbles-klippen appear folded with NE-SW and NW-SE anticline axes direction (Figures 2 and 4). Fault breccia and

foliated cataclasites dominate along the contact (Figures 4, 6B and 6G). The latter is outlined by low-angles and listric geometry (Figure 6A). Along the contact,

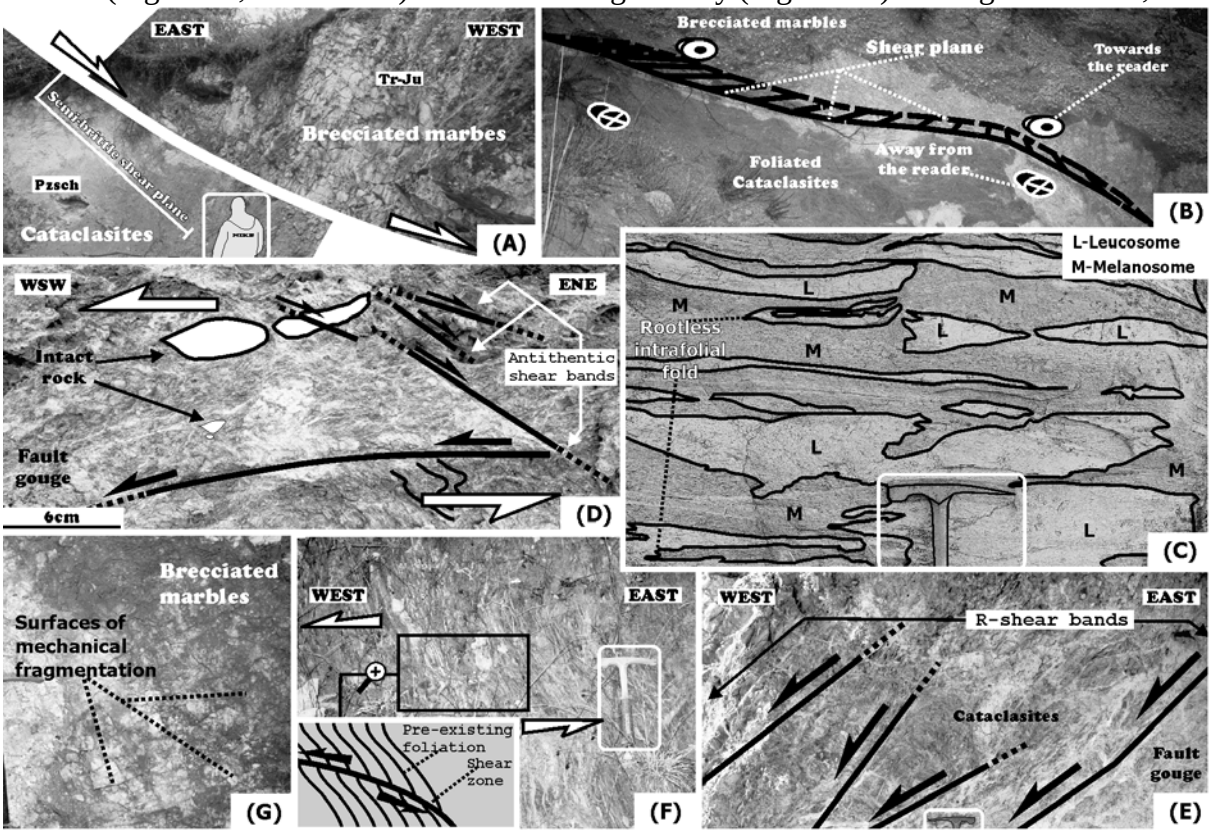

Figure 6. Contact Triassic-Jurassic marbles – pre-alpine rocks. A) View of Anarrachi klippe, B) View in Aetos settlement, C) pre-Alpine migmatites, D) Shears bands, E) Synthetic shear bands, F) Semi-brittle shear zone, G) Mechanical fragmentation due to cataclasis.

green to grey ultra-cataclasites of 5-20m thickness go over upwards in white to grey fault gouge with meta-carbonate fragments (Figure 6G, 6E). Rockslided rocks of fault breccia characterize the perimeter of the klippen within the cataclastic zone. Several anastomosed S-planes, a dense network of sub-parallel shear bands with sinistral asymmetry, tectonic pieces of intact rock bodies and asymmetric boudinages constitute the basic structures along the contact. R-shear planes, synthetic to the shear direction, dominate and show sinistral sense of shear (Figures 6E and 6D). Back-rotation folds are observed in limited and localized packages. In eastern Askion, variable geometric differences of the produced shear bands are found within the contact zones, controlled by both strain and microstructures. Co-axial structures along the contacts are observed in few locations in the Askion mountain, and their mode decreases towards southwest (Figure 2). The contact among Permo-Triassic rocks and pre-Alpine sub-units has the identical kinematic characteristics as the former contacts and display a westward tilting (Figure 2).

4.3 Shear planes within the pre-Alpine Pelagonian Basement

The relation of the granitoid mylonites with the adjacent sub-units appear identical kinematic features with the above analyzed shear-contacts. A well-expressed low-angle shear plane (from 100 up to 200) occurs in the center of the mountain, bringing granitoid mylonites onto Schist sub-unit. The eastward termination of this shear zone is exactly estimated in the tectonic boundary of Almopia Unit with the pre-Alpine basement (Figure 7). Thus, granitoid mylonites wedge out eastward, displaying

a similar geometry with the Permo-Triassic rocks.

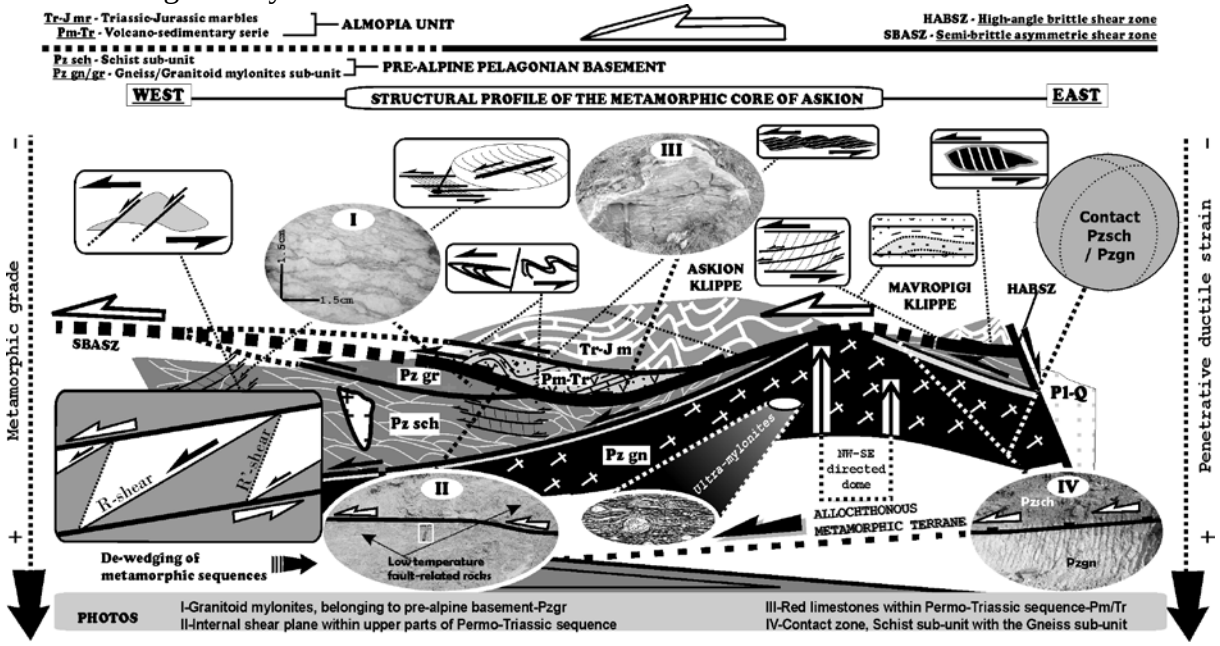

Figure 7. Structural profile of Askion mountain, illustrating the kinematics.

In the eastern flank of Askion mountain, Schist sub-unit overlies Gneiss sub-unit through a sub-horizontal shear plane (Figure 7 photo IV). A NW-SE directed anticline dome is the result of this geometry. Cataclastic phenomena, related to the mechanical fragmentation of the involved rocks, dominate. Marbles, locally karstified and faulted, compose the higher sub-unit.

4.4 Asymmeric nappe-stretching and Architecture

The asymmetric nappe-stretching and thinning are also proven in the study area. (i) The emplacement of Triassic-Jurassic marbles onto distinctive pre-Alpine tectonites eliminating Permo-Triassic rocks, (ii) the imposition of Triassic-Jurassic marbles above Permo-Triassic rocks through a semi-brittle shear plane, (iii) the determination of stretching structures along the contacts and (iv) the evidence for overprinting of semi-brittle/brittle structures on ductile penetrative structures, constitute criteria for the asymmetric nappe-stretching (toward WSW). Shear band and foliation boudinages with WSW-ward sense of shear along footwalls reinforce the above (Figure 6D). Internal and external asymmetry for either the intervening rocks within previous contacts or for the footwall-related rocks prove the former conclusion. Co-existing fault breccia and cataclasites show that nappe-transports were continued until the formation of these rocks. The architecture of Askion mt. is depicted in Figure 7.

5. DISTRIBUTED SHEAR STRAIN ALONG FOOTWALLS AND HANGINWALLS & DATING OF STRETCHING

Our analysis points out the apparently stronger and well-defined deformation of footwalls, indicating their harder tectonic strain. Footwall formations show a noted amount of intense strain, revealing the large amount of absorption of structural transports (Figures 5D, 5C, 6E, 6D). Thus, the nappe-emplacements, apart from the major shear plane in which the dominant displacement takes place, also arrange internal shear band-networks, which become much rare away from the contacts. In the Askion mountain, a marked variation in the spatial distribution of the shear bands as well as in their orientation is obvious. Heterogeneous strain together with the rheological variety of the involved rocks could be considered

responsible for this complication. Domains of denser shear-band networks are closely connected to strain localization of increased intensity. At variance, Triassic-Jurassic marbles have been deformed as a massive sub-unit due to competency contrast. Few discrete brittle shear planes were observed, corroborating a marked differentiation of distributed shear strain between footwalls and hangingwalls.

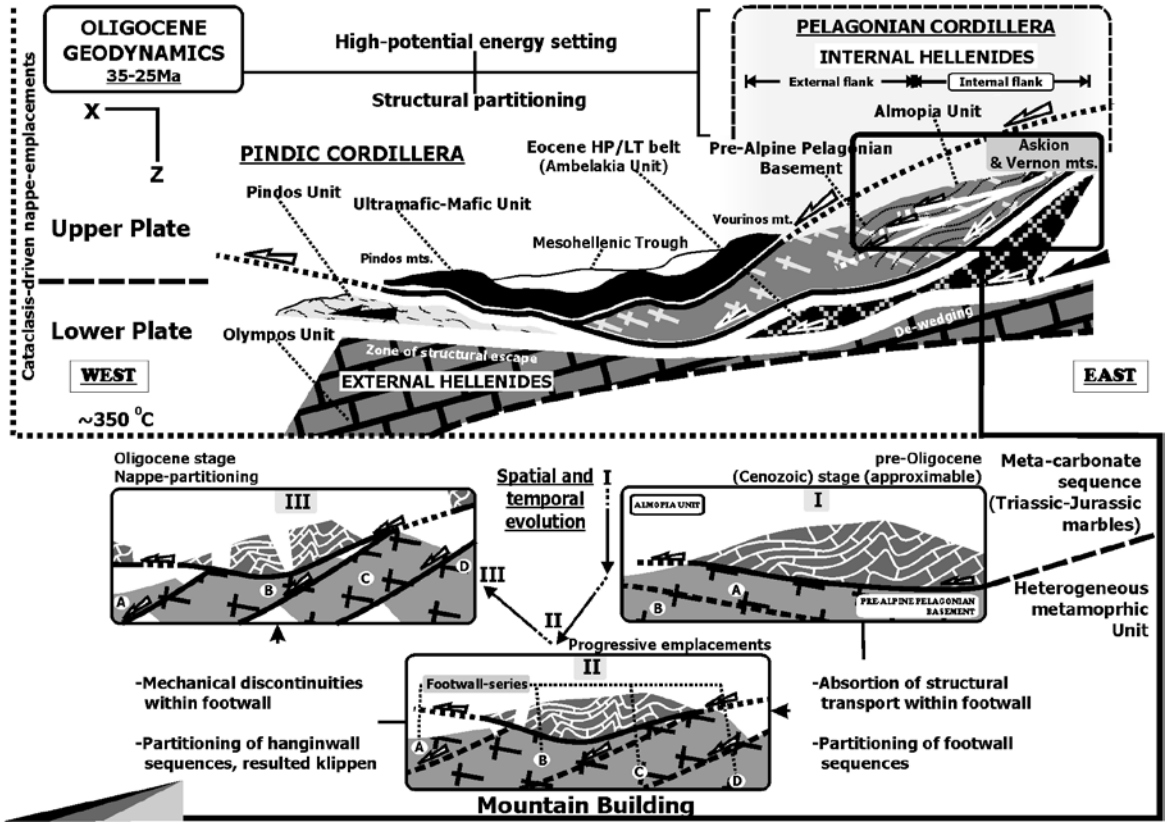

Figure 8. Oligocene geodynamics of Northern Greece (Western Macedonia).

Age determination of the contacts is of particular interest. Mn+1 and Mn+2 alpine metamorphic events at epidote-amphibolite and greenschist conditions, respectively, are closely connected with penetrative textures (Spyropoulos, 1992; Mposkos and Krohe, 2004). K-Ar ages of pre-alpine schists and gneisses reveal Eohellenic ages between 148Ma-111Ma (Most, 2003), for the dominant penetrative textures. Isotopic ages (K-Ar ages) between 100 Ma and 85Ma in mica schists and gneisses represent secondary textures (Most, 2003). Semi-brittle fabrics and post-metamorphic fold systems of WSW-ward asymmetry, overprinting previous ductile fabrics, have Late Tertiary ages (Spyropoulos, 1992; Most, 2003; Diamantopoulos and Panousopoulos, 2004). Thus, the action of the semi-brittle contacts is determined in Late Tertiary. Bearing in mind our analysis and the process of the emplacement of Internal onto External Hellenides, the Oligocene age of nappe-emplacements is revealed. Particularly during the Oligocene, the island-arc geodynamic regime in Internal Hellenides is recognized, showing the syn-orogenic nature of the contacts coeval with the westward orogenic migration (Aubouin, 1965).

6. CONCLUSION & DISCUSSION

Having in mind the above, the mutual relation of the nappe-emplacements is supported with the Oligocene geodynamics of Internal Hellenides. Their kinematic asymmetry towards west-southwest has been suggested (Aubouin, 1965; Godfriaux and Ricou, 1991;

Ferriere et al., 1998; Most, 2003) and is strongly reinforced by our data. Thus, nappe-emplacements during mountain building characterize this orogenic stage. Semi-brittle mechanical discontinuities activate and convey the entire nappe-pile, causing an asymmetric architecture (Figure 8). Thus, structural partitioning of Internal Hellenides took place during their emplacement onto External in a high-potential energy setting of the developed mountain belt. In addition, although our analysis marks the semi-brittle/brittle nature of the shear planes, their evolution during the poly-orogenic processes of Internal Hellenides requires further speculation. Diamantopoulos & Panousopoulos (2004) noted a negative inversion (from shortening to extension) for alpine times but the present analysis reveals our difficulty in determining pre-Cenozoic processes. If the contacts were initially activated in Cretaceous, as Mercier (1968) supported, the problem of their evolution during post-Cretaceous times towards surface arises and needs solution. In conclusion, the architecture of the study area is outlined by discrete shear planes, coinciding with the boundaries of the metamorphic sub-units. Low-temperature fault-related rocks, the non-coaxial lengthening and the low-angle orientation enumerate the basic structural features of the examined contacts. Oligocene structural perturbations of WSW-ward asymmetry are connoted to occur coeval with the emplacement of Internal onto External Hellenides. Structural partitioning of Internal Hellenides in semi-brittle up to brittle conditions provides a satisfied mechanism for mountain building. A remarkable deformation differentiation between hanginwalls and footwalls is also proven along the contacts.

ACKNOWLEDGEMENTS

Professor Mposkos Evripides, Professor Krohe Alexander and Dr Perraki Maria are really thanked for providing corrections of the manuscript as well as for helpful discussions.

REFERENCES

Aubouin, J., 1965. Geosynclines. *Developments in Geotectonics* 1, Elsevier.

Brunn, J. H., 1990. Geology of the Ophiolitic Northern Pindos and Western Macedonia. *Annales Geologique des pays Helleniques*, XXXIV/2, 1-85.

Celet, P., Cadet, J.-P., Charvet, J., Ferriere, J., 1976. Volcano-sedimentary and volcano-detritic phenomena of Mesozoic age in Dinaric and Hellenic ranges: A comparison. *Histoire Structurale des Bassins Mediterraneens, Symposium International*, 33-46.

Diamantopoulos, A., Panousopoulos, A. 2004. On the structural geology and the tectonics of the pre-Cretaceous metamorphic rocks on eastern Askion mountain (Western margin of Ptolemais-Kozani graben, NW Macedonia, Greece). *ISES*, Turkey, 695-703.

Ferriere, J., Reynaud, J.-Y., Migiros, G., Proust, J.-N., Bonneau, M., Pavlopoulos, A., Houze, A. 1998. Initiation d'un basin transporte': l' exemple du «sillon meso-hellenique» au Tertiaire (Grece). *C. R. Acad. Sci. Paris, Sciences de la terre et planettes* 326, 567-574.

Godfriaux, I., Ricou, L. E., 1991. Direction et sens de transport associes an charriage synmetamorphe sur L' Olympe. *Bull. Geo. Soc. Greece*, XXV/1, 207-229.

Hansen, E., 1971. Strain Facies. *Springer*.

Kornprobst, J., 2002. Metamorphic rocks and their Geodynamic significance. *A petrological handbook. Kluwer Academic Publishers*.

Laubscher, B., 1969. Mountain building. *Tectonophysics* 7, 551-563.

Malavieille, J., 1993. Late orogenic extension in mountain belts: Insights from the Basin and Range and the Late Paleozoic Variscan Belt. *Tectonics*, 12, 1115-1130.

Mercier, J. L., 1968. Etude géologique des zones Internes des Hellenides en Macedoine Centrale (Grèce), Annales Geologique des Pays Helleniques, XX, 1-792.

Most, T., 2003. Geodynamic evolution of the Eastern Pelagonian Zone in north-western Greece and the Republic of Macedonia. Implications from U/Pb, Rb/Sr, K/Ar, Ar/Ar, geochronology and fission track thermochronology. *Tubingen, Phd, Germany*.

Mposkos, E., Krohe, A., 2004. New evidences of the Low-P/High-T pre-Alpine metamorphism and medium-P alpine overprint of the Pelagonian Zone documented in metapelites and orthogneisses from the Voras Massif, Macedonia, Northern Greece. *Bull. Geo. Soc. Greece*, XXXVI/1, 558-567.

Mountrakis, D., 1982. Etude géologique des terrains métamorphiques de Macedoine orientale (Grèce). *Bull. Geol. Fr.*, XXIV, 697-704.

Passchier, C. W., Trouw, R. A. J., 2005. Microtectonics. *Springer*.

Papanikolaou, D., Stoyanov, R. 1983. Geological correlations between the Greek and Yugoslav parts of the Pelagonian Metamorphic Belt. *IGCP* No 5, Newsletter No 5.

Robertson, A. H. F., 2004. Overview of the genesis and the emplacement of Mesozoic ophiolites in the Eastern Mediterranean Tethyan region. *Lithos* 65, 1-67.

Spyropoulos, N., 1992. The geological structure of the Pelagonian Zone in Askion mountain. *Phd Thesis, Department of Geology, Thessaloniki, Greece* (unpublished).

Turner, R. J., Weiss, L. E., 1963. Structural analysis of metamorphic tectonites, University of California, Berkley, McGraw-Hill Book Company, Inc.

Vanderhaeghe, O., Teyssier, Ch., 2001. Crustal-scale rheological transitions during late-orogenic collapse. *Tectonophysics* 335, 211-228.

DIRECT DETECTION OF OIL AT GACHSARAN PROVEN FIELD; CASE HISTORY FROM IRAN

Ercan A. Ö.[1] and Tabatabaee S.H.[2]

[1] Honorary President of Geophysical Society Of Turkey and Consultant of National Iranian Oil Company of Ministry of Petroleum

[2] National Iranian Oil Company of Ministry of Petroleum (NIOC) and Chairmen of Geophysical Prospecting and Land Seismic.

Postal Address: **Subsurface Exploration Inc.** Süleyman Seba Cad. Acısu Sok. 5/2 Maçka-BEŞİKTAŞ, İSTANBUL, TÜRKİYE

e-mail: ahmetercan@ahmetercan.net, web: www.ahmetercan.net

Abstract: 8.6 percent of world oil resources are in Iran. Average cost of one barrel of oil is 4.5 $. Average depth of the deepest oil deposits is 7 kilometers. Iran is one of the main petroleum producers and also one of the countries which exploits contemporary geophysical techniques in the Middle East region. Main aim of this study is direct detection of oil hydrocarbons by a special geophysical technique. To accomplish that, FEM, TEM and IP integrated geophysical techniques were successfully applied to measure IP phase shift, which might relate to the existence of oil traps. Target penetration for this prospecting is about 6 kilometers.

Key Words: petroleum, polarization, İran, IP, direct detection of oil.

INTRODUCTION

Gachsaran field is a proven oil field in the Khuzestan region of İran. Gachsaran oil field is on the south-western end of Khaviz anticline, divided by a nearly east west extending left strike slip fault (Figures 1, 2, 3 and 4). Gachsaran oil field

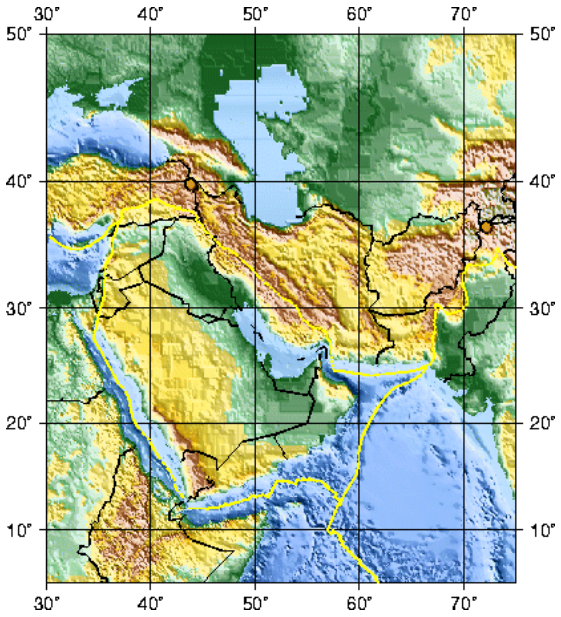

Figure 1. Physical map of Middle East, in respect of Turkey's border with Iran

was discovered by a British earth scientist in 1960. Total production capacity of the field is about 3000 barrels per day. The first reservoir rock is the Asmari formation. Depth to the gas-oil contact is about 800 meters and OWL oil water contact is about 2000 meters. Depth to Jurassic formations is about 3.5 kilometers. Reservoir is situated at the crown part of the anticline type structure. This dome like structure is sliced by an easterly trust fault on which one observes Neocene deposits. However, widely seen geological unit is Gachsaran (evaporates) in the area. Extension of the hidden anticline type of reservoir rock is about N45W, which is in accordance with elongation of the induced polarization phase anomaly. Average width of Gachsaran oil field is about 1 to 1.8 kms and length is about 6.5 kms.

Khaviz in between this Gachsaran and Dehdash twin oil fields is also productive. This area is like a main body with two wings at two sides.

Depths of drillings in Gachsaran oil field are around 3 to 3.5 kms. Cap rock is the first member of Gachsaran, which is identified as marl. Reservoir rock is Limestone in upper Asmari, which has a thickness of 50 to 100 meters. Continuing middle reservoir is basically limestone at

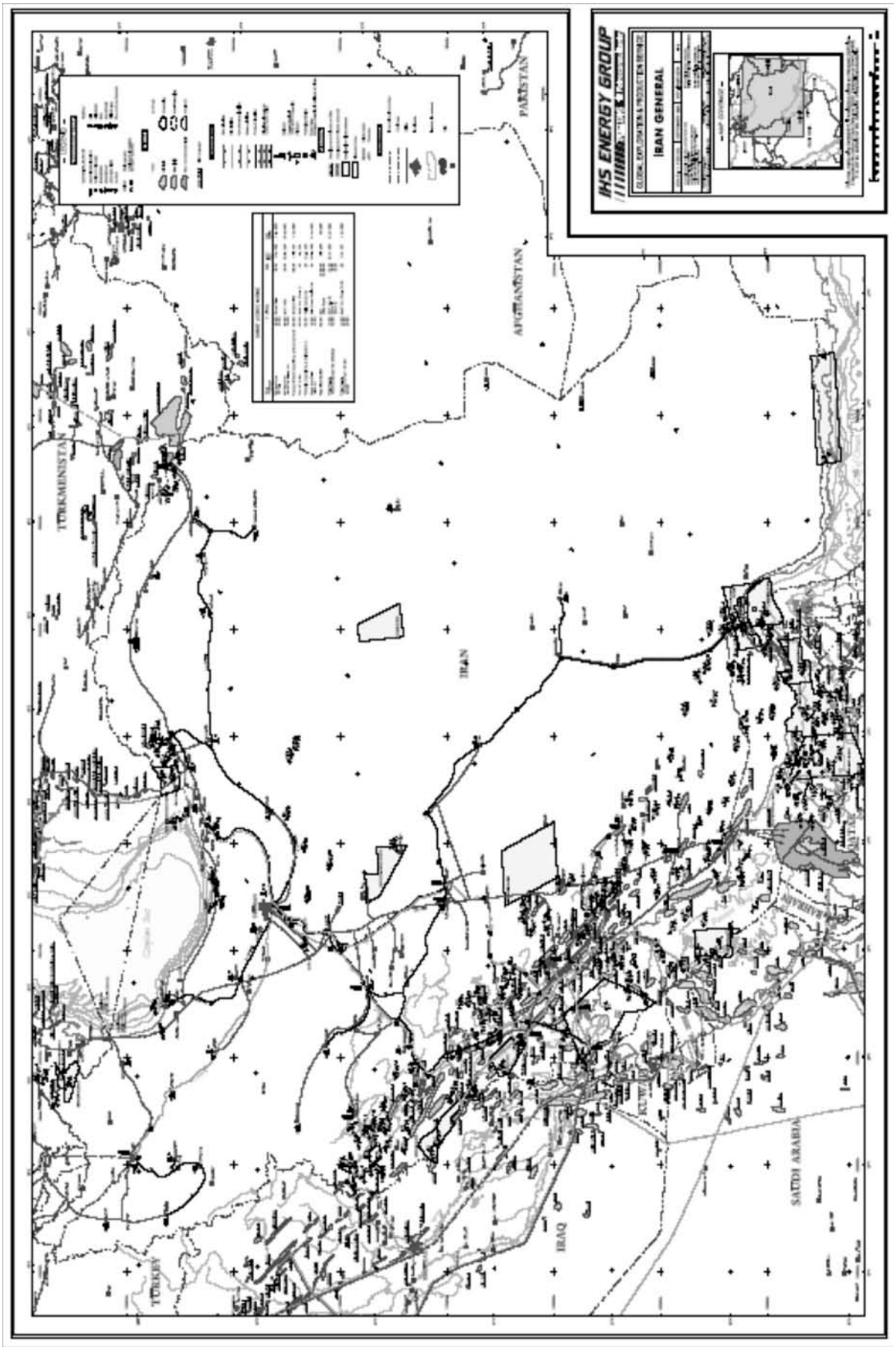

Figure 2. Oil fields of Iran and surroundings

Figure 3. Location map of neighbouring Dehdasht area and Gachsaran oil filed

the top and dolomite at the bottom with a thickness of 300 to 350 meters. Oil water interface is in the middle Asmari, which coincides with the surface depth of the dolomite. Second half of the Middle Asmari and Low Asmari are saturated with saline water.

So hydrocarbon related saline water layer thickness in Asmari is not less than 300 meters, which reveals why we observed conductive property of the rock in the neighboring Dehdash area and why we have recorded high polarization over the possible reservoir around Koohbord Mountain. Origin of such an IP phase polarization anomaly is clearly electrolytic in type. So there is also a good chance of expectation that such water oil contact zone could have large Zeta potential and therefore natural current flow near and around the reservoir which could be delineated by NP surveying as well. We conducted CSEM+IP techniques at Gachsaran oil field. Previous geophysical applications in the field site was seismic reflection and sparse gravity

Figure 4. The tectonic map of Iranian Gulf area and the study field

Methodology Of Oil Prospecting

1. *In geophysical investigation, the most proper approach is to start with a known field and then expand into an unknown prospecting site.*
2. *To do that one should follow steps given below*
    a. *Library work*
    b. *Infrared imaging*
    c. *Airborne magnetic and electromagnetic maps*
    d. *A photogrameter map*
    e. *A topographic map*
    f. *A geologic and tectonic map and structural sections*
    g. *A geochemical map*
    h. *Drilling and Borehole geophysics data*
    i. *Previous surface geophysical data (gravity, ground magnetics, seismic reflection, MT, CSAMT, FEM or TEM etc.)*
3. *Combination of all these methods and getting an idea what to do and how to do for future geophysical work.*

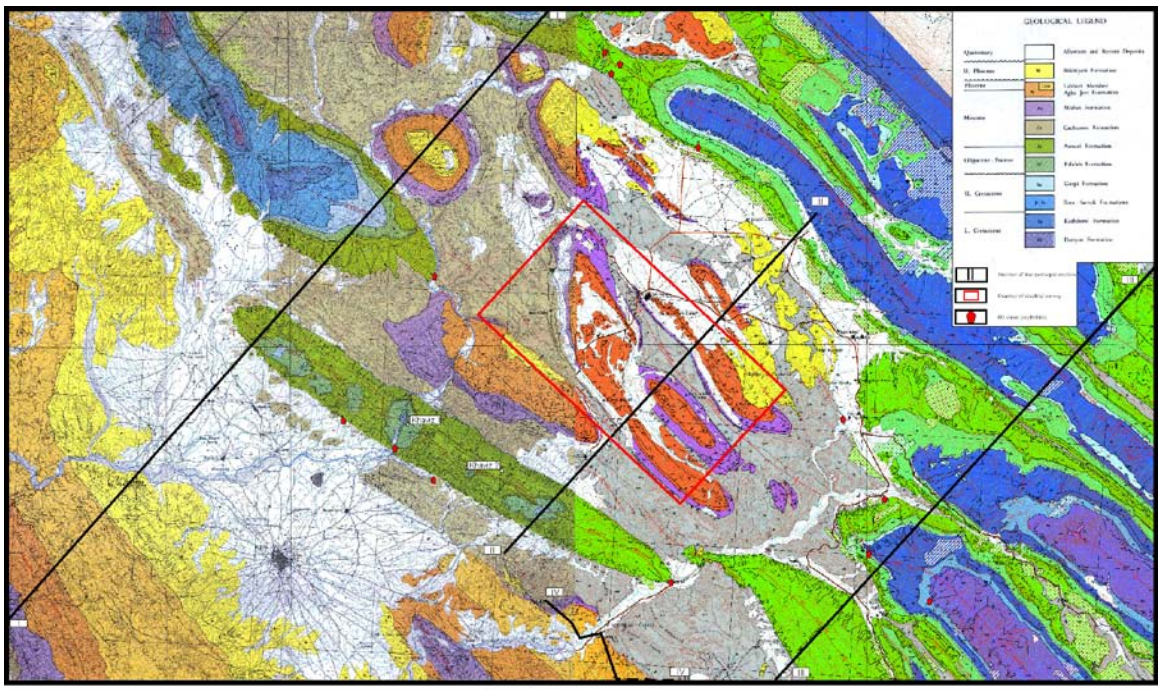

Figure 5. The surface geology of Gachsaran and Dehdasht fields. Khaviz mountain separates these two fields.

GACHSARAN FIELD

Topography and Geology

Gachsaran oil field is situated 30 kilometers away from Deh Dasht prospect, on the western part of the Khaviz Mountain which separates the two fields in Southern Iran (Figure 3). There are about 44 completed wells in the area, only ¼ was successful to encounter an oil reservoir, and others are dry. Performed borehole locations take place in strips which are parallel to the main strike of geology and direction of Khaviz anticline, which elongates approximately in N45W. (Figure 5). The region is completely covered by high velocity overburden which is well known evaporates with large scale cavities in it. This formation embraces Khaviz anticline from Abrigek town, on the north, to the Khairabad River on the south, along the surface trace of the thrust fault. This formation also represents high resistivity as well as low background electrolytic polarization which is close to zero. Topographic altitude of the Khaviz anticline axis is about 1600 meters maximum, which dips beneath the overburden on the south, nearby the Khaydarabad River. This river bed itself is a left lateral strike slip fault, extending approximately in N45E, which is almost vertical to general extend of the topography. However, trust faults which may have vertical offset of 1 km take place on the western (Gachsaran) and on the eastern sides of the Khaviz, as known from geological and gravitational studies. Nevertheless, the seismic reflection technique which was employed in the field had a very weak performance because of the screening effect of the surface evaporates which are observed on the very rocky foothills which have approximate elevations of 500 to 600 meters. Western plane of the field is largely covered by Agha Jari sandstone as well as Baktyari, which lies as crown on the top of hills.

Typical Geological Section.

Typical stratigraphic section of the field site is as follows;

1. *Quaternary **Alluvium and Recent Deposits (Q –Al)**– shown with white color on the map.*

   Discordance
2. *Upper Pliocene **Bakhtiyari (Ba)**–Conglomerate- **shown with yellow color***

   Discordance
3. *Pliocene- Miocene **Agha Jari(Aj) and Labhari(Lbar) Member**– Sandstone and sandy limestone- **shown with orange color***
4. *Miocene **Mishan(Mn)**- Limestone- **shown with violet color***
5. *Miocene **Gachsaran(Gs)** - Evaporates (anhydrites, chalk and gypsums), salt, marl, shale, stiff limestone with karsification- **shown with gray color**- cap rock*
6. *Miocene-Oligocene-Eocene **Asmari**-Limestone- **shown with green color**-**First Reservoir** rock with underlying Jehrun. Depth to Asmari is about 1.9 to 2.3 kms.*
7. *Oligocene-Eocene **Jehrun**-Sandy limestone- **First reservoir** rock with overlying Asmari*
8. *Oligocene- Eocene **Pabdeh Formation (Pa)**- Shale, marl and limestone - **shown with dark green***

   Discordance
9. *Upper Cretaceaus **Gurpi Formation (Gu)-** Shale, marl and limestone **Shown with blue***
10. *Upper Cretaceaus **Ilam-Servak (Il-Sa)**- Limestone- **Second reservoir. Shown with intermediate blue***
11. *Lower Cretaceaus **Kazhdomi** (akrep)- Shale. **Source rock of Asmari (1st reservoir).Shown with dark blue***
12. *Lower Cretaceaus **Khami Group** (Dariyan(Dr), Fehlivan, Gadvan)- Dolomite, Limestone, Shale- **Third reservoir.Shown with dark blue-to violet.Gadvan is source rock of Dariyan***
13. *Jurassic. **Hizh-Surmeh-** Limestone and Dolomite*
14. *Triassic**.Nayriz** - **Khanehkat**–Dolomite*
15. ***Dehrem Group**- Sandstone- **Fourth reservoir- producing only natural gas**. Because of high temperature and pressure oil is transformed to be in gas form. Depth to Dehrem is about 4 to 5 kms.*

Only first seven of these formations give surface exposures in the Gachsaran oil field. Gachsaran and Agha Jari units are the most dominant units which are widely observed in the field site. Gachsaran unit causes absorption of

seismic energy to penetrate beneath, because of its high velocity and karsifications properties(Figures 5, 5b, 6 and 7). This problem of obstruction of energy penetration is known to be the screening effect. Therefore, seismic reflection survey, in the past, was not able to give a clear decisive interpretation about the existence of a possible reservoir structure at Gachsaran oil field.

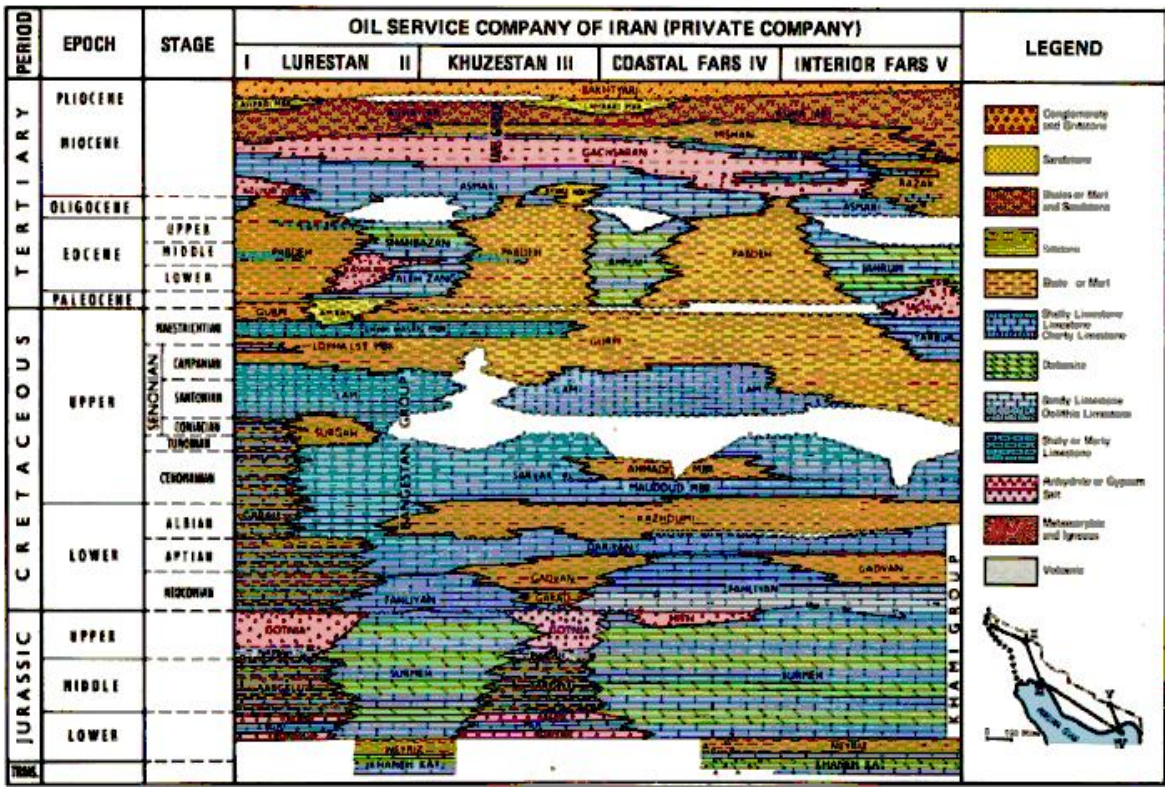

Figure 5b. A typical stratigraphic section in Iran and at some specific fields

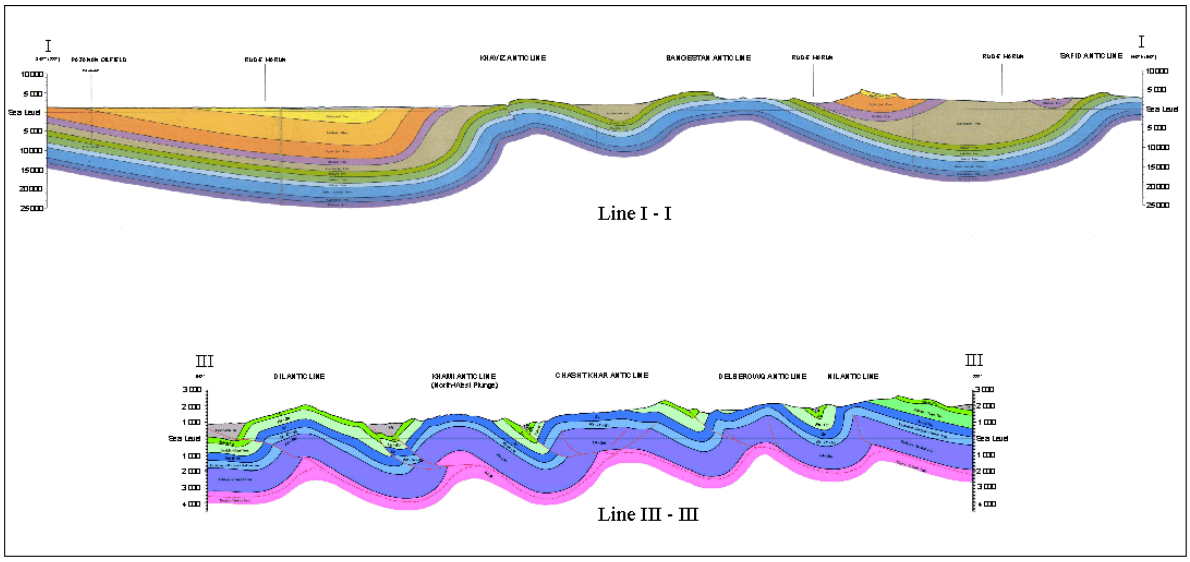

Figure 6. General geological section of the area

Figure 7. Geological cross section of Gachsaran oil field

Geology and Tectonics in Relation with Geophysical Investigations

The north-easterly compressive forces derived by the opening of the Red Sea, orogenesis of the Zagros mountain started along the Alp- Himalaya mountain chain. According to the stress axis and direction, anticline and syncline axis as well as strikes of napes elongated parallel to the costal line of Persian Gulf, which has an extension in the NW-SE direction. According to this effective active tectonic, oceanic crust and hydrocarbon deposits had also deformed and then trapped in the same direction (Figures 4, 6 and 7).

Macro-Anisotropy and Directivity

In accordance with such an active tectonic, strike direction of layers extend in NS or NW and SE directions. Such an alignment of the folding and strike can lead to macro-anisotropy which could produce fictitious anomalies which may extend in NW-SE and NE-SW directions. Such an event could mislead one to arrive at misinterpretations. In addition to these, the napping feature observed on the surface could also produce secondary polarization anomalies which will have no relation with actual anomalies directly pointing the petroleum reservoir itself (Figures 6 and 7).

In order to overcome such a structural limitation it seems to be necessary to collect data with a 3D vector scheme. In such an approach, two pairs of perpendicular vector components of E-field, E_{xy} and E_{xx}, and E_{yx} and $E_{yy,}$ should be measured for two different transmitters, which will be oriented perpendicular to each other. Then vector average sum of these two total vector fields will be mapped to remove the influence of the macro-anisotropy created by the geological structure.

Geophysical Properties Of the Oil Filed

Electromagnetic and Induced Polarization Response of Gachsaran Field.

Electrical resistivity stratigraphy is an essential parameter effecting

1. *Depth of penetration;*
2. *Depth of polarization.*

The resistivity structure does not necessarily follow up with that of geology. Their estimated values can not be used to name deep layers of geological formations, on a one to one bases. Sometimes groups of layer appear as a single layer in the same resistivity value

and sometime one single formation with content of different facieses, or porosities, or clay contaminations, or fluid saturation can be observed as a multi layer in the resistivity sounding section. However, there could also be some typical formations which are recognized with their high, intermediate or low resistivities.

In order to recognize the electro-response of the media in Gachsaran, the first step is to be informed about geological stratigraphy and resistivity stratigraphy to understand the correlation between each other.. To do that lithological samples and geophysical well logging data are combined in neighboring Khaviz Mountain oil field.

Average Electrical Resistivity Structure in the Gachsaran Oil Field.

In electromagnetic and polarization studies there are four essential resistivity stratifications which are considered in preliminary evaluation capabilities to communicate with the subsurface. Three layered media are grouped in four different types of distribution and response curves which are named as H, K, A, Q

1. **Q-Type is defined as ro1>ro2>ro3**

In this case resistivity reduces as one goes deeper. This a case like in Gachsaran resistive unit confronted in the western side of the field. For such media, there will not be any problem of penetration either with FEM or TEM methods for detection of phase. Especially TEM is successful in such areas unless the thickness of the resistive overburden is too big.

2. **A-Type is defined as ro1<ro2<ro3**

In this case, resistivity increases as one goes deeper. This a case like on successions of Quaternary and Neogene aged Bakhtiyari and Gachsaran or Agha Jari as observed on the northern portion of the field side. On such media, there will not be any problem of penetration either in FEM or TEM applications for detection of phase. However, energy level will drastically reduce in deeper parts for FEM. Especially TEM will be successful in such areas to map the depth of resistive basement. Energy level for FEM will reduce about 10 folds below the skin depth.

3. **K-Type is defined as ro1<ro2>ro3**

In this case, resistivity is high in the intermediate layer. This is a case like on successions of Neogene aged Bakhtiyari and Gachsaran and Asmari as observed in Gachsaran oil field at Mensurabad town on the western side of Khaviz anticline. On such media, there will be some problem of penetration in FEM to penetrate beneath the intermediate layer. Because, almost all energy will be saturated on the interface of the conductive overburden with the underlying intermediate resistive layer. TEM applications will not have similar difficulty if the second resistive layer is thin. Otherwise TEM will also have penetration trouble as FEM does, for the detection of phase from deeper reservoirs. TEM energy beneath the intermediate resistive layer will drastically reduce in deeper parts of the conductive third layer as well. Especially FEM or DC soundings will be successful in such areas to map the depth of resistive second layer.

4. **H-Type is defined as ro1>ro2<ro3**

In this model, resistivity is low in the intermediate layer. Such a section is mostly confronted in arid areas where the climate is so hot and moisture content in

the surface layer is very small. Khyrabad area is represented to respond as a good example for this case. Because, CSEM+IP prospecting was run in the dry season of this area, which is the summer months of June, July, August and September.

Any of Neogene aged Bakhtiyari or Gachsaran or Agha Jari will produce an H-type resistivity model as observed in Gachsaranon on the eastern side of the Khaviz anticline.

Electrical Resistivity Section Is H-Type In Dehdasht and Khyrabad.

Average section representing Gachsaran oil field is somewhat as follows:

1. The layer has a resistivity of 20 to 100 ohm meters, with a thickness of 100 to 300 meters. TEM and FEM will not have any difficulty penetrating this dry upper layer. No matter what type of formation is taking place on the surface, because of the dryness of the rock it is always resistive. **RESISTIVE**
2. The layer is conductive down to the bottom of Asmari, which is the first reservoir rock represented with low resistivity of 10 to 30 ohm meters. Approximate depth is about 2000 meters with beddings of some numbers of thin resistive layers of 40 to 300 ohm meters. I suppose that FEM will be limited to collect information till to the bottom of Asmari and Jehrum units. TEM's communications and information gathering depth may go behind of Khami group, which is the 3rd reservoir at about 4 to 5 kms depth. **CONDUCTIVE**
3. The layer is resistive, which is called as EM basement, with resistivity of 300 to 400 ohm meters. This could be Servak for FEM or even another deeper layer. **RESISTIVE.**

So as we know from theory TEM will pass through a resistive thin layer in succession; however, FEM will run into a shielding effect for such a resistive layer (Figure 8).

For HREIP surveying depth of penetration of FEM could be around 4 to 5 kms and it can reach up to 10 kms for TEM. Especially TEM or DC soundings will be successful to map the depth of bottom resistive third layer at depths beyond 6 or 7 kms.

Estimated Polarization Capabilities of Geological Units at Gachsaran Oil Field

	Metal Factors mho/cms		**Chargeability msec**
Quaternary Alluviums and Gravels	0- 200	1-4	Low
Conglomerates *Bakhtiyari*	0- 200	3-9	Moderate
Groundwater *Near Surface*	0	0	None Polarizable
Saline water *Oil Water Contact*	0		High Polarizable For Low Salinity

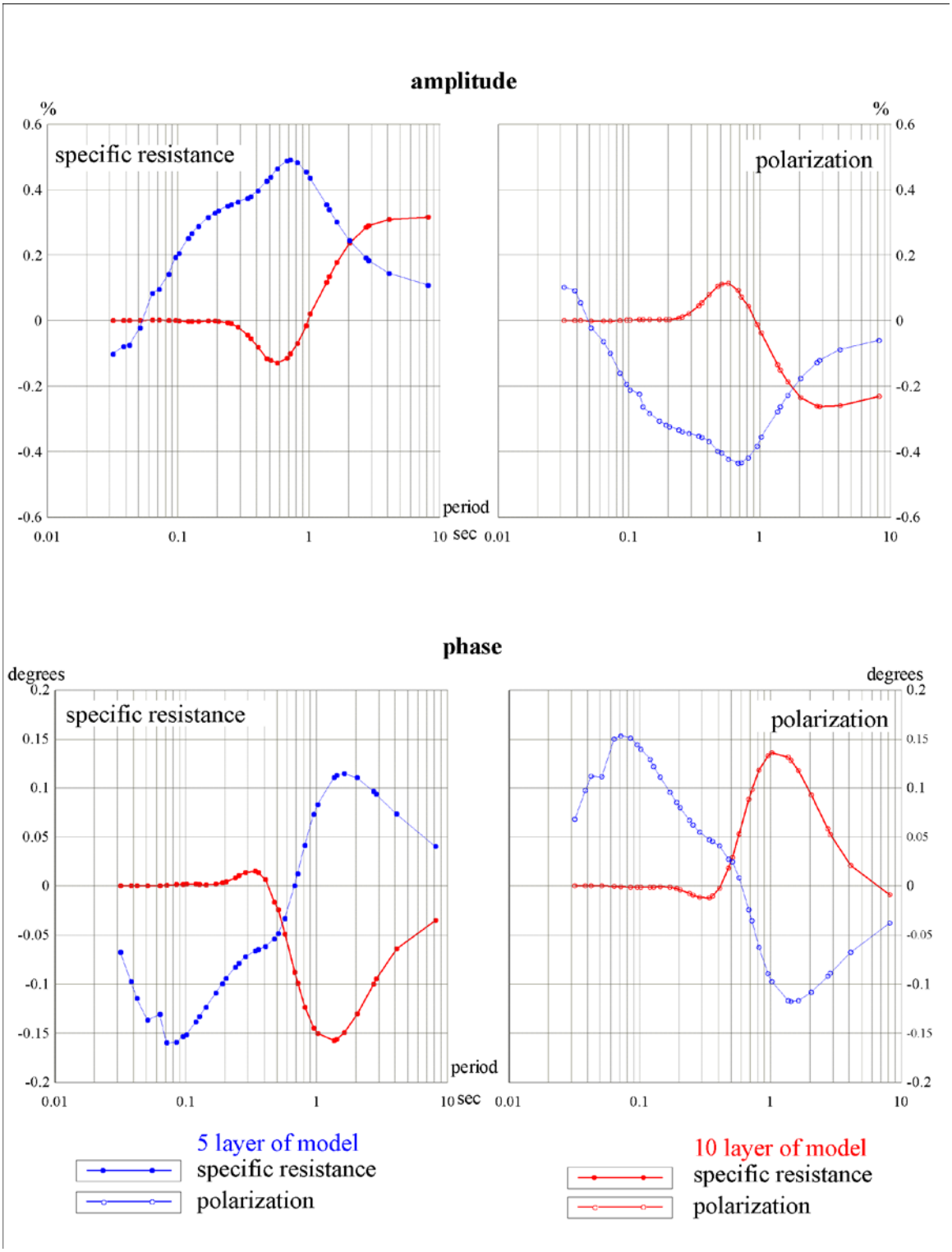

Figure 8. Samples curves for electromagnetic and IP soundings

Clay Content	1- 300	<%2 High Polarizable
		<%10 Moderate Polarizable.
		>%10 Low or None Polarizable.

Limestone

(Asmari,Jehrun)(1.Reservoir Rock), Servak(2. Reservoir Rock), Mishan, Surmeh

	0	10 – 20	High
Schist			
	10- 60	5 – 20	High
Sandstone			
(Agha Jari, Dehrem	0	3 – 12	Moderate
Shale			
Khami Group-source rock, Pabdeh and Gurpi Formations			
	0	50 – 100	Low to High
Sandstone- Siltstone	0	100- 500	Very High
Argillites	0	3 – 12	Moderate
Quartzite	0	5 – 12	Moderate
Salt, Anhydrites, Gypsum			
Evaporates			
Gachsaran Formation	0	0	
Cap Rock			
Disseminated Sulfite	10 - 100	0	
Surface Contamination			
Zone			
Sulfide 2 % – 8 %	500 – 1000	0	
Sulfide 8 % – 20 %	1000 – 2000	0	
Sulfide >20 %	2000 – 3000	0	

Metal Factor is frequency dependency capacity of electronic polarization.

Chargeability shows the magnitude of the electrolytic polarization.

Trap and Reservoir. Oil-water contact depth varies from 2.4 kms to 2 kms estimated from drills. Typical trap is in the form of anticline - hydrodynamic type with approximate width of 8 and length of 15 kilometers. Basic part of the oil field is on the south-eastern side and only northern head passes about 0 to 9 kilometers to the north of Khaydarabad River. Field may have two structures, like a shape of a fork, which characteristically lies beneath the high mountains on the surface which are covered with Gachsaran evaporate, acting as cap rock.

Asmari is main productive, widely spared rock in İran. Barren portion of Asmari is about 25 to 75%. Average porosity in barren zones is less than 5% and penetration is less than 1 mDarcy. Productive portion of Asmari is about 8 to 14%. Average porosity in productive zones is not less than 5% and average penetration is 10 mDarcy; however, in some places exceeds 20 mDarcy.

Gachsaran oil field's initial production reserves of oil are 1485 billion tones, and 162 billion cubic meters of gas. Size of the anticline is 7 by 67 kms in the form of two domes containing gas, oil and water. Oil-water contact depth is 2.2-2.24 kms. Oil and gas column is about 2.1 km. Khami, at the depth of 3.6 kms, contains gas. Productive Asmari series has a thickness of 480 meters where the fractured reservoir has a porosity of 8%, penetration of 16 mDarcy.

Geophysical Method and Configuration. Frequency Domain Electromagnetic and Induced Polarization techniques were used in conjunction. Gradient configuration was set. An oscillating long line source A4B4, in the

N45E direction, was laid out with a length of 8 kilometers, and 7 receiving profiles were laid parallel to the excitation source, which have varying lengths of 5 to 7 kilometers. Southern heads of profiles start from Khaydarabad River and the northern ends end mostly at Khaviz Mountain, if there is not any drastic topographic obstacle. Profiles 57 and 58 cross the river and 59 takes place on the southern side of the river (Figure 7). Aim is to measure polarization characteristics of several anticline type traps which are known to take place at depths of 1.6 to 4.5 kilometers and riding over each other. Source of polarization is thought to be induced generation of electrolytic polarization in and around the kerosene water underlying each reservoir rock for every trap. So there are approximately 4 traps and 4 kerosene water layers, each with a thickness larger than 300 meters. Upper reservoir rock is named as Asmari sandy limestone which gives large surface exposures on Khaviz anticline with higher secondary porosity and permeability ratio.

Measuring profiles, where 24 channel Ex electric and Bz induction dipoles take place, are separated with an interval of 1 kilometers, in line with the transmitting antenna. Profile lengths vary between 5 to 7 kilometers and the antenna length is 50 meters, which can also be rearranged digitally for 100, 150, or 200 meters as well. Frequency sweep was used between 0.125 to 62.5 Hz with for 15 logarithmically separated harmonics with a current intensity of 28 amps.

Adjustments for Field Conditions. Width of the anomaly is about 1.8 kms; therefore, source length will be about 7 kms (at least 3 times longer). Eastern end will be situated nearby Khaviz Mountain's western flank and western end will be in a dry creek near the city of Gachsaran. Extension of source line and observation lines will be the same, in approximately EW. Total number of observation profiles will be about 5. Some will be on the northern and some will be on the southern side of the river. We already knew that especially in near field measurements, at Gachsaran, source will produce very strong Eddy currents along and around the casing of existing boreholes and at pipelines as well, which will create strong fake anomalies. Therefore, the contractor should be asked to remove such effects before setting the final interpretation. Also, it is well known from experience that maximum polarization is obtained at the optimum current level. At low and high values of excitation current I polarization is low. However, electrochemical and electro kinetic and electrolytic polarization capabilities increase to attain to a maximum value in an intermediate level of currents. Therefore, we repeated preliminary surveying at test station to find out the optimum current intensity. Then, this optimum current level was kept stationary throughout the prospecting. Otherwise, there will be no recognized level of magnitude of polarization at the surface projection of oil reservoirs, so we would therefore have missed some of the targets or some targets would expose fade anomalies as well.

DATA PROCESSING

Data Processing in Frequency Domain. Primary goal of processing of field data in frequency domain is the reception of amplitude and phase FS curves with the regard for hardware amendments and geometrical factors, the division of effects of induced polarization (IP) and an induction and the subsequent performance of various transformations and filtration of the data.

1. Spectral Characteristics Received Ex Field. After performing filtration, field data were collected in time domain for various frequencies by using the square waves, for the duration of some time, exposed to Fourier transform. As a result of which amplitudes and absolute phases of the first, the third and higher harmonics are obtained.

2. Spectral Characteristics Transmitting I-Current Field. Records of the form of a current are exposed to similar processing and by its results amendments are made to amplitude and phase frequency curves, i.e. the account for frequency characteristics of the measuring channel and a source line current is carried out.

3. Estimation of the Phase Difference. Phase parameters at all kinds of measurements are determined by subtraction from the phase shift on an observation point of value of a phase of a current measured in source line.

Absolute Phase FI(f)

$$FI(f)= FI\ Ex(f)- FI\ Ix(f) \qquad (1)$$

From the results of field data, processing amplitude and phase curves of frequency soundings are constructed.

Two Frequency Phases. For component Ex on absolute phases of the first and third harmonics the so-called two-frequency phase parameter is calculated under the formula:

$$FI(f)= \Delta\varphi(\omega) = 1{,}5 * (\varphi 1) - 0{,}5 * (\varphi 3) \qquad (2)$$

Where (φ1) is the absolute phase shift of the first harmonic; (φ3) is the absolute phase shift of the third harmonic.

Apparent Resistivity. Processing of results of spectral amplitude measurements on each frequency helps calculate the apparent electric resistivity ρ(ω) in Ohm.m. The measurement of an electric field ρ(ω) is determined under the formula:

$$\rho(\omega)Ex = K*\Delta V/I. \qquad (3)$$

Where K is the geometrical factor of array, m;

ΔV is the received voltage on a dipole , V;

I is the transmitted current in a source line, A.

The algorithm of calculation of the geometrical factor changes depending on the measured component of a field. In particular, for the most widely used technique in HRES-IP electric components Ex and Ey and a source as a grounded line, the geometrical factor is calculated with the formula:

$$K=2*\pi / (1/AM-1/BM-1/AN+1/BN) \qquad (4)$$

Where AM, BM, AN, BN are distances between grounded electrodes A, B, M and N of source and the reception line.

As a result of initial field data processing values of apparent resistivity and two-frequency phase parameter for all observation points and all frequencies are received. Those values serve as an initial material for further processing and interpretation.

Data processing in time domain. The purpose of processing of materials in time area is the construction of time electro-prospecting sections for the detailed analysis of geoelectric characteristics of an interval of depths including a target complex of rocks of a geological section. In time domain, data registered by a transient technique at excitation of an electromagnetic field in a two-polar mode with a pause or last period of the sweep are exposed to processing. Decay curve of lowest frequency is used. The complex of programs of processing includes a set of statistical procedures and special algorithms.

Final Processing and Preparation of Files of the Data on a Line for Interpretation. After initial data processing files such as "*.DAT" are formed, where all work registered on a line from one of a component of a field, in frequency or time domain is collected. At the performance of field research, the part of work (for example, at the increased level of noise) is repeated, on separate intervals of lines control measurements are carried out, there are parts of a site on which qualitative registration of a field is impossible (nearby an electrified railway, an industrial zone etc.), there are infringements of work of station, failures of synchronization, a mistake of the operator and other not regular situations which lead to a reduction of quality in registration.

In this connection, before the beginning of interpretation it is necessary to execute an estimation of quality of measurements on a site, to reject sounding of poor quality, to get an average from repeated soundings if they are equivalent in quality.

Extra Information That Maybe Derived From IP. IP does not necessarily aim quantitative information relating to the structure, but it produces qualitative results, which are direct detection of oil by using the phase component. Geophysical structure can be deduced from;

Ex(f) **(5)**

∂ **Bz (f) /** ∂ **t**

of FEM components or from decay curves of transient fields for low frequencies

Ex(f=0;t) **(6)**

∂ **Bz (f=0;t) /** ∂ **t** **(7)**

The last way is to utilize DC part of the signal to measure resistivity R as a function of distance,

R(x,y:f=0) = V(x,y:f=0)/ I(x,y:f=0) **(8)**

But the commercial approach is to use only the first step to set up frequency soundings of the resistivities and the phase.

ρ **(x,y;f)= ABS (**ρ **(x,y;f)). Exp (-i**φ **)** **(9)**

In this approach absolute value of resistivity and phase is plotted for interpretation.

Understanding of Complex Resistivity. The phase and imaginary values of the resistivity are mostly created by displacement currents. Therefore φ represents the qualitative component of the property (target reservoir). ABS (ρ), absolute resistivity (or real component of ρ) is created dominantly by conduction currents. Therefore ρ represents quantitative portion of the property (target). In summary, structural map (tectonic) could accurately be derived by ρ, resistivity, and type of fillings in pores or in cavities, or in fracture zones could be derived from φ, phase. However, in many cases, if ρ, resistivity is high, also φ, phase is high (Figures 9, 10, and 11).

INTERPRETATION

Estimated parameters are apparent phase and apparent resistivity.

a. Apparent resistivity lies between 1 to 10 ohm.m maximum for the frequency which approximately coincides with the reservoir depth. There is a resistivity increase adjacent to Khaviz Mountain, on the SE and on the northern portion of the field which may be caused by existence of a stiff limestone cap rock of Gachsaran. However, elongations of high resistivity anomalies are in accordance with general geologic and topographic strike direction. There is low resistivity exposure on the western and south western parts of the field over the Agha Jari sandstone, which is situated on low altitude zone. Horizontal resistivity variation seems to have no relation with reservoir characteristics if it is compared with the locations of productive and dry wells. However, most dry wells take place on conductive zones. There is no dry well on the resistive portion of the field. It appears that chance of catching a productive well on the conductive zone is 50%. Productive zone usually takes place on or adjacent sides of the resistive anomalies. Higher resistivity could be caused mostly from existence of cap rock rather than resistive oil reservoir. A Resistivity high does not only generate from higher resistivity of an oil reservoir but cap rock as well. Therefore, a resistivity map by itself is not a reliable way to delineate the location of drills for oil.

b. Apparent phase values lie between -12 to +10 degrees. Anomalies are dipolar in form, in which a positive anomaly in the middle is associated with two negatives on the flanks, as expected.

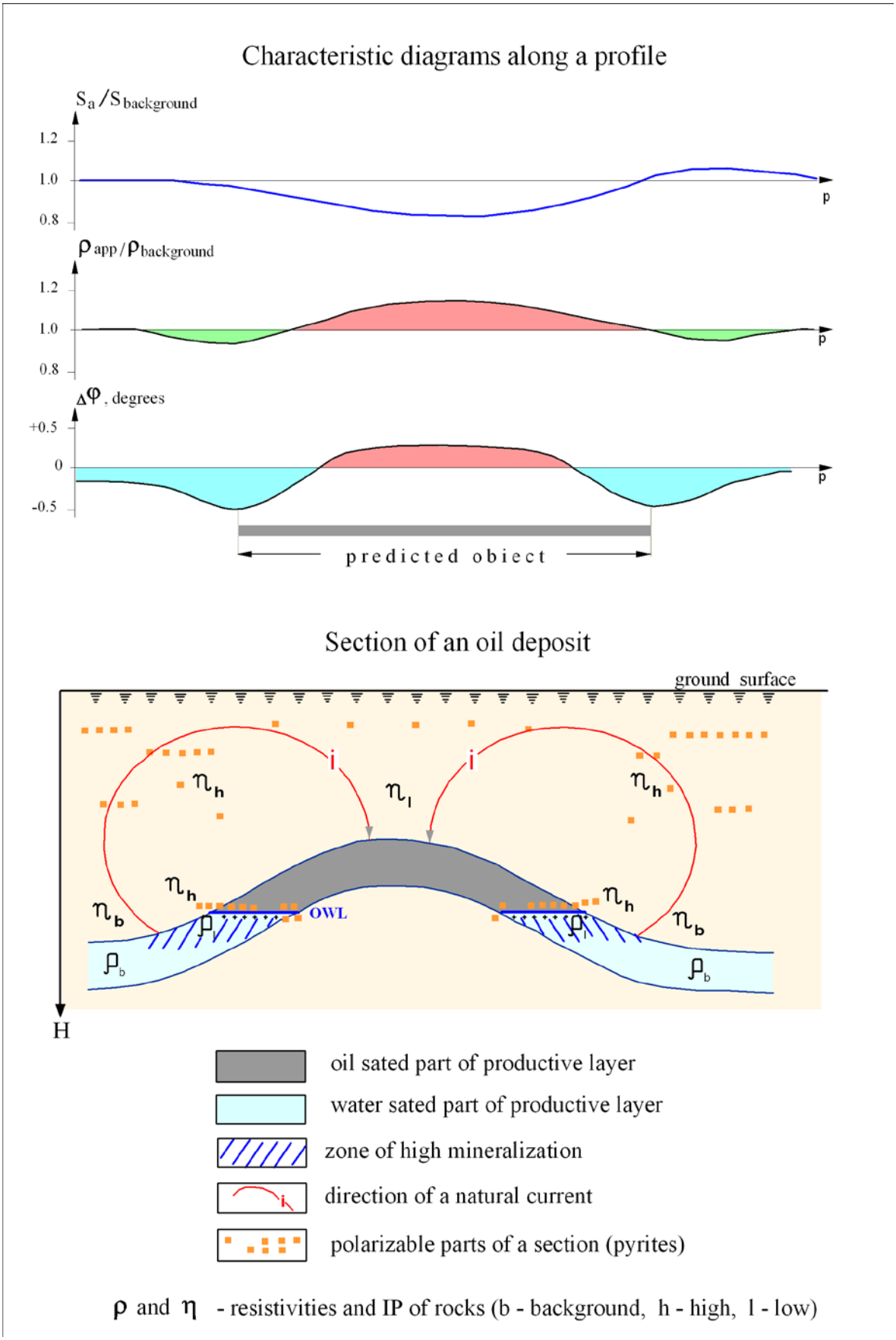

Figure 9. A typical anomaly on a possible oil reservoir

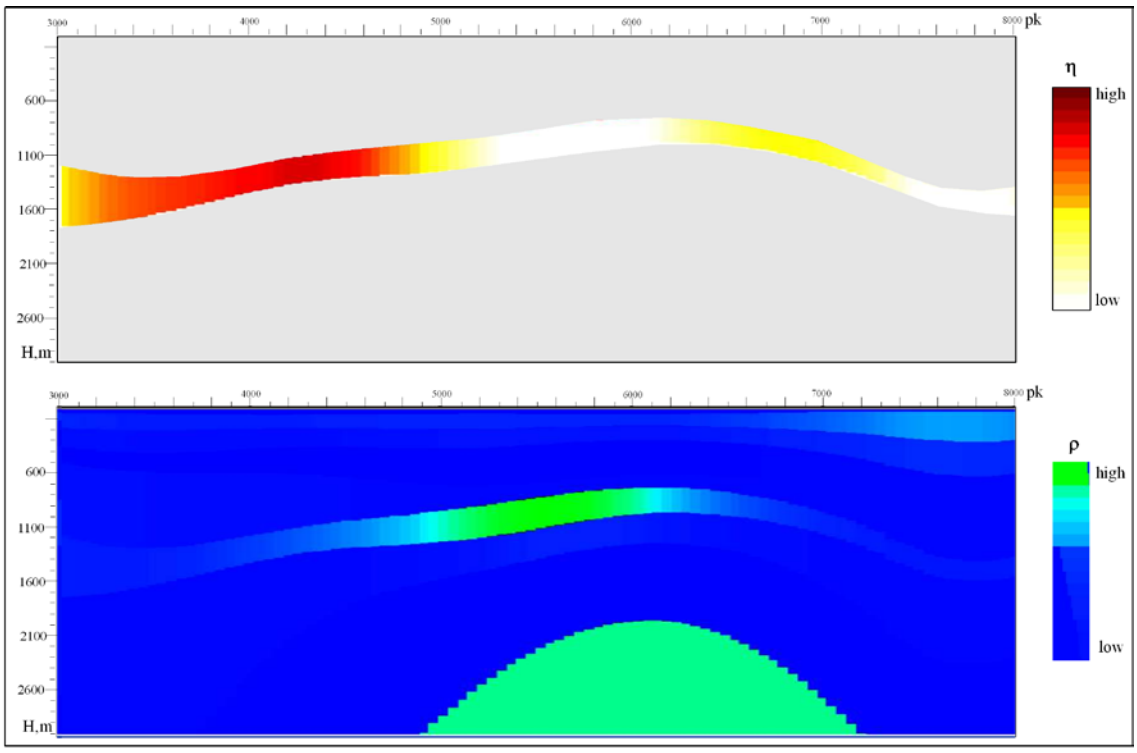

Figure 10. A theoretically expected phase anomaly over a productive reservoir

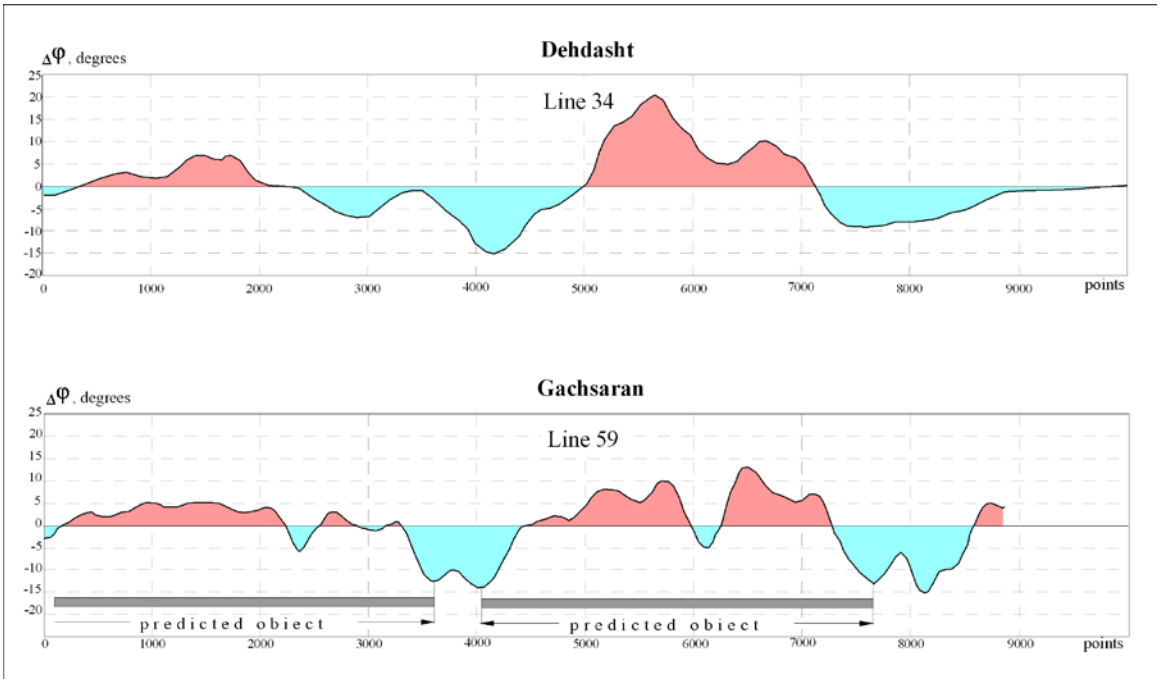

Figure 11. Phase section correlation between Gachsaran and Dehdasht fields

Widths of negative troughs are about 1 to 1.25 kilometers and positive rise in the middle is about 1.5 to 2.5 kilometers. Extensions of anomalies are in N45W as surface manifestations of geology and topographic highs. There are 31 wells superimposed on the phase map. 18 of them, which had already proven to be producing oil, coincide with higher phase anomalies (G39, G38, G37, G21, G26, G22, G27, G30, G29, G28, G32, G33, G34, G35, G31, G36 and G44). However, 8 of them are also on the anomaly zone but dry (G6, G16, G20, G15, G14, G2, G10, G11), 5 are off side of the anomaly zone and they are dry as expected (G9,

G1, G3, G4, G5). One is outside of the anomaly zone but has oil (G23). However, this location takes place on the extrapolated region of the negative anomaly. So, the performance ratio is 73% because 22 out of 30 are consistent with polarization interpretation. It means that 7 out 10 wells will hit the oil target directly by using electrolytic polarization technique of oscillating long line EM+ IP method.

Benefits Of HRES-IP Method At Gachsaran Production Field

Actual names of the operation at Gachsaran are FEM and FIP (frequency domain electromagnetic and frequency domain induced polarization).

1. Therefore, by using the FEM, we were able to determine the structure, (Quantitative).

2. We were also able to determine constituents of matters in pores, (Qualitative).

3. Measurements were converted to be in complex domain of apparent resistivity.

4. Complex resistivity was presented in two components, such as absolute resistivity and phase.

5. Using the absolute apparent resistivity; we undoubtly found lateral discontinuities, such as anticlines and synclines axis.

Confidence of determination is not less than 95%, if there is not any obscuring conductive overburden, such as ground water saturated Quaternary alluvial deposits or the Agha Jari sandstone. In such unfavorable places, confidence reduces down to 10% if alluvium overlaps the sandstone where the layers are fully saturated. If sandstone lays on the surface by itself, reliability is about 65%. If there is a resistive overburden, such as evaporates of Gachsaran formation, reliance is not less that 95%.

Therefore, this technique is perfect to enlighten “structural geophysics” beneath a resistive overburden.

6. According to our manual 2D modeling of abs(ρ), we constructed a 2D modeling which is complementary to the structural geology given before.

7. In our final interpretation, it is clear that rather recent formations, namely Agha Jari(shown in brown) and Mishan (shown in violate), consistently take place on N450 W extension of syncline axis, so does Holocene alluvial.

8. In contrast, high resistive and high velocity evaporates, consistently lay out the anticline axis. Determination capability of an anticline is much higher than synclines, because of screening or saturation effect of higher groundwater saturation along the synclines.

9. So, EM and IP techniques are superior to seismic techniques at especially sites where surface is covered by high velocity and high resistivity rocks. This is true, if such disconformities take place in an intermediate layer in the stratum. So this technique is well capable of collecting information beneath a problematic layer which acts as a seismically shielding layer.

10. Long line source gradient measurement used in the field site is very useful for mapping surface and subsurface geophysical structures as well as assisting to catch the continuation of the hidden geology.

11. If a resistive layer such as evaporates lies on the surface, penetration depth is certainly deeper than 2.5 to 4 kilometers.

12. Groundwater’s layer thickness and limits of highly saturated regions are easily recognized as a screening layer at shallow depths, which is represented by a low absolute resistivity (shown in dark green on sections), and high phase (shown in a reddish color in sections). Such areas are confronted especially on the northern extension of Khaviz Mountain as well as northern part of Gachsaran Town. Therefore, complex resistivity is a powerful tool for detecting groundwater existence.

Findings from 2D Interpretation

1. Structural geophysics was constructed with higher certainty. We determined a few anticlines extending in approximately N45W direction, along the profiles whose length is about 14 kilometers. Wavelengths or widths from crest to crest are about 2.5 to 4.5 kilometers. Geophysical locations of anticline axes are verified by geological observations. In addition, there is some degree of correlation between seismically found anticline crest and electrically found one as well. In addition, no disagreement was observed between seismic and electromagnetic anticlines. This could be seen on superimposed reconstructed anomalies.
2. Syncline axis does not necessarily take place at the mid point of two crests. Syncline axes closely approach the eastern part of each anticline.

Phase Anomalies

1. Positive phase anomalies appear on western part of Khaviz Mountain with magnitudes varying between 20 and 25 degrees. Shape is bi-polar as expected. Anomaly border is limited with Agha Jari and Mishan. Outside of this anomaly, there also exists an extension of this anomaly on the western side over the same geological formations. However, the phase is rather smaller (about 10 degrees) there.
2. An interesting new target is on the northern portion of the field site. The phase anomaly appears on Agha Jari and Mishan as we expected. However, although the feature of anomaly is the same, its amplitude is negative. Therefore, our interpretation of this was that it shifted downward because of some surface variations in resistivity.
3. In summary, possible prospect could be taking place over an anticline axis which has a grater phase anomaly in the order of 15 degrees.
4. This 2D manual interpretation of HRES-IP and its correlation with the seismicity and geology of the region indicate that the performed drills are located on right places.

CONCLUSION AND DISCUSSIONS

Topographic altitude of Khaviz anticline (prospect) axis is about 1600 meters at maximum, which dips beneath the overburden on the south, near by Khaydarabad River. This river bed itself is a left lateral strike slip fault, but trust faults which may have a vertical offset of 1 km take place on the western (Gachsaran) and on the eastern sides of the Khaviz, as known from geological and gravitational studies. Nevertheless, the seismic reflection technique which was empoyed in the field had a very weak performance because of the screening effect of the surface evaporates which are observed on the very rocky foothills.

Oil-water contact depth varies from 2.0 kilometers to 2.4 kilometers, which are estimated from drills. Typical trap is in the form of anticline - hydrodynamic type with an approximate width of 8 and a length of 15 kilometers.

Horizontal resistivity variation seems to have no relation with reservoir characteristics. Most dry wells take place on conductive zone. Productive zones usually take place on or adjacent sides of the resistive anomalies. Higher resistivity could have resulted mostly from the existence of cap rock rather than a resistive oil reservoir. The receptivity map by itself is not a reliable way to delineate location of drills for oil.

Apparent phase values lies between -12 to +10 degrees. Phase anomalies are dipolar in form, in which a positive anomaly in the middle is associated with two negatives on the flanks, as expected. The IP phase technique was experienced to be successful.

ACKNOWLEDGEMENTS

We thank NIOC who let us publish this scientific material and we also thank Geoneftagas for compiled and interpreted field data, we extend our appreciation for NIOC geophysicist collogues who assisted to draw figures and put a great effort in the interpretation.

MANTLE-DERIVED OIL AND GAS OF THEKURA RIFT (AZERBAIJAN)

Galant Y.

P.O.Box 164, Yokneam-Moshava, 20600, ISRAEL; E-mail – bakinez1@mail.ru

Abstract: Rift structures come into interest because of about 80% of the world's oil and gas resources extracted from them. Rift structures are the most important geotectonic elements as a fluids channel from mantle to the surface of Earth. In the Kura rift several oil reserves exist that are connected with magmatic rocks. The roof of the mantle is placed at about 20 km depth. Volcanic rocks are mainly in the forms of basalts and andesite-basalts. The forming period of these rifts is the Upper Jurasic–Upper Cretaseous. For an understanding of the sources of hydrocarbonaceous fluids, the following structures have been analyzed for basalts: Muradhanly, Zardob, Duzdag, Mil, Mamedtepe, Middlemugan, Jarli, Sor-Sor. 139 samples of basalts, andesite-basalts, and tuffs have been selected and 695 analyses have been executed. Average content of components H_2, H_2O, CO, CO_2, CH_4 and Sum (ml/gr of rocks) is as follows respectively: 0.62, 22.12, 8.08, 0.29, 0.006 and 31.56 for basalts; 0.309, 22.597, 13.469, 1.93, 0.011 and 40.589 for andesite-basalts; for 4.66, 18.6, 15.71, 0.5, 0.048, and 35.3 tuffs. According to the dominant components, fluid mixtures have been assignated as the three types of gas-geochemical structures in the Earth's crust below the Kura rift: C- structure, H-structure, C-H-structure. According to known models of fluid degassation (Letnikov and Komarov, 1980; Letnikov, 2003), they were considered to be the enrichment by hydrogen of the upper-mantle (H-structure) and the enrichment by carbon of the middle mantle (C-structure). Fluids that saturate mantle can introduce a certain budget of hydrocarbon in the process of oil and gas fields' formation in the Kura rift.

Key words: fluids, basalt, H-C-structures.

1. INTRODUCTION

According to geological-statistical data, about 80% of world's oil and gas resources which have been investigated and extracted are concentrated in rift class oil-gas bearing basins. The rift itself is still forming because the intrusion of mantle diapir possesses a significant amount of energy. Rift structures are the most important geotectonic elements of the Earth's crust in the continents as well as in the oceans. As disjunctive dislocations of different ages, mainly of rectangular forms, these structures are widespread all over the globe. In places of their intersections, disjunctive knots structured in a complicated manner occur; these knots are the zones of increased permeability of the Earth's crust. For example, fluids flow from the middle Pacific Ocean rift is estimated as 1.6 to 3.7*10*8 m^3/year (Beskrovny, 1985). Values of methane in the mantle can approximately be estimated as 4*10*24 m^3.

Oil and gas provinces are associated with rift structures all over the world. In epi-, intro-, and exocontinental-oceanic rift and paleorift systems, the sedimentary basins contain 80 percent of the world reserves of economically recoverable oil and natural gas. At the present time fluid outgassing of the Earth is considered to be playing a significant role at a lot of geological processes. Besides different geological appearances, fluid streams form oil fields. Studying the hydrocarbon flows in new rift zones of the oceans shows that these are juvenile streams from the mantle. At the present time there are existing models showing that hydrogen-carbons which have developed inside the core of the Earth flows through the mantle into the lithosphere, and they form hydrocarbon accumulations (Letnikov, 2002). The process of Earth's degassation is considered to have permanently existed for 4.5 billion years. The main direction of degassation can use the riftogenic structures and the depth faults reaching Earth's core (Marakushev, 2002). Riftogenic structures are one of the main

elements of the Earth (Figure 1). The geochemical aspect of degassation is not known well, although degassation of the mantle may be investing a huge budget of hydrocarbon fluids and many geological epochs can be perniciously forming oil-gas deposits. A strong interest caused the study of the Kura rift (Figure 2) where oil deposits are discovered associated with basalts. The roof of the mantle is placed at about 20 km depth. Volcanic rocks are mainly basalts and andesite-basalts.

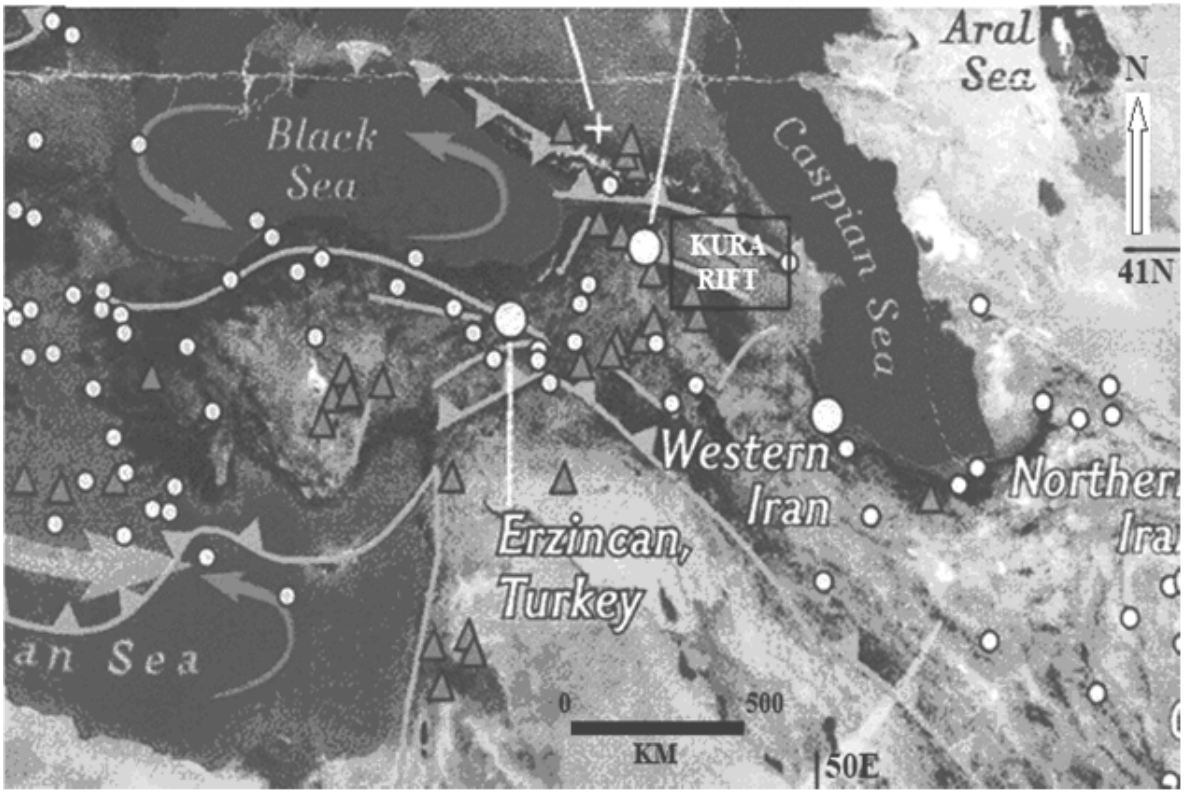

Figure 1. Rifts of Meditteranean Sea (Fragment of Map: Phisicial Earth). Produced by National Geographic Maps, Washington D.C. May 1998

2. GEOLOGY

The formation period of the rift is the Upper Jurassic- Upper Cretaceous. Kura rift is situated between the Greater Caucasus to the south and the Lesser Caucasus to the north in the area of Tran Caucasian microcontinent that was a part of the Tethys Ocean until the Oligocene times (Khain et al., 1991). The Kura basin comprises several sub-basins of different origin, with up to 15 km of sediment separated by areas with less sediment (Marie-Fransoise Brunet et al., 2003). According to data, the Saalti superdeep well (8324 m) located on the North-West–South-East stretching of Talesh-Vandam mantle diapir (gravity anomaly is possible) section of the well is several kilometers of Mesozoic sediments from late Cretaceous until middle Miocene times (Shihalibeily et al., 1998; Ali-Zade et al., 1999). Several super-well volcanic complexes are recognized on the section Saalti, the two most important of which are widespread:

Lower-Middle Jurassic volcano-sedimentary series of at least 4784 m, with basalts, andesites, dolerites, diorites (possibly covering nearly the whole Lower Kura basement).

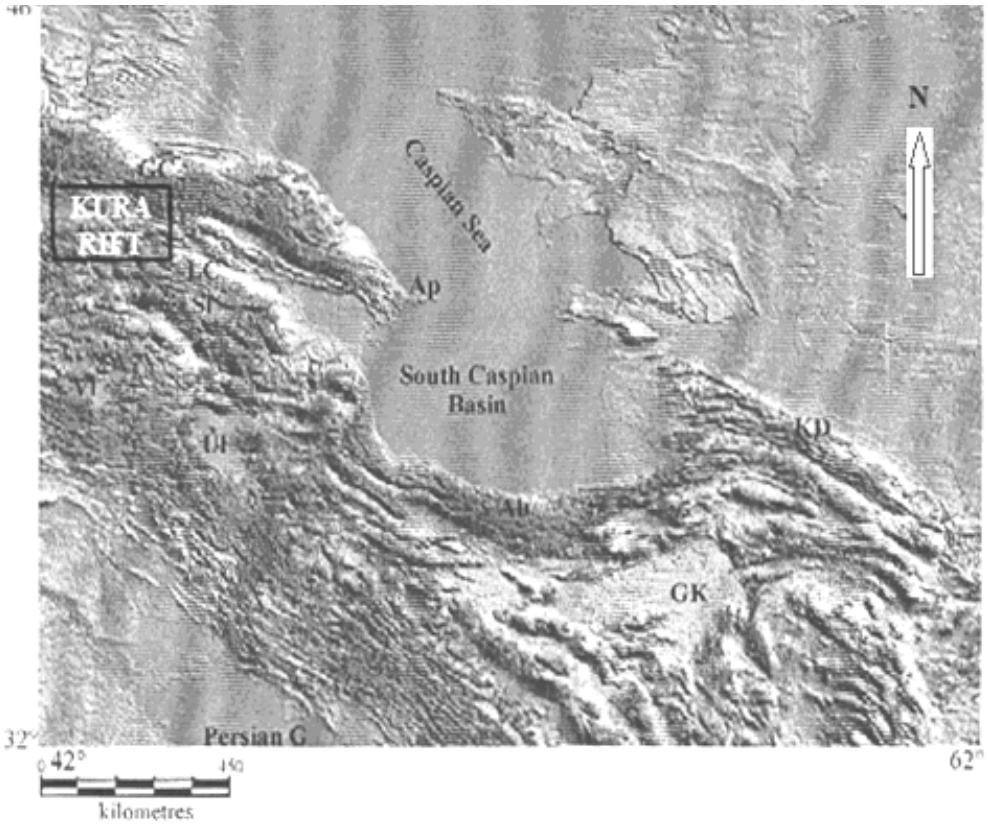

Figure 2. Location of the Kura Rift . (Brunet *et al*., 2003)

390 m of late Jurassic and 320 m of early Cretaceous carbonates with basalts sills (Ali-Zade et al., 1999).

3. METHODS

8 areas were involved in the analysis: 1) Murad-Hanli, 2) Zardob, 3) Duzdag, 4) Mill, 5) Mamedtene, 6) Srednemugansky, 7) Djarli, 8) Sor-sor; and 30 wells, from which 139 samples of basalts, andesite-basalt, and tuffs were selected. 5 components were defined, and accordingly 695 analyses were performed in the Institute of Earth's Crust – Siberian branch of Academy of Science, Russia. Rock samples were heated, and outgassing fluids were analyzed on the chromatograph.

4. DISCUSSION

The results of the analysis are given in Table (1)1, Table (2), and in Figure (3A) and Figure (3B). As it can be observed from the tables and from the graphs (Figures 3A, 3B), the contents of CH_4, CO, $H_2+CO+CH_4$ increase along the line of examined rocks as: basalts→andesite - basalts→tuffs. Maximum contents of the components of H_2O, CO_2, Sum, H_2O+CO_2 are present in the andesite basalts. Contents of H_2 consequently decrease along the line of tuff→basalt→andesit-basalt. The relationships of oxidized fluids were examined for the rocks and the reconstructed $K=H_2O+CO_2/H_2+CO+CH_4$ decreases in the order of basalts→andesit - basalts→tuffs (Figure 3A). Commonly total gases also fall in this way (basalt→andesit-basalt→tuffs). H_2O+CO_2 makes up 72.6% of the total oxidized fluids, and, consequently, total reconstructed gases ($H_2+CO+CH_4$) are 27.4%. Furthermore, the total oxidized gases comprise 66.0% of the total in the andesite-basalts, and reconstructed to 34.0%. In tuffs the total oxidized gases is 54.0%, and reconstructed to 46.0% (Figure 3B).

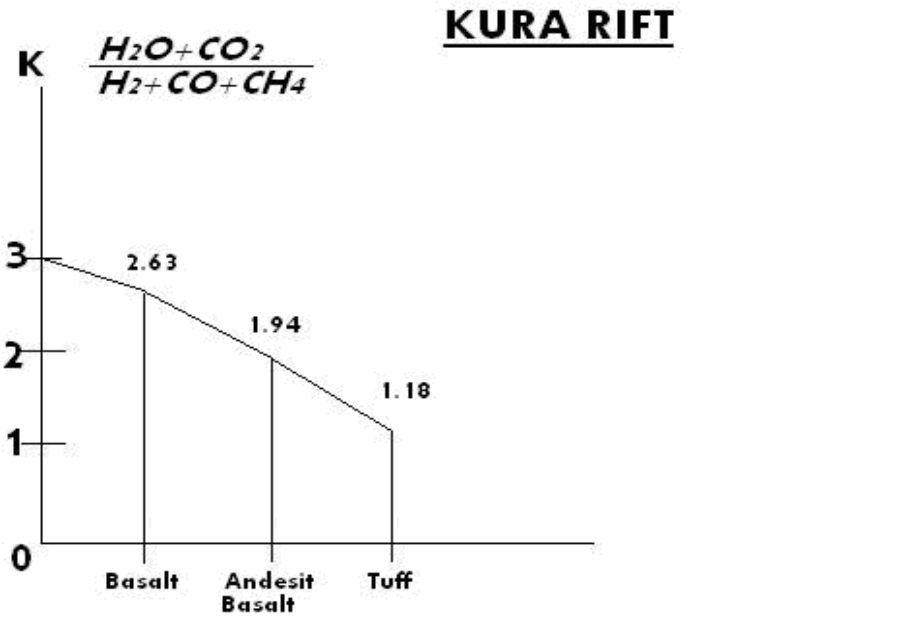

Figure 3 A. Variation of the Coefficient of oxidation of fluids in rocks in the Kura Rift

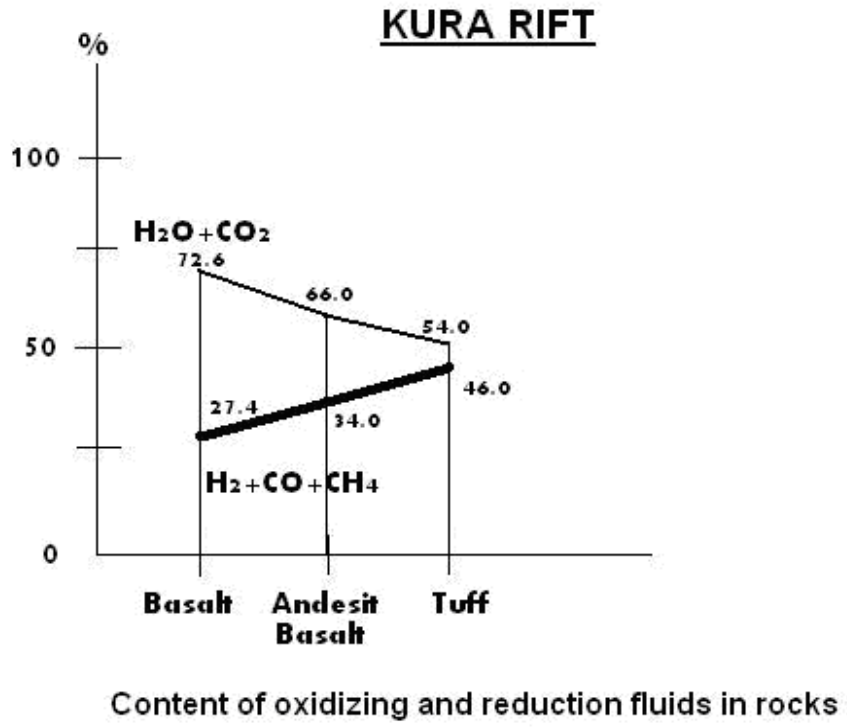

Figure 3 B. Content of oxidizing and reduction fluids in rocks in the Kura Rift

Table 1. Fluids of Magmatic rocks

Component mg/gr of rocks (from to average) / Rocks Range of fluids	H_2O	H_2O	CO	CO_2	CH_4	SUM
Basalt $H_2O>CO>H_2>CO_2>CH_4$	2.5-0.11 0.62	76.0-1.5 22.12	59.7-0.71 8.08	1.8-0.03 0.29	0.05-0.001 0.006	96.5-2.58 31.56
Andesit Basalt $H_2O>CO>CO_2>H_2>CH_4$	1.6-0.11 0.309	76.7-2.3 22.597	52.4-0.34 13.469	15-0.03 1.93	0.04-0.001 0.011	95-4.2 40.589
Tuff $H_2O>CO>H_2>CO_2>CH_4$	0.12-1.9 4.66	36.4-3.6 18.6	39.6-1.2 15.71	3.05-0.07 0.5	0.12-0.02 0.048	49.03-12.07 35.3

Table 2. Oxidizing and reduction fluids of magmatic rocks

Component mg/gr of rocks (from to average) / Rocks Range of fluids	$H_2+CO+CH_4$	H_2O+CO_2
Basalt $H_20>CO>H_2>CO_2>CH_4$	60.96-0.71 8.7	74.68-1.6 22.902
Andesit Basalt $H_20>CO>CO_2>H_2>CH_4$	52.4-0.34 13.788	76.86-2.68 26.801
Tuff $H_2O>CO>H_2>CO_2>CH_4$	39.75-1.2 126.206	36.47-4.12 19.079

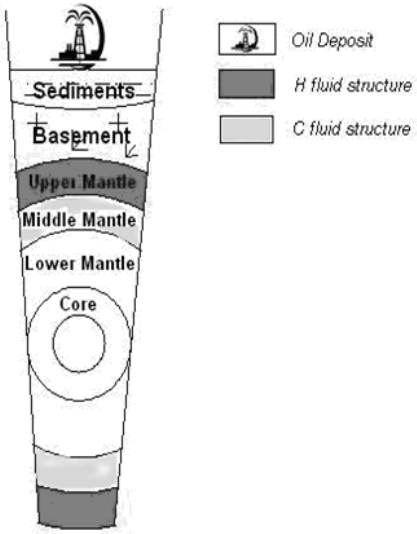

Figure 4. Schematic section for the Kura Rift as the case for the fluid saturation in the mantle

The results of the analysis show in basalts the range of fluids classified as $H_2O>CO>H_2>CO_2>CH_4$ with the content of components sequentially as (sum of medium/ml/gr of rocks) – 22.12; 8.08; 0.62; 0.29; 0.006; in andesite-basalts the range of fluids classified as: $H_2O>CO>CO_2>H_2>CH_4$ with the content of components sequentially as (sum of medium/ml/gr of rocks) 22.60; 13.47; 1.93; 0.309; 0.011; in tuffs the range of fluids being $H_2O>CO>H_2>CO_2>CH_4$, with the content of components sequentially as 18.6; 15.71; 4.66; 0.5; 0.048.

In general the analyses of prevalent fluids composition show that three types of geochemical structures can be assigned in the Earth crust of Kura rift: C-structure, H-structure, and C-H-structure (Figure 4). From 30 wells (sites of sampling): C-

structure is outlined in 5 wells (17%), H-structure in 20 wells (66%), and C-H structure in 5 wells (17%). To put it another way, the part of H-structure is placed 66%, and the part of C-structure with C-H structure 34%. What does it mean? According to known models of fluid degassation (Lethnikov, 2002), it could be considered enrichment by hydrogen of upper-mantle (H-structure), and by carbon of middle- mantle(C-structure). Most deep faults and zones of heightened permeability are characterized by carbon, which is the specific character of fluids of C-structures. The production of these structures are being hydrocarbons, and also carbonates, kimberlites, alkaline rocks, graphite.

H-structure is characterized by the prevailing of water in fluid composition that develops in the crust or in the upper mantle.

5. CONCLUSION

As it can be deduced from the above geological situation of the Kura rift, drawing nearer of the mantle diapir to the Earth's surface, the existence of range of different sequence faults, as well as geochemical conditions and the existence of saturation by hydrogen and carbon at the upper and middle mantle zones allow us to form an accurate understanding of the formation of oil deposits on account of degassation. Thus, migrating fluids could form deposits of oil associated with the basalts in the Kura rift.

ACKNOWLEDGMENTS

Author would like to express his gratitude to his family, Dayan, Yana and Sahar, Galant, Rivka for their help in designing the paper

REFERENCES.

Ali-Zade, A., Khain, V. and Ismail-Zade, A., 1999. The Saatly Ultra-Deep Well. The study of deep structure of the Kura intermountain depression according to the data of the drilling of the Saalty ultra-deep well SG-1. Naphta-Press, Baku, Azerbaijan.

Beskrovny, N.,1985. Inorganic origin of oil and gas. *Survey of VIEMS*, Moscow, Russia.

Brunet, M-F., Korotaev, M., Ershov, A., and Nikitin, A., 2003. The South Caspian Basin: a review of its evolution subsidence modeling. *Sedimentary Geology*, 156, 119-148.

Galant, Y., 2004. Hydrocarbon components of the Saalti superdeep well, *5-th International Symposium of Eastern Meditteranean Geology*, A.Chatzipetros, S.Pavlides, Aristotle University of Thessaloniki, Vol. 3, 1392-1393, Thessaloniki, Greece.

Galant, Y., 1988. On hydrocarbon outgasing from Barum massive of Somhit-Agdam zone of the Lesser Caucasus. *Lectures of the USSR Academy of Sciense, Academy of Sciense*, 301, №2, 434-435, Moscow, Russia.

Letnikov, F., 2002. The Degasation of the Earth as a global process of self-organization. Outgassing of the Earth: Geodynamics, Deep Fluids, Oil and Gas, A.Dmitrievsky, B.Valiaev, *Institute of problems of oil and gas*, 6-7, Moscow, Russia.

Letnikov, F., and Komarov, Y., 1980. Fluid regime of forming of mantle rocks. *Nauka*, Novosibirsk, Russia.

Marakushev, A., 2002. Geological consequence of the Earth`s core outgassing. Outgassing of the Earth: Geodynamics, Deep Fluids, Oil and Gas, A.Dmitrievsky, B.Valyaev, *Institute of problems of oil and gas*, 8-10, Moscow, Russia.

Shikalibeily, E.,Abdulaev, R., and Ali-Zade, A., 1988. Geological results of the super-deep well of Saalty. *Sovetskaya Geologya*, 11, 61-66.

RESOURCES, QUALITY AND ECONOMIC IMPORTANCE OF SOLID FOSSIL FUELS AND PEAT DEPOSITS IN TURKEY

İnaner H.[1], Coşar Y.Z.[2] and Nakoman E.[1]

[1]Dokuz Eylül University, Faculty of Engineering, Department of Geological Engineering, 35160 Buca, İzmir, Turkey, hulya.inaner@deu.edu.tr, eran.nakoman@deu.edu.tr
[2]General Directorate of Mineral Research and Exploration (MTA), Ankara

Abstract: As fossil fuel resources, hard coal, lignite, bituminous shale, asphaltite, peat, petrol and natural gas are found in Turkey. As domestic resources, they are important for energy production, domestic heating and for the industry. During investigations carried out by the General Directorate of Mineral Research and Exploration of Turkey, peat formations have been discovered within the boundaries of 19 provinces. Among the most important of these findings are Kayseri-Ambar, Hakkari-Yüksekova and Bolu-Yeniçağa peat formations. Kayseri-Ambar peat seam possesses 105 million tons of proven reserve on the received basis, Hakkari-Yüksekova peat seam 74,5 million tons of proven reserve again on the received basis, 18,8 million tons on the air dried basis. They display different chemical properties. It is necessary to continue investigations to determine Turkey's peat potential. Some peat seams that are being operated by the private sector with inappropriate methods are also used as plant soil. Peat lands burned, dried or used as building sites present another problem. A lot remains to be done in the way of new legislation and education to protect established peat lands. It is essential that work be commenced immediately in the way of inventory preparation, protection, discovery of new formations and making logical use of existing ones.

Keywords: Peat, reserve, chemical properties, conservation, Turkey

1. INTRODUCTION

Turkey possesses fossil fuel resources of hard coal, lignite, bituminous shale, asphaltite, peat, petrol and natural gas (Figures 1 & 2). Among these, the hard coal and lignite have the greatest importance in energy production and for the national economy. The hard coal reserve of Turkey is estimated to be 1.1 billion tonnes with a calorific value between 5650-7250 kcal/kg. Lignites occur in the Eocene, Oligocene, Miocene and Pliocene basins all around Turkey. The majority of Turkish lignite deposits are worked in open-pit mines with the total lignite coal reserve estimated to be around 8.9 billion tonnes as displayed in Table 1 (by 2006 estimates). Lignites are mined by TKİ (Turkish Coal Enterprises) at a rate between 60-65 million tonnes per year.

Because of their low calorific values, most of the lignites produced are used in the electrical power plants. Whilst the total capacity of hard coal based power plants is 300 MW, that of the lignite based ones is 5913 MW. The total reserve of the asphaltite deposits is estimated to be 82 million tonnes. Bituminous shales amount to a total reserve of approximately 1,641 million tonnes, but are not being utilized economically at present. Peat deposits are estimated to be in the order of 190 million tonnes, and are generally used only as plant soil. Among the above mentioned solid fossil fuels, lignite has the greatest importance and potential. Based on the reserve estimation data available at present, it is safe to say that Turkey has enough solid fossil fuel reserves to meet most of its energy needs for many years to come. Prospection and evaluation studies for peat and other solid fuels are continuing at present as raw materials for domestic energy sources both for now and for the future. Safe utilization of solid fuels both for people and for the environment is another study under way. We evaluate especially the peat resources of Turkey in this paper.

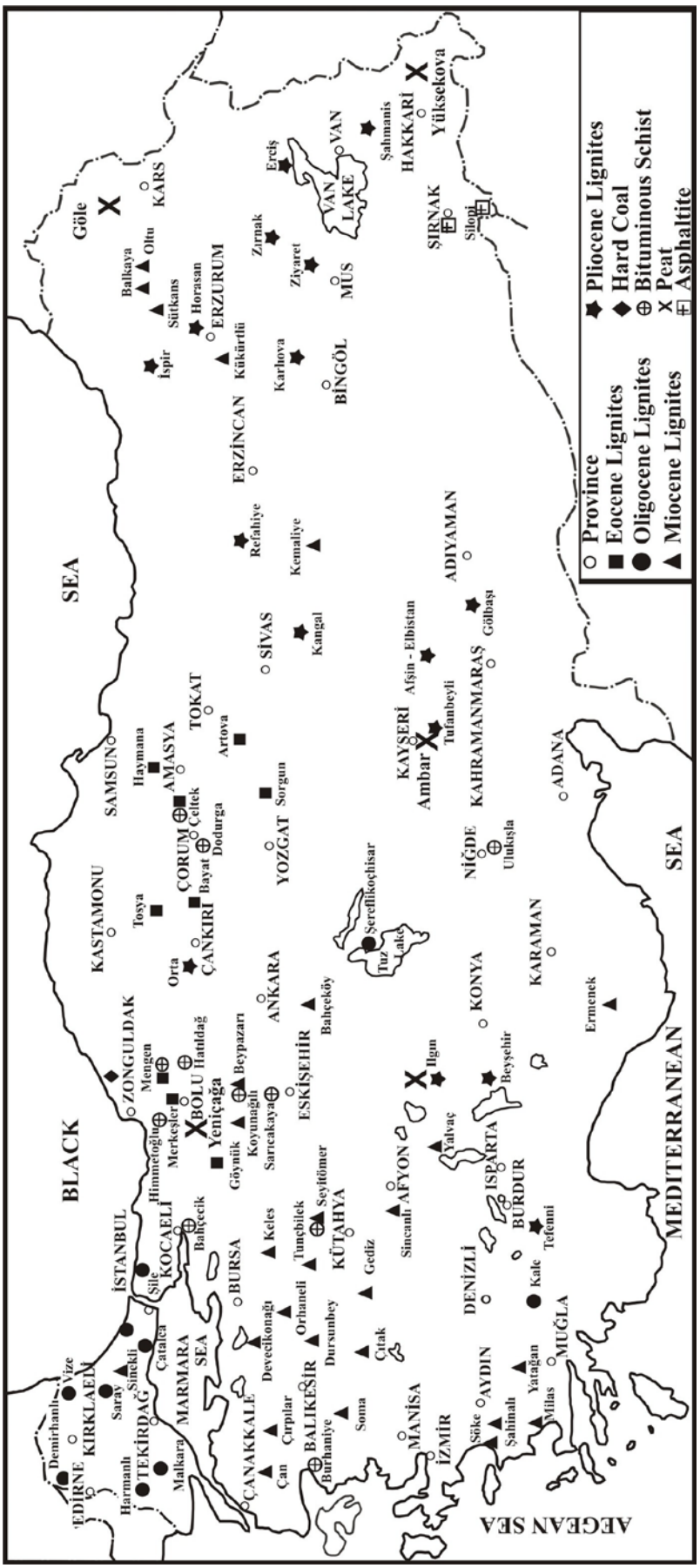

Figure 1. Solid fossil fuel deposits of Turkey

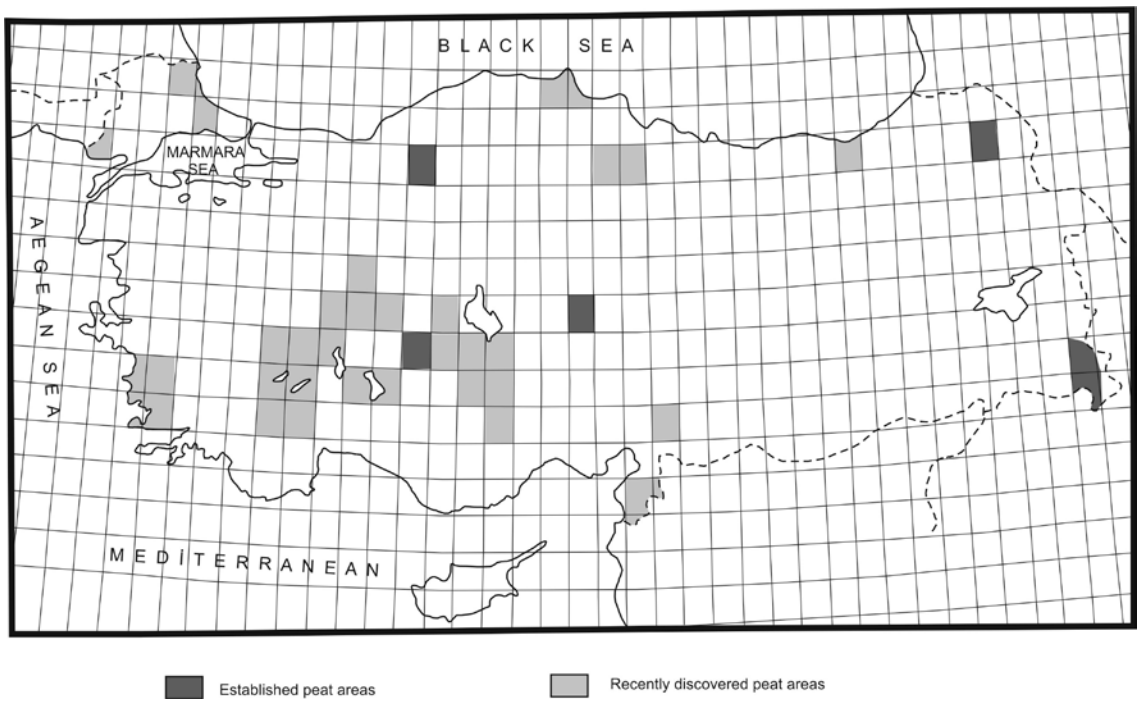

Figure 2. Location map of established and recently discovered peat areas of Turkey (Öz, 1994)

Because of their low calorific values, most of the lignites produced are used in the electrical power plants. Whilst the total capacity of hard coal based power plants is 300 MW, that of the lignite based ones is 5913 MW. The total reserve of the asphaltite deposits is estimated to be 82 million tonnes. Bituminous shales amount to a total reserve of approximately 1,641 million tonnes, but are not being utilized economically at present. Peat deposits are estimated to be in the order of 190 million tonnes, and are generally used only as plant soil. Among the above mentioned solid fossil fuels, lignite has the greatest importance and potential. Based on the reserve estimation data available at present, it is safe to say that Turkey has enough solid fossil fuel reserves to meet most of its energy needs for many years to come.. Prospection and evaluation studies for peat and other solid fuels are continuing at present as raw materials for domestic energy sources both for now and for the future. Safe utilization of solid fuels both for people and for the environment is another study under way. We evaluate especially the peat resources of Turkey in this paper.

Table 1. Solid Fossil Fuels of Turkey (2006 Energy Statistics)

Solid Fossil Fuels	Reserves (million tonnes)
Hard Coal	793
Lignite	8995
Bituminous shales	1641
Peat	190
Asphaltite	79

2. PEAT DEPOSITES OF TURKEY

Peat deposits are distributed in different parts of Turkey (Figure 2). To determine Turkey's peat potential in a short time, they have been categorized by MTA (General Directorate for Mineral Research and Exploration of Turkey) as 'established peat areas' and 'recently discovered peat areas' (Öz 1994). Established peat areas are located in Bolu, Kayseri, Hakkari, Konya and Kars provinces. Recently discovered peat area

are located in Afyon, Aksaray, Aydın, Burdur, Denizli, Edirne, Eskişehir, Hatay, Istanbul, Isparta, Kocaeli, Konya,

Table 2. List of established and recently discovered peat areas of Turkey (Öz, 1994).

	Province	*Peat Field*
Established	*Bolu*	Yeniçağa-Reşadiye Lake
	Hakkari	Yüksekova
	Kayseri	Ambar Village
	Konya	Ilgın-Çavuşçu Lake
	Kars	Göle
Recently discovered	*Afyon*	Bataklı Çayır- Değirmendere Çayırı
		Çay-Karamık Swamp
		Eber Lake
		Akşehir Lake
		Dinar Gökçeli
		Salda Lake
		Karataş Lake-Pınarbaşı Swamp
		Söğüt Swamp
	Aksaray	Esmakaya-Bezirci Bataklığı
		Obruk Lake
	Aydın	Söke-Avşarköyü-Azapgölü-Sazlıköy
	Burdur	Burdur Lake
		Söğüt (Manav Gölü)
	Denizli	Çardak-Kurugöl and Beylerik Lake
		Gölcük Village –Gölcük Lake
		Bayındır-Akgöl
		Işıklı Lake
		Gökgöl (Kocagöl)
		Acı Lake
	Edirne	Eynez Dalyan Lake
		Gala Lake
	Eskişehir	Çifteler
	Hatay	Amik Lake
	İstanbul	Silivri-Danamandıra Village
	Isparta	Hoyran Lake
		Eğridir Lake
		Kestel Lake
	Kocaeli	Sapanca Büyük Derbent
		Gökçeören Lake Swamp
	Kırklareli	Erikli Lake
		Mert Padina-Hamam-Saka-Lakes
	Konya	Altınekin (Zırvarık) Musalar Lake
		Cihanbeyli-Bolluk Lake
		Cumra Eski Hotamışgölü Sazlıdağ Bataklığı
		Ereğli Akgöl Savran Swamp
		Beyşehir Lake
		Yunak Akgöl Lake
	Kahraman maraş	Gavur Lake+Swamp
	Nevsehir	Acı Lake
		Sultan Sazlığı
	Samsun	Havza Ladik
		Bafra Kızılırmak Deltası
	Trabzon	Sürmene Ağaçbaşı Yaylası

Kahramanmaraş, Samsun and Trabzon provinces (Figure 2 & Table 2). Charactristics of some important peat deposits are given below.

2.1. Kayseri-Ambar peat deposit

Kayseri Ambar peat deposit is located in the west of Kayseri (Figure 3). Prospection studies in this area were started in 1966 with OTTO-GOLD and MTA cooperations. 56 boreholes were drilled for the determination of peat potential in the field. The distribution area is approximately 25 km^2. Tuff can be observed in two layers in the field surrounded by andesites and volcanic talus (Nakoman, 1998). Total proven reserve is 105 million tonnes. Average thıckness of the peat is 4, 66 m (Demirok, 1982). Chemical properties of the Kayseri Peat Deposit are given in Table 3.2.1. Kayseri-Ambar peat deposit

There are buildings over a big part of the peat deposit. It is necessary to protect the peat deposit from construction and other human activities to preserve the deposit for future generations.

2.2. Hakkari-Yüksekova peat deposit

This peat deposit is located in the south of Yüksekova village of Hakkari province (Figure 4). Peat distribution area is approxsimately 19 km^2. Prospection studies were carried out between 1968 and 1969. There are 61 drilled holes in this deposit. Proven reserve was calculated on original and air dried basis by MTA researchers as 74.507.800 and 18.846.875 tonnes respectively (Öz, 1994). Calorific value has reached 3000 kcal/kg on dried basis (Ünalan, 2003).

Table 3. Chemical properties of Kayseri-Ambar peat deposit (Demirok, 1982)

Analysis	**As Received Basis**	**Air Dried Basis**	**Dried Basis**
Moisture (%)	64.97	10.01	
Ash (%)	24.31	56.52	63.25
LCV (kcal/kg)		1453	

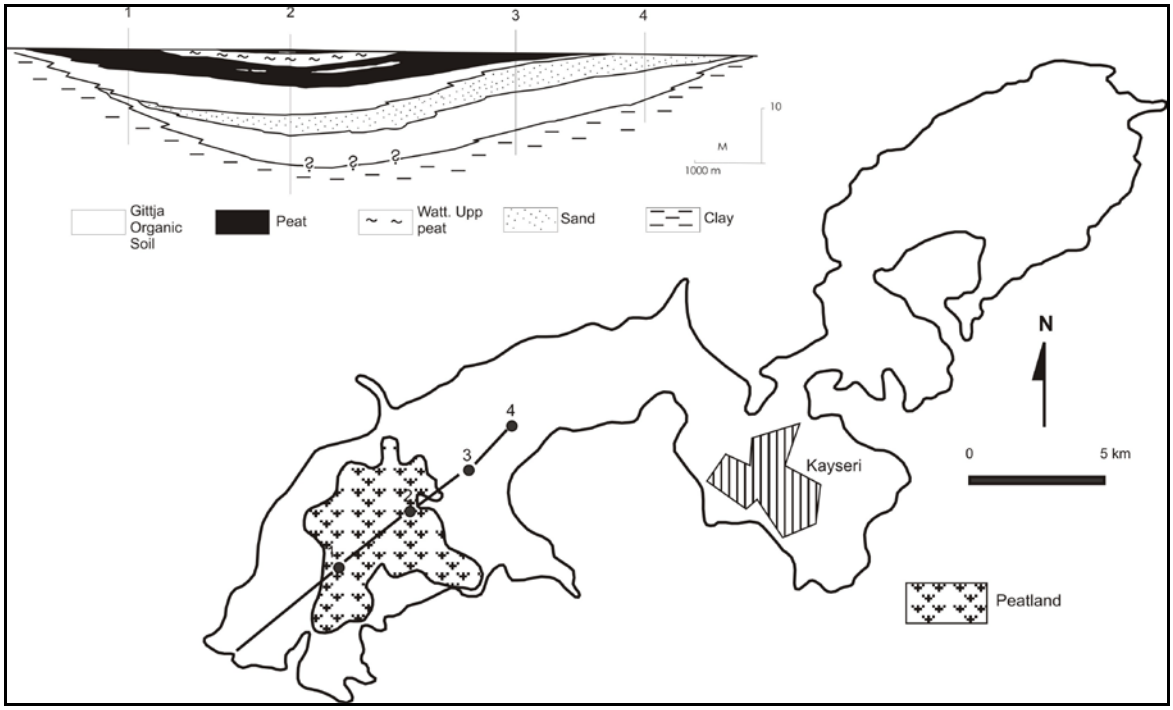

Figure 3. Map and section of Kayseri-Ambar peat deposit (Öz, 1994)

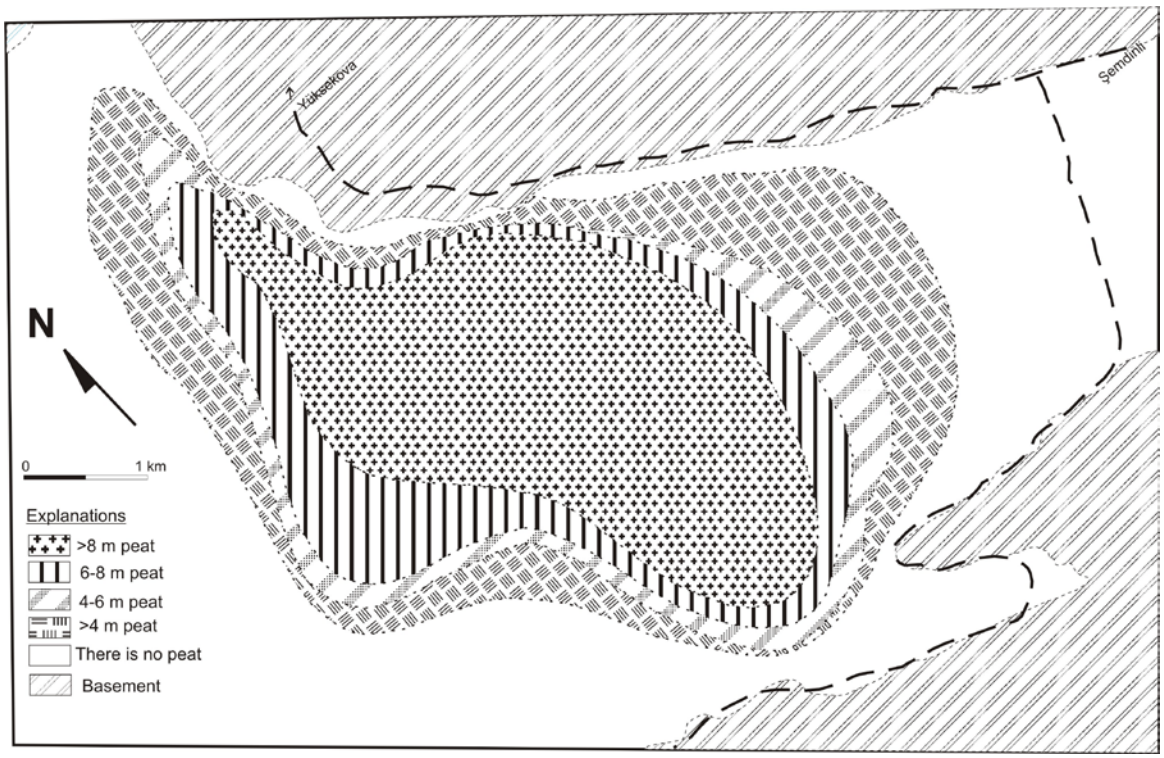

Figure 4. Map of Hakkari-Yüksekova peat deposit (Öz, 1994)

2.3. Bolu-Yeniçağa peat deposit

Bolu-Yeniçağa peat deposit is located in the south of Yeniçağa village in the Bolu province (Figure 5). Distribution area is 5 km^2 as the peat area, 2.5 km^2 of which is under water. Average thickness is between 0-15 m. There are six channels in the area. Peat has been mined as plant soil with unsuitable mining methods. This must change immediately if we want to preserve the peatland and the wild life on it. Chemical properties of peat deposit is given in Table 4.

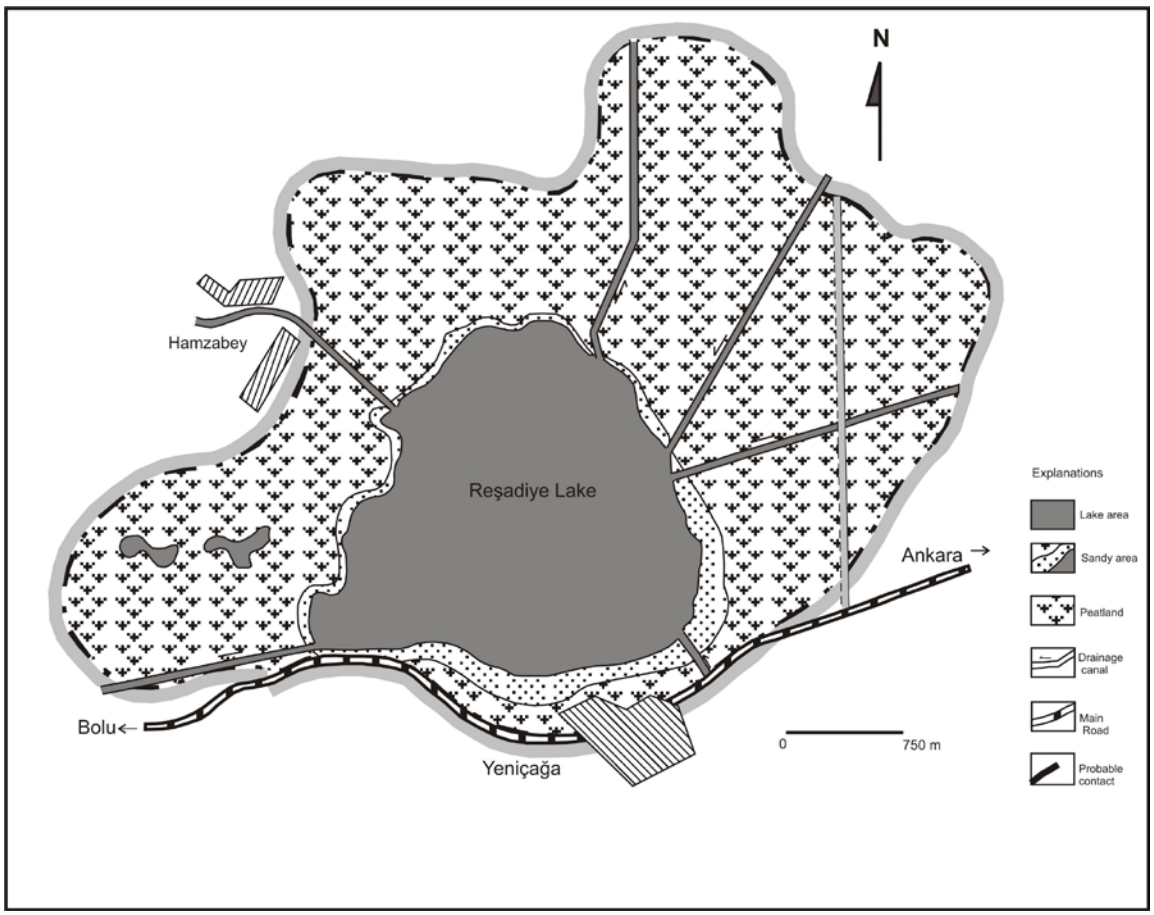

Figure 5. Map of Bolu-Eniçağa peat deposit (Öz, 1994)

Table 4 Chemical properties of Bolu-Yeniçağa peat deposit (Öz, 1994)

Analysis	As Received Basis	Air Dried Basis	Dried Basis
Moisture (%)	49.20	5.20	
Ash (%)	29.90	55.89	58.96
LCV (kcal/kg)	415	1294	1401
UCV (kcal/kg)	771	1441	1520

Kavuşan & Serdaroğlu (1999) evaluated the Yeniçağa peat samples to be "ligneous" and "per-hydrous peat" according to the Van Krevelen and Mott classifications, respectively.

2.4. Kars-Göle peat deposit

Peat deposit is located on the south of the town of Göle in the Kars province. Distrubution area is approximately 150-200 km^2. According to as received and air dried basis analysis results it has a 6,5-7,5 ph watered environment and 80% original moisture (Öz, 1994). Thickness could not be measured. Although new and detailed studies are required, results of the prelimanary analysis and the distrubition of the deposit make it feasible to consider the deposit for energy production and agricultural use (Table 5).

Table 5. Chemical properties of Kars-Göle Peat Deposit (Öz, 1994)

Analysis	As Received Basis	Air Dried Basis	Dried Basis
Moisture (%)	34.28	8.00	
Ash (%)	48.67	68.12	74.05
LCV (kcal/kg)	432	844	970
UCV (kcal/kg)	688	963	1047

2.5. Konya-Ilgın-Çavuşçu peat deposit 14

Konya-Ilgın-Çavuşçu peat deposit is a small occurrence located 5 km to the south of the town of Ilgın in the Konya province. General Directorate of State Hydraulic Works (DSİ) has built a drainage system and dried the swamp area. Peats remained above water level

and is burned by the villagers. It can neither be used as agricultural land because of the high amounts of clay it contains. Educating the villagers to make them understand why this peat land must be protected and preserved still remains a problem to overcome. Water level was controlled by DSİ. There is lignite under the lake water but it has not been evaluated yet (Öz, 1994). Chemical properties of the peat deposit is given in Table 6.

Table 6. Chemical properties of Konya-Ilgın-Çavuşçu peat deposit (Öz, 1994)

Analysis	As Received Basis	Air Dried Basis	Dried Basis
Moisture (%)	49.20	5.20	
Ash (%)	29.90	55.89	58.96
LCV (kcal/kg)	415	1298	1401
UCV (kcal/kg)	771	1441	1520

3. RESULTS

Peat deposits have been found in different parts of Turkey and are estimated to be in the order of 190 million tonnes, and are generally used only as plant soil. New explorations and evaluations are necessary for determining their economic values and chemical properties. It is necessary to prepare a peat inventory. Some private companies have been mining peat deposits; however, mining methods must be controlled better for a more effective use. It is necessary to take legal precautions to preserve the peat deposits. We must prevent wrong use and the destruction of peat deposits by villagers and mine owners. Also DSİ has been causing damage to peatlands by builging drenage channels and drying these lands. This must be stopped by governmental action. The most important thing is also to grow better educated people who are conscious of their value and importance for the country.

REFERENCES

Demirok, Y. 1982 Kayseri-Ambar Köyü Civarı Turba (Gitya-Linyit) Yatağına ait ön değerlendirme raporu. *MTA Fizibilite Dairesi Enerji Hammaddeleri Servisi* Der. No. 7214 p. 6. (unpublished)

Energy Statistics, 2006. Dünya ve Türkiye Energy İstatistikleri *Dünya Energy KonseyiTürk Milli Komitesi*. p. 263.

Kavuşan, G. ;& Serdaroğlu, A. 1999. The physical and chemical properties of Yeniçağa-peat deposit, Bolu-Turkey. *3rd European Coal Conference, 1997 Publication* pp. 301-310.

Nakoman, E. 1998. Kömür. *Dokuz Eylül Üniversitesi Mühendislik Fakültesi Yayını*, p. 348.

Ünalan, G. 2003. General evaluation of Energy resources of Turkey. Jeoloji Mühendisliği Dergisi *Geological Engineering Journal*, Volume 27, Number 1, pp.17-41

Öz, D. 1994. Turba ve turbiyerlerin genel tanıtımı, etüdü ve Türkiye turbiyerlerinin coğrafik lokaliteleri. *Maden Tetkik ve Arama Genel Müdürlüğü (MTA), Enerji Hammadde Etüt ve Arama Dairesi Başkanlığı*, Derleme no: 9845, p. 70. (unpublished)

(This page is left blank intentionally.)

GEOLOGICAL HERITAGE, GEOPARKS, GEOTOURISM AND TURKEY

İnaner H.

Dokuz Eylül University, Faculty of Engineering, Department of Geological Engineering, Buca, İzmir, Turkey. hulya.inaner@deu.edu.tr

Abstract: Geological heritage, geoparks and geotourism are new but very important concepts in Turkey, which is a very fortunate country with respect to cultural as well as natural beauties, and geomorphologically it is a bridge between Asia and Europe, and also at the crossroads between cultures. Although the first publication on the geological heritage was made in the journal of Geosphere and Man (Yeryuvarı ve İnsan) during 1970s in Turkey, we have not been very effective in protecting and advertising our geological heritage. Voids in our laws and other factors would have not allowed this. Some of the heritages have been preserved in the MTA Natural History Museum. However, nowadays in situ protection has gained popularity. Association for the Conservation of Geological Heritage (Jeolojik Mirası Koruma Derneği, JEMİRKO) was established in 2000 in Turkey. First, an inventory of our geological heritage was prepared by the Association, and this inventory is continuously revised. In Turkey, there are 37 national parks which are important from geological, biological and cultural points of view. Besides these, there are very many areas having incredible beauties from a geological viewpoint to be geoparks in the country. Geoparks are also the potential geotourism sites. Thus important responsibilities have been bestowed upon us to protect them for the future of the country.

Key words: Geological heritage, geopark, geotourism, Turkey

INRODUCTION

Turkey has a colourful geological history between Asia and Europe (Figure 1). There are a lot of places which deserve to be preserved for their geological beauty (Figure 2). Studies about geological heritage began in the beginning of 1970's in Turkey. The work on geological heritage has been carried out individually or by the General Directorate of Mineral

Figure 1. Location Map of Turkey

Research and Exploration (MTA). These amateurish studies were published in various journals in Turkey by geoscientists. General Directorate of Preservation of Cultural and Natural Heritage (The Ministry of Cultural Affairs and Tourism), General Directorate of Nature protection and National Parks, and The Authority for the Protection of Special Areas (Ministry of Environment and Forestry) have made some inventory studies about cultural, historical and natural sites. You can see these lists in their web pages. The geological heritage has been shadowed by the numerous cultural objects and archaeological works in Turkey (İnaner and Savasçın 1999). Some national parks, natural parks and specially protected areas are important in respect of geological heritage in addition to cultural, archaeological, biological and natural heritage.

There are only two examples of geological heritage ('Pamukkale' by the name Hierapolis-Pamukkale and Fairy Chimneys by the name Göreme National Park and Rock Sites of Cappadocia) on The UNESCO World Heritage List (Figure 3). There are 2 natural (Kekova and Mount Güllük-Termessos National Park) and 17 cultural sites in the tentative

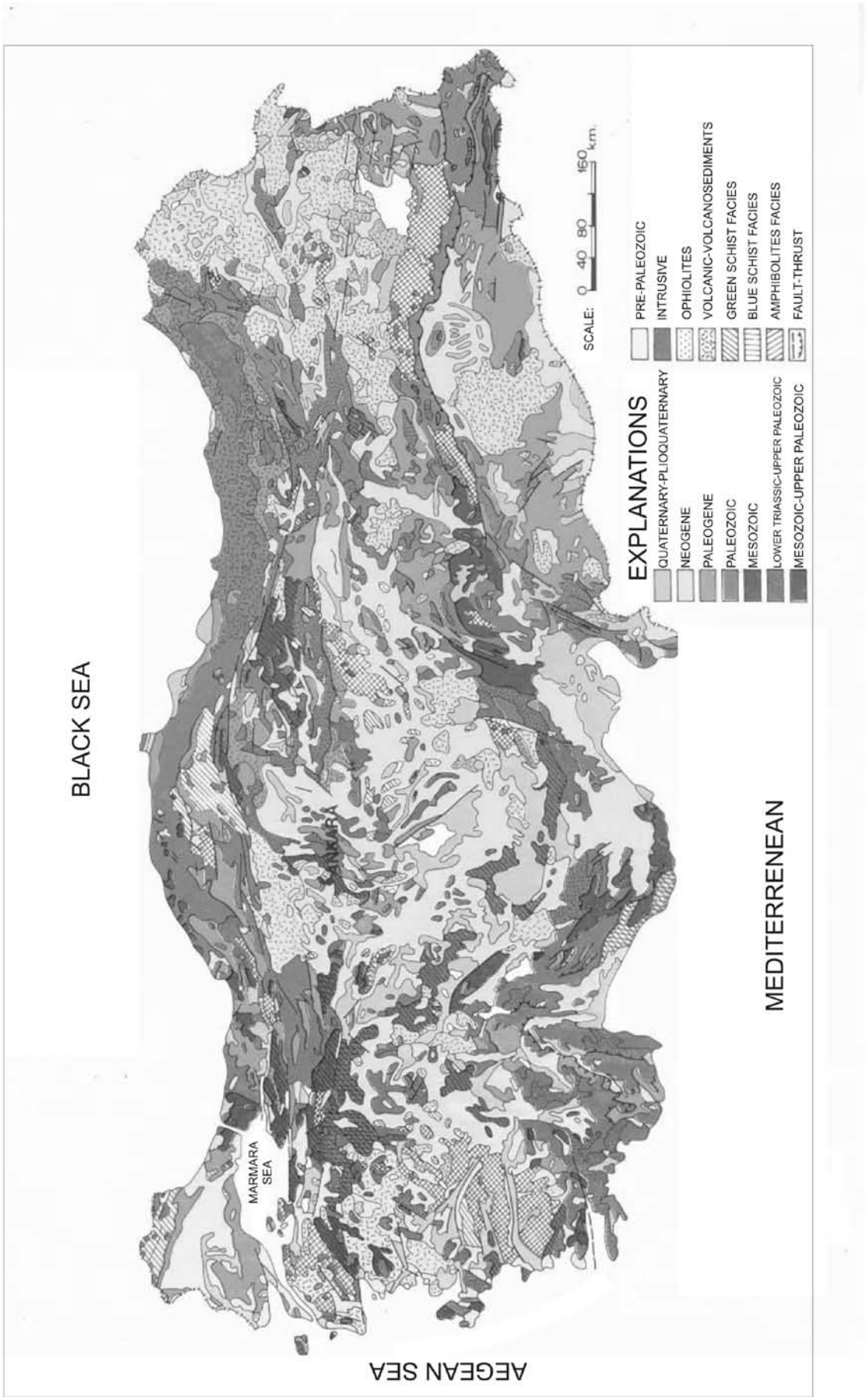

Figure 2. Geological Map of Turkey (from MTA)

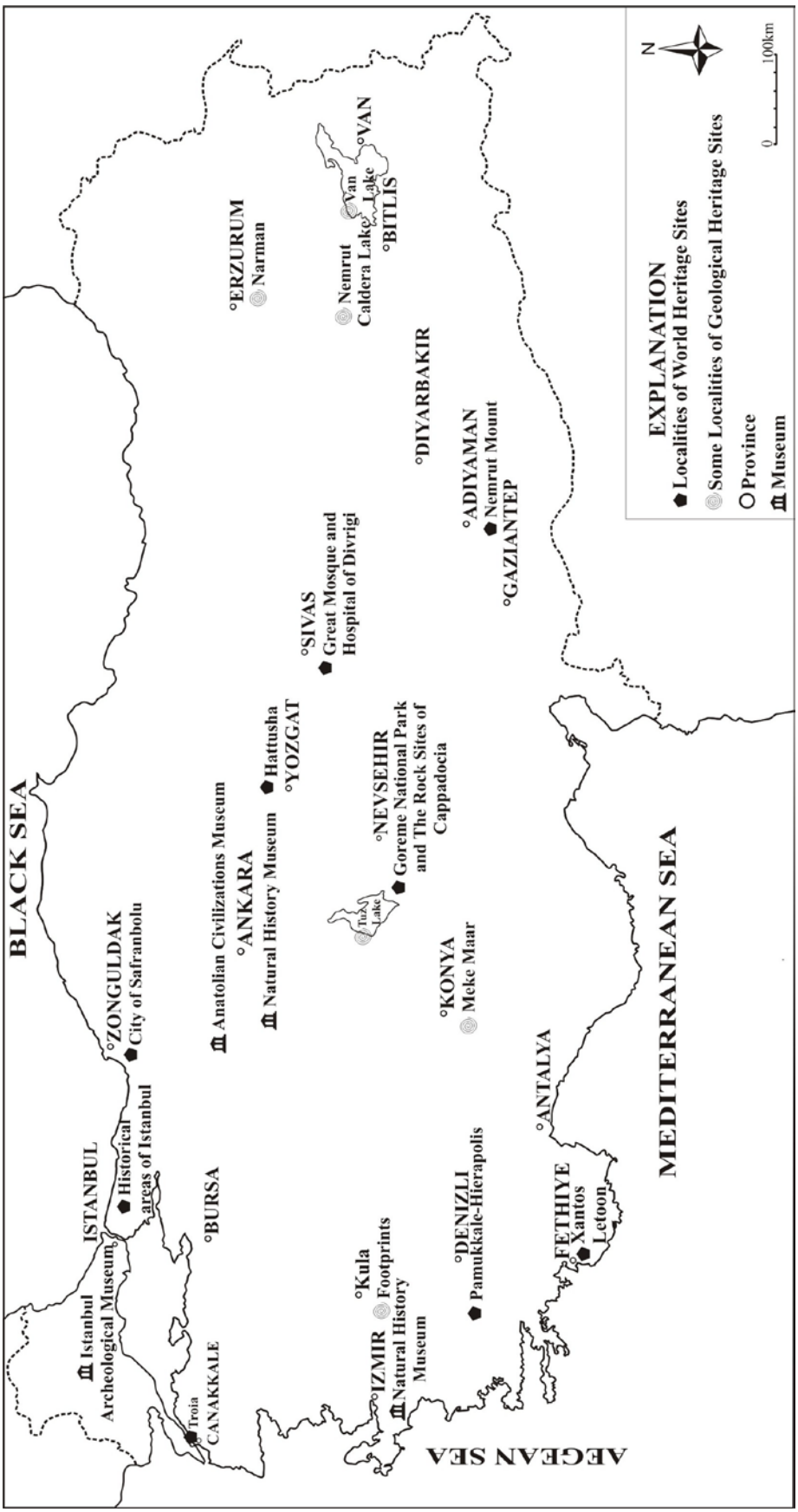

Figure 3. Location Map of Turkey's some important geological heritage sites and Natural and Cultural Heritage Sites included in World Heritage List

list, which was prepared by Ministry of Cultural Affairs of Turkey for UNESCO World Heritage List (Inaner&Savaşçın, 2000).

As you can see in Figure 3, the most important examples of natural geological heritage are in Natural Historical Museum of General Directorate of Mineral Research and Exploration (MTA) in Ankara and some universities' museums, especially in İzmir Aegean University Natural History Museum (Inaner & Savaşçın, 1999). The important thing, however, is to preserve them in situ.

Table 1. Registered site areas list of Turkey (http://www.kultur.gov.tr)

Kind of Sites	Number
Archaeological Sites	6371
Natural Sites	1058
Urban Sites	205
Historical Sites	375
Urban and Historical Sites	36
Total	8182

The laws were made by the Turkish Government to protect the natural and cultural assests. Ministries of Cultural Affairs and Tourism, Forestry, and Environment have carried out studies in these areas. There are responsible directorates in the ministries for the conservation these areas.

There are 6371 archaeological sites, 1058 natural sites, 205 urban sites, 137 historical sites, 375 other sites, 36 urban and archaeological sites, 8182 sites in total in Turkey's Ministry of Cultural Affairs' Internet site (http://www.kultur.gov.tr) and in 2007 Activity Report of Ministry of Cultural Affairs and Tourism (Table 1). Dictrict Councils for the Preservation of Natural and Cultural Heritage are responsible from these sites.

There are 37 national parks, 19 natural parks, 33 natural conservation areas, 102 natural monuments, 191 sites in total in Turkey's Ministry of Forestry, General Directorate of the Nature Protection and National Parks' Internet site (http://www.milliparklar.gov.tr) (Tables 2 &3). According to the Law of National Parks a total area of 857.029 Ha has been under protection, which is expected to be enlarged in the near future.

Table 2. Protected areas list of Turkey (http://www.milliparklar.gov.tr)

Sites	Number	Total Area (Ha)
National Parks	37	857.029
Nature Parks	19	72.342
Areas for Nature Protection	33	64.663
Natural Monument	102	344
Total	191	994.378

The number of Conservation Areas is 32 in Turkey. These areas are important generally in respect of their fauna and flora. There are 102 Natural Monuments in the General Directorate of National Parks. There are 14 specially protected areas, 116 wetland areas in Turkey's Ministry of Environment's internet site (http:/www.cevre.gov.tr.dogal.html) (Table 4). The Authority for the Protection of Special Areas (APSA) is responsible for the management, the conservation of nature and protection of environmental values in 14 Specially Protected Areas (Inaner & Saroglu, 2001).

Association for the Conservation of Turkey's Geological Heritage (JEMIRKO) was founded in 2000. The association intends to carry out some very important studies on geological heritage sites and will try to obtain the collaboration of related universities, museums, Ministries of Cultural Affairs, Forestry, Environment, Tourism, and General Directorate of Mineral Research and Exploration (MTA), other related Directorates, Institutes and Chambers of Engineering. Preliminary inventory studies of geological heritage of Turkey have been completed by the Association for the Conservation of Turkey's Geological Heritage (JEMIRKO) (Figure 4). Our researchers are continuing with

Table 3. National Parks and properties of Turkey (http://www.milliparklar.gov.tr)

No	Province	Name	Area (Ha)	Date of Establishment	Characteristics
1	Adana	Karatepe-Aslantaş	7715	1958	Archeological ruins, Natural flora associations, recreation
2	Adıyaman	Nemrut Mt.	13850	1988	Historical open air museum
3	Afyon	Başkomutan TMP	35500	1981	War history
4	Ağrı Iğdır	Ağrı Mountain	87380	2004	Acheological ruins, hole of meteor, Noah's Ark, flora, fauna
5	Ankara	Soğuksu	1050	1959	Natural flora associations, recreation
6	Antalya	Beydağları Sahil MP Olimpus	34425	1972	Archeological ruins, Natural flora associations, scenery, recreation
7	Antalya	Köprülü Kanyon	36614	1973	Archeological ruins, Natural flora associations, Geological structures
8	Antalya	Altınbeşik Cave	1156	1994	Geologic and geomorphologic stuructures
9	Antalya	Güllük Dağı Termesos	6702	1970	Archeological ruins, Natural flora and fauna associations, recreation
10	Artvin	Hatilla Valley	16988	1994	Geologic and geomorphologic structures, Rich vegatation
11	Artvin	Karagöl-Sahara	3766	1994	Hydrographic structure, Rich vegatation
12	Aydın	Dilek Yarımadası	27675	1994	The most preserved bush flora of Mediterenean, Geological structure, Natural fauna and flora associations, recreation
13	Balıkesir	Kuşcenneti	64	1959	Rich bird families, Natural flora associations, Bird observation
14	Balıkesir	Kaz Mt.	21300	1994	Flora, Biologic diversity and fauna
15	Bartın Kastomonu	Küre Mountains	37000	2000	Geological and geomorphological structures, waterfall, canyon, cave, flora, fauna
16	Bolu	Yedi Göller	2019	1965	Natural fauna and flora associations, scenery, recreation
17	Bursa	Uludağ	12732	1961 1996	Geological structure, Natural flora associations, Mountain and snow sports
18	Çanakkale	Gelibolu Yarımadası historical MP	33000	1973	War history, Natural flora and fauna associations, Geomorphological structures
19	Çanakkale	Troia History	13350	1996	Historical ruins and Geological structures
20	Çorum	Boğazköy-Alacahöyük	2634	1998	Archeologic ruins (Capital city of Hitites)
21	Denizli	Honaz Mt.	9219	1995	Geology, Geomorphology, Archeology and Flora richness (Endemic Species)
22	Edirne	Gala Lake	6090	2005	Delta, wetland area, flora, fauna
23	Erzurum Kars	Sarıkamış-Allahüekber Mountains	22980	2004	Historical, geological, flora, fauna
24	Isparta	Kızıldağ	59400	1969	Natural flora associations, recreation
25	Isparta	Kovada Lake	6534	1970	Natural flora and fauna associations, scenery, recreation
26	Kastomonu	Ilgaz Mountain	1088	1976	Natural flora associations, Mountain and snow sports scenery, recreation

Table 3 continued

No	Province	Name	Area (Ha)	Date of Establishment	Characteristics
27	Kayseri	Sultan Sazlığı	24523	2006	Wetland, Fauna, Bird observation
28	Konya	Beyşehir Lake	88750	1993	Historical ruins, Geomorphological features, Natural flora associations, Rich bird families and hidrological features
29	Manisa	Spil Mountain	5505	1968	Geological structure, Natural flora and fauna associations, recreation
30	Muğla	Marmaris	33350	1996	Geomorphological stuructures, Flora and Fauna richness
31	Muğla	Saklıkent	12390	1996	Geomorphological stuructures, Flora and Fauna richness
32	Nevşehir	Göreme TMP	9572	1986	Ancient sites (Churches, Chapels, and Fairy Chimneys), Geological structures, Recreation
33	Niğde Adana Kayseri	Aladağlar	54524	1995	Geomorphological stuructures, Flora and Fauna richness
34	Rize	Kaçkar Mt.	51550	1994	Geologic and geomorphologic structures, Flora and Fauna
35	Trabzon	Altındere Valley	4800	1987	Cultural assests (Sürmela Monastery), Natural flora associations, scenery, recreation
36	Tunceli	Munzur Vadisi	42000	1971	Geological structure, Natural flora and fauna associations
37	Yozgat	Yozgat Çamlığı	264	2001	Natural fauna and flora associations, recreation

Table 4 The Names of Specially Protected Area in Turkey (http://www.ockkb.gov.tr)

Number	Name	Province	Area (km^2)	Properties
1	Foça	İzmir	28	Cultural, Historical, Natural
2	Gökova	Muğla	521	Cultural, Natural
3	Datça-Bozburun	Muğla	1474	Cultural, Natural, Flora, Fauna
4	Köyceğiz-Dalyan	Muğla	385	Cultural, Historical, Natural, Flora, Fauna
5	Fethiye-Göcek	Muğla	613	Cultural, Historical, Natural,
6	Patara	Antalya	190	Cultural, Historical, Natural, Fauna,
7	Kekova	Antalya	260	Cultural, Historical, Natural
8	Belek	Antalya	135	Cultural, Historical, Natural Flora, Fauna
9	Göksu Deltası	İçel	236	Cultural, Historical, Natural Flora, Fauna
10	Pamukkale	Denizli	44	Cultural, Historical, Natural
11	Gölbaşı	Ankara	245	Natural, Flora, Fauna
12	Ihlara	Aksaray	58	Cultural, Historical, Natural Flora, Fauna
13	Tuz Gölü	Ankara-Konya-Aksaray	7414	Biodiversity, Wetland area, Flora, Fauna, Salt production, Natural, Cultural
14	Uzungöl	Trabzon	149	Flora, Fauna, Natural

their studies. As we have numerous places of geologic heritage, it will take some time to complete these studies. Collaborations between related organizations and universities give us big hopes for carrying out and completing these research studies (Inaner, 2006).

The first aim of the Association for the Conservation of Turkey's Geological Heritage (JEMIRKO) is to make a list of Turkey's geological heritage sites, which we would like to complete as soon as possible. We will try to give examples to some important geological heritage localities in this study. Many more sites of natural geological heritage have not had the opportunity to go into this list (Inaner, 2006).

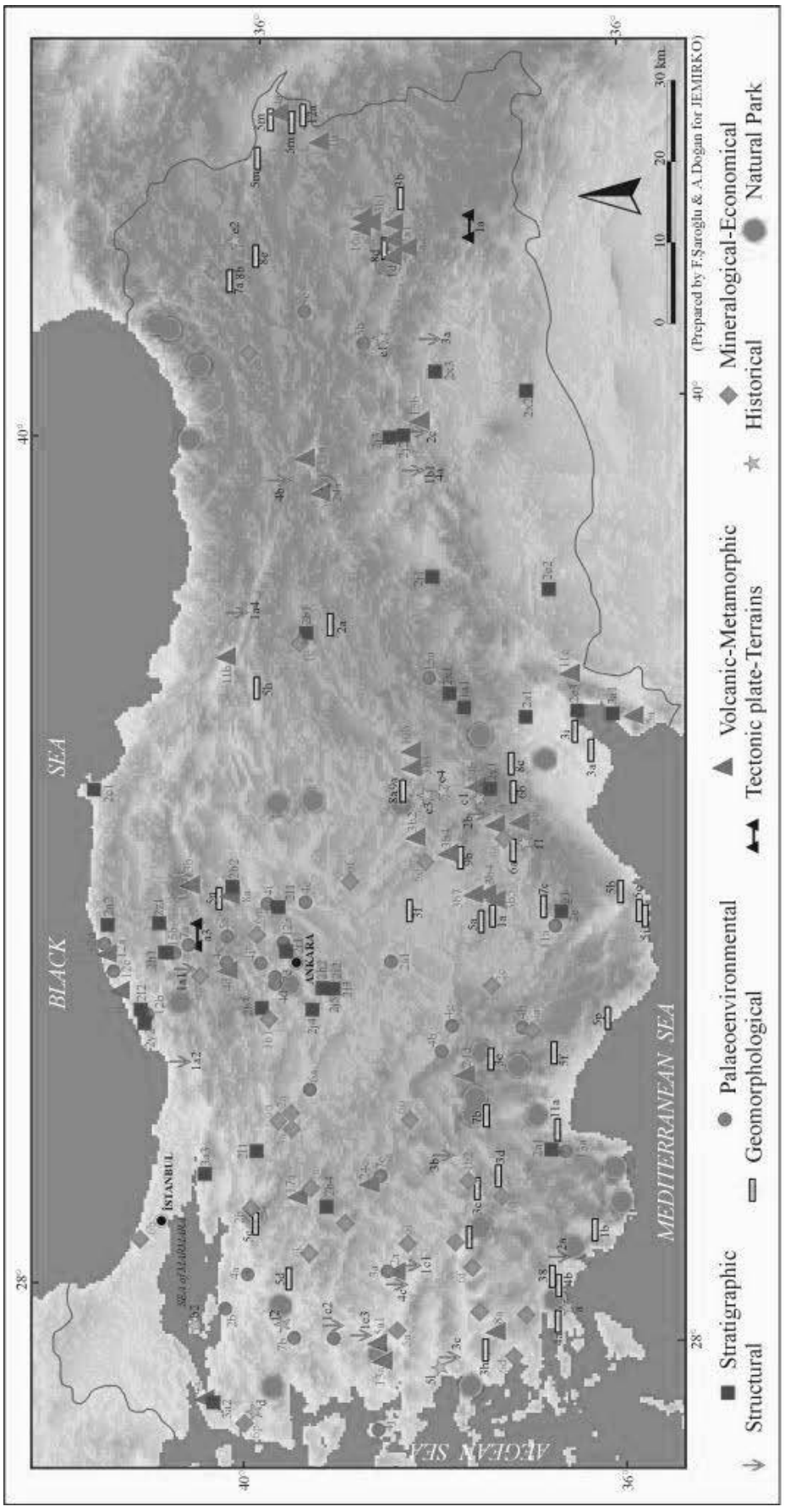

Figure 4. Inventory Map of Geological Heritage Sites of Turkey (prepared by F. Saroglu & A. Dogan for JEMIRKO, Kazancı and Saroglu, 2003)

Some parts of Göreme, Mount Nemrut and Troya National Parks are in the list of UNESCO. Mount Uludağ, Seven Lakes, Dilek Peninsula, Mount Spil, Munzur Valley, Gelibolu Peninsula, Köprülü Canyon, Beyşehir Lake, Kaçkar Mountains, Hatilla Valley, Altınbeşik Cave, Mount Honaz, Mount Aladağlar, Marmaris, Saklıkent are important in respect of geological heritage in addition to cultural and natural heritage.

19 Natural Parks in Turkey are Afyon-Akdağ, Antalya-Kurşunlu waterfall, Aydın- Bafa Lake, Balıkesir-Ayvalık Islands, Bolu-Abant Lake, Çorum-Çatak, Gümüşhane-Artabel Lakes, Isparta-Yazılı Canyon and Gölcük Lake, İstanbul-Polonezköy and Türkmenbaşı, Kocaeli-Beşkayalar and Ballıkayalar, Konya-Kocakoru Forest, Muğla-Kıdrak and Trabzon-Uzungöl.

There are 102 Natural Monuments in the General Directorate of Conservation and National Parks, but only Samandra Waterfalls, Asarlıktepeleri, Fossil Ardıç and Güney Waterfall are important in respect of geological heritage.

There are 14 specially protected areas, and 116 wetland areas in Turkey's Ministry of Environment's internet site (http:/www.cevre.gov.tr.dogal.html).

The Authority for the Protection of Special Areas (APSA) is responsible for the management, the conservation of nature and protection of environmental values in fourteen Specially Protected Areas. These are Fethiye-Göcek, Köyceğiz-Dalyan, Patara, Kekova, Göksu Deltası, Gölbaşı, Pamukkale, Ihlara Valley, Foça, Belek, Datça-Bozburun, Gökova, Tuzgölü and Uzungöl (Table 4).

GEOLOGICAL HERITAGE

Geological heritage sites were classified according to ProGEO criteria with other SW European Countries. Some important geological heritage sites for Turkey and other SE European counries are given by Drandaki (2001). These are given in Figure 3 as Pamukkale, Cappadoccia, Meke Maar, Nemrut Caldera Lake, Narman red sandstones, Van Lake, Tuz Lake and human footprints of Kula volcanism (İnaner and Şaroğlu, 2001).

GEOPARKS

21 geological parks in Europe and 12 in China are currently registered in the UNESCO's Global Network of Geological Parks.

According to national and international initiatives, like the "International Declaration of the Rights of the Memories of the Earth" (Digne, France 1991), the IGCP, IUGS, ProGEO, Malvern Group, UNESCO's Division of Earth Sciences and the Council of Europe, an international group of experts on Geoparks recommended the establishment of a "Global Network of National Geological Parks (Geoparks) seeking UNESCO's assistance" in order to promote the three goals of conserving a healthy environment, educating in Earth Sciences at large, and fostering sustainable local economic development (http://www.unesco.org).

The members of the Global Network of Geoparks are:

1. *Mount Lushan Geopark – P.R. China*
2. *Geopark Wudalianchi – P.R. China*
3. *Songshan Geopark – P.R. China*
4. *Yuntaishan Geopark – P.R. China*
5. *Danxiashan Geopark – P.R. China*
6. *Stone Forest Geopark – Shilin Geopark – P.R. China*
7. *Zhangjiajie Sandstone Peak Forest Geopark – P.R. China*
8. *Huangshan Geopark – P.R. China*
9. *Reserve Géologique de Haute Provence – France*
10. *Petrified Forest of Lesvos – Greece*

11. *Vulkaneifel European Geopark – Germany*
12. *Maestrazgo Cultural Park – Spain*
13. *Psiloritis Natural Park – Greece*
14. *Astroblème Châtaigeraie Limousine - France*
15. *Nature park Terra Vita European Geopark – Germany*
16. *Coper Coast – Ireland*
17. *Marble Arch Caves & Cuilcagh Mountain Park – Northern Ireland, United Kingdom*
18. *Madonie Natural Park – Italy*
19. *Rocca di Cerere Cultural Park - Italy*
20. *Kamptal Geopark – Austria*
21. *Nature Park Eisenwurzen – Austria*
22. *22.European Geopark Bergstrasse–Odenwald - Germany*
23. *North Pennines AONB Geopark – United Kingdom*
24. *Abberley and Malvern Hills Geopark – United Kingdom*
25. *Park Naturel Régional du Luberon – France*
26. *North West Highlands – Scotland, UK*
27. *Geopark Swabian Albs – Germany*
28. *Geopark Harz Braunschweiger Land Ostfalen – Germany*
29. *Mecklenburg Ice age Park - Germany*
30. *Xingwen National geopark– P.R. China*
31. *Hexigten National geopark– P.R. China*
32. *Yandangshan National geopark– P.R. China*
33. *Taining National geopark– P.R. China*

Although Turkey has all these geological, natural, cultural and historical sites, there is no registered geopark in Turkey. However, there are 37 national parks.

JEMIRKO's executive committee determined seven potential geopark areas for Turkey (Kazancı and Şaroğlu, 2003). Project studies are continuing on these areas. JEMİRKO is collaborating with Ministries, General Directorate of Mineral Reseach and Exploration (MTA), Chamber of Geological Engineering (JMO), universities and other organizations for geological heritage and geoparks research.

According to Kazanci and Saroglu (2003) names and properties of potential geopark areas of Turkey are as follows:

1. The Karapınar Geopark: It is located in Konya province in central Turkey. It covers many kinds of geological and cultural sites including maars, maar lakes, volcanic cones, stratovolcanes, sinkholes, dried and living lakes, old lake plains, eolien dunes, modern evaporates and salt formations, ophiolitic and sedimentary sequences from Eocene to Holocene. The area has been declared under conservation.

2. The Mut Geopark: It is located in the central Mediterrenean region of Turkey. Apart from extraordinary erosive landforms, it includes a very thick, large but underformed Miocene sequence. It is the largest paleobay of the Mediterrenean. JEMIRKO and MTA have been working on a project for determining the properties of the Mut region.

3. Narman Red Happiness Valley Geopark: It is located in the Erzurum province in Narman-Erzurum in eastern Turkey, and is comprised of red coloured Pliocene sandstone-conglomerates of typically non-marine facies. There are fairy chimmneys and canyon type valleys. It is not protected by any scheme of conservation.

4. Kula Volcanic Geopark: Kula is a lovely town located in the Manisa province along the Izmir-Ankara road in Western Turkey. This small town is famous by its extinct volcanoes, human and domesticated animal footprints dating from Pre-Neolithic times, fairy chimneys, roasted chickpea, textile industry, historical Kula houses, thermal water

resources which have been in use since Roman times, well known mineral water springs, Kula carpets and blankets, handicrafts such as copper plate production, leather production, shoemaking, tombs, old mosques and old churches.

Upon the lapilli tuff ashes lying beneath the scorias of Kula alkaline volcanism still active even today in Western Anatolia, human footprints can be found together with those of some domesticated animals. Thanks to these footprints, we now know that this last volcano was active at least 10,000 years ago or later than that, for the existance of domesticated animals in Pre-Neolithic times (approximately 10,000 years ago) is out of the question.The area has recently been declared under conservation. Unfortunately the footprints are decaying and number of them is decreasing rapidly.

5. Cappadoccia Geopark: It is in central Turkey. Erosive landform, many tuff cones, calderas, lava and pyroclastic flows are the basic elements. Colorful lithology and trenched morphology create a wonderful landscape appereance. It has been already in the World Heritage List.

6. Denizli Travertine Geopark: Different types of travertine of late Quaternary can be visited. The area includes remnants of many mammalian species including Hominids. Pamukkale part of it is already in the World Heritage List. Pamukkale is a health tourism center with termal waters and other specialities.

7. Nemrut Volcano and Lake Van Geoparks: It is in Eastern Turkey and includes many cultural, volcanic, sedimentary and structural sites. North Anatolian fault begins from here and Lake Van is the largest waterbody with natrium sulphate. Van Lake is the largest soda lake in the world. Lake is not covered by any scheme of conservation.

JEMİRKO is currently concentrating on a project to determine the geological heritage areas of National parks, which we hope will provide us with new methods to determine new geopark areas.

GEOTOURISM

Geotourism is defined as tourism that sustains or enhances the geographical character of a place—its environment, culture, aesthetics, heritage, and the well-being of its residents (www.nationalgeographic.com/travel/sustainable/).

Geotourism is a new kind of tourism but there are a lot of geotorism or geotrip destinations in European countries. A lot of people are interested in different kinds of tourism nowadays. Turkey happens to be very lucky in this respect.

If you look at the web page of Ministry of Tourism, you will see different categories of tourism areas in Turkey; for hunting, winter sports, faith tours, silk road, thermal resorts, congress tourism, golf, youth tourism, yachting, botanics, spelunking, highlands, air sports, mountaineering, rafting, underwater diving and ornitology. Some of them are directly related with geotourism like winter sports, thermal resorts, botanics, spelunking, highlands, mountaineering, rafting, underwater diving and ornitology. It is necessary to develop new organizations for new kinds of tourism. Geotourism must be placed within these tourism kinds for devoloping tourism in Turkey. Geoparks are also potential geotorism areas for all over the world. Turkey must provide these new organizations for the benefit of the tourism sector for the future. Slovenia is a country well advanced in geotourism. A lot of geotourism books are published yearly in Slovenya. Colloborations with ProGEO member countries will be useful for all of us. It is posibble to find new roads for geotourism between these countries.

CONCLUSION

Turkey, a land which has been home to various cultures and civilizations for thousands of years, contains innumerable

natural and cultural sites. Most of these geological heritage sites have not yet obtained their deserved place in the museums and the related publications.

We are continuing our efforts to promote the concept of geological heritage in Turkey by workshops, symposiums, conferences, TV programs, and hope to collect in the near future all localities together in a list, and we realized that, because of the high number of such localities in Turkey, we have a great amount of work to do to accomplish this task we have set up in front of us. We hope to declare geoparks for Turkey in the near future. JEMIRKO and its members are ready for collaborations on new projects about education, geological and cultural conservation, tourism and geoparks

Turkey is one of the richest countries in the world in respect of natural geological heritage. There are a lot of very important scientific and natural geological heritage examples in Turkey. These beauties have not been classified completely yet. They are waiting to be discovered.

Geological heritage, geoparks and geotourism will provide us with new opportunities, and governments, universities, non governmantal organizations, chambers and the public, we all share this same responsibility to make proper use of this chance for a better future. And for this the first step should be educating all the concerned parties and especially the public to make them understand their importance for future generations.

REFERENCES

Drandaki, I.T.(2001)- Geological Heritage Conservation in South-Eastern European Countries. *IGME*. 26p.

Inaner, H., Savascin, M.Y. 1999 Natural and cultural geological heritage of Anatolia. *Towards the Balanced Management and Conservation of the Geological Heritage in the new Millenium. D. Barrettino,M. Valleco&E. Gallego (Eds.)* p. 459

Inaner, H., Savascin, M.Y. 2000 Natural and cultural geological heritage of Turkey. International Earth Sciences Colloquium on the Aegean Region, *IESCA-2000 Abstracts,* p.266

Inaner, H., Saroglu, F. 2001 Preliminary Inventory Studies of Geological Heritage of Turkey. *Workshop ProGEO WG1,* 26 September─2 October 2001. (unpublished)

Inaner, H. 2006 Geological Heritage of Turkey. *4th European Geopark's meeting*, 2─5 October 2003, Anogia, Greece. *Proceedings Volume*, Crete 2006, pp. 43-50

Kazancı N., Saroglu, F. (2003)- Annual report on the protection of geological heritage in Turkey, p. 17. (unpublished)

Ministery of Cultural Affairs and Tourism 2007 Activity Report of 2006. T.C. Ministery of Cultural Affairs and Tourism Head of Devolopment of Stratregy, Ankara, p. 308

(This page is left blank intentionally.)

BEYPAZARI-OYMAAĞAÇ GRANITOID: ITS GEOLOGY, PETROGRAPHY, GEOCHEMISTRY AND TECTONIC SIGNIFICANCE

Küçükuysal (İpekgil) C. and Lünel A. T.

Geological Engineering Department, Middle East Technical University, Ankara,Turkey
ipekgil@metu.edu.tr

Abstract: Beypazarı-Oymaağaç granitoid (BOG) is a low-temperature and shallow-seated batholith that plays an important role in the better understanding of both Palaeo- and Neo-tethyan evolution in northwest Ankara (Central Anatolia, Turkey). The pluton is composed of granitoid rocks, ranging from granite to granodiorite. Petrographically these rocks are composed essentially of quartz, K-feldspar, plagioclase, hornblende and opaques while sphene, zircon, apatite and pistacite form the common accessories. K-feldspars occur as megacrystals, whereas plagioclases are characterized by strong zoning common with corroded cores. The granitoid is calcic, metaluminous and characterized by the enrichment in LREE relative to HREE and the depletion in HFSE. ORG-normalized spider-diagram displays relatively high Rb and Th, and low Zr and Y. The characteristic negative anomalies in Ba and Nb are consistent with a crustal component. The presence of abundant dioritic mafic microgranular enclaves, aplite and pegmatite dykes imply I- / H_{LO}-type origin. The batholith has an arc-related geochemical affinity but it also displays ORG-normalized patterns characteristic to post-collisional calc-alkaline granitoids. The BOG is therefore interpreted as typical representative of the magmatic arc environment and formed through magma mingling processes of the upper continental crust material and the basic magma related to the subduction process.

Key words: Oymaağaç Granitoid, Beypazarı, Petrology, Arc Magmatism

1. INTRODUCTION

Turkey is an east-west trending segment of the Alpine-Himalayan orogenic belt and is located on the boundary between Gondwana in the south and Laurasia in the north. Within this belt, Central Sakarya region is a key area where tectonic elements of both the Palaeo- and Neotethyan assemblages crop out (Göncüoğlu *et al.*, 2000). The Beypazarı district located in Central Sakarya is a large area of volcano-sedimentary rocks in western central Anatolia, Turkey; approximately 100 kilometers northwest of Ankara. The Beypazarı-Oymaağaç Granitoid (BOG) within the Pontide is located in the 100 km northwest of Ankara. The intrusive body has an extension greater than 100 km^2 and can be called also as batholith. This batholith is a granitoid body having a composition ranging from granite to granodiorite. Beypazarı-Oymaağaç Granitoid is located to the south of Beypazarı region (Figure 1). Beypazarı-Oymaağaç Granitoid is located approximately 50 km south of Beypazarı region. The study area covers 40 km² around Oymaağaç village. The purposes of the present study are to determine the origin, source characteristics, evolution petrogenesis and emplacement mechanisms of the Beypazarı-Oymaağaç Granitoid (BOG).

2. METHODS OF THE STUDY

This study is composed of 3 major steps: (1) field work, (2) laboratory work and (3) data interpretation. First of all, geological mapping was carried out in an area of about 40 km² at a scale of 1:25 000 during the summer of 2003. During mapping, the occurrences of rock units, their contact relations between them and the structural features were studied in detail. About 100 samples from the Beypazarı-Oymaağaç Granitoid were collected. Secondly, the least altered samples were selected and 90 thin sections were prepared in the Thin Section Preparation Laboratory of the Geological Engineering Department of the Middle

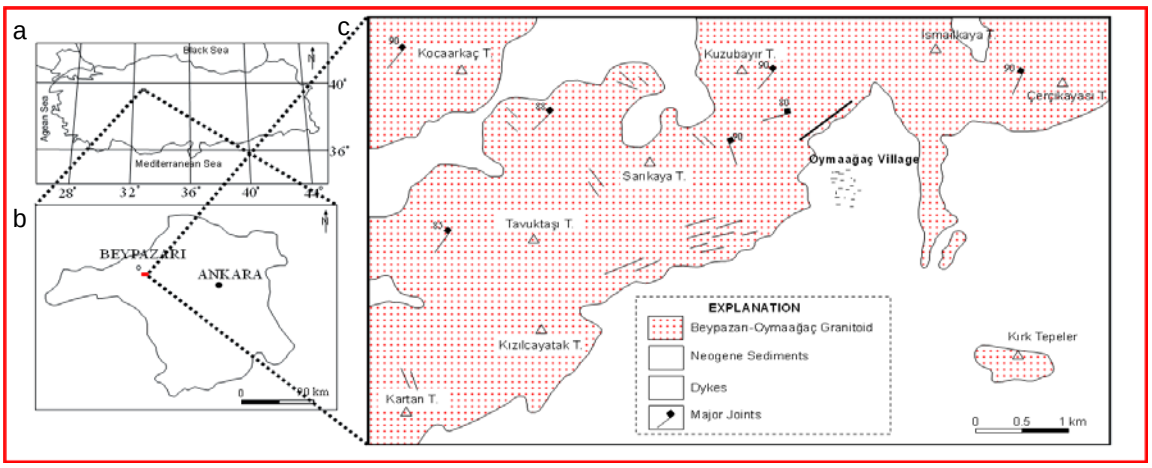

Figure 1. a & b) Maps showing geographic location of the study area; c) the geological map of Beypazarı-Oymaağaç Granitoid (BOG)

East Technical University. The determination of the rock forming minerals of the granitoid body was carried out by studying the optical properties under the polarized microscope. After the petrographic study was completed, 25 samples were chosen for geochemical analysis. They were analysed for both major and trace element compositions in ACME Laboratories, Canada. The final step concerns the interpretation of the piled-up data which involves a discussion of the results of the petrographical and geochemical analyses.

3. PETROGRAPHY

Petrographical study forms the first part of the laboratory work of the research. The least altered samples were selected and 90 thin sections from fresh surfaces were prepared. Petrographic studies were carried out by a polarizing microscope. The mineralogical and textural properties of BOG were determined. James Swift Automatic Point Counter Model F was used to make modal analyses of representative samples with point counts of 2500 points per sample.

Oymaağaç pluton is pink, pale gray and also greenish in color. Under polarising microscope, BOG is phaneritic and holocrystalline in terms of its granularity and crystallinity. Considering the fabric of the granitoid, it is hypidiomorphic and porphyritic according to its crystal face and distribution of grains. The essential minerals of BOG are quartz, plagioclase, alkali-feldspar, hornblende, pyroxene and biotite. The accessory minerals include sphene, zircon, pistacite, zeolite and apatite. Epidote, chlorite, sericite, kaolinite and calcite are secondary minerals found in the batholith. The enclaves in BOG are up to 30 cm in diameter and have a sharp contact with the host granitoid. The petrographic analyses of the enclaves reveal that they are dioritic in composition. Aplite dykes are pale gray to pink in color. Their size varies from 10 cm to 5 m in width and from 10 m to hundered meters in length. They are holocrystalline and hypidiomorphic and show myrmekitic and graphic textures. The pegmatite located around 1 km nortwest of Oymaağaç Village is pale pink in color. It is holocrystalline, hypidiomorphic and porphyritic. Additionaly, it displays graphic and myrmekitic textures. It is composed of very large quartz crystals, alkali-feldspar, plagioclase and biotite. 60 representative thin sections were analysed by James Swift Automatic Point Counter Model F. Petrographically BOG is composed essentially of 22-60% quartz, 20-25% K-feldspar, 15-49% plagioclase, 5-18% hornblende and 0.8-6% opaques. BOG shows a normal zonation in color and mineral composition from centre towards the margins of the pluton. Modal analyses data reveal that the granitoid has a

compositional range from granite to granodiorite.

4. GEOCHEMISTRY

25 fresh samples selected from the Beypazarı-Oymaağaç Granitoid were analysed geochemically by ICP-ES and ICP-MS techniques at ACME Laboratories, Canada. BOG is classified as subalkaline according to total alkalies vs. SiO_2 classification scheme of Irvine and Baragar (1971) (Figure 2a). The AFM diagram of Irvine and Baragar (1971) shows that all samples have calc-alkaline nature (Figure 2b). (Figure 2c) The molecular Al_2O_3 / ($CaO+Na_2O+K_2O$) ratio of BOG range defines its metaluminous nature (Maniar and Picolli (1989) TiO_2, Fe_2O_3, MnO, MgO and CaO decrease, whereas K_2O and Rb increase with increasing SiO_2 content.

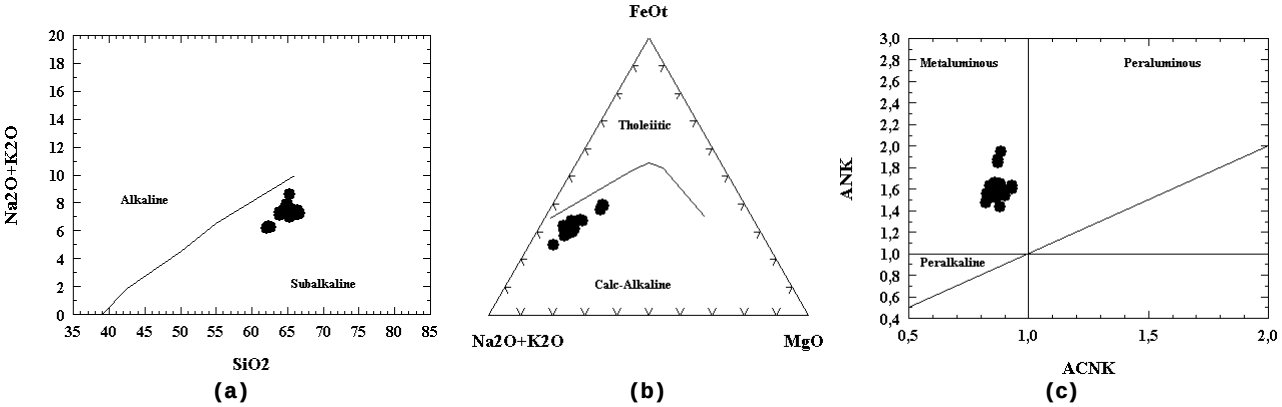

Figure 2. a) Alkalies (Na_2O+K_2O) versus SiO_2 diagram with the Irvine and Baragar (1971) fields, showing the subalkaline character of all samples, b) the AFM diagram of Irvine and Baragar (1971) showing the calc-alkaline nature of all samples from BOG and c) Alumina Saturation Index showing metaluminous character of the studied samples (Maniar and Picolli (1989))

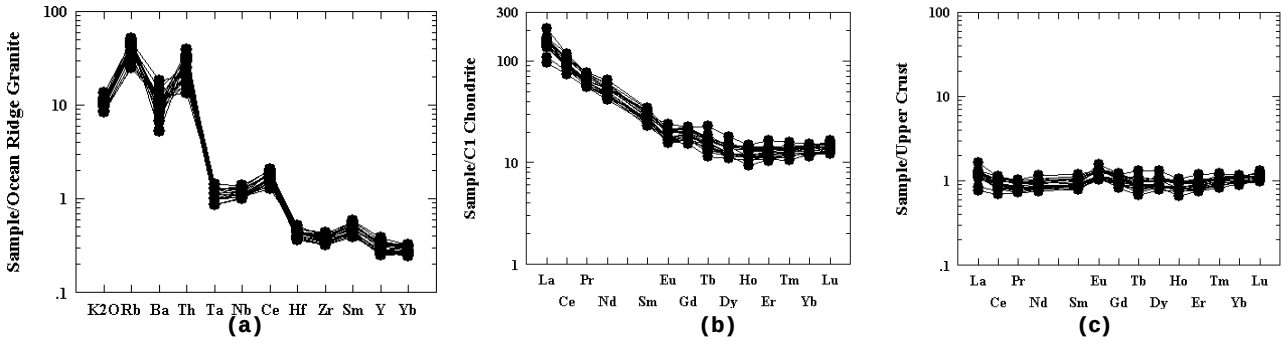

Figure 3. a) ORG-normalized trace element patterns; b) Chondrite-normalized REE atterns and c) upper crust normalized REE patterns of BOG (normalizing values are from Taylor and Mc Lennan (1985))

These geochemical variations indicate the fractional crytallization. However, resulting from alterations, there are some irregular variations in Na_2O, Sr and Ba with increasing SiO_2. The ORG-normalized spider diagram of Beypazarı-Oymaağaç Granitoid reveals that K_2O, Rb, Ba and Th are enriched with respect to ORG; Ta and Nb are quite similar to ORG; Hf, Zr, Sm, Y and Yb are all less than ORG (Figure 3a). Oymaağaç batholith is enriched in Rb and Th; depleted in Zr and Y, indicating that it has had very much interaction with the crust. Negative Ba and Nb anomalies are characteristic of the continental crust and may be an indicator of crustal involvement in magma processes. Negative anomaly in Ba also suggests the fractionation of K-feldspars and hornblende (the main depositer for Ba and Ce), suggesting lower water pressures

and/or shallower emplacement depths (Rollinson, 1993). The pluton is also normalized to chondrite. BOG appears to be enriched in HREE, MREE and LREE with respect to chondrite with a steep La/Sm ratio (Figure 3b). Then, it is normalized to upper crust (Figure 3c). BOG displays very close values to upper crust, revealing that it may be of upper crustal origin.

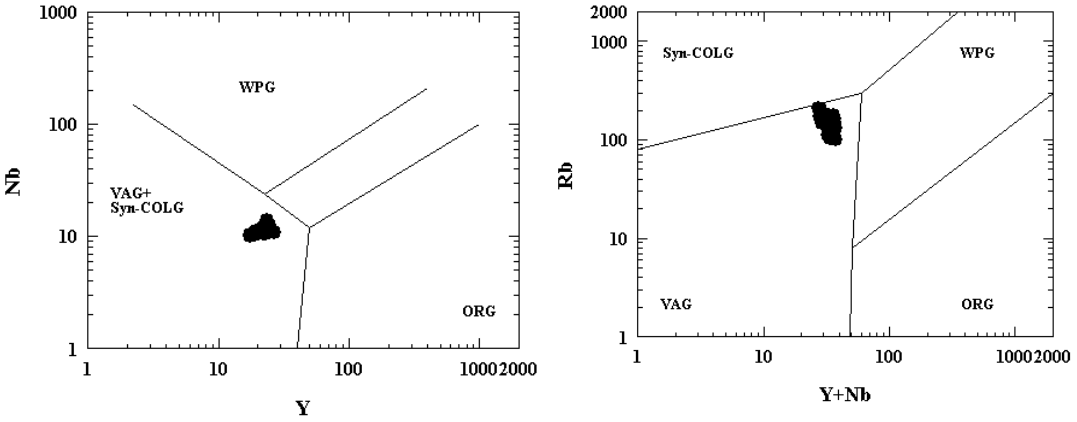

Figure 4. a) Nb-Y diagram and b) Rb-Y+Nb tectonicdiscrimination diagams of Pearce *et al.*, 1984

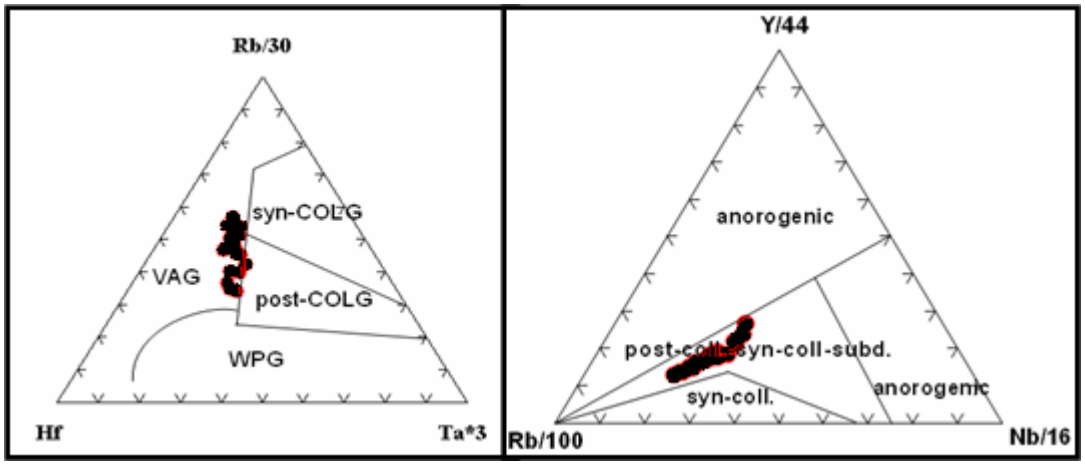

Figure 5. a) Rb/30-Hf-Ta*3 diagram of Harris *et al.*, 1986 and b) Y/44, Rb/100-Nb/16 diagram of Thieblemont and Cabanis (1990)

To discriminate the tectonic setting of Beypazarı-Oymaağaç Granitoid, Nb vs Y and Rb vs Y+Nb diagrams of Pearce *et al.*, 1984, are employed (Figures 4a & b). BOG samples plot in the fields of VAG+syn-COLG and VAG very close to the triple junction of VAG, syn-COLG and WPG, respectively. The patterns in Figure 3a (ORG-normalized diagram) display a well-defined decrease from LILE to HFSE. Compared with the patterns in Figure 1 of Pearce *et al.*, 1984, BOG displays a trend very similar to the collision granites. (Rb/30)-Hf-(Ta*3) triangular diagram of Harris *et al.*, 1986, is employed to better understand whether the samples plot in VAG or post-COLG fields (Figure 5a). From this diagram, it may be concluded that the samples from BOG plot along the boundary of VAG and collisional granites. Y/44-Rb/100-Nb/16 discrimination diagram of Thiéblemont and Cabanis (1990) shows that the studied samples fall in the field of collision-subduction regions (Figure 5b).

Being the coeval products of the calcalkaline volcanism in the Pontides during Late Cretaceous, Beypazarı-Oymaağaç Granitoid and Galatia Volcanics (GV) are discussed together in their geochemical signatures. Figures 6a & 6b show MORB-normalized trace element characteristics and chondrite-normalized REE patterns, respectively. In both diagrams, Beypazarı-Oymaağaç Granitoid and the samples from Galatia Volcanics plot almost the same trends. The geochemical interpretations suggest that they were most probably generated from the same source, but controlled by different geodynamics of magma genesis.

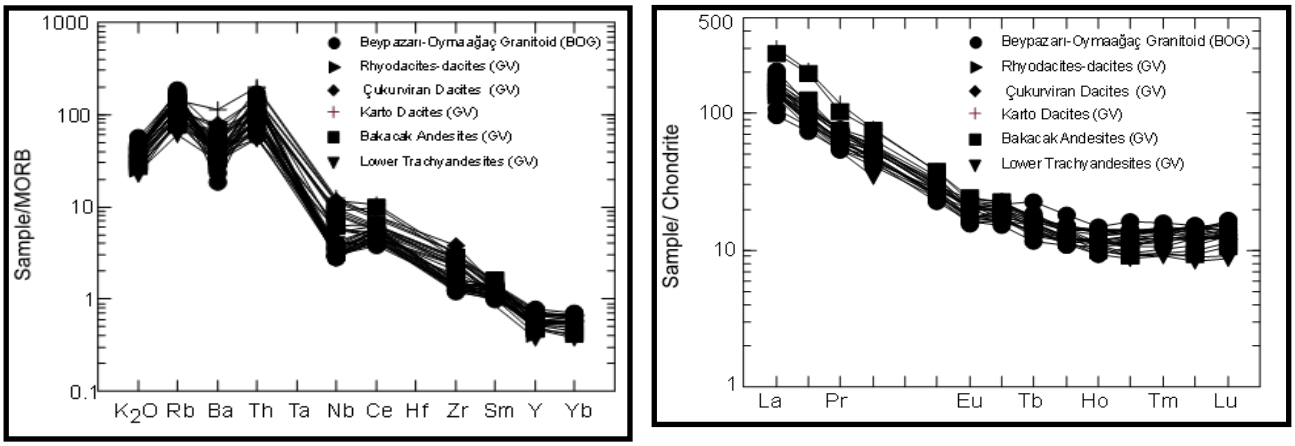

Figure 6. a) MORB-normalized trace element diagram and b) chondrite-normalize REE patterns of BOG and GV (the geochemical data of Galatia Volcanics are taken from Keller *et al.*,1992, Tankut *et al.*, 1998 and Koçyiğit *et al.*, 2003.)

5. CONCLUSIONS

The major conclusions about the origin, source characteristics, evolution petrogenesis and emplacement mechanism of BOG are summarized below.

1) *BOG is characterized as a composite pluton including mafic microgranular enclaves, aplite dykes and pegmatite with host granitoid.*

2) *Petrographic studies on BOG reveal the compositional range from granite to granodiorite. Due to some mineralogical differences through the batholith, BOG may be said to show petrographically normal zoning.*

3) *Mafic microgranular enclaves are found throughout the batholith. They are holocrystalline and dioritic in composition. They have a sharp contact with the host batholith and are elongated in the direction of the flow lines of the granitic magma. MMEs display abundant evidence of variable mixing/mingling processes.*

4) *The pluton has the general features of I-/H_{LO}-type, calc-alkaline, and metaluminous granitoid series.The geochemistry of BOG on major and trace elements reveals that it was formed in an arc-matured environment and has a geochemical signature of collisional granitoids. Beypazarı-Oymaağaç Granitoid and Galatia Volcanics, which are both coeval, are comparable with each other in terms of source of the magmatism in the study area. Additionally, the calcalkaline and alkaline rocks in the Galatia Volcanic Province points to the polyphase magmatism in the Beypazarı region.*

(5) As a whole for the origin for BOG, it can be concluded that it formed from upper continental crust material which mingled with the basic magma related to the subduction process. The tectonic setting of the batholith is suggested as magmatic arc.

ACKNOWLEDGEMENT

The present study is a 1.5-year research project and is supported by BAP-2004-07-

02-00-61 (Scientific Research Projects) at the Middle East Technical University.

REFERENCES

Göncüoğlu, M.C., Turhan, N., Şentürk, K., Özcan, A., Uysal, Ş., Yalınız, M.K., 2000. A geotraverse across northwestern Turkey: tectonic units of Central Sakarya region and their tectonic evolution. *Geological Society,London, Special Publications*., 173, 139-161.

Harris, N.B.W., Pearce, J.A., Tindle, A.G., 1986. Geochemical characteristics of collision-zone magmatism: In: Coward MP, Ries AC (eds) Collision Tectonics. *Geol. Soc. Spec. Publ. Lond*., 19, 67–81.

Irvine, I.C. and Baragar, W.R.A., 1971. A guide to chemical classification of the common volcanic rocks. *Canadian Journal of Earth Sciences*, 8, 523-548.

Keller, J., Jung, D., Eckhardt, F.J. & Kreuzer, H. 1992. Radiometric ages and chemical characterization of the Galatean andeiste massif, Pontus, Turkey. *Acta Vulcanologica, Marinelli Volume,* 2, 267-276.

Koçyiğit, A., Winchester, J.A., Bozkurt, E. & Holland, G. 2003. Saraçköy volcanic suite: implications for the subductional phase of arc evolution in the Galatean Arc Complex, Ankara, Turkey. *Geological Journal,* 38, 1-14.

Maniar, P.D., and Picolli, P.M., 1989. Tectonic discrimination of granitoids. *Geological Society America Bulletin,* 101, 635-643.

Pearce, J.A., Harris, N.B.W., Tindle, A.G., 1984. Trace element discrimination diagrams for the tectonic interpretation of granitic rocks. *Journal of Petrology*, 25, 956-983.

Rollinson, H., 1993. Using geochemical data: evaluation, presentation, interpretation. Longman Scientific and Technical, UK.

Tankut, A., Wilson, M. & Yihunie, T. 1998. Geochemistry and tectonic setting of Tertiary volcanism in the Güvem area, Anatolia, Turkey. *J. Volcanol. Geotherm. Res*. **85**, 285-301.

Taylor, S.R., McLennan, S.M., 1985. The continental crust: its composition and evolution. Blacwell Scientific Publications, Oxford.

Thiéblemont, D. and Cabanis, B. 1990. Utilisation d'un diagramme (Rb/100)-Tb-Ta pour la discrimination géochimique et l'étude pétrogénétique des roches agmatiques acides. *Bull. Soc. Geol., France,* 8, 23-35.

GEOCHEMICAL CONSTRAINTS ON THE SOURCE CHARACTERISTICS AND ATTENDANT TECTONICS OF THE BOROUJERD GRANITOID MASS, SANANDAJ- SIRJAN ZONE, WESTERN IRAN

Khalaji A. A.*, Esmaeily D. and Valizadeh M.V.

School of Geology, College of Sciences, University of Tehran, Tehran, Iran
*Corresponding author: Tel.: +98 21 66491623; fax: +98 21 66491623. E-mail address: khalagi@khayam.ut.ac.ir (A. Ahmadi Khalaji).

Abstract: The granitoid Boroujerd mass belongs to the Sanandaj – Sirjan Zone (SSZ) in western Iran. It is elongated and parallel to the prevailing schistose in the metamorphic rocks by the trend of NW–SE and consists of quartz diorites, granodiorites, monzogranites and acidic dikes (aplites and pegmatites). The statistical technique of discriminant analysis, using major elements differences alone, shows that this mass has characteristics of orogenic granitoids. The granitoid Boroujerd has geochemical characteristics typical of arc intrusives and plot as volcanic arc granites on various discriminant diagrams. This granitoid is typically representative of a volcanic arc environment, spatially related to an active continental margin. High Th/Yb (>5) ratios correlated to high values (>10, up to ca. 100) for La/Yb show the analogies of these intrusive rocks to modern continental arc felsic magmas. Probably, it is the result of the subduction of Neo-Tethyan oceanic crust below the Iranian microcontinent. All available data are compatible with the idea that these rocks represent the products of convergent margin processes during the Mesozoic.

Key words: Sanandaj-Sirjan Zone, Granitoid Boroujerd, Continental arc, Neo-Tethyan

1. INTRODUCTION

Subduction of the Tethyan oceanic lithosphere under the southwestern border of Central Iran, caused plutonic and volcanic activity between the Jurassic and the Quaternary within and adjacent to the Sanandaj-Sirjan Zone (Berberian and King, 1981; Berberian, 1983; Mohajjel et al., 2003).

The Sanandaj-Sirjan Zone, characterized by metamorphic and complexly deformed rocks associated with abundant deformed and undeformed plutons in addition to widespread Mesozoic volcanic rocks, has a length of 1500 km and a width up to 200 km from northwest to southeast Iran (Figure 1a). It separates the stable Central Iran block, from the Afro-Arabian plate (Stöcklin, 1968). According to Mohajjel et al. (2003), the major structures in the Sanandaj Sirjan Zone formed during three separate events (1) subduction along the active margin of Central Iran at the northeastern margin of Tethys, (2) ophiolite obduction along the northeastern margin of Tethys, and (3) continental collision of Arabia and Central Iran in the Miocene. The ophiolites of the Neyriz and Kermanshah regions indicate obduction of oceanic fragments along the Zagros suture. Continental collision in the Sanandaj–Sirjan Zone reached a climax in the Miocene after opening of the Red Sea and the Gulf of Aden. The Sanandaj-Sirjan magmatic-arc, including the Boroujerd complex, was formed over the 'northern' steeply dipping Neotethyan subduction zone during Late Triassic to Late Cretaceous time (e.g., Berberian and King, 1981; Shahabpour, 2005) (Figure 1b).

In this paper, we present new geochemical data on granitoid plutons from the Boroujerd area of the Sanandaj-Sirjan Zone. The data in this paper are important for the understanding of the presence of a subduction zone in SW of Iran during the Mesozoic.

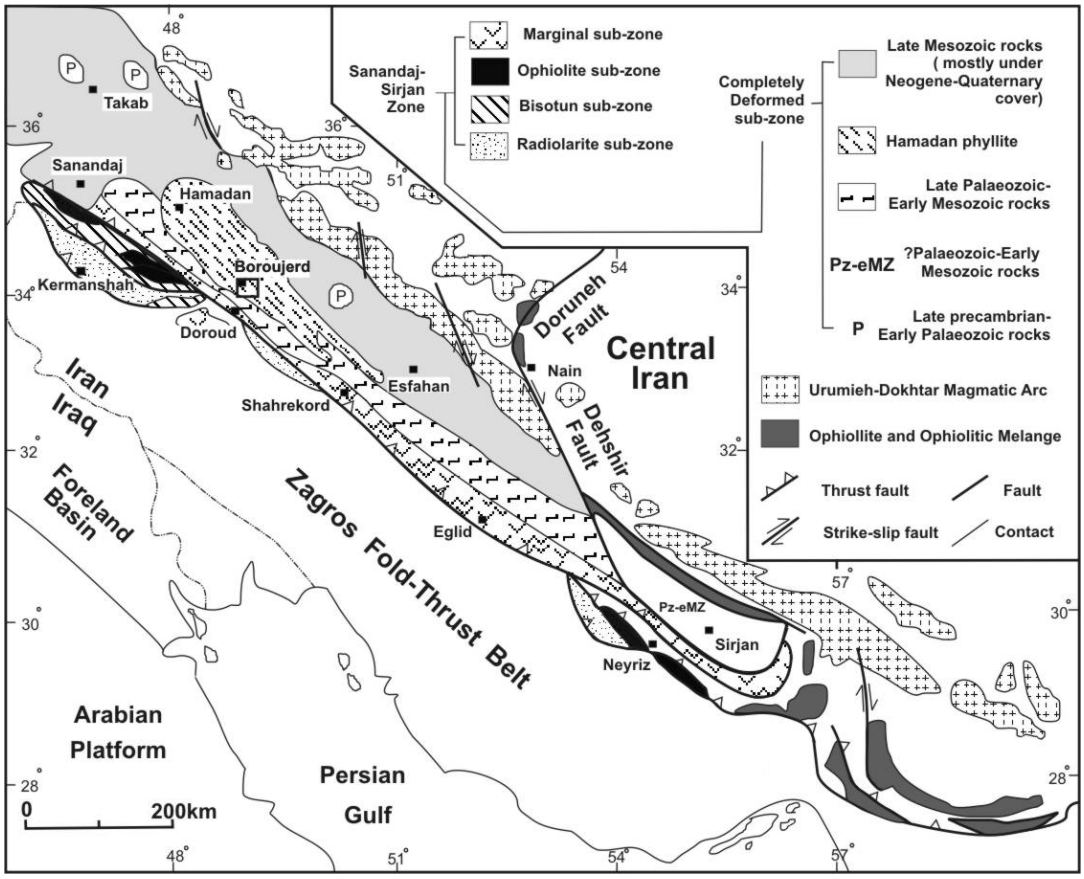

Figure 1 a. Tectonic setting of zones in the western of Iran (Mohajjel et al., 2003) and located of studied area

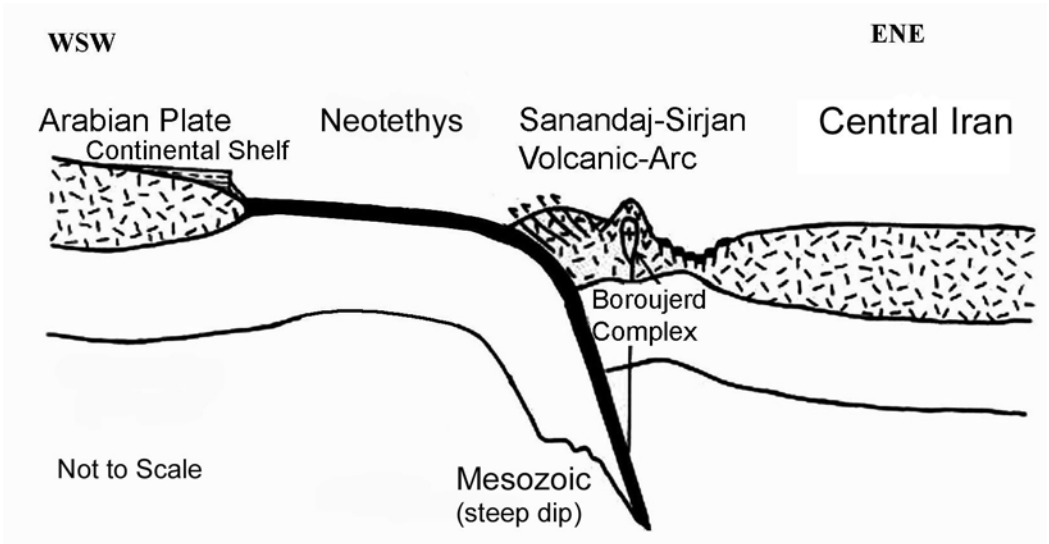

Figure 1 b. Tectonic setting of the Sanandaj-Sirjan zone granitoids (Shahabpour, 2005)

2. GEOLOGICAL SETTING

The Boroujerd area is characterised by the predominance of metamorphic rocks of Jurassic age and the presence of the Boroujerd huge granitoid complex. The oldest distinguishable rocks of the area are pre-Jurassic in age (Ahmadi, 2005).They are low- to very low-grade metamorphic rocks, such as Meta volcanic and tuff, Meta cherty limestone, Meta sandstone, slates and phyllites. The country rocks into which the Boroujerd complex was emplaced consist of the metamorphic complex of Jurassic age. Contact effects

are especially noticeable to the north of the pluton. The contact metamorphism of the northern margin is better developed and exposed then those of the southern margin. This suggests that the southern contact of Boroujerd complex is controlled by a fault system parallel to the contact (Ahmadi, 2005).

The results of U-Pb single zircon geochronology of granitoids (the analyses were measured on a VG sector 54 mass spectrometer at the University of MIT) show a maximum age interval of 172 Ma to 169 Ma, correlating with middle Jurassic (Ahmadi, 2005).

3. FIELD DESCRIPTION AND PETROGRAPHY

The Boroujerd granitoid rocks consist of granodiorites, quartz diorites, monzogranites and acidic dikes.

The granodiorites are widespread throughout the area and the biggest intrusion in the area with an elongate shape extending north-west. A foliation due to orientation of the minerals (especially biotite) is seen in them. They have a granular to weakly porphyritic texture showing a simple mineralogy: plagioclase, biotite, quartz and alkali feldspar. Apatite, zircon, allanite and opaques are common accessory minerals and some muscovite is present as secondary mineral.

The quartz diorites are exposed within the granodiorites and have gradual boundaries with them**.** These rocks have granular texture to porphyritic with plagioclase megacrysts and composed predominantly of plagioclase, amphibole, biotite, alkali feldspar and quartz.

The monzogranites widely scattered as separate and small outcrops through the southern part. These rocks are light in colour and fine to coarse-grained and display a porphyritic texture with feldspar megacrysts and a granular texture in margin. The mineral assemblages include perthitic alkali feldspar, plagioclase, quartz, biotite, and minor muscovite. Zircon, allanite, apatite are common accessory minerals.

4. SAMPLING AND ANALYTICAL METHODS

A total of about three hundred rock samples from different localities, including granodiorites, quartz-diorites, monzogranites and enclaves were collected. Two hundred thin sections of these samples were prepared and studied by optical microscope. Representative samples (34 samples) were then selected for whole rock geochemistry. Major and trace element abundances were determined by inductively coupled plasma atomic emission spectrometry (ICP-AES) and inductively coupled plasma-mass spectrometry (ICP-MS) at the ALS Chemex laboratories in Vancouver, Canada. The results of the analyses are reported in Table 1.

5. TECTONOMAGMATIC SETTING AND DISCUSSION

Numerous studies suggest that major and trace elements could be used as discriminatory tools to distinguish among different tectonic settings of granitoid magmas (e. g., Pearce et al., 1984; Hariss et al., 1986). Agrawal (1995) with the application of multiple discriminat analysis (a statistical technique) on the data, developed a numerical of classification that, using major elements alone, distinguishes the various tectonic setting of granitoids. The results of discriminant analysis for the various groups are summarizaed in table 2a. With the help of the discriminant coefficient given in table 2a, a discriminant score for granite can be obtained from the linear discriminant equation:

$$Di = B1X1 + B2X2 + ….. + BpXp + Bo$$

Where X is the major element value, B is the discriminant function coefficient, B_0 is constant. Only those major elements selected (Table 2a) in the discriminant equation were included in the discriminant equation for obtaining the discriminant score (D_i).

Tablo 1. Major and element contends from the Boroujerd granitoids

Quartz diorites											
Sample	G14	G16	G18	G19	B2A31	GM25	G12	G11	AG2	B2A28	B2A33
SiO[2]	63.4	60.7	59.9	59.2	58.9	57.9	56.3	55.5	55.4	53.2	52.6
TiO[2]	0.6	0.6	0.6	0.8	0.7	0.6	0.9	0.7	1.3	0.7	0.6
Al_2O_3	16.6	14.9	15.4	15.9	16.2	15.3	17.1	15.9	16.8	15.6	15.2
Fe_2O_3 t	6.0	6.4	6.6	7.1	7.1	6.9	8.0	7.8	8.6	8.7	8.7
MnO	0.1	0.1	0.1	0.1	0.1	0.1	0.2	0.2	0.2	0.2	0.2
MgO	3.3	4.3	4.6	4.8	4.7	6.5	5.1	6.5	4.6	7.6	8.4
CaO	5.6	5.2	5.6	5.5	5.9	6.1	6.9	6.4	7.3	7.8	8.9
Na_2O	1.4	2.2	2.3	2.4	2.5	2.4	2.5	2.5	2.7	2.3	1.9
K_2O	2.3	3.5	3.0	2.8	2.0	2.5	2.1	2.2	1.8	2.1	1.8
P_2O_5	0.2	0.1	0.1	0.2	0.1	0.1	0.2	0.1	0.3	0.1	0.1
Ni	37.0	53.0	57.0	63.0	49.0	115.0	75.0	101.0	38.0	86.0	103.0
Cr	260.0	280.0	260.0	330.0	320.0	420.0	360.0	450.0	150.0	490.0	690.0
Co	20.0	20.3	20.6	22.9	23.8	48.0	27.8	28.7	54.5	31.9	36.4
V	176.0	144.0	144.0	148.0	150.0	170.0	204.0	210.0	168.0	217.0	274.0
Cs	9.9	6.0	6.2	7.5	4.7	10.0	5.4	4.6	4.2	3.2	3.5
Rb	103.0	128.0	105.0	111.0	77.4	106.5	88.2	101.0	66.6	78.8	65.9
Sr	299.0	263.0	269.0	261.0	231.0	347.0	347.0	388.0	334.0	197.0	202.0
Ba	242.0	596.0	388.0	372.0	361.0	407.0	355.0	454.0	296.0	236.0	238.0
Th	4.0	24.0	7.0	13.0	5.0	11.0	9.0	10.0	7.0	5.0	5.0
U	2.5	3.0	2.0	1.8	2.3	2.1	2.4	2.6	1.9	1.4	1.2
Ta	0.8	1.0	0.9	0.9	0.9	0.9	0.9	0.7	1.1	0.5	0.5
Nb	8.0	12.0	10.0	12.0	10.0	10.0	12.0	9.0	13.0	7.0	8.0
La	13.8	68.3	19.4	33.8	16.4	28.8	27.2	24.1	19.0	16.6	20.0
Ce	32.9	146.5	44.2	72.3	41.5	55.6	57.6	50.1	44.4	39.4	50.7
Pr	3.8	14.8	5.4	7.9	5.7	6.7	6.7	5.8	5.1	4.4	6.1
Nd	14.8	49.4	20.9	28.7	24.0	24.0	25.0	21.8	19.8	16.2	23.9
Sm	3.9	8.3	4.4	5.6	5.4	4.8	5.0	4.4	4.8	3.5	5.0
Eu	0.1	1.1	0.7	1.2	0.8	1.1	0.4	0.1	1.1	0.8	0.1
Gd	3.8	7.8	4.6	5.6	5.3	4.6	5.1	4.1	4.5	3.8	5.2
Tb	0.6	1.0	0.7	0.8	0.8	0.7	0.7	0.6	0.6	0.5	0.8
Dy	3.7	5.7	4.2	4.4	5.1	3.8	4.3	3.5	3.8	3.5	4.6
Ho	0.7	1.1	0.9	0.9	1.0	0.8	0.8	0.8	0.7	0.7	1.0
Er	2.1	3.4	2.6	2.6	3.2	2.3	2.6	2.2	2.1	2.1	2.9
Tm	0.3	0.5	0.4	0.4	0.5	0.3	0.4	0.3	0.3	0.3	0.4
Yb	1.9	3.4	2.5	2.6	3.2	2.3	2.5	2.2	2.0	2.0	2.8
Lu	0.3	0.5	0.4	0.4	0.5	0.3	0.4	0.3	0.3	0.3	0.4
Y	20.4	30.7	22.5	23.3	30.2	21.6	23.4	19.8	18.2	18.4	26.6
Hf	4.0	4.0	5.0	5.0	4.0	5.0	5.0	5.0	3.0	2.0	2.0
Zr	117.0	115.0	139.0	179.5	123.5	164.0	161.5	175.5	90.0	77.6	71.6
Zn	96.0	70.0	62.0	69.0	58.0	68.0	127.0	118.0	79.0	63.0	114.0
Ga	19.0	18.0	17.0	19.0	18.0	18.0	22.0	20.0	19.0	16.0	18.0
Sn	5.0	3.0	2.0	2.0	2.0	6.0	3.0	4.0	3.0	1.0	2.0
W	9.0	5.0	3.0	4.0	14.0	217.0	8.0	5.0	269.0	1.0	3.0
Eu/Eu*	0.1	0.4	0.5	0.7	0.5	0.7	0.2	0.1	0.7	0.7	0.0
(La/Yb)N	4.9	13.4	5.2	8.7	3.4	8.4	7.3	7.3	6.4	5.6	4.8

Table 1 continued

Quartz diorites											
Sample	G14	G16	G18	G19	B2A31	GM25	G12	G11	AG2	B2A28	B2A33
SiO[2]	63.4	60.7	59.9	59.2	58.9	57.9	56.3	55.5	55.4	53.2	52.6
TiO[2]	0.6	0.6	0.6	0.8	0.7	0.6	0.9	0.7	1.3	0.7	0.6
Al_2O_3	16.6	14.9	15.4	15.9	16.2	15.3	17.1	15.9	16.8	15.6	15.2
Fe_2O_3 t	6.0	6.4	6.6	7.1	7.1	6.9	8.0	7.8	8.6	8.7	8.7
MnO	0.1	0.1	0.1	0.1	0.1	0.1	0.2	0.2	0.2	0.2	0.2
MgO	3.3	4.3	4.6	4.8	4.7	6.5	5.1	6.5	4.6	7.6	8.4
CaO	5.6	5.2	5.6	5.5	5.9	6.1	6.9	6.4	7.3	7.8	8.9
Na2O	1.4	2.2	2.3	2.4	2.5	2.4	2.5	2.5	2.7	2.3	1.9
K_2O	2.3	3.5	3.0	2.8	2.0	2.5	2.1	2.2	1.8	2.1	1.8
P_2O_5	0.2	0.1	0.1	0.2	0.1	0.1	0.2	0.1	0.3	0.1	0.1
Ni	37.0	53.0	57.0	63.0	49.0	115.0	75.0	101.0	38.0	86.0	103.0
Cr	260.0	280.0	260.0	330.0	320.0	420.0	360.0	450.0	150.0	490.0	690.0
Co	20.0	20.3	20.6	22.9	23.8	48.0	27.8	28.7	54.5	31.9	36.4
V	176.0	144.0	144.0	148.0	150.0	170.0	204.0	210.0	168.0	217.0	274.0
Cs	9.9	6.0	6.2	7.5	4.7	10.0	5.4	4.6	4.2	3.2	3.5
Rb	103.0	128.0	105.0	111.0	77.4	106.5	88.2	101.0	66.6	78.8	65.9
Sr	299.0	263.0	269.0	261.0	231.0	347.0	347.0	388.0	334.0	197.0	202.0
Ba	242.0	596.0	388.0	372.0	361.0	407.0	355.0	454.0	296.0	236.0	238.0
Th	4.0	24.0	7.0	13.0	5.0	11.0	9.0	10.0	7.0	5.0	5.0
U	2.5	3.0	2.0	1.8	2.3	2.1	2.4	2.6	1.9	1.4	1.2
Ta	0.8	1.0	0.9	0.9	0.9	0.9	0.9	0.7	1.1	0.5	0.5
Nb	8.0	12.0	10.0	12.0	10.0	10.0	12.0	9.0	13.0	7.0	8.0
La	13.8	68.3	19.4	33.8	16.4	28.8	27.2	24.1	19.0	16.6	20.0
Ce	32.9	146.5	44.2	72.3	41.5	55.6	57.6	50.1	44.4	39.4	50.7
Pr	3.8	14.8	5.4	7.9	5.7	6.7	6.7	5.8	5.1	4.4	6.1
Nd	14.8	49.4	20.9	28.7	24.0	24.0	25.0	21.8	19.8	16.2	23.9
Sm	3.9	8.3	4.4	5.6	5.4	4.8	5.0	4.4	4.8	3.5	5.0
Eu	0.1	1.1	0.7	1.2	0.8	1.1	0.4	0.1	1.1	0.8	0.1
Gd	3.8	7.8	4.6	5.6	5.3	4.6	5.1	4.1	4.5	3.8	5.2
Tb	0.6	1.0	0.7	0.8	0.8	0.7	0.7	0.6	0.6	0.5	0.8
Dy	3.7	5.7	4.2	4.4	5.1	3.8	4.3	3.5	3.8	3.5	4.6
Ho	0.7	1.1	0.9	0.9	1.0	0.8	0.8	0.8	0.7	0.7	1.0
Er	2.1	3.4	2.6	2.6	3.2	2.3	2.6	2.2	2.1	2.1	2.9
Tm	0.3	0.5	0.4	0.4	0.5	0.3	0.4	0.3	0.3	0.3	0.4
Yb	1.9	3.4	2.5	2.6	3.2	2.3	2.5	2.2	2.0	2.0	2.8
Lu	0.3	0.5	0.4	0.4	0.5	0.3	0.4	0.3	0.3	0.3	0.4
Y	20.4	30.7	22.5	23.3	30.2	21.6	23.4	19.8	18.2	18.4	26.6
Hf	4.0	4.0	5.0	5.0	4.0	5.0	5.0	5.0	3.0	2.0	2.0
Zr	117.0	115.0	139.0	179.5	123.5	164.0	161.5	175.5	90.0	77.6	71.6
Zn	96.0	70.0	62.0	69.0	58.0	68.0	127.0	118.0	79.0	63.0	114.0
Ga	19.0	18.0	17.0	19.0	18.0	18.0	22.0	20.0	19.0	16.0	18.0
Sn	5.0	3.0	2.0	2.0	2.0	6.0	3.0	4.0	3.0	1.0	2.0
W	9.0	5.0	3.0	4.0	14.0	217.0	8.0	5.0	269.0	1.0	3.0
Eu/Eu*	0.1	0.4	0.5	0.7	0.5	0.7	0.2	0.1	0.7	0.7	0.0
(La/Yb)N	4.9	13.4	5.2	8.7	3.4	8.4	7.3	7.3	6.4	5.6	4.8

Table 1 continued

Microgranodioritic enclaves				Monzogranites							
Sample	AGH2	B2A24	AD	G22	AG19	GM11	AB6	AG18	G24	GM10	G23
SiO[2]	64.2	62.3	55.0	75.1	73.7	71.4	71.1	70.8	70.7	70.0	69.7
TiO[2]	0.7	0.6	0.8	0.1	0.3	0.3	0.2	0.4	0.2	0.3	0.2
Al_2O_3	15.7	16.7	18.5	12.8	12.8	14.0	14.5	13.5	14.6	14.1	14.9
Fe_2O_3 t	6.0	6.2	7.7	1.1	2.2	3.0	2.0	2.8	2.2	3.5	2.5
MnO	0.1	0.1	0.1	0.0	0.1	0.1	0.0	0.1	0.1	0.1	0.1
MgO	1.8	2.4	2.3	0.1	0.4	0.6	1.2	0.6	0.4	0.7	0.5
CaO	3.6	3.4	1.8	0.5	0.9	1.8	0.9	1.0	1.7	2.1	1.8
Na_2O	3.3	3.3	2.5	3.7	3.8	3.0	4.2	3.9	3.8	2.8	4.1
K_2O	2.2	2.7	8.3	4.6	3.8	4.1	2.1	4.1	4.6	4.0	4.2
P_2O_5	0.3	0.1	0.1	0.0	0.1	0.1	0.1	0.1	0.0	0.1	0.0
Ni	22.0	19.0	46.0	7.0	7.0	11.0	13.0	20.0	9.0	12.0	8.0
Cr	100.0	100.0	130.0	130.0	10.0	20.0	150.0	10.0	80.0	20.0	110.0
Co	14.2	14.2	14.6	1.2	54.1	32.9	3.3	54.7	3.7	53.4	3.5
V	64.0	130.0	172.0	3.3	17.0	24.0	23.0	27.0	11.0	29.0	11.0
Cs	9.5	7.0	13.3	3.7	0.8	2.7	2.3	1.1	4.5	6.2	4.5
Rb	162.5	149.5	290.0	189.0	129.0	146.5	63.8	123.5	157.0	166.5	152.5
Sr	260.0	294.0	205.0	27.8	121.5	229.0	114.0	168.0	124.5	239.0	132.5
Ba	353.0	250.0	1105.0	38.5	320.0	399.0	276.0	631.0	408.0	404.0	372.0
Th	17.0	18.0	14.0	19.0	31.0	15.0	16.0	32.0	11.0	20.0	13.0
U	1.9	3.0	1.7	3.8	5.8	2.6	2.5	5.3	2.4	2.7	2.6
Ta	1.7	0.9	1.0	1.5	3.2	1.4	1.1	2.6	0.9	1.4	1.1
Nb	19.0	12.0	14.0	9.0	32.0	11.0	10.0	28.0	10.0	11.0	11.0
La	37.3	37.7	30.5	7.3	42.7	32.9	32.5	59.5	20.1	39.7	25.1
Ce	74.7	71.3	63.5	18.0	74.6	64.6	64.1	101.5	40.5	77.4	54.5
Pr	7.8	7.8	6.8	2.4	7.2	6.9	6.5	9.7	4.2	8.3	5.6
Nd	27.2	27.1	24.2	9.8	23.0	23.7	22.3	29.6	15.0	28.7	20.3
Sm	5.4	4.7	4.7	4.0	4.5	4.5	4.5	5.2	3.3	5.2	4.4
Eu	1.1	0.8	1.4	0.1	0.9	0.7	0.7	0.1	0.4	0.5	0.2
Gd	5.8	4.9	3.8	5.7	4.6	4.1	4.2	5.3	3.6	5.1	4.2
Tb	0.8	0.6	0.4	1.2	0.7	0.6	0.6	0.7	0.6	0.7	0.6
Dy	5.2	3.2	2.4	8.8	4.2	3.5	3.7	4.0	3.5	3.9	4.1
Ho	1.0	0.6	0.5	2.0	0.8	0.7	0.7	0.8	0.7	0.8	0.8
Er	3.0	1.8	1.4	6.0	2.5	1.9	2.2	2.5	2.1	2.2	2.7
Tm	0.5	0.2	0.2	1.0	0.4	0.3	0.3	0.4	0.3	0.3	0.4
Yb	3.1	1.6	1.3	6.6	2.9	2.0	2.4	2.6	2.1	2.2	2.6
Lu	0.4	0.2	0.2	0.9	0.4	0.3	0.3	0.4	0.3	0.3	0.4
Y	27.2	17.1	12.7	59.5	22.8	19.2	20.2	22.8	20.3	21.0	23.3
Hf	7.0	5.0	5.0	4.0	5.0	4.0	4.0	6.0	4.0	4.0	5.0
Zr	235.0	145.5	157.5	81.5	178.0	116.5	106.0	230.0	128.0	137.0	149.0
Zn	56.0	53.0	69.0	16.0	30.0	29.0	13.0	79.0	39.0	35.0	47.0
Ga	24.0	20.0	22.0	16.0	19.0	17.0	17.0	20.0	17.0	17.0	17.0
Sn	2.0	1.0	4.0	3.0	3.0	2.0	3.0	4.0	4.0	2.0	4.0
W	6.0	4.0	2.0	8.0	469.0	225.0	8.0	416.0	11.0	429.0	11.0
Eu/Eu*	0.6	0.5	1.0	0.0	0.6	0.5	0.5	0.0	0.4	0.3	0.1
(La/Yb)N	8.0	15.8	15.7	0.7	9.8	11.0	9.1	15.3	6.4	12.1	6.5

Table 2 a. Discriminant Coefficients, Mean Discriminant Scores and Cut- off Values for the various groups of the granites (Agrawal, 1995)

X	B	M_i(mean score)	C_i (cut of value)	B_0(constant)
Fe_2O_3	0.929241			
MgO	-2.570311	-0.4898	0.2915	-11.754220
Na_2O	1.246346			
K_2O	1.266569			

Tablo 2 b. The results of discriminant analysis for the various samples from the Boroujerd granitoids

SAMPLE	D_i	D_i-C_i	M_i-C_i	R
AGH1	-2.22306	-2.51456	-0.7813	3.218431
AS2	-1.86802	-2.15952	-0.7813	2.764011
AGH6	-2.94696	-3.23846	-0.7813	4.144964
AD4	-2.18494	-2.47644	-0.7813	3.169639
AGH2	-3.829	-4.1205	-0.7813	5.273903
B2A24	-4.65729	-4.94879	-0.7813	6.334051
AB6	-5.09146	-5.38296	-0.7813	6.889753
GM11	-1.65822	-1.94972	-0.7813	2.495484
GM10	-1.64418	-1.93568	-0.7813	2.477511
AG18	-0.73966	-1.03116	-0.7813	1.319805
AG19	-1.32556	-1.61706	-0.7813	2.06971
G22	-0.60362	-0.89512	-0.7813	1.145683
G23	-0.25604	-0.54754	-0.7813	0.700801
G24	-0.25279	-0.54429	-0.7813	0.696648
AKY13	-3.31919	-3.61069	-0.7813	4.621385
B1A55	-2.31954	-2.61104	-0.7813	3.341921
B4A19	-2.77037	-3.06187	-0.7813	3.918948
G4	-2.55118	-2.84268	-0.7813	3.638399
G5	-2.89941	-3.19091	-0.7813	4.084108
G6	-2.74668	-3.03818	-0.7813	3.888618
B2A28	-17.6983	-17.9898	-0.7813	23.02548
B2A31	-11.7115	-12.003	-0.7813	15.3628
B2A33	-20.5805	-20.872	-0.7813	26.71446
G11	-15.2941	-15.5856	-0.7813	19.94827
G12	-11.8718	-12.1633	-0.7813	15.56797
GM25	-15.9385	-16.23	-0.7813	20.7731
AG2	-9.93547	-10.227	-0.7813	13.08968
G14	-9.95933	-10.2508	-0.7813	13.12022
G16	-9.59563	-9.88713	-0.7813	12.65472
G18	-10.5938	-10.8853	-0.7813	13.93234
G19	-11.0159	-11.3074	-0.7813	14.47252
GM5	-12.778	-13.0695	-0.7813	16.72791
MA3	-10.5025	-10.794	-0.7813	13.81547
AD	2.931517	2.640017	-0.7813	-3.37901

The discriminant rule, R, for given granite can be obtained with the help of this equation:

$$R = \frac{(D_i - C_i)}{(M_i - C_i)}$$

Where D_i is the discriminant score, C_i and M_i are constants (Table 2a).

If the discriminant rule, R, is positive, sample is assigned to the orogenic, otherwise to the anorogenic. Thus, the Boroujerd granitoids have characteristics of orogenic granitoids (R is greater than zero, Table 2b).

Granitoids of the Boroujerd aera are also compatible with pre-plate collision setting on R_1 vs. R_2 discrimination diagram (Figure 2a) of Batchlor and Bowden (1985).

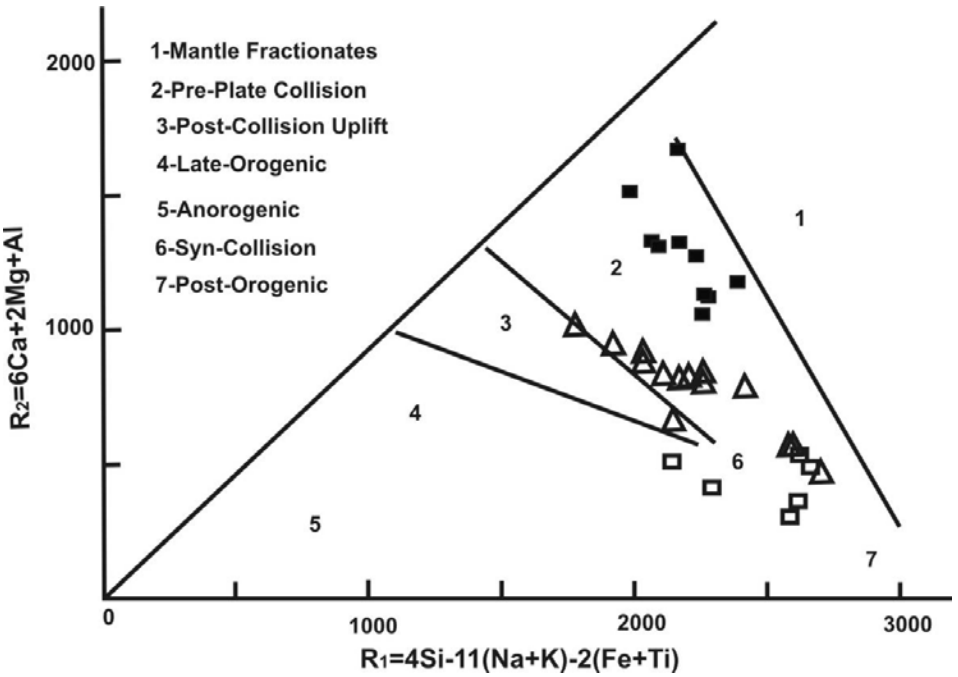

Figure 2 a. Plot of samples from the Boroujerd granitoids on R1 vs. R2 discrimination diagram (Batchlor and Bowden, 1985) which indicates a pre-plate collision affinity for the Boroujerd granitoids

■: quarz diorites, □: monzogranites, Δ: granodiorites

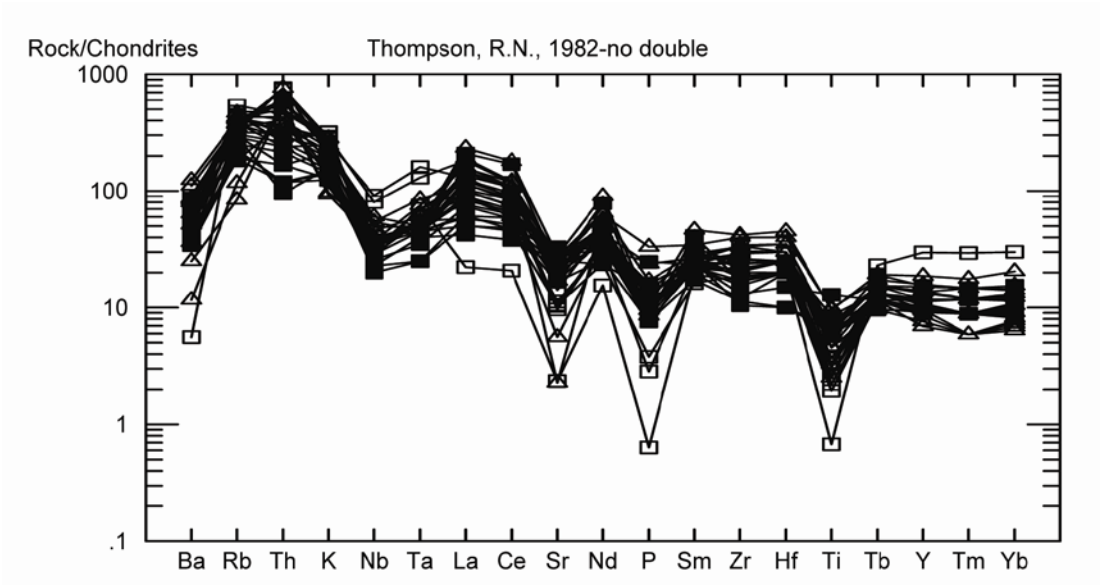

Figure 2 b) Chondrite-normalised (Thompson, 1982), trace element abundance diagram (spidergrams) for representative samples of the studied granitoids. Symbols as in Figure 2 a.

Trace elements distribution patterns of granodioritic, quartz-dioritic and monzogranitic units from the Boroujerd complex are normalized to chondrites (Figure 2b). Accordingly, all studied samples show Ta, Nb, Ti, P and Sr depletion and are enriched in LILE (Rb, K, and Th). In comparison with HFSE (Nb, Ta, Hf, Zr, Sm, Y, and Yb), the LREE (La, Ce, Nd) show enrichment. These features are a general characteristic of calc-alkaline arc granitoids (e.g. Rogers and Hawkesworth, 1989; Sajona et al., 1996). Granitoids of the Boroujerd aera are also compatible with volcanic arc settings (Figure 3a) on the tectonic discriminant diagram of Harris et al. (1986). On the tectonic discriminant diagram of Pearce et al. (1984) all analyzed samples fall into the VAG field (Figure 3b). These VAG belong to the group of 'active continental margin' rocks (Group C after Pearce et al., 1984).

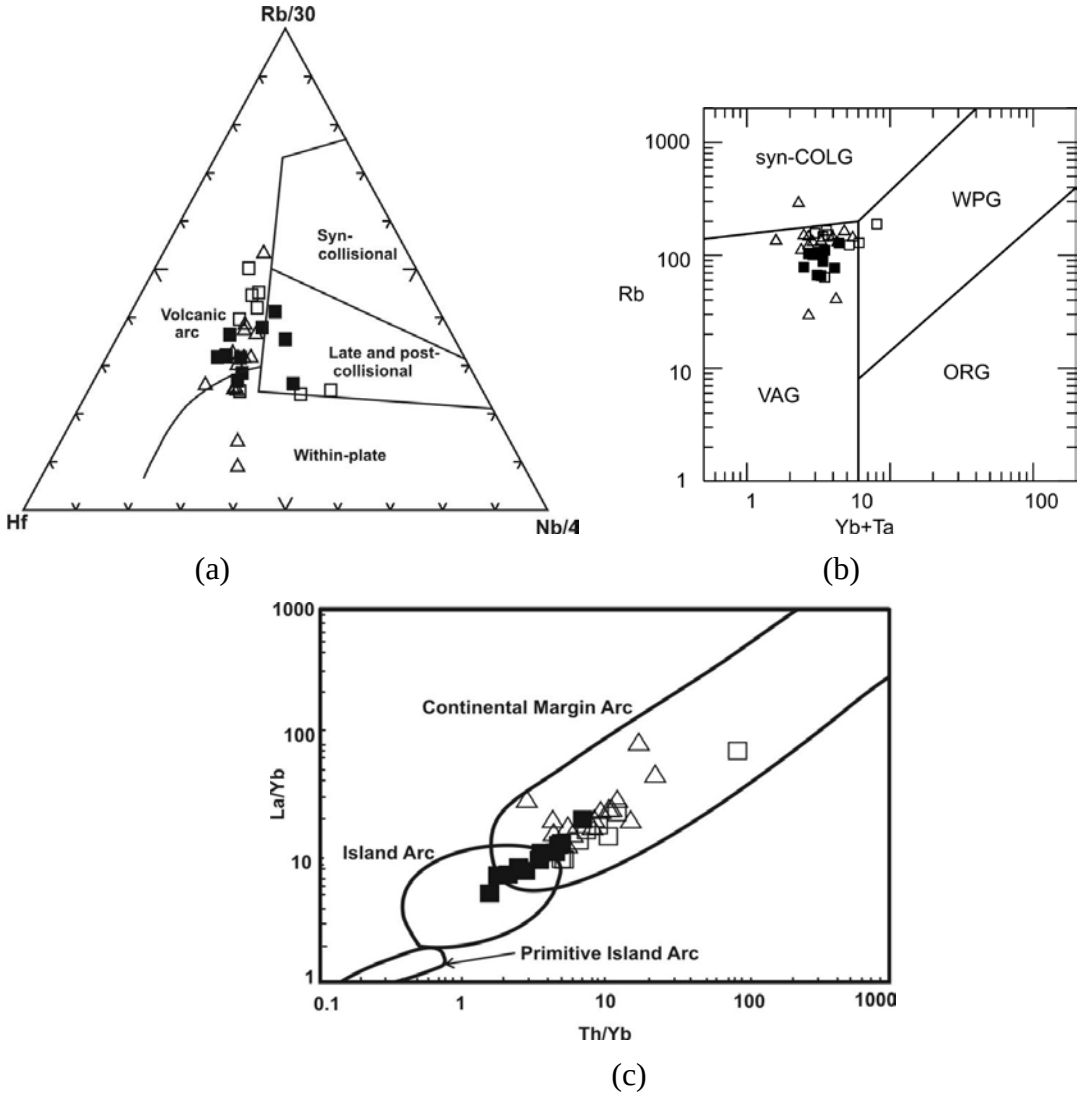

Figure 3. (a) Ternary diagram (Harris et al., 1986) for rocks of the Boroujerd complex;.(b) Studied granitoids in the tectonic discriminant diagram (Pearce et al., 1984), ORG, oceanic ridge granites; syn-COLG, syncollision; VAG, volcanic arc granites; WPG, within plate granites; (c) La/Yb vs. Th/Yb diagram (Condi, 1989). Symbols as in Fig.2.

High Th/Yb (>5) ratios correlated to high values (>10, up to ca. 100) for La/Yb (Figure 3c), and Th/Ta vs. Yb and Th/Yb versus Ta /Yb (Schandl & Gorton, 2002) diagrams show the analogies of these intrusive rocks to continental arc felsic magmas.

6. CONCLUSIONS

The Boroujerd granitoid mass belong to the Sanandaj-Sirjan zone and display geochemical characteristics typical of the volcanic arc granites related to an active continental margin. This conclusion is in good agreement with the general model of Berberian (1983) and Shahabpour (2005), which assumed that the Sanandaj-Sirjan calc-alkaline magmatic arc formed over a high angle subducting oceanic slab in the Neotethyan subduction zone during Late Triassic to Late Cretaceous time (Fig.1b).

AKNOWLEDGEMENTS

This work was supported by grant no 6105013/1/01 from the University of Tehran of I.R. Iran, received by M.V. Valizadeh.

REFERENCES

Ahmadi, A., 2005. Petrology of the granitoids rocks of the Boroujerd area. PhD Thesis, *School of Geology, College of Sciences, University of Tehran*, Tehran, Islamic Republic of Iran. (unpublished).

Agrawal, S., 1995. Discrimination between late-orogenic, post-orogenic and anorgenic granites by major element compositions. *The journal of geology* 103, 529 – 537.

Batchelor, R.A. and Bowden, P., 1985. Petrogenetic interpretation of granitoid rock series using multicationic parameters. *Chemical Geology* 48, 43–55.

Berberian, M., 1983. Generalized tectonic map of Iran. In: Berberian, M., (Ed.), Continental Deformation in the Iranian Plateau, *Geological Survey of Iran*, Report No. 52.

Berberian, M. and King G.C.P., 1981. To wards a paleogeography and tectonic evolution of Iran. *Canadian Journal of Earth Sciences*, vol. 18, No. 2. pp.210-265.

Condie, K.C., 1989. Geochemical changes in basalts and andesites across the Archean–Proterozoic boundary: identification and significance. *Lithos* 23, 1–18.

Harris, N.B.W., Pearce, J.A. and Tindle, A.G., 1986. Geochemical characteristics of collision-zone magmatism. In: Coward, M.P., Ries, A.C. (Eds.), Collision Tectonics. *Geological Society London, Special Publication* 19, 67–81.

Mohajjel, M., Fergusson, C.L. and Sahandi, M.R., 2003. Cretaceous–Tertiary convergence and continental collision, Sanandaj-Sirjan zone, Western Iran. *Journal of Asian earth Sciences* 21, 397–412.

Pearce, J.A., Harris, N.B.W. and Tindle, A.G., 1984. Trace element discrimination diagrams for the tectonic interpretation of grantitic rocks. *Journal of Petrology* 25, 956 – 983.

Rogers, G. and Hawkesworth, C.J., 1989. A geochemical traverse across the North Chilean Andes: evidence for crust generation from the mantle wedge. *Earth and Planetary Science Letters* 91, 271–285.

Sajona, F.G., Maury, R.C., Bellon, H., Cotton, J. and Defant, M., 1996. High field strength elements of Pliocene-Pleistocene island-arc basalts Zamboanga Peninsula, Western Mindanao (Philippines), *Journal of Petrology* 37, 693–726.

Schandl, E. S., and Gorton, M. P., 2002. Appplication of high field strength elements to discriminate tectonic setting in VMS environments. *Economic Geology* 97, 629–642

Shahabpour, J., 2005. Tectonic evolution of the orogenic belt in the region located between Kerman and Neyriz. *Journal of Asian Earth Sciences* 24, 405-417.

Thompson, A.B., 1982. Magmatism of the Bristish Terciary volcanic Province, *Scottish Journal of Geology* 18, 50–107.

PETROLOGY AND GEOCHEMISTRY OF THE BOROUJERD GRANITOID ROCKS SANANDAJ - SIRJAN ZONE, WESTERN IRAN

Khalaji A. A.*, Esmaeily D. and Valizadeh M.V.

School of Geology, College of Sciences, University of Tehran, Tehran, Iran
*Corresponding author: Tel.: +98 21 66491623; fax: +98 21 66491623. E-mail address: khalagi@khayam.ut.ac.ir (A. Ahmadi Khalaji).

Abstract: The Boroujerd area belongs to the Sanandaj-Sirjan Zone (SSZ). The Boroujerd granitoid rocks consist of granodiorites, quartz diorites and monzogranites. They are of sub-alkaline affinity, belong to the high-K calc-alkaline series, metaluminous to weakly peraluminous, and display features typical of I-type granites.

Trace and rare-earth elements distribution patterns for the Boroujerd granitoid rocks indicate a distinctive depletion in Nb, Ta, Sr, Ba, P and Ti relative to other trace elements and a greater enrichment in LILE compared to HFSE. These geochemical characteristics suggest that these rocks derived from a crustal source.

The most reasonable model for the origin of the Boroujerd granitoid rocks involves partial melting of crustal protoliths having different compositions, leaving restites with variable proportions of amphibole and plagioclase as a result of melting under variable H_2O contents. Mantle-derived basaltic magmas emplaced into the lower crust are the most likely heat sources for partial melting.

Key words: Sanandaj-Sirjan Zone, Boroujerd, Iran, Granitoid rocks, Geochemistry

1. INTRODUCTION

The Boroujerd area belongs to the Sanandaj – Sirjan zone that has a length of 1500 km and a width up to 200 km from northwest to southeast Iran. This area is characterised by the predominance of metamorphic rocks and the presence of the Boroujerd huge granitoid complex (Figure 1).

The objectives of this paper are: (1) to present new chemical data of granitic rocks from the Sanandaj – Sirjan Zone; (2) to discuss the petrogenesis of the granitic rocks.

2. FIELD DESCRIPTION AND PETROGRAPHY

The Boroujerd granitoids include quartz diorite, granodiorite and monzogranite. The granodiorites are widespread throughout the area and the biggest intrusion in the area (Figure 1). They are gray and generally medium to coarse–grained rocks and have a granular to weakly porphyritic texture showing a simple mineralogy: plagioclase (30-40%), biotite (10-20%), quartz (25-30%) and alkali feldspar (<20%). Apatite, zircon, allanite and opaques are common accessory minerals and some muscovite is present as secondary mineral.

The quartz diorites are exposed within the granodiorites and have gradual boundaries with them. These rocks have granular texture to porphyritic with plagioclase megacrysts and composed predominantly of plagioclase (40-50%), biotite (15-20%), green amphibole (10-15%), quartz (<15%) and alkali feldspar (<5%). Zircon, titanite and apatite are conspicuous accessory minerals.

The monzogranites widely scattered as separate and small outcrops through the southern part (Figure 1). These rocks are light in colour, fine to coarse-grained that display a granular texture (in center) and a porphyritic texture with feldspar megacrysts in the margin. The mineral assemblages include quartz (30-35%) alkali feldspar (30-35%), plagioclase (25-35%), biotite (5-10%) and some secondary muscovite. Zircon, allanite and apatite are common accessory minerals. Quartz intergrowths with K-feldspar and

plagioclase form micrographic and/or granophyric texture and myrmekites, respectively.

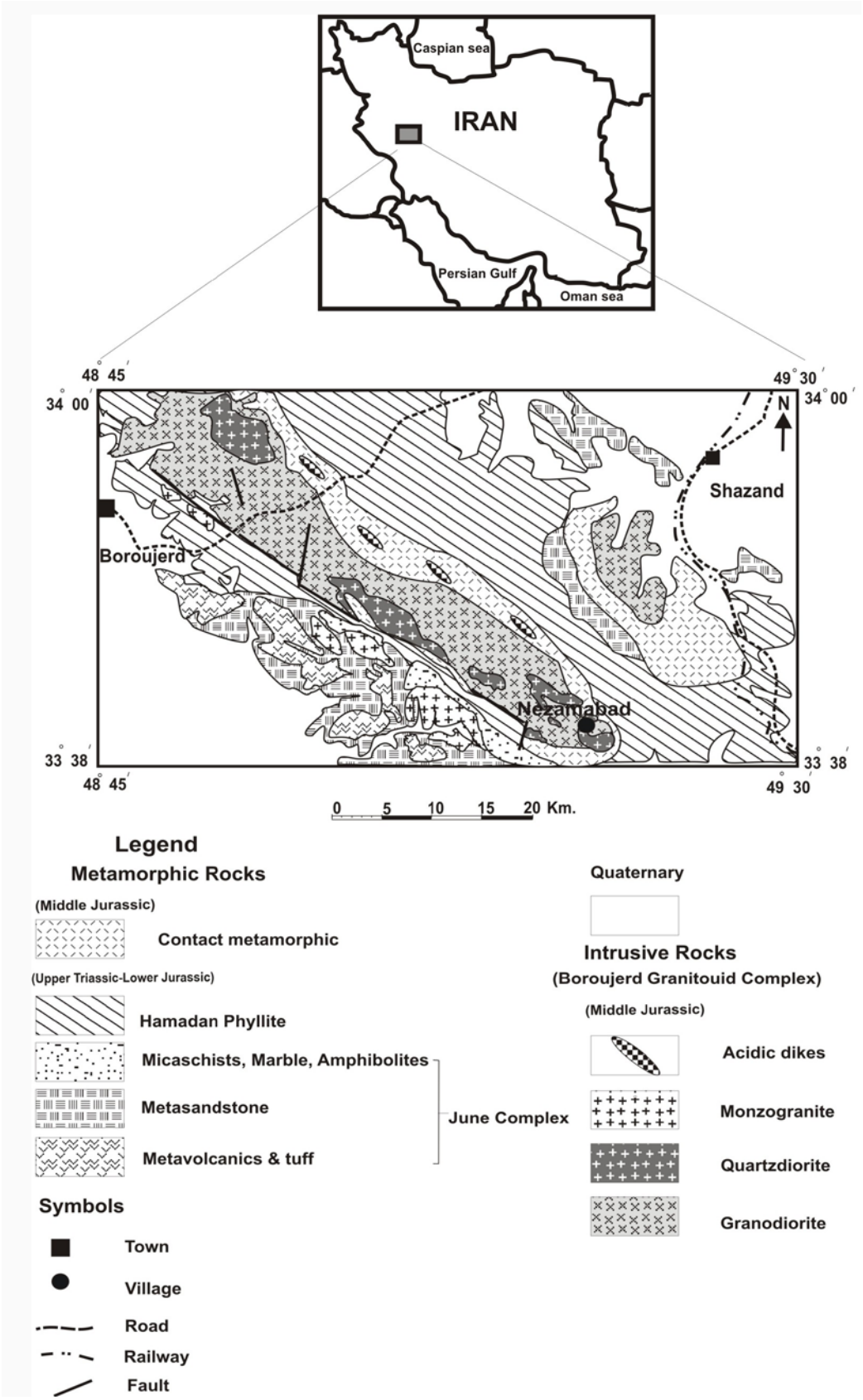

Figure 1. Geological map showing the distribution of the granitoid rocks in the Boroujerd area

3. SAMPLING AND ANALYTICAL METHODS

A total of about three hundred rock samples from different facies, including granodiorites, quartz diories, monzogranites and enclaves were collected. Two hundred thin sections of these samples were prepared and studied by optical microscope. Representative samples (34 samples) were then selected for whole rock geochemistry. Major and trace element abundances were determined by inductively coupled plasma atomic emission spectrometry (ICP-AES) and inductively coupled plasma-mass spectrometry (ICP-MS) at the ALS Chemex laboratories in Vancouver, Canada.

4. GEOCHEMICAL CHARACTERISTICS OF THE BOROUJERD GRANITOID ROCKS

A total of 34 whole-rock samples from different facies of the Boroujerd complex have been analyzed for major and trace element contents (Table 1).

The samples exhibit a wide range in SiO_2 content from approximately 52 to 63 wt% for quartz diorites, 55 to 71 wt% for the granodiorites, and 69 to 75 wt% for the monzogranites. TiO_2, Al_2O_3, Fe_2O_3, MgO, MnO, CaO, and P_2O_5 abundances decrease with increasing SiO_2, whereas K_2O and Na_2O (alkali) increase. The generally negative correlation between SiO_2 and MgO, CaO, Fe_2O_3, MnO, and positive correlation between SiO_2 and K_2O and Na_2O (alkali) could have resulted from fractional crystallization.

Transition elements (Ni, Cr, Co, V) show a pronounced negative correlation with silica contents, i.e. they behave as compatible elements. The decrease of V with increasing SiO_2 is evidence for the fractionation of Fe-Ti oxides. Sr, Ba and Zn show a negative trend, whereas Rb, U, Ta, Nb and Th define a positive correlation.

The A/CNK vs. A/NK diagram (Maniar and Piccoli, 1989) defines the rocks as metaluminous to slightly peraluminous, and of I-type character (Figure 2). It is also shown that P_2O_5 decreases with increasing SiO_2, which is considered as an important criterion for distinction of I- from S-type granitoids by Chappell and White (1992). All samples are of subalkaline affinity and belong to the calc-alkaline series. The K_2O vs. SiO_2 plot further shows almost all samples to be of high-K affiliation (Figure 3).

Representative REE analyses are given in Table 1 and chondrite-normalized REE patterns are shown in Figure 4. We have used the chondrite-normalizing values for REE of Nakamura (1974). Chondrite-normalized REE patterns (Figure 4 and Table 1) show light REE (LREE) enrichment and significant negative Eu anomalies (Eu/Eu*=0–1.1), probably resulting from fractional crystallization of plagioclase during magmas differentiation. The granodioritic samples exhibit very strongly fractionated REE patterns ($[La/Yb]_{n=}$8–71), the LREE/HREE ratios vary within a range of La_N/Yb_N from 8 to 71, flat heavy REE patterns (HREE), and have variable Eu anomalies, (Eu/Eu*=0.2–1.1). The quartz dioritic samples have strongly fractionated REE patterns ($[La/Yb]_n$=3–13) and flatter heavy REE patterns with strong to moderate negative Eu anomalies (Eu/Eu*=0–0.7). The monzogranitic samples are characterized by strongly fractionated and flat heavy REE patterns ($[La/Yb]_n$=5–15) and have strong to moderate negative Eu-anomalies (Eu/Eu*=0–0.6). In general, the Boroujerd complex shows unfractionated HREE patterns. The negative Eu anomaly in the REE patterns (Figure 4) suggests substantial plagioclase in the residual assemblage and this would indicate melting under low $a_{H2O.}$

Tablo 1. Major element contents from the Boroujerd granitoids

Granodiorites												
Sample	MA3	AS2	GM5	AGH1	G6	G4	G5	AGH6	B1A55	AD4	AKY13	B4A19
SiO[2]	71.4	70.6	67.2	64.9	64.3	63.8	63.4	62.8	60.6	59.7	58.5	57.8
TiO[2]	0.3	0.3	0.5	0.5	0.6	0.6	0.6	0.7	0.7	0.6	1.0	1.0
Al_2O_3	14.7	14.5	15.5	16.0	16.7	16.9	16.1	16.9	17.5	20.2	18.0	18.3
Fe_2O_3 t	1.0	3.5	2.0	4.5	5.5	5.6	5.2	5.7	6.5	4.3	8.0	8.7
MnO	0.0	0.1	0.0	0.1	0.1	0.1	0.1	0.1	0.1	0.0	0.1	0.1
MgO	2.9	0.9	3.9	1.4	1.6	1.6	1.5	1.8	1.8	1.3	2.4	2.5
CaO	0.3	2.2	0.7	2.5	3.9	3.8	3.8	3.8	4.1	5.2	4.1	4.3
Na_2O	4.8	3.0	4.2	3.1	3.1	3.0	2.9	3.4	2.9	3.6	2.5	2.6
K_2O	1.3	4.1	1.4	4.0	3.4	3.6	3.4	3.0	3.4	3.4	3.2	3.3
P_2O_5	0.1	0.1	0.2	0.1	0.2	0.1	0.1	0.2	0.3	0.2	0.4	0.1
Ni	12.0	13.0	18.0	18.0	17.0	16.0	19.0	21.0	22.0	10.0	32.0	47.0
Cr	20.0	120.0	40.0	150.0	120.0	120.0	90.0	110.0	150.0	100.0	180.0	160.0
Co	55.3	6.4	41.9	10.2	12.0	11.1	11.1	11.8	12.8	8.9	18.6	19.6
V	31.0	36.0	55.0	60.0	88.0	88.0	81.0	78.0	97.0	50.0	155.0	152.0
Cs	0.5	5.2	0.9	9.3	3.8	3.5	3.0	4.5	5.8	4.3	4.1	4.7
Rb	40.8	142.5	29.3	146.0	130.5	133.5	122.0	111.0	134.5	133.5	129.5	142.5
Sr	26.9	200.0	65.9	256.0	322.0	319.0	295.0	320.0	338.0	484.0	294.0	330.0
Ba	80.2	441.0	172.5	577.0	598.0	596.0	551.0	549.0	765.0	1150.0	763.0	853.0
Th	23.0	24.0	23.0	21.0	12.0	10.0	17.0	32.0	2.0	14.0	15.0	25.0
U	2.2	2.7	1.6	1.9	2.4	3.3	2.5	2.3	1.4	2.3	1.9	2.2
Ta	1.5	1.1	1.2	1.0	0.9	1.0	0.9	1.0	0.9	0.8	0.9	1.0
Nb	13.0	12.0	16.0	14.0	14.0	13.0	14.0	17.0	15.0	15.0	19.0	21.0
La	52.3	48.7	28.6	47.3	29.4	44.2	40.7	62.1	19.5	64.0	51.0	76.4
Ce	94.1	93.6	52.2	91.1	59.9	92.6	82.5	104.5	40.8	118.5	103.0	155.0
Pr	10.6	10.0	6.0	9.6	6.4	9.3	8.6	11.8	4.1	11.6	11.0	16.2
Nd	35.8	33.1	21.2	32.3	22.4	31.0	30.0	40.9	15.1	38.8	39.2	56.6
Sm	6.3	6.6	3.9	5.3	4.0	4.8	5.2	5.9	2.3	6.2	7.0	9.4
Eu	0.6	1.2	0.2	1.2	1.0	1.1	0.9	0.9	1.3	2.2	1.3	0.8
Gd	5.7	6.6	3.7	6.0	4.1	4.3	4.7	5.9	2.2	6.3	6.8	8.3
Tb	0.8	0.8	0.5	0.7	0.5	0.6	0.6	0.6	0.2	0.8	0.9	1.0
Dy	4.5	5.1	2.7	3.8	2.9	3.4	3.6	3.0	1.1	3.6	5.3	6.3
Ho	0.9	1.0	0.6	0.7	0.6	0.7	0.7	0.6	0.2	0.5	1.1	1.4
Er	2.8	3.1	1.6	2.0	2.1	2.1	2.0	1.6	0.7	1.2	3.6	4.5
Tm	0.4	0.4	0.2	0.2	0.3	0.3	0.3	0.2	0.1	0.1	0.5	0.6
Yb	2.7	2.9	1.5	1.7	2.0	2.3	1.8	1.4	0.7	0.8	3.4	4.5
Lu	0.4	0.4	0.2	0.2	0.3	0.4	0.3	0.2	0.1	0.1	0.5	0.6
Y	27.8	27.2	15.2	19.2	18.8	20.2	19.6	13.8	6.7	15.0	31.6	37.4
Hf	5.0	5.0	6.0	5.0	6.0	6.0	6.0	7.0	6.0	9.0	8.0	9.0
Zr	147.5	162.5	210.0	179.5	203.0	203.0	198.5	227.0	232.0	341.0	274.0	287.0
Zn	10.0	27.0	18.0	43.0	56.0	52.0	51.0	48.0	58.0	53.0	83.0	124.0
Ga	15.0	17.0	15.0	21.0	22.0	20.0	21.0	20.0	20.0	25.0	22.0	26.0
Sn	2.0	2.0	2.0	2.0	1.0	1.0	1.0	1.0	2.0	2.0	1.0	2.0
W	550.0	5.0	420.0	15.0	6.0	9.0	4.0	7.0	8.0	5.0	10.0	5.0
Eu/Eu*	0.3	0.6	0.2	0.7	0.8	0.7	0.6	0.5	1.8	1.1	0.6	0.3
(La/Yb)N	13.0	11.2	12.7	18.6	9.8	12.9	15.1	29.7	18.6	53.5	10.0	11.4

Table 1 continued

Quartz diorites											
Sample	G14	G16	G18	G19	B2A31	GM25	G12	G11	AG2	B2A28	B2A33
SiO[2]	63.4	60.7	59.9	59.2	58.9	57.9	56.3	55.5	55.4	53.2	52.6
TiO[2]	0.6	0.6	0.6	0.8	0.7	0.6	0.9	0.7	1.3	0.7	0.6
Al_2O_3	16.6	14.9	15.4	15.9	16.2	15.3	17.1	15.9	16.8	15.6	15.2
Fe_2O_3 t	6.0	6.4	6.6	7.1	7.1	6.9	8.0	7.8	8.6	8.7	8.7
MnO	0.1	0.1	0.1	0.1	0.1	0.1	0.2	0.2	0.2	0.2	0.2
MgO	3.3	4.3	4.6	4.8	4.7	6.5	5.1	6.5	4.6	7.6	8.4
CaO	5.6	5.2	5.6	5.5	5.9	6.1	6.9	6.4	7.3	7.8	8.9
Na_2O	1.4	2.2	2.3	2.4	2.5	2.4	2.5	2.5	2.7	2.3	1.9
K_2O	2.3	3.5	3.0	2.8	2.0	2.5	2.1	2.2	1.8	2.1	1.8
P_2O_5	0.2	0.1	0.1	0.2	0.1	0.1	0.2	0.1	0.3	0.1	0.1
Ni	37.0	53.0	57.0	63.0	49.0	115.0	75.0	101.0	38.0	86.0	103.0
Cr	260.0	280.0	260.0	330.0	320.0	420.0	360.0	450.0	150.0	490.0	690.0
Co	20.0	20.3	20.6	22.9	23.8	48.0	27.8	28.7	54.5	31.9	36.4
V	176.0	144.0	144.0	148.0	150.0	170.0	204.0	210.0	168.0	217.0	274.0
Cs	9.9	6.0	6.2	7.5	4.7	10.0	5.4	4.6	4.2	3.2	3.5
Rb	103.0	128.0	105.0	111.0	77.4	106.5	88.2	101.0	66.6	78.8	65.9
Sr	299.0	263.0	269.0	261.0	231.0	347.0	347.0	388.0	334.0	197.0	202.0
Ba	242.0	596.0	388.0	372.0	361.0	407.0	355.0	454.0	296.0	236.0	238.0
Th	4.0	24.0	7.0	13.0	5.0	11.0	9.0	10.0	7.0	5.0	5.0
U	2.5	3.0	2.0	1.8	2.3	2.1	2.4	2.6	1.9	1.4	1.2
Ta	0.8	1.0	0.9	0.9	0.9	0.9	0.9	0.7	1.1	0.5	0.5
Nb	8.0	12.0	10.0	12.0	10.0	10.0	12.0	9.0	13.0	7.0	8.0
La	13.8	68.3	19.4	33.8	16.4	28.8	27.2	24.1	19.0	16.6	20.0
Ce	32.9	146.5	44.2	72.3	41.5	55.6	57.6	50.1	44.4	39.4	50.7
Pr	3.8	14.8	5.4	7.9	5.7	6.7	6.7	5.8	5.1	4.4	6.1
Nd	14.8	49.4	20.9	28.7	24.0	24.0	25.0	21.8	19.8	16.2	23.9
Sm	3.9	8.3	4.4	5.6	5.4	4.8	5.0	4.4	4.8	3.5	5.0
Eu	0.1	1.1	0.7	1.2	0.8	1.1	0.4	0.1	1.1	0.8	0.1
Gd	3.8	7.8	4.6	5.6	5.3	4.6	5.1	4.1	4.5	3.8	5.2
Tb	0.6	1.0	0.7	0.8	0.8	0.7	0.7	0.6	0.6	0.5	0.8
Dy	3.7	5.7	4.2	4.4	5.1	3.8	4.3	3.5	3.8	3.5	4.6
Ho	0.7	1.1	0.9	0.9	1.0	0.8	0.8	0.8	0.7	0.7	1.0
Er	2.1	3.4	2.6	2.6	3.2	2.3	2.6	2.2	2.1	2.1	2.9
Tm	0.3	0.5	0.4	0.4	0.5	0.3	0.4	0.3	0.3	0.3	0.4
Yb	1.9	3.4	2.5	2.6	3.2	2.3	2.5	2.2	2.0	2.0	2.8
Lu	0.3	0.5	0.4	0.4	0.5	0.3	0.4	0.3	0.3	0.3	0.4
Y	20.4	30.7	22.5	23.3	30.2	21.6	23.4	19.8	18.2	18.4	26.6
Hf	4.0	4.0	5.0	5.0	4.0	5.0	5.0	5.0	3.0	2.0	2.0
Zr	117.0	115.0	139.0	179.5	123.5	164.0	161.5	175.5	90.0	77.6	71.6
Zn	96.0	70.0	62.0	69.0	58.0	68.0	127.0	118.0	79.0	63.0	114.0
Ga	19.0	18.0	17.0	19.0	18.0	18.0	22.0	20.0	19.0	16.0	18.0
Sn	5.0	3.0	2.0	2.0	2.0	6.0	3.0	4.0	3.0	1.0	2.0
W	9.0	5.0	3.0	4.0	14.0	217.0	8.0	5.0	269.0	1.0	3.0
Eu/Eu*	0.1	0.4	0.5	0.7	0.5	0.7	0.2	0.1	0.7	0.7	0.0
(La/Yb)N	4.9	13.4	5.2	8.7	3.4	8.4	7.3	7.3	6.4	5.6	4.8

Table 1 continued

Microgranodioritic enclaves				Monzogranites							
Sample	AGH2	B2A24	AD	G22	AG19	GM11	AB6	AG18	G24	GM10	G23
SiO[2]	64.2	62.3	55.0	75.1	73.7	71.4	71.1	70.8	70.7	70.0	69.7
TiO[2]	0.7	0.6	0.8	0.1	0.3	0.3	0.2	0.4	0.2	0.3	0.2
Al_2O_3	15.7	16.7	18.5	12.8	12.8	14.0	14.5	13.5	14.6	14.1	14.9
Fe_2O_3 t	6.0	6.2	7.7	1.1	2.2	3.0	2.0	2.8	2.2	3.5	2.5
MnO	0.1	0.1	0.1	0.0	0.1	0.1	0.0	0.1	0.1	0.1	0.1
MgO	1.8	2.4	2.3	0.1	0.4	0.6	1.2	0.6	0.4	0.7	0.5
CaO	3.6	3.4	1.8	0.5	0.9	1.8	0.9	1.0	1.7	2.1	1.8
Na_2O	3.3	3.3	2.5	3.7	3.8	3.0	4.2	3.9	3.8	2.8	4.1
K_2O	2.2	2.7	8.3	4.6	3.8	4.1	2.1	4.1	4.6	4.0	4.2
P_2O_5	0.3	0.1	0.1	0.0	0.1	0.1	0.1	0.1	0.0	0.1	0.0
Ni	22.0	19.0	46.0	7.0	7.0	11.0	13.0	20.0	9.0	12.0	8.0
Cr	100.0	100.0	130.0	130.0	10.0	20.0	150.0	10.0	80.0	20.0	110.0
Co	14.2	14.2	14.6	1.2	54.1	32.9	3.3	54.7	3.7	53.4	3.5
V	64.0	130.0	172.0	3.3	17.0	24.0	23.0	27.0	11.0	29.0	11.0
Cs	9.5	7.0	13.3	3.7	0.8	2.7	2.3	1.1	4.5	6.2	4.5
Rb	162.5	149.5	290.0	189.0	129.0	146.5	63.8	123.5	157.0	166.5	152.5
Sr	260.0	294.0	205.0	27.8	121.5	229.0	114.0	168.0	124.5	239.0	132.5
Ba	353.0	250.0	1105.0	38.5	320.0	399.0	276.0	631.0	408.0	404.0	372.0
Th	17.0	18.0	14.0	19.0	31.0	15.0	16.0	32.0	11.0	20.0	13.0
U	1.9	3.0	1.7	3.8	5.8	2.6	2.5	5.3	2.4	2.7	2.6
Ta	1.7	0.9	1.0	1.5	3.2	1.4	1.1	2.6	0.9	1.4	1.1
Nb	19.0	12.0	14.0	9.0	32.0	11.0	10.0	28.0	10.0	11.0	11.0
La	37.3	37.7	30.5	7.3	42.7	32.9	32.5	59.5	20.1	39.7	25.1
Ce	74.7	71.3	63.5	18.0	74.6	64.6	64.1	101.5	40.5	77.4	54.5
Pr	7.8	7.8	6.8	2.4	7.2	6.9	6.5	9.7	4.2	8.3	5.6
Nd	27.2	27.1	24.2	9.8	23.0	23.7	22.3	29.6	15.0	28.7	20.3
Sm	5.4	4.7	4.7	4.0	4.5	4.5	4.5	5.2	3.3	5.2	4.4
Eu	1.1	0.8	1.4	0.1	0.9	0.7	0.7	0.1	0.4	0.5	0.2
Gd	5.8	4.9	3.8	5.7	4.6	4.1	4.2	5.3	3.6	5.1	4.2
Tb	0.8	0.6	0.4	1.2	0.7	0.6	0.6	0.7	0.6	0.7	0.6
Dy	5.2	3.2	2.4	8.8	4.2	3.5	3.7	4.0	3.5	3.9	4.1
Ho	1.0	0.6	0.5	2.0	0.8	0.7	0.7	0.8	0.7	0.8	0.8
Er	3.0	1.8	1.4	6.0	2.5	1.9	2.2	2.5	2.1	2.2	2.7
Tm	0.5	0.2	0.2	1.0	0.4	0.3	0.3	0.4	0.3	0.3	0.4
Yb	3.1	1.6	1.3	6.6	2.9	2.0	2.4	2.6	2.1	2.2	2.6
Lu	0.4	0.2	0.2	0.9	0.4	0.3	0.3	0.4	0.3	0.3	0.4
Y	27.2	17.1	12.7	59.5	22.8	19.2	20.2	22.8	20.3	21.0	23.3
Hf	7.0	5.0	5.0	4.0	5.0	4.0	4.0	6.0	4.0	4.0	5.0
Zr	235.0	145.5	157.5	81.5	178.0	116.5	106.0	230.0	128.0	137.0	149.0
Zn	56.0	53.0	69.0	16.0	30.0	29.0	13.0	79.0	39.0	35.0	47.0
Ga	24.0	20.0	22.0	16.0	19.0	17.0	17.0	20.0	17.0	17.0	17.0
Sn	2.0	1.0	4.0	3.0	3.0	2.0	3.0	4.0	4.0	2.0	4.0
W	6.0	4.0	2.0	8.0	469.0	225.0	8.0	416.0	11.0	429.0	11.0
Eu/Eu*	0.6	0.5	1.0	0.0	0.6	0.5	0.5	0.0	0.4	0.3	0.1
(La/Yb)N	8.0	15.8	15.7	0.7	9.8	11.0	9.1	15.3	6.4	12.1	6.5

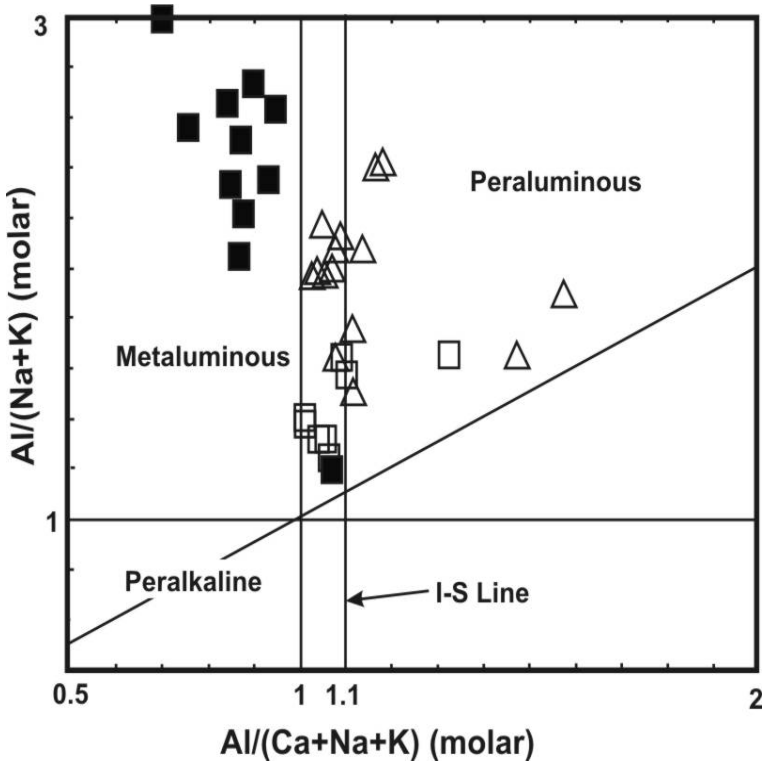

Figure 2. A plot of Shand's index for the Boroujerd granitoids. Discrimination fields for different types of granitoids (Maniar and Piccoli, 1989) are shown.
■: quarz diorites, □: monzogranites, Δ: granodiorites

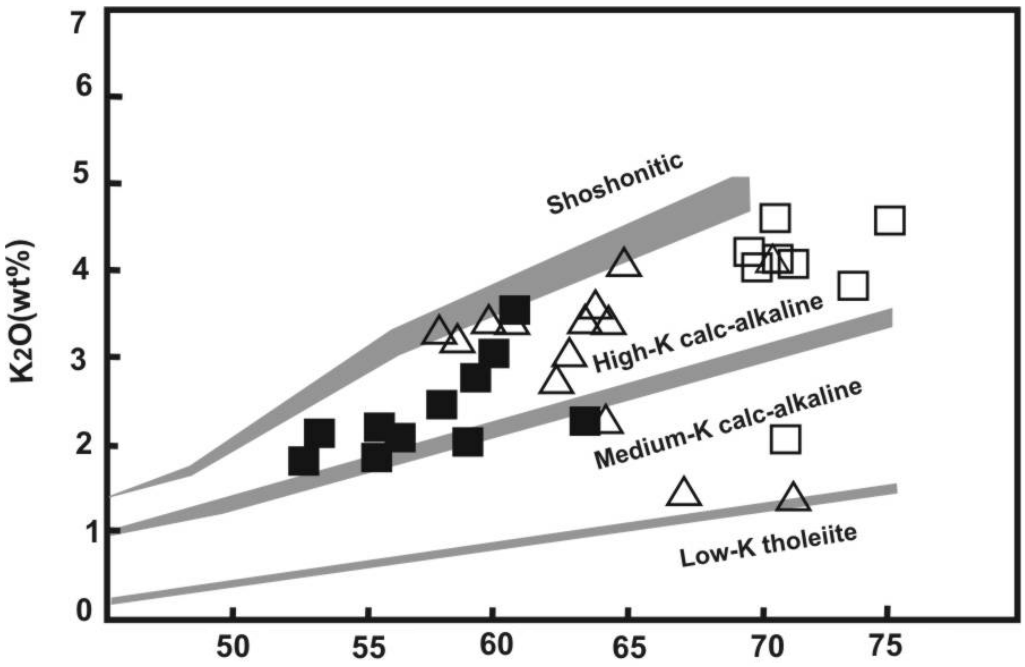

Figure 3. K_2O vs. SiO_2 diagram after Rickwood (1989). Symbols as Fig.2

Representative intrusive rock samples (granodiorites, quartzdiorites and monzogranites) from the Boroujerd complex are normalised to chondrites of Thompson (1982). Trace element distribution patterns show that all granitoids studied have Ta and Nb depletion. Troughs are also observed at Ti, P and Sr. All the granitoids studied are enriched in LILE (Rb, K, and Th) and the

LREE (La,Ce, Nd) compared to HFSE (Nb, Ta, Hf, Zr, Sm, Y, and Yb), which is a general characteristic of calc-alkaline granitoids. The patterns of the granitoids display significant troughs at P, Sr, less pronounced Ti troughs, and lower Y, Yb, and Nb values, resulting in a trace element distribution pattern characteristic of calc-alkaline arc granitoids.

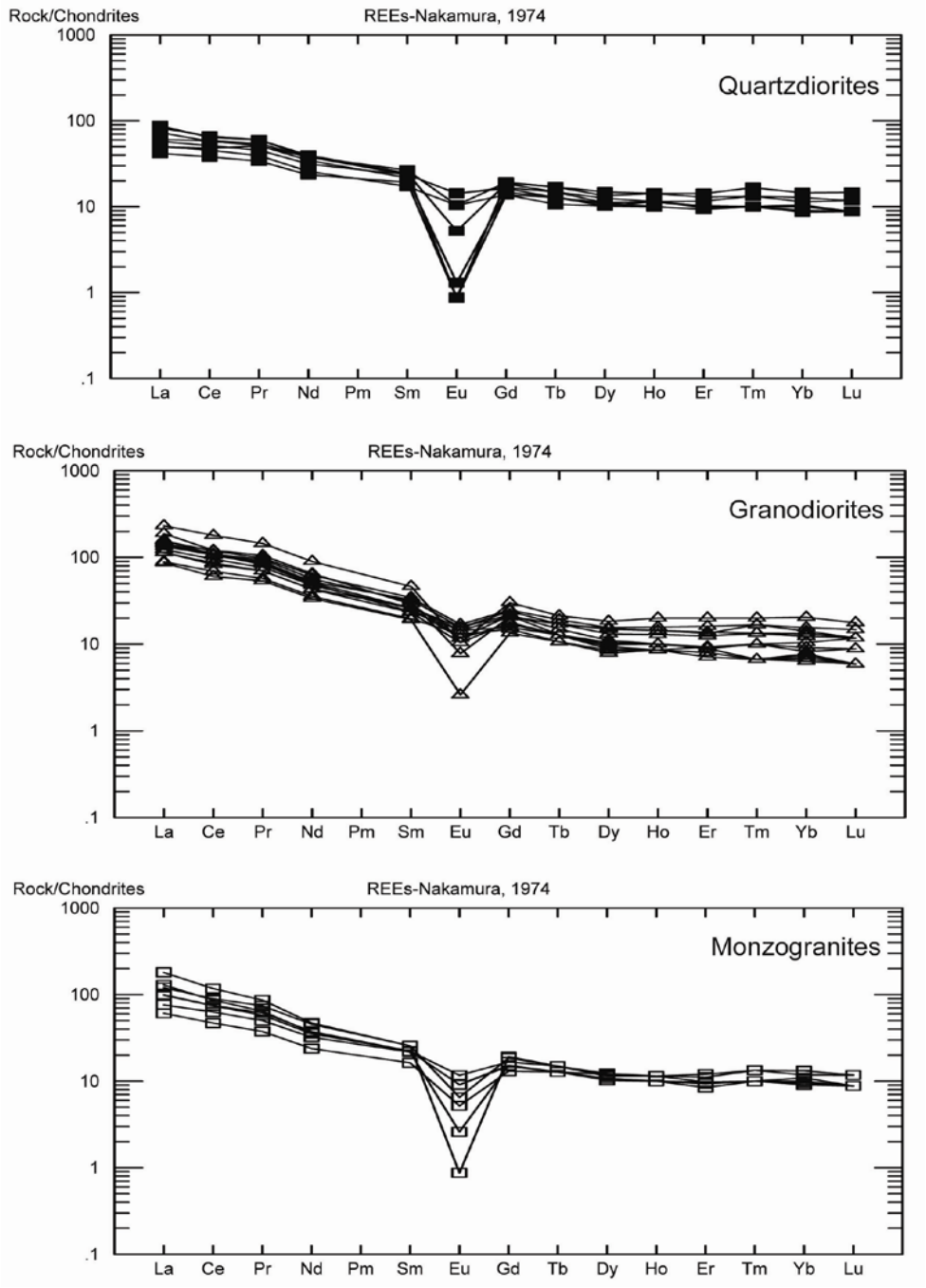

Figure 4. Chondrite-normalised REE patterns (values from Nakamura, 1974). Symbols as in Fig.2.

6. DISCUSSION

Granitoids of the Boroujerd aera are high-K, calc alkaline rocks and are characterized by pronounced negative Ba, Sr, Nb, Ta, P and Ti anomalies and are enriched in Rb, Th, K, Ce, La and Nd. These features are compatible to those of typical crustal melts, e.g. granitoids of the Lachlan Fold belt (Chappell and White, 1992).

Roberts and Clemens (1993), on the basis of the data on the experimental

partial melting of common crustal rocks, stated that high-K, I-type, calc-alkaline granitoid magmas can be derived from the partial melting of hydrous, calc-alkaline mafic to intemediate metamorphic rocks in the crust.

The negative Eu and Sr anomalies may suggest that plagioclase was stable in the source; instead, the unpartionated HREE (and Y) patterns could perhaps present the magmas produced outside of the garnet stability field.

It should be considered that not all granitoids in the world fit into alphabetical classification of Chappell and White (1974), as claimed by Patiño Douce (1999). Also, in the study of Alaskan granitoids Barker et al. (1992) reached the same conclusion. He suggested that the Alaskan granitoids, which show I-type characters, is generated by melting of sediments mainly consisting of greywackes and the finer-grained argillite. Moreover, Altherr et al. (2000) showed that high-potassium, calc-alkaline I-type granitoids in northern Schwarzwald (Germany) are derived from metagreywackes.

We think that the most reasonable model for the origin of the Boroujerd granitoids involves partial melting of crustal protoliths having different compositions, leaving restites with variable proportions of amphibole and plagioclase as a result of melting under variable H_2O contents. Mantle-derived basaltic magmas emplaced into the lower crust are the most likely heat sources for partial melting.

7. CONCLUSIONS

The Boroujerd granitoid complex is made of three units including granodioritic, quartz-dioritic and monzogranitic units. Fractional crystalization could play an important role in the formation of the whole spectrum of granitoid types present in the Boroujerd area. The geochemical characteristic, mineralogy and petrography of these units are comparable with the typical I-type granites. The Boroujerd granitoid rocks are of sub-alkaline affinity, metaluminus to slightly peraluminus, high-K calk-alkaline series, and display geochemical characteristics typical of the volcanic arc granites related to an active continental margin.

It could be suggested that the Boroujered granitoids originated by partial melting of crustal protoliths in a deforming active margin. In such a setting, mantle melts emplaced into the lower crust most likely supplied the heat required for crustal anatexis.

ACKNOWLEDGEMENTS

This work was supported by grant no 6105013/1/01 from the University of Tehran of I.R. Iran, received by M.V. Valizadeh.

REFERENCES

Altherr, R., Holl, A., Hegner, E., Langer, C. and Kreuzer, H., 2000. High-potassium, calc-alkaline I-type plutonism in the European Variscides: northern Vosges (France) and northern Schwarzwald (Germany). *Lithos* 50, 51–73.

Barker, F., Farmer, G.L., Ayuso, R.A., Plafker, G. and Lull, J.S., 1992. The 50 Ma granodiorites of the eastern Gulf of Alaska: melting in an accretionary prism in the fore arc. *Journal of Geophysic Research* 97, 6757–6778.

Chappell, B. W, 1999. Aluminium saturation in I- and S-type granites and the characterization of fractionated haplogranites. *Lithos,* 46, 535-551.

Chappell, B.W., and White, A.J.R., 1992. I and S-type granites in the Lachlan Fold Belt. *Transactins of the Royal Society of Edinburgh. Earth Sciences.* 83, 1–26.

Chappell, B.W. and White, A.J.R., 1974. Two contrasting granite types. *Pacific Geology* 8, 173–174.

Maniar, P.D. and Piccoli, P.M., 1989. Tectonic discrimination of granitoids. *Geological Society of America Bulletin* 101, 635–643.

Nakamura, N, 1974. Determination of REE, Ba, Fe, Mg, Na, and K in carbonaceous and ordinary chondrites. *Geochimica et Cosmochimica Acta* 38, 757–775.

Patiño Douce, A.E. 1999. What do experiments tell us about the relative contributions of crust and mantle to the origins of granitic magmas? In: A. Castro, C. Fernandez and J.L. Vigneresse, (Eds), Understanding granites: intergrating new and classical techniques. *Geological Society London, Special Publication* 168, pp. 55–75.

Rickwood,P.C., 1989. Boundary lines within petrologic diagrams which use of major and minor elements. *Lithos* 22, 247–263.

Roberts M.P. and Clemens, J.D., 1993. Origin of high-potassium, calc-alkaline, I-type granitoids. *Geology* 21, 825–828.

Thompson, A.B., 1982. Magmatism of the Bristish Terciary volcanic Province. *Scottish Journal of Geology* 18, 50–107.

GIS-BASED ENGINEERING GEOLOGICAL MAPPING IN THE INNER BAY OF IZMIR (TURKEY)

Kıncal C. and Koca M. Y.

Dokuz Eylul Univ., Engineering Faculty, Geological Engineering Dept., 35100, Bornova-Izmir/Turkey

Abstract: Geographical Information Systems based settlement suitability have been completed using 25 sheets of 1/5000 scale maps having detail scale of 1/1000 which are in the 1/25000 scale L18-a2 topographic map in Izmir Municipality area. Engineering geological maps for the above mentioned area were prepared using field and laboratory works. All the data were digitised and stored using MapInfo Professional 5.5 GIS software. Drainage network and flood affected areas were considered when preparing landuse maps. The slope zoning map and the digital elevation model have been prepared using elevation data with 5.0 m intervals in the 1/5.000 scale maps. Borehole database has been formed by gathering collected soil data including index properties and Standard Penetration Test results data in the alluvial plain. Database was formed by four different methods of (i) applied liquefaction analysis in 422 borehole locations for the liquefaction potential assessment of the ground, (ii) soil zoning maps using borehole data, (iii) SPT-zoning map for the bearing capacity calculations, (iv) groundwater table map. Land-use map for the Inner bay of Izmir and its nearby environs has been prepared consequently using all the analysis.

Key words : Land-use map, Geographical Information Systems, Engineering Geology, The Inner Bay of Izmir.

STUDY AREA

Study area is in the 1/25000 scale L18-a2 titled topographic map, located in the eastern part of the Izmir Bay, known as "Bornova Plain" (Figure 1). 25 sheets of 1/5000 scale geological maps which belong to the study area having detail of 1/1000 scale was mapped in the field.

THEMATIC MAP PREPARATION

Seismic measurements performed in the field (Vs and Vp-wave values, Poisson's ratio and site amplification values), corrected SPT-N'_{30} values obtained from 422 boreholes, 442 sonic velocity values performed in the laboratory, liquefiable soil level determination according to four different methods, index properties of alluvial soils, 18-different type of soils described using borehole logs were entered into the database using a PC-based computer and MapInfo Professional 5.5 software. Digitized topographic and geological maps were overlaid with maps below;

- ***Geological Map Layer***

25 sheets of 1/5000 scale geological maps which belong to the study area having detail of 1/1000 scale were mapped in the field and digitised using MapInfo Professional 5.5 software (Kıncal, 2005; Figure 2). The important point is the use of the poligon-tool when digitising a geological map. Because geological units constitute a geometrical area on the map plain, each map unit was drawn like a "closed polygon" while digitising in GIS software. While digitising, three columns, which are the symbol, the name and the age of the unit, form the database.

- ***Slope Map Layer***

Slope values (%) were used while preparing slope zoning maps in the study area. Slope values (%) were classified as 0-8.7%, 8.7-17.6%, 17.6-36.4%, 36.4-57.7%, 57.7-100 and >100%. In the first step, the slope map was prepared using L18-a2 titled 1/25000 scale topographical map with 10 meter intervals and in the second step, the slope map was prepared using 25 sheets of 1/5000 scale topographical maps with 5 meter intervals with the help of MapInfo Professional 5.5 software (Figure 3). If two slope maps were compared, the 1/5000 scale slope map would be useful because of its accuracy.

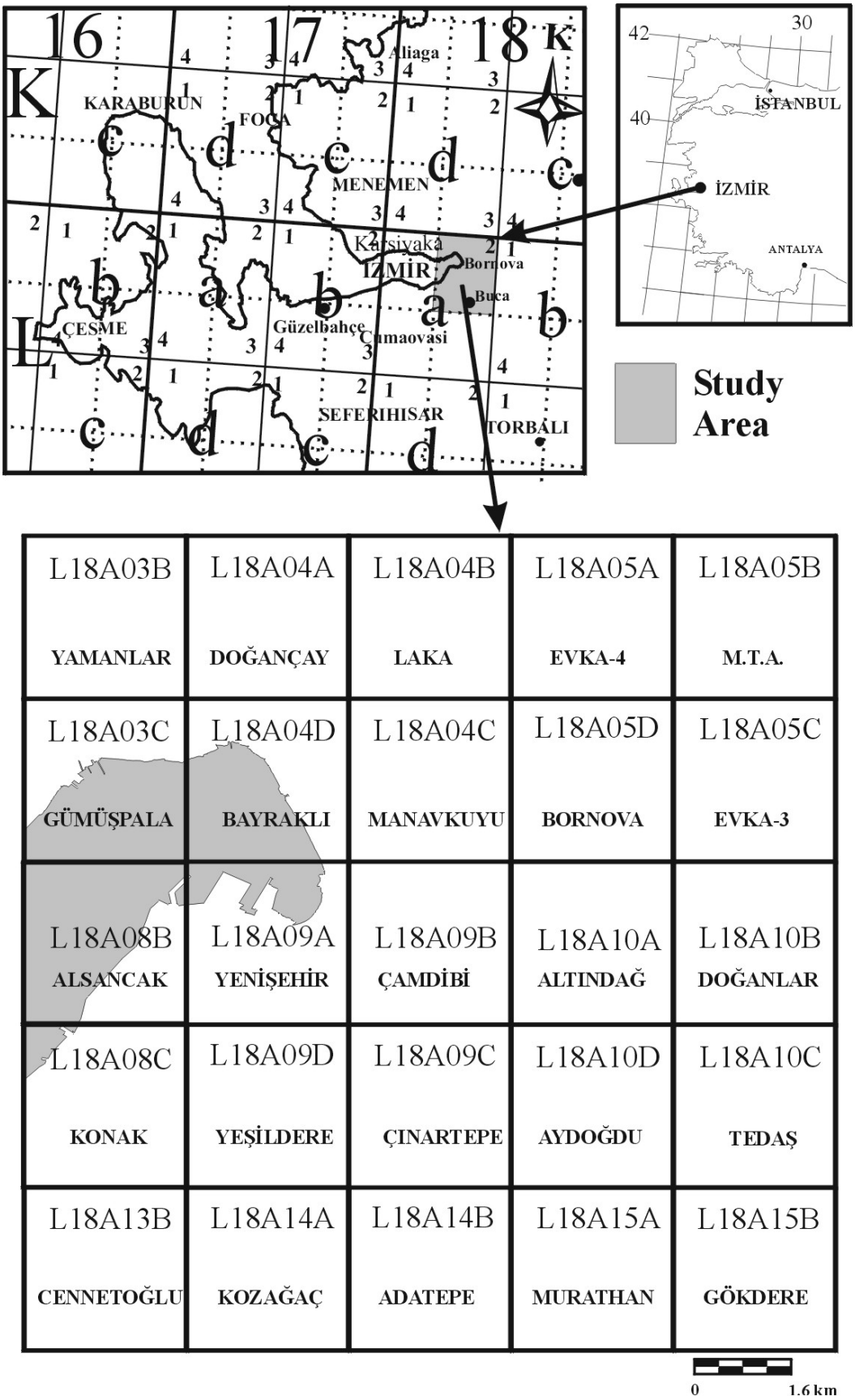

Figure 1. Location map of the study area.

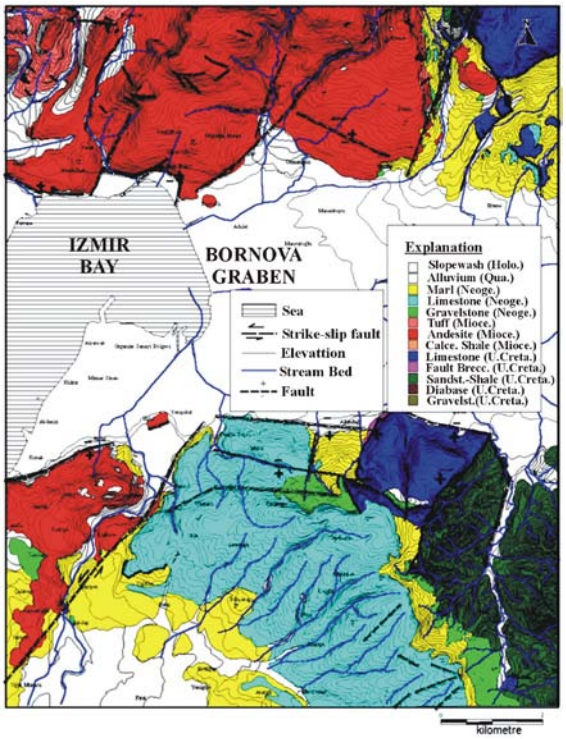

Figure 2. Digital geological map and Hazard Map-IV

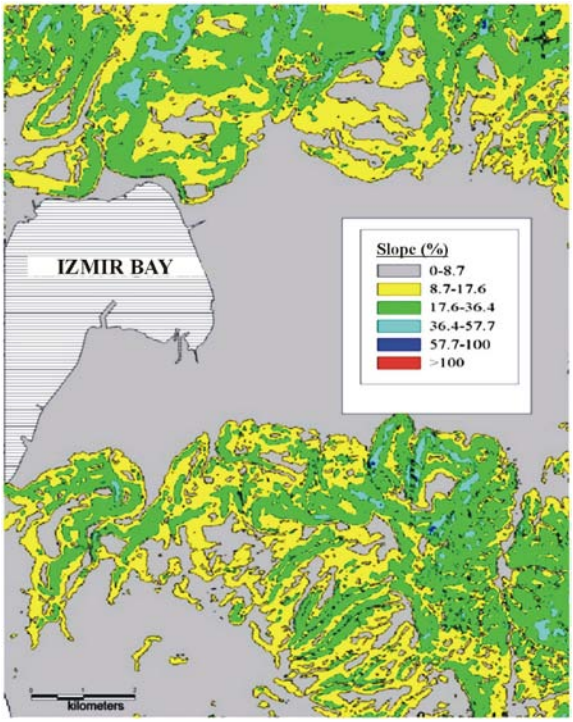

Figure 3. Digital slope map having 5 m detail

- ***Borehole Map Layer***

167-soil site investigation study reports were obtained from the drilling companies and UTM coordinate of each of the 422 boreholes in the mentioned reports were determined in the field and were entered into the database. Borehole locations (X, Y, Z) were registered to the database using GIS.

Borehole map layer was prepared for the graben site soils of Inner Bay of Izmir because of the reasons given below;

1. *Geological profile determination using soil descriptions.*
2. *Soil classification made according to bearing capacity using SPT-N'_{30} values.*
3. *Comparing bearing capacity values obtained from SPT-N'_{30} values and obtained from seismic data.*
4. *Forming a map layer to use in overlay analysis according to settlement suitability.*

- ***Groundwater Level Map Layer***

Hydrogeological study which was the groundwater level change determination from past to present, was performed in the Inner Bay of Izmir. A past groundwater level map was prepared by Camp-Harris, Mesana (1971). In this study, measurements were based on 1967 values. Also, a present groundwater level map was prepared using the borehole data between in 1990-2004 years.

A recent groundwater level map was prepared using the present data. Finally, the past and present groundwater level maps were overlaid and a thematic map was prepared.

The past groundwater level map has low accuracy and sensitivity because of the less total number of boreholes. But, the present one was prepared using 422 soil boring measurements. So, the last one is much more sensitive then the older one. It is known that underground water level falls because of the uncontrolled water discharge. Also, the recent groundwater

level map was used during the determination of liquefaction susceptibility analysis.

- ***Stream Bed Map Layer***

The stream bed map was prepared and digitised using 25 sheets of 1/5000 scale topographic maps to analyse drainage network in the study area (Figure 4). As is well known, stream beds are very important when a field is analyzed according to settlement suitability. Settling is not allowed in the stream bed and slope beginning from stream floor was evaluated as "unsuitable areas for settlement" because of the flood hazard.

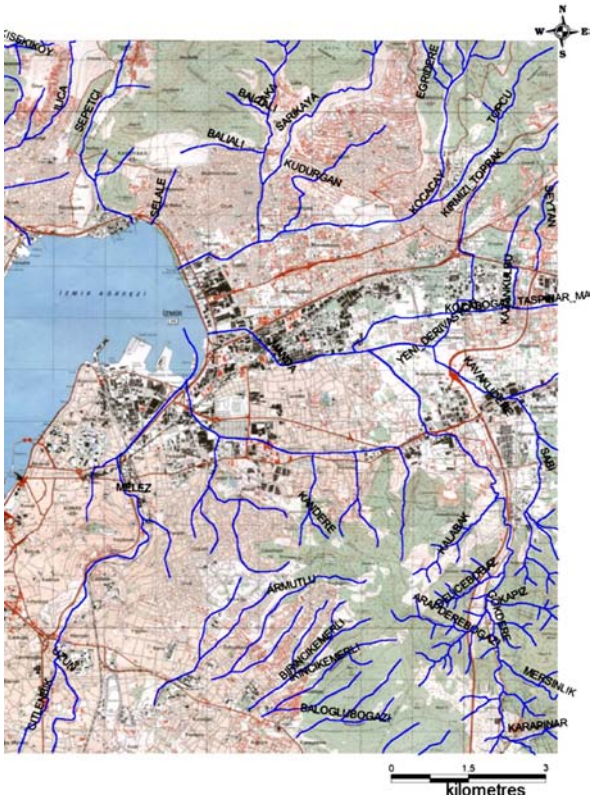

Figure 4. Digital drainage map

- ***Location Info Map Layer***

Location info database was prepared by using a location map which was formed by text format data to give information and connect with the relevant data. This database was also used to give location information with the results of finished analyses.

- ***Fault Planes Map Layer***

Fault lines database was formed in two phases;

1) Existing fault lines in the study area were drawn directly based on field work while preparing 1/5000 scale geological maps in the field.

2) Lines which were thought to be fault lines from satellite images, were determined and transferred to the database as probable faults by using Erdas Imagine 8.3 software. Effect area (buffer zone) of Izmir fault was determined as 30 meters which is the largest number in the study area considering the other fault plane's continuity. Normal faults with high angle which have E-W direction in the study area were considered as "effective faults". In dynamic conditions, node points of faults were determined as "risky points".

Fault line directions and continuities were determined by using digital fault lines in the database. Then, the buffer zone of each line/polyline type object was prepared using MapInfo Professional 5.5 software.

- ***Vs and Vp-Wave Velocity Map Layers***

Seismic data were obtained in the field (Kıncal, 2005). Longitudinal (Vp) and Shear (Vs) wave velocities were measured from time-distance diagram on the each seismic profile.

Vp and Vs-wave velocity zoning maps were prepared for 3.0, 6.0 and 10.0 meter depths. Vs-wave velocity values in 6.0 and 10.0 meters are very close to each others. So, Vs-wave velocity maps given for these depths are almost similar.

Vs-wave velocities are below 250 m/s in Karacaoglan, Mevlana and Manavkuyu Districts.

- ***Landslide Map Layer***

Active landslide areas in the study area are located in the south and east slopes of the Kadifekale Hill (Figure 5). Rainfalls affect the landslides mentioned above (fossil landslide areas).

- ***Stone Quarry Map Layer***

Stone quarries were determined and mapped by remote sensing techniques using orthophotos of the study area.

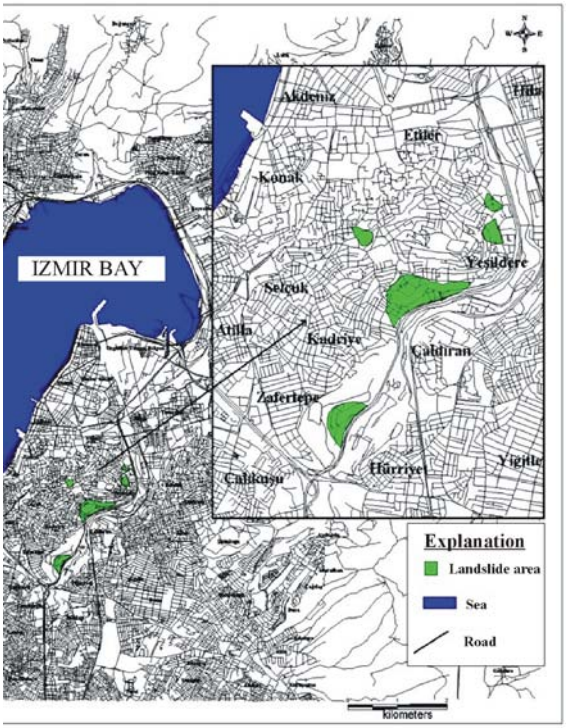

Figure 5. Active landslide map

MAP OVERLAYING

Maps were overlaid with some configurations which are mentioned in detail below and obtained according to Figure 6. Overlaid different map combinations are given below;

HAZARD MAPS PRODUCED BY GIS

To obtain the settlement suitability map in the Inner Bay of Izmir, related 3 and/or 4-thematic maps were overlaid using GIS. Twenty one thematic maps were transformed to five hazard maps.

Hazard Map-I : Hazard map-I was obtained using Vs and Vp wave velocities, Poisson's ratio and site amplification like seismic data. In dynamic conditions, this map shows the areas of loose/soft soil layers where the damage of an earthquake will be expected at maximum (Figure 7).

Hazard Map-II : SPT-N'_{30} zoning, bearing capacity and groundwater level maps were overlaid together. This map shows the low bearing capacity values and weak soils under the water-saturated conditions (Figure 8).

Hazard Map-III : This map formed by liquefaction susceptibility analysis' results, soil types zoning map, groundwater level map and topographical map, shows liquefaction susceptible water saturated soil locations under the dynamic conditions (Figure 9).

Hazard Map-IV : It was obtained by overlaying five thematic maps. On this hazard maps, stream beds, flood areas, slopes with high angles (α>36.4%), active landslide areas and stone quarry locations are presented. All of the areas mentioned above were determined as "unsuitable areas" for settlement (Figure 2).

Hazard Map-V : This map was obtained by overlaying fault planes, topography and geological thematic maps. In this study, fault zones and its effected areas were determined as "unsuitable areas" (Figure 10).

Each hazard map was obtained overlaying related thematic maps with a single explanation, explanation, which is important to determine which bound values overlay with the others.

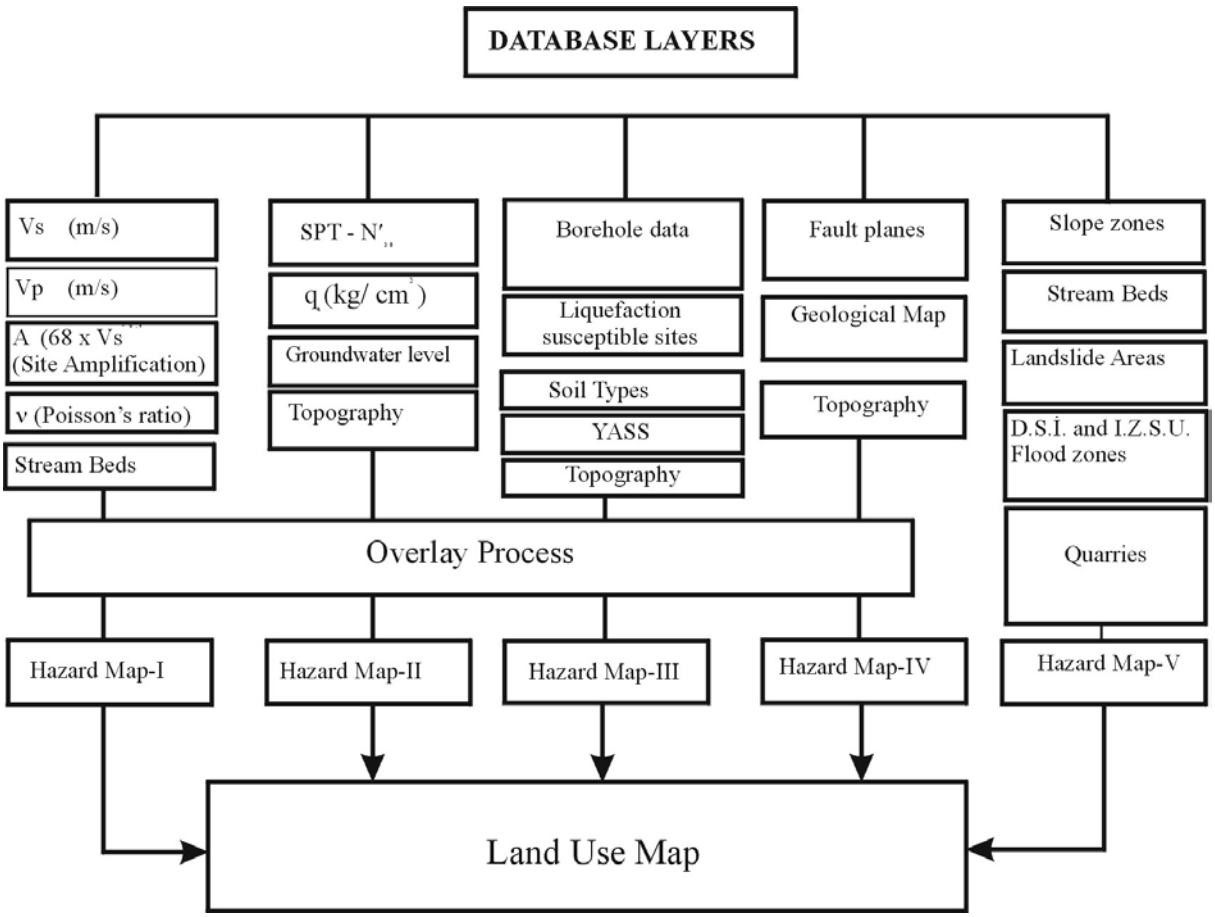

Figure 6. Flowchart used to obtain hazard maps and land-use map of the study area.

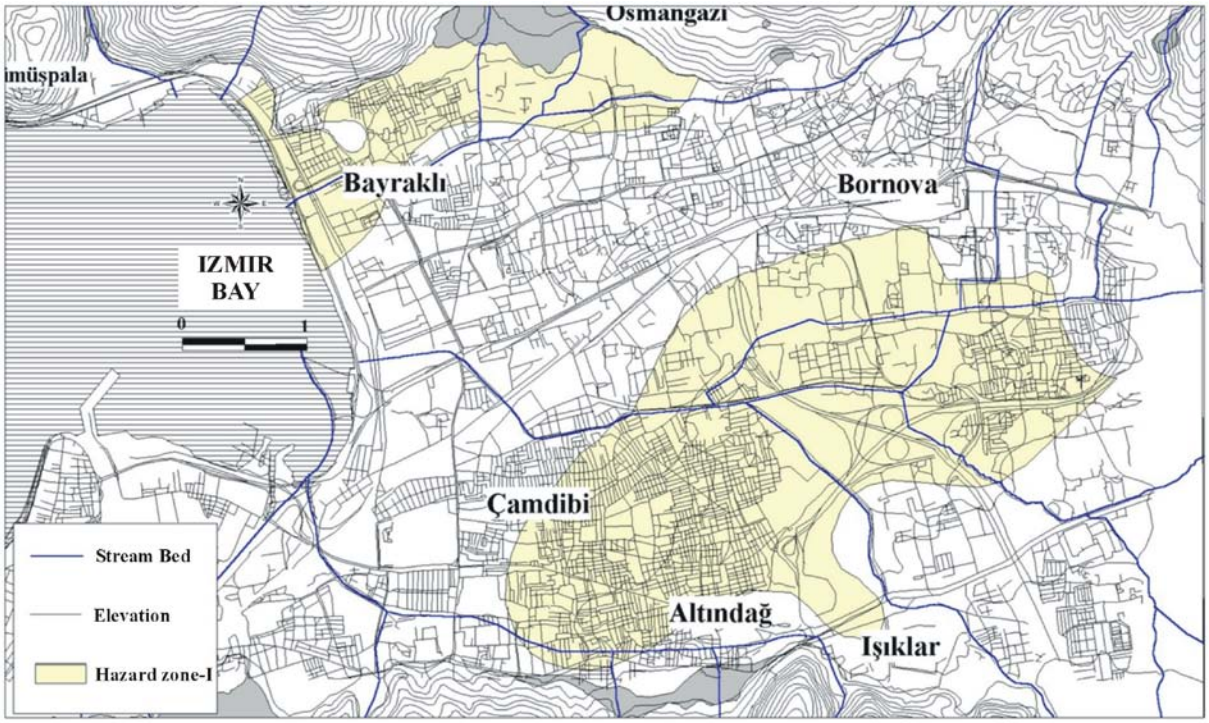

Figure 7. Hazard map-I.

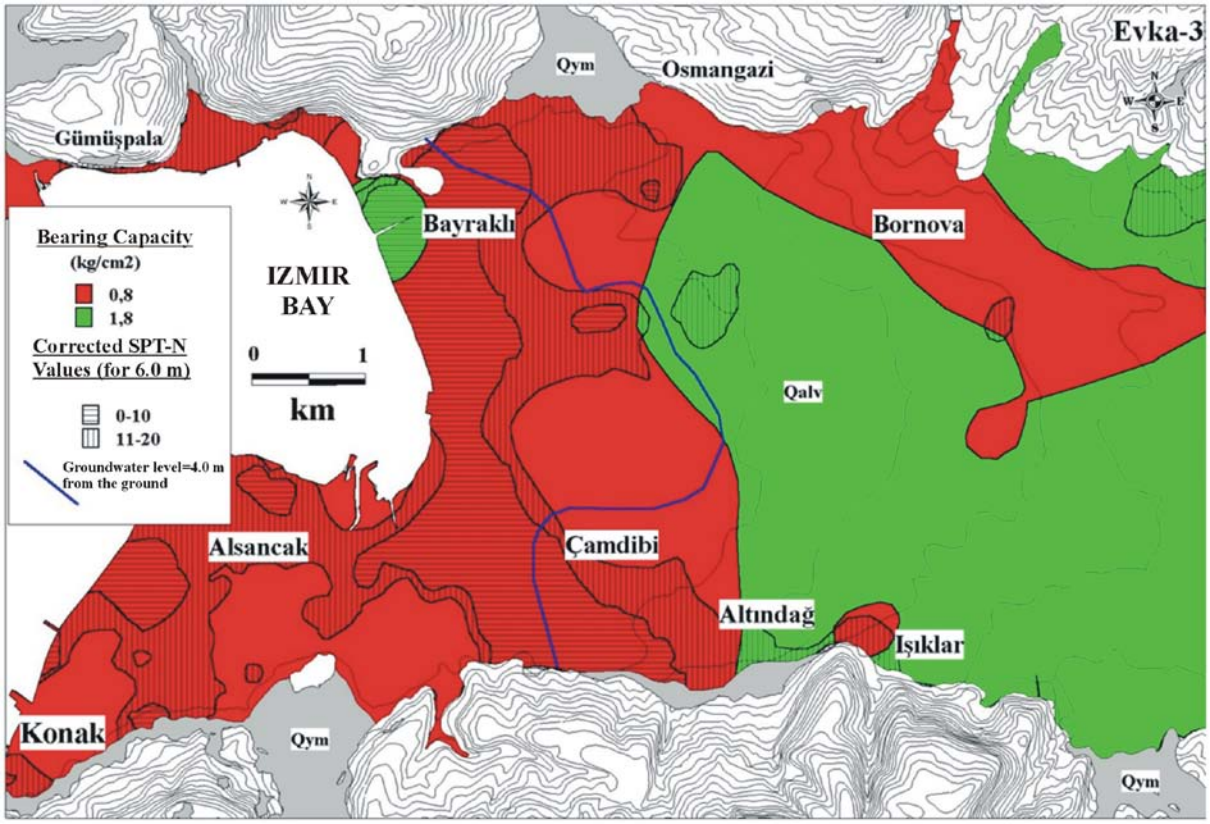

Figure 8. Hazard map-II.

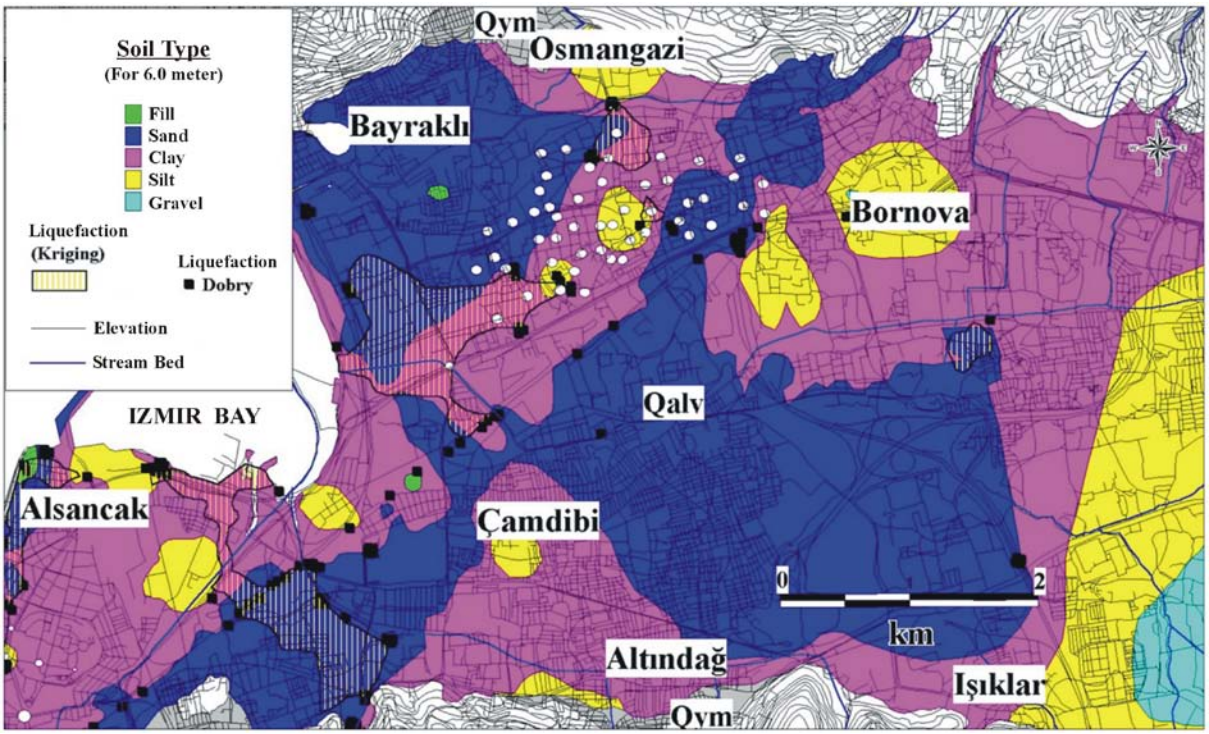

Figure 9. Hazard map-III.

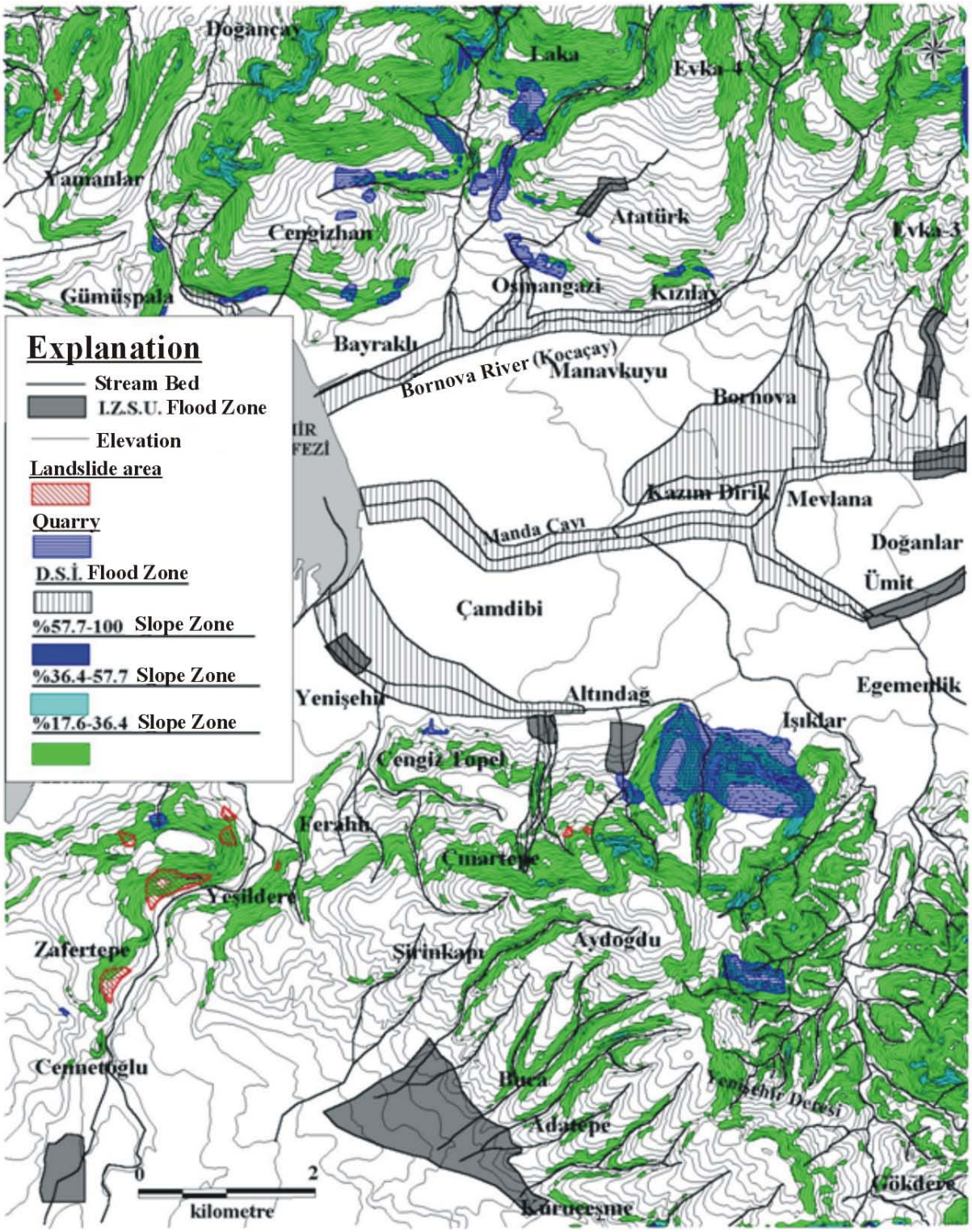

Figure 10. Hazard map-V.

RESULTS

GIS based settlement suitability aimed hazard maps have been completed using 25 sheets of 1/5000 scale maps having a detail scale of 1/1000 which are in the 1/25000 scale L18-a2 topographic map in Izmir (Turkey) Municipality area.

A database which was formed by four different liquefaction susceptibility analysis methods, soil zoning maps using borehole data, SPT-zoning maps for the bearing capacity calculations, groundwater table map, quarry zones, map of landslides, fault planes map, was used

to querry and finally prepare hazard maps with different weights for searching new and existing safe areas to settle on.

REFERENCES

Camp-Harris-Mesara. 1971. Izmir Project, Camp, Dresser&McKee (Boston), Frederic R.Harris Inc. (New York), Mesara Mühendislik Firması (Ankara), *Report on Feasibility and Master Plan for Water Supply*, Vol.1, Izmir-Turkey.

Erdas Imagine 8.3, Program Manual.

Kıncal, C. 2005. Engineering Geological Evaluation of the Geological Units Exposed in Inner Bay Area (Izmir)'s Vicinity Using Geographical Information Systems and Remote Sensing, *PhD Thesis*, p.342, Izmir (In Turkish). (unpublished)

MapInfo Corporation. 1995. MapInfo Professional User's Guide, *MapInfo Corporation*, Troy, NY.

(This page is left blank intentionally.)

LIQUEFACTION ANALYSIS APPLIED TO THE INNER BAY SOILS OF BORNOVA PLAIN, IZMIR/TURKEY

Kıncal C. and Koca M. Y.

Dokuz Eylül Univ., Engineering Faculty, Geological Engineering Dept., 35160, Buca-Izmir/Turkey

Abstract: Soil liquefaction susceptibility of the sandy soils under fully water saturated conditions in the Inner Bay of Izmir and in the Bornova (Izmir) Plain was determined according to four well known methods by using geotechnical data from 422 boreholes. Geotechnical data, including borehole records and laboratory test results of the samples taken from the boreholes and geophysical seismic data were taken into account in the liquefaction analysis. The liquefaction assessments were performed by using the field performance data obtained from Standard Penetration Tests (SPT). Additionally, the groundwater table map has been prepared by using groundwater level recorded in each recently drilled borehole in the Bornova (Izmir) Plain.

Corresponding attribute data were given to each layer in the database so the interaction of graphic and non-graphic data using MapInfo Professional 5.5 software was provided. Appropriate risk points were allocated for each digital map layer in the database. This grading system then was used in multi-criteria decision analysis and overlay processes in Geographical Information Systems (GIS) to prepare risk maps forming the land-use map of the study area.

Key words: Soil liquefaction analysis, Geographical Information Systems, Engineering Geology, Standard Penetration Test, Bornova (Izmir).

STUDY AREA

Study area is in the 1/25000 scale L18-a2 titled topographic map, located in the eastern part of Izmir Bay (Turkey), known as "Bornova Plain" (Figure 1).

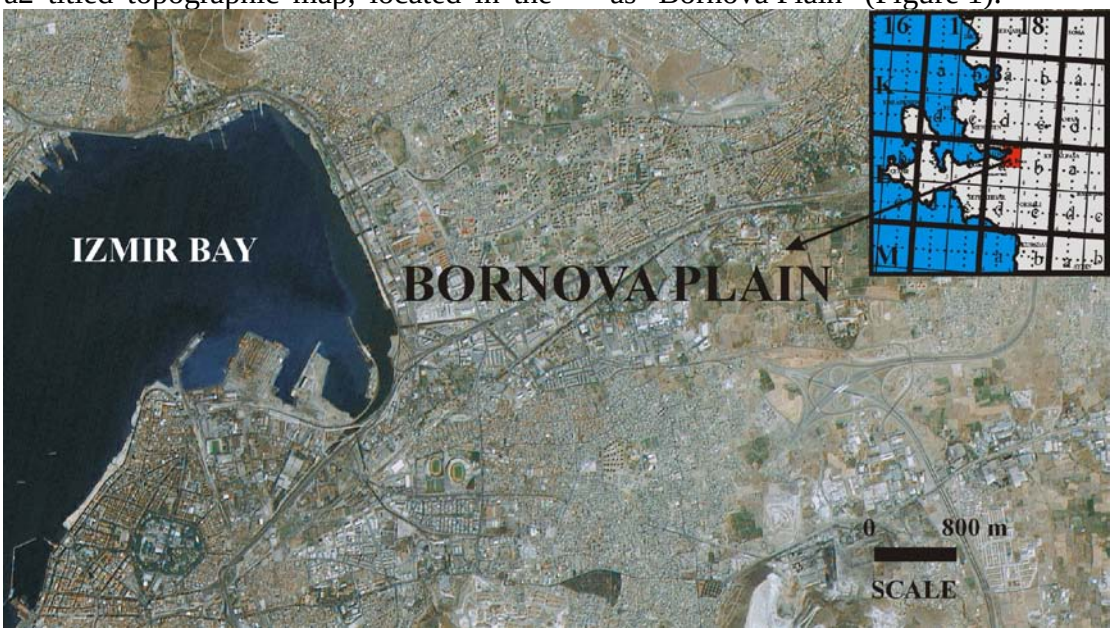

Figure 1. Location map of the study area.

SOIL LIQUEFACTION

Liquefaction analyses were performed according to Treshold Acceleration Criterion (Dobry et al., 1981), Dynamic Shear Stress (Seed and Idriss, 1971), Empiric Method (Iwasaki et al., 1984) and Tokimatsu-Yoshimi Approach (1983) by using laboratory test results and records from 422 boreholes which had been opened before in the Bornova Plain. The conclusion of these analyses and the liquefaction zoning map were prepared according to each method. For 0-20.0 meter depth, soil layers which have

liquefaction susceptibility were determined and transformed to thematic maps in GIS. In liquefaction analyses, corrected SPT-N values (SPT-N'_{30}) were used. While thematic maps were prepared, the current groundwater level data was used.

Damages occurred in some buildings, in the Inner Bay of Bornova during the Urla earthquake which occurred in 10 April 2003. The areas where damaged buildings were located were compared with liquefaction analysis results that were obtained in this study and the results are found to conflict with each other.

The earthquakes transform water saturated sandy soils to muddy water suddenly. As a result of strong vibrations, water saturated or partly saturated homogenous sandy soils are transformed to liquid phase, which can be defined as liquefaction (Port and Harbor Research Institute, 1997).

Before an earthquake (in static position) in sandy soils, there are contact points between the grains, and loads are carried by transferring through these contact points (Figure 2). By this way, soil shear strength provides support for any structure on the surface of the soil. Shear waves reshape the structure of the sandy soils, and contact points between grains disappear because of the earthquake waves. (Figure 3).

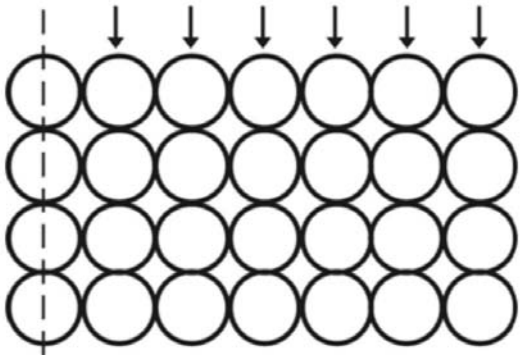

Figure 2. Cubic type orientation of the soil particles (Port and Harbour Research Institute, 1997).

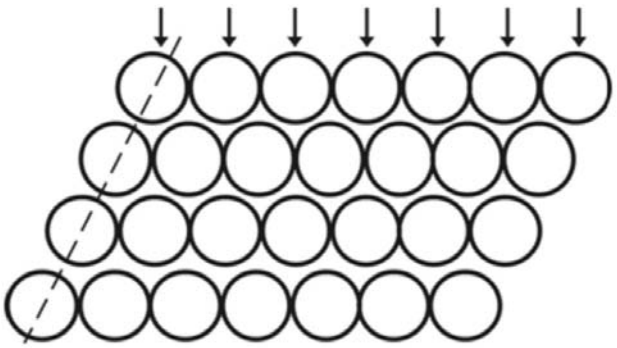

Figure 3. Shear status (Port and Harbour Research Institute, 1997).

FACTORS THAT CAUSE LIQUEFACTION

These are factors that cause liquefaction of sands (Prakash, 1981; Pusat, 1989; Yılmaz, 2004):

- *Grain size distribution,*
- *Uniformity degree (coefficient)*
- *Stiffness of layer (Initial relative stiffness),*
- *Vibration properties,*
- *Location of drainage and dimensions of layer,*
- *Size and properties of probable loads,*
- *Type of soil formation,*
- *Time of being under the load,*
- *Past of deformation,*
- *Stuck air,*
- *Void ratio,*
- *Effective pressure,*
- *Percent of clay size (content),*

Gravity acceleration must be included in these factors. Aydan et al. (1996) states that liquefaction might occur in any kind of coarse grain soils.

PREPARATION OF THE LIQUEFACTION SUSCEPTIBILITY MAPS

By utilizing laboratory test results and records from boreholes which were drilled before in the alluvial field in the study area, liquefaction analyses were performed according to four different methods, and potential liquefaction borehole locations were shown for each method one by one (Figures 4, 5, 6 and 7).

These methods are;

1. *Threshold Acceleration Criterion (Dobry et al., 1981),*
2. *Dynamic Shear Stress (Seed and Idriss, 1971),*
3. *Empiric Method (Iwasaki et al., 1984)*
4. *Tokimatsu-Yoshimi Approach (1983).*

Locations of those boreholes that do and do not cut liquefaction susceptible soil layers were marked on the groundwater table map which was prepared by taking into account the groundwater table data measured in 232 boreholes between years 1990-2004 (Figures 4, 5, 6 and 7). Liquefaction susceptible soil layers were cut in black dotted borehole locations. According to four different methods, obtained results were almost similar. Where groundwater table was below 10 meters and low and near the Izmir bay, it was understood that soil layers have liquefaction susceptibility (Kıncal, 2005).

A series of analyses were performed by using laboratory and field tests on potential liquefaction soils before preparing the liquefaction maps, in probable liquefiable zones in each borehole.

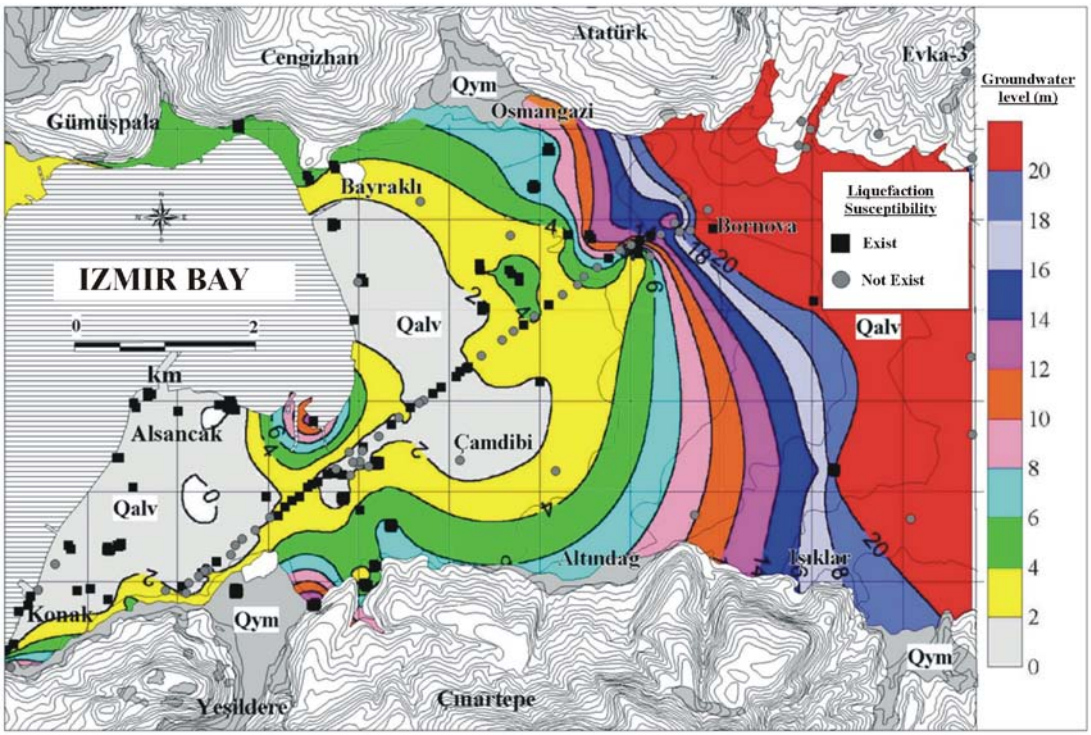

Figure 4. Liquefaction susceptibility analysis results suggested by Dobry (1981).

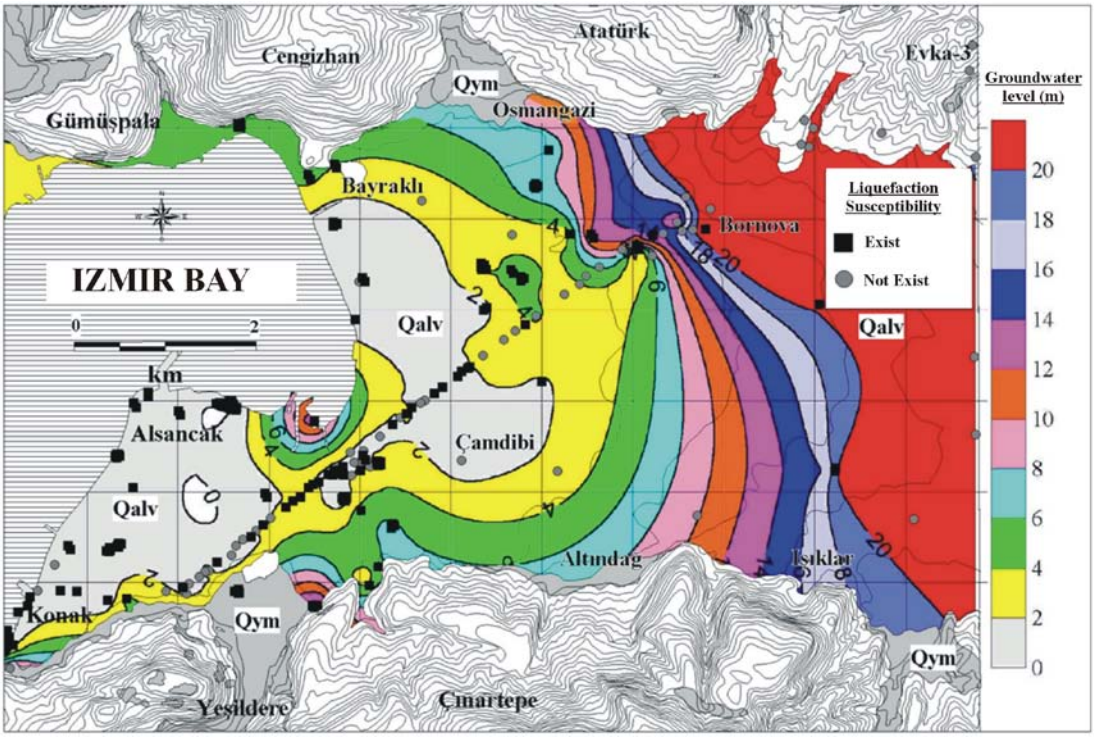

Figure 5. Liquefaction susceptibility analysis results suggested by Seed and Idriss (1971).

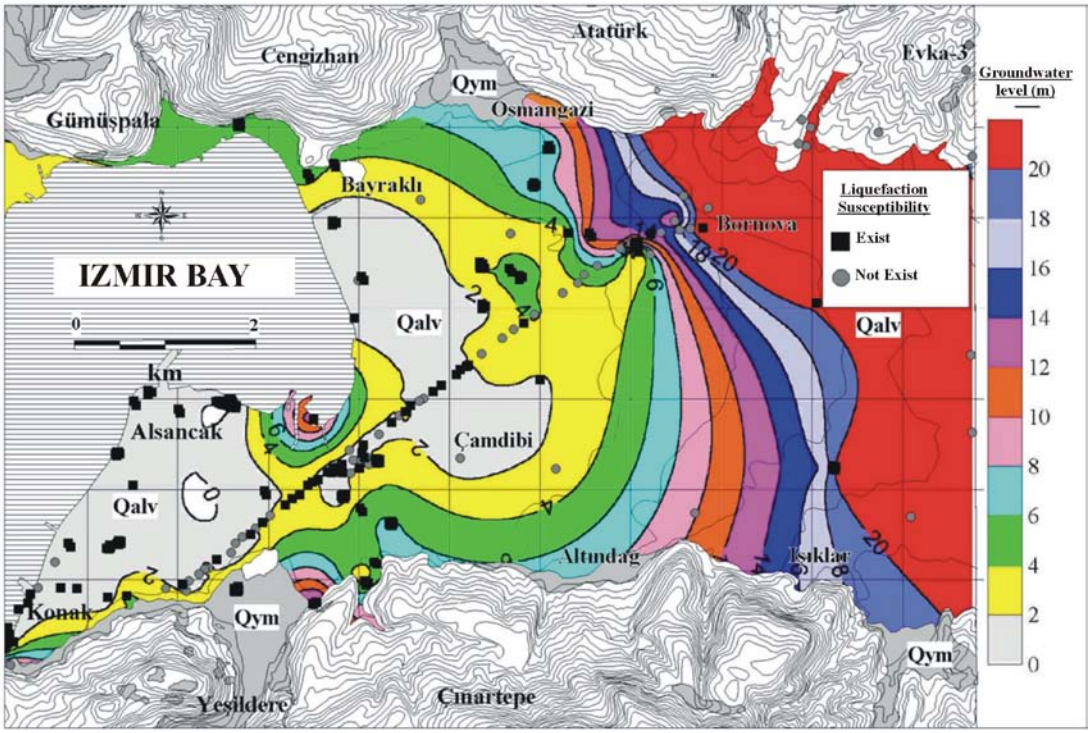

Figure 6. Liquefaction susceptibility analysis results suggested by Tokimatsu-Yoshimi Approach (1983).

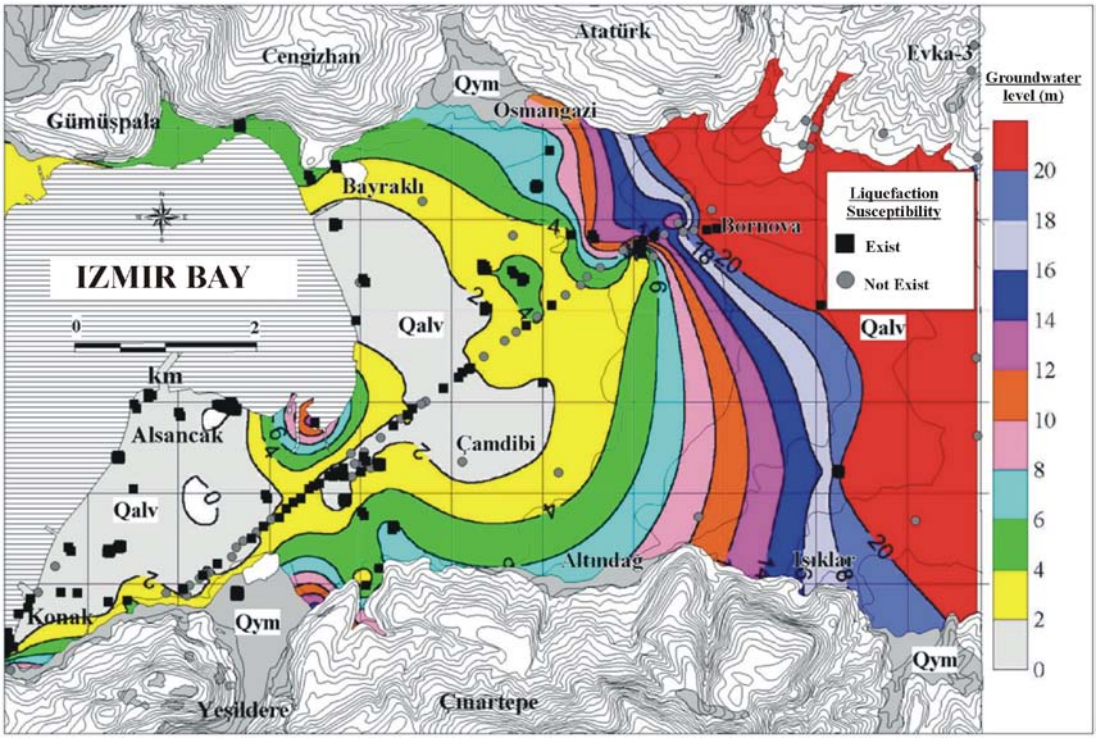

Figure 7. Liquefaction susceptibility analysis results suggested by Iwasaki et al. (1984).

RISK MAP PREPARATION

The "Risk Map" was obtained using below digital maps in GIS, by taking into consideration those boreholes that cut probably liquefiable soil layer;

- *Liquefaction analyses results which were made according to Dobry et al. (1981)*
- *Map of liquefaction susceptible areas prepared using four different liquefaction analysis*
- *Detailed soil type data layers determined from the borehole logs which were previously drilled in the study area*
- *Groundwater level map*
- *Elevation map*
- *Bearing capacity map (Figure 8).*

Liquefaction analyses were performed with four different methods using laboratory test results and borehole data previously drilled. Four different thematic maps were prepared using the results of the liquefaction analysis with the help of GIS. During the preparation of the Risk Map, only the thematic map which belongs to Dobry et al. (1981) was used as a layer in liquefaction susceptibility analyses. Because only field data like V_S and V_p-wave velocities must be used in susceptibility mapping work, Dobry et al. (1981) method was chosen.

In the thematic map shown in Figure 9, 14-different soil types can be seen for the 6.0 meter depth. Also, on this map bearing capacity zoning and groundwater level data can be seen easily. 18-soil types were decreased to 5 (1.fills, 2.sandy, 3. clayey, 4.silty and 5.gravelly soils) to obtain the Risk Map to avoid soil type complications.

In dynamic conditions, groundwater level is between 0-2 meters in the sites which have liquefaction susceptibility. Liquefiable soils are located in sandy soils and fill sites (Figure 8). Liquefiable soil layers in the sandy-clayey soils can be observed for 6.0 m depth in Figure 8 (pink colored zones).

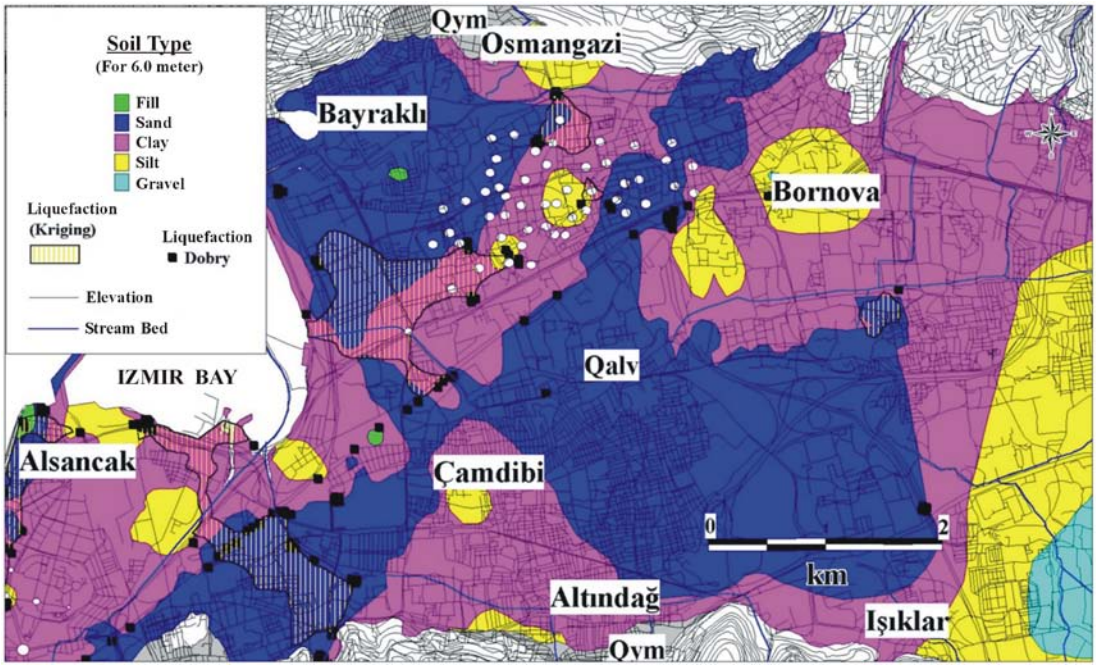

Figure 8. Risk Map which represent liquefaction potential boreholes on soil map.

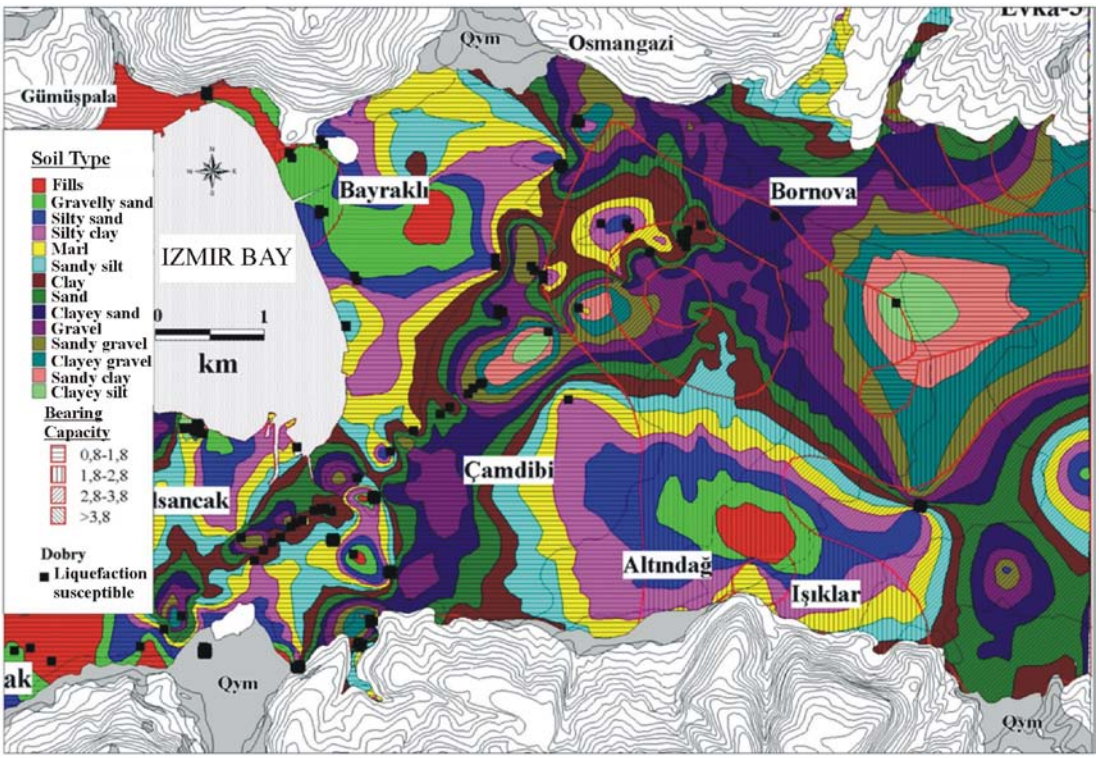

Figure 9. Detailed soil overlay map which also shows liquefaction susceptible soils analyzed in boreholes and bearing capacity values calculated from seismic measurements.

If liquefiable sandy soils exist over and/or under the 6.0 meter depth, zone in the 6.0 m depth has liquefaction susceptibility. Black dots in Figure 8 show that liquefiable soil layer exists in any depth of soil profile of 0-20 meters. For example, if there are sandy soil layers that have liquefaction susceptibility between 0-5 meters and 7-20 meters and also there is a clayey zone observed in 6 meters depth, this zone must not be understood as "liquefiable soil layer". Indeed, it should be known that over and under the 6.0

meters depth, any sandy soil layer in any depth has liquefaction susceptibility.

Fields which have liquefaction susceptibility (Figure 10), overlay with the sites that were effected by Urla earthquake in April 10, 2003 and partly damaged buildings located in Figure 10.

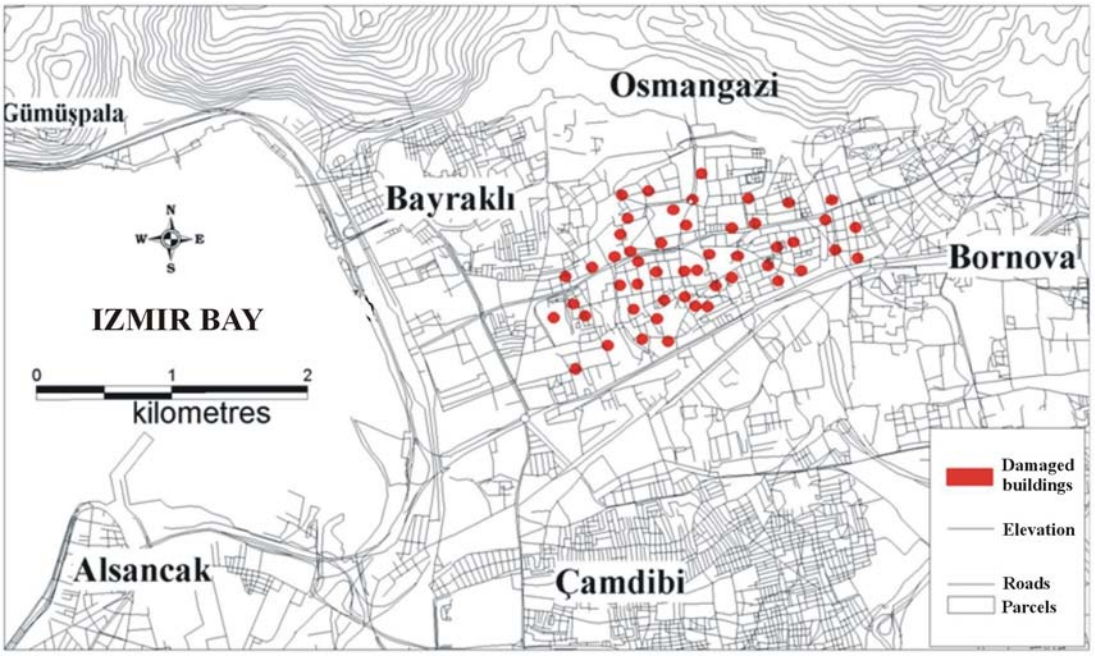

Figure 10. Damaged buildings during the 10 April 2003 earthquake.

The investigation methods of soil liquefaction susceptibility are updated non-stop in the light of advances in liquefaction techniques. Although the base of liquefaction susceptibility investigation methods is based on basic methods of Seed and Idriss (1971), because dynamic effects and a variety of soil parameters were used, their changeable numbers may cause different results. Because there is no one single reliable method for determining the susceptibility of soil liquefaction, analyzing the soil with a few methods and then comparing the results is the most suitable method. Because, while a specific soil level has liquefaction susceptibility according to a method, the same soil level does not have the same results according to another method. For decreasing the possibility of error to a minimum, liquefaction susceptibility of any soil level was investigated by four different methods. Analyses were made by using different methods which use different soil parameters. Dobry et al. (1981) was chosen one of the methods used in this study because it takes into account the in-situ shear wave velocity (V_s) measurements and measured / estimated threshold deformation values. Other three methods are related with SPT-N'_{30} values.

Tokimatsu and Yoshimi (1983) and Seed and Idriss (1971) methods resemble each other. Tokimatsu and Yoshimi (1983) method is different, in that horizontal soil acceleration and number of cycles belonging to soil movements like seismic earth movements which cause liquefaction are taken into account. Also in this method, shear strength ratio - SPT-N'_{30} relationship was obtained graphically by considering the amount of materials under the number-200 sieve. This graphic is important to determine soil liquefaction susceptibility. Liquefaction potential index (I_L) concept suggested by Iwasaki et al. (1984) is different from the other methods, as it takes into account the intensity of liquefaction degree for a given area, and it suggests the classification of liquefaction potential in a wide range. This classification is made in a wide range

[0< IL≤5, 5< IL≤15 and IL>15 (liquefaction susceptibility is very high)] because it is easier to make such classifications based on thematic maps of liquefaction susceptibility.

In this study, liquefaction susceptibility analyses were completed for 0-20 meter depths according to four different methods, and four thematic maps were obtained by overlaying the groundwater level map and map that boreholes cut soil layers which have liquefaction susceptibility located in (Figure 4, 5, 6 and 7). But, only the thematic map of Dobry et al. (1981) was used to prepare the Risk Map about soil liquefaction susceptibility. Because, Vs-seismic wave velocity measurements like field values are used in Threshold Acceleration Criterion to determine liquefaction susceptibility of existing soils in the study area (seismic measurements do not represent point values, they present mass values).

RESULT

The Risk Map was obtained by overlaying results of liquefaction analyses, soil map, groundwater level and elevation thematic maps which belong to soils exposed in the Bornova Plain (Izmir-Turkey). This map represents those soil layers that have water-saturated liquefaction susceptibility in dynamic conditions in Bornova Plain (Izmir-Turkey).

REFERENCES

Aydan, Ö., Sezaki, M. ve Yarar, R. (1996). The Seismic Characteristics of Turkish earthquakes, *11 th World Conf. on Earthquake Engrg.*, Mexico, Paper No. 1025.

Dobry, R., Stokoe, K. H., Ladd, R. S., and Youd, T. L. (1981). Liquefaction from S-wave Velocity, Preprint 81-544, ASCE, National Convention, St.Louis, Missouri.

Iwasaki, T., Tadashi, A., and Tokida, K. (1984). Simplified procedures for assessing soil liquefaction during earthquakes, *Soil Dynamics and Earthquake Engineering*, 3(1): 48-58.

Kıncal, C. (2005). Engineering Geological Evaluation of the Geological Units Exposed in Inner Bay Area (Izmir)'s Vicinity Using Geographical Information Systems and Remote Sensing, *PhD Thesis*, p.342, Izmir (In Turkish). (unpublished)

Port and Harbour Research Institute. (1997). Handbook on Liquefaction Remediation of Reclaimed Land, Balkema Pub. Co., Rotterdam, Netherlands, 312p.

Prakash, S. (1981). Soil Dynamics, Mc-Graw Hill Book Pub. Co., USA, 426 p.

Pusat, Ö. (1989). Sıvılaşmanın Etüdü, İzmir İçin Sismik Risk Analizi ve Sıvılaşma Uygulamaları, *Yüksek Lisans Tezi, DEÜ, FBE*, İzmir, 85s. (unpublished)

Seed, H. B. and Idriss I. M. (1971). Simplified procedure for evaluating soil liquefaction potential, *J. of Geotech. Engrg. Div.*, ASCE, 97(9): 1249-1273.

Tokimatsu, K., and Yoshimi, Y. (1983). Empirical correlation of soil liquefaction based on SPT-N value and fines content, *Soils and Foundations*, 23(4): 56-74.

Yılmaz, R. (2004). Fundamental Construction, *Birsen Publication, p. 207*, İstanbul (In Turkish).

ENGINEERING GEOLOGICAL MAP PREPARATION IN ALLUVIAL FIELDS : CASE STUDY, BORNOVA PLAIN (IZMIR-TURKEY)

Kıncal C.[1] and Çakıcı S.[2]

[1]Dokuz Eylul University, Engineering Faculty, Department of Geology, 35100, Bornova/Izmir-Turkey
[2]Ege Temel Boring Company, Doğanlar District, Okul Street No: 145, 35040, Pınarbaşı/Izmir-Turkey

Abstract: Site suitability maps are a special type of engineering geological maps, and are necessary when you are planning to construct a building on a field, and include detailed geological elements. Geotechnical data in 352 previously drilled borings in the total number of 167 geotechnical reports were used to prepare SPT-resistance and soil zoning maps in 3.0, 6.0 and 10 meters from the ground surface in Bornova Plain. Standard Penetration Test (SPT) values chosen from borings were used to form a database to analyze the site settlement suitability. UTM (Universal Transverse Mercator) coordinates of the boreholes were determined and digitized to be used in Geographical Information Systems (GIS). SPT-resistance map was used in overlay analysis in GIS for choosing the suitable sites. Soil thematic map layer was used to check the SPT-N'_{30} values when geotechnical decisions were made.

Boring data layer was used in alluvial soils existing in the Bornova (Izmir-Turkey) Graben Site located in the eastern part of the Izmir Gulf, 1) to reveal the soil distribution horizontally and vertically, 2) to make soil classification considering SPT-N'_{30} values according to their bearing capacity and compare it with the data exposed from seismic measurements, 3) to use geotechnical data to complete liquefaction analysis and finally 4) to make overlay analysis when making settlement suitability analysis in GIS. Borehole database has been formed by gathering collected soil data including index properties and SPT data in the alluvial plain.

Key words : Drilling, SPT-Resistance map, Soil Thematic Map, Geographical Information Systems, Bornova Plain (Izmir-Turkey).

1. METHODOLOGY

Soil and earthquake database has been established based on available geotechnical reports. Geotechnical data from 422 boreholes which were drilled in the alluvium were gathered from Ege Temel drilling company in Izmir. Index and engineering properties of the soils taken from drillings were determined in the laboratory works such as specific gravity, natural water content, cohesion, angle of friction, initial void ratio and then all data were entered (SPT blow counts ans CPT resistance i.e.) to a database using Microsoft Excel software (Kıncal, 2005).

167 soil investigation reports which belong to the study area were taken from borehole companies and UTM coordinates of each borehole were determined and then digitized using GIS (Figure 1). The liquefaction analyses were completed using 352 boring logs which belong to 167-soil investigation reports; first of all, borehole locations (X, Y, Z) were determined.

Software used to prepare maps using geographically registered different kinds of data was Surfer version 8.0. Kriging is a geostatistical gridding method that has proven useful and popular in many fields. This method produces visually appealing maps from irregularly spaced data. Kriging attempts to express trends suggested in any data, so that, for example, high points might be connected along a ridge rather than isolated by bull's-eye type contours. Kriging is a very flexible gridding method. You can accept the Kriging defaults to produce an accurate grid of your data, or Kriging can be custom-fit to a data set by specifying the appropriate variogram model. Within Surfer, Kriging can be either an exact or a smoothing interpolator depending on the user-specified parameters. It incorporates anisotropy and underlying trends in an

efficient and natural manner (Cressie, 1991; Abramowitz and Stegun, 1972). Powefull thematic maps were prepared using Surfer 8.0 program to investigate engineering properties of the alluvial fields.

Bornova graben area includes both rock and soil formations. Precise determination of dynamic characteristics of these formations are essential to reliable microzonation analysis.

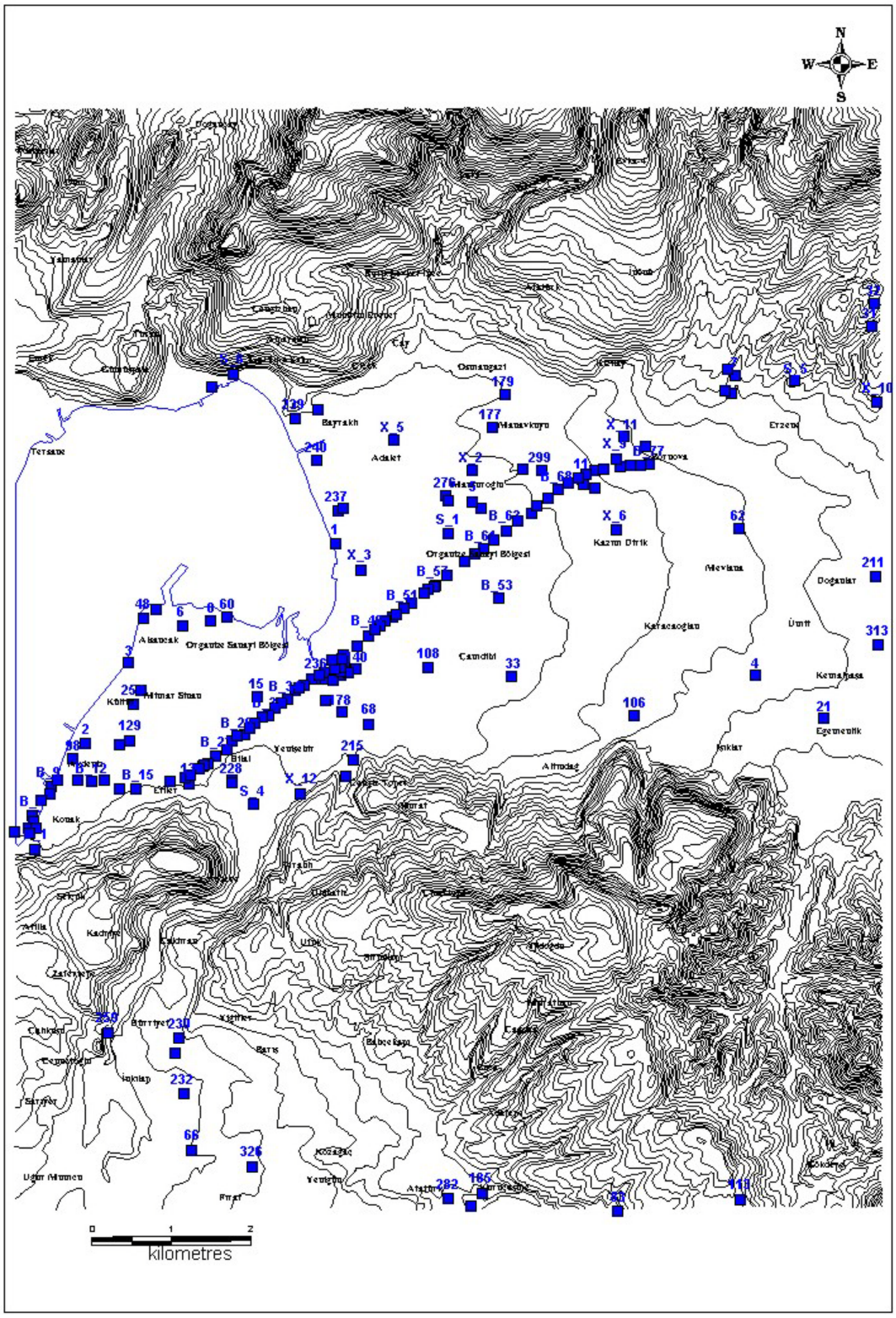

Figure 1. Location map of the soil investigation reports in the study area (boreholes)

2. GEOLOGY AND GEOMORPHOLOGY

Study area is in the 1/25000 scale L18-a2 titled topographic map, located in the eastern part of the Izmir Bay, known as "Bornova Plain" (Figure 2). Ilıca, Sepetçi, Şelale, Baliali, Sarıkaya, Kudurgan, Eğridere, Kocaçay, Topçu, Bornova, Kırmızı Toprak, Şeytan and Kazan Kulbu rivers are located in the north and Sabi, Mersinlik, Kapız, Arapdereboğazı, Deliceboğaz, Kalabak, Gökdere, Kandere Çitlenbik and Uzundere (Meles) rivers are located in the south of the study area. Northern river's waters flow from north to south and southern river's waters flow from south to north directions.

Çilekdağı (221 m), Zeytinlidağ (272 m), Kirişdağı (273 m), Kale (371 m), Küçükkale (442 m), Dede (148 m), Döşeme (427 m.), Alaca (252 m) and Akgedik Hills (188 m) are located in the north and Kalabak (379 m), Canavar (288 m), Boz (265 m), Buca (312 m), Çıtırlık (217 m) and Beyti Hills (376 m) are located in the south of the study area.

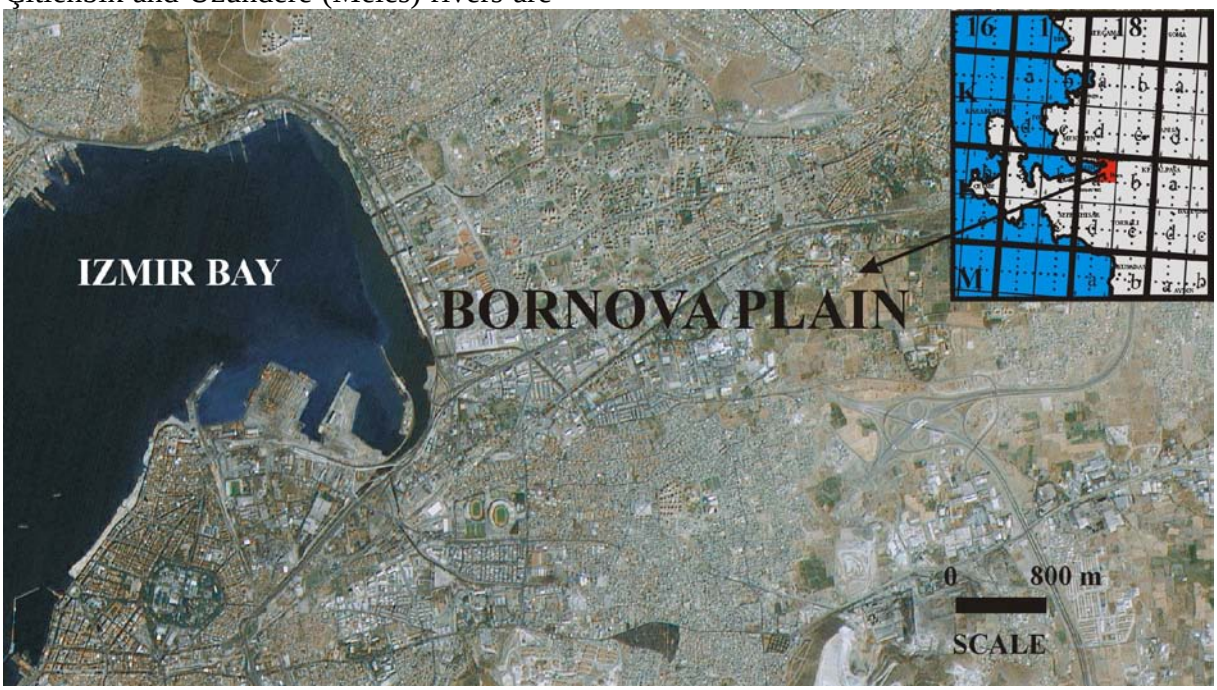

Figure 2. Location map of the study area.

Alluvium can be seen in the surrounding stream beds of the study area and in the Bornova Plain (Figure 3). Alluvium is exposed in the large horizontal/near horizontal fields. Alluvium is mostly seen in the Alsancak, Gökdere, Yenişehir, Çamdibi, Altındağ, Doğanlar, Bayraklı, Manavkuyu, Bornova and Evka-3 Districts.

Alluvial plains exist in and around Izmir Bay basically developed on the same terrestrial fills but they are different from a geomorphological point of view. Balçova and Alsancak in the south and Karşıyaka in the north are simple delta plains which developed in front side of the mountain rivers (Kayan, 2000).

Gediz Delta is a complicated geomorphologic formation which was formed by Gediz River's alluvium that collects all the waters of Western Anatolia. Bornova Plain in the east starts with the Izmir Bay shore and is not a typical delta plain because there isn't any large river which starts in Bornova and ends in Izmir Bay.

Figure 3. Alluvium exposed in the eastern part of the study area, Gökdere District (520740/4252620)

First of all, Bornova Plain is a basin between mountains which is located next to the east of Izmir Bay. But when alluvial morphology is investigated carefully, different soils on the base can be realized. These areas are associated with the hydro-geomorphologic properties of streams which flow to the Bornova Plain. There are 3 big mountain streams that flow to Bornova, while short streams flow from the mountain slopes. These are Kocaçay in the north; which flows from Yamanlar Mountain and forms Bornova accumulation cone, in the south; Gökdere (Arap stream) which comes from west of the Kurudağ Hill and forms Işıkkent accumulation cone, and in the east; Kavaklıdere (Manda River) which flows from the area of Kemalpaşa Mountain and Kurudağ Hill. These three large rivers form three big accumulation cones on the plain (Kayan, 2000).

Bornova and Işıkkent accumulation cones make the base narrow by flowing from north and south and separate the east and west part of the basin with its morphology. Manda River leaves its coarse material in the east of the Bornova Plain and ends up in the area between Işıkkent and Bornova accumulation cones, filling it up easily but unable to continue, its path being blocked by little thinner alluvium it deposits. For this reason, the east of the plain was formed as a higher filling area. This is why the typical development of a delta on the coast of Bornova could not be seen (Kayan, 2000). Kayan's (2000) study was re-modeled in this study and X-X′ cross-section was taken, existing soils seen in the ground are presented just for about 1.0 meter (Figure 4).

3. GEOTECHNICAL STUDIES

Geotechnical data in the 352 previously drilled borings were used to prepare SPT-resistance and soil zoning maps in 3.0, 6.0 and 10 meters from the ground in the Bornova Plain (Izmir). Standard Penetration Test (SPT) values which were choosen from borings were used to form a database to investigate the site settlement suitability. Boring logs which belong to soil boreholes were examined and maps prepared using soil types which were observed at 3.0, 6.0 and 10.0 meter depths.

In engineering geological works, SPT-resistance maps and soil zoning maps are very important to analyze any field. So, these kinds of maps must be prepared before any project applications in real life to help decision makers with risk management.

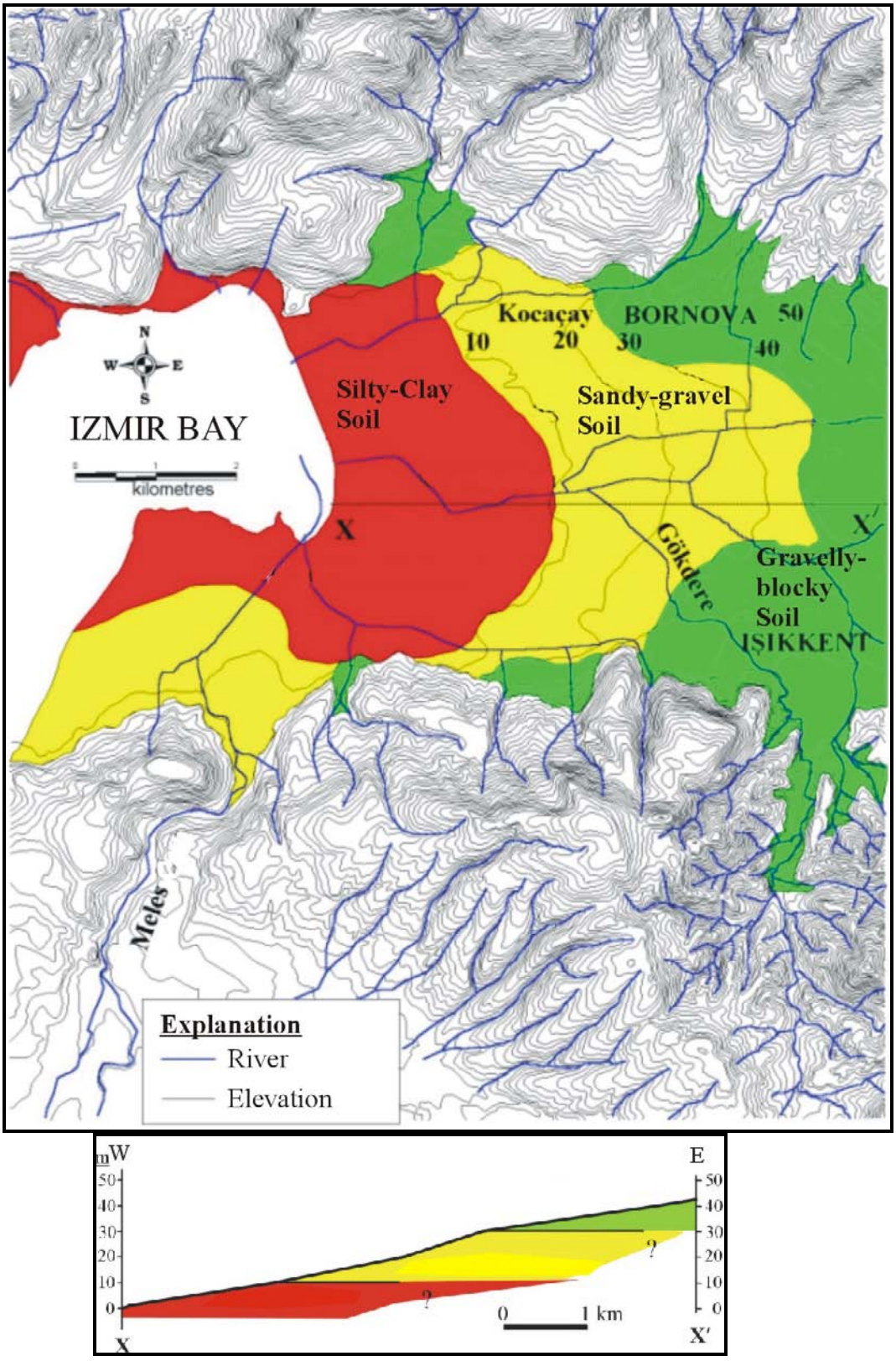

Figure 4. Alluvial geomorphologic map of the Bornova Plain and E-W directioned geological cross-section (existing soils seen under the ground level are presented just for about 1.0 meter, modified from Kayan, 2000).

3.1 Field Tests

Standard Penetration Test results are used to determine relative density and bearing capacity of the non-cohesive soils. Suggested relationship between SPT-N and relative density values for non-cohesive soils is presented in Table 1. Also corrections which are made on SPT-N_{30} values can be seen in Table 2 below.

Table 1 : Suggested relationship between SPT-N and relative density values for non-cohesive soils (Terzaghi ve Peck, 1948).

SPT-N value	Relative Density	Dry Density (kN/m³)	Internal Friction Angle (Ø)
0-4	Very loose	<14	<30
4-10	Loose	14-16	30-32
10-30	Moderately dense	16-18	32-35
30-50	Dense	18-20	35-38
>50	Very dense	>20	>38

SPT-N_{30} values must be corrected against groundwater and depth effects. Corrected SPT-N_{30} values entered into database while interpreting them with relative density.

3.2 Calculation of SPT-N′$_{30}$ Values and Depth Relations

Corrections were made on SPT-N Values obtained from drillings in the Bornova Plain.

Boring pipe length (C_R), inner tube (C_S), energy rate (E_E) and overburden corrections were made as suggested by Robertson and Wride (1998). Overburden stress corrections which were suggested by Lia and Whitman (1986) should be applied when the stress is less than 170 kPa.

Although there are many equations about overburden stress corrections, the ones which are in widespread use are Liao and Whitman (1986), Tokimatsu and Yoshimi (1983), and Peck et al. (1974). Overburden corrections which were suggested by Peck et al. (1974) were used in this study. On the SPT-application points, depending on average effective geostatic pressure, below formulas are used;

$$\text{SPT-N}' = C_N x N_{30},\ C_N = 0.77 \log\left[\frac{20}{\sigma'_0}\right] \text{(Peck et al.., 1974)}$$

σ'_0 : (Ton/ft^2) ; effective geostatic pressure, C_N: Overburden correction

In-situ tests, in the study area were upgraded because of the difficulty of taking undisturbed soil samples from non-cohesive soils.

SPT-N′$_{30}$ zoning maps were prepared for 3.00, 6.00 and 10.00 meter depths, and they are presented respectively in Figures 4, 5 and 6. On these maps, the area whose SPT-N′$_{30}$ values are less than 20, are shown in green and brown. For non-cohesive soils, SPT-N′$_{30}$ $\leq$ 20 values point out the "moderately dense, loose and very loose" soils. Especially the zones which are shown with brown (SPT-N′$_{30}$ $\leq$ 10), are the problematic areas as regards bearing capacity and soil liquefaction. In addition to existing cohesive soils in these areas, consolidation settlement problems must be considered. SPT-N′$_{30}$ $\leq$ 15 values represent very soft – soft and/or moderately hard consistency (q_u<2.0 kg/cm^2).

When we look at the SPT-N′30 zoning map which was prepared for 6.0 m depth, SPT-N′30 values lower than 20 in the 2 km-large area from seaside to land are observed in Kultur and Mimar Sinan Districts, from the industrial zone to Altındağ district, approximately a 1 km large area.

For almost half of these areas, SPT-N′30 values are below or equal to 10 and the soil layers have either loose-very loose or moderately hard-soft soil properties.

Almost the same zones are the problematic areas about soil problems on the SPT-N'_{30} zoning map which were prepared for 3.0 and 10.0 m depths (Figures 5 and 7). When we look at the zoning map of SPT-N'_{30} that was prepared for 3.0, 6.0 and 10.0 meter depths, generally for all the alluvial areas in the west, SPT-N'_{30} values were determined as less than 20 (Figure 5, 6 and 7). The most important region with respect to bearing capacity is the profile which includes soils section for 0-10 meter depths. This profile is known as "significant depth" (Yılmaz, 2004) and stress increases decrease to lowest levels below this profile.

Table 2 : SPT-N_{30} Corrections (Pa: atmosphere pressure, 98 kPa ve σ'_v: vertical overburden pressure) (Robertson ve Wride, 1998)

Correction Type	Equipment	Correction Factor
C_N **overburden pressure**		$(P_a / \sigma'_v)^{1/2} < 170$ kPa
E_E (energy ratio)	Donut type beetle Automatic-Trip Donut type beetle	0,5-1,0 0,8-1,3
C_B (borehole diameter)	65-115 mm 150 mm 200 mm	1,0 1,05 1,15
C_R (Boring pipe length)	<3 mm 3-4 mm 4-6 mm 6-10 mm 10-30 mm	0,75 0,80 0,85 0,95 1,0
C_S (sampler correction)	Standard sampler Sampler without inner tube	1,0 1,1-1,3

Relative density values can be calculated using SPT-N'_{30} values which were depth-corrected.

Parameters like Ø (internal friction angle), E_s (deformation moduli) and γ_n (natural unit weight) can be calculated using correlative relationships (Das, 1995). Field SPT tests in non-cohesive soils are given healty results and relationship between SPT-N'_{30} and density is presented in Table 1.

SPT-N_{30} values in 3.0, 6.0 ve 10.0 meters were collected using previously drilled boreholes in the Bornova Plain and SPT-Resistance maps were prepared.

3.3 Determining Soil Types in Alluvial Deposits

352 out of 422 boreholes were drilled in the Bornova Plain alluvial soils. Boring logs which belong to soil boreholes were examined and maps prepared using soil types which were observed at 3.0, 6.0 and 10.0 meters depths (Figure 8, 9 and 10). Looking at the soil-type zoning map prepared for 3.0 meters, the gravel levels are only seen in the east sides of Işıklar, the whole 2.0 km^2-area at the east of Konak, the north of Işıklar and Altındağ, the east of Çamdibi, the west and northwest of Bornova, approximately 15.0 km^2-area at the east of Osmangazi and all the area between Bayraklı and the Aegean Sea. Cohesive soils are covered approximately 10 km^2 - area between Bornova and Evka-3 and Alsancak, the south of Çamdibi, Altındağ and Işıklar and the area around the Justice department

building (Figure 8).

Looking at the soil types zoning maps for 6.0 and 10.0 meter depths, there are similar structures that can be seen in Figures 9 and 10. The main difference between Figure 8 (soil type zoning map for 3.0 meters depth) and Figures 8-9 is that gravelly soil levels (approximately a 25 km^2-large area which is from the east of the Bornova District and the south of Çamdibi and Işıklar Districts) cover a larger area.

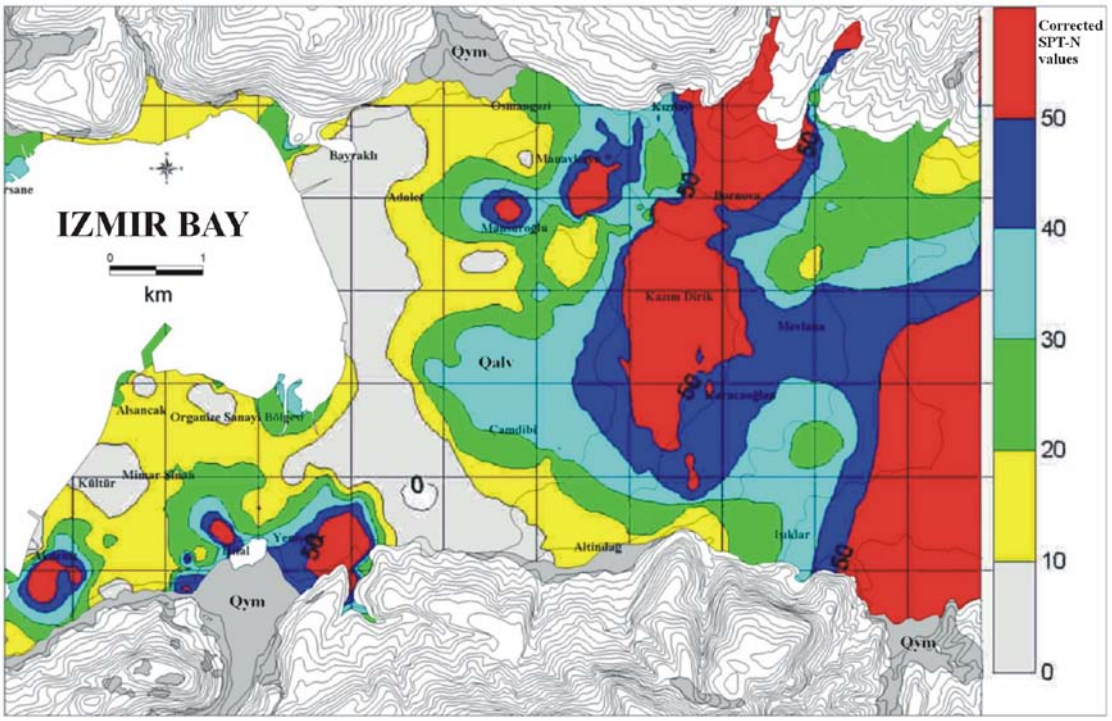

Figure 5 : SPT-N'_{30} zoning map prepared for 3 meters depth (Qym : Slopewash, Qalv : Alluvium).

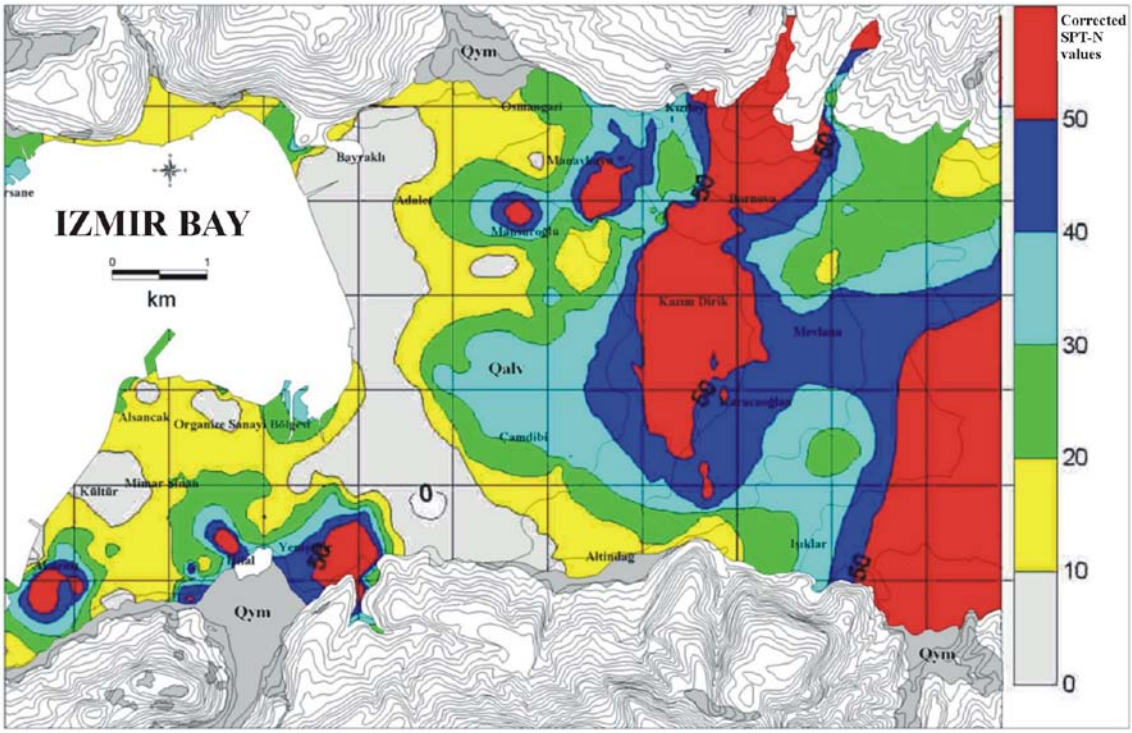

Figure 6 : SPT-N'_{30} zoning map prepared for 6 meters depth (Qym : Slopewash, Qalv : Alluvium).

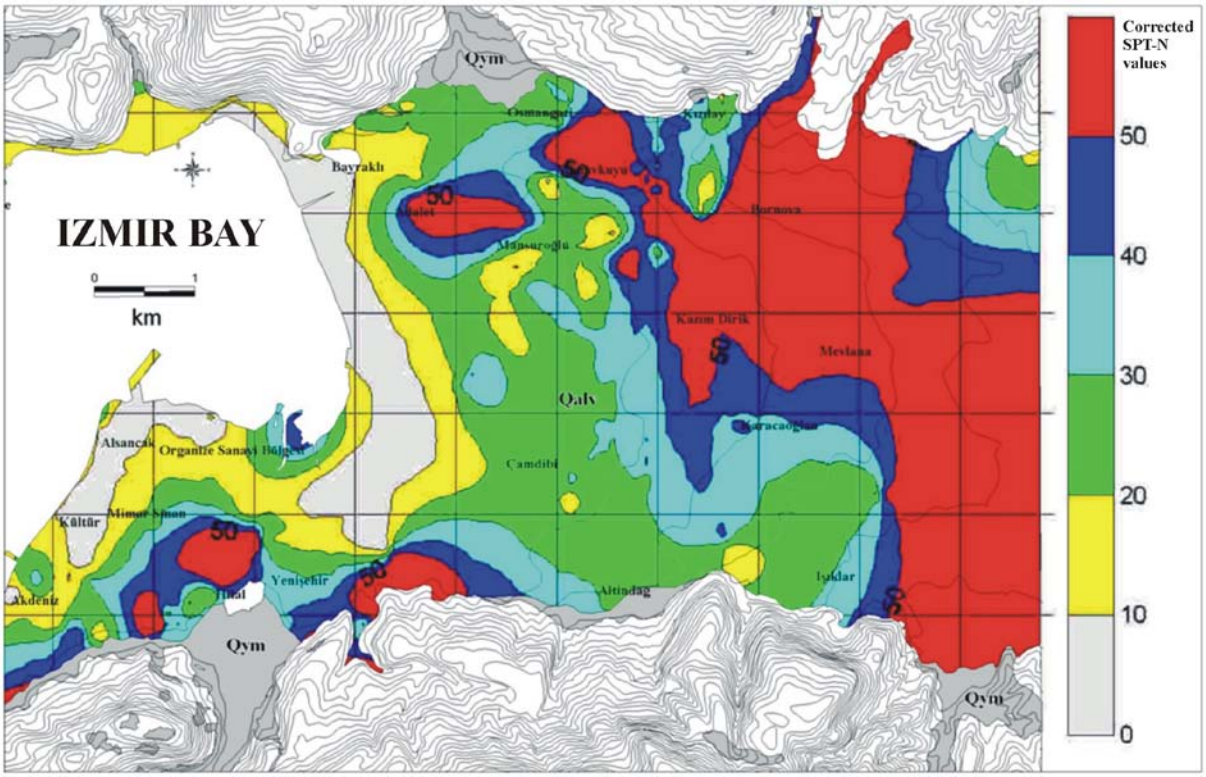

Figure 7 : SPT-N'_{30} zoning map prepared for 10 meters depth (Qym : Slopewash, Qalv : Alluvium).

The area covered by gravelly soils seen in maps prepared for 6.0 and 10.0 meters is equal to the area for 3.0 meters multiplied by 5.

Table 3 : Geotechnical problems depend upon soil properties in different soil types.

	Soil Type	SPT-N′$_{30}$	Soil description	Supposed Geotechnical Problem	
Cohesive soils	Clay (CL, CH)	≤ 8-10	Very soft and soft	Sudden settlement + Consolidation settlement	Different settlement problems
	Silt (ML, MH)	≤ 8-10			
	Clayey Silt	≤ 8-10			
	Silty Clay	≤ 8-10		Bearing capacity problems	
Non-Cohesive soils	Gravel (GP, GW, GC and GM)	≤ 10	Loose-very loose	Sudden settlement+	
	Sand (SP, SW, SM, SC)	≤ 10			
	Gravelly Sand	≤ 10		Bearing capacity problems	
	Sandy Gravels	≤ 10			

4. RESULTS

Cohesive soils (Table 3) over approximately 10 km^2 in the area between Bornova and Evka-3 and Alsancak, the south of Çamdibi, Altındağ and Işıklar and the area around the Justice department building (Figure 8). SPT-N′$_{30}$ zoning map was prepared for the 6.0 m depth, SPT-N′$_{30}$ values lower being than 20 in 2 km-large area from seaside to land area (from west to east), Kultur and Mimar Sinan Districts, from Industrial Zone to Altındağ District approximately 1 km large area (Figures 5, 6 and 7).

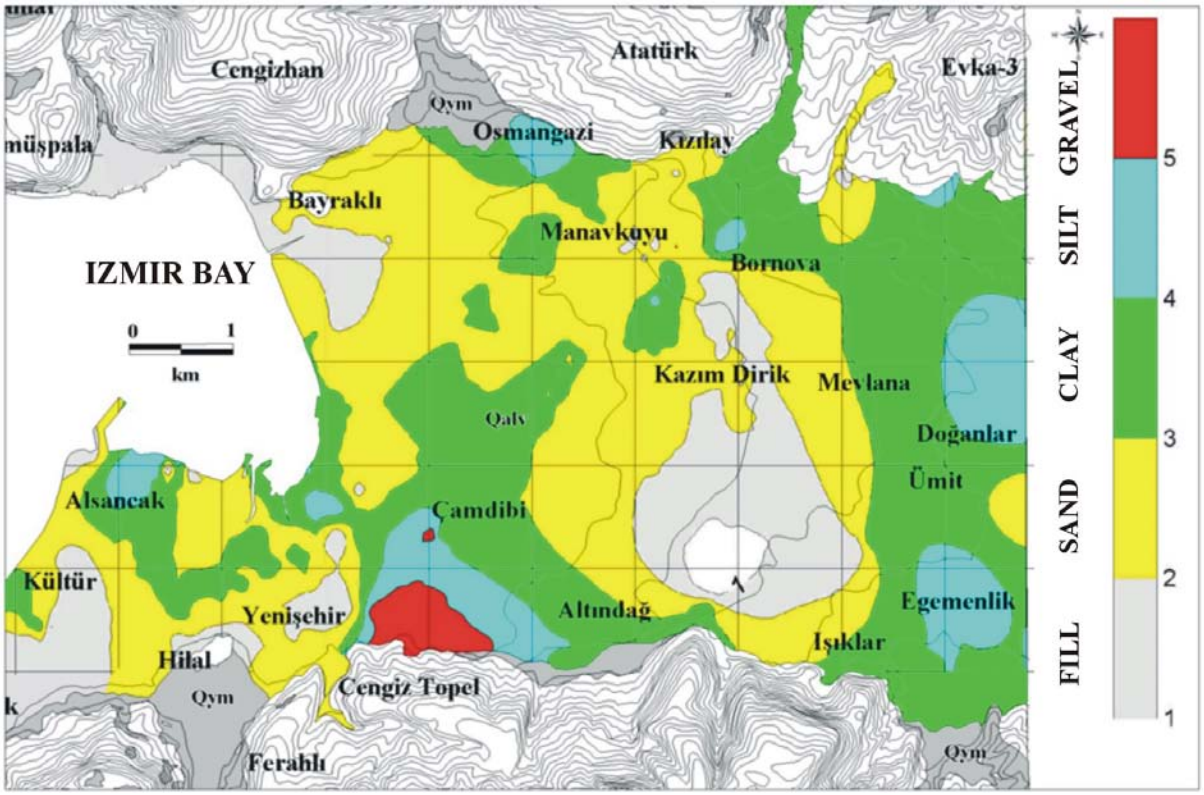

Figure 8 : Soil type zoning map prepared for the 3 meter depth (modified from Kıncal, 2005).

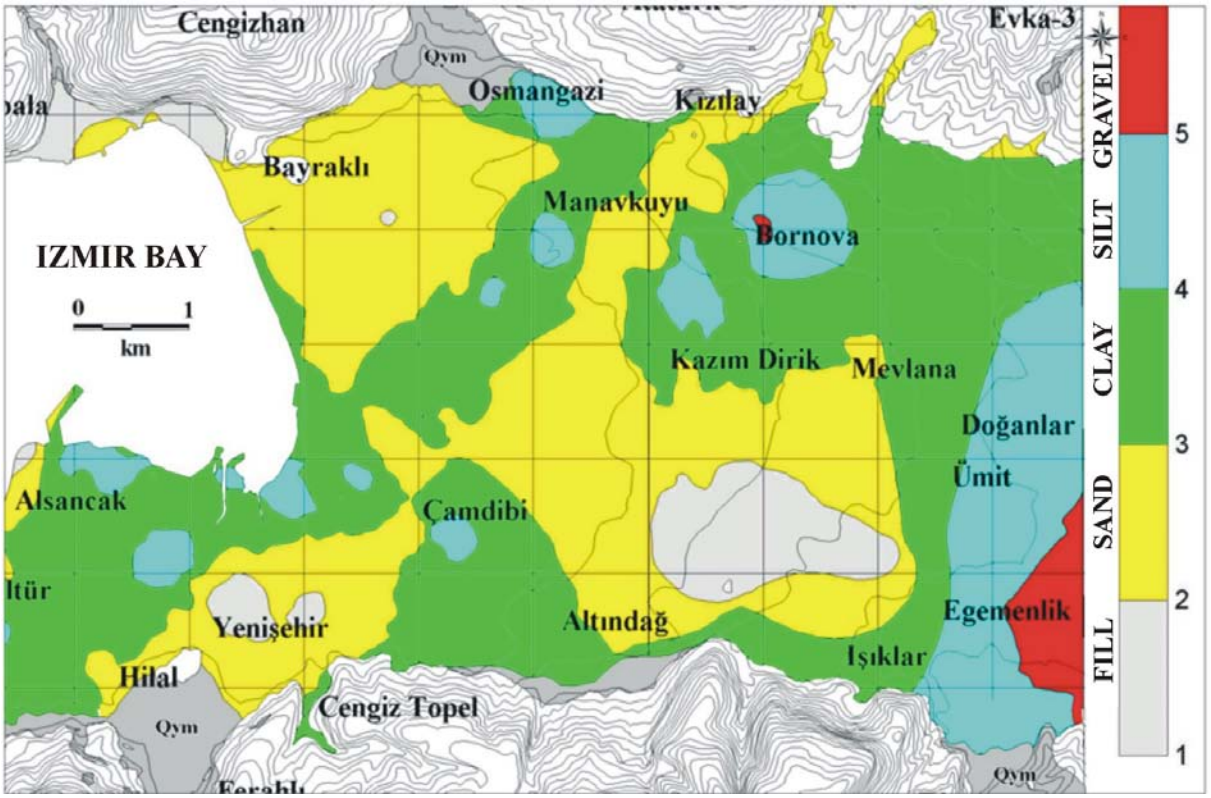

Figure 9 : Soil type zoning map prepared for the 6 meter depth (modified from Kıncal, 2005).

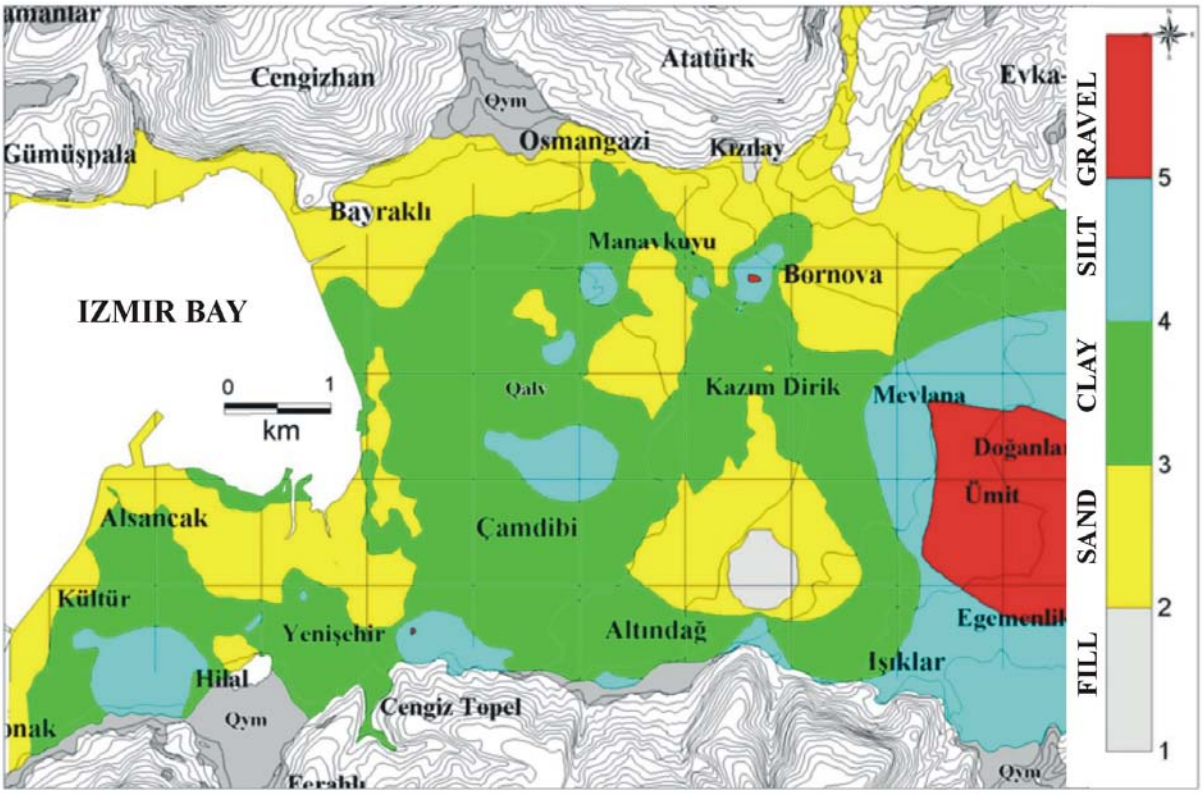

Figure 10 : Soil type zoning map prepared for the 10 meter depth (modified from Kıncal, 2005).

For non-cohesive soils, SPT-$N'_{30} \leq 20$ values point out the "moderately dense, loose and very loose" soils. Especially the zones which have the values of SPT-$N'_{30} \leq 10$, are the problematic areas in respect of bearing capacity and soil liquefaction. In addition to existing cohesive soils in these areas, consolidation settlement problems must be considered (Figures 5, 6 and 7).

Alluvial soils in western part of the Bornova graben area should now be taken into consideration to carry high liquefaction resistance of the graben area cohesionless soils. To cope with settlement, liquefaction and other soil problems, soil improvement techniques must be applied before any construction.

5. REFERENCES

Abramowitz, M., and Stegun, I. (1972). *Handbook of Mathematical Functions*, Dover Publications, New York.

Cressie, N. A. C. (1991). *Statistics for Spatial Data*, John Wiley and Sons, Inc., New York, 900 pp.

Das, B. M. (1995). *Principles of Foundation Engineering, 3rd ed.*, PWS Publishing Company, Boston, USA, p 828.

Kayan, İ. (2000). Morpho-tectonic units and alluvial geomorphology of the Izmir and its surroundings; *Syposium of Earthquake Potential of the Western Anatolia*, p.103 (In Turkish).

Kıncal, C. (2005). Engineering Geological Evaluation of the Geological Units Exposed in Inner Bay Area (Izmir)'s Vicinity Using Geographical Information Systems and Remote Sensing, *PhD Thesis*, p.342, Izmir (In Turkish). (unpublished)

Liao, S. S. C., and Whitman, R. V. (1986a). Overburden correction factors for correction in sand, *J. of Geotech. Engrg. Div.*, ASCE, 112(3): 373-377.

Peck, R. B., Hanson, W.E., and Thornburn, T.H. (1974). *Foundation Engineering, 2nd Ed.*, Wiley, New York.

Robertson, P. K., and Wride, C. E. (1998). Evaluating cyclic liquefaction potential using the cone penetration test, *Canadian Geotech. J.,* Ottawa, 35(3): 442-459.

Terzaghi, K. and Peck R.B. (1948), Soil Mechanics in Engineering Practice, John Wiley & Sons. Inc., 729 p. New York

Tokimatsu, K., and Yoshimi, Y. (1983). Empirical correlation of soil liquefaction based on SPT-N value and fines content, *Soils and Foundations,* 23(4): 56-74.

Yılmaz, R. (2004). Fundamental Construction, p. 207 Birsen Publication, Istanbul (In Turkish).

SEISMIC RISK DETERMINATION OF BORNOVA PLAIN SOILS IN IZMIR (TURKEY) USING S-WAVE AND P-WAVE VELOCITY MEASUREMENTS

Kıncal C.[1], Özyalın Ş.[2] and Zarif H.[3]

[1]Dokuz Eylul Univ., Engineering Faculty, Geological Engineering Dept., 35100, Bornova-Izmir/Turkey
[2]Dokuz Eylul Univ., Engineering Faculty, Geophysical Engineering Dept., 35100, Buca-Izmir/Turkey
[3]Istanbul Univ., Engineering Faculty, Geological Engineering Dept., 34850, Avcılar-Istanbul/Turkey

Abstract: The city of Izmir located on the western coast of Anatolia has long been recognized as a major industrial center and port carrying high seismic risk. The region has faced major earthquake disasters both in the historical and modern times. Seismicity nearby and in the Bornova graben area, which is the eastern part of the Izmir Gulf, is being governed by normal and oblique faults. These active faults have produced significant seismic activity. Bornova graben area and its surroundings include both rock and soil formations. Precise determination of dynamic characteristics of these soil formations are essential to reliable microzonation analysis and/or obtaining a land use map of the study area. Currently satisfactory data are not available regarding damping and wave velocity characteristics (Vp and Vs and Vp/Vs ratio, i.e....) of regional rocks and soils.

Seismic work has been conducted to measure Vs and Vp-seismic wave velocities in the Bornova graben area limited by active faults. The goal of this study is to realize seismic measurements for the depths of 0-3, 3-6 and 6-10 meters and to prepare the 1/5000 scaled seismic risk map for each depth. Obtained results for the different depths have been correlated with each other in this study. Maps of seismic velocities (Vp and Vs) were prepared using the field data with the help of Surfer 8.0 and MapInfo Professional 5.5 softwares.

Key words : Engineering Geology, Seismicity, Geographical Information Systems, The Inner Bay of Izmir (Bornova Graben).

1. INTRODUCTION

Geotechnical investigation of about 40 km2 has been carried out in the area known as Bornova Plain between Osmangazi, Kazım Dirik districts in the north and Konak, Ozkanlar, Altındag, Isiklar districts in the south (Figure 6). Seismic measurements were conducted with geotechnical purposes. In this context, seismic measurements were taken from 29 stations in the Bornova Plain (Figure 6). Bornova Plain is placed on the Bornova graben. As is well known, this graben area is limited by the normal faults from north and south. Graben faults mentioned above are still active. This shows that it is still tectonically active in this region. Additionally, Izmir and its surroundings are among the 1st degree earthquake zones in Turkey. So, soil behaviour under dynamic conditions must be known in the Bornova graben area, which is heavily under construction.

In the study area, Quaternary alluvium, which is the products of alluvial fans (fan deposits), and slopewash are placed in the graben area. Considering the borehole data and geological cross-sections taken in N-S directions (Kıncal, 2005), the thickness of alluvium is estimated as 250-300 m. The sedimentary and volcanic rocks form the outcrops seen in the hills in the northern and southern parts of the graben area. The units in the study area are limestones, marl, claystones, tuffs, agglomerates and andesitic lavas from base to the top respectively. These rocks are overlain discordantly by the alluvial deposits in the study area.

The study area is slightly sloped and the elevation increases from west to east and reaches 35-40 meters in height. The area is inclined 5-10° from west (side of the gulf) to east (Figure 6).

Based on several seismic risk assessment studies the city has attracted the attention of national and international authorities, and was subjected to more detailed earthquake hazard analysis (Radius Project, 1999). Deterministic and

probabilistic seismic hazard studies revealed high risk for the city indicating significant possible life and economic losses. Despite these studies, however, it is not possible to state that due attention has been paid to the study of engineering aspects of earthquake hazard. For instance, not too many microzonation studies have been performed considering dynamic properties (Vp, Vs, υ, G (Bulk moduli)) of local soil and rock formations.

Seismic work has been conducted to measure Vs and Vp-seismic wave velocities in the Bornova (Izmir) graben area. Maps of seismic velocities such as Vs and Vp, were prepared using the field data with the help of Surfer 8.0 software, then digitised with MapInfo Professional 5.5 software to obtain a thematic layer. Seistronix Ras24 Remote Acquisition System was used to gather seismic signals in the field. Physical properties of soils existing in the Bornova Plain and determination of in-situ dynamic soil parameters are very important in engineering applications. Seismic measurements were taken from 29 stations in the Bornova Plain. Vp and Vs-wave velocities were determined using time-distance diagrams in every seismic profile.

Izmir is among the highest earthquake risk zones in Turkey. So, soil behaviour under dynamic conditions must be known in the Bornova graben (Izmir), which is heavily under construction. Seismic waves were created artificially in the study area to measure Vs and Vp records using Seistronix Ras24 Remote Acquisition System. Seismic refraction method was applied to prepare the existing soils model in the study area. Seismic risk maps which form the land-use map of the study area prepared using GIS analysis. MapInfo Professional 5.5 software were used during digital map preparation and vector analysis.

Vs and Vp-wave velocity maps were prepared in GIS with the help of seismic measurements in 29-stations in Bornova (Izmir) graben site. In addition, sonic wave velocity measurements were implemented in the laboratory using core samples which represent all rock units exposed in the study area. Vp-wave velocities are recorded during the tests.

1.1 Seismicity of Izmir and Its Surrounding Area

Izmir is the 3rd largest city in Turkey and it is one of the most densely populated cities in western Anatolia. This study aims to investigate the regional earthquakes of Izmir, located between latitudes 37.80-39.15 N and longitudes 26.31-28.02 E. From BC 17 to A.D 2003, the city of Izmir has experienced 170 seismic events, represented by magnitudes greater than 4.0.

Before assessing the earthquake potential and seismic risk evaluation of Izmir, it is vital to understand the recent tectonic regime of Western Anatolia, where the whole region is currently under tensional stresses. Utku and Ozyalin (2000) studied the relationships between the past earthquakes of Izmir and correlated these earthquakes with the tectonics of the region and finally calculated the seismic risk numbers, statistically (WEB_1, 2004). In this study, we aimed to show the distribution of the seismic events and investigate the possibility of future earthquakes by using earthquake risk assessment.

1.2 The Earthquake Potential of Izmir City

Figure 1 shows the distribution of earthquakes with magnitudes greater than 4.0. In the time interval between BC 17 and AD 2003, there are 3 earthquakes with magnitudes greater than 7.0. The data given here is not clear enough to make precise interpretations of the seismotectonics of the region, since some earthquakes are recorded by instruments and the rest of them are extracted from available historical data.

Through the time interval between 1900 and 2004, the earthquakes recorded by the seismograms are given in Figure 2. In 1994 there were 11 earthquakes, 10 earthquakes in 1966, 9 earthquakes in

1982 and 9 earthquakes in 1979. In Figure 2, the distribution of great earthquakes in respect of years is also shown. The largest earthquake was recorded in 1919 with Ms= 7.0.

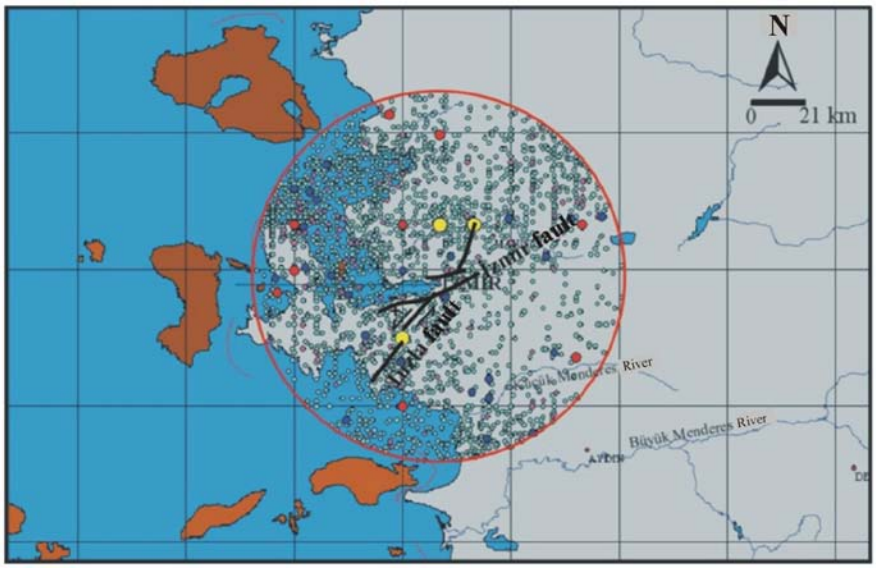

Figure 1. Seismotectonics of the Izmir region and the epicenter distribution of the earthquakes between BC 17 and AD 2003. (Modified from Utku and Ozyalin, 2000). Yellow dots; earthquakes Ms>7.0, Red dots; earthquakes 7.0>Ms>6.0, Blue dots; earthquakes >5.0

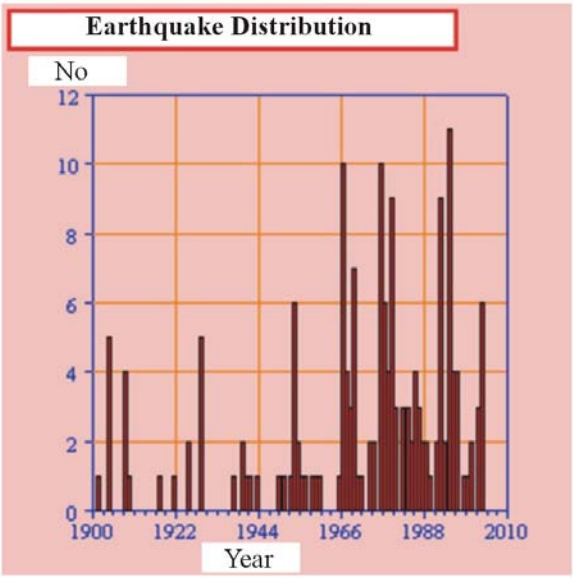

Figure 2. Earthquake distribution between 1900 and 2004 (Modified from Utku and Ozyalin, 2000)

2. THE EARTHQUAKE RISK ANALYSIS OF IZMIR AND ITS SURROUNDING AREA

In order to construct an earthquake risk analysis of the region, Utku and Ozyalin (2000) have used the Q 100 computer program. By using such computational method, it is aimed to define the earthquakes nearby of Izmir and investigate the destruction effect of these earthquakes.

2.1 Risk Analyse Methodology

Risk analysis is formed by some calculations about probability. A theoretical distribution is chosen which best fits with the data that risk analysis will be applied. The most effective distribution in this area is the Gumbel Extremity Values Distribution. Q100 is a

piece of software (Utku and Ozyalin, 2000) which uses the first type of this distribution function;

$$G(M) = \exp[-\alpha.\exp(\beta.M)],\ M>0 \ldots\ldots (1)\ \text{(Gumbel, 1958)}$$

α and β are regression coefficients. M : magnitude of an earthquake.

2.2 The Results of the Risk Analysis

In the first step of the analysis, the magnitude-amplitude relationship was examined annually. This relationship was obtained, as shown below, by using a kind of the historical rule about earthquakes which took place before in the study area.

$$\text{Log } N = 3.75-0.86M,\ r=0.99 \ldots..(2)$$

M, magnitude of an earthquake; N, the number of earthquakes whose magnitude is at least equal to "M"; R, correlation coefficient.

Using the Formula-2, conformity of the relationship is very good as seen in Figure 3. Using the Formula and the graphical relationship, it can be seen that the seismo-tectonic region has high seismic activity and also has high damage risk. Historical earthquakes which were above the magnitude of 7.0 are the indicators for this region.

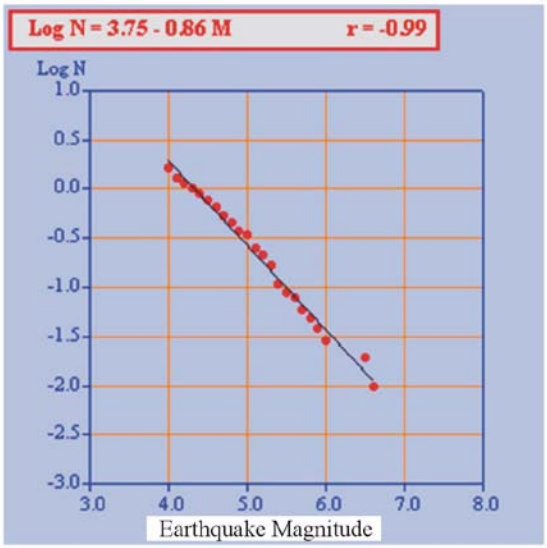

Figure 3. Relationship between M-earthquake magnitude and number of earthquakes (N) at least M-magnitude (edited from Utku and Ozyalin, 2000)

In the second step of the risk analysis, characteristic earthquake magnitudes are calculated for the seismo-tectonic field;

- Average highest magnitude is 4.5 annually
- Earthquake magnitude which is close to each other is 4.0 annually.
- The highest earthquake magnitude that will happen in 100-years period is : 6.9.

In the third step, exceeding probabilities of the probable earthquake magnitudes in the known economical periods (30, 50, 75 and 100 years) of the structures were calculated. In Figure 4, the probability of any earthquake with the magnitude from 4.0 occurring in the seismo-tectonic field is given related to economical periods of the structures mentioned above.

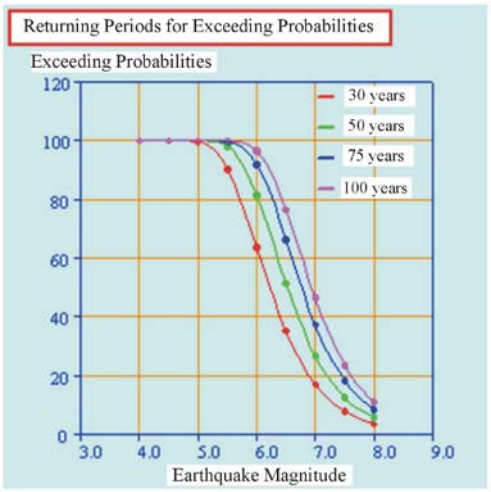

Figure 4. Exceeding probabilities of the earthquake magnitudes in the seismo-tectonic field depend on economical periods of the structures

In the fourth step, returning periods of the earthquakes which may ocur in the seismo-tectonic field were determined. Results of this study can be seen in Figure 5. According to Figure 5, a magnitude of 5.5 earthquake is experienced every 12 years.

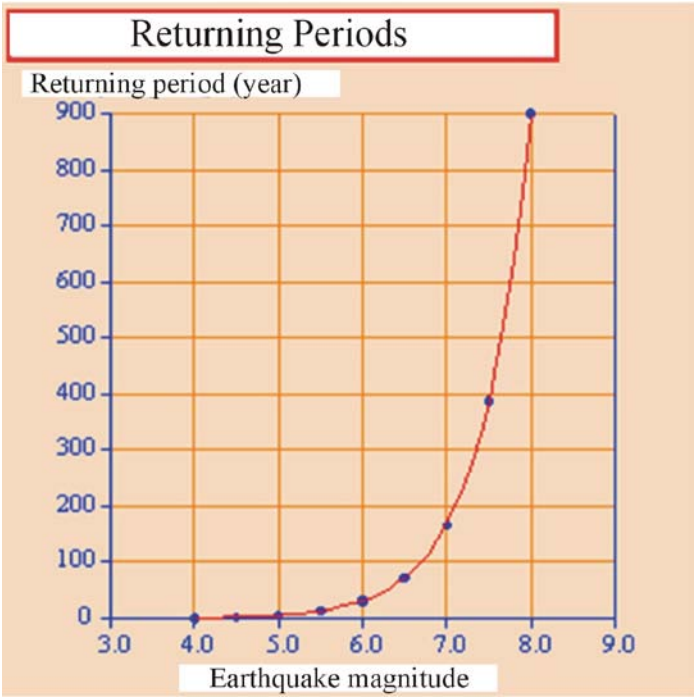

Figure 5. Changes of the earthquake magnitudes against the returning periods in the seismo-tectonic field

3. Vs AND Vp-WAVE VELOCITIES ZONING MAP LAYERS

Results were obtained using geophysical seismic wave field data (Figure 6). Vp and Vs-wave velocities were determined using time-distance diagrams in every seismic profile. On the other hand, changes in the Vp/Vs ratio is important. An increase in the Vp/Vs ratio is very important from the point of view of the increase of void ratio, porosity and/or crack ratio (Kıncal, 2005). Porosity defines the pore space, or voids, in a rock / a soil as a ratio of the total volume of rock/soil and voids (Craig, 1982). The general tendency is for moisture content and porosity to increase, and for density to

decrease and Vp/Vs ratio to increase. On the other hand, the changes in density and moisture content are a direct result of the increasing porosity, which itself is due to solution and to an increase in weathering of each soil grains and particles. The velocity of wave propagation is controlled by the elastic properties of earth materials. This holds for both compressional and shear waves.

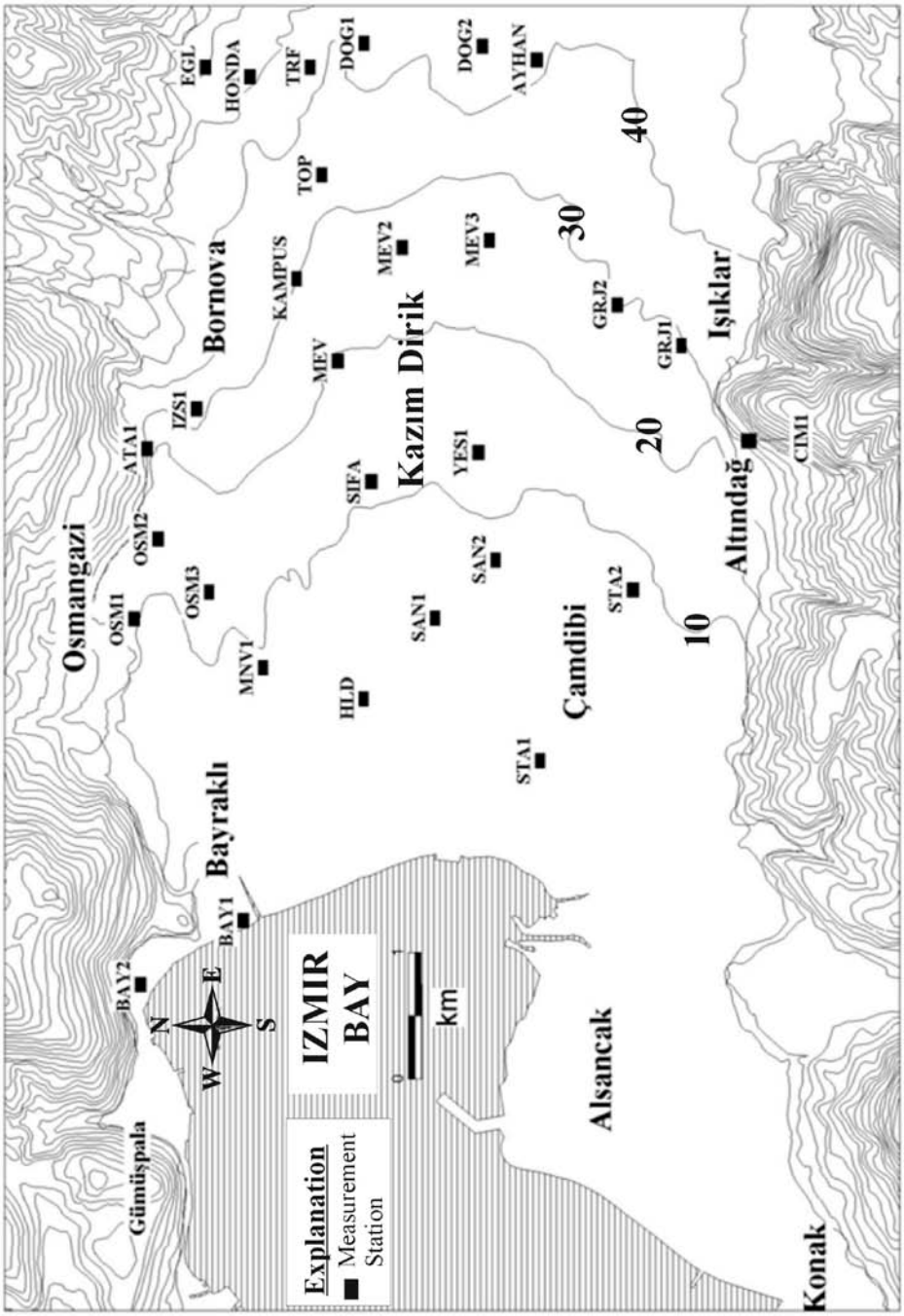

Figure 6. Location map of the seismic wave measurement stations

Vs-wave velocity zoning maps prepared for 3.0, 6.0 and 10.0 meter depths are presented in Figure 7 and Vp-wave velocity zoning maps prepared for 3.0, 6.0 and 10.0 meters depths are presented in Figure 8. Vs-wave velocity values are nearly the same values for 6.0 and 10.0 meter depths, so the maps prepared for them are nearly the same.

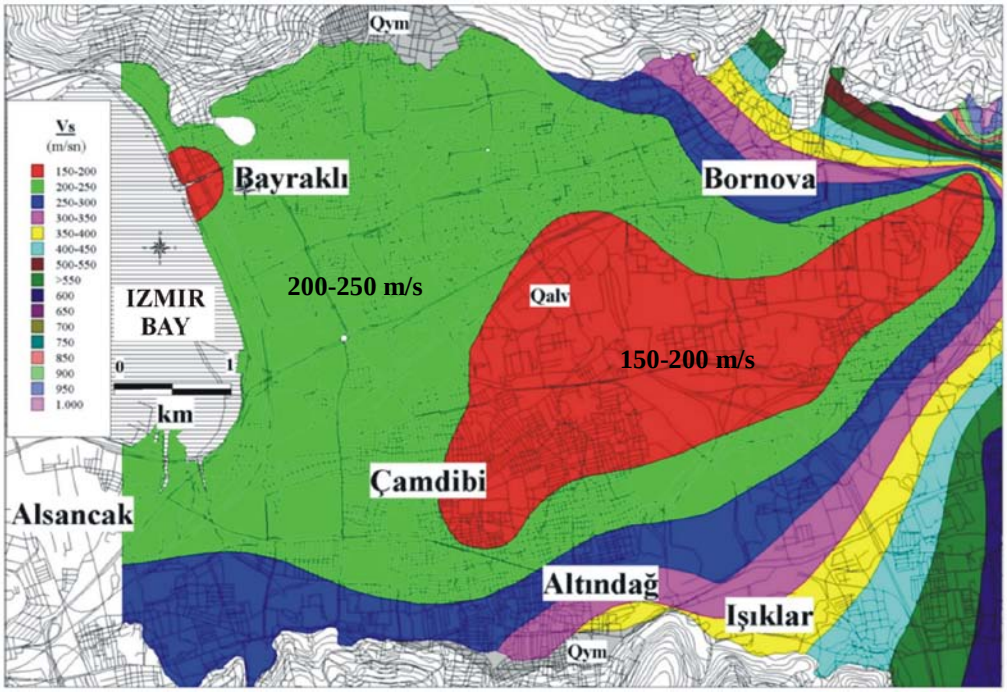

(3 m)

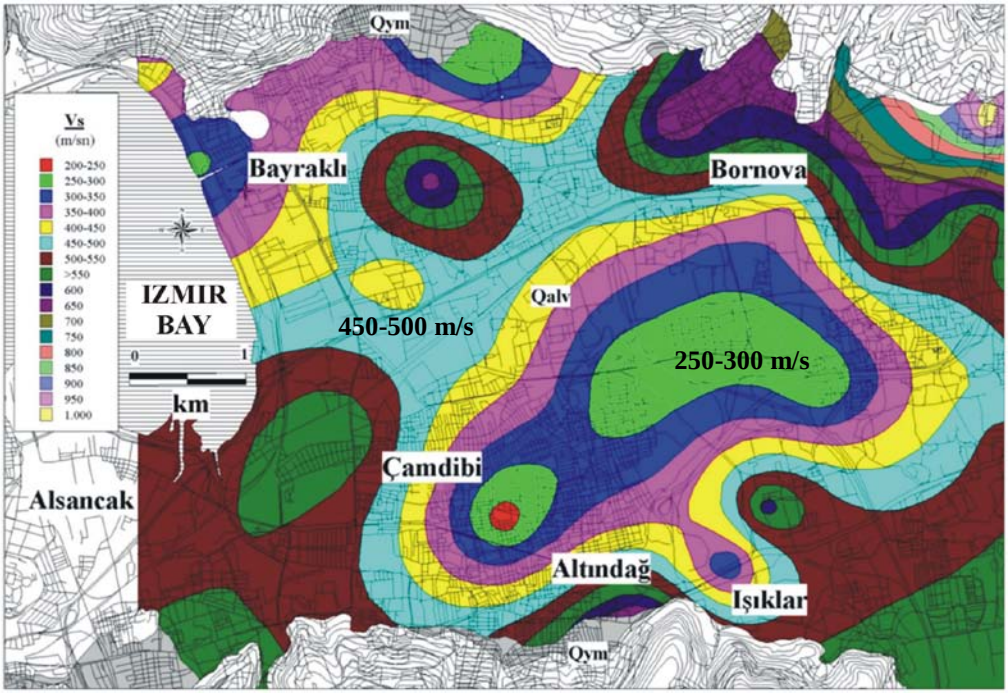

(6 and 10 meters)

Figure 7. S-wave velocity (Vs) maps.

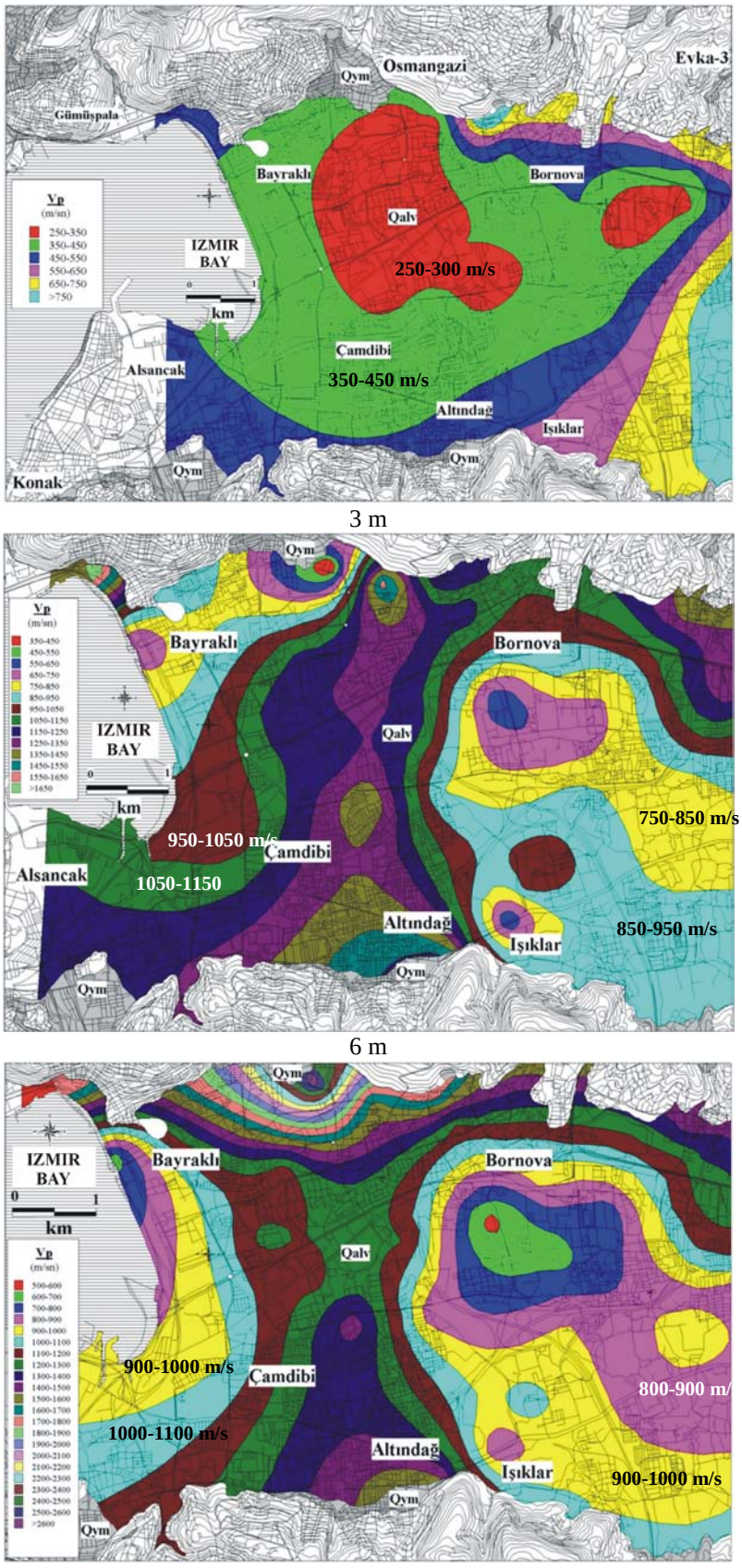

Figure 8. P-wave velocity (Vp) maps.

Zones in Karacaoglan, Mevlana and the ones between Manavkuyu and Izmir Bay area, have shear wave velocity values below 250 m/s.

3.1 Comparison of the Vp and Vs-wave velocity maps for 3.0 meter depth

All locations in the north of the Altındağ-Işıklar and in the south of the Kazım Dirik districts, about 4 km^2; the south of Bayraklı, about 1.0 km^2 and the districts of Yenişehir, Hilal and Kültür are covered with fills (Figure 6).

Sandy soils cover these areas as a ring. The area which is from the south of the Bayrakli and Manavkuyu to the Izmir Bay, is covered by the same type of sandy soil. Vs-wave velocity values are between 0-200 m/s in fill sites and 200-400 m/s in sandy soils. In the Vp-wave velocity map, wave velocity values are 200-400 m/s in all fill sites and sand soil sites. In the mentioned areas, Vs-wave velocities are below the 400 m/s (Figure 7 and 8). For this reason, loose fine sands and fill site-type soil properties are mostly conformed with the Vs and Vp-seismic wave velocity values.

3.2 Relations between Vp-Vs seismic wave velocities and soil types for 3-6 meter depths

Sites covered with fill materials in the soil-type map prepared for 3-6 meters are nearly half of the area of soil-type map prepared for 0-3 meters, 2.0 km^2. Bayraklı-Işıklar area, which contain above mentioned fills, is covered by mainly sandy soils that is 2.0 km wide and 6.5 km long. In addition, Hilal and Yenişehir Districts are covered by sandy soils as well. Clayey soils cover outside of these areas.

In the area covered by fills in Vs-wave velocity map and in the surrounding sandy soils, Vs-wave velocity values are between 200-400 m/**s** (Figure 7). The other field which has also low Vs-wave velocities has a strip shape from the Bayrakli-Osmangazi Districts to the Izmir Bay and it is about 3.0 km long (Figure 7). Moderately stiff sands are located in the area which has the Vs-wave velocities between 200-400 m/s.

In the outside of the sandy soils area which covers about ¾ of the total study area, Vs-wave velocity values are between 400-800 m/s (Figure 7).

Soil-type map conformed with Vs-wave velocity map prepared for 3-6 meters depth (Figure 7 and 8). The lowest Vp-wave velocities are measured in Osmangazi-Bayrakli and Kazim Dirik-Mevlana Districts which are about 2 km^2 (Figure 8). In the outside of this area Vp-wave velocities are more then 800 m/s. In the maps prepared for 3-6 meters, there is a Vp=2.Vs distribution. It means that good seismic signal measurements have been taken from the field.

3.3 Correlation of Vp and Vs-wave velocity maps prepared for 6.0-10.0 meter depths

Conformity between the soil maps of 0-3 meters and 3-6 meters is realized. Soil map for 6-10 meters is different then both other maps. When the depth of 0-10 meters from the ground are investigated, it is understood that sandy soils in the depth of 0-6 meters are dominant, whereas clayey soils are dominant for 6-10 meters.

No fill site appeared in the depths of 6-10 meters. Gravelly clays and/or clayey-soils are dominant in the depths of 3-6 meters in Alsancak and Yenişehir districsts but, loose sands are dominant in the depths of 6-10 meters in the same districts. Vp and Vs-wave velocity maps are mostly the same prepared for 3-6 meters and 6-10 meters (Figures 7, 8, and 9).

Generally, Vp have above 800 m/s wave velocity values in the depths of 6-10 meters. And also the relationship between Vp and Vs is $Vp \cong 2.Vs$.

4. CORRELATION BETWEEN THE CORRECTED STANDARD PENETRATION TEST AND VS-SHEAR WAVE VELOCITY

Vs-wave velocity values for the 3.0 meter depth are below 400 m/s in the west side areas of the Mevlana-Isiklar-Bornova

line. Vs-wave velocity map for the 10.0 meter depth is a little different then the 3.0 meter one. The areas have Vs-wave velocity values of below 400 m/s in Osmangazi-Bayrakli and Camdibi-Kazim Dirik-Mevlana and Karacaoglan districts.

SPT-N′$_{30}$ values are below 20 for 0-3 meter depths in the strip shape area which is 2.5 km wide and 3.0 km long in the east side of the Izmir Bay area. In the areas which have the SPT-N′$_{30}$ values below 20, Vs-wave velocity values are below 250 m/s (Figure 7).

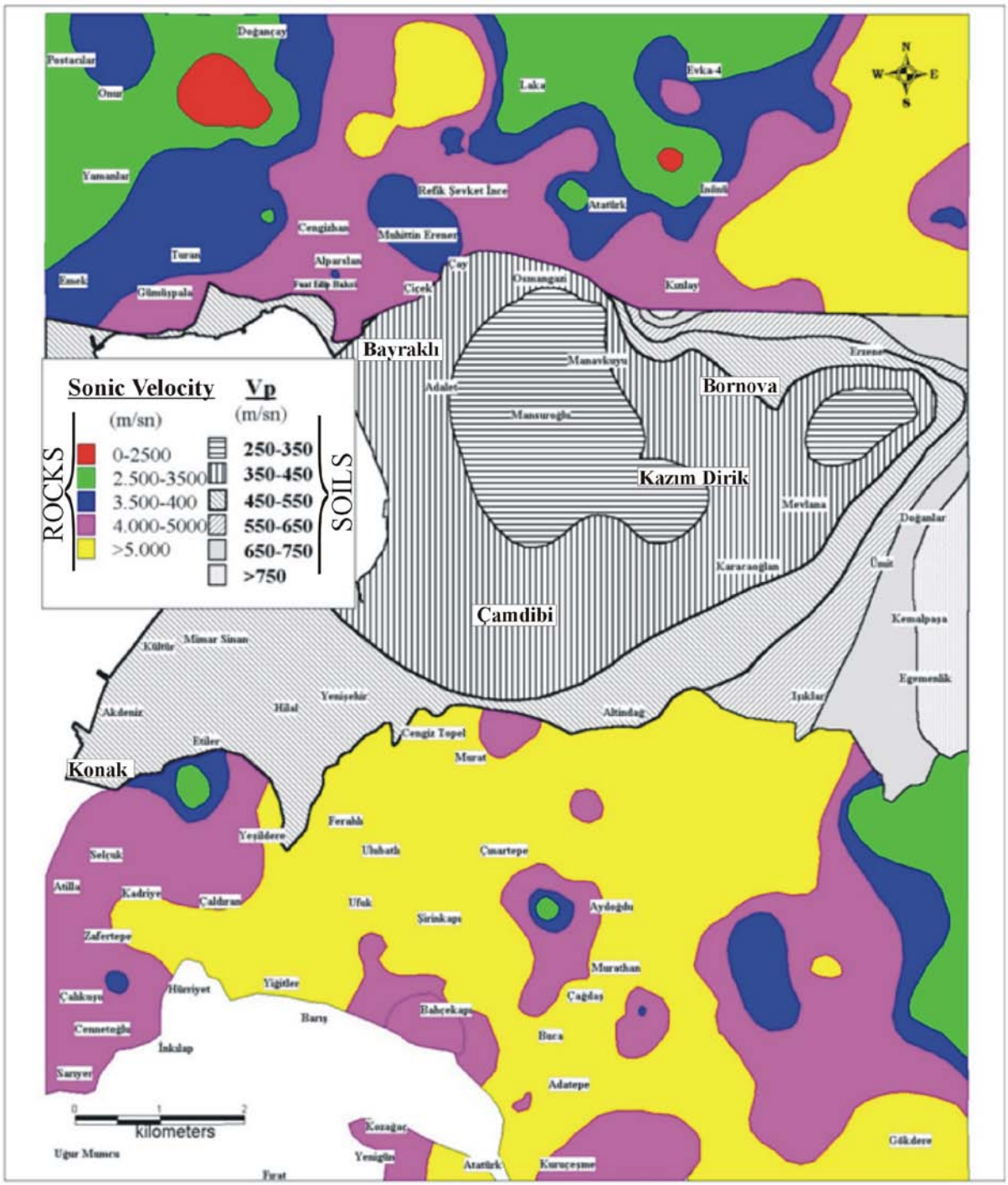

Figure 9. Correlation of Vp-wave velocity map (for soils) &Sonic wave velocity map (for rocks)

Earthquake activity of Izmir and its surroundings, together with earthquake risk analysis, was carried out and earthquake predictions were estimated. It was statistically concluded that Izmir is an earthquake-active area and must always

be prepared for earthquakes with the magnitude between 5.5 and 6.5. In addition, an earthquake with 6.9 magnitude seems likely to occur with 136 year intervals according to the statistical calculations.

With the correlation of Vp-wave velocity values obtained from both core samples from rocks and alluvium, Vp-wave velocity map was created by GIS, and this thematic map is presented in Figure 9.

5. RESULTS

Seismic risk of Izmir and its surroundings is very high. It has also high destruction potential. Risk analysis which was conducted for the seismo-tectonic field is a micro-risk analysis. As a result of all this, it is safe to say that Izmir and its surroundings have very active seismicity, and consequently, it also has a high earthquake risk potential. The fault system in the field is the best indicator of this risk potential. Izmir area must be ready to an earthquake with the magnitude between 5.5 to 6.5. The above limit is the magnitude of 6.9 in the seismo-tectonic field. This big an earthquake should be expected every 136 years, and has the probability of 60% according to the risk analysis.

It is determined that the Bornova graben area is located on an active earthquake zone, and two normal faults which extend parallel to each others, exist in the area. This area is mainly located on an alluvial-plain, and is limited by active graben faults.

The maps for the engineering purposes were prepared using the Vp and Vs seismic wave measurements for different depths in the alluvial fan deposites in the graben area. These depths are determined for 0-3 m, 3-6 m and 6-10 meters. On the basis of the information from the borehole records, SPT-blow counts and Vp, Vs seismic waves were employed in the assessment of liquefaction susceptibility and other engineering problems. Soil liquefaction phenomenon in the graben area is due to the presence of fine-grained sandy layers in the alluvial sequence, low seismic wave values (Vp<350 m/s, Vs<250-300 m/s), and high ground water level which become liquefied during the dynamics condition especially for 0-3 meter depths (Figure 10). Therefore, building and structural foundations have the risk of sinking into the liquified materials, causing tilting, differential settlement, and related damage.

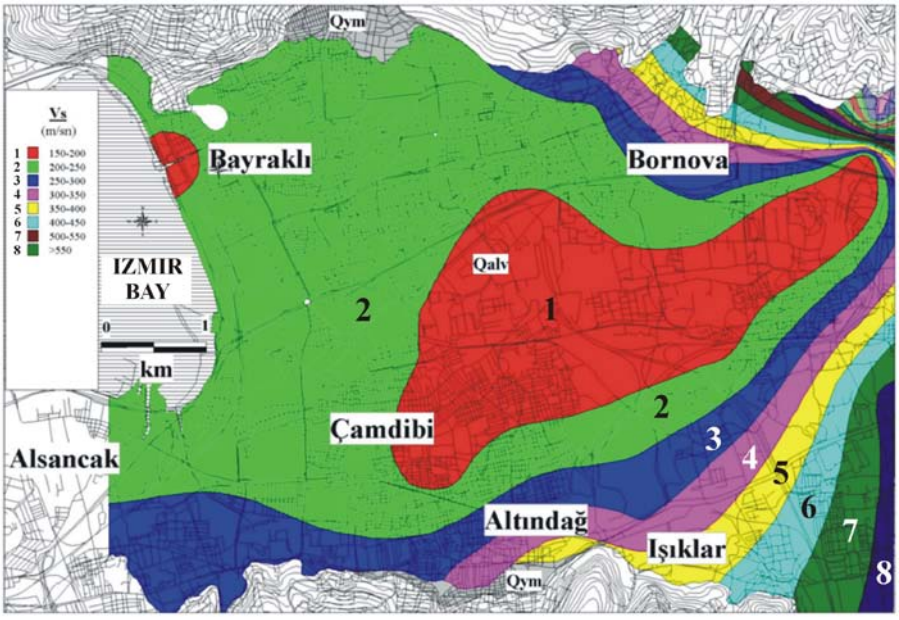

Figure 10. Risky zones numbered using S-wave velocity (Vs) measurements just for the 3.0 meter depth from the ground surface

6. REFERENCES

Craig, R.F. (1992). Soil Mechanics. Department of Civil Engineering University of Dundee, ELBS with Chapman & Hall. London, p. 427

Gumbel, E. J. (1958). Statistics of Extremes, *Columbia University Press,* USA.

Kıncal, C. (2005). Engineering Geological Evaluation of the Geological Units Exposed in Inner Bay Area (Izmir)'s Vicinity Using Geographical Information Systems and Remote Sensing, *PhD Thesis*, p. 342, Izmir (In Turkish). (unpublished)

MapInfo Corporation. (1995). *MapInfo Professional User's Guide*, MapInfo Corporation, Troy, NY.

Radius Project (1999). Earthquake Scenario and Master Plan of Izmir City, İzmir (In Turkish).

Surfer 8.0, Golden Software, Online manual.

Utku, M. ve Özyalin, Ş. (2000). Q100 software : Earthquake Risk analysis. National Geophysical Meeting *2000, Extended Abstracts*, pp. 46-47, 23-25 November 2000, Mining Research and Exploration Institute, Ankara.

WEB_1 (2004), Web Page of the Kandilli Earthquake Research and Observation Institute, http://www.koeri.boun.edu.tr, *Boğaziçi Univ.,* İstanbul, 02/12/2004.

CHARACTERIZATION OF FEED COAL, FLY ASH AND BOTTOM ASH FROM SEYITOMER POWER PLANT, KUTAHYA, TURKEY

Kırdım Ö.[1], Karayiğit A. İ.[1], Querol X.[2]

[1]Hacettepe University, Department of Geological Engineering, 06532, Beytepe-Ankara, Turkey, Tel:+90-312-2977798, Fax:+90-312-2992034, Email:aik@hacettepe.edu.tr

[2]Institute of Earth Sciences, "Jaume Almera", CSIC, C/ Lluis Sole i Sabaris s/n, 08028, Barcelona, Spain

Abstract: The Seyitomer lignite basin is one of the most important coal basins of Turkey, located in western Anatolia. Lignite production is performed by open-cast mining methods. Annual coal production is about 6.5 Mt and all production is being burned at Seyitomer power plant with 600 MW capacity. Workable coal seam is located to the bottom level of the lacustrine Seyitomer Formation of Miocene age. A total of 24 samples (feed coal, fly ash and bottom ash) were systematically collected once a week over an eight-week period from the boiler units. Proximate analyses of all samples were studied. X-ray powder diffraction (XRD) was used to determine major mineralogy of all samples. Accessory mineralogy/micron sized minerals was determined with Scannining Electron Microscopy-Energy Dispersive X-ray Analyzer (SEM-EDX) on selected samples. The feed coal samples have high moisture (av. 31.87%) on an as-received basis, very high ash yield (av. 46.35%), relatively high total sulfur content (av. 1.62%), low net calorific value (av. 2663 kcal/kg) on an air-dried basis. Mean values of ash yields of the fly ash and bottom ash samples on an air-dried basis are 96.57% and 85.89%, respectively. Major minerals in feed coal samples are clay minerals (smectite, illite, kaolinite, chlorite and pyrophyllite), quartz, feldspar, pyrite, siderite, opal-CT, and minor/trace amounts of calcite, aragonite, ankerite and gypsum. Accessory minerals in feed coal samples are FeNi-sulfur (pentlandite), rutile, apatite, barite and sphalerite. Amorphous matter (glass) forms the main constituent of the fly ash and bottom ash samples. Accessory minerals in fly ash and bottom ash samples are FeNi-sulfur (pentlandite), rutile, apatite, barite and mellilite. In addition, siderite and celsian in the bottom ash samples were also determined.

Key words: Mineralogy, XRD, SEM-EDX, Seyitomer, Turkey.

1. INTRODUCTION

Turkish coal reserves are estimated to be in the order of 8.3 Gt of lignite (low-rank coal) and 1.4 Gt of bituminous coal, and total annual lignite production was about 55.3 Mt in 2005. The total power generation capacity from coal in Turkey is about 8445 MW, 96% of which is generated from lignite and 4% from bituminous coals (http://www.enerji.gov.tr). The Seyitomer lignite basin, which is one of the most productive lignite basins in western Anatolia-Turkey, includes two lignite seams (lower and upper) in the Seyitomer Formation of Miocene age. The lower seam is mineable, and the upper has no economic value. This basin has a coal reserve of 172 Mt. The lower seam reaches 36.75 m thickness in some boreholes, but it averages 15 m in the basin (Celik and Karayigit, 2004). The lower seam is currently exploited in an open-cast mine with a dragline, excavator and truck system in the Seyitomer field and supply feed coal to the Seyitomer power plant with 600 MW capacity, which has four boiler units each with 150 MW. The power plant burns approximately 6.5 Mt lignite per year (http://www.tki.gov.tr). Figure 1 shows location of the Seyitomer lignite field and some other Turkish coal-fired power plants.

2. STRATIGRAPHY

Stratigraphy of the Seyitomer lignite field was summarized from Celik and Karayigit (2004). A generalized stratigraphic sequence of the Seyitomer lignite field and a simplified geological map are presented in Figures 2 and 3, respectively. The metamorphic and

ophiolitic rocks and less granites of Pre-Neogene age form the basement of the basin. The Miocene-Pliocene aged basin fill rests unconformably on the basement rocks. The first sedimentary system in the field begins with fluvial regime of the Egrioz Formation (Figure 2), which consists of conglomerate, trough cross-bedded conglomerate, sandstone, mudstone and thin coal seam.

Figure 1. Location of the Seyitömer lignite field and some other Turkish coal-fired power plants

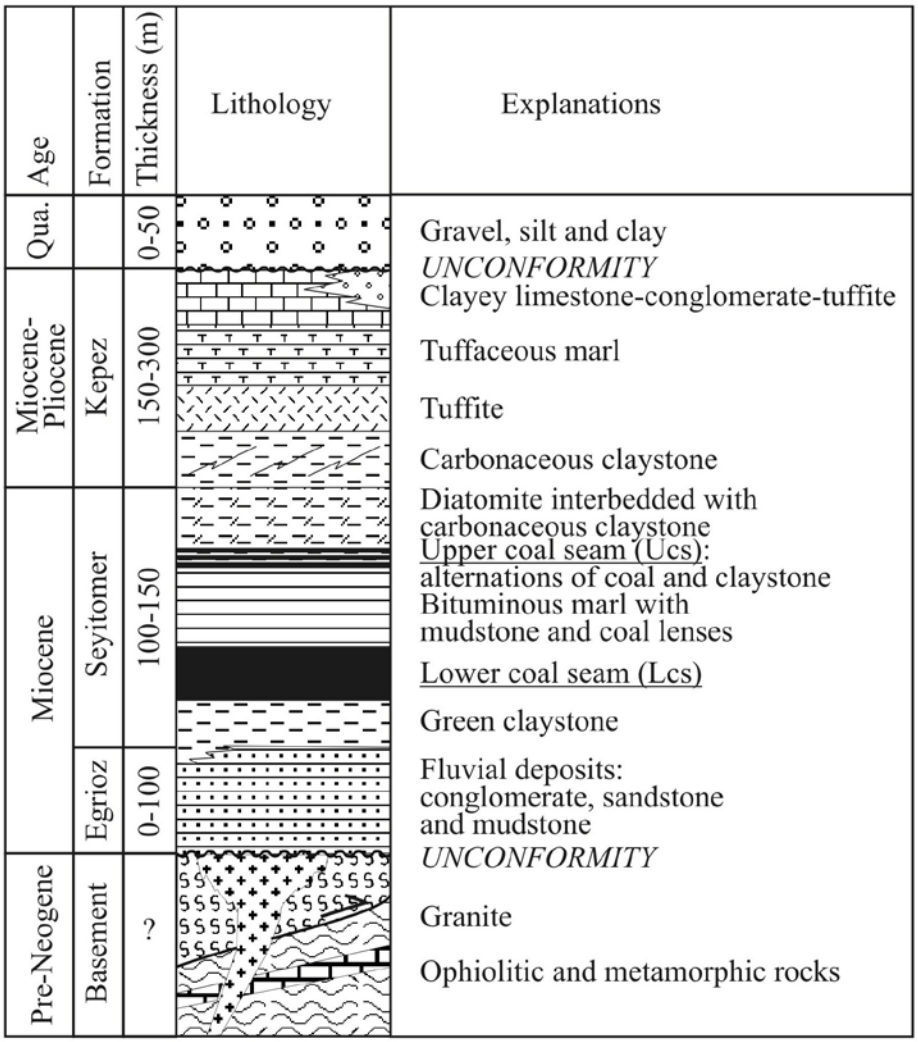

Figure 2. Generalized stratigraphic column section of the Seyitömer lignite field (Çelik and Karayiğit, 2004)

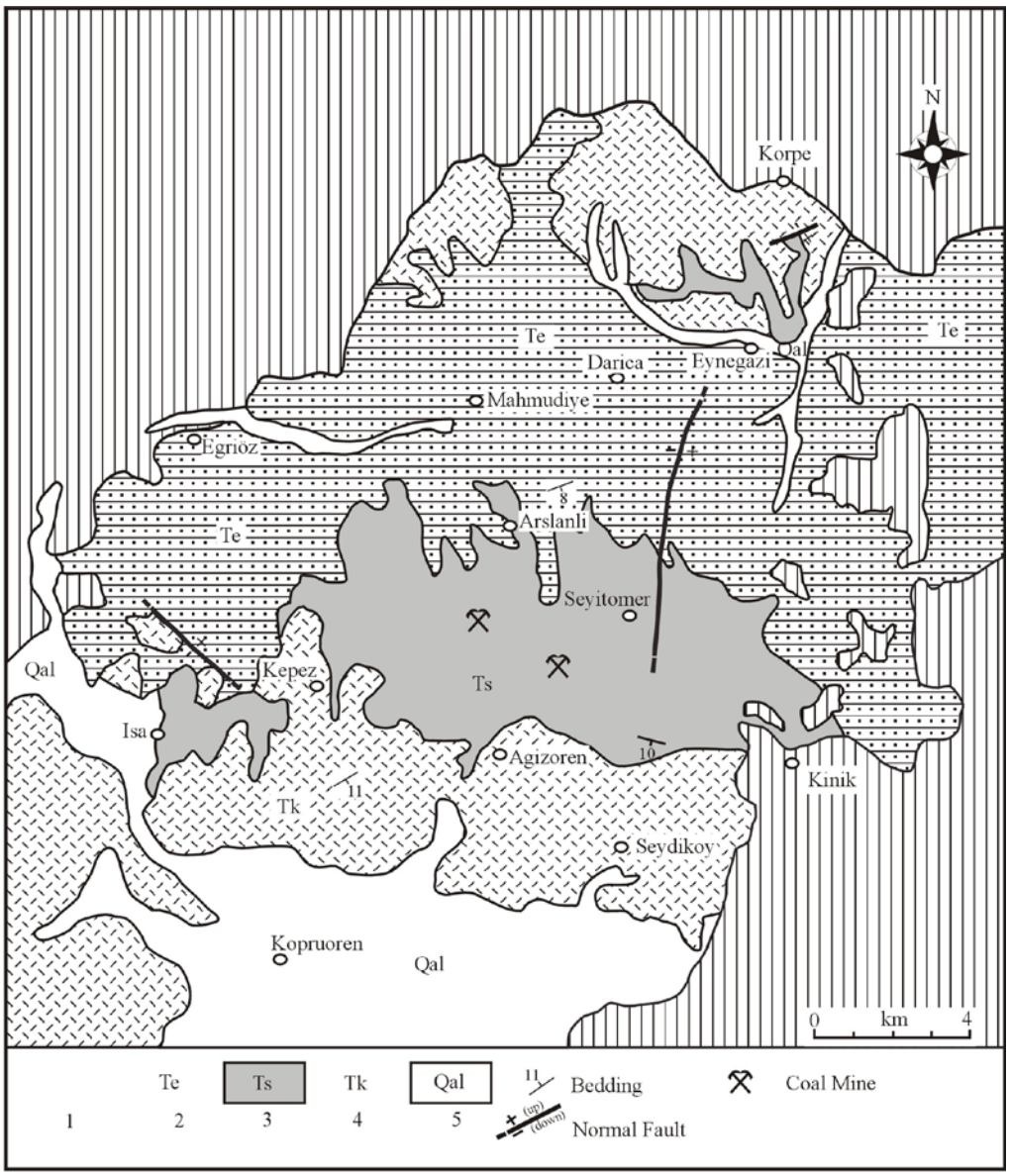

Figure 3. Simplified geological map of the Seyitömer lignite field. Abbreviations: 1) Pre-Neogene basement rocks, 2) Eğriöz F., 3) Coal-bearing Seyitömer F., 4) Kepez F., 5) Alluvium (Çelik and Karayiğit, 2004)

The coal-bearing Seyitomer Formation of Miocene age in the lignite field was conformably underlain by fluvial deposits of the Egrioz Formation and conformably overlain by the Kepez Formation of Miocene-Pliocene age. The coal-bearing Seyitomer Formation in lateral-vertical direction was developed in lacustrine facies, and is represented, from the base to the upwards, by green claystone, lower coal seam, bituminous marl with mudstone and sapropelic coal lenses, upper coal seam, diatomite interbedded with carbonaceous claystone and fossiliferous marl (Celik and Karayigit, 2004). The palynological studies suggest a Miocene age for the coal-bearing Seyitomer Formation, and coal formation was rich in subtropical forest taxa together with some riparian and hill-side forest elements (Yavuz, 2001).

The Kepez Formation that developed in a partly-fluvial lacustrine environment, from the base to the upwards, consists mainly of carbonaceous claystone, tuffite, tuffaceous marl, clayey limestone and conglomera-tuffite. The facies units of the Kepez Formation were interpreted as freshwater carbonates, volcanic fall

deposits, and river deposits (Çelik and Karayiğit, 2004).

3. MATERIAL AND METHODS

A total of 24 samples (feed coal, fly ash and bottom ash) weighing about 1-2 kg were systematically collected once a week over two months in 2004. The feed coal was sampled from the boiler mills and was crushed, blended, and split to obtain 0.5 kg sub-samples for analysis. Fly ash was sampled from the electrofilter sampling point. The ash was split for analysis. Bottom ash samples were obtained from the boiler doors under the boiler. These samples, before being delivered to laboratories in Ankara-Turkey, were dried in air at the power plant due to wet quenching in the combustion boiler. The samples in the study were analyzed using proximate analysis, X-ray powder and clay diffraction (XRD) and Scannining Electron Microscopy-Energy Dispersive X-ray Analyzer (SEM-EDX).

Standard proximate analyses were carried out in the Department of Geological Engineering at Hacettepe University-Ankara, Turkey, following American Society for Testing and Materials' (1991) recommended guidelines. Mineralogical characterization of the feed coal, fly ash and bottom ash powder was determined by X-ray diffraction spectrometer (XRD) with Cu Kα radiation and a 4-60 deg. 2θ range at CSIC-Barcelona, Spain and a 0-50 deg. 2θ range at Hacettepe University-Ankara. SEM-EDX analyses were especially used for accessory minerals. The analyses were performed on carbon coated samples in the Department of Geological Engineering at Hacettepe University, Ankara. Detailed information about analysis techniques was given by Kırdım (2006).

4. RESULTS AND DISCUSSION

4.1. Proximate analyses

The feed coal samples have high moisture (av. 31.87%) on an as-received basis, very high ash yield (av. 46.35%), high volatile matter (av. 29.91%), relatively high total sulfur content (av. 1.62%), low net calorific value (av. 2663 kcal/kg) on an air-dried basis. Fly ash samples have very low moisture (av. 0.26%), volatile matter (av. 3.15%); bottom ash samples include detectable contents of volatile matter (av. 6.75%) and net calorific value (av. 828 kcal/kg). Mean values of ash yields of the fly ash and bottom ash samples on an air-dried basis are 96.57% and 85.89%, respectively. Bottom ash samples have lower ash yields than the fly ashes which are related to much more formation of chars and unburned/relatively unburned coal particles in bottom ashes.

4.2. Mineralogy

X-ray powder diffraction traces of selected feed coal, fly ash and bottom ash samples are presented in Figure 4. Selected microphotographs of minerals in the feed coals, fly ashes and bottom ashes are presented in Figures 5, 6 and 7.

Major minerals in feed coal samples are clay minerals (smectite, illite, kaolinite, chlorite and pyrophyllite), quartz, feldspar, pyrite, siderite, opal-CT. Minor/trace amounts of calcite, aragonite, ankerite, gypsum were also identified in some feed coal samples. SEM-EDX studies indicated that quartz, feldspars, massive and framboidal pyrites are abundant in feed coal samples. Accessory minerals are FeNi-sulfur (pentlandite), rutile, apatite, barite and sphalerite. Traces of Ca and S in organic matter; K, Mg, Fe in kaolinites; Ti in chlorites; Ni in pyrites; Ca and Mn in siderites; Mn in ankerites; Sr in barites were determined with SEM-EDX.

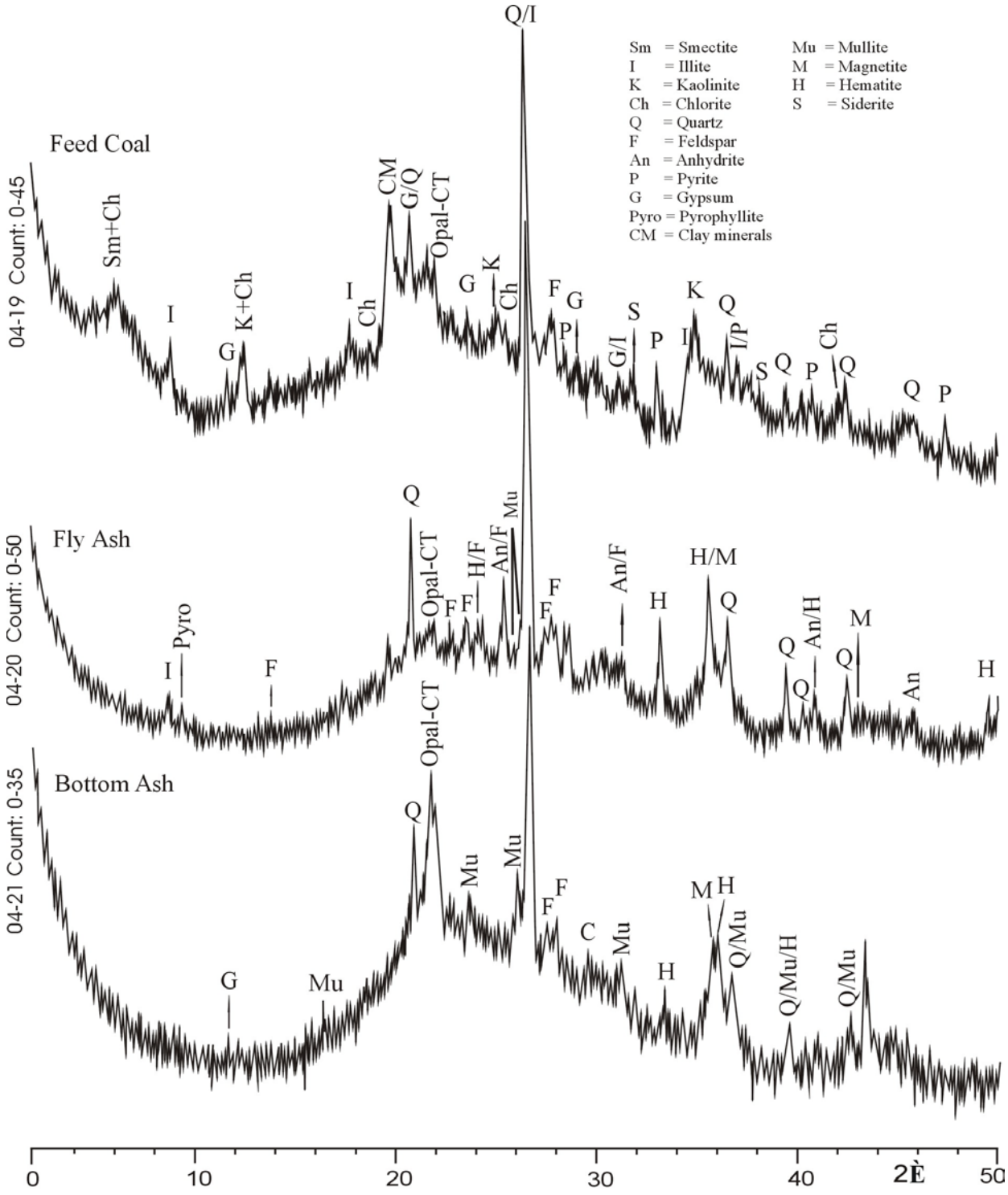

Figure 4. X-ray powder diffraction traces of selected feed coal, fly ash and bottom ash samples

The XRD peak intensities (count values) of the fly ash and bottom ash samples from Seyitomer are very low, suggesting that non-crystalline amorphous phases are the main constituents of fly ash and bottom ash samples. The common crystalline constituents in fly ash and bottom ash samples include the minerals quartz, feldspar, anhydrite, hematite and magnetite. Minor/trace amounts of portlandite, mullite, tridymite, opal-CT, gypsum and calcite were also identified in fly ash and bottom ash samples.

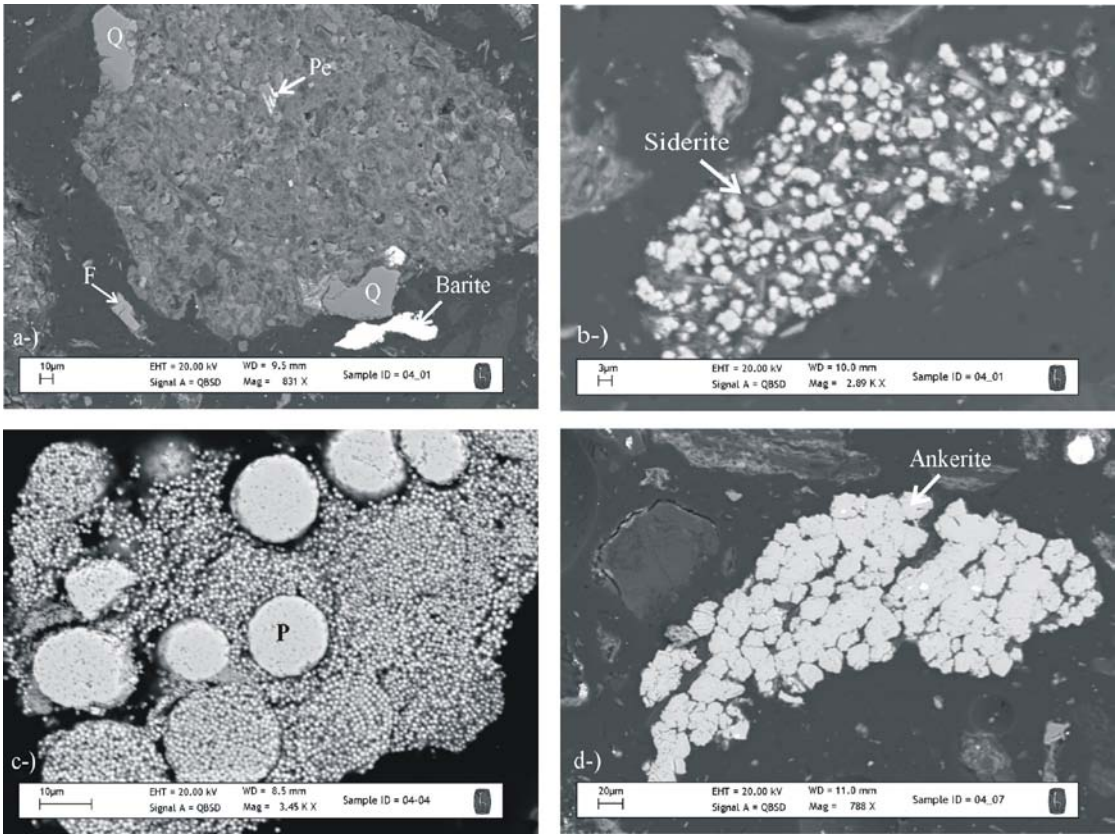

Figure 5. Selected SEM microphotographs of micron sized minerals in feed coals; a) Pe (Pentlandite), F (Feldspar - NaKAl-silicate), barite with Sr traces and Q (Quartz), b) Siderite with Ca and Mn traces, c) P (Framboidal pyrite), d) Ankerite

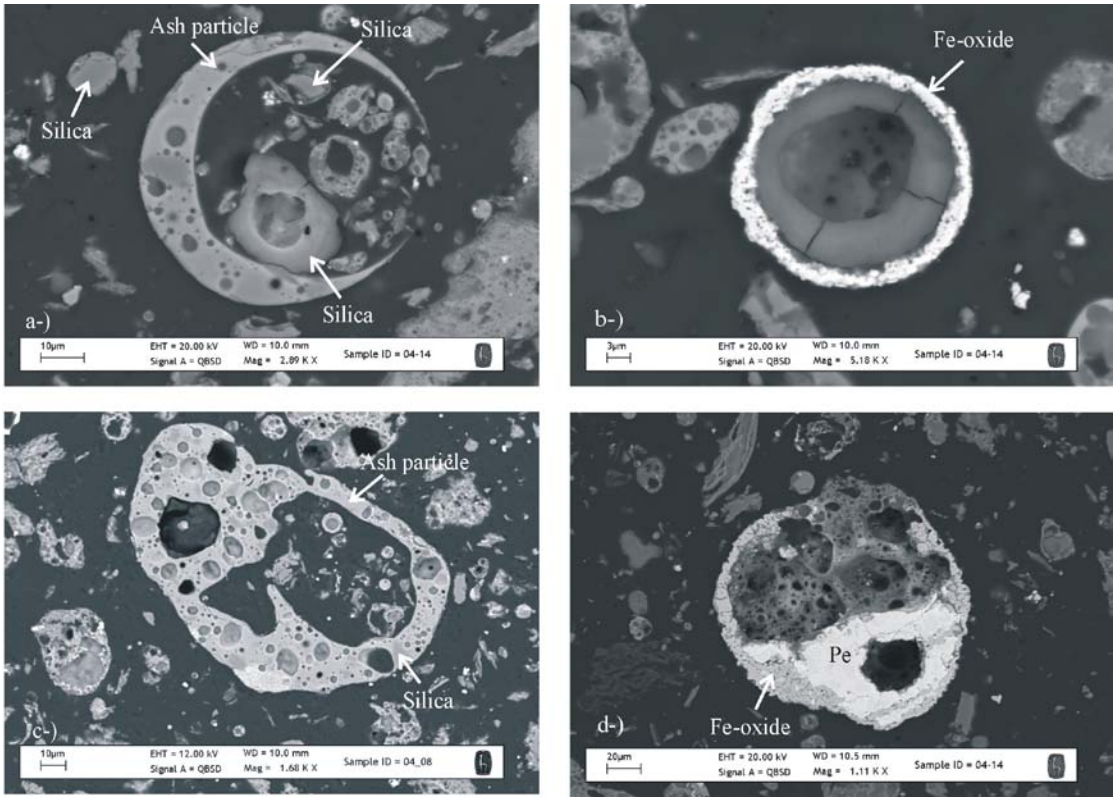

Figure 6. Selected SEM microphotographs of micron sized minerals in fly ash samples; a) Ash particle with NaFeCaKMgAl-silicate composition and silica, b) Fe-oxide, c) Ash particle with FeMgAl-silicate composition and Q (Quartz), d) Pe (Pentlandite) and Fe-oxide

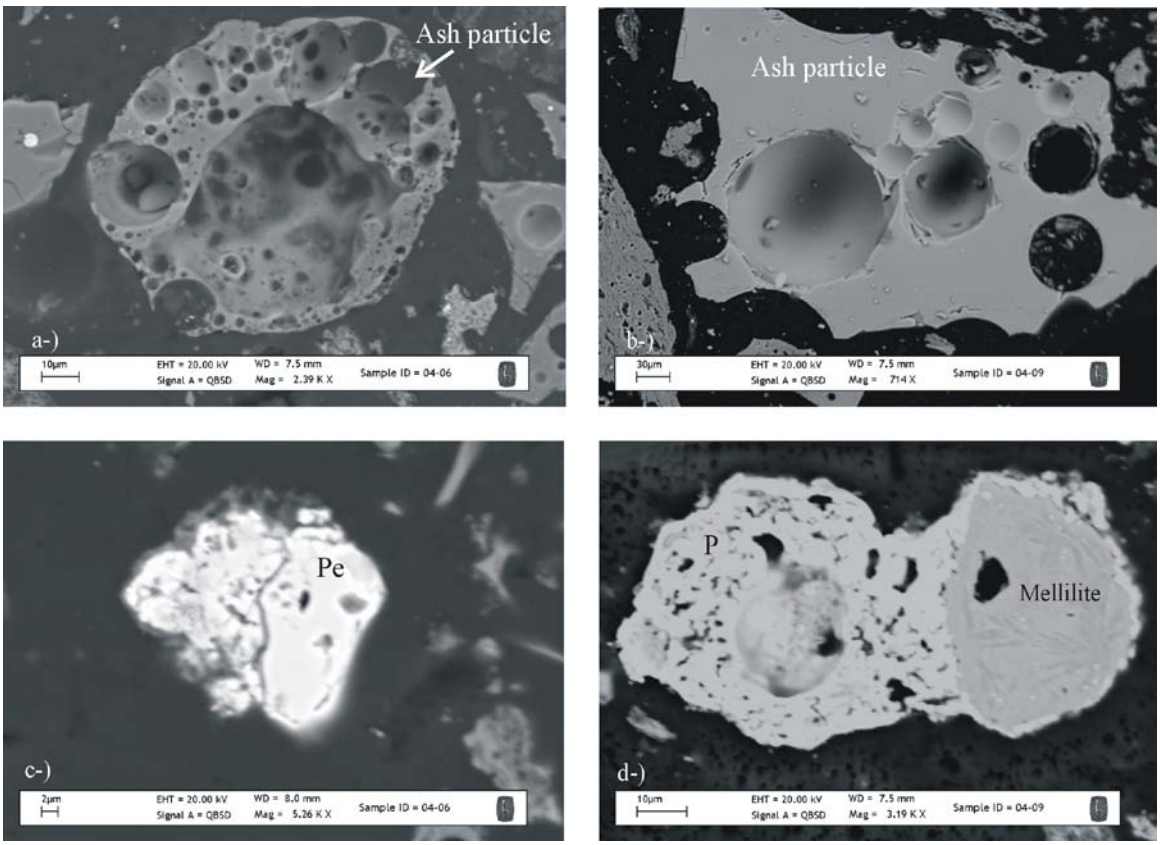

Figure 7. Selected SEM microphotographs of micron sized minerals in bottom ash samples; a) Ash particle with KFeCaMgAl-silicate composition, b) Ash particle with KFeMgCaAl-silicate composition, c) Pe (Pentlandite), d) Mellilite and P (Pyrite)

However, quartz, feldspar and anhydrite contents are relatively higher in the fly ash than in the bottom ash samples. Accessory minerals in fly ash and bottom ash samples are FeNi-sulfur (pentlandite), rutile, apatite, barite, mellilite. In addition, siderite and celsian in the bottom ash samples were also determined. SEM-EDX studies indicate that silica, feldspar and Fe-oxide are abundant in fly ash and bottom ash samples. Unburned carbons (char) in fly ash and bottom ash include Ca and S traces. Amorphous (glass) matter in fly ash and bottom ash is mainly composed of KCaFeMgAl-silicate. Mullites in fly ash samples include minor/trace amounts of Mg, K and Fe.

The XRD peak intensities (count values) of the fly ash and bottom ash samples from Seyitomer are very low, suggesting that non-crystalline amorphous phases are the main constituents of fly ash and bottom ash samples. The common crystalline constituents in fly ash and bottom ash samples include the minerals quartz, feldspar, anhydrite, hematite and magnetite. Minor/trace amounts of portlandite, mullite, tridymite, opal-CT, gypsum and calcite were also identified in fly ash and bottom ash samples. However, quartz, feldspar and anhydrite contents are relatively higher in the fly ash than in the bottom ash samples. Accessory minerals in fly ash and bottom ash samples are FeNi-sulfur (pentlandite), rutile, apatite, barite, mellilite. In addition, siderite and celsian in the bottom ash samples were also determined. SEM-EDX studies indicate that silica, feldspar and Fe-oxide are abundant in fly ash and bottom ash samples. Unburned carbons (char) in fly ash and bottom ash include Ca and S traces. Amorphous (glass) matter in fly ash and bottom ash is mainly composed of KCaFeMgAl-silicate. Mullites in fly ash samples include minor/trace amounts of Mg, K and Fe.

5. ACKNOWLEDGEMENTS

This work was supported by TUBITAK under a project study (105Y042). The authors gratefully acknowledge TUBITAK for the project support, EUAS and Seyitomer power plant staff for the sampling.

6. REFERENCES

American Society for Testing and Materials, 1991. *Annual book of ASTM standards*. Section 5: Petroleum Products, Lubricants, and Fossil Fuels. 5.05: Gaseous Fuels: Coal and Coke.

Celik, Y. and Karayigit, A.I., 2004. Chemical properties and petrographic composition of the lacustrine Seyitomer lignites (Miocene), Kutahya, Turkey. *Energy Sources*, 26, 339-352.

http://www.enerji.gov.tr
http://www.tki.gov.tr

Kirdim, O., 2006. Mineralogy and petrography of feed coals and combustion residues from the Seyitomer (Kutahya-Turkiye) thermal power plant. *Yuksek Lisans Tezi, Hacettepe Univ., Fen Bilimleri Enst.*, Ankara, 149s.

Yavuz, N., 2001. Palynological investigation of the Seyitomer coals. *Fourth International Turkish Geology Symposium*, Adana. Abstracts, pp 253.

THE MINERALOGY AND GEOCHEMISTRY OF A BENTONITE DEPOSIT BETWEEN YENİKÖY AND AKÇAKERTİL (BİGADİÇ)

Kocabaş C. and Çoban F.

Balıkesir University, Faculty of Engineering - Architecture, Department of Geological Engineering, 10145 Çağış, Balıkesir, Turkey

cumhurkocabas@yahoo.com, fcoban@balikesir.edu.tr

Abstract: A bentonite deposit in the Neogene sedimentary sequence of Bigadiç lacustrine basin was studied with X-ray diffractometer (XRD) and scanning electron microscope (SEM) for determining the mineralogical variations in the alteration zone. Major, trace and rare earth element contents (REE) were analyzed to interprete the element mobilization. Yeniköy bentonite deposit is characterized by two different zones. The first is grey bentonite in the lower part and the second is white bentonite in the upper part of the deposit. Rhyolitic character of the bentonite was determined. The deposit consists mainly of montmorillonite, feldspar, quartz, calcite, dolomite and illite. The removal of alkalis control the formation of smectite. The behavior of Si depends on the chemistry of the parent rock. In the alteration profile a net gain of Al, Fe, Mg, Ca, Ti was determined. Enrichment in Ga, Nb, Sr, Zr and Sc and depletion in Rb and Cs were determined. Total rare earth element (REE) content was enriched during alteration. Yeniköy bentonite formed from in-situ alteration of volcanic glass, and diagenetic factors affected the mineralization during alteration process.

Key words: Yeniköy, lacustrine, bentonite, glass, in-situ.

1. INTRODUCTION

Bentonite is a formation composed essentially of a clay like mineral formed by the devitrification of a glassy igneous material, usually a tuff or volcanic ash (Grim and Güven, 1978). Bentonite is formed mainly in situ alteration of volcanic glass in an aqueous environment and hydrothermal alteration (including deuteric alteration) of igneous rocks. The geology and mineralogy of Bigadiç lacustrine basin was investigated by Helvacı (1995). Yeniköy bentonites was formed in the lower tuff unit. Field observations and analyses indicate that conversion of volcanic glass into smectite involves mobilization of elements from altered glass to bentonite. The loss of alkalis and a high Mg-activity promote formation of smectite. Leaching of Si from asidic rock also leads to bentonite. The study examines smectites derived from acidic rocks and it aims to: a) establishing the mineralogy and geochemical features of bentonite; b) determininig the mode of origin of the deposit; c) invastigating the effect of the nature of the parent rock to alteration.

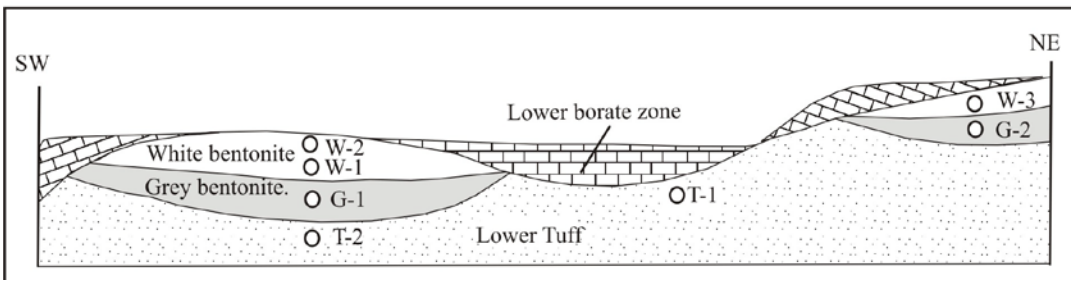

Figure 1. Schematic cross-section of sampling

2. METHODS OF THE STUDY

Representative samples were collected 25-30 cm beneath the surface to minimize weathering and contamination. Shematic cross-section of sampling sites is given in Figure 1. Whole- rock mineralogy studied by using Philips 1140 model X-ray powder diffractometer with Ni-filtered

CuKα radiation and scanning speed was 1º 2θ/ min. Chemical analyses were determined in the Acme Analytical Laboratories (Canada). Major oxides and several minor elements are reported on a 0.2 g sample analysed by ICP-emission spectrometry following a $LiBO_2$ fusion and dilute nitric digestion. Loss on ignition (LOI) is by weight difference after ignition at 1000 º C. Scanning electron microscope studies were conducted on 50-300 °A thin carbon film-coated sample chip, using a LEO-VP 1431 model electron microscope in the Laboratories of Afyon Kocatepe University.

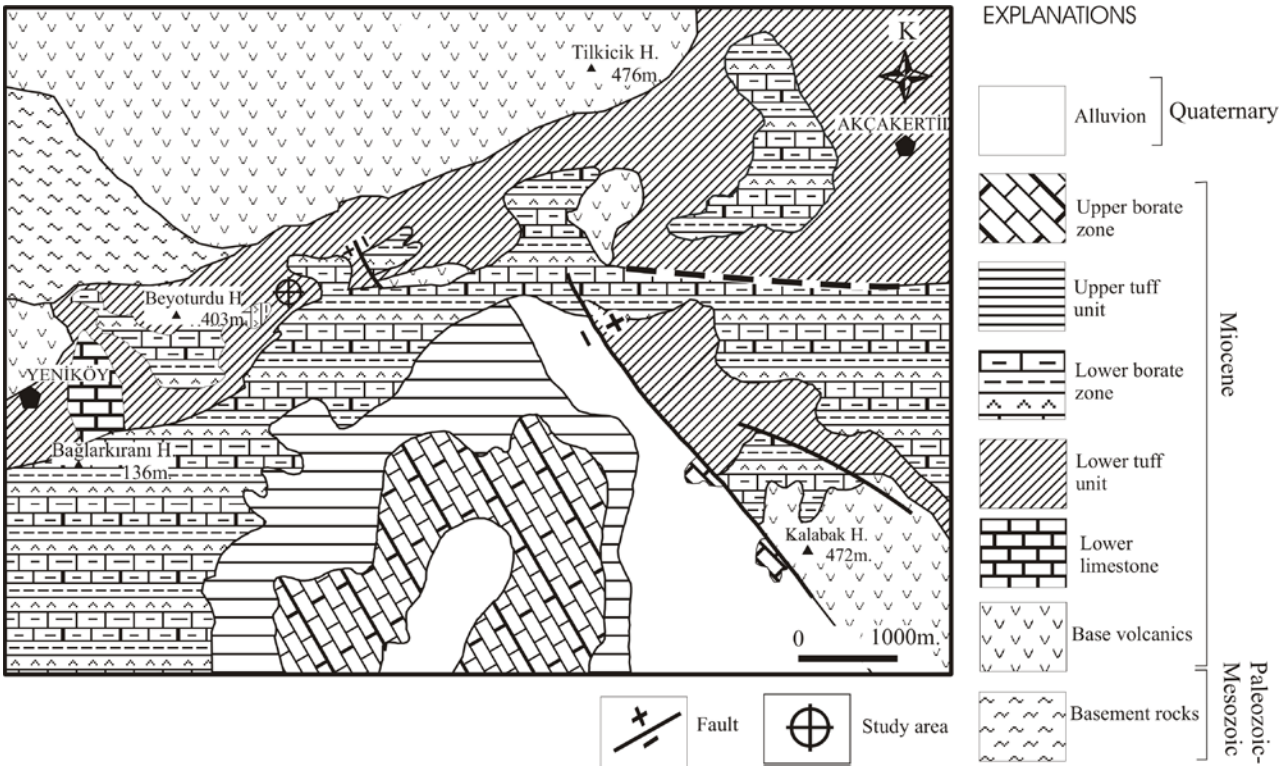

Figure 2. Geological map of the study area (After Helvacı, 1995)

3. GEOLOGICAL SETTING

In the Bigadiç volcano-sedimentary basin, the Miocene rocks overlie the Paleozoic- Mesozoic basement complex (Helvacı, 1995). Volcano-sedimentary basin includes the following units from bottom to the top; basement rocks, base volcanics, lower limestone, lower tuff, lower borate zone, upper tuff, upper borate zone and alluvion respectively (Figure 2). The basement rocks involve Paleozoic metamorphic rocks and Mesozoic ophiolite complex. The base volcanic unit rests unconformably on basement rocks and contains andesite, trachyte, their tuffs and aglomerates. The base volcanics are overlain uncomformably by lower limestone. Lower limestone is composed of marl, limestone, dolomitic limestone and tuff . The lower tuff unit, including bentonite formation overlies the lower limestone comformably. Lower tuff has glassy texture. It has occurred by volcanic activity throwing the fine grained dust to the lacustrine. Lower borate zone overlies lower tuffs comformably and includes limestone, claystone, marl and tuff intercalations. Borate minerals occur as nodules, thin beds and lenses in this unit. They are composed of colemanite, ulexite, howlite, propertite and hydroboracite (Helvacı, 1995). Lower borate zone is followed by upper tuff including high zeolite content, especially clinoptilolite (Esenli, 1990). It has a comformable and graditional contact with the lower borate-bearing unit. Upper tuff is in the form of coarse grained glassy ash at the bottom

and fine grained glassy dust at the top of the sequence. The upper tuff unit has been covered by upper borate zone comformably. Upper borate-bearing unit is composed of alternating beds of limestone, claystone, marl and tuff. This unit is composed of borate beds at intermediate levels (Helvacı 1995). Alluvion covers all units as the youngest in the study area.

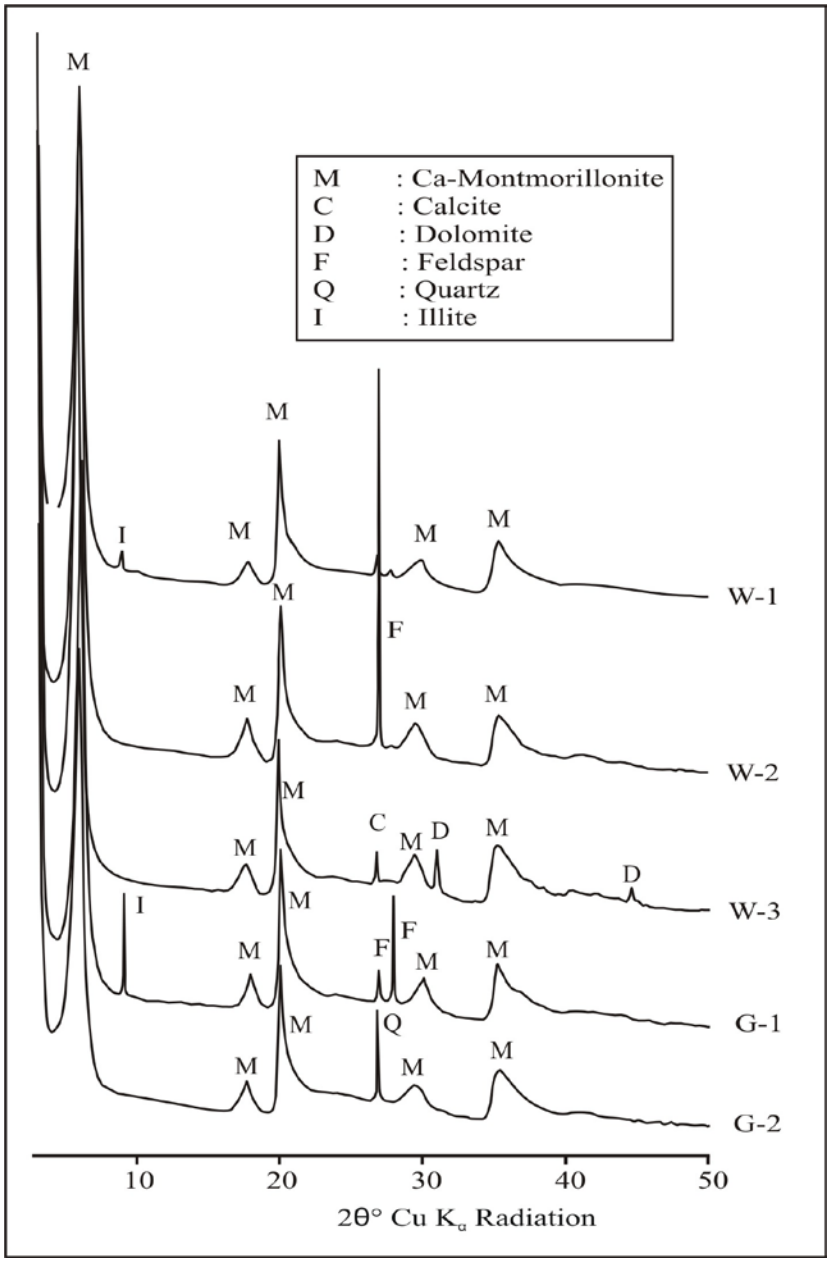

Figure 3. X-ray diffraction (XRD) of bentonites (G: grey bentonite, W :white bentonite)

4. RESULTS AND DISCUSSION

4.1. Mineralogy

Yeniköy bentonite deposit is characterized by two different zones. The first is grey bentonite in the lower part of the deposit and the second is white bentonite in the upper part of the deposit. Five samples are studied with X-ray diffraction (XRD). The first zone consists of montmorillonite, quartz, feldspar, illite. The second zone consists of montmorillonite, calcite, dolomite, feldspar, illite. The XRD investigation has shown that bentonite's main mineral is Ca-montmorillonite. The other minerals accompanying montmorillonite are quartz, feldspar, illite, calcite and dolomite (Figure 3). d_{001} values of bentonites range

from 14.7 to 15.2, indicating the presence of Ca- smectites (Grim, 1962).

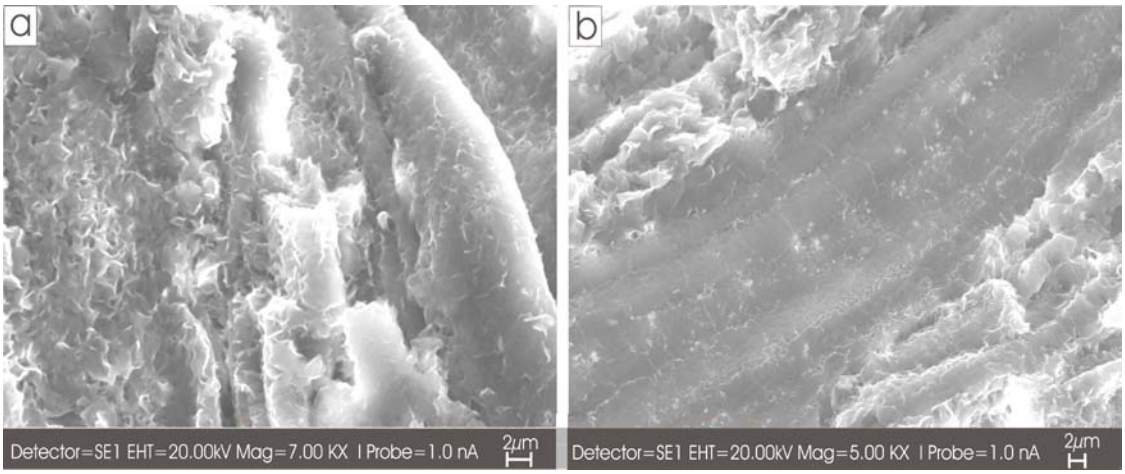

Figure 4. Scanning electron micrograph (SEM) of bentonites a) thin film bands over volcanic glass b) Amorphous silicious material formed as veins

Optical microscope investigation reveals that quartz and feldspar are residuel minerals in bentonite. Illite, calcite and dolomite may have occured by diagenetic processes.

Based on SEM observations, the montmorillonite, the main constituent mineral of bentonite, was grown as thin film bands over volcanic glass and it has a sheet like structure (Figure 4a). The curled edges indicate bentonite texture. An amourphous silicious material can be seen in the bentonite as a vein shape (Figure 4b).

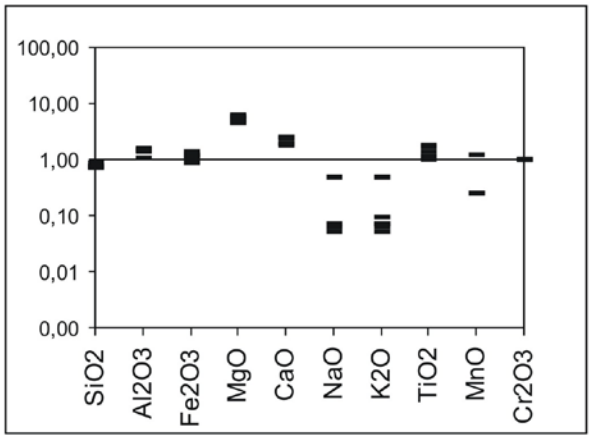

Figure 5. Normalization diagram showing mobility of major elements during the conversion to bentonite

Table 1. Major element content of bentonites and tuffs (T-1: Tuff, T-2: less altered tuff, G: Grey bentonite, W: White bentonite)

	T-1	T-2	G-1	G-2	W-1	W-2	W-3
MAJOR ELEMENTS (%)							
SiO_2	68.58	58.60	52.58	50.88	51.81	52.66	50.50
AL_2O_3	12.26	13.25	18.33	18.09	18.87	17.04	17.68
FE_2O_3	1.17	1.40	1.62	1.02	1.34	1.32	1.39
MGO	0.79	3.64	3.96	4.67	3.51	4.36	4.94
CAO	0.87	2.21	1.63	2.00	1.53	1.72	2.13
NA_2O	1.39	0.69	0.10	0.07	0.09	0.10	0.09
K_2O	5.53	2.68	0.53	0.40	0.40	0.35	0.29
TiO_2	0.07	0.07	0.13	0.08	0.12	0.10	0.08
MNO	0.04	0.05	0.01	0.01	0.01	0.01	0.01
CR_2O_3	0.001	0.001	0.001	0.001	0.001	0.001	0.001
LOI	9.1	17.3	21.0	22.7	22.2	22.2	22.3
TOTAL	99.82	99.91	99.92	99.94	99.90	99.88	99.43

4.2. Chemistry

The major element contents of bentonites and tuffs are given in Table 1. Alteration into bentonite in Yeniköy involves removal of alkalis and enrichment of Al, Fe, Mg, Ca and Ti. Si is depleted from fresh rock to the bentonite formation. Normalization diagram made

over fresh rock (T-1) shows mobility of major elements during conversion to bentonite of an acidic rock (Figure 5). Al remained stable in higher pH conditions and enriched in-situ during alteration.

In the alteration profiles depletion of Cs, Rb, U, Zr and enrichment of Sr, Sc, Cr and Co are sensitive indicators of conversion of glassy material into clay (Zielinski, 1982). It was determined that Cs and Rb were leached with Na and K, and Sr and Sc are enriched in Yeniköy bentonites. If an element is lost when plotted in a diagram with an immobile element, the regression line on the ordinate will be positive. If it is gained the regression line on the ordinate will be negative (Chrisditis,1998). Hence, Na, K, Si, Rb and Cs are lost (Figure 6a-6e). When two immobile elements plotted versus one another, they display a straight line passing from the origin (Figure 6f). Such behavior indicates that Al and Ga are immobile elements and enriched in-situ. The plotted point that connect the fresh rock (T-1) with the origin is a measure of the mobilization of Mg and Si and their concentration varying over Al (Figure 7). The degree of enrichment in Mg versus Al (Figure 7a), and the degree of depletion in Si versus Al (Figure 7b) is determined from fresh rock to bentonite. On the other hand, Rb may substitute for K, Ga may substitute for Al. While Rb is leached, Ga is concenrated in a residue.

Table 2. Trace element and REE contents of bentonites and tuffs (T-1: Tuff, T-2: less altered tuff, G: Grey bentonite, W: White bentonite)

	T-1	T-2	G-1	G-2	W-1	W-2	W-3
TRACE ELEMENTS (PPM)							
BA	228.3	201.6	206.3	353.2	487.3	61.4	4041.1
GA	14.8	16.3	21.5	21.9	21.3	19.2	20.8
NB	17.7	18.8	21.6	27.7	24.8	24.2	25.1
RB	641.2	227.9	15.4	14.8	12.6	9.6	8.9
SR	83.7	113.4	155.9	101.1	134.8	132.7	149.7
ZR	96.0	98.9	188.5	128.9	161.0	131.7	118.2
Y	30.5	31.2	32.8	26.1	31.2	35.7	41.4
SC	3	3	4	4	4	4	4
CS	80.1	16.7	6.4	5.0	5.6	4.4	2.3
REE (PPM)							
LA	28.9	24.6	52.2	28.7	61.1	30.8	21.3
CE	56.7	45.5	90.6	58.3	110.3	60.3	41.0
ND	22.6	20.8	31.9	25.8	40.0	26.8	15.3
SM	5.0	5.2	7.0	6.9	8.7	6.3	3.8
EU	0.27	0.26	0.46	0.3	0.58	0.30	0.21
DY	4.83	4.95	6.19	5.57	6.52	5.67	3.65
ER	2.99	3.08	3.18	2.80	3.26	3.43	2.36
YB	3.05	3.40	2.72	3.03	3.32	3.55	2.47
LU	0.29	0.51	0.44	0.45	0.47	0.59	0.42

When we plotted the bentonites and tuffs in the diagram (Wichester and Floyd, 1977) in respect of Zr/ TiO_2 and Nb/Y contents, asidic (Rhyolite) composition of the samples were determined (Figure 8).

The trace element and REE contents of samples are given in Table 2. Total abundance of rare earth element (REE) enriched in bentonites when compared with the fresh rock (tuff). Both light rare earth elements (LREE) (La-Sm) and heavy rare earth elements (HREE) (Lu-Dy) enriched during alteration. Normalization diagram over fresh rock (T-1) shows mobility of REE in alteration profile (Figure 9). As indicated by REE, enrichment in LREE is greater than HREE. Under alkaline conditions the

stability of HREE complexes is greater than that of LREE (Muchangos, 2000).

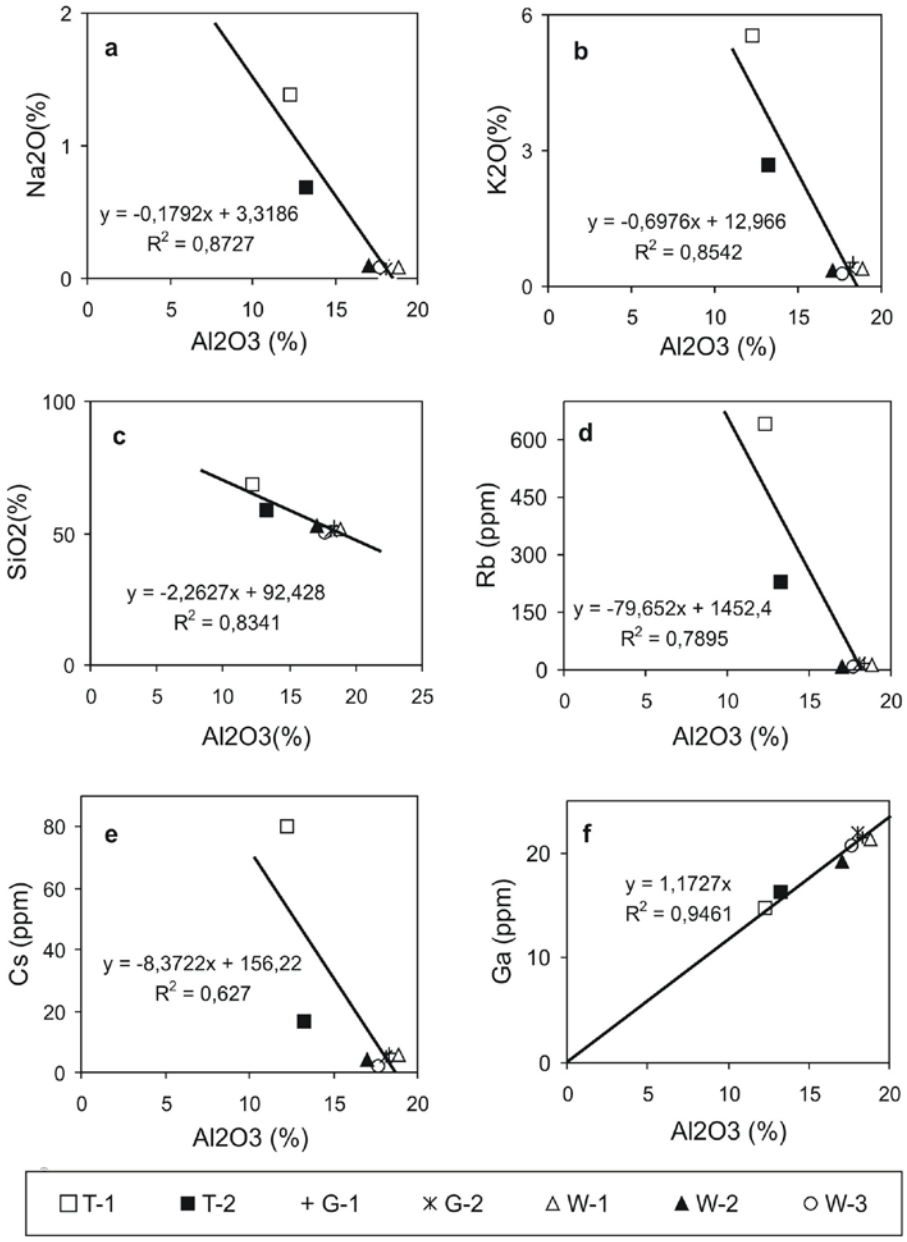

Figure 6. Mobility of some major and trace elements relative to Al during alteration

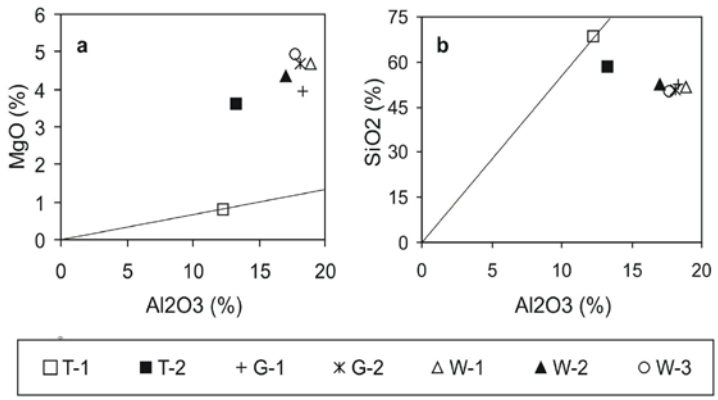

Figure 7. a) Enrichment in Mg relative to Al and b) depletion in Si relative to Al

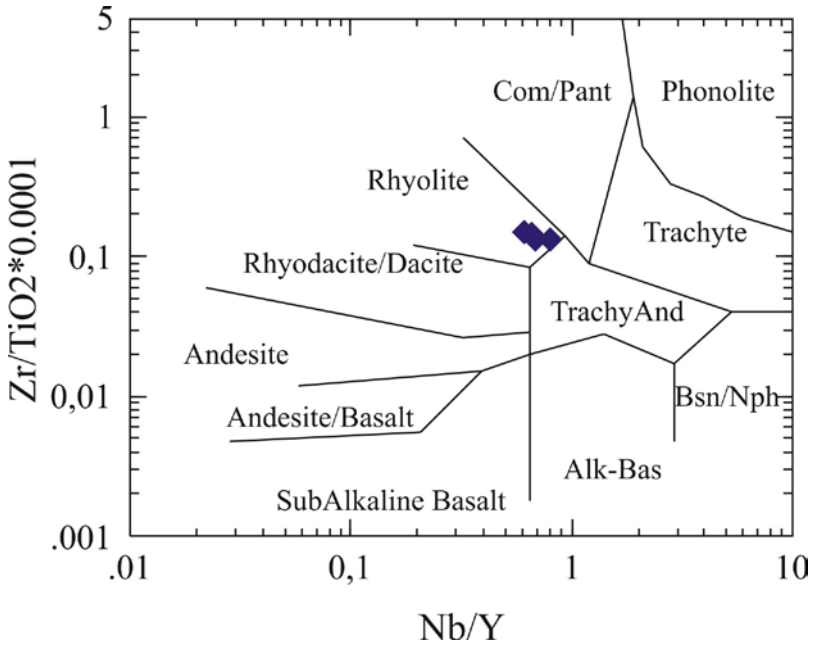

Figure 8. Diagram of Winchester and Floyd (1977) determining rhyolitic composition of bentonites

On the other hand, a negative Eu anomaly indicates a feature of the upper continental crust (Lipin and McKay, 1989). It is indicative of equilibration of the melt with a feldspar residium prior to eruption. Because of high pH values of the lacustrine water rare earth elements precipitated as compounds, exchanged for H^+ or were adsorbed on the mineral surfaces of bentonites (Lipin and McKay, 1989).

5. CONCLUSIONS

The bentonite formation in Yeniköy was formed in the alkaline lake of Bigadiç lacustrine basin. The high Mg content promotes the alteration into bentonite and it may be originating from ultrabasic rocks of basement complex at the bottom. Ca-montmorillonite is the main clay mineral of the deposit. Illite was formed by the diagenetic processes during alteration. Illite mineral was determined in grey bentonite. The higher K value may promote formation of illite. Excess Si was not precipitated as Si-polymorphs like opal-CT in bentonite. It is leached in open system. Montmorillonite mineral was also determined by the SEM investigation. It grows as thin film bands over volcanic glass. Characteristic sheet like structure also indicates montmorillonite mineral.

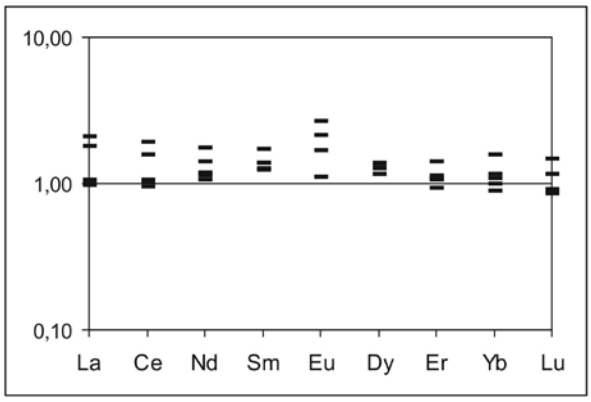

Figure 9. Normalization diagram showing mobility of REE during conversion to bentonite

The Yeniköy bentonite was formed from alteration of volcanic glass of possible rhyolitic composition. The vertical development of alteration zone indicates in-situ alteration of volcanic glass. The alteration mechanism includes migration of major and trace elements from the parent rock. Alkalis are leached and Mg was taken up. Due to the higher pH conditions Al remained stable and enriched in-situ during alteration . The excess Mg may be transported from an external source. The origin of the Mg rich fluids could not be hydrothermal. Because there is no evidence of hydrothermal alteration. Low Si and low Fe, Ti contents are due to the asidic composition of parent rock. Cs and Rb are leched with alkalis and Sr, Sc are enriched.

REE pattern indicates an enrichment in total REE content during alteration. LREE are more enriched relative to HREE. On the other hand a negative Eu anomaly reflects the upper continental crust feature. REE elements came out of solution and precipitated in bentonites in alkaline conditions.

ACKNOWLEDGEMENTS

We thank Ahmet Yıldız for helping us to obtain SEM observations and Işık Ece for getting us XRD pattern in İstanbul Technical University.

REFERENCES

Christidis, G., 1998. Comparative Study Of Major and Trace Elements During Alteration of An Andesite and A Rhyolite To Bentonite, In The Islands of Milos and Kimilos, Aegean, Greece. *Clays and Clay Minerals*, 46, 379-399.

Ercan et al., 1984. Bigadiç Çevresinin (Balıkesir) Jeolojisi ve Magmatik Kayaçların Petrolojisi. *Türkiye jeoloji Kurultayı Bülteni*, s. 5, 75-85

Esenli, F., 1990. Zeolithic Diagenesis and its Chemical Reactions; Examples from Turkey and The World. İstanbul Technical University ,48, 68-73.

Grim, R.E., 1962. Applied Clay Mineralogy. *International Series in Earth Sciences*, Mc Graw-Hill Book Co. Inc., Newyork.

Grim, R. E. and Güven, N., 1978. Bentonites- Geology, Mineralogy, Properties and Uses.*Developments in Sedimentology, Elsevier Scientific Publishing Company*, New York, USA.

Helvacı, C.,1995. Stratigraphy, Mineralogy and Genesis of the Bigadiç Borate Deposits, Western Turkey. *Economic Geology*, 90, 1237-1260.

Lipin, B.R. and McKay, G.A., 1989. Geochemistry and Mineralogy of Rare Earth Elements. Reviews in Mineralogy .*Mineralogical Society of America*, Michigan, USA.

Muchangos, A.C., 2000. The mobility of rare-earth and other elements in process of alteration of rhyolitic rocks to bentonite (Lebombo Volcanic Mountainous Chain, Mozambique). *Journal of Geochemical Exploration, Elsevier*, 88, 300-303.

Winchester, J.A. and Floyd, P.A., (1977). Geochemical discrimination of different magma series and their diffentiation products using immobile elements. *Chem. Geol*., 20, 325-343.

Zielinski, R.A., 1982. The Mobility of Uranium and Other Elements During Alteration of Rhyolite Ash To Montmorillonite: A Case Study In The Troublesome Formation, Colorado, U.S.A. *Chemical Geology*, 35, 185-204.

CEMENT CHARACTERISTICS OF THE CARBONIFEROUS SANDSTONES OF CENTRAL POLAND

Kozłowska A.

Polish Geological Institute, Rakowiecka 4, 00-975 Warszawa, Poland, aleksandra.kozlowska@pgi.gov.pl

Abstract: The main cements of the Carboniferous fluvial sandstones from the north-western part of the Lublin Trough adjoining the Mazowsze Region are quartz, clay minerals and carbonates. Kaolinite/dickite is the dominant authigenic clay mineral, whereas illite occurs locally. Carbonate cements are represented by common siderite and ankerite, and subordinate Fe-dolomite and dolomite. Diagenetic history of the studied sandstones includes two stages: eodiagenesis and mesodiagenesis with the presumed boundary between the stages corresponding to a temperature of 50°C. The isotopic composition of oxygen in meteoric pore waters gradually changed through time toward higher $\delta^{18}O$ values. The Carboniferous deposits underwent diagenesis at a maximum temperature of approximately 120°C.

Key words: cements, sandstones, Carboniferous, Central Poland

1. INTRODUCTION

Data on cements of sandstones are important in determing their reservoir quality. The aim of this study was to acquire information about the timing and geochemical conditions of precipitation and dissolution of diagenetic minerals as well as the source of them.

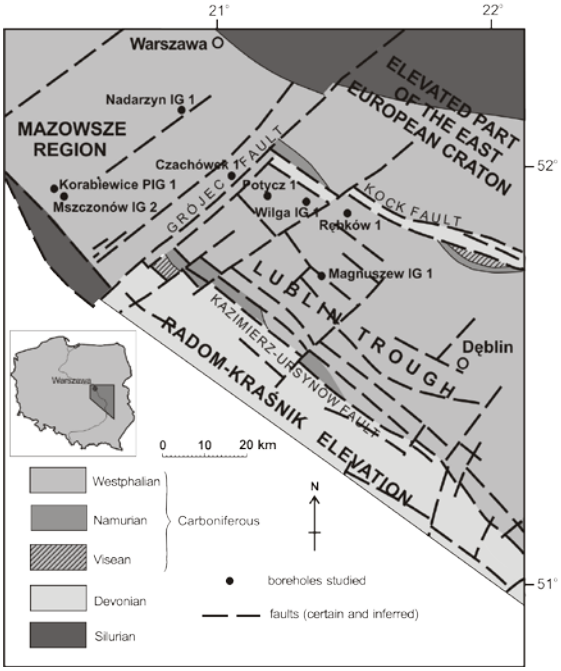

Figure 1. Location of boreholes against simplified geology (without Permian, Mesozoic and Cenozoic) of the Mazowsze and Radom-Lublin zone (after Żelichowski and Porzycki, 1983)

The study area, which covers the north-western part of the Lublin Trough adjoining the Mazowsze Region (Figure 1), is composed of Upper Carboniferous (Namurian, Westphalian) fluvial sandstones (Waksmundzka, 1998). The examinations were performed on rocks from 8 boreholes located in the area between Warszawa and Dęblin (Korabiewice PIG 1, Mszczonów IG 2, Nadarzyn IG 1, Czachówek 1, Potycz 1, Rębków 1, Wilga IG 1 and Magnuszew IG 1). The Carboniferous rocks occur at depths ranging from 1.8 to 5.0 km in this area. They directly overlie the Silurian or Devonian deposits and are overlain by Permian rocks.

2. RESEARCH METHODS

278 thin sections, most of which prepared with blue epoxy resin for porosity identification, were examined with a standard petrographic microscope. Quantitative data on mineralogy and pore spaces were obtained by 300 point counts per slide for all the samples. Staining with ferricyanide solution was used to characterize different carbonate cements (Dickson, 1965). 150 samples were studied by using a Cambridge Image Technology Ltd. CCL 8200 mk3 cold-cathode chamber. Two scanning electron microscopes, (SEM) – JSM-35 JEOL and LEO 1430, were used to study the texture, pore types and authigenic minerals on broken rock surfaces and polished sections coated with carbon and gold.

Energy dispersive spectrometer analysis (EDS ISIS) was employed to study the composition of representative authigenic minerals. Samples for clay mineralogical analysis were run in a Philips PW 1840 X-ray diffractometer. Clay mineral analyses of sandstones were performed on the <0.2 μm, <0.3 μm and <2 μm fractions for illite and <2 μm and 2-10 μm fractions for kaolinite. Mineral identification was based on comparison with JCPDS files. Infrared studies were used to identify kaolinite subgroupe minerals on a FT-IR FTS135 one-bunch spectrometer. It was made by assessing the position and relative intensity of the OH-stretching bands in the 3000 – 4000 cm^{-1} region. Fluid inclusion investigations were performed on thick rock slices polished on both sides, using freezing-heating stage – Fluid Inc. System. The reproducibility of temperature measurements on standards is ±0.1ºC. Carbon and oxygen isotope analyses of carbonate cements were performed on 46 samples. Powdered bulk-rock samples were reacted with phosphoric acid (McCrea, 1950). The evolved CO_2 was analysed using a NI1305 mass spectrometer. Carbon and oxygen isotope data are represented in the normal δ notation relative to PDB. Precision was ±0.08‰ for both $\delta^{13}C$ and $\delta^{18}O$.

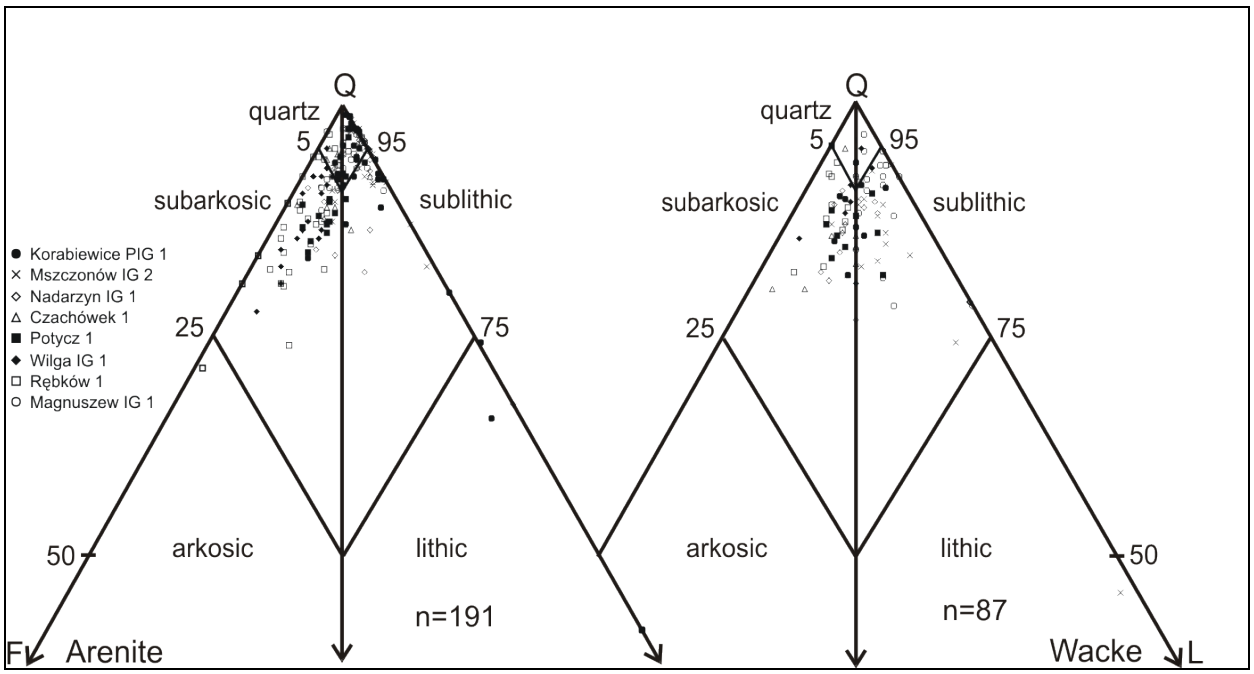

Figure 2. Carboniferous sandstones classification according to the triangle of Pettijohne *et al.* (1972)

3. RESULTS OF INVESTIGATIONS

3.1. Texture and framework grain composition of sandstones

The Carboniferous sandstones are represented mostly by subarkosic, quartz and sublithic arenites and wackes (Figure 2). Lithic and arkosic arenites, as well as lithic wackes, are subordinate. Arenites are represented by fine- to coarse-grained rocks characterized by unoriented structure. Wackes are represented by very fine- and fine-grained sandstones showing oriented structures. The main component of the samples is both mono- and polycrystalline quartz. Detrital quartz grains account for 60-70 vol%. The amount of feldspars represented by K-feldspar is about 6 vol%. They are commonly blue in CL, sporadically yellow-brown and yellow-green. The content of micas, mainly muscovite, biotite and chlorite, ranges from 0 to 2 vol% in arenites and above 10 vol% in wackes. Heavy minerals are rare. The amount of rock fragments is about 2 vol%.

Magmatic (mainly volcanic), metamorphic and clastic sedimentary rocks are the dominant lithic grains. Detrital grains of sandstones are largely subrounded, in particular in coarse fraction. Pore space between grains is filled completely or partly by matrix and/or by cements. Of cements, the most significant role is played by quartz, authigenic clay minerals and carbonates. Sulphates, iron hydroxides, hematite and pyrite account for a small percentage. The intergranular and intragranular petrographic porosity in sandstones ranges from 1 to 24.8 vol%, average about 10 vol%.

3.2. The main authigenic minerals

3.2.1. Quartz

Quartz cement occurs as syntaxial overgrowths developed on quartz grains. The amounts of the cement vary from about 3 to 10 vol%, reaching at places above 20 vol%. Generally, in polarization microscope authigenic quartz is difficult to discriminate from a quartz grain. Sometimes the boundary between a quartz grain and a quartz overgrowth is marked by fluid inclusion, early siderite or hematite. The real image of quartz cement filling the pore space can be observed in cathodoluminescence (CL). Two generations of authigenic quartz overgrowths have been identified (Kozłowska, 2004). The older generation overgrowths are characterized by dark-brown luminescence. The younger generation overgrowths show no luminescence. Sometimes authigenic quartz shows an irregular sector structure. Quartz cement also fills microfractures within quartz framework grains, suggesting that mechanical compaction took place before silification. In SEM images, authigenic quartz overgrowths are very well visible as rhombohedral crystals and prisms on detrital quartz grains. Quartz cement is dissolved and replaced by carbonates, sporadically by anhydrite. Homogenization temperatures of fluid inclusions of quartz overgrowths were measured for 22 samples. The homogenization temperatures of fluid inclusions in authigenic quartz indicate that quartz cement precipitated at temperatures of 50-150ºC (Kozłowska, 2004; Kozłowska and Poprawa, 2004). The salinity of fluid inclusions ranges between 5 and 15 eq. wt.% NaCl.

3.2.2. Clay minerals

Authigenic clay minerals observed under the polarization microscope and scanning electron microscope (SEM) and identified in X-ray method are represented by kaolinite/dickite, illite, chlorite and I/S mixed-layer clay minerals. Kaolinite is dominant, illite is subordinate, chlorites and I/S mixed-layer clay minerals are local diagenetic clay minerals.

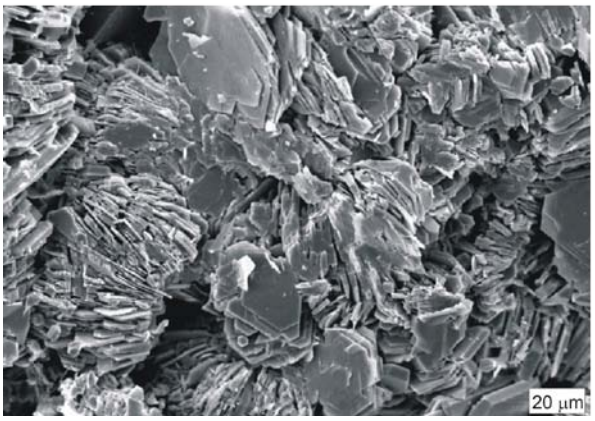

Figure 3. Vermiform kaolinite. SEM image; Nadarzyn IG 1 borehole, depth 3463.4 m

3.2.2.1. Kaolinite/Dickite

Kaolinite cement fills mainly intergranular and intragranular space. Its content is about 5 vol% up to a maximum of 11 vol%. The term kaolinite refers to minerals of the kaolinite subgroup (e.g. kaolinite, dickite). Kaolinite has been identified as 2 morphological types of vermiform kaolinite and blocky kaolinite (Kozłowska, 2004). Vermiform kaolinite (Figure 3) is early diagenetic and occurs mainly in upper parts of the Carboniferous sections. Vermiform kaolinite is mostly coarse grained. It consists of large platy crystals, often with irregular edges, which are usually curvilinear in shape, reaching several hundreds of µm in length. Blocky

kaolinite (Figure 4) which developed at later diagenetic stages is dominant at larger depths. Blocky kaolinite is typically finer in comparison to the vermiform one. It consists of plates with smooth edges which are distinctly shorter in their length. X-ray analyses show mainly the presence of kaolinite from sandstones of different depths. Kaolinite that is referred to as well ordered kaolinite occurs down to a depth of 3 km. Beneath this depth, more weakly ordered kaolinite is predominant. Infrared spectroscopy is recommended as the most sensitive technique for differentiating kaolinite and dickite in sandstones where large amounts of non-clay minerals are present and for estimating relative abundances of the polytypes under these circumstances (Ehrenberg *et al*., 1993).

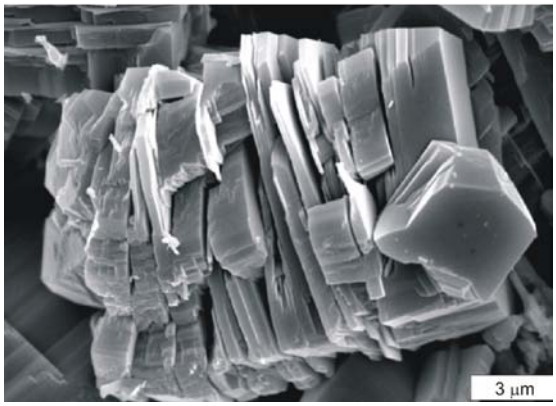

Figure 4. Blocky kaolinite. SEM image; Czachówek 1 borehole, depth 3442.4 m.

An infrared analysis shows that below 3 km, locally at slightly shallower depths, kaolinite-dickite intergrowths are observed. The average dickite content is about 20%. It was estimated comparing the pattern of absorption bands with a series of computer-generated well crystallized kaolinite and dickite mixtures (Ehrenberg *et al*., 1993; Beaufort *et al*., 1998). The obtained results suggest that, the onset of transformation of kaolinite to dickite can be observed with increasing burial depth in the studied sandstones. The initial temperature for dickite to be formed is estimated at 120ºC (Ehrenberg *et al*., 1993). Kaolinite has been altered into illite and replaced by carbonates, locally by anhydrite. The oxygen isotope data for kaolinite show $\delta^{18}O$ values ranging from 9.59 to 14.11‰$_{SMOW}$ (average 12.19‰$_{SMOW}$ for vermiform kaolinite and 10.34‰$_{SMOW}$ for blocky kaolinite). The calculated growth temperatures of vermiform kaolinite (25-50ºC) and blocky kaolinite (50-80ºC) (Osborn *et al*., 1994) and the oxygen izotope data for kaolinites indicate that vermiform and blocky kaolinites precipitated from meteoric pore waters which varied in oxygen isotopic composition. For vermiform kaolinite the pore waters are more ^{18}O depleted.

3.2.2.2. Illite

Illite creates plate and filamentous crystals very easily observable in SEM image. Filamentous illite covers quartz, kaolinite and carbonate cements and it occurs at depths below 3 km. This form of occurrence suggests a very late crystallization of illite. From observations and literature data it seems that the temperature above 100ºC is most possible for the precipitation of illite (Bjørlykke and Aagard, 1992; Chuchan *et al*., 2001). K/Ar age determinations of fibrous illite show that it began to crystallize 205.4 to 167.3 My ago, i.e. during the Late Triassic and Middle Jurassic (Kozłowska, 2004; Kozłowska and Poprawa, 2004).

3.2.3. Carbonates

Carbonate cements are represented by common siderite and ankerite, and subordinate Fe-dolomite and dolomite. Their content in the sandstones ranges from 0 to 38 vol%. Carbonate cements occur mainly as porous, rarely basic, cements.

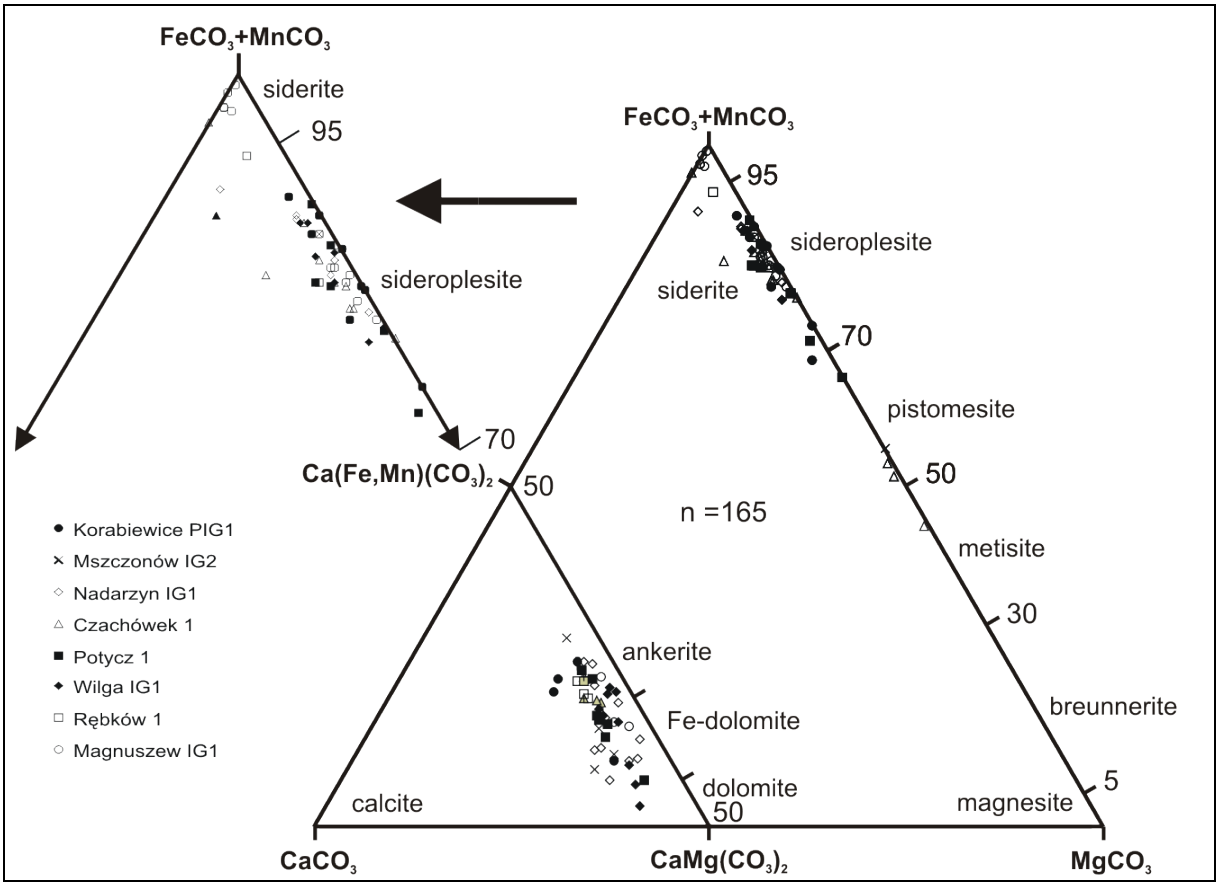

Figure 5. A triangle plot of chemical composition of carbonate cements in mole percentage calculated from EDS ISIS measurements

3.2.3.1. Siderites

Siderite is often a link within an isomorphic series of $FeCO_3$ – $MgCO_3$ (Figure 5). Most of the siderites fall within an interval of siderite-pistomesite. The overage amount of siderite is about 4 vol%. There are two generations of siderite: early and late (Kozłowska, 2003; 2004). The early siderite is sideroplesite and siderite in chemical composition. It occurs as very fine-crystalline grains or spherolites. It has been replaced by later carbonate generations. The late siderite is represented by sideroplesite, sporadically by pistomesite, which crystallized as dispersed rhombohedrons or it composes base cement. Backscattered electron image (BEI) revealed a complexity of composition of late siderites (Figure 6). Rhombohedral specimens show even 4 distinct grey shades according to the Mg content. The darker the colour, the higher the Mg content. Late siderite has replaced early siderite, authigenic quartz and kaolinite. The results of $\delta^{18}O$ determinations of the early and late siderites shows values varying from –3.44 to –15.45‰$_{PDB}$, average about –8.5‰$_{PDB}$ for both of them. If we consider precipitation of the early siderite at a temperature between 15-40ºC (Backer *et al*., 1995; Rezaee and Schulz-Rojahn, 1998), it may be suggested that this

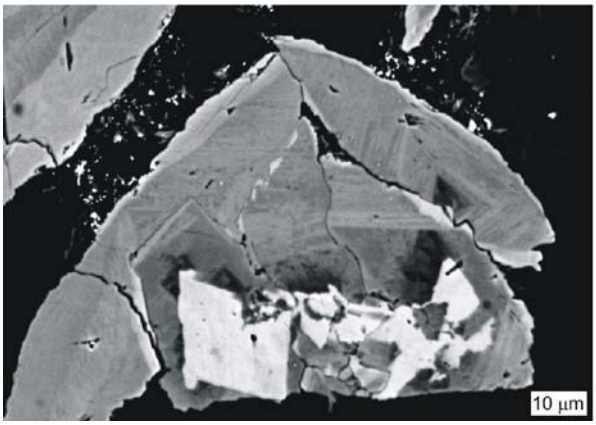

Figure 6. Rhombohedrons of late siderite in pore space of sandstones. Back-scattered electron image; Korabiewice PIG 1 borehole, depth 4828.5 m.

mineral precipitated from modified meteoric waters strongly depleted in ^{18}O. Late siderite which crystallized at higher temperatures of about 70ºC (Kozłowska, 2004) precipitated from meteoric pore waters ranging from about -7 to -1‰$_{SMOW}$. The $\delta^{13}C$ values range between -16.12 to 1.37‰ $_{PDB}$, average -5.51‰$_{PDB}$, and between -13.89 to -3.78‰ $_{PDB}$, average -9.62‰$_{PDB}$, for early and late siderites, respectively. The obtained $\delta^{13}C$ values show that porous waters were enriched in carbon generated in a microbial methanogenesis zone for early siderite and in a thermal decarboxylation zone for late siderite (Morad, 1998).

3.2.3.2. Dolomite/Fe-dolomite/ankerite

Dolomite, Fe-dolomite and ankerite are the minerals of an isomorphic series of $CaMg(CO_3)_2$ – $Ca(Fe,Mn)(CO_3)_2$ and they mostly represent ankerite (Figure 5) (Kozłowska, 2003; 2004). The average amount of ankerite is about 1 vol% of the rock, but locally its content reaches about 10 vol%. Ankerite occurs as basic cement or isolated rhombohedral crystals. Some crystals show characteristic features of saddle ankerite, such as: sweeping extinction and slightly curved crystal boundaries (Spötl and Pitman, 1998). Ankerite has replaced authigenic quartz, siderite, kaolinite and has been replaced by anhydrite. Homogenization temperatures were measured for 30 fluid inclusions in the ankerite cements. The overall range of the homogenization temperatures in ankerite cement is 55–129ºC (Kozłowska, 2004; Kozłowska and Poprawa, 2004). The salinity of fluid inclusions ranges between 5 and 13 eq. wt.% NaCl. The $\delta^{18}O$ data from ankerite, ranging from -1.19 to -12.81‰$_{PDB}$, average -6.63‰$_{PDB}$, show that ankerite precipitated from pore waters which were a mixture of marine and meteoric waters ($\delta^{18}O$ values from about -4 to 10‰$_{SMOW}$). The $\delta^{13}C$ values vary from -13.96 to -1.19‰$_{PDB}$, average -6.63‰$_{PDB}$. The $\delta^{13}C$ values of ankerite suggested that carbon originated from two different sources – thermal decarboxylation of organic matter and microbial methanogenesis zones, as postulated by Morad (1998).

4. DISCUSSION

Diagenetic history of the Carboniferous sandstones includes two stages: eodiagenesis and mesodiagenesis, with the presumed boundary corresponding to a temperature of about 50°C (Figure 7). The main diagenetic processes observed in the rocks are the following: compaction, cementation, dissolution, replacement and alteration. At the beginning of eodiagenesis, iron hydroxides and hematite formed under oxidizing conditions (Walker *et al.*, 1978). Mechanical compaction also operated from the very beginning. Early siderite is a dominant mineral of older cements of Carboniferous rocks. It precipitated in anoxic environments such as swamps and flood plains in sediment rich in reactive minerals containing iron under low dissolved sulphate conditions (Morad, 1998). Higher content of magnesium in the fluvial siderites can be connected with transformation of detrital magnesian minerals by meteoric porous waters infiltration (Hawkins, 1978). Pyrite precipitated locally in association with siderite. During eodiagenesis, potassium feldspar and mica grains started to undergo dissolution and alteration processes. Vermiform kaolinite crystallization was connected with transformation of detrital feldspar and mica grains with a participation of meteoric waters (Bjørlykke, 1989). Regeneration quartz overgrowths began to precipitate at the end of eodiagenesis and they continued to grow during mesodiagenesis. The main silica-providing sources were meteoric water, dissolution of aluminosilicates, smectite to illite transformation in I/S mixed-layer clay minerals, pressure solution and illitization of kaolinite (Worden and Morad, 2000). During mesodiagenesis,

mechanical compaction still operated and also detrital grains were subjected to dissolution. Vermiform kaolinite was replaced by blocky kaolinite. It was either the result of dissolution-crystallization reaction involved by the replacement of vermiform crystals by blocky ones (Ehrenberg *et al*., 1993; McAulay *et al*., 1993; Beaufort *et al*., 1998) or it precipitated directly from pore fluids enriched in Al and Si which circulate in the rock. Alteration of smectite to illite commenced at the beginning of mesodiagenesis (Boles and Franks, 1979). Carbonate cements precipitated at that time in the following order: dolomite, Fe-dolomite, late siderite and ankerite. The formation of the late diagenetic high-Mg siderite was most likely connected with a high concentration of magnesium in the formation water (Morad *et al*., 1994). Altered minerals rich in Mg^{2+} could be the source of magnesium (Macaulay *et al*., 1992), or magnesium could be liberated from kerogen during burial processes (Desborough, 1978). Due to no traces of an early diagenetic calcite in the sandstones, the formation of dolomite and ankerite should not be associated with dolomitization of calcite at the late diagenetic stage. The source of Mg^{2+}, Fe^{2+}, Mn^{2+} and Ca^{2+} for late diagenetic carbonates could be the transformation of detrital clay minerals in shales related to their compaction (Boles and Franks, 1979). During late mesodiagenesis, mechanical compaction was replaced by chemical compaction. Anhydrite crystallized from solutions associated with Zechstein evaporates (Kozłowska, 2004). Quartz cement, quartz grains as well as carbonate and sulphate cements underwent dissolution. Alteration of kaolinite to dickite occurred at the end of mesodiagenesis. Also late Fe-chlorite and fibrous illite crystallized at that time. The origin of authigenic illite was mainly connected with alteration of kaolinite and recrystallization of detrital clay minerals of matrix (Kozłowska, 2004). It is possible that mesodiagenesis was the time of hydrocarbon generation.

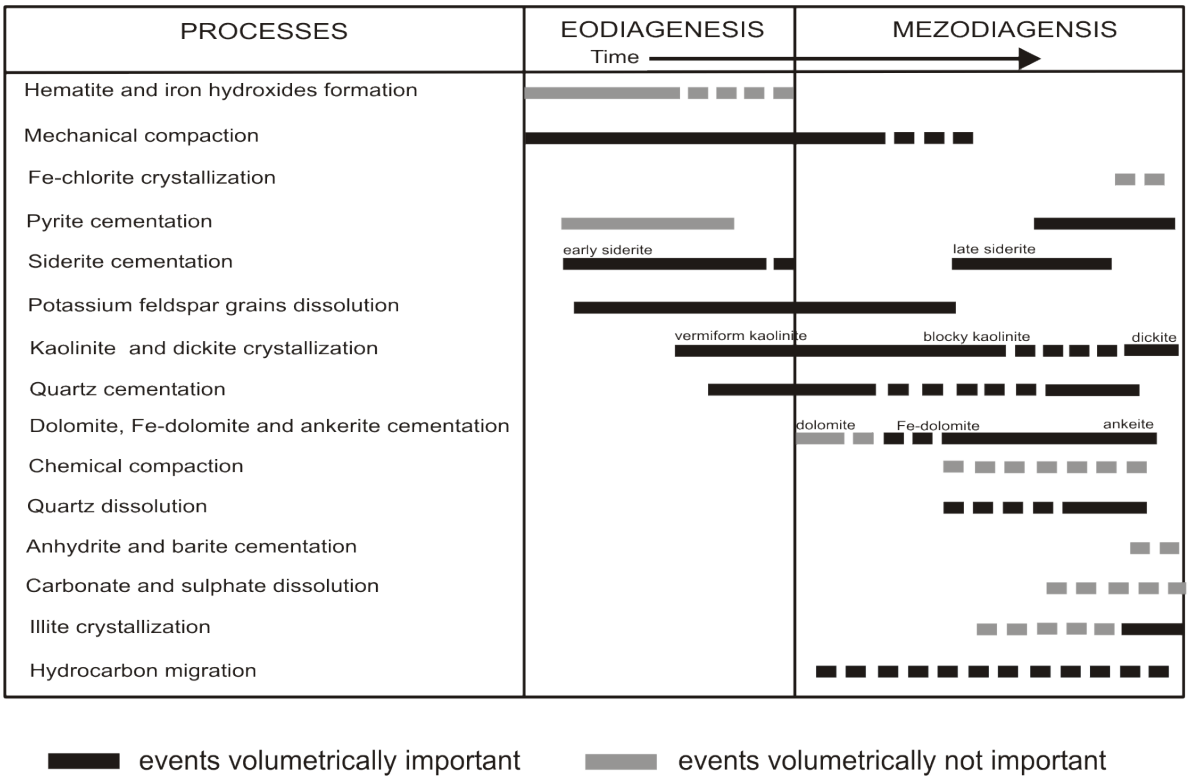

Figure 7. The diagenetic sequence of Carboniferous sandstones

The variation in paragenetic sequences is reflected not only in the different temperatures of crystallization, but also in the pore-water evolution. It was attempted to reconstruct the evolution of isotopic relationships of oxygen in pore water on the basis of the results of isotopic studies and analyses of fluid inclusions, taking into account a hypothetical sequence of authigenic minerals. The collected data are illustrated in a graph demonstrating the relationship between $\delta^{18}O$ of pore water and the crystallization temperature of authigenic minerals (Figure 8). This graph shows that, during eodiagenesis, the cements precipitated locally from meteoric waters strongly depleted in ^{18}O. During mesodiagenesis, pore waters had become enriched in ^{18}O until positive $\delta^{18}O$ values were reached.

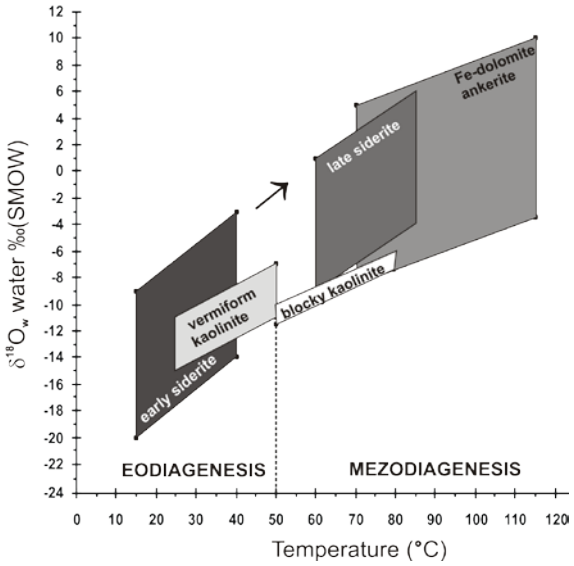

Figure 8. Evolution of $\delta^{18}O$ isotope in pore water from Carboniferous sandstones related to the increase in temperature (based on the results of isotopic and fluid inclusion analyses)

5. CONCLUSIONS

1. The Carboniferous sandstones are represented mostly by subarkosic, quartz and sublithic arenites and wackes. The main component of the sandstones grain framework is both mono- and polycrystalline quartz. Feldspar, lithoclasts and micas occur in minor proportions. Heavy minerals are rare. Quartz, clay minerals and carbonates are the most common cements in the sandstones. Sulphates, iron hydroxides, hematite and piryte account for a small percentage. Average porosity of the sandstones is approximately 10 vol%.

2. Quartz cement occurs as 2 generations of syntaxial overgrowths developed on quartz grains. In CL image the older generation of the overgrowths is characterized by dark brown luminescence, whereas the younger generation shows no luminescence. The main authigenic clay minerals are represented by kaolinite/dickite and illite. Two morphological types of kaolinite were identified: vermiform kaolinite occurring mainly in upper parts of the Carboniferous section, and blocky kaolinite dominant at larger depths. Below the depth of 3 km, locally at slighty shallower depths, kaolinite – dickite intergrowths are observed, in which the average dickite content is about 20%. Carbonate cements are represented by common siderite and ankerite, and subordinate Fe-dolomite and dolomite. Two generations of siderite were identified with the early siderite generation having the lower content of magnesium than the late one.

3. Diagenetic history of the Carboniferous sandstones includes two stages: eodiagenesis and mesodiagenesis with the suggested boundary corresponding to a temperature of 50ºC. The results of investigations indicate that the Carboniferous deposits underwent diagenetic processes at temperatures up to 120ºC. This can be inferred from results of vitrinite reflectance studies (Grotek, 2005) and measurements of homogenization temperatures of fluid inclusions in the cements. Moreover, the occurrence of kaolinite-dickite intergrowths suggests that these rocks were heated to the temperature of approximately 120ºC. The reconstruction of evolution of oxygen in pore water during diagenetic history shows that

isotopic composition of oxygen in modified meteoric pore water gradually changed toward higher $\delta^{18}O$ values.

ACKNOWLEDGEMENTS

This study is based on results of a research project No 6 PO4D 038 18 financially supported by the Polish Committee for Scientific Research. I wish to thank Stanisław Hałas for providing stable isotope determinations. My cordial thanks are due to Anna Maliszewska for making corrections and comments to the text.

REFERENCES

Backer, J. C., Kassan, J. and Hamilton, P. J., 1995. Early diagenetic siderite as indicator of depositional environment in the Triassic Rewan Group, Southern Bowen basin, Eastern Australia. *Sedimentology*, 43, (1), 77-88.

Beaufort, D., Cassagrabere, A., Petit, S., Lanson, B., Berger, G., Lacharpagne, J. C. and Johansen, H., 1998. Kaolinite - to - dickite reaction in sandstone reservoirs. *Clay Minerals*, 33, (2), 237-316.

Bjørlykke, K., 1989. Sedimentology and Petroleum Geology. *Springer Verlag*, Berlin.

Bjørlykke, K. and Aagaard, P., 1992. Clay minerals in North Sea sandstones. *Society of Economic Paleontologists and Mineralogists Special Publication*, 47**,** 65-80.

Boles, J. R. and Franks, S. G., 1979. Clay diagenesis in Wilcox sandstones of Southwest Texas: implications of smectite diagenesis on sandstones cementation. *Journal of Sedimentary Petrology*, 49, (1), 55-70.

Chuhan, F. A., Bjørlykke, K. and Lowrey, C., 2001. Close system diagenesis in reservoir sandstones: examples from the Garn Formation at Haltenbanken area, offshore Mid-Norway. *Journal of Sedimentary Research*, 71, (1), 15-26.

Desborough, G. A. , 1978. A biogenic – chemical stratified lake model for the origin of oil shale of the Green River Formation: on alternative to the playa – lake model. *Geological Society of American Bulletin*, 89, (7), 961-971.

Dickson, J. A. D., 1965. A modified staining technique for carbonates in thin section. *Nature*, 205, 587.

Ehrenberg, S. N., Aagaard, P., Wilson, M. J., Fraser, A. R. and Duthie, D. M. L., 1993. Depth - dependent transformation of kaolinite to dickite in sandstones of the Norwegian Continental Shelf. *Clay Minerals*, 28, (3), 325-352.

Grotek, I., 2005. Alteration of the coalification degree of the organic matter dispersed in the Carboniferous sediments along border of the Eastern-European Craton in Poland. *Biuletyn Państwowego Instytutu Geologicznego*, 413, 5-80.

Hawkins, P. J., 1978. Relationship between diagenesis, porosity reduction, and oil emplacement in late Carboniferous sandstones reservoirs, Bothamsall Oilfield, E Midlands. *Journal of the Geological Society*, 135, (1), 7-24.

Kozłowska, A., 2003. Genesis of carbonate minerals in the Upper Carboniferous sandstones in Central Poland. *Prace Specjalne Polskiego Towarzystwa Mineralogicznego*, 22, 115-118.

Kozłowska, A., 2004. Diagenesis of the Upper Carboniferous sandstones occurring at the border of the Lublin Trough and the Warsaw Block. *Biuletyn Państwowego Instytutu Geologicznego*, 411, 5-86.

Kozłowska, A. and Poprawa, P., 2004. Diagenesis of the Carboniferous clastic sediments of the Mazowsze region and the northern Lublin region related to their burial and thermal history.

Przegląd Geologiczny, 52, (6), 491-500.

Macaulay, C. I., Haszeldine, R. S. and Fallick, A. E., 1992. Distribution, chemistry, isotopic composition and origin of diagenetic carbonates: Magnus sandstones, North Sea. *Journal of Sedimentary Petrology*, 63, (1), 33-43.

Mc Aulay, G. E., Burley, S. D. and Johnes, L. H., 1993. Silicate mineral authigenesis in the Hutton and NW Hutton fields: implications for sub - surface porosity development. *The 4th Conference of Petroleum Geology of Northwest Europe*, J. R. Parker, The Geological Society, London, 1377 – 1394.

Mc Crea, J. M., 1950. On the isotopic geochemistry of carbonates and a paleotemperature scale. *Journal of Chemical Physics*, 18, 849-857.

Morad, S., 1998. Carbonate cementation in sandstones: distribution patterns and geochemical evolution. *Special Publication of the International Association of Sedimentologists*, 26, 1-26.

Morad, S., Ben Ismail, H. N., De Ros, L. F., Al-Aasm, I. S. and Sherrhini, N. E., 1994. Diagenesis and formation water chemistry of Triassic reservoir sandstones from Southern Tunisia. *Sedimentology*, 41, (6), 1253-1272.

Osborne, M., Haszeldine, R. S. and Fallick, A. E., 1994. Variation in kaolinite morphology with growth temperature in isotopically mixed pore - fluids, Brent Group, UK North Sea. *Clay Minerals*, 29, (4), 591-608.

Rezaee,, M. R. and Schulz-Rojahn, J. P., 1998. Application of quantitative back-scattered electron image analysis in isotope interpretation of siderite cement: Tirrawarra sandstone, Cooper Basin, Australia. *Special Publication of the International Association of Sedimentologists*, 26, 461-481.

Spötl, C. and Pitman, J. K., 1998. Saddle (baroque) dolomite in carbonates and sandstones: a reappraisal of burial – diagenetic concept. *Special Publication of the International Association of Sedimentologists*, 26, 437-460.

Waksmundzka, M. I., 1998. Depositional architecture of the Carboniferius Lublin Basin. *Prace Państwowego Instytutu Geologicznego*, 165, 89-100.

Walker, T. R., Waugh, B. and Grone, A. J., 1978. Diagenesis in first-cycle desert alluvium of Cenozoic age, southwestern United States and northwestern Maxico. *Geological Society of American Bulletin*, 89, (1), 19-32.

Worden, R. H. and Morad, S., 2000. Quartz cementation in oil field sandstones: a review of the key controversies. *Special Publication of the International Association of Sedimentologists*, 29, 1-20.

FAULTING AND SHAKING CHARACTERISTICS OF EARTHQUAKES IN DENİZLİ PROVINCE (TURKEY)

Kumsar H.[1] and Aydan Ö.[2]

[1]Pamukkale University, Department of Geological Engineering, Denizli, Turkey
e-mail: hkumsar@pau.edu.tr

[2]Tokai University, Department of Marine Civil Engineering, Shizioka, Japan
e-mail: aydan@scc.u-tokai.ac.jp

Abstract: The development of graben-horst systems in the western Turkey is still continuing as the upper most crust in the western Anadolu has been streched by the subduction of the African continent beneath the plate of Anadolu. The Denizli region in the western Turkey, is a seismically very active region where Gediz and Büyük Menderes grabens join together near by Sarayköy at northwest of Denizli. The antique cities in Denizli basin were affected by the strong earthquakes causing heavy damages of the structures in Denizli Province. Some stress concentration is taking place in Denizli province. From the crustal deformation measurements by GPS and computations of mean stress variations, the highest mean stress concentration with a tensile character occurs in the Denizli, which may be interpreted such that an earthquake due to normal faulting with or without lateral strike-slip component is likely. The recent seismic activity of the region confirms this conclusion. The seismic activity of this region has been increasing at an alarming rate. This study is mainly concerned with the faulting and shaking characteristics of Denizli province within the area bounded by latitudes 28.5-29.5E and longitudes 37.5-38.5N. It also covers several aspects of the region such as geology, tectonics, seismicity, faulting characteristics, recurrence and characteristics of strong motions recorded since 1976. As a result of the frequency and magnitude relations it can be said that earthquake with a magnitude of about 6.0 may strike the region at any time by taking into account its regional seismicity.

Key words: Denizli, earthquake, characteristics

1. INTRODUCTION

The development of graben-horst systems in the western Turkey is still continuing as the upper most crust in the western Turkey has been streched by the subduction of the African continent beneath the plate of Anadolu. The Denizli region in the western Turkey, is a seismically very active region where Gediz and Büyük Menderes grabens join together. The authors pointed out that some stress concentration is taking place in Denizli province (Aydan 2000 and Aydan et al. 2000a,b). The recent seismic activity of the region confirms this conclusion. The seismic activity of this region has been increasing at an alarming rate. This study is mainly concerned with the faulting and shaking characteristics of Denizli province within the area of bounded by latitudes 28.5-29.5E and longitudes 37.5-38.5N. This article covers several aspects of the region such as geology, tectonics, seismicity, faulting characteristics, recurrence and characteristics of strong motions recorded since 1976.

2. GEOLOGY AND TECTONICS

Denizli basin is a graben area located at the eastern sections of Büyük Menderes and Gediz grabens in the Aegean extensional province. The rock units are classified in three main groups in terms of their age; 1) basement rocks of pre-Neogene, 2) Neogene units and 3) Quaternary and Holocene units (Figure 1). The pre-Neogene formations are made up of mainly gneiss, schist and marbles of Paleozoic metamorphic rocks, and Mesozoic carbonates (Uysal, 1995). Neogene rocks are deposited within the all of the graben basins in western Anadolu. Quaternary sediments are deposited along

river and stream beds in the basins. There are hot and mineral water springs discharging through fracture and fault zones bounding Denizli basin at the north. The chemical composition of these waters, whose temperatures vary between 28°C - 98°C, is composed of calcium bicarbonate (Özkul *et al.,* 2000).

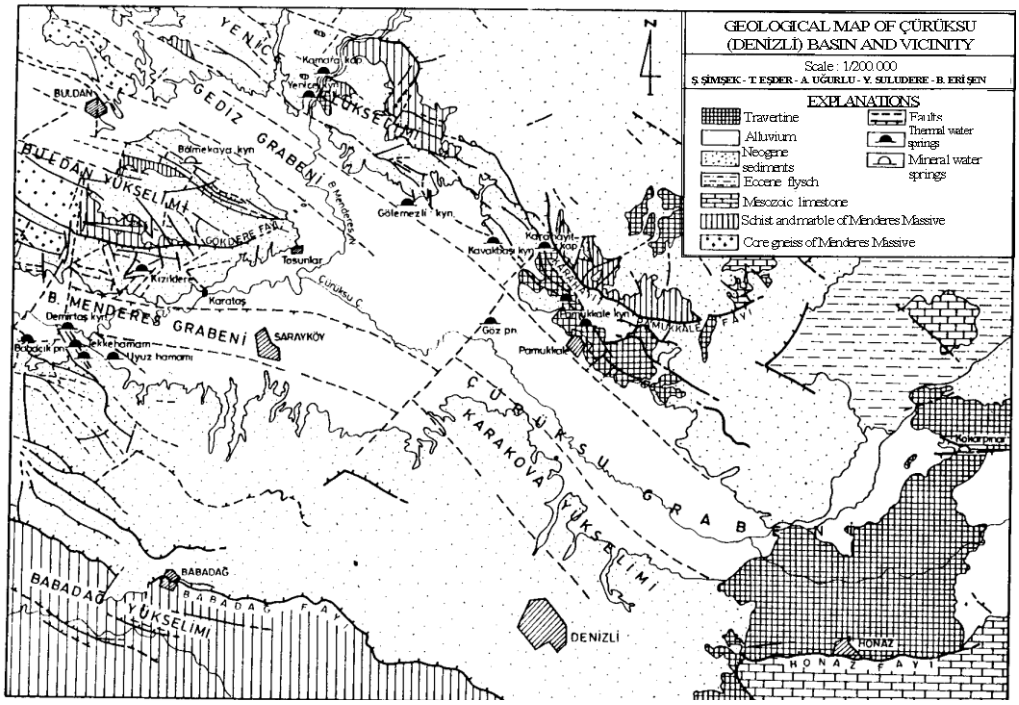

Figure 1. Geological map of Denizli basin and its tectonic structure (after Eşder, 1994)

As a result of the extensional tectonic regime, normal faults and extension cracks trending E-W and NW-SE developed, and horst and graben systems formed. This extensional province is one of the fast extending area in the world. The faults bounding the basin from north and south are segmented. The prominent faults of the province are Pamukkale fault (35km), Buharkent-Sarayköy fault (39km), Babadağ-Honaz fault (29km) and Çal- Çivril fault (42km).

3. SEISMICTY

The antique cities such as Hierapolis, Tripolis, Laodekia, Colessea and Aphrodisias in Denizli basin were affected by the strong historical earthquakes (Ceylan, 2000). Since antique cities were ruined by the historical earthquakes, it is most likely that the region can produce very large earthquakes in due time. The seismicity of the province was studied through earthquake catalogues prepared by ITU (Ergin *et al.*, 1967; Eyidoğan *et al.*, 1991), Kandilli Observatory (Ayhan *et al.*, 1981), Earthquake Engineering Department (Gençoğlu *et al.*, 1990), Turkish Earthquake Foundation (TDV), TEDBASE (Aydan *et al.*, 1996; Aydan, 1997), Denizli Municipality and USGS-NEIC. The seismicity of the province is divided into two broad groups, namely, historical seismicity and instrumented seismicity.

3.1 Historical Seismicity

The antique cities in Denizli basin were affected by the strong earthquakes in the history. The strong earthquakes in the history are summarized in Table 1. Magnitudes were inferred from the empirical relation suggested by Ergin *et al.*, (1967). As noted from this table, earthquakes of magnitude 7 class do occur in Denizli province. The province is also affected by 7.5 class earthquakes in neighboring provinces.

Table1. Historical earthquakes that affected Denizli

Date	Io	M	Epicenter	Comments
17	X	7.5	Sart	Heavy damage at Hierapolis, Laodicea, Tripolis, Aphrodisias
47	VII	5.7	Aphrodisias	Aphrodisias damaged
60	IX	7.0	Pamukkale	Hierapolis heavily damaged
102-116	VII	5.7	Aphrodisias	Aphrodisias damaged
300	VII	5.7	Pamukkale	Apollion temple is collapsed, new restorations and new constructions
359	VII	5.7	Aphrodisias	Aphrodisias damaged
494	VIII	6.4	Laodicea	Heavy damage and collapses
647	VIII	6.4	Laodicea	Heavy damage and collapses
700	VII	5.7	Hierapolis	Partial damage at theatre, roman bath house, collapse of walls and columns
1354	VII	5.7	Tripolis	Damage and collapses
1358	IX	7.0	Hierapolis	Heavy damage and collapses at Hierapolis and city was abandoned
1651	VIII	6.4	Honaz	Honaz heavily damaged and 700 dead
1653	X	7.5	Ödemiş	Heavy damage in K. Menderes, B. Menderes, Gediz basins and 2000-3000 dead.
25 Feb. 1702	VIII	6.4	Denizli	Heavy damage at Denizli & Sarayköy, 12000 dead
19 Nov. 1717	VIII	6.4	Denizli	6000 dead, heavy damage at collapses
1878	VIII	6.4	Çivril	1300 dead
16 Jan. 1886	VII	5.7	Denizli	Heavy shaking
20 Sep. 1989	IX	7.0	Aydın	Damage in Denizli
June 1907	VI	5.2	Denizli	Heavy shaking

3.2 Instrumental Seismicity

The magnitude of the earthquakes occurred between 1900-2005 are not greater than 6 within Denizli Basin except the one in 1945 with a magnitude of 6.8 (Figure 2 and Figure 3). However, the magnitude of this earthquake is disputed (Eyidoğan *et al.,* 1991). Figure 2 shows the cumulative magnitude and the magnitude of earthquakes as a function of time between 1900 and 2005. The tendency of the cumulative magnitude has been increasing at an alarming rate. If there is no problem with the recording of the seismic activity before 1990, the energy release is quite high between 1990 and 2005. The shape of the curve resembles to the tertiary phase of creep tests of geo-materials.

Recently a seismic activity in Buldan and surrounding in Denizli started on 23rd of July 2003. An earthquake with a magnitude of 5.2 occurred at 07:56AM on 23 July 2003. On the 26th of July 2003, another earthquake with a magnitude of 5.6 occurred near Buldan at 11:26AM on the local time. Buldan earthquakes caused some short surface ruptures following the earthquake with a magnitude of 5.6.

3.3 Earthquake Occurence Frequency and Magnitude Relation

The seismicity of the region bounded between latitudes 36.67-38.83N and longitudes 27.16-31.08E was also studied by Gençoğlu *et al.,* (1990) for a period between 1900 and 1986. The empirical relation of Gutenberg-Richter (1942) of the following form is used

$$\log N = a - bM \qquad (1)$$

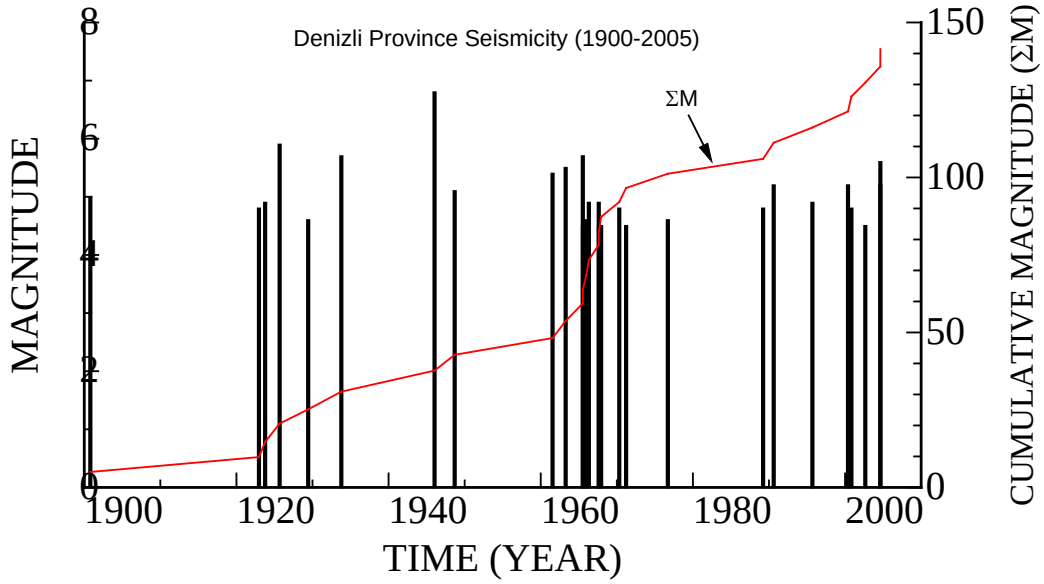

Figure 2. Seismic activity of Denizli province (M>4 earthquakes only)

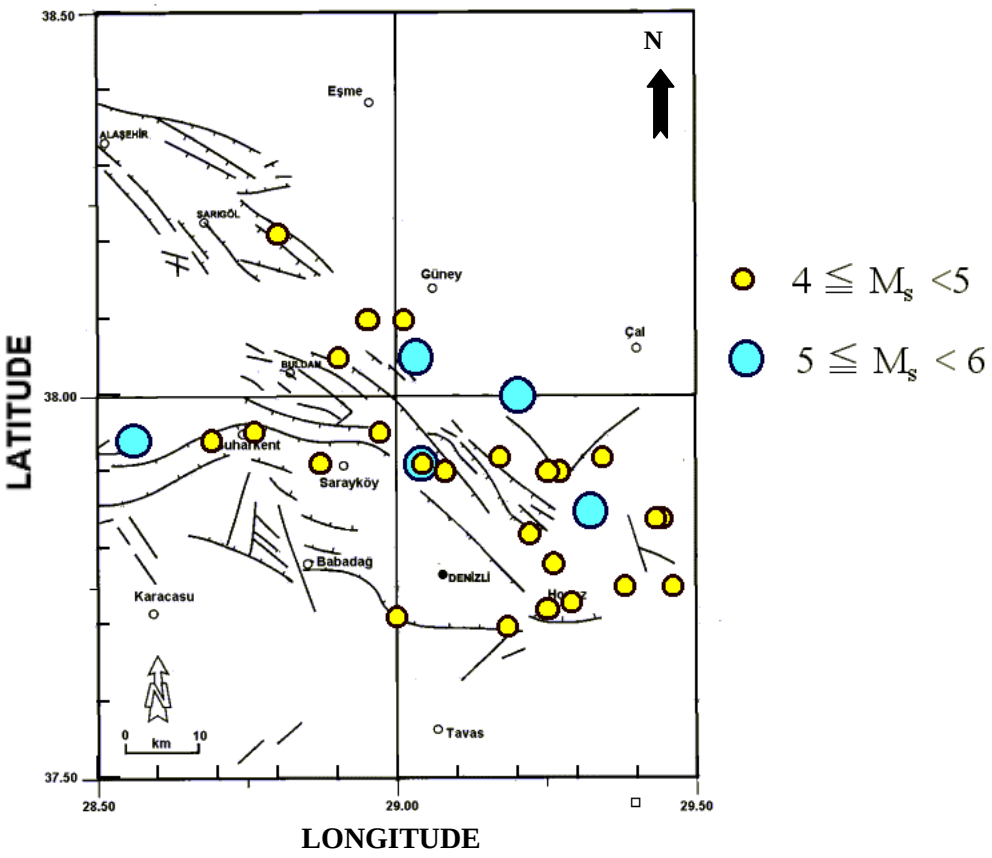

Figure 3. Epicenters of earthquakes which occurred between 1900 and 2005 in Denizli Basin and their relation to tectonics of the region (Tectonic map taken from MTA, 1992.)

Coefficients obtained by Gençoğlu *et al.*, (1990) and by Aydan *et al.*, (2002) together with observed data are shown in Figure 4. The maximum magnitudes of

earthquakes inferred from these relations ranges between 6.43 and 6.53. The inferred *b* coefficients in the relation are very similar to each and it is close to the *b* coefficient of the global seismicity. Furthermore, the computed results indicate that M 7-7.5 class earthquakes may occur at time intervals ranging between 400 to 800 years.

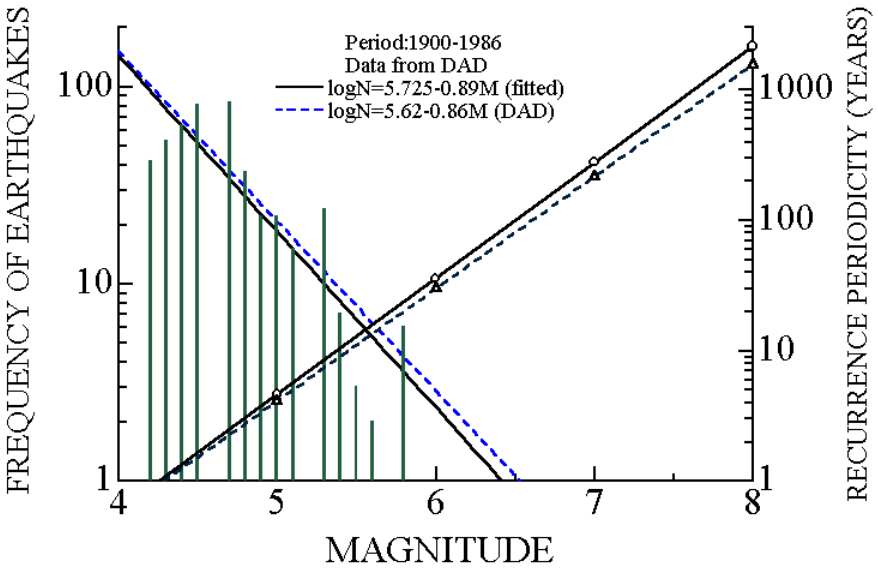

Figure 4. Earthquake recurrence and frequency magnitude relation (DAD-ERDdata)

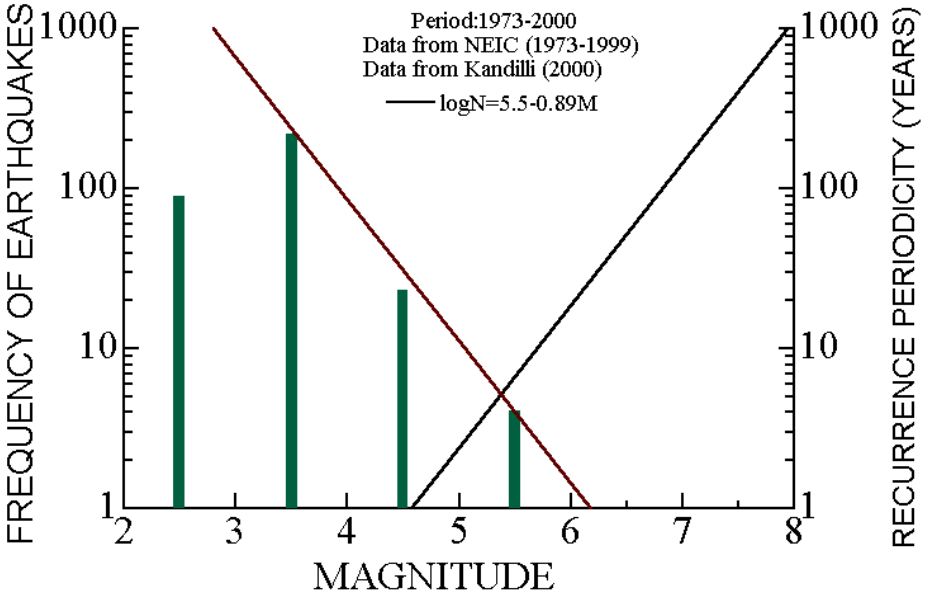

Figure 5. Earthquake recurrence and frequency magnitude relation(NEIC ve KOERI data)

Figure 5 shows the frequency and magnitude relations obtained for observations of the seismic activity between 1973-2000 compiled from catalogues NEIC and KOERI. This figure is somewhat different from the one in a previous study (Aydan *et al.*, 2002). In this study the coefficient *b* is chosen to be the same as that obtained for DAD data set. Since the seismic network of Turkey improved, it is now easy to locate earthquakes having magnitudes greater than 3. The data for earthquakes having magnitude greater 3 for a smaller region can be closely represented by the *b*-value obtained for longer period of observations with magnitudes greater than 4. This is actually the confirmation of the

fundamental assumptions of Gutenberg-Richter (1942) in the derivation of their empirical relation. Since the period is shorter, the maximum magnitude of the earthquake is 6.18. However, if the magnitude of the 1945 earthquake was less than 6.8 (Gençoğlu assigned a magnitude of 5.1 to the 1945 earthquake), then, an earthquake having magnitude greater than 6.0 may occur at any time.

Although it is rather difficult to speculate on this type of calculations, there is no doubt that an earthquake with a magnitude of about 6.0 may strike the region at any time by taking into account its regional seismicity.

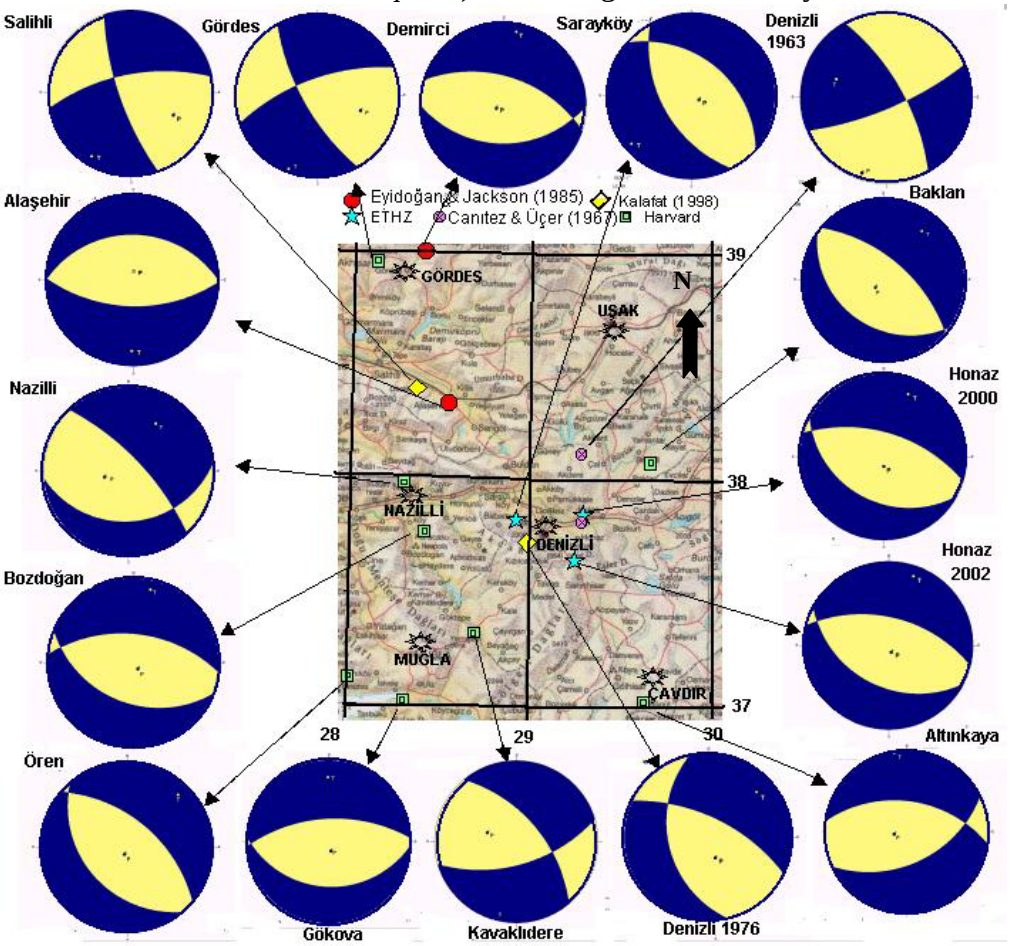

Figure 6. Faulting mechanisms of earthquakes within Latitudes 37-39 and Longitudes 27-29

3.4 Faulting Mechanisms of Past Earthquakes

Faulting mechanisms of earthquakes occurred within the region bounded by Latitudes 37-39 and Longitudes 27-29 are obtained by several researchers and institutes, specifically Canıtez and Üçer (1967) for 1963 Denizli and 1965 Honaz earthquakes, Kalafat (1998) for 1965 Salihli and 1976 Denizli earthquakes, Eyidoğan and Jackson (1995) for 1969 Demirci and Alaşehir earthquakes, ETHZ for earthquakes between 2000-2002 and Harvard for earthquakes between 1986 and 1999 and they are shown in Figure 6. Although the dominant faulting mechanism is normal faulting, the lateral strike slip components are also observed. For northern boundary faults, the lateral strike slip component is dextral while it is sinistral for southern boundary faults in the basins.

The focal plane solutions of the recent Buldan earthquakes indicated that the earthquakes with magnitudes of 5.2, 5.6 and 5.0 are related with normal faulting with large sinistral lateral movements while the earthquake with a magnitude of 4.9 is almost due to normal faulting (Aydan, 2003; Aydan and Kumsar, 2004).

4 CHARACTERISTICS OF POSSIBLE EARTHQUAKES FROM ACTIVE FAULTS

4.1 Inferred Faulting mechanisms of Possible earthquakes from Faults

The striations and internal structure of the faults are just evidences of stress state caused them, and they may also indicate the type of earthquake they produced. Therefore, the data for the faults for a given region may be used to infer the possible mechanism and characteristics of earthquakes. For such a study, the young faults must be given priority. The methodology for the inference of the possible mechanism of the faults require data on dip, dip direction and striation orientation (Aydan, 2000). A large scale map of the active faults of Turkey is prepared by MTA. The faults in the region around Denizli are associated with B. Menderes, Gediz. Honaz-Çivril and Karacasu-Dandalaz basins. Their strikes can be grouped as NW-SE, E-W and NE-SW. Figure 7 also shows the distribution of active faults in the Denizli province together with inferred faulting mechanisms using the measurements done by the authors and the method proposed by Aydan *et al.,* (2002). Faulting mechanism must be in the form of normal faulting with a small amount of sinistral or dextral slip for the region.

4.2 Inference of Characteristics of Possible Earthquakes

Aydan and his co-workers (Aydan *et al.,* 1996, Aydan 1997; Aydan and Kumsar, 1997; Aydan and Hasgür 1997; Aydan *et al.,* 2002) proposed various empirical relations among several parameters of the earthquakes based on Turkish earthquake data only. The methodology proposed by Aydan *et al.,* (2002) is the determination of characteristics of earthquakes through the utilization of the surface trace length of the fault. Although the actual length of faults may be longer than their surface trace length, it may be useful for determining the earthquake characteristics. First the magnitude of earthquake is either obtained graphically or non-linear back analysis of the empirical relations of Aydan (1997). Once the magnitude of the earthquake is determined, then the other characteristics of the expected earthquakes can be obtained from the other empirical relations.

For example the trace length of the Pamukkale fault is about 35 km. For this fault trace length, it is expected that an earthquake with a magnitude of 6.3 may occur. Its faulting mechanism is likely to be similar to those shown for Gölemezli and Karahayıt (see Figure 7). The computed characteristics of possible earthquakes for each fault are given in Table 2.

Table 2. Inferred characteristics of the earthquakes for Denizli region

Fault		Magnitude M_s	Depth (km)	Amax (Gal) (R=25km)	RVHA	UMAX (cm)
Name	Length (km)					
Pamukkale	35	6.30	19.96	432	0.51	35.0
Babadağ – Honaz	29	6.17	19.11	385	0.51	29.0
Buharkent-Sarayköy	39	6.37	20.44	461	0.51	38.0
Çal-Çivril	42	6.42	20.79	483	0.51	42.0

4.3 Shaking Characteristics of Past Earthquakes

One of the first strong motion station was established in Denizli in 1973 and the record was taken during the earthquake of August 19, 1976 with a magnitude of 5.1 (DAD). This earthquake was very close to Denizli city center and it was probably associated with Babadağ–Honaz fault with a dominant normal faulting mechanism. The NS component of this earthquake was 340gal and it is yet the largest strong

motion record in Denizli. Figure 8 shows acceleration response spectra of three components of several earthquakes including the 1976 earthquake. The relative acceleration response spectra exceed the designated relative acceleration of Turkish Seismic Design Code. The results also indicate that if the ground accelerations are similar to those of the 1976 earthquake, RC buildings having a story number more than 8 may be severely affected by the earthquakes.

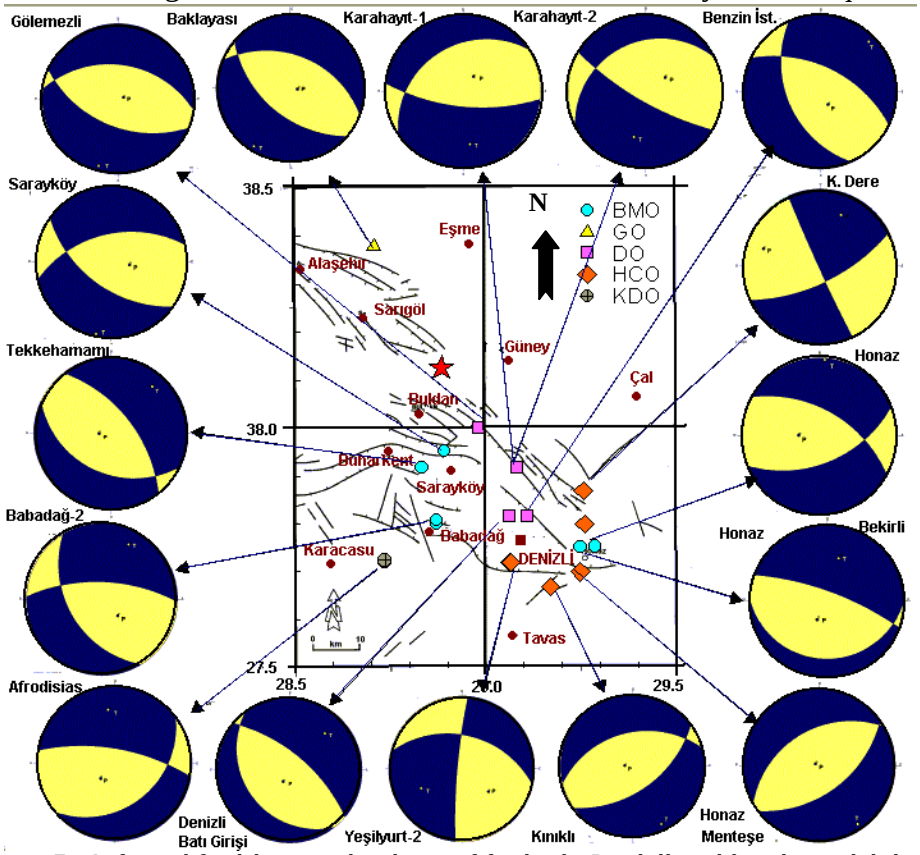

Figure 7. Inferred faulting mechanisms of faults in Denizli and its close vicinity

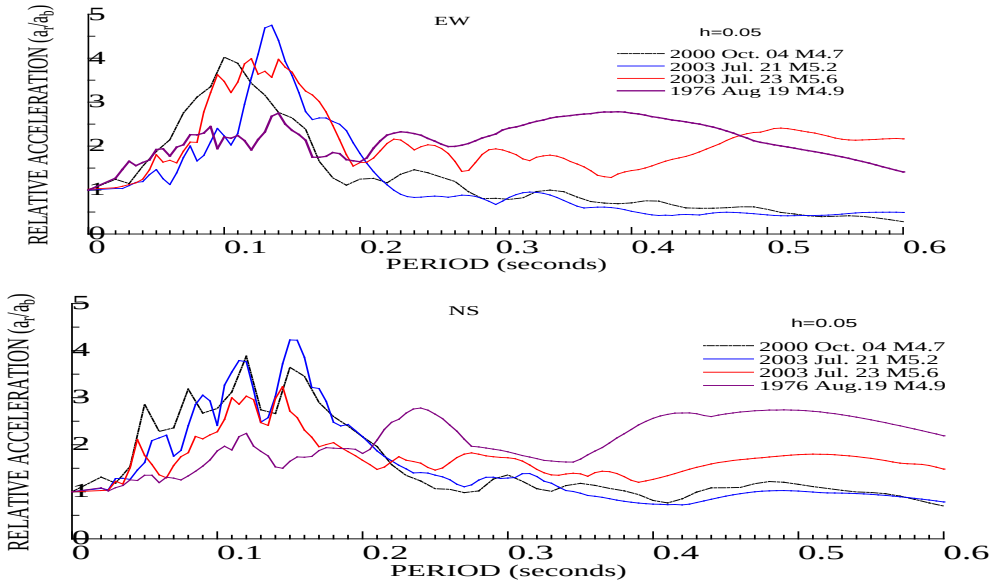

Figure 8. Acceleration response spectra of several earthquakes nearby Denizli

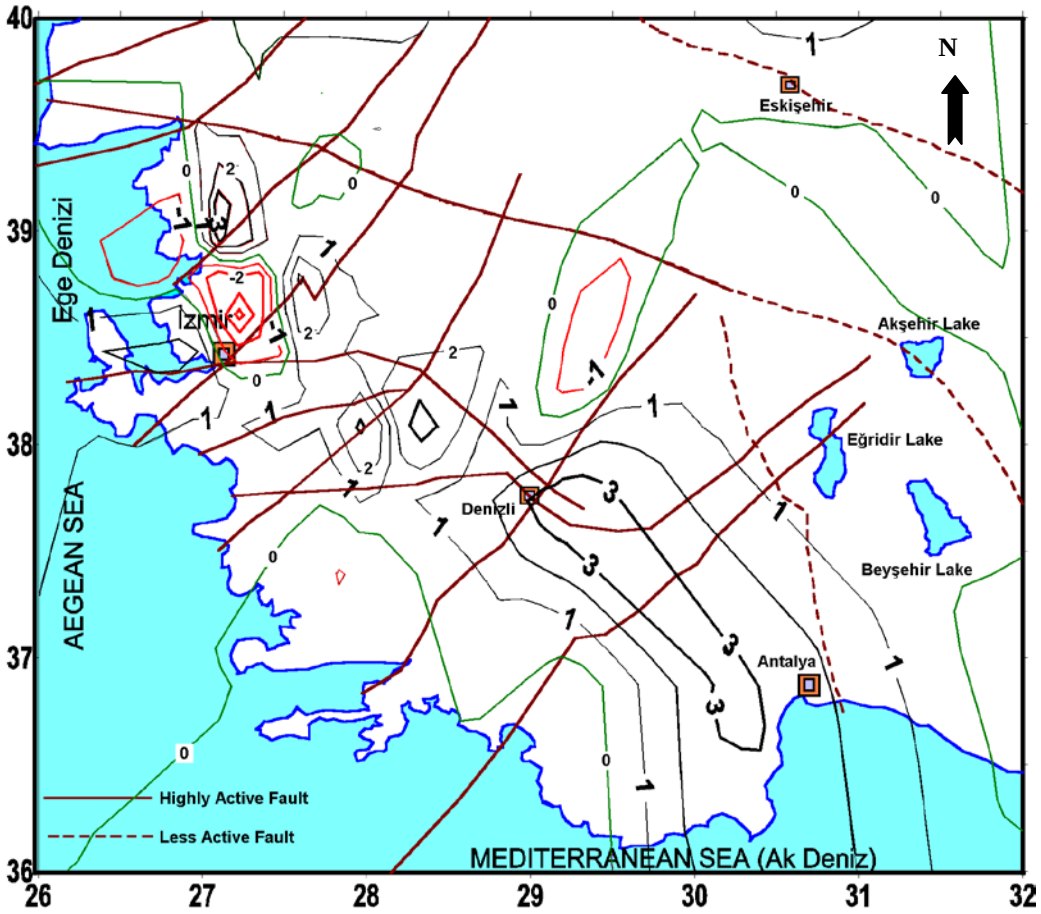

Figure 9. Mean stress rate distributions computed from GPS measurements between 1988-1994 (Aydan et al. 2000b)(contours show the mean stress rate value in kPa/year)

5. CURRENT CRUSTAL STRAINING IN THE VICINITY OF DENİZLİ

From the crustal deformation measurements by GPS (Reilenger et al., 1997) and computations of mean stress variations, it is clarified that the region is undergoing a stretching strain regime (Aydan 2000, 2003; Aydan *et al.*, 2000a). Figure 9 shows the mean stress rate distribution in the Western Turkey, in which the highest stress rate concentration occurs in the Denizli. The concentration of the mean stress rate nearby İzmir has a compressive while it is tensile in Denizli area. The mean stress rate is particularly of great concern since it has a tensile character and such a stress field should result on the reduction of the normal stress and increase in shear stress on the faults. Under these circumstances, any earthquake should be due to normal faulting with or without lateral strike-slip component.

6. CONCLUSIONS

Several aspects such geology, tectonics, faulting and shaking characteristics and current crustal straining of Denizli province are presented. The conclusions from this study may be summarised as follows:

- *The faulting mechanism of regional earthquakes indicated that the classical horst-graben concept is not sufficient to explain the earthquake mechanism in Denizli province.*
- *Although the dominant faulting mechanism is normal faulting, the lateral strike slip components also observed. For northern boundary faults, the lateral strike slip component is dextral while it is sinistral for southern boundary faults in the basins.*
- *The magnitude of earthquakes*

inferred from fault traces may range between 6.3 and 6.5.

- *The regional seismicity has an average recurrence period of 40 years with an activity period of 10 years. The region presently has been experiencing one of the seismic activities.*
- *An earthquake with a magnitude of greater than 6.0 may strike the region at any time by taking into account the past seismicity of the region.*
- *From the crustal deformation measurements by GPS and computations of mean stress variations, the highest mean stress concentration with a tensile character occurs in the Denizli, which may be interpreted such that an earthquake due to normal faulting with or without lateral strike-slip component is likely.*
- *The relative acceleration response spectra of past earthquakes of Denizli province exceed the designated relative acceleration of Turkish Seismic Design Code.*

REFERENCES

Aydan, Ö., 1997. Seismic characteristics of Turkish earthquakes," *Turkish Earthquake Foundation*, TDV/TR 97-007.

Aydan, Ö., 2000. A stress inference method based on GPS measurements for the directions and rate of stresses in the earth' crust and their variation with time. *Yerbilimleri*, 22, 21-32.

Aydan, Ö. (2003): The earthquake prediction and earthquake risk in Turkey and the applicability of Global Positioning System (GPS) for these purposes. *Turkish Earthquake Foundation*, TDV/KT 024-87, 1-73 (in Turkish).

Aydan, Ö. and Hasgür, Z., 1997. Acceleration characteristics of Turkish earthquakes. *The 4th National Earthquake Engineering Conference*, 30-37.

Aydan, Ö. and Kumsar, H., 1997. A site investigation of Oct. 1, 1995 Dinar Earthquake," *Turkish Earthquake Foundation*, TDV/DR 97-003, 116.

Aydan, Ö., Sezaki, M. and Yarar, R. 1996. The seismic characteristics of Turkish Earthquakes, *The 11th World Conf. on Earthquake Eng.*, CD-2, Paper No:1270.

Aydan, Ö. ve Kumsar, H., 2004. Features of the 2003 Buldan earthquakes and an evaluation of damaged Roman underground tombs in Yenice (Denizli). *Bulletin of Engineering Geology of Turkey*, No.20, 61-73 (in Turkish).

Aydan, Ö., Kumsar, H. and Ulusay, R., 2000a. The implications of crustal strain-stress rate variations computed from GPS measurements on the earthquake potential of Turkey. *International Conference on GIS on Earth Science Applications* 2000, Menemen.

Aydan, Ö., Ulusay, R. and Kumsar, H., 2000b. "An approach for earthquake occurrences in Western Anatolia through GPS measurements," *The Symp. on Earthquake Potential of Western Anatolia*, 279-292.

Aydan, Ö, Kumsar, H. and Ulusay R., 2002. How to infer the possible mechanism and characteristics of earthquakes from the strations and ground surface traces of existing faults. *JSCE, Earthquake and Structural Engineering Division*, Vol. 19, No.2, 199-208.

Ayhan, E., Alsan, E., Sancaklı, N. and Üçer, S.B., 1981. A catalog of earthquakes for Turkey and

surrounding area (1881-1980). Boğaziçi University (in Turkish).

Canıtez, N. and S.B. Üçer, 1967. Computer determinations for the fault plane solutions in and near Anatolia, *Tectonophysics*, 4(3), 235-244.

Ceylan, A,. 2000. Buldan-Tripolis antik kenti ve Buldan nekropolü kazı çalışmaları – (Scavia Tripolis nella necropoli di Buldan – Tripolis), *Lykos Vadisi Türk Arkeoloji Araştırmaları*, Ed. by F. D'Andria and F. Silvesterelli, pp 69-95.

Ergin, K., Güçlü, U. and Uz, Z., 1967. A catalog of earthquakes for Turkey and surrounding area. ITU, Faculty of Mining Engineering, No. 24.

Eşder, T., 1994. Denizli dolayındaki jeotermal sistemler ve jeotermal enerjinin Denizli için önemi. *I. Kızıldere Jeotermal Sahasından Denizli İl Merkezinin Isıtılabilirliği ve Sorunları Paneli*, PAÜ-Denizli, s 19-33.

Eyidoğan, H., Güçlü, U., Utku, Z., Değirmenci E., 1991. Türkiye Büyük Depremleri Makro-sismik Rehberi (1900-1988). ITU, Maden Fakültesi, 198p.

Eyidoğan, H. and J. Jackson, 1995. A seismological study of normal faulting in the Demirci, Alaşehir and Gediz earthquakes of 1969-1970 in the Western Turkey. Implications for the nature and geometry of deformation in the continental crust. *Geophys. J. R. Astr. Soc.*, 81, 569-607

ETHZ. Automatic Moment Tensor Solutions. http://www.seismo.ethz.ch/mt/

Gençoğlu, S., İnan, E., Güler, H. 1990. Türkiye'nin Deprem tehlikesi. TMMOB, Jeoloji Mühendisleri Odası, 1-701p. Ankara.

Gutenberg, B. and Richter, C.F., 1942. Earthquake magnitude, intensity, energy and acceleration. *Bulletin of Seismological Society of America*, 32, 163-191.

Harvard University Seismology web: http://www.seismology.harvard.edu

MTA, 1992. Active fault map of Turkey, Maden Tetkik Arama Genel Müdürlüğü, Ankara, Turkey.

Özkul, M., Kumsar, H., Gökgöz, A., 2000. Caratteri geologici, geografici ed hidrogeologici del bacino del fiume Çürüksu (Çürüksu havzasının jeolojisi). *Ricerche Archeologiche Turche Nella Valle del Lykos* (Lykos Vadisi Türk Arkeoloji Araştırmaları), *a cura di F. D'Andrida e F.Silvestrelli*, Italy 327-348.

Reilinger, R.E, S.C. McClusky, M.B., Oral, R.W., King, M., Toksöz, N., Barka, A.A., Kınık, I., Lenk, O. and Şanlı I., 1997. Global positioning system measurements of present-day crustal movements in the Arabia-Africa-Euroasia plate collision zone, *J. Geophysical Research*, 102(B5), 9983-9999.

Uysal, Ş., 1995. Denizli ve çevresinin jeoloji haritası, MTA Genel Müdürlüğü, Ankara.

(This page is left blank intentionally.)

SEISMIC RISK OF QUATERNARY SOIL DEPOSITS FOR LONG DISTANCE EARTHQUAKES IN İZMİR METROPOLITAN AREA

Kuruoğlu M. and Özden G.

Dokuz Eylül Univ., Dept. of Civil Eng., Buca-İzmir,
mehmet.kuruoglu@deu.edu.tr, gurkan.ozden@deu.edu.tr

Abstract: Today's growing population of metropolitan areas increasingly forces local and national authorities to take risks in their decisions of new urbanization area designations in seismically active regions. Alluvial sites in or nearby coastal regions have traditionally been known as high-risk areas of seismicity. Historically, people avoided urbanizing on such grounds as much as possible. However, technological advances in construction technologies combined with the growing need for more residential and industrial buildings have been resulted in dense population on marginal lands. The city of İzmir demonstrates major examples of this kind of urbanization.

Following the devastating Marmara Earthquake occurred in 1999 and some other smaller scale events, an interest and fear have been grown in national scale regarding the safety of buildings and facilities on alluvial sites of seismically active regions. This interest fed by fear originating from inadequate knowledge about soil and structure behavior provoked several speculations regarding safety of buildings on marginal lands. Unfortunately, well-engineered structures were also affected by such speculations sometimes losing their economic values significantly.

Today the need for reliable microzonation is greater than ever in metropolitan areas like İzmir. City officials are mostly uninformed and subject to easy manipulation regarding their decisions for prospective urban areas on thick alluvial soil deposits. The goal of this study is to investigate seismic risk of Quaternary age soil deposits for long distance earthquakes in İzmir metropolitan area. The development of a new strategy was attempted with the combined use of deterministic and probabilistic methods for the city of İzmir.

Key words: Seismic risk, Quaternary, Site response, Microzonation, İzmir

1. INTRODUCTION

Seismic hazard analyses involve the quantitative estimation of the risk of a site either using deterministic methods when a particular earthquake scenario is assumed or utilizing probabilistic approaches where uncertainties in earthquake size, location, and occurrence times are questioned. It is well known that local soil conditions play a significant role on seismic ground motion parameters that would directly govern structural design (Seed et al., 1987 & 1990; Ansal et al., 2001). Estimation of ground motion parameters via appropriate numerical site response analyses can better take local soil characteristics into consideration. The success of numerical site response analyses, however, largely depends on the reference motion defined at the bedrock of the soil profile. The probabilistic nature of ground motion parameters, however, may not be present in numerically computed data if the reference motion is taken arbitrarily harming the reliability of the results achieved in numerical analyses. This aspect of microzonation studies has been already taken attention of researchers (Marcellini et al., 2001). It appears that best answers to this problem can be provided by means of the combined use of deterministic and probabilistic methods (McGuire, 2001). For instance, it would be appropriate to know the probabilistic risk of a scenario motion in microzonation and performance based structural analysis studies. It is even better to conduct deterministic analyses with probabilistic information available so that results could be related to the national and/or regional seismic code requirements.

The decision for the most critical rupture location(s) for a site can be made following the below given procedure suggested for generation of the reference

motion: Firstly, the seismicity for the site is investigated, and seismic sources surrounding the site are determined. During this stage, dynamic soil characteristics in the site have to be known. Effects of close and long distance earthquakes on the site are evaluated depending on dynamic soil characteristics. Then, probabilistic analyses are performed to obtain probability of potential rupture locations at closest distance(s) to the site. A decision is then made regarding critical close and long distance rupture locations.

The city of İzmir was subject to major destructive earthquakes from historical ages to recent times due to the tectonic activity in Western Anatolia. The 1688, 1739 and 1778 earthquakes caused significant damage in İzmir during historical period (Ambraseys and Finkel, 1995; Oikonomos and Slaars, 2001). Major instrumental seismic period earthquakes occurred in İzmir and surrounding area are the 1928 Torbalı (M=6.5), 1939 Dikili (M=6.5), 1949 Karaburun (M=6.6), 1974 İzmir (M=5.5), 1977 İzmir (M=5.3), 1992 Doğanbey (M=6.0), and 2003 Urla (M=5.6) earthquakes (BU-KOERI, 2003; GDDA-ERD, 2003). Major seismic sources producing destructive earthquakes in the vicinity of İzmir can be defined as the İzmir Fault and faults located in the Karaburun Peninsula (Figure 1).

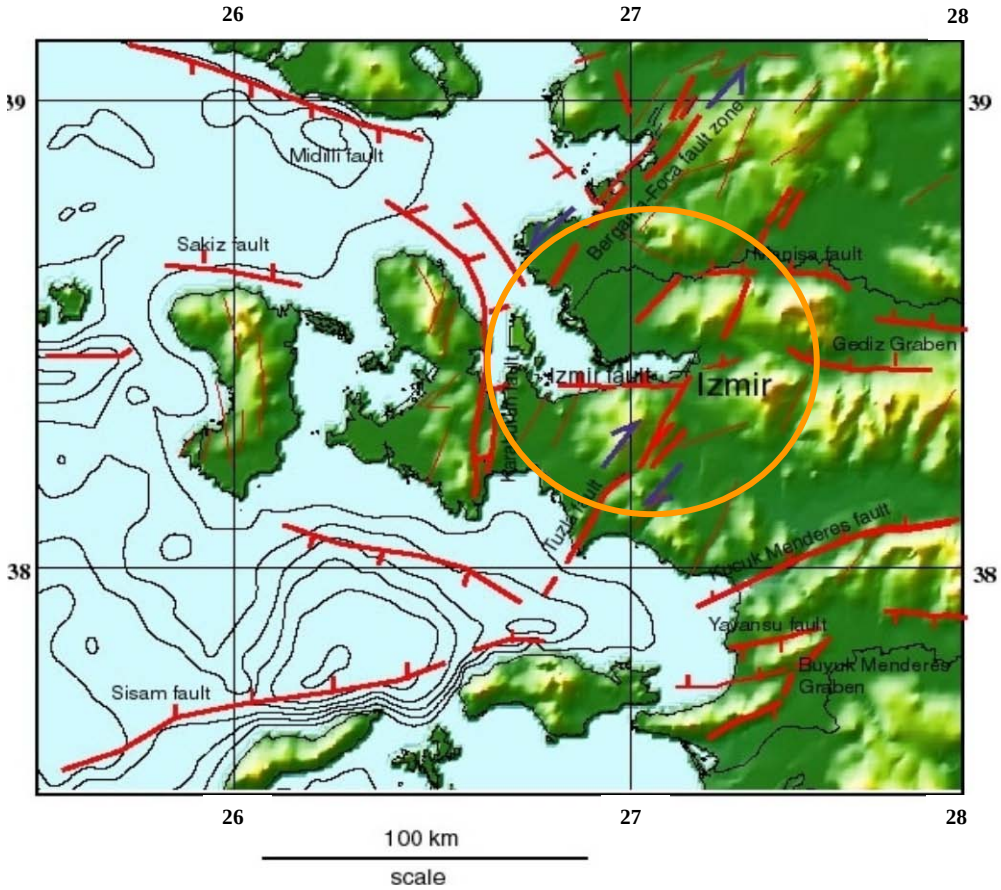

Figure 1. Critical faults and seismic risk area for seismic risk analyses of İzmir

Recent seismic vulnerability studies have shown that the İzmir Fault shall be considered as a major seismic source that would impose significant impact on the city in close distance (Ansal, 1995; RADIUS, 1999). Based on the evaluation of earthquake activities in both historical and instrumental periods (Ambraseys and Finkel, 1995; BU-KOERI, 2003; GDDA-ERD, 2003), it would be appropriate to evaluate the Karaburun Fault as a critical long distance seismic source as well. One should note that the epicenter of the 2003 Urla Earthquake was also in the peninsula

and this earthquake generated considerable damage on several buildings located on alluvial sites in Manavkuyu region indicating presence of dominating long period harmonics during the earthquake (GDDA-ERD, 2003).

Although the scenario earthquake based deterministic risk analysis of İzmir was performed considering the scenario motion that would take place on the İzmir Fault (RADIUS, 1999), such an analysis has not yet been performed for critical long distance seismic source. In an attempt to pursue such an analysis, a soil properties database has been established and the spatial uncertainties were calculated for the Karaburun Fault.

The "Soil Properties" database has been constructed using a readily available database platform. This database includes the geotechnical data obtained from 238 boring locations and 106 CPT locations in alluvial regions along the northern coast of İzmir Bay. Index and engineering properties of soils in project area have been stored in "Geotechnical Properties" database. The geotechnical data stored in the constructed database were acquired through relatively shallow boreholes. The deepest borehole in the database was 55m long. However, bedrock in the study area exists between 150-250m elevations. The gap between end of borehole logs and the bedrock level was filled using the porosity-depth (Poland, 1984) and undrained shear strength-effective stress (Skempton and Sowa, 1963) models.

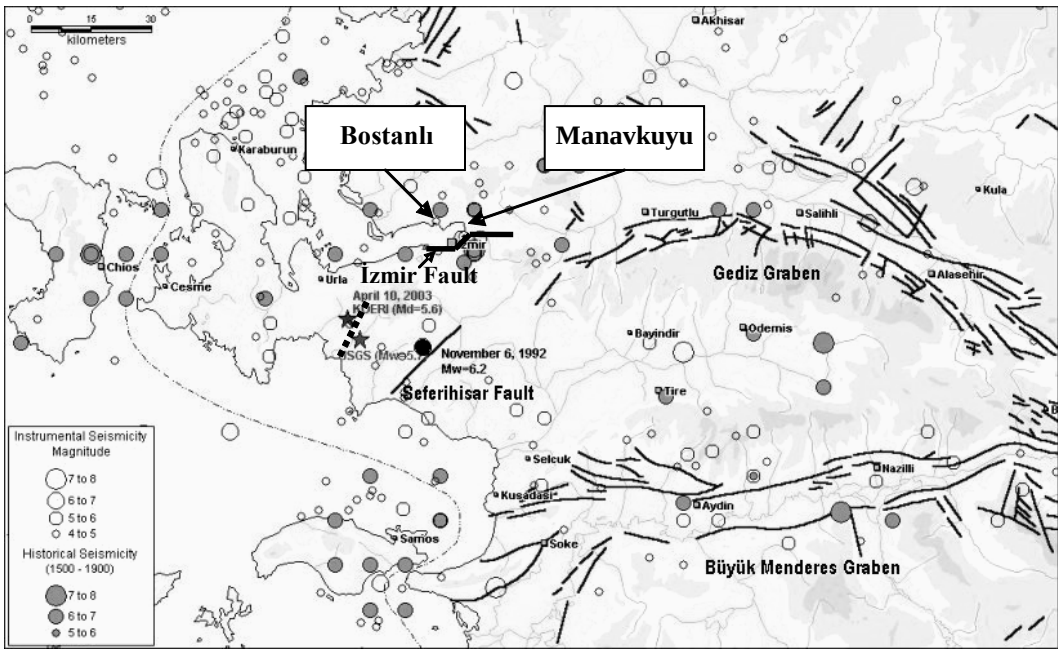

Figure 2. Bostanlı and Manavkuyu regions

2. ALLUVIAL SITES IN BOSTANLI AND MANAVKUYU REGIONS

Manavkuyu and Bostanlı are two major districts of the city where thick and saturated Quaternary age alluvial deposits constitute the dominant soil profile. Geological and geotechnical characteristics of both regions are quite similar to each other. The 2003 Urla Earthquake caused the widespread damage on several buildings located on alluvial sites in Manavkuyu region. Locations of the regions and the epicenter of the 2003 Urla Earthquake are shown in Figure 2.

The central segment of the Karaburun Fault has been found to be the most critical long distance seismic source for Bostanlı area. The maximum bedrock acceleration values for a scenario earthquake (M=6.5) originating from the central segment of the Karaburun Fault were estimated using the recently

developed attenuation relationships (Abrahamson and Silva, 1997; Boore et al., 1997; Campbell, 1997; Sadigh et al., 1997; Spudich et al., 1997).

3. DYNAMIC SITE RESPONSE ANALYSES

The original ground motion of 10.04.2003 Urla Earthquake (M_w=5.6) was recorded in the eastern section of İzmir (GDDA-ERD, 2003). The maximum acceleration was recorded as 0.079g on the ground surface. Deconvolution was performed in order to compute bedrock motion from ground surface motion for idealized soil profile in the location of the recording station. This process has been made following one-dimensional site response analysis method (Bardet et al., 2000), and the maximum bedrock acceleration was calculated as 0.031g. Frequency histogram of the 2003 Urla Earthquake at the bedrock is shown in Figure 3. The fundamental frequency is found as 0.78 Hz, and the Fourier amplitude distribution give maximum value on 0.4-2.8 Hz band. The frequency histogram is typical for long distance earthquakes with low frequency content. Therefore, the acceleration record of the 2003 Urla Earthquake strong motion can be used as a representative long distance strong motion record for the alluvial sites of the city.

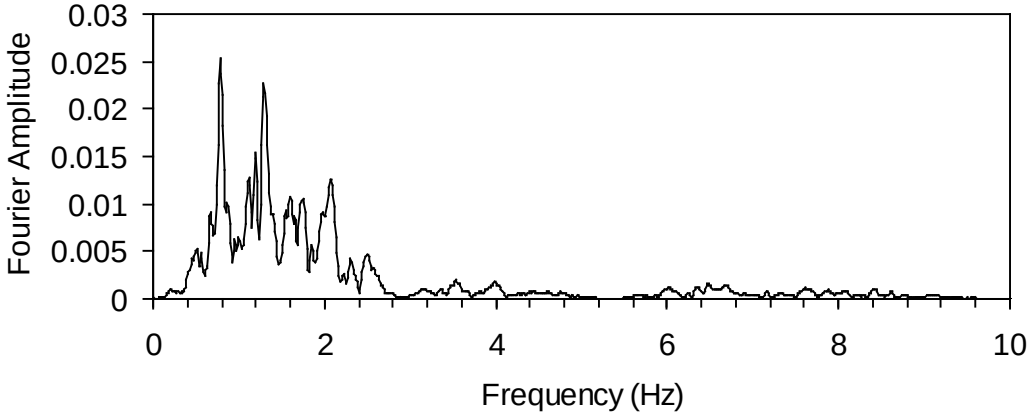

Figure 3. Frequency histogram of the 10.04.2003 Urla Earthquake (M = 5.6, f_0 = 0.78 Hz)

Table 1. Results of Dynamic Site Response Analyses for Long Distance Earthquakes (Özden and Kuruoğlu, 2004)

Boring No.	10.04.2003 Urla Earthquake (M_w=5.6)					Urla Scenario Earthquake (M=6.5)				
-	$a_{max,s}$ (g)	$a_{max,s}$ / $a_{max,r}$	$S_{a,max,s}$ (g)	$S_{a,max,s}$ / $S_{a,max,r}$	T_0 (s)	$a_{max,s}$ (g)	$a_{max,s}$ / $a_{max,r}$	$S_{a,max,s}$ (g)	$S_{a,max,s}$ / $S_{a,max,r}$	T_0 (s)
140	0.191	4.24	0.670	5.07	0.82	0.402	4.32	1.40	5.12	0.82
141	0.179	3.98	0.635	4.80	0.82	0.364	3.91	1.29	4.73	0.82
169	0.172	3.82	0.651	4.92	0.82	0.391	4.20	1.37	5.02	0.82
133	0.14	3.41	0.588	4.88	0.64	0.297	3.38	1.00	3.87	0.74
134	0.137	3.34	0.535	4.44	0.64	0.302	3.43	0.98	3.78	0.74
135	0.156	3.80	0.576	4.78	0.64	0.287	3.26	0.96	3.70	0.82

Two parcels were selected at Bostanlı and Manavkuyu regions to examine the effect of long distance earthquakes on the results of dynamic site response analysis. Boreholes tagged as #140, #141 and #169 in the database are located in Bostanlı, whereas #133, #134 and #135 boreholes belong to Manavkuyu (Kuruoğlu, 2004). Dynamic site-response analyses have been performed for 10.04.2003 Urla Earthquake (M_w=5.6) record and its the scaled up version (i.e. scaled up for the scenario earthquake M=6.5). Results of analyses are given for long distance earthquakes in Karaburun Peninsula in Table 1. The maximum ground surface

acceleration, $a_{max,s}$ (g); the maximum bedrock acceleration, $a_{max,r}$ (g); the amplification ratio ($a_{max,s}$ / $a_{max,r}$); the maximum ground surface spectral acceleration, $S_{a,max,s}$ (g); the maximum bedrock spectral acceleration, $S_{a,max,r}$ (g); the spectral amplification ratio ($S_{a,max,s}$ / $S_{a,max,r}$); and the fundamental period of earthquake motion, T_0 (s) are presented in this table.

This long distance earthquake has shown significant amplification effect in Bostanlı and Manavkuyu regions. The amplification ratio ($a_{max,s}/a_{max,r}$) was found as 3.8-4.2 in Bostanlı, and determined as 3.4-3.8 in Manavkuyu. The average amplification ratio value has been obtained as 4.15 in Bostanlı and 3.5 in Manavkuyu taking all borehole data into consideration. The spectral amplification ratio ($S_{amax,s}/S_{amax,r}$) was computed as 4.8-5.1 in Bostanlı, and found as 4.4-4.9 in Manavkuyu areas. The average spectral amplification ratio has been determined as 5.1 in Bostanlı and 4.7 in Manavkuyu. One should note that these amplification ratio levels are much larger than those accepted in a previous seismic hazard evaluation of the city (RADIUS, 1999; Düzgün et al, 2001).

High values of amplification are expected since Urla Earthquake ground motion has lower frequency harmonics resulting in resonance effects in saturated, deep Quaternary alluvial soil profiles along the İzmir Bay area. Long distance and large scale earthquakes can cause major problems in soft coastline deposits. Maximum ground surface spectral accelerations have also attained high values. Spectral accelerations have values of at least 1.0g, and can reach to 2.0g in some boring locations. Maximum ground surface accelerations can reach to 0.4g and may be greater than 0.4g at some boring locations for scenario earthquake motion.

Response spectra of acceleration for close and long distance scenario earthquake motions were presented in Figure 4 for borehole locations in Table 1. The effective peak acceleration can be determined as 0.6g (S_A/2.5) for these locations.

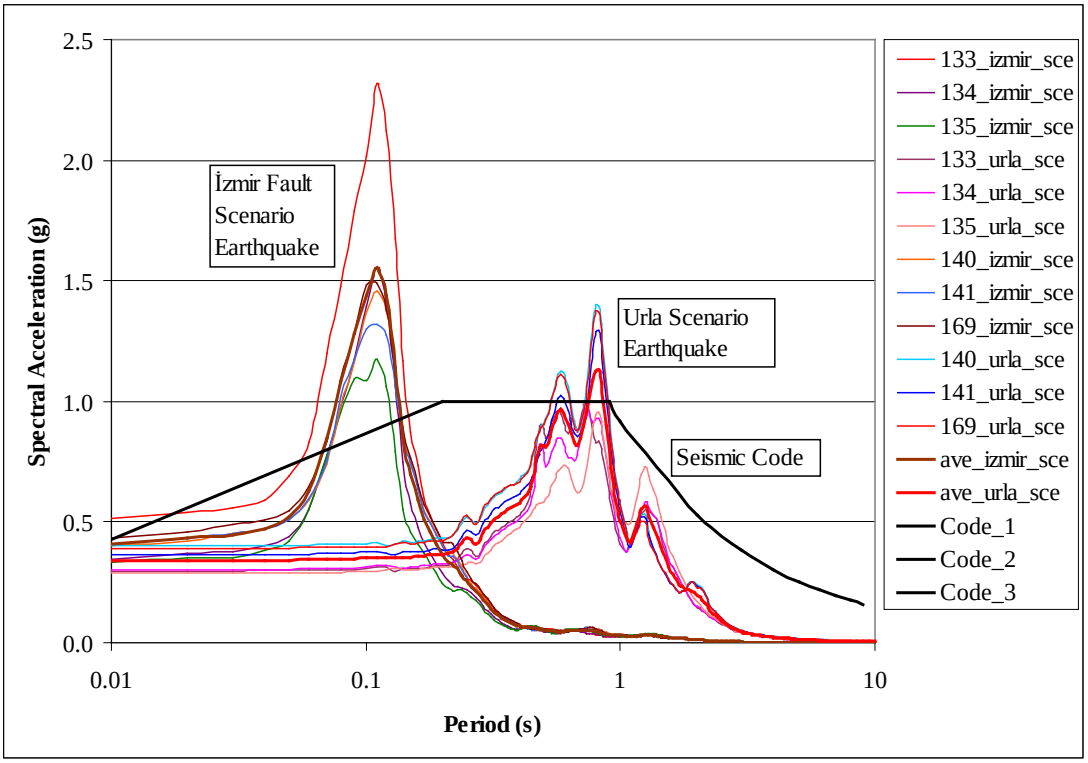

Figure 4. Acceleration response spectra for close and long distance scenario earthquakes

It has been shown in Figure 4 that, fundamental period of earthquake motion is 0.11s for close distance scenario earthquake motion, and is about 0.74-0.8s for long distance scenario earthquake motion. These values cover the characteristic period interval (T_A=0.2s and T_B=0.9s) for Z4 type of soils (saturated and deep alluvial deposits) defined in the Seismic Code of Turkey (1998).

In order to enrich the acceleration spectrum graph in terms of frequency content, acceleration records of Coalinga and Loma Prieta earthquakes have been also added in strong ground motion database. Dynamic site response analyses have been performed for idealized soil profiles of Bostanlı and Manavkuyu regions using close and long distance scenario earthquake motions, and acceleration records of Coalinga and Loma Prieta earthquakes. Maximum spectral acceleration values computed for these earthquakes exceed 2.0g in Bostanlı close to the fundamental period of 0.4s. Spectral accelerations calculated for the İzmir Fault scenario earthquake motion were less than those computed using Coalinga and Loma Prieta earthquakes. Majority of the structures in Manavkuyu area are high-rise buildings with 8 to 10 stories. Conditions of these buildings following the earthquake were assessed by the governmental agencies. Fundamental periods of damaged buildings were calculated according to national seismic code provisions and found to be in the range of 0.7-0.85s and 0.45-0.5s for 8-10 and 4-5 story high apartment buildings, respectively. The dominant period of motion at ground surface for the Urla Earthquake is within the 0.7-1.0s range. It is highly likely that near resonance conditions took place during the earthquake causing buildings to undergo several loading cycles. This explains the reason of major damage at high-rise buildings with 8 to 10 stories. It would be appropriate to design such high rise buildings taking locally produced elastic design spectra such as the ones presented in this study into consideration as the Seismic Code of Turkey recommends in a general manner. Besides, it would be more beneficial to add additional requirements to the code for alluvial sites similar to those here.

4. CONCLUSIONS

In this study, site-specific analyses have been used in decision of design ground motion for the city of İzmir. In this way, the effect of local site conditions and earthquake characteristics were taken into consideration and this study has become a microzonation study for the northern coast of İzmir Bay area. Results of site-response analyses are interpreted according to national seismic code and commonly used provisions in the United States (ATC 3-06, 1984; UBC, 1991; NEHRP, 2001).

Location of the site and characteristics of the earthquake have significant effect on maximum ground surface accelerations. In the Seismic Code of Turkey (1998), effective ground surface acceleration coefficient A_0 has been suggested as 0.4g for Z4 type soils (alluvial soil deposits, soft/very soft clays, loose/very loose sands). In current national engineering practice, effective peak ground acceleration is taken as maximum ground surface acceleration. However, effective ground acceleration can be close to or greater than maximum ground acceleration for long distance earthquakes. Fundamental period and frequency content of the ground motion at bedrock level are major characteristics to cause the difference (Özden and Kuruoğlu, 2004).

It would be appropriate to design high rise buildings taking locally produced elastic design spectra such as the ones presented in this study into consideration as the Seismic Code of Turkey recommends in a general manner. Besides, it would be more beneficial to add additional requirements to the code for alluvial sites similar to those here.

The period corresponding to maximum spectral acceleration is very close to the fundamental period of the 8-10 story high structures in Manavkuyu region. Therefore, various levels of damages were observed at buildings in Manavkuyu following the Urla Earthquake. Although amplification values are greater in Bostanlı than those in Manavkuyu, important damage was not observed in Bostanlı. The reason for this observation can be explained by the fact that the fundamental periods of 18-22 story buildings in Bostanlı are away from the period range corresponding to maximum spectral acceleration values. Besides, 8-10 story high buildings are scarce in Bostanlı area, and were build on long pile foundations probably enlarging their natural periods.

Parcel based site-specific analyses and microzonation studies taking into account geotechnical characteristics of saturated, thick and soft Quaternary alluvial formations and bedrock depth may be encouraged in national seismic code and local provisions. Such additional regulations would be highly beneficial for high-rise structures in İzmir and similar provinces with marginal soil conditions.

REFERENCES

Abrahamson, N.A. and Silva, W.J., 1997. Empirical Response Spectral Attenuation Relations for Shallow Crustal Earthquakes, *Seismological Research Letters, 68, No.1,* 94-127

Ambraseys, N.N. and Finkel, C.F., 1995. The Seismicity of Turkey and Adjacent Areas, A Historical Review: 1500-1800, *Eren Publ.*, İstanbul, Turkey, ISBN: 975-7622-38-9

Ansal, A.M., 1995. Seismicity in Engineering Design, *Turkish Engineering News, 379,* 26-32 (in Turkish)

Ansal, A., İyisan, R., and Yıldırım, H., 2001. The Cyclic Behaviour of Soils and Effects of Geotechnical Factors in Microzonation, *Soil Dynamics and Earthquake Engineering, 21*, 445-452

ATC 3-06, 1984. ATC 3-06 Amended Tentative Provisions for the Development of Seismic Regulations for Buildings, *Applied Technology Council*, CA, USA, Second Printing, Sec. 1.4.1, 298-305

Bardet, J.P., Ichii, K., and Lin, C.H., 2000. EERA – A Computer Program for Equivalent-linear Earthquake Site Response Analyses of Layered Soil Deposits, *Univ. of Southern California, Dept. of Civil Engineering*, August 2000

Boore, D.M., Joyner, W.B., and Fumal, T.E., 1997. Equations for Estimating Horizontal Response Spectra and Peak Acceleration from Western North American Earthquakes, A Summary of Recent Work, *Seismological Research Letters, 68, No.1*, 128-153

BU-KOERI, 2003. Kandilli Observatory and Earthquake Research Institute, *Boğaziçi University*, İstanbul

Campbell, K.W., 1997. Empirical Near-Source Attenuation Relationships for Horizontal and Vertical Components of Peak Ground Acceleration, Peak Ground Velocity, and Pseudo Absolute Acceleration Response Spectra, *Seismological Research Letters, 68, No.1*, 154-179

Düzgün, M., Hepcanlı, E., and Tüzün, C., 2001. RADIUS – Risk Evaluation Tools Against Seismic Disasters for Municipal Areas, *İzmir Metropolitan Municipality Publ.*, December 2001, İzmir, 65 p. (in Turkish)

GDDA-ERD, 2003. General Directorate of Disaster Affairs, Earthquake Research Department, Ankara

Kuruoğlu, M. 2004. Geographic Information System (GIS) Based Database Development and Evaluation Study for Soils of Northern Coast of İzmir Bay, *PhD Thesis, Dokuz Eylül*

University, Graduate School of Natural and Applied Sciences, İzmir, Turkey, 151 p.

Marcellini, A., Daminelli, R., Franceschina, G., and Pagani, M., 2001. Regional and Local Seismic Hazard Assessment, *Soil Dynamics and Earthquake Engineering, 21*, 415-429

McGuire, R.K., 2001. Deterministic vs. Probabilistic Earthquake Hazards and Risks, *Soil Dynamics and Earthquake Engineering, 21*, 377-384

NEHRP, 2001. NEHRP Recommended Provisions for Seismic Regulations for New Buildings and Other Structures: Part 2-Commentary, *Building Seismic Safety Council, Federal Emergency Management Agency*, 2000 Edition, Washington, USA, 59-62

Oikonomos and Slaars, 2001. Etude sur Smyrne, *İletişim Publ.*, İstanbul, 68 p., Original publication: 1868, ISBN: 975-470-864-9, 244 p., (in Turkish)

Özden, G. and Kuruoğlu, M., 2004. Peak Ground Acceleration for Liquefaction Analysis, Tenth National Congress for Soil Mechanics and Foundation Engineering, İstanbul Technical University, İstanbul, *Proceedings*, 447-456 (in Turkish)

Poland, J.F., 1984. Guidebook to Studies of Land Subsidence due to Ground Water Withdrawal, *UNESCO Report*

RADIUS, 1999). Earthquake Scenario and Master Plan for the Metropolitan Area of İzmir, *Final Report*, Edt: Erdik, M., Boğaziçi University, İstanbul

Sadigh, K., Chang, C.Y., Egan, J.A., Makdisi, F., and Youngs, R.R., 1997. Attenuation Relationships for Shallow Crustal Earthquakes based on California Strong Motion Data, *Seismological Research Letters, 68, No.1*, 180-189

Seed, H.B., Romo, P.R., Sun, J., Jaime, A. and Lysmer, J., 1987. Relationships between soil conditions and earthquake ground motions in Mexico City in the earthquake of September 19, 1985, Earthquake, *Engineering Research Center, University of California, Berkeley*, Report No: UCB/EERC-87/15. 112 p.

Seed, R.B., Dickenson, S.E., Reimer, M.F., Bray, J.D., Sitar, N., Mitchell, J.K., Idriss, I.M., Kayen, R.E., Kropp, A., Harder, L.F., and Power, M.S., 1990. Preliminary report on the principal geotechnical aspects of the October 17, 1989 Loma Prieta Earthquake, *Engineering Research Center, University of California, Berkeley*, Report No: UCB/EERC 90/05, Vol. 2, 351-376

Seismic Code of Turkey, 1998. *Ministry of Public Works and Settlement*, Ankara.

Skempton, A.W. and Sowa, V.A., 1963. The Behaviour of Saturated Clays During Sampling and Testing, *Géotechnique, 13*, 269-290

Spudich, P., Fletcher, J.B., Hellweg, M, Boatwright, J., Sullivan, C., Joyner, W.B., and Hanks, T.C., 1997. SEA-96-A new predictive relation for earthquake ground motions in extensional tectonic regimes, *Seismological Research Letters, 68, No.1*, 190-198

UBC, 1991. Uniform Building Code, *International Conference of Building Officials*, Whittier, California

CRETACEOUS CALCAREOUS NANNOPLANKTON BIOSTRATIGRAPHY OF THE SOUTHERN ROMANIAN BLACK SEA REGION

Melinte M. C.

National Institute of Marine Geology and Geoecology (GeoEcoMar Bucharest), No. 23-25, Street Dimitrie Onciul Street, RO-024053, Bucharest, Romania, e-mail: melinte@geoecomar.ro

Abstract. Calcareous nannoplankton investigations carried out on 22 drillings from the onshore area of the Southern Romanian Black Sea and from one drilling from offshore area of the Southern Romanian Black Sea are presented. The oldest sedimentary sequence, identified as latest Jurassic (Tithonian)-early Cretaceous (Berriasian-Valanginian) - corresponding to the NK1, NK2 and NK3 calcareous nannoplankton zones, is represented by marine shallow water carbonates. The next cycle, late Barremian-early Aptian (corresponding to the NC5 and NC6 calcareous, nannoplankton zones) is also represented again by marine shallow water carbonates. A fluvial-lacustrine formation, middle-late Aptian in age, was intercepted only by the drillings from the onshore. The youngest Cretaceous deposits from the onshore area, Santonian – Maastrichtian in age (proved by the presence of the CC18-CC26 calcareous nannoplankton zones), are mainly composed of chalks, with intercalations of glauconitic sands towards the base. A continuous sedimentation was identified within the Cretaceous/Tertiary boundary interval, only in the chalk deposits offshore the Southern Romanian Black Sea. The Cretaceous climate around the NW Black Sea region was warm, as proved by the character of nannofloral assemblages, but several cooling episodes, in the middle Berriasian, late Valanginian, latest Barremian and Maastrichtian (early and latest) are expressed in the nannofloral fluctuation pattern.

Key words: Cretaceous, nannofloras, biostratigraphy, palaeoclimate, Southern Romanian Black Sea.

1. INTRODUCTION

This paper focuses on the calcareous nannoplankton biostratigraphy of the Cretaceous subsurface deposits from both onshore and offshore areas of the Southern Romanian Black Sea. The investigated region belongs to the eastern part of the Moesian Platform (the Dobrogea sector). The analyzed wells are placed in the subsided block of the South Dobrogea, which is separated from the uplifted block of the Central Dobrogea by the Capidava-Ovidiu Fault (Săndulescu, 1984).

Former stratigraphical studies of the Cretaceous sediments, cropping out in the South Dobrogea, were published by Reuss (1865), Anastasiu (1898), Chiriac (1968), Neagu et al. (1977), Neagu (1986, 1987), Bărbulescu and Neagu (1988), Avram et al. (1988). Although the surface stratigraphy of the Southern Dobrogea has been intensively studied, the data on the subsurface of Southern Dobrogea are scarce. One of the first published papers belongs to Băncilă (1973). In the ’80, the investigation of the subsurface of southern Romanian Black Sea onshore was revitalized, by the drilling of 22 wells in this region, which offered new data on Cretaceous subsurface deposits of the southern Romanian Black Sea onshore (Avram et al., 1993; Ion et al., 1998).

This paper aims to decipher the subsurface Cretaceous stratigraphy of the onshore and offshore regions of the Southern Romanian Black Sea, based on calcareous nannofloral investigations. Another scope of this work is to interpret the nannofloral fluctuation, in terms of paleobiogeographical changes, which took place within the Cretaceous.

2. MATERIAL AND METHODS

Both quantitative and semiquantitative calcareous nannofloral analyses of 22 drillings from the onshore and of one drilling from the offshore of the Southern Romanian Black Sea were performed (Figure 1).

Fig.1

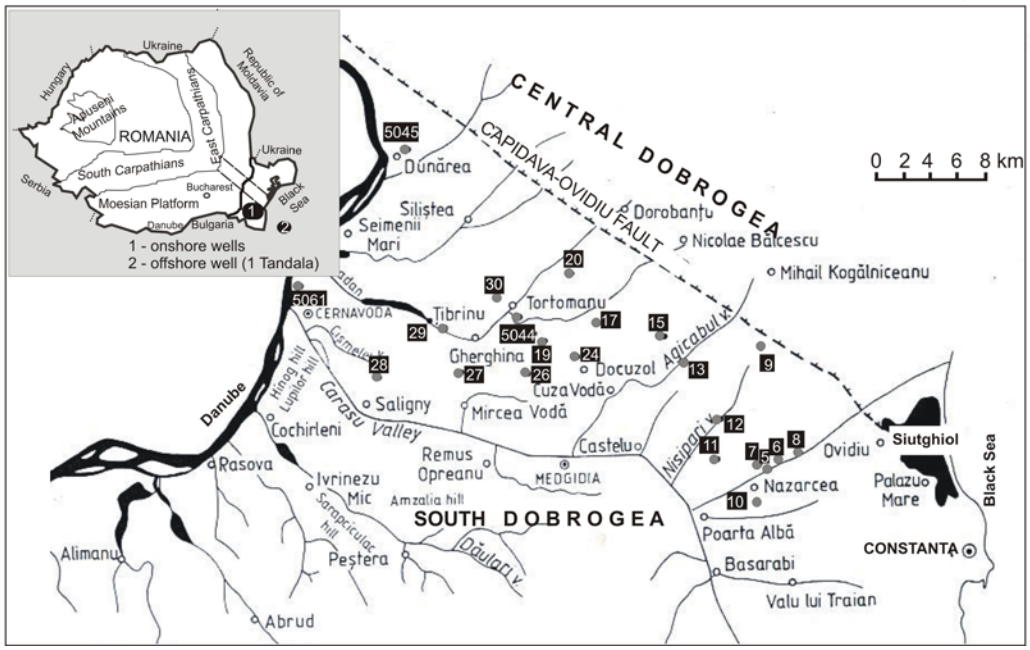

Figure 1. Location of the studied drillings (compiled after Avram et al., 1993 and Ion et al., 1998)

The investigated cores have been taken, in each drilling, at a distance between 25-40 cm. Smear-slides were prepared directly from untreated samples, in order to retain the original sample composition. The calcareous nannofloral analyses were made under a light polarizing microscope at 1600x magnification. For the semiquantitative analyses, at least 300 specimens were counted, the investigation being completed to 200 fields of view in each smear-slide.

3. RESULTS

3.1. Early Cretaceous

The oldest deposits traversed by the drillings from the onshore area of the Romanian Black Sea belong to the Cernavodă Formation and yielded two main facies: a north-western facies, mainly composed of evaporitic rocks, variegated clays, marls and sandstones (the Amara Member, 150-180 m in thickness) and a south-eastern one, mainly made by calcarenites and calcilutites (the Alimanu Member, 150-180 m in thickness) – Figure 2.

The age of the two above-described members is early Berriasian-late Valanginian, as proved by the identified calcareous nannofloral assemblages. The successive first occurrences (FO) of the nannofossils *Cretarhabdus angustiforatus* (Black) Bukry and *Calcicalathina oblongata* (Worsley) Thierstein led to the identification of the NK1, NK2 and NK3 calcareous nannoplankton zones of Bralower et al. (1989).

For semiquantitative studies, four taxonomical groups were counted: (1) *Watznaueria barnesae* (Black) Perch-Nielsen, an extreme cosmopolitan species, resistant to diagenesis; (2) the Tethyan oligotrophic *Nannoconus* species, indicating warm surface waters (Melinte and Mutterlose, 2001); (3) Tethyan taxa, more confined to low to middle latitudes (other than *Nannoconus*), including *Polycostella senaria* Thierstein, *Diazomatolithus lehmanii* Noël, *Conusphaera mexicana* Trejo and *Calcicalathina oblongata*; (4) Boreal taxa (*sensu* Mutterlose, 1992), including *Micrantholithus speetonensis* Perch-Nielsen, *Sollasites horticus* (Stradner) Čepek and Hay, *S. lowiei* (Bukry) Rood et al. and *Crucibiscutum salebrosum* (Black) Jakubowski, nannofossils which indicate cooler water surfaces and a eurytrophic environment.

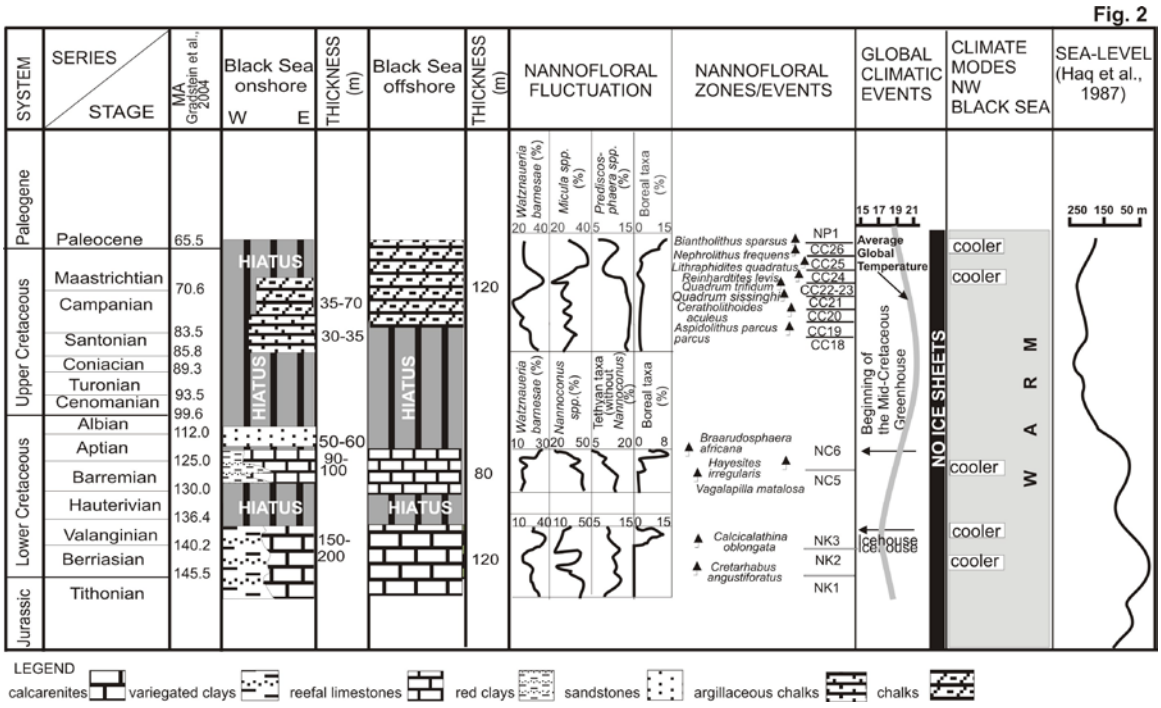

Figure 2. Litho- and biostratigraphy of the Cretaceous deposits from the Southern offshore and onshore areas of the Romanian Black Sea and nannofloral and climatic fluctuations. Global climatic events after Worsley and Martini (1970), Weissert and Lini (1991), Erba (1994), Melinte and Mutterlose (2001). Average Global Temperature from www.scotese.com

As in other Romanian sections (i.e. in the Southern Carpathians - Melinte and Mutterlose, 2001), the Berriasian of the Southern Romanian Black Sea onshore area is characterized by nannofloral assemblages dominated by *Watznaueria barnesae* (with an abundance 20-40%) and by *Nannoconus* spp. (which the abundance is between 20-50%) – Figure 2. The cosmopolitan species are significantly more abundant than the Tethyan ones only in the middle Berriasian, while in the early Berriasian and in the late Berriasian - early Valanginian interval the nannofloras are dominated by the Tethyan taxa (including the genus *Nannoconus*, which represents around 50%). In the late Valanginian, a pronounced shift of the nannoconids was remarked, coincident with the appearance of the Boreal nannofossils, which increase up to 12% from the nannofloras. Nannofossil proxy of the surface water fertilization, as *Biscutum constans* (Gorka) Black, *Diazomatolithus lehmanii* Noël and *Zeugrhabdothus erectus* (Deflandre) Reinhardt, become more abundant (jointly amounting up to 15%), within the late Valanginian.

In the investigated offshore drilling (Tandala 1), the oldest recorded deposits (120 m in thickness) are latest Jurassic (Tithonian) - earliest Cretaceous (Berriasian-Valanginian) in age. Lithologically, these sediments are similar with the Lower Cretaceous south-eastern facies recorded in the drillings from the onshore area – calcarenites and calcilutites with common dasycladacean algae of the Alimanu Member (Cernavoda Formation). The Berriasian-Valanginian age is argued by the presence of the NK1, NK2 and NK3 calcareous nannoplankton zones (Figure 2). The semiquantitative investigations revealed similar trends in fluctuation as in the offshore drillings: high abundance of Tethyan taxa (including *Nannoconus*) within the early Berriasian, late Berriasian and early Valanginian, and significant decrease of them, synchronously with the occurrence of Boreal taxa and increase of *Watznaueria barnesae*, within the late Valanginian.

The next lithological unit traversed by the drillings from the onshore area, is the Ramadan Formation (90-100 m in thickness), which displays two main facies (Figure 2): red clays in the western part, and reefal limestones and calcarenites, rich in orbitolinids and miliolids in the eastern part. The identified nannofloras indicate, for the Ramadan Formation, a late Barremian-early Aptian age, based on the successive FO of the nannofossils *Vagalapilla matalosa* (Stover) Thierstein, *Hayesites irregularis* (Thierstein) Covington and Wise and *Braarudosphaera africana* Black. The latest bio-event approximates, in the Tethyan Realm (including the study area), the Barremian-Aptian boundary interval (Barragan and Melinte, *in press*).

For semiquantitative nannofloral studies, four taxonomical groups were selected: (1) *Watznaueria barnesae*, a eurytrophic cosmopolitan and ecologically robust form, one of the first species to settle in new biotopes; (2) *Nannoconus* spp., taxa which are believed to be restricted to lower photic zone and relatively high temperature of surface water (Melinte and Mutterlose, 2001; Bersezio *et al*., 2002); (3) Tethyan taxa (other then nannoconids), which are also more confined to low to middle latitudes, including *Assipetra terebrodentarius* (Applegate *et al*. *in* Covington and Wise) Rutledge and Bergen *in* Bergen, *Hayesites irregularis*, *Conusphaera mexicana*, and *C. rothii* (Thierstein) Jakubowski; (4) Boreal taxa (*sensu* Mutterlose, 1992) including *Sollasites horticus*, *Crucibiscutum salebrosum*, *Zeugrhabdotus sysiphus* (Gartner) Crux and *Vagalapilla matalosa*, species indicating cooler water surfaces.

The late Barremian nannofossil assemblages (upper part of NC5 Calcareous Nannoplankton Zone of Roth, 1978) are dominated by the Tethyan taxa, which make, together with *Nannoconus* spp., almost 70% of total nannofloras – Figure 2. Within the latest Barremian (around the boundary between the NC5/NC6 Calcareous Nannofossils Zones of Roth, 1978) a significant shift in the Tethyan nannofossil abundance was remarked (from 70% up to 45%), bioevent coincident with the increased abundance of cosmopolitan nannofossil *Watznaueria barnesae* and that of Boreal taxa. The shift of the Tethyan nannofossils is even more pronounced within the earliest Aptian (lower part of the NC6 Calcareous Nannoplankton Zone), interval in which they represent only 25% of total nannofloras – Figure 2.

In the Tandala Well, the reefal limestones and calcarenites, rich in orbitolinids and miliolids were assigned, based on nannofloral investigations, to the late Barremian - early Aptian interval (the NC5 and NC6 Calcareous Nannoplankton Zones of Roth, 1978). The nannofloral semiquantitative analyses allow the identification of a similar trend for the calcareous nannoplankton fluctuation, as in the deposits studied from the onshore area (Figure 2).

The Ramadan Formation is unconformably overlaid, in the southern offshore area of the Romanian Black Sea, by the Gherghina Formation, mainly made by sands with thin coal lenses and kaolinitic clays. The late Aptian-early Albian age of this lithological unit is argued by its rich charophyte content (Iva, 1990). No similar formation, in age and/or lithology, with Gherghina Formation was recorded in the offshore area of the Southern Romanian Black Sea.

3.2. Late Cretaceous

The oldest Upper Cretaceous unit intercepted in the drillings from the onshore area of the Black Sea is the Murfatlar Formation, made by 30-35 m of grey-whitish argillaceous chalk, with reddish clays in the lower part, overlain by yellowish clays and whitish, massive chalky limestones. The calcareous nannoplankton assemblages, characteristic for CC18, CC19, CC20 and CC21 calcareous nannoplankton zones of

Sissingh (1977) argue for a Santonian – Early Campanian age of this formation (Figure 2).

The youngest Upper Cretaceous unit intercepted by the studied drillings from the onshore area of the Southern Romanian Black Sea is the Nisipari Formation (35-70 m in thickness), made by chalky marls and clays, overlain by thin glauconitic sands, and whitish massive chalky limestones. The age of this formation, late Campanian - late Maastrichtian, is proved by the identification of the CC22-CC26 calcareous nannoplankton zones of the Sissing (1977) – Figure 2.

For semiquantitative nannofloral studies, four taxonomical groups were counted: (1) *Watznaueria barnesae*, a eurytrophic cosmopolitan and ecologically robust form; (2) *Micula* spp., the dominant genus in the Upper Cretaceous nannofloral assemblages, taxa being more confined to low to middle latitudes, indicating also an oligotrophic environment; (3) *Prediscosphaera* spp., another important component of the recorded calcareous nannoplankton, mainly represented by the species *P. cretacea* (Arkhangelsky) Gartner. One species of the genus, *P. stoveri* (Perch-Nielsen) Shafik and Stradner was counted together with the Boreal taxa; (4) Boreal taxa**,** represented by *Nephrolithus frequens* Górka, *Cribrosphaerella daniae* Perch-Nielsen, *Kamptnerius magnificus* Deflandre and *Prediscosphaera stoveri*, which are nannofossils more confined to high latitudes and cooler surface waters (Worsley and Martini, 1970).

The Santonian (the lower part of the Murfatlar Formation) is dominated by the *Watznaueria barnesae* and *Micula* spp., which make together around 50% of the total nannofloras. In the latest Santonian an increase of the abundance of *Micula* spp (up to 35%) was noticed, synchronously with the shift in abundance of *Watznaueria barnesae*. A similar nannofloral composition characterizes the upper part of the Murfatlar Formation (Early Campanian) and the lower part of the Nisipari Formation (late Campanian – earliest Maastrichtian in age). The nannofloral composition significantly changed within the early Maastrichtian, the abundance of *W. barnesae* increasing up to 40% - Figure 2. Concomitantly, the genera *Micula* and *Prediscosphaera* sharply decrease. An important fluctuation in the abundance of the calcareous nannofloras took place within the latest Maastrichtian (CC25 and CC26 Calcareous Nannoplankton Zone), when the assemblages are clearly dominated again by the genera *Micula* and *Prediscosphaera*, jointly amounting to 50% of the total nannofloras. The latest Maastrichtian (upper part of the Nisipari Formation) is characterized by the increase of Boreal taxa (up to 15%), decrease of *Micula* and *Prediscosphaera* genera and abundance of *Watznaueria barnesae* around 30%.

The Upper Cretaceous deposits identified on the Black Sea offshore (within the Tandala Well) consists of white chalky limestones, with a remarkable high calcareous nannoplankton concentration. The nannofloral analyses led to the identification of the CC20, CC21, CC22, CC23, CC24, CC25 and CC26 calcareous nannoplankton zones, Early Campanian *pro parte*-latest Maastrichtian in age (Figure 2). The whole Upper Cretaceous succession identified in the Tandala Well is 120 m thick. The Campanian calcareous nannofloras are dominated by Tethyan taxa, as *Ceratolithoides aculeus* (Stradner) Prins and Sissingh *in* Sissingh, *Quadrum sissinghi* Perch-Nielsen and *Quadrum trifidum* (Stradner *in* Stradner and Papp) Hattner and Wise, making together with the *Micula* and *Prediscosphaera* genera over 60% of the total nannofloras. Early Maastrichtian calcareous nannofossils are mainly made by cosmopolitan taxa, while in the latest Maastrichtian the Boreal nannofossils represent an important

component of the nannofloras (almost 20%).

Based on the identified nannofloras, a continuous sedimentation could be assumed within the Cretaceous/Tertiary boundary interval, in the chalk deposits of the Tandala Well. This finding is supported by the presence of the nannofloral mass extinction, in the upper part of the chalky limestones. Over 95% of the Cretaceous nannofossils disappeared, bioevent known to point out the K/T boundary in the whole Tethyan Realm (Perch-Nielsen, 1985, Burnett, 1998; Melinte, 1999; Gardin, 2002; Lamolda et al., 2005). The occurrence of the nannofossil *Biantolithus sparsus* Bramlette and Martini led to the identification of the early Danian NP1 Calcareous Nannoplankton Zone of the Martini Zonation (1971). Notably, significant successive blooms of the calcareous dinoflagellate genus *Thoracosphaera* and of the nannofossil *Braarudosphaera bigelowii* occur at the top of the chalk.

4. DISCUSSION

A warm homogenous Cretaceous climate was previously assumed by some authors (i.e., Barron, 1983; Hallam, 1985, Herman and Spicer, 1996). A more varied Cretaceous climate, including the development of seasonal polar ice caps, was suggested by other scientists (Weissert and Lini, 1991; Kemper, 1987; Hay, 1995). The provincialism showed by some groups of organisms (i.e. ammonites, belemnites, calcareous nannoplankton) argues also for Cretaceous climatic belt and latitudinal bioprovinces, related to the palaeogeographical distribution of the Tethyan and Boreal Realms. Being planktonic organisms, the calcareous nannofossils are good proxy of palaeoceanographic conditions at the surface waters. Their variations in abundance and diversity express changes in palaeoclimate, nutrient supply, detrital input and geochemistry (Erba, 1994; Melinte and Mutterlose, 2001; Mutterlose et al., 2005).

The fluctuations of Cretaceous nannofloras identified in the studied drillings in the Southern Romanian Black Sea region indicate rather a stable warm climate and oligotrophic conditions at the surface waters. The early Cretaceous studied intervals (Berriasian – Valanginian and late Barremian - early Aptian) contain bipolar nannofloras, dominated by *Watznaueria barnesae* and *Nannoconus* spp. Shift in nannoconids, accompanied by increased abundance of the cosmopolitan nannofossil *Watznaueria barnesae* and by the occurrence of Boreal species, express climatic changes in three particular intervals: middle Berriasian, late Valanginian and late Barremian. Remarkably, all the three intervals correspond to a global high-stand sea-level (Haq et al., 1987). We can assume that these three early Cretaceous intervals are characterized by a shift from an arid and warm climate to a cooler and humid one. Notably, palaeotemperatures based of the belemnites (McArthur et al., 2004), and of the nannofossil assemblages (Melinte and Mutterlose, 2001; Mutterlose et al., 2003) indicate also icehouse conditions in the Late Valanginian. A late Barremian cooling, accompanied by a sea-level trangression was also previously identified in several regions of the Tethys Realm (Rawson, 1994; Erba, 1994; Barragan and Melinte, 2006).

The Late Cretaceous nannofloras from the NW Black Sea region is characterized by bipolar assemblages, dominated by *Watznaueria barnesae* and *Micula* spp. The changes in nannofloral abundance in two Maastrichtian intervals, expressed in higher abundance of Boreal nannofossils and shift of the Tethyan ones, indicate cooler episodes, within the early Maastrichtian and at the top of this stage. The later cooling event is probably related to the global climatic deterioration from the end of Cretaceous, just below the Cretaceous/Tertiary boundary event.

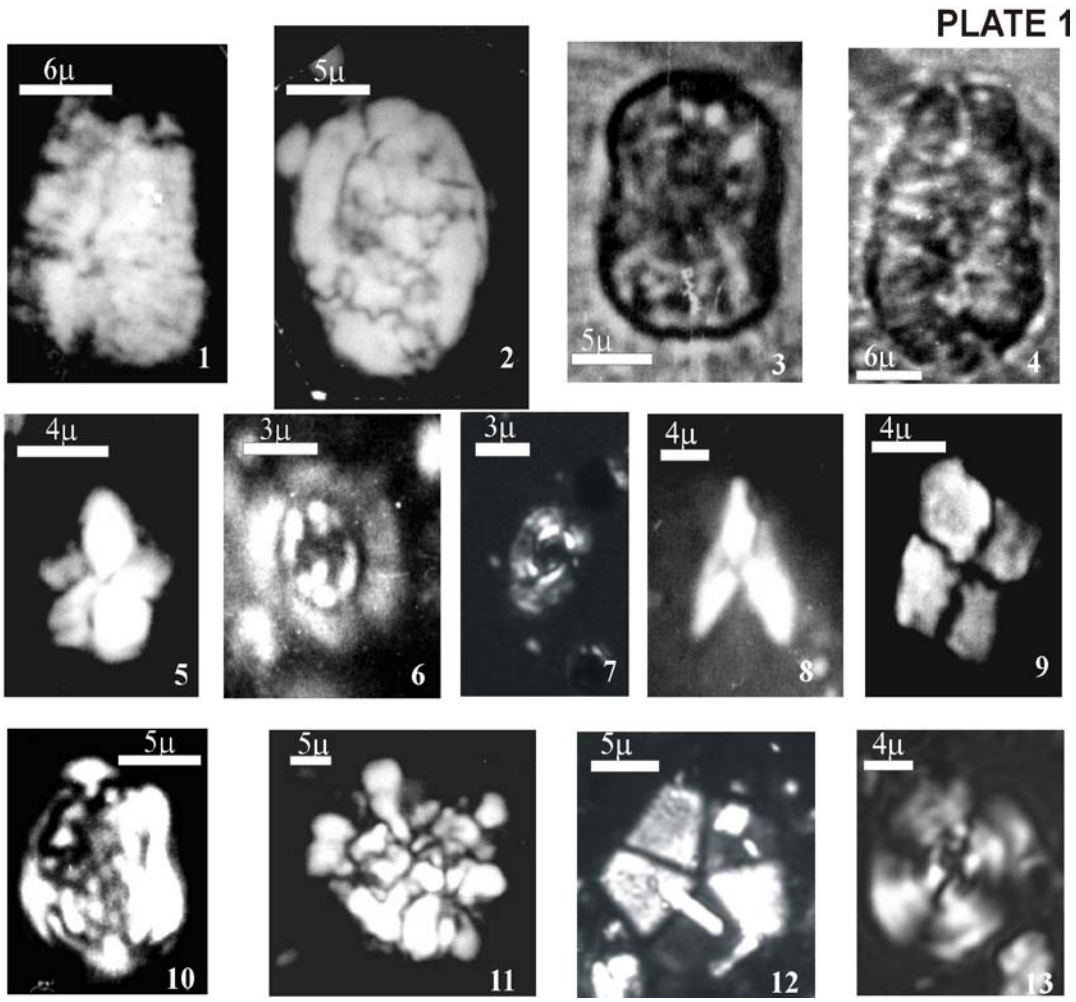

Plate 1. Fig. 1. *Nannoconus steinmanii* Kamptner, 1931 - early Berriasian, Cernavoda Formation.

Fig 2. *Calcicalathina oblongata* (Worsley, 1971) Thierstein, 1971 - late Valanginian, Cernavoda Formation.

Fig. 3. *Nannoconus globulus* Brönnimann, 1955 - late Barremian, Ramadan Formation.

Fig. 4. *Nannoconus kampneri* Brönnimann, 1955 - late Valanginian, Cernavoda Formation.

Fig. 5. *Braarudosphaera africana* Stradner, 1961 – early Aptian, Ramadan Formation.

Fig. 6. *Prediscosphaera cretacea* (Arkhangelsky, 1912) Gartner, 1968 - early Campanian, Murfatlar Formation.

Fig. 7. *Biscutum constans* (Górka, 1957) Black *in* Black and Barnes, 1959 - late Valanginian, Cernavoda Formation.

Fig. 8. *Ceratolithoides aculeus* (Stradner, 1961) Prins and Sissingh *in* Sissingh, 1977 – late Campanian, Nisipari Formation.

Fig. 9. *Quadrum sissinghi* Perch-Nielsen, 1984 – late Campanian, Murfatlar Formation.

Fig. 10. *Nephrolithus frequens* Górka, 1957 - latest Maastrichtian, Nisipari Formation.

Fig. 11. *Thoracosphaera* sp. - early Danian, Nisipari Formation.

Fig. 12. *Braarudosphaera bigelowii* (Gran and Braarud, 1935) Deflandre, 1947 - early Danian, Nisipari Formation.

Fig. 13. *Watznaueria barnesae* (Black, 1959) Perch-Nielsen, 1968 - late Valanginian, Cernavoda Formation.

5. CONCLUSIONS

The Cretaceous history of the NW Black Sea region, deciphered based on calcareous nannofloral investigations, reflects multiple depositional episodes of different sedimentological regimes, separated by several hiatuses of varying duration. The oldest sedimentary sequence recovered by the studied drillings is latest Jurassic (Tithonian) - earliest Cretaceous (Berriasian - Valanginian) in age, followed by a hiatus of more than 15 MA. The next depositional cycle is late Barremian - early Aptian in age, followed (in the offshore area of the Southern Romanian Black Sea) by a hiatus of around 45 MA, covering the early Aptian - early Campanian interval. In the onshore region of the Black Sea, after a shorter hiatus (up to 10 MA), a fluvial-lacustrine formation was deposited, within the Aptian/Albian boundary interval. The Upper Cretaceous deposition covers the Campanian – earliest Paleocene interval in the offshore area and the Santonian - latest Maastrichtian interval in the onshore region of the Southern Romanian Black Sea.

Based on the data presented herein, we assumed that the Cretaceous climate around the Black Sea region was a subtropical one, warm and arid, with several episodes of cooling. Three early Cretaceous cooler intervals are suggested by the nannofloral fluctuation, within the middle Berriasian, late Valanginian and latest Barremian. Within the late Cretaceous, the warm climate starts to deteriorate in the Maastrichtian, stage characterizes by a relative cooler episodes, in the early part and towards its top, prior the K/T boundary.

REFERENCES

Anastasiu, V., 1898. Contribution à l'étude géologique de la Dobrogea. Thèse de Doctorat, *G. Carré & C. Naud*, Paris.

Avram E., Drăgănescu, A., Szasz, L, Neagu T., 1988. Stratigraphy of the outcropping Cretaceous deposits in Southern Dobrogea (SE Romania). *Mémoires*, 33, 4-43.

Avram E., Szasz, L., Antonescu E., Baltres A., Iva M., Melinte M., Neagu T., Radan S., Tomescu C., 1993. Cretaceous terrestrial and shallow marine deposits in northern South Dobrogea (SE Romania). *Cretaceous Research*, 14, 265-305.

Barragan, R., Melinte, M.C., 2006. Palaeoenvironmental and palaeobiological changes across the Barremian-Aptian boundary interval in the Tethys Realm (Mexico and Romania). *Cretaceous Research* (in press).

Barron, E. J., 1983. A warm equable Cretaceous: The nature of the problem. *Earth-Science Reviews*, 19, 305-338.

Băncilă I., 1973. Asupra prezenţei unor formaţiuni gipsifere purbeckian-wealdiene în regiunea Feteşti-Constanţa. *Studii şi Cercetări de Geologie, Geofizică şi Geogrfaie, Seria Geologie*, 18, 115-125.

Bărbulescu, A., Neagu, T., 1988. Brachiopodes crétacés de la Dobrogea de Sud. Nouvelles contributions à l'étude des Terebratulides néocrétacés. *Analele Universităţii Bucureşti*, 37, 41-55.

Bersezio, R., Erba, E., Gorza, M., Riva, A., 2002. Berriasian-Aptian black shales of the Maiolica Formation (Lombardian Basin, Southern Alps, Northern Italy): local to global events. *Palaeogeography, Palaeoclimatology, Palaeoecology*, 180, 253-275.

Bralower, T.J., Monechi, S., Thierstein, H.R., 1989. Calcareous nannoplankton zonation of the Jurassic-Cretaceous boundary interval and correlation with the geomagnetic polarity timescale.

Marine Micropaleontology, 14, 153-234.

Chiriac, M., 1968. Carte géologique de la Roumanie 1/200,000, Feuille 46-Constanţa. Note explicative, p. 1-44, *Institut de Géologie et Géophysique*, Bucarest.

Erba, E., 1994. Nannofossils and superplumes: the early Aptian "nannoconid crisis". *Palaeoceanography*, 9, 481-501.

Gardin, S., 2002. Late Maastrichtian to early Danian calcareous nannofossils at Elles (Northwest Tunisia). A tale of one million years across the K-T Boundary. *Palaeogeography, Palaeoclimatology, Palaeoecology*, 178, 211-231.

Haq B.U., Hardenbol, J., Vail, P.R., 1987. The chronology of fluctuating sea-level since the Triassic. *Science*, 235, 1156-1167.

Hallam, A., 1985. A review of Mesozoic climates. *Journal of Geological Society of London*, 142, 433-445.

Hay, W.W., 1995. Cretaceous Paleocenoagraphy. *Geologica Carpathica*, 46, 5, 257-266.

Herman A.B., Spicer, R.A., 1996. Paleobotanical evidence for a warm Cretaceous Arctic Ocean. *Nature*, 380, 330-333.

Ion, J., Iva, M., Melinte, M.C., Florescu C., 1998, Subsurface Santonian-Maastrichtian deposits in NE South Dobrogea (Romania). *Romanian Journal of Stratigraphy*, 77**,** 4, 47-63.

Iva, M., 1990, Early Cretaceous Characeae of South Dobrogea. *Meeting of the IGCP Projects 245 and 262*, Bucharest, Abstracts, p. 59.

Kemper, E., 1987. Das Klima der Kreide-Zeit. *Geologisches Jahrbuch*, 96 A, 5-185.

Lamolda, M.A., Melinte, M.C., Kaiho, K., 2005. Nannofloral extinction and survivorship across the K/T boundary at Caravaca, southeastern Spain. *Palaeogeography, Palaeoclimatology, Palaeoecology*, 224, 27-52.

McArthur, J.M., Mutterlose, J., Price, G.D., Rawson, P.F., Ruffell, A, Thirwall, M.F., 2004. Belemnites of Valanginian, Hauterivian and Barremian age: Sr-isotope stratigraphy, composition ($^{87}Sr/^{86}Sr$, $\delta^{13}C$, $\delta^{18}O$, Na, Sr, Mg), and palaeo-oceanography. *Palaeogeography, Palaeoclimatology, Palaeoecology*, 202, 253-272.

Melinte, M. C., 1999. Cretaceous/Tertiary Boundary in the East Carpathians (Romania), based on nannofloral evidence. *Acta Paleontologica Rumaniae*, 2, 269-273.

Melinte, M., Mutterlose, M., 2001. A Valanginian (Early Cretaceous) 'boreal nannoplankton excursion' in sections from Romania. *Marine Micropaleontology*, 43, 1-25.

Mutterlose, J. 1992. Migration and evolution pattern of floras and faunas in marine Early Cretaceous sediments of NW Europe. *Palaeogeography, Palaeoclimatology, Palaeoecology*, 94, 261-282.

Mutterlose. J., Bornemann A., Herrle, O., 2005. Mesozoic calcareous nannofossils – state of the art. *Paläontologische Zeitschrift*, 79/1, 113-133.

Neagu, T., 1986, Barremian-Lower Aptian milliolid fauna in South Dobrogea (Romania). *Revista Española de Micropaleontologia*, 18, 313-348.

Neagu, T., 1987. White Chalk foraminiferal fauna in South Dobrogea (Romania), 1. Planktonic Foraminifera. *Revista Española de Micropaleontologia*, 19, 281-314.

Neagu, Th., Pană, I., Dragastan O., 1977. Biostratigraphie de la série des

calcaires éocretacées de l'aire Alimanu-Cernavodă-Ostrov. *Revue Roumaine de Géologie, Géophysique et Géographie, Série de Géologie*, 21, 131-144.

Reuss, A. E., 1865. Foraminiferen und Ostracoden der Kreide am Kanara-See bei Küstendsche (Dobrudscha). *Sitzungsberichte der Kaiserlich-Königliche Akademie des Wissenchaften*, 53, 1-265.

Rawson, P. F., 1994. Sea level changes and their influence on ammonite biogeography in the European Lower Cretaceous. *IIIrd Conference International "Fossili, Evolutione, Ambiente"*, Pergola, 1990. *Palaeopelagos Special Publication 1*, 317-326.

Roth P.H., 1978, Cretaceous nannoplankton biostratigraphy of the northwestern Atlantic Ocean. In Benson et al. (Eds.): *Initial Reports Deep Sea Drilling Project*, Washington (U.S. Govt. Printing Office), 22, 731-759.

Săndulescu, M., 1984. Geotectonica României. *Editura Tehnică*, Bucureşti.

Sissingh, W., 1977, Biostratigraphy of Cretaceous calcareous nannoplankton. *Geologie en Mijnbouw*, 56, 37-65.

Weissert, H., Lini, A., 1991. Ice age interludes during the time of Cretaceous greenhouse climate? In: Müller, D.W., McKenzie, J.A., Weissert H. (Eds.), *Controversies in Modern Geology*. Academic Press, London, pp. 173-191.

Worsley, T.R., Martini E., 1970. Late Maastrichtian nannoplankton provinces. *Nature*, 225, 1242-1243.

MINERALOGY, GEOCHEMISTRY AND UTILITY OF TRIAS SEDIMENTS IN SIZMA - YÜKSELEN (KONYA)

Menlikli G. F.[1] and Baykal A.[2]

[1]Mineral Research and Exploration General Directorate, Agean Regional Directorate 35040 Bornova, İzmir Turkey,
ferlizmen@yahoo.com

[2]Dokuz Eylül University, Department of Geological Engineering 35100 Bornova, İzmir Turkey,
alev.baykal@deu.edu.tr

Abstract: In this study, fine-grained and plastic metashales and calc-schists belonging to Lower Triassic aged Morbel Tepe Member, which are widespread in the study area and lying between Sızma and Yükselen towns in Konya have been investigated in particular. In addition, metasandstones and recrystallized limestones belonging to the same unit and other units which have contact relationship with this unit have been investigated from mineralogical, petrographic and geochemical point of view.

The petrographic studies indicated the existence of four groups of rocks which are volcanic, metavolcanic, sedimentary and metasedimentary rocks .

According to the results of XRD investigations, the metashales and calc-schists consist of illite and chlorite as clay minerals. The XRD data indicates that the degree of crystallinity is high in illites in metashales and calc-schists, therefore they are in epizone region representing a low grade metamorphism. The illites are detrital and in 2M polytypes because of the low grade metamorphism. The chlorites are in IIb polytypes, trioctahedral and detrital because of the low grade metamorphism.

The results of the geochemical studies revealed a similar composition for the metashales and calc-schists. However, the metashales contain more SiO2 and Al2O3 than the calc-schists and the calc-schists contain more CaO than the metashales.

When the properties of samples were evaluated with respect to uses in cement industry, it was determined that the samples meet the requirement of 2/1 ratio of Al2O3/Fe2O3. According to the result of the plasticity experiments, however, the plasticity of Morbel Tepe clays is 11.4%.

Key words: Low grade metamorphism, Illite.

1. INTRODUCTION

The study area is between Sızma and Yükselen towns in 25 km northwest of the Konya city center (Figure 1). It covers an area about 50 km^2. It is located on the ILGIN L28-c4 sheet. The probable use of the purplish metashales and yellowish calc-schists as industrial raw material is the subject of the present study. The metashales are dominant in the Morbel Tepe Member and the calc-schists are not very widespread and the rocks of both units show fine-grained, plastic property; and traditionally have been used as plaster material in the surrounding towns (Figure 2) and can be considered as potential industrial raw material. For this reason, these rocks have been investigated in particular. In addition, metasandstones and recrystallized limestones belonging to the same unit and other units which have contact relationship with this unit have been investigated in terms of mineralogy, petrography and geochemistry.

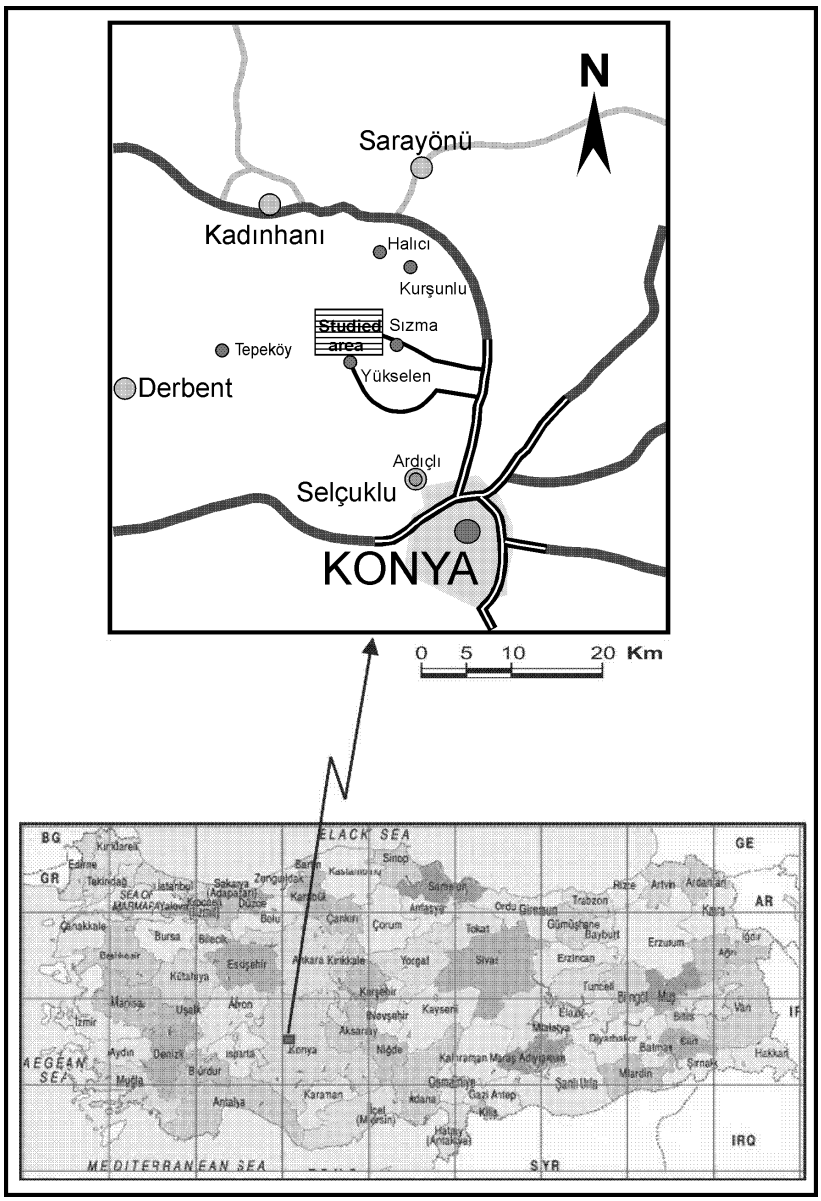

Figure 1. Location map of the study area.

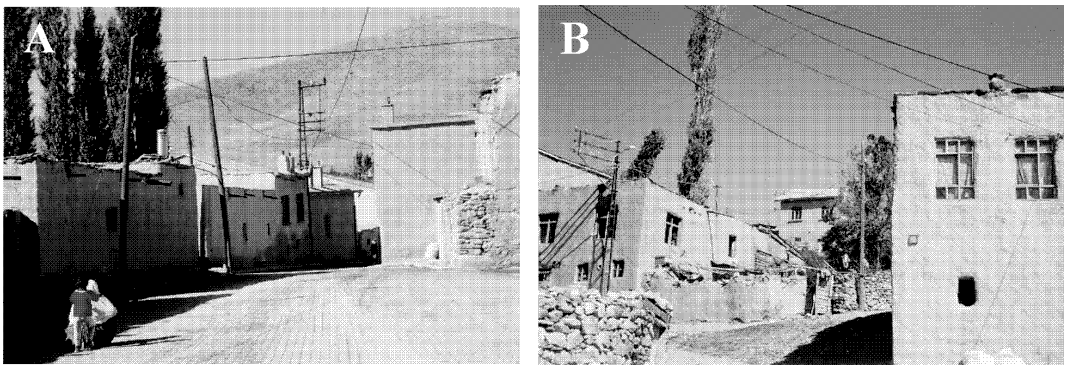

Figure 2. The yellow coloured calc-schists (A) and the purple coloured metashales (B) are used as a plaster material in Sızma (A) and Yükselen (B) towns.

2. GEOLOGY

In general Paleozoic, Mesozoic, Neogene and Quaternary formations appear in stratigraphic sequence in the area (Figure 4) (Özcan et al., 1990). The study area has sedimentary, metasedimentary, volcanic and metavolcanic rocks (Figure 5). Lower

Triassic aged Morbel Tepe Member is widespread in the study area. The Morbel Tepe Member consists of purple coloured metasandstones and metashales which are intercalated with gray coloured recrystallized limestones or yellow-gray-green coloured calc-schists (Figure 3). These rocks are folded and fractured because of tectonism and have a schistosic structure because of metamorphism (Figures 6 & 7). This unit is overturned in the study area.

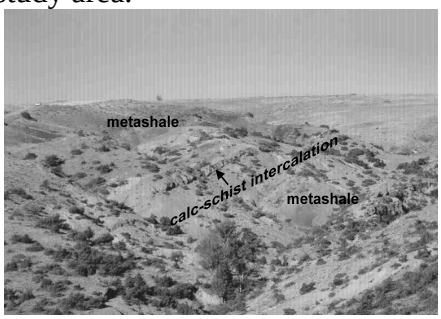

Figure 3. A view of the Morbel Tepe Member

3. MINERALOGY AND PETROGRAPHY

3.1 Polarization microscope studies

Sızma Metavolcanite Member (Chs)

This unit consists of light - dark gray, dark green coloured metavolcanic rocks which are acidic and intermediate volcanic in origin. These rocks have a schistosic structure because of metamorphism.

These altered metavolcanic rocks have primary texture features. Argillized, carbonatized, chloritized, sericitized feldspar minerals and opaque minerals which are parallel to the schistosity occur in recrystallized fine-grained matrix (Figure 8). Some samples have uralitized pyroxenes (Erkan, 1978) (Figure 9) or amphiboles which are opaque in their margins and close to their cleavages.

Morbel Tepe Member (TRam)

Metasandstones which have schistose structure consist of quartz, feldspar, lesser muscovite and sericite minerals. Poorly graded grains touch each other in some places and are cemented by calcite and lesser dolomite. These rocks have also accessory minerals such as tourmaline, apatite and zircon and opaque minerals which are parallel to the schistosity (Figure 10).

Metashales which have schistosic structure consist mostly of quartz, feldspar and rarely mica minerals and accessory minerals such as tourmaline and apatite. The elongated and parallel grains are cemented by carbonate minerals. There are also opaque minerals as thin layers which are parallel to the schistosity (Figure 11).

The schistose calc-schists are composed mainly of microspary calcite, lesser dolomite, minor quartz and rare muscovite minerals. Chlorite, silica, Fe_2O and carbonate minerals are present in the tiny fractures. Some of the samples are widely chloritized.

Recrystallized limestones are mainly composed of calcite, lesser dolomite and minor quartz minerals. Fe_2O and carbonate minerals are present in the tiny fractures.

Seyrantepe Member (TRas)

This unit includes dolomitic limestones having a brownish yellow weathered surface. But fresh rocks are gray, or pinkish gray in colour. The limestones are mainly composed of calcite and lesser dolomite and minor quartz minerals. These rocks are present in the fractures which are parallel and/or cut each other.

Sulutaş Member (Tds)

The volcanic rocks are determined as dacite according to their mineralogical and textural features (Figure 12).

These rocks showing a porphyritic texture consist of plagioclase with zoning and polysynthetic twinning, amphibole, biotite and corrode quartz phenocrystals. There are trace amounts of K-feldspar phenocrysts. Plagioclase phenocrysts exhibit slightly normal and reverse zoning. The plagioclase phenocrysts are completely carbonatized and carbonatized in some places beginning either from the centre or from the margin related to the zoning (Erkan, 1978). The cryptocrystalline groundmass is widely

chloritized, argillized and silicified and includes also plagioclase microlites.

Karacaören Formation (Tk)

Conglomerates consist of rounded metaclasts of metasandstone and metashale fragments, and limestone and calc-schist fragments varying from sand to gravel dimension. Matrix is formed by carbonate minerals and colored by Fe_2O.

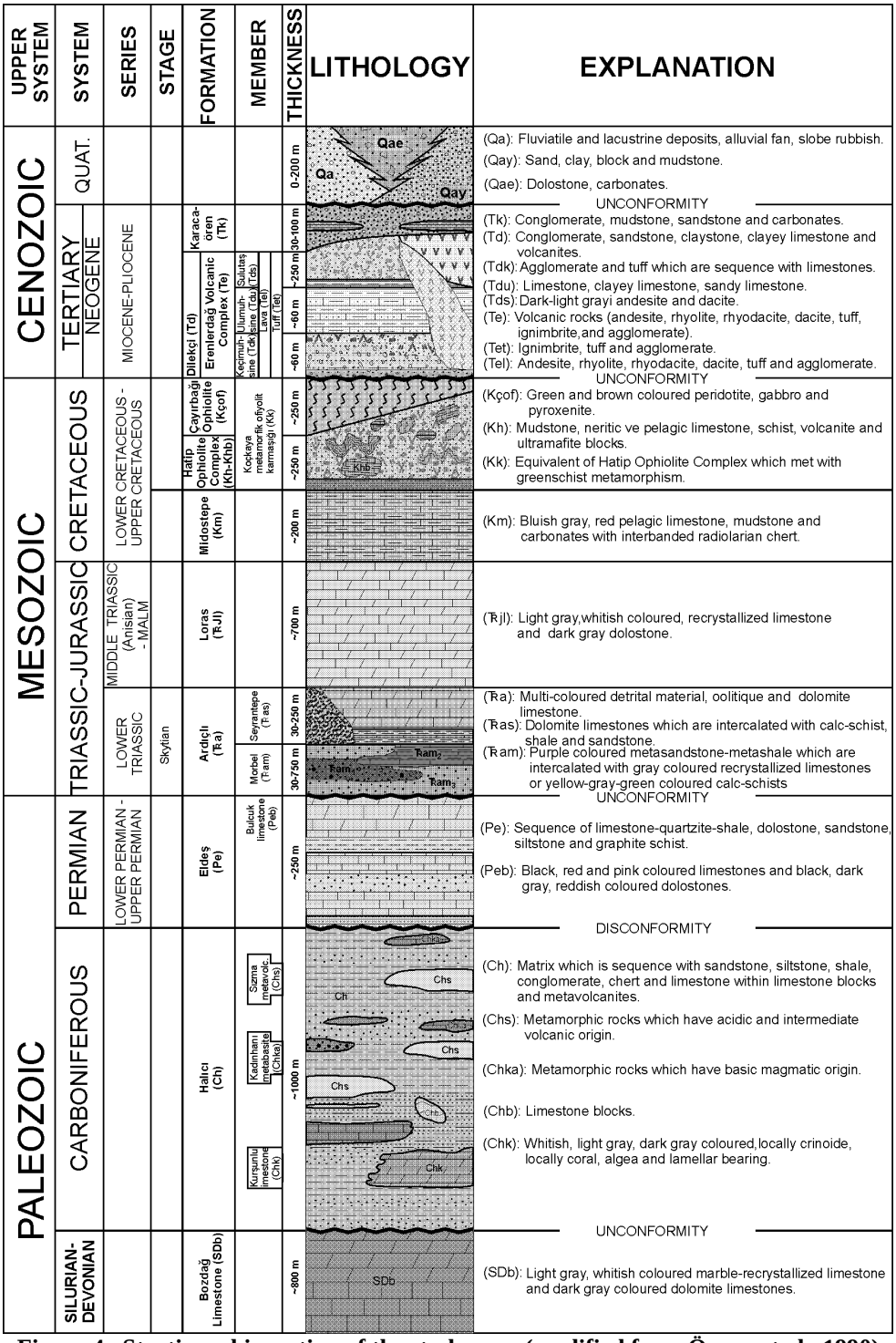

Figure 4. Stratigraphic section of the study area (modified from Özcan et al., 1990)

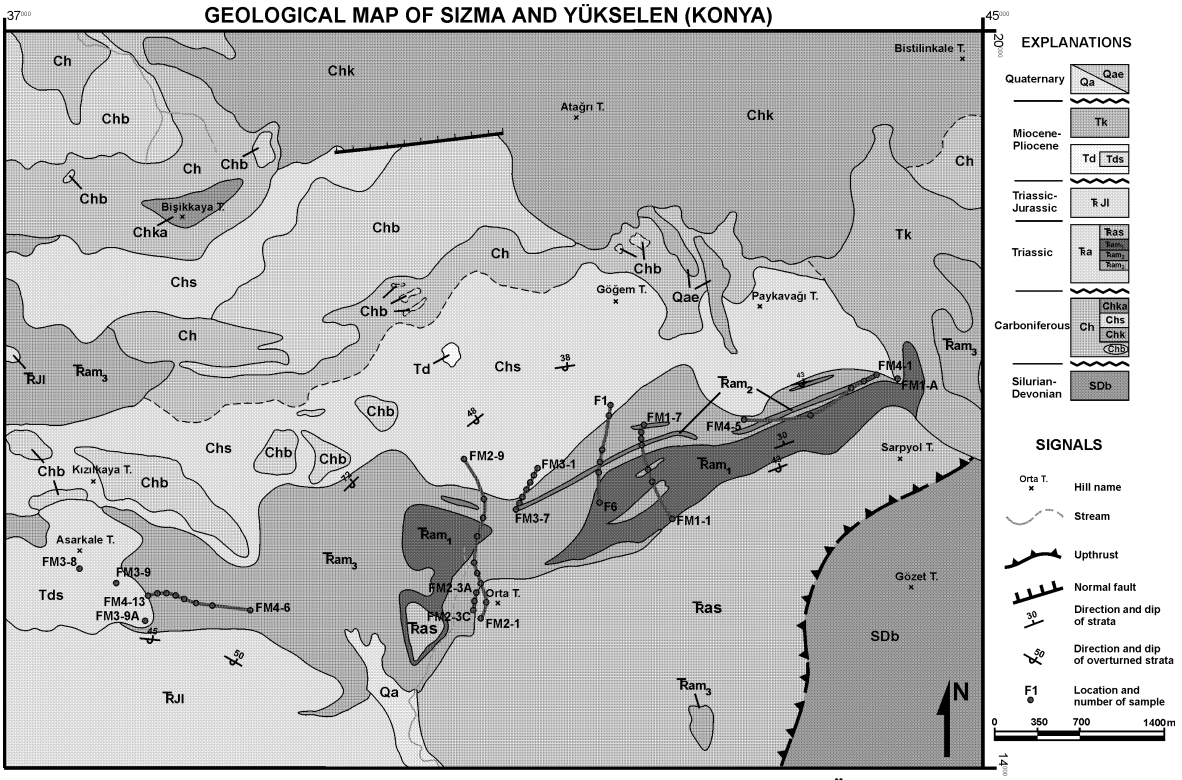

Figure 5. Geological map of Sızma and Yükselen region (modified from Özcan et al., 1990)

3.2 X-ray diffraction (XRD) and scanning electron microscope (SEM) studies

The results of XRD of whole rock and detail clay analyses and images of SEM of Morbel Tepe Member are shown in Figures 13, 14, and 15. Metashales and calc-schists consist of quartz, calcite and feldspar and illite and chlorite as clay minerals.

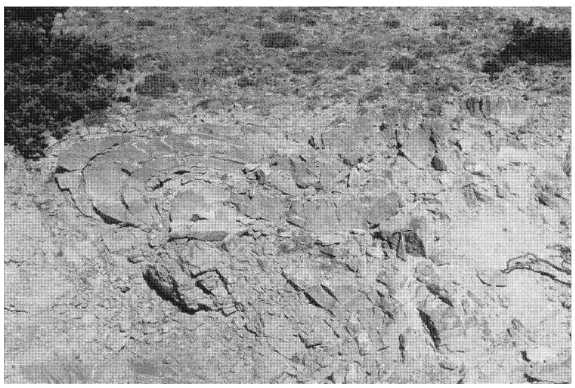

Figure 6. Tectonic folds in recrystallized limestone

An oriented mount of illite/muscovite gives an integral series 00l spacings of which the (001) for 2M structures (the 002) is prominent at about 10 Å. A reflection at about 5 Å is also readily observed (Carroll, 1970) (Figure 14).

Figure 7. Shear fractures in metasandstone

The reflection of (060) of the dioctahedral illites is 1.50 Å and 1.53-1.55 Å for the trioctahedral chlorites (Weaver & Pollard, 1973).

Fe-rich chlorites give weak reflections at 1st and 3rd basal reflections but strong 2nd and 4th order at basal reflections (Carroll, 1970). After the heating the chlorite for 1 hour at 550-600 ºC, 1st peak (14 Å) stays fixed (with no changes) but 2nd peak (7 Å) is destroyed (Figure 14).

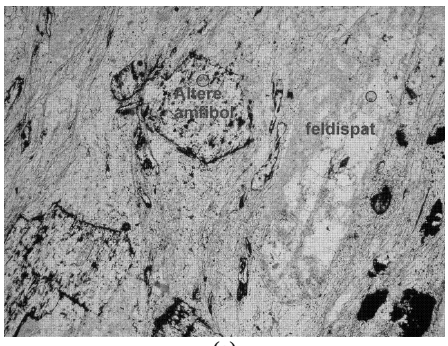

(a)

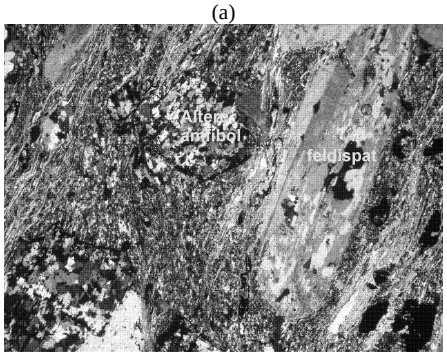

(b)

Figure 8. Photomicrographs of metavolcanic rock (a) plain light (b) polarized light (4 X 0,10)

(a)

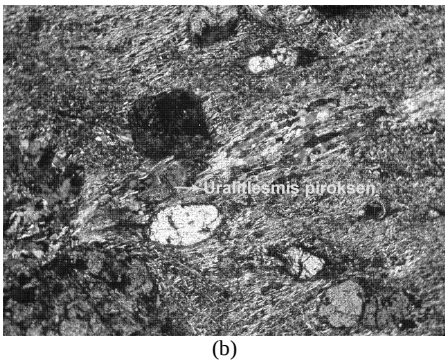

(b)

Figure 9. Photomicrographs of uralitized pyroxene (a) plain light (b) polarized light (4 X 0,10)

4. GEOCHEMISTRY

According to the geochemical studies (Table 1), the metashales are composed of SiO_2 32-66%, Al_2O_3 11-18%, CaO 0-17%, Fe_2O_3 6-7%, K_2O 1-5 %, MgO 1-2%, Na_2O 0-1%, K.K. 3-21% and the calc-schists are composed of SiO_2 18-47%, Al_2O_3 6-14%, CaO 11-38%, Fe_2O_3 3-9%, K_2O 1-3%, MgO 1-4%, Na_2O 0-1%, MnO 0-4%, and LOI 12-31%.

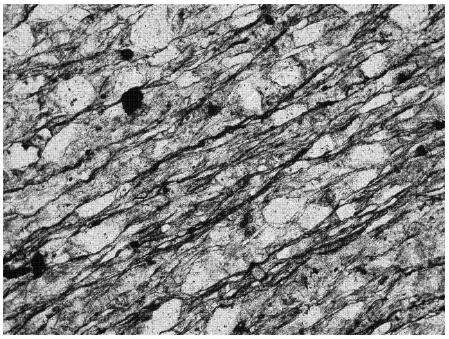

(a)

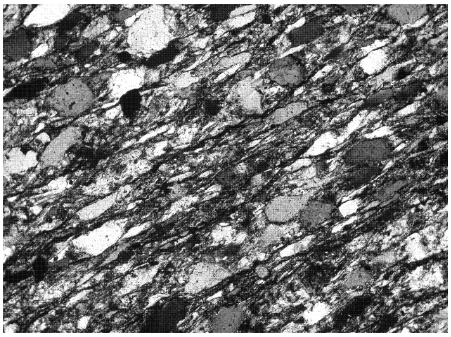

(b)

Figure 10. Photomicrographs of metasandstone (a) plain light (b) polarized light (4 X 0,10)

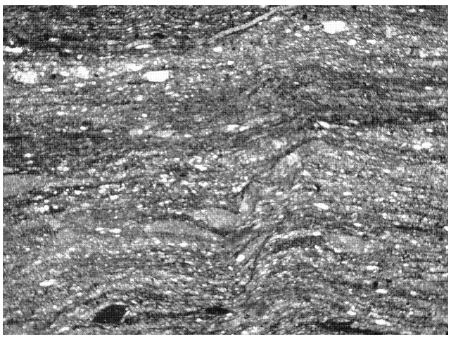

(a)

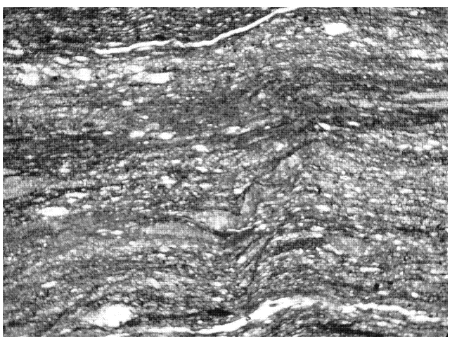

(b)

Figure 11. Photomicrographs of metashale (a) plain light (b) polarized light (4 X 0,10)

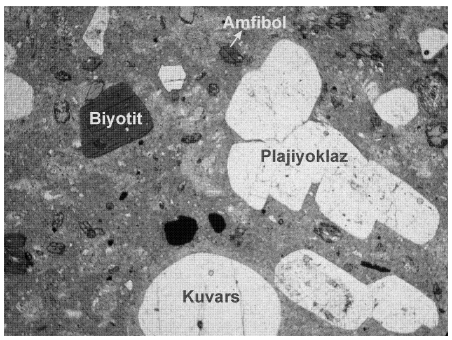

(a)

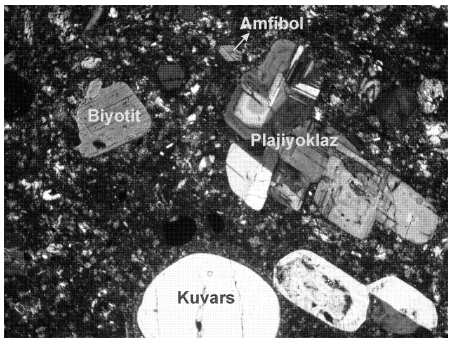

(b)

Figure 12. Photomicrographs of dacite (a) plain light (b) polarized light (4 X 0,10)

5. INVESTIGATION AND UTILIZATION OF THE CLAY MINERALS IN THE STUDIED AREA

According the data of XRD, metashales and calc-schists (Morbel Tepe clays) include illite and chlorite as clay minerals.

The value of peak width at half-height for the illite (001) XRD reflection is known as the Kubler index or the illite crystallinity index (Kubler, 1984). The narrow peak width shows high crystallinity and the grade of metamorphism. Generally, the micas rapidly reach a maximum crystallinity in the epizone, corresponding to a minimum width of the 10 Å peak (Dunoyer De Segonzac, 1970). The 10 Å reflection of 2M illite/mica is usually narrower and sharper than that of the 1M form (Wilson, 1987). I (001) is the height of the illite (001) peak and I (002) is the height of the illite (002) peak. The crystallinity values of the illite belonging to the Morbel Tepe clays are given in Table 2.

According to the crystallinity data of illite, the degree of crystallinity of illites in metashales and calc-schists is high; therefore, they are in epizone region representing a low grade metamorphism (Figure 16). The illites are in 2M polytypes, dioctahedral and detrital because of the low grade metamorphism. The chlorites are in IIb polytypes, trioctahedral and detrital because of the low grade metamorphism.

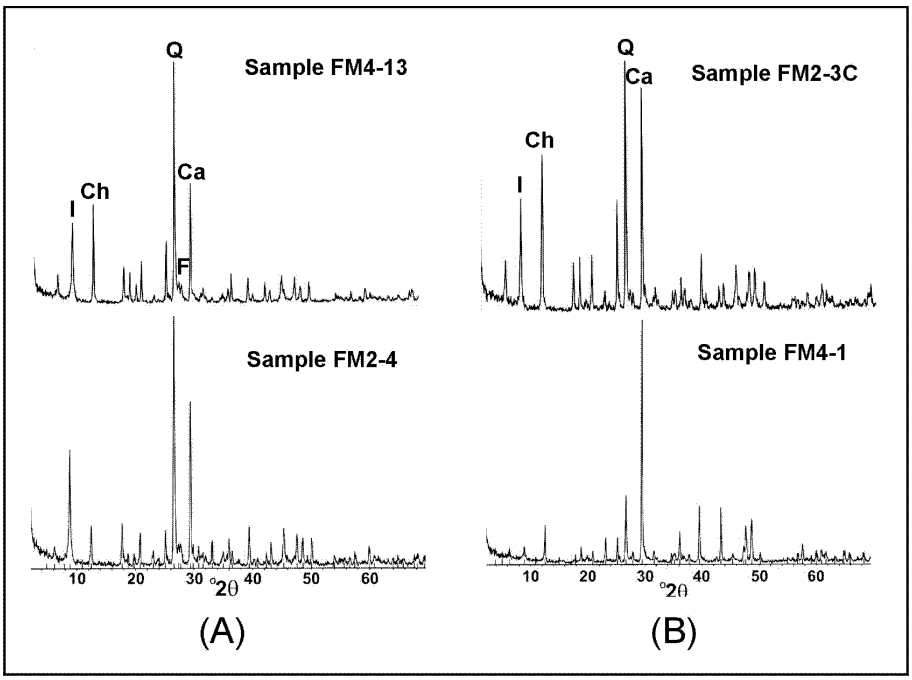

Figure 13. X-ray diffractograms of metashales (A) and calc-schists (B). Q: quartz, Ca: calcite, I: illite, Ch: chlorite, F: feldspar.

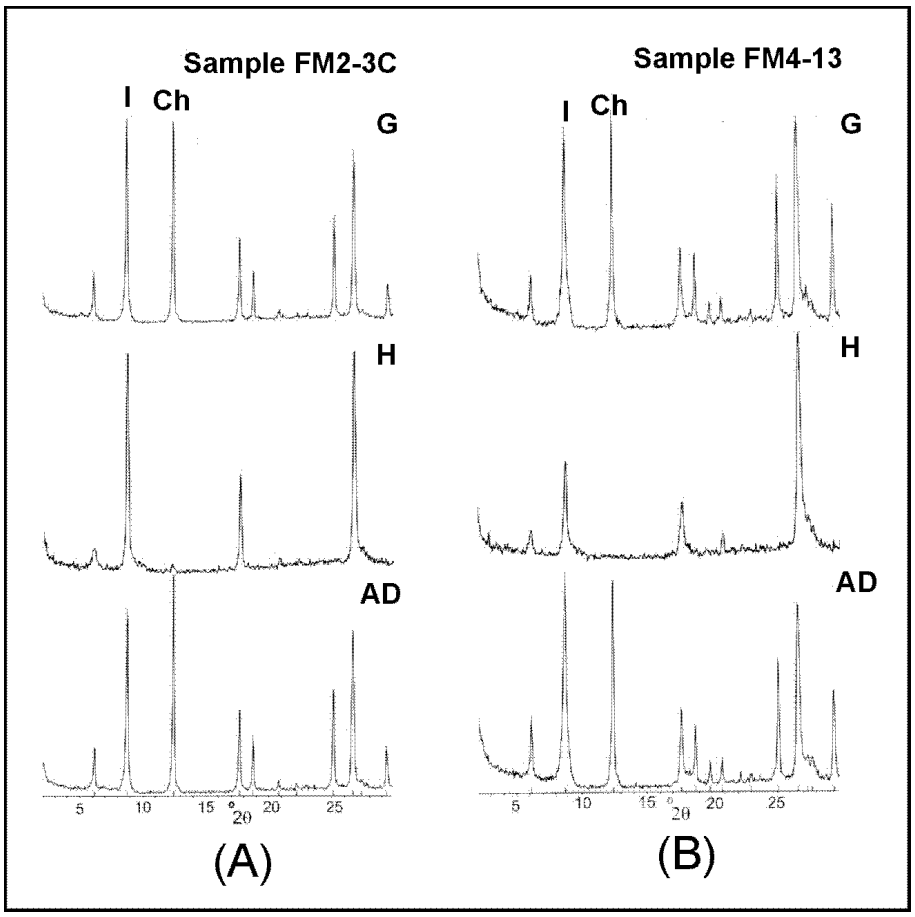

Figure 14. Detail clay XRD of metashale and calc-schist.
I: illite, Ch: chlorite, AD: air-dried, G: glycolated, H: heated (550 °C)

Table 1. Chemical analyses of the samples (major elements)

UNIT	SAMPLE	SiO_2 %	Al_2O_3 %	Fe_2O_3 %	MgO %	CaO %	Na_2O %	K_2O %	TiO_2 %	MnO %	LOI %
Morbel Tepe clays	FM1-3	48.51	12.81	6.03	1.77	13.87	1.04	1.16	0.8	0.06	13.64
	FM2-3	42.38	12.45	5.76	1.45	16.67	0.76	2.08	0.71	0.06	16.22
	FM2-4	39.25	13.89	6.76	1.6	16.67	0.74	2.84	0.71	0.07	16.75
	FM2-5	46.7	13.5	9.1	3.8	11.4	0.4	2.4	0.9	0.1	11.75
	FM2-7A	45.45	12.27	5.6	2.74	14.41	1.5	1.97	0.61	0.1	14.36
	FM2-8	44.24	17.67	6.76	2.49	10.45	0.89	3.5	0.7	0.05	12.45
	FM3-5	64.85	17.04	7.15	1.38	0.15	0.69	4.44	0.93	0.01	3.02
	FM 3-6	49.32	17.05	8.31	2.43	8.72	1.4	3	0.85	0.05	8.09
	FM4-9	47.09	14.25	6.69	1.39	13.3	0.71	2.62	0.84	0.05	12.67
	FM4-13	45.38	14.25	5.68	1.91	14.27	0.69	2.25	0.83	0.06	14.13
	F4	65.8	16.41	6.45	1.42	0.23	0.52	4.98	0.93	0.01	2.72
	F5	46.52	17.94	6.49	2.02	9.16	0.99	3.82	0.66	0.06	11.65
	FM1-6	29.7	11.19	5.02	2.25	25.28	1.06	1.14	0.55	0.09	23.2
	FM2-3A	31.41	10.74	4.98	1.34	25.06	0.38	2.56	0.58	0.08	22.07
	FM2-3B	32.26	10.74	6.49	1.29	24.58	0.37	2.47	0.6	0.06	20.8
	FM2-3C	32.26	12	6.88	2.79	21.6	0.3	1.93	0.6	0.06	21.68
	FM3-7	18.3	6.15	2.49	1.41	38	0.36	0.63	0.33	0.14	31.34
	FM4-1	22.57	8.13	3.7	2.6	32.45	0.44	1.06	0.41	0.06	28.1
	FM4-8	19.44	7.41	3.07	0.73	36.15	0.25	1.49	0.36	0.12	30.29
Halıcı metavolcanites	FM3-2	63.62	14.16	5.99	3.64	2.58	2.57	1.42	0.76	0.04	3.99
	FM3-3	57.3	14	6	3.8	5.8	0.2	4.7	0.8	0.1	6.6
	FM3-4	57.63	13.44	4.9	3.1	8.21	0.49	2.84	0.66	0.05	8.05
	FM7-1	58.49	13.26	8.32	2.53	5.87	1.48	0.05	0.53	0.13	5.91
Asarkale volcanites	FM3-8	64.84	16.64	3.68	0.75	4.45	3.65	3.6	0.52	0.04	1.93
	FM3-9	65.35	16.09	4.02	1.72	3.57	3.64	3.83	0.6	0.07	1.01
	FM3-9A	64.71	16.79	3.21	0.69	4.63	3.51	3.67	0.5	0.04	2.05

Table 2. Data of I(002) / I(001) and KI of Morbel Tepe clays

Sample	I(002) / I(001)	KI ($\Delta^o 2\theta$)	Clay Minerals
F4	0.22	0.1	Illite
FM2-3A	0.37	0.11	Illite, Chlorite
FM2-3B	0.36	0.15	Illite, Chlorite
FM2-3C	0.45	0.15	Illite, Chlorite
FM2-4	0.37	0.3	Illite, Chlorite
FM2-8	0.35	0.2	Illite, Chlorite
FM3-5	0.2	0.1	IllIte
FM3-6	0.31	0.3	Illite, Chlorite
FM4-7	0.29	0.2	Illite, Chlorite
FM4-13	0.32	0.2	Illite, Chlorite

Table 3. Results of liquid limit

1.CAN NO			I	II	III
2.WEIGHT OF WET SOIL+CAN	(g)		117.2	135.4	132.5
3.WEIGHT OF DRY SOIL+CAN	(g)		106.2	123.5	120.5
4.WEIGHT OF MOISTURE	(g)	2-3	11	11.9	12
5.WEIGHT OF CAN	(g)		61.4	78.1	78
6.WEIGHT OF DRY SOIL	(g)	3-5	44.8	45.4	42.5
7.WATER CONTENT	(w%)	4/6	24.6	26.2	28.2
8.NUMBER OF BLOW	(N)		60	30	16

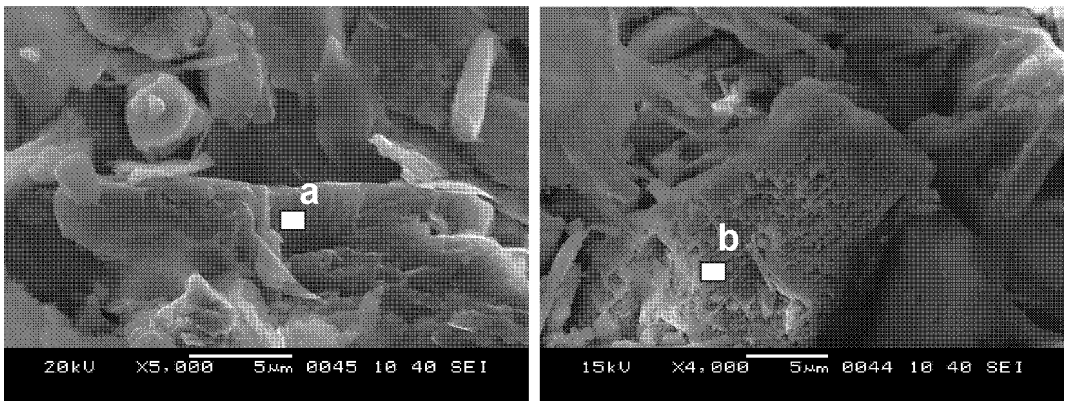

Figure 15. SEM photographies of clay minerals (a: phillosilicates resulted by alteration b: the argillization occured along the cleavage as a result of alteration)

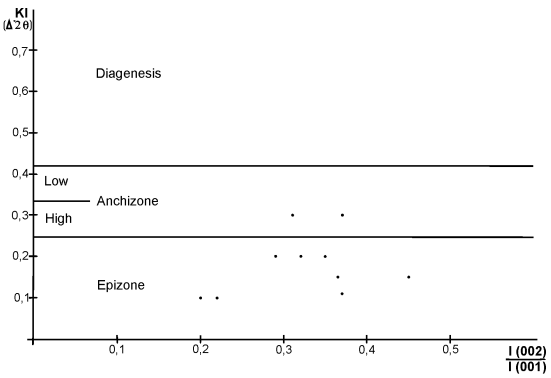

Figure 16. Diagram of KI - I(002)/I(001) (Kubler 1984)

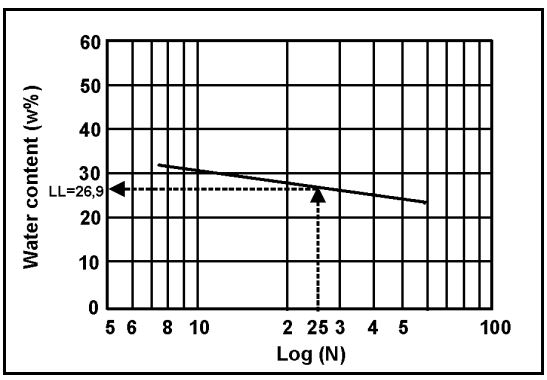

Figure 17. Graph of the flow curve

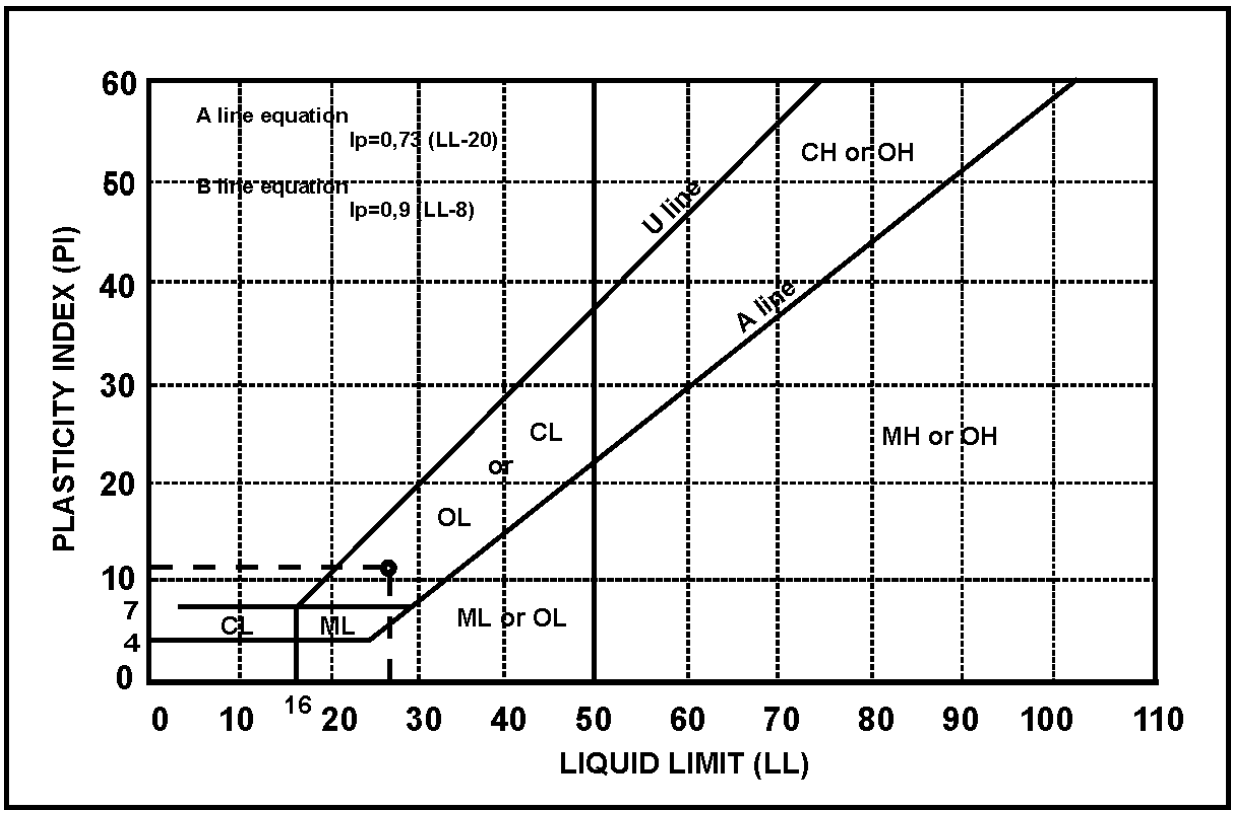

Figure 18. Casagrande plasticity graph

5.2 Determination of the Atterberg limits

The Atterberg limits comprise the liquid limit, plastic limit and shrinkage limit. These limits are also called consistency limits (Aytekin, 2000). This document covers the determination of the liquid limit and the plastic limit only.

The Casagrande Liquid Limit Test is used to obtain the water content at which a soil changes from a viscous liquid to a plastic state (Table 3).

On the plotted flow curve which is drawn with respect to water content versus log of blow, the value of water content at 25 blow is designated as the liquid limit. In this study liquid limit was obtained as 26.9% (Figure 17).

The Plastic Limit Test is used to find the water content at which a soil changes from a plastic state to a semi-solid (Table 4).

Table 4. Results of plastic limit

1.CAN NO			I	II
2.WEIGHT OF WET SOIL+CAN	(g)		17.4	17.3
3.WEIGHT OF DRY SOIL+CAN	(g)		17	16.9
4.WEIGHT OF MOISTURE	(g)	2-3	0.4	0.4
5.WEIGHT OF CAN	(g)		14.2	14.5
6.WEIGHT OF DRY SOIL	(g)	3-5	2.8	2.4
7.WATER CONTENT	(w%)	4/6	14.3	16.6

Table 5. Unified soil classification system (USCS) (Kumbasar & Kip, 1999)

MAIN GROUPS (except 7,5 cm coarse material)			GROUP SYMBOL	TYPICAL NAMES
COARSE-GRAINED SOILS	GRAVEL	Pure pebble	GW	Well graded gravel, pebble-sand mixtures (few or none fine grains)
			GP	Poorly graded gravel, pebble-sand mixtures (few or none fine grains)
		Pebble	GM	Silty gravels, poorly graded pebble-sand-silt mixtures
			GC	Clayey gravels, poorly graded pebble-sand-clay mixtures
	SAND	Pure sand	SW	Well graded sands or pebbly sands (few or none fine grains)
			SP	Poorly graded sands and pebbly sands (few or none fine grains)
		Sand	SM	Silty sands, poorly graded sand-silt mixtures
			SC	Clayey sands, poorly graded sand-clay mixtures
FINE-GRAINED SOILS	Silt and Clay Liquid Limit < 50		ML	Inorganic silt and very fine sands, very little plastic rock dust silty or clayey fine sands
			CL	Inorganic clays (low-middle plasticity) pebbly clays, sandy clays, silty clays, lean clays
			OL	Organic silts and low plasticity organic silt-clay mixtures
	Silt and Clay Liquid Limit > 50		MH	Inorganic silts, diatomaceous or micaceous fine sandy or silty soils, elastic silts
			CH	High plasticity inorganic clays, fat clays
			OH	Middle-high plasticity organic clays
More organic soils			Pt	Peat and the other more organic soils

The plastic limit of a soil is the lowest water content at which the soil is plastic. The determination of the plastic limit is normally obtained in conjunction with the determination of the liquid limit.

According the determination, average water content (plastic limit) is 15.5%. The formula of plasticity index is as follows:
PI (plasticity index) = LL (liquid limit) – PL (plastic limit).

According to this formula, plasticity index is 11.4%.

The sample is located in the CL area in the Casagrande plasticity graph (Figure 18). The sample is silty clay which has low-middle plasticity in the unified soil classification system (Table 5).

6. RESULTS

The petrographic studies indicated the existence of four groups of rocks, which are volcanic, metavolcanic, sedimentary and metasedimentary rocks .

According to the results of XRD investigations, the metashales and calc-schists consist of illite and chlorite as clay minerals. The XRD data indicate that the degree of crystallinity of illites in metashales and calc-schists is high; therefore, they are in epizone region representing a low grade metamorphism. The illites are in 2M polytypes, dioctahedral and detritial because of the low grade metamorphism. The chlorites

are in IIb polytypes, trioctahedral and detritial because of the low grade metamorphism.

- *The results of the geochemical studies revealed a similar composition for the metashales and calc-schists. However, the metashales contain more SiO_2 and Al_2O_3 than the calc-schists and the calc-schists contain more CaO than the metashales.*
- *When the samples are evaluated with respect to their properties from the viewpoint of cement industry, it was determined that the samples meet the requirement of 2/1 ratio of Al_2O_3/Fe_2O_3. According to the results of the plasticity experiment, however, the plasticity of Morbel Tepe clays is 11.4%.*

As a conclusion, it is not convenient to determine the clay according to its chemical, mineralogical analyses and plasticity. It is also necessary to combine it with a convenient limestone, prepare a different composition, and perform the firing tests.

REFERENCES

Aytekin, M. (2000). Deneysel Zemin Mekaniği (1.Baskı). Trabzon: Akademi Yayınevi.

Carroll, D. (1970). Clay minerals: A guide to their x-ray identification. USA: *The Geological Society of America*.

Dunoyer De Segonzac, G. (1970). The transformation of clay minerals during diagenesis and low-grade metamorphism: A review. *Sedimentology,* 15, 281-346.

Erkan, Y. (1978). Kayaç oluşturan önemli mineraller. Ankara: *Hacettepe Üniversitesi Yayınları* A 26.

Kubler, B. (1984). Les indicateurs des transformations physiques et chimiques dans la diagenese, temperature et calorimetrie. In Thermometrie et barometrie geologiques, ed. M. Lagache, *Soc. Franç. Miner. Crist.*, Paris, 489-596.

Özcan, A., Göncüoğlu, M.C., Turhan, N., Şentürk, K., Uysal, Ş. & Işık, A. (1990). Konya-Kadınhanı-Ilgın dolayının temel jeolojisi. *MTA Rapor No: 9535*.

Weaver, C. E. & Pollard L. D. (1973). The chemistry of clay minerals. Amsterdam: Elseiver Scientific Publishing Company.

Wilson, M. J. (1987). A handbook of determinative methods in clay mineralogy. New York: Chapman and Hall.

A STRIPE METHOD FOR PRODUCING ENGINEERING GEOLOGICAL MAP OF BURDUR (TURKEY) URBAN AREA

Özçelik M.[1], Şener E.[1] and Ertunç A.[2]

[1]Süleyman Demirel University Dept. of Geological Engineering, 32260, Isparta, Turkey
[2]Çukurova University Dept. of Geological Engineering , 01330, Balcalı, Adana, Turkey
ozcelik@mmf.sdu.edu.tr , esener@mmf.sdu.edu.tr , aertunc@cu.edu.tr

Abstract: The purpose of this research is to obtain a basic knowledge of geological structures, the types and distribution of lithologic units and their geotechnical properties. Such knowledge is essential for the planning of the land use especially for design, construction and maintenance of engineering works.

In this study three different 1:5000 scaled "Engineering Geological Maps" of the Burdur Urban Area have been prepared. The first of these maps is a "Documentation Map" on which borehole locations, foundation excavation points, surface observation points are marked. On the second map, which is an "Engineering Geological Map", shows the lithological properties of the geological units at five different levels, 1 – 3 m., 3 – 7 m., 7 – 13 m., 13 – 20 m, > 20 m. Finally, the Section map is prepared from 17 geological cross-sections of different location 400 meter intervals to give a three-dimensional model of the investigation area. The stripe method has been used as a mapping method and supported with cross sections. This method shows the distribution depth and thickness of layers in three-dimensional representation. A stripe drawn on a map provides a window appearance which includes surface layer and deep layers, simultaneously.

These maps provide valuable information on foundation problems, canalization, land planning and environmental problems. The results obtained from the Engineering Geological Map of the area include the exposures determined by local observation, the level of the water table along with observation positions (i.e. boreholes and wells). It is expected that such a map will satisfy the requirements of the local authorities, planners, architects and engineers.

Key words: Stripe Method, Engineering Geological Map, Burdur

INTRODUCTION

An engineering geological study of the city of Burdur and its surrounding area (Figure 1) was carried out by the Department of Geology (during the years of 2000 and 2001) jointly with the department of Geophysics and Civil Engineering of Suleyman Demirel University. A major part of the project was the geological remapping and engineering geological mapping of the area.

An engineering geological map provides information on the probable presence of one or more geologic materials at a given depth over a specified area. The value of such a map is due to the information provided about the distribution, depth and thickness of all geological materials within the depth of mapping. This information is significant for many specific uses. Engineering geological mapping is a basic requirement for the fullest possible understanding of specific features at a site.

2. GEOLOGY

The geologic map of the study area along with its surroundings was prepared at a scale of 1:25000 by members of geology department (Figure 2). This map allowed clearer and more detailed understanding of the lithological and stratigraphical of the area then what is known due to previous surveys. New lithostratigraphical divisions were defined on the basis of current knowledge and mapping criteria and shown as map units.

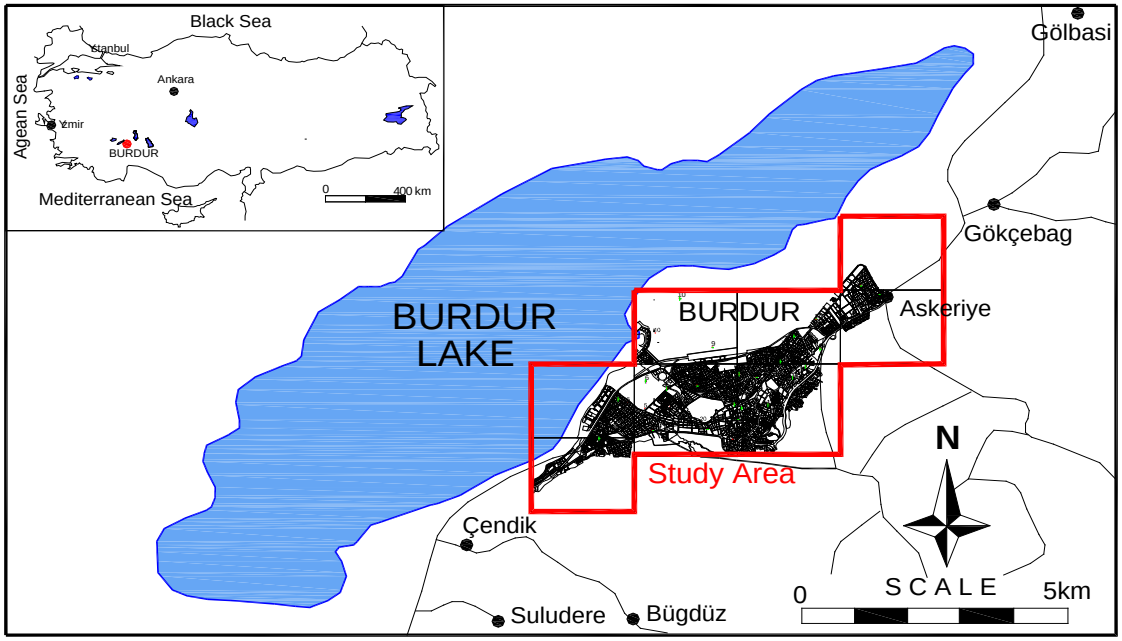

Figure 1. Location map of the study area

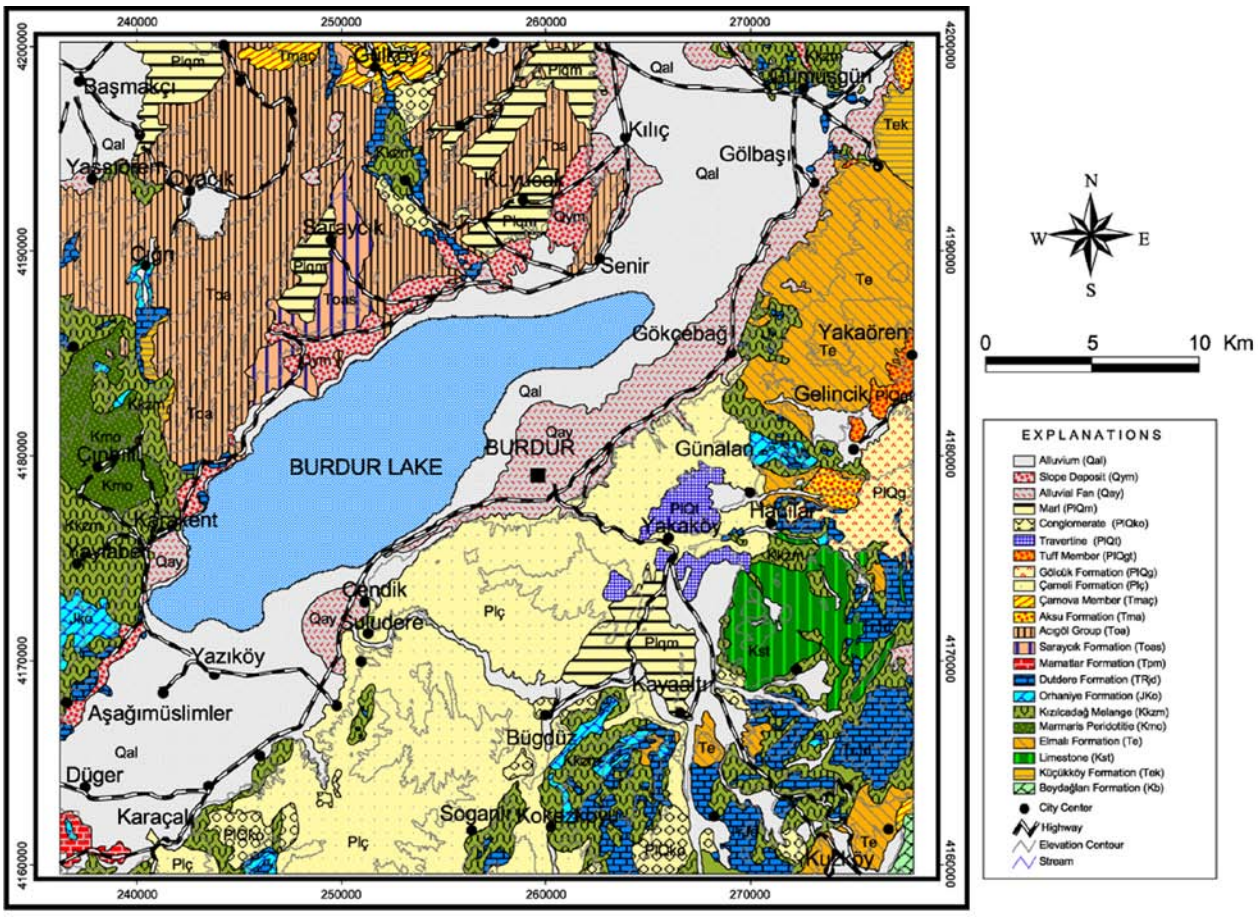

Figure 2. Geological Map of the Burdur Urban Area and its Surroundings (modified by Şenel 1997)

Stratigraphical and lithological features of the units in the study area were determined by field study and observations as well as description of the borehole cores. The stratigraphic

coloumnar section of the geological units of the study area is given in Figure 3.

This unit is composed of mainly polygenic pebbles and strongly cemented conglomerate. This formation takes its name from Karaburun Hill located south-west of Burdur city.

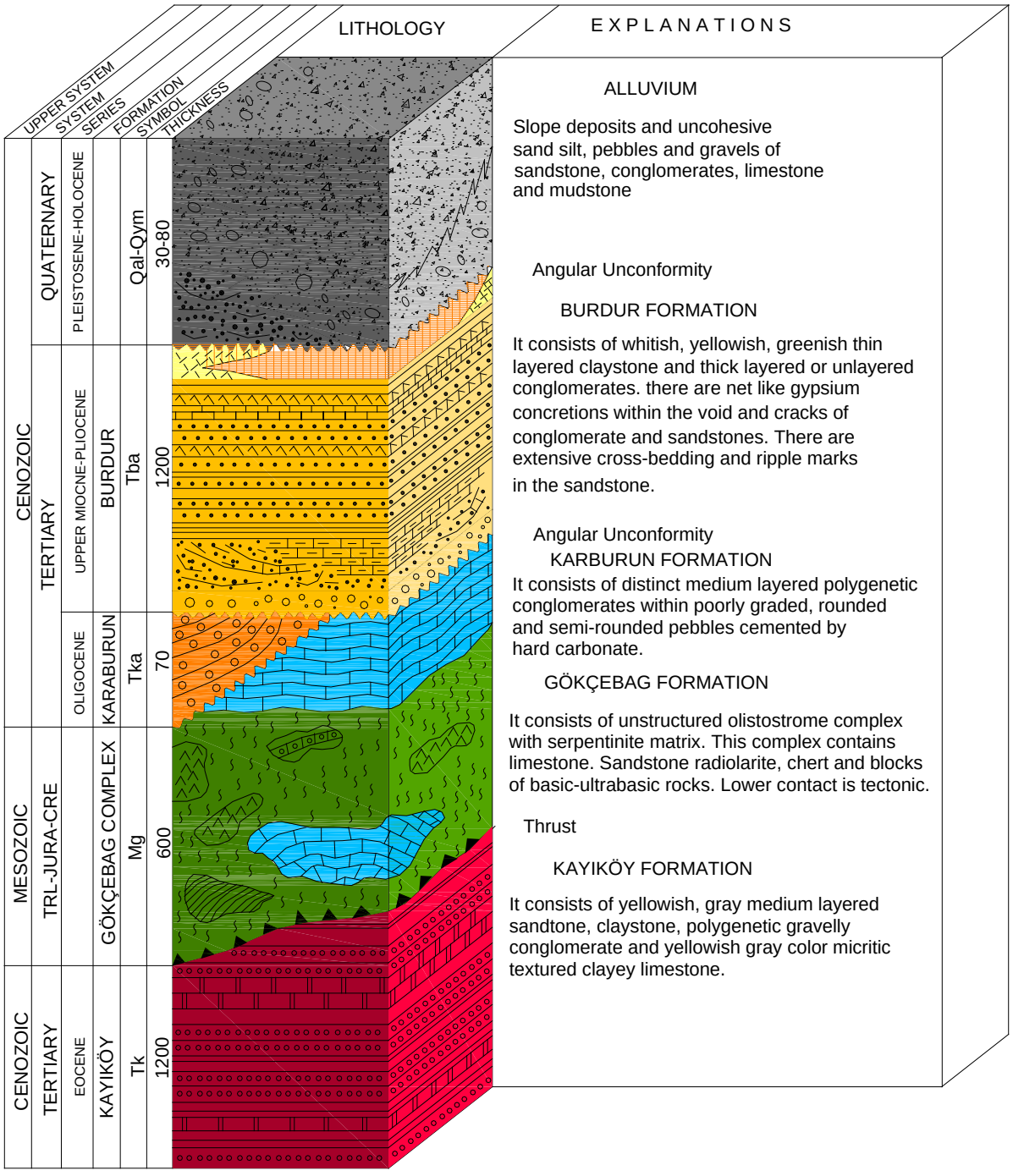

Figure 3. Generalized Stratigraphic column of the Burdur Urban Area and its Surroundings (modified by Ertunç et al. 2001)

This formation has been located south of the Burdur lake depression and Burdur city centre and its surrounding area. Burdur formation is mainly composed of reddish brown poorly packed, poorly graded pebble stone, rarely interbedded whitish-yellowish sandstone, greenish claystone, marl, clayey limestone, and intermingled with thin interbedded coal,

whitish-yellowish tufit upper level of which can be seen.

Alluvium can be seen at the surface in most of the study area. The alluvium cut by drillhole SK-21 has a thickness of 33m. This is a maximum value in this area. The thickness of the alluvium increases to the north of Bağlar quarter. Particles in size of clay, silt, sand and gravel forming the alluvium lie in horizontal position and show vertical and horizontal transition to one another. Levels are formed by the particles of these four sizes at different ratios. Descriptions of materials forming the alluvium are summarized from the drill holes.

Lacustrine sediments are the sediments within the influence area of Burdur Lake and below 915 meter elevation. They consist of clay, silt, sand layers and various combinations of them. They exhibit vertical and horizontal variations. They are unaffected by recent tectonism. Here, exposed areas with a clay layer over 10m. thick is defined as lacustrine clay. The other places which contain sands extensively are mapped as lacustrine sands. Alluvial fans mainly formed as a result of weathering of Burdur Formation units. This unit is mainly composed of clay sediments.

3. ENGINEERING GEOLOGY

Engineering geological maps are characterized by great variability because of a wide range of subjects of engineering geological investigation. Generally, the main purpose of engineering geological maps is presentation of engineering geological conditions because they determine the terms of design, constructions and maintenance of engineering works.

Engineering geological maps can be differentiated according to extension and contents of presented information: engineering geological maps created as a result of regional studies aimed at providing information for land use planning, and site investigation maps concentrated on the presentation of geologic information that affects the design and construction of a particular project at a specific location. Moreover, the different phases of design require a different degree of engineering geological condition proficiency, as well as a different degree of completeness of their content and data precision (Dearman, 1991).

Despite all this variety and individuality, engineering geological maps must embody certain conventions and a certain degree of standardization. A guide to the preparation of engineering geological maps (Anon, 1976), issued by IAEG Commission No.1 named “Engineering Geological Maps” is largely accepted by most engineering geologists as the world standard (Culshaw, 1998).

There are numerous publications of working party reports (Anon., 1972; 1976; IAEG 1981a; 1981b) issues by IAEG Commissions No.1 (Engineering Geological Maps) and No.2 (Landslides and other mass movements on slopes), which are used as a base for developing international (Varnes, 1984; Anon.,1996a; 1996b) and national (Anon., 1981) standards related to specific purpose geological mapping.

The publication of engineering geological standards is especially extensive in Europe in the last decade, due to the publication of European norms (Eurocode 7).

3.1. Documentation Map

A documentation map shows documentation points according to their nature; that is whether they are borehole locations, foundation excavation points, outcrops, road cuttings, etc. The location from which samples have been taken for laboratory tests are shown in a distinctive way. This map is a base map for an Engineering Geological Map.

Initially, a 1/25.000 scale basic geology map of the area was prepared and the lithological units were determined. Geotechnical, hydrogeological and

geophysical studies were carried out in the area where the basic geological investigations were made and 24 boreholes were drilled at different locations in Burdur city centre. Cored boreholes were drilled at 24 locations in order to determine the geotechnical properties of the ground, to establish the geological profile at the area to carry out in-situ tests.

3.2. Engineering Geological Map

In engineering geological studies, ground classification is expressed on engineering geological maps. The extent and variation of lithological units are predicted from borehole records, geotechnical data or from mapping explanatory drilling. When these maps are backed up by laboratory test results, they become very useful (Dearman, 1991).

The results of the examination of preliminary sources of information and the site inspection may be incorporated. In a provisional map the section of the area is investigated. The map will be a valuable aid and it will be possible to map only some of the information mentioned in this section, from the data obtained from preliminary sources. The map will need to be revised and completed when the full site investigation has been carried out. The geological map can form a good basis for one type of engineering geological map, refinements and additions being made to be mapped (Figure 4).

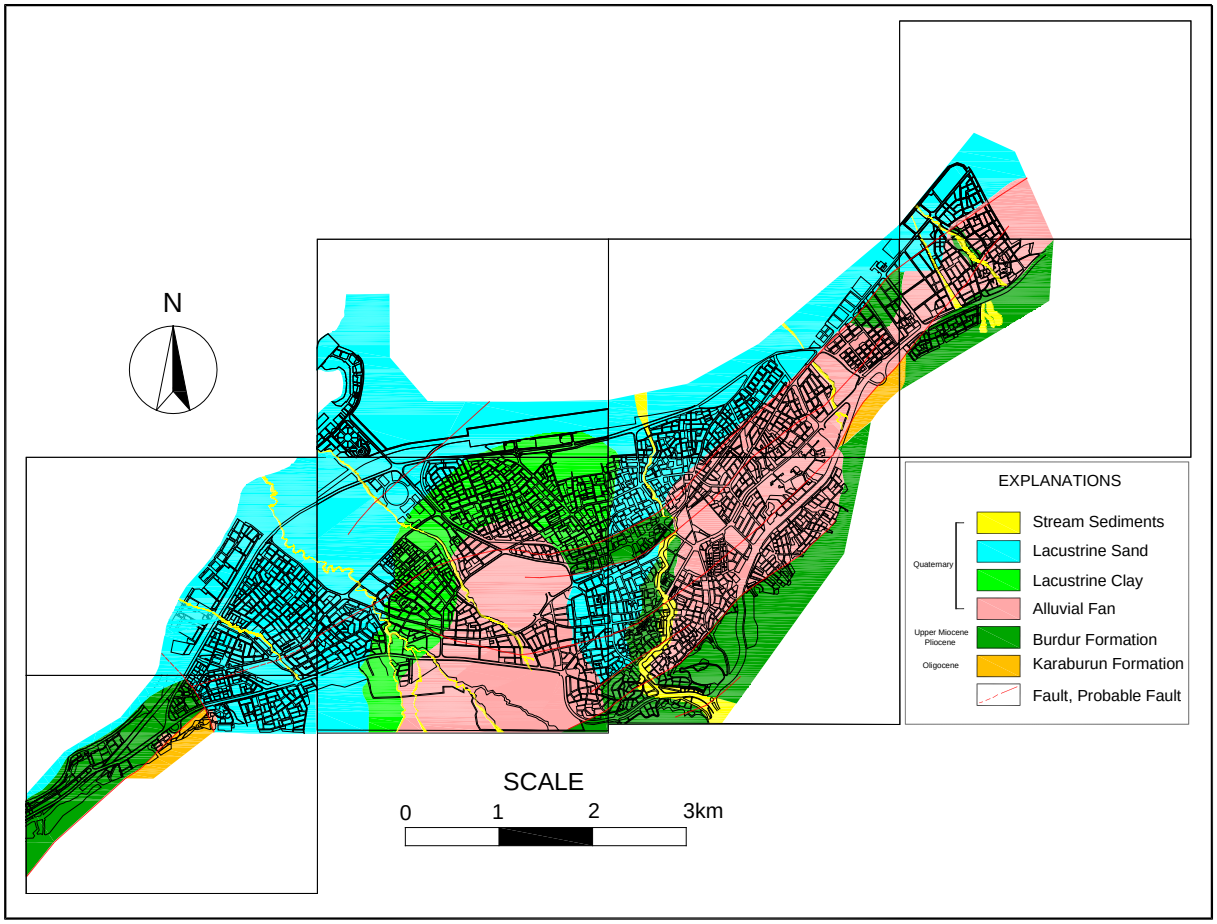

Figure 4. Engineering Geological Map of the Burdur Urban Area (Ertunç et al. 2001)

Boundaries and features, and further detailed keys should be added indicating the engineering character of the materials present. Overlays to the map may also be useful. Direct observations should be distinguished from inference and interpretation, and care should be taken to show the degree of certainty of the

position of boundaries and features by using suitable conventions. Local observations, outcrops and exposures should be included, and the groundwater conditions should be indicated. The position of boreholes and other site investigations works should be marked. More than one map or overlay may be needed to show various features of the area. A section map can also help.

3.2.1 Preparation of the Engineering Geological Map with Stripe Method

In engineering geological studies, ground classification or grading is generally expressed on engineering geological maps. The extent and variation of soils are predicted from borehole records. When these maps are backed up by laboratory test results they become very useful.

Various approaches have been used to show earth materials in three-dimensional way. Each approach has been tailored to fit specific needs and geologic conditions for engineering geology (Varnes, 1974). A number of methods have been developed in different countries.

Engineering geological studies with depth limits within 2 to 20 m can be useful here, since much general construction and most borrow extraction occur within this range. With this thickness of superficial deposits there is a strong likelihood that more than one soil type might be present, with the certainty also that individual layers would not be uniform in thickness. The surface layer presents no difficulties. Different colors, and thickness ranges still leave the map visually attractive and easy to understand. It is the next step, representing the following layers, that is difficult.

The stripe method is used to represent the lithology in five thickness zones distinguished either by a pattern representing lithology, for which there are variations for spacing, or by shades of the same color with the deepest shade for the thickest unit.

A vertical stripe with a symbol or a distinctive pattern designates the second layer, which of course can also crop out. Where the second layer lies beneath the top layer, a very wide stripe is used for the thickness range 1-3 m, a wide stripe used for the thickness range 3-7 m, a narrow stripe for 7-13 m, a narrower stripe used for the thickness range 13-20 m and interrupted stripe for > 20 m where thickness ranges are approximate, the boundaries of the stripes and rectangles are drawn as pecked lines. As a result of the evaluation of data obtained from the examination of cores and field studies together, engineering geological maps were prepared (Figure 5). A section map, prepared chiefly on account of numerous borehole logs, gives information about the occurrence of the strata and distribution of the types of the unit at greater depth.

3.2.2. Engineering Geological Characteristics of Units

The engineering geological characteristics of units are summarised in Table 1, some of the common engineering geological problems are likely to be encountered in these units. The tables highlight the important unit characteristics such as liquid limit (WL), plastic limit (WP).

Table 1. Selected engineering properties of different geological units

Engineering Properties	Units	Lacustrine Sediments		Alluvial Fan
		Clay	Sand	
W_L		22-252,3	323-528	366-614
W_P		196,2-252,3	206,1-263	176-288
P_I		23,8-2	98-289,3	1382-326
Above Groudwater W_O (%)	Clay	4-46	11-48	17-38
	Sand	14-29	4-20	11-21
	Silt	-------	10-21	-------
Under W_O (%) groundwater	Clay	-------	34-49	17-41

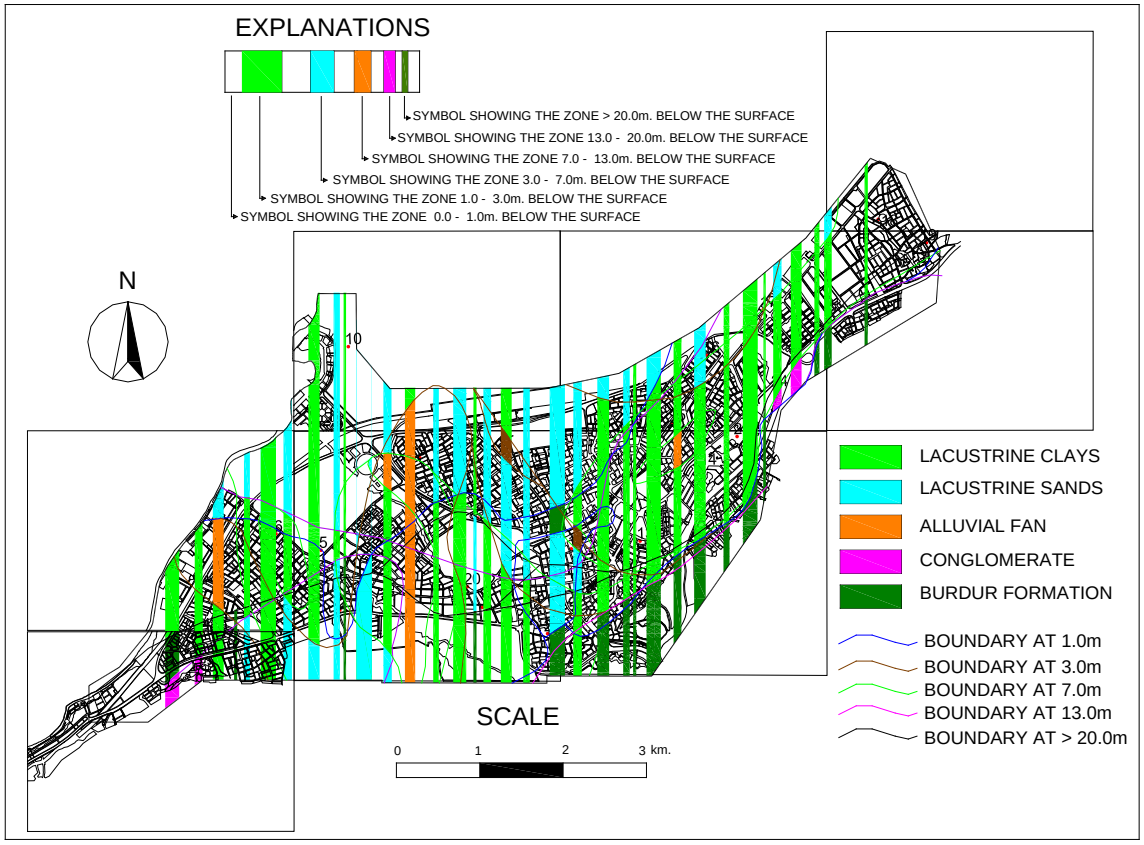

Figure 5. Engineering Geological Map of the Burdur urban area produced using the Stripe method

3.2.3. Section Map

A section map of the site showing the surface topography and with the boreholes marked at their correct position and levels, brings out the relation between the one borehole and the next, and between the boreholes and the site as a whole. This may allow a correlation to be made between the units in the borehole and, when taken with other information on the site and interpolation is made between the boreholes, to determine the ground conditions.

It may be useful to prepare other sections running in different directions in addition to the horizontal section. Section map will be useful in situations such as dipping state in cuttings and embankments, on sidelong ground, and appropriately oriented sections may be required at the sites of important structures or extensive works.

A section map is prepared chiefly on account of the numerous borehole logs, gives information about the occurrence of the strata and distribution of the types of rock and soil greater depth (scale of height 1/1000). 17 cross-sections were prepared of the study area, in the NW-SE direction. The aims of these sections were to describe the geological structures completely (Figure 6).

4. CONCLUSIONS

Engineering geological maps are special maps designed to highlight the engineering relevance of the geology of an area. There are many ways that this has been done, but only a few portray the depth dimension and even less do this in an adequate way. These maps require a considerable number of observation points for their completion and this means that a borehole sampling plan is necessary. Careful documentation and advance detailed planning is the basic pre-request for using these maps with confidence for engineering purposes.

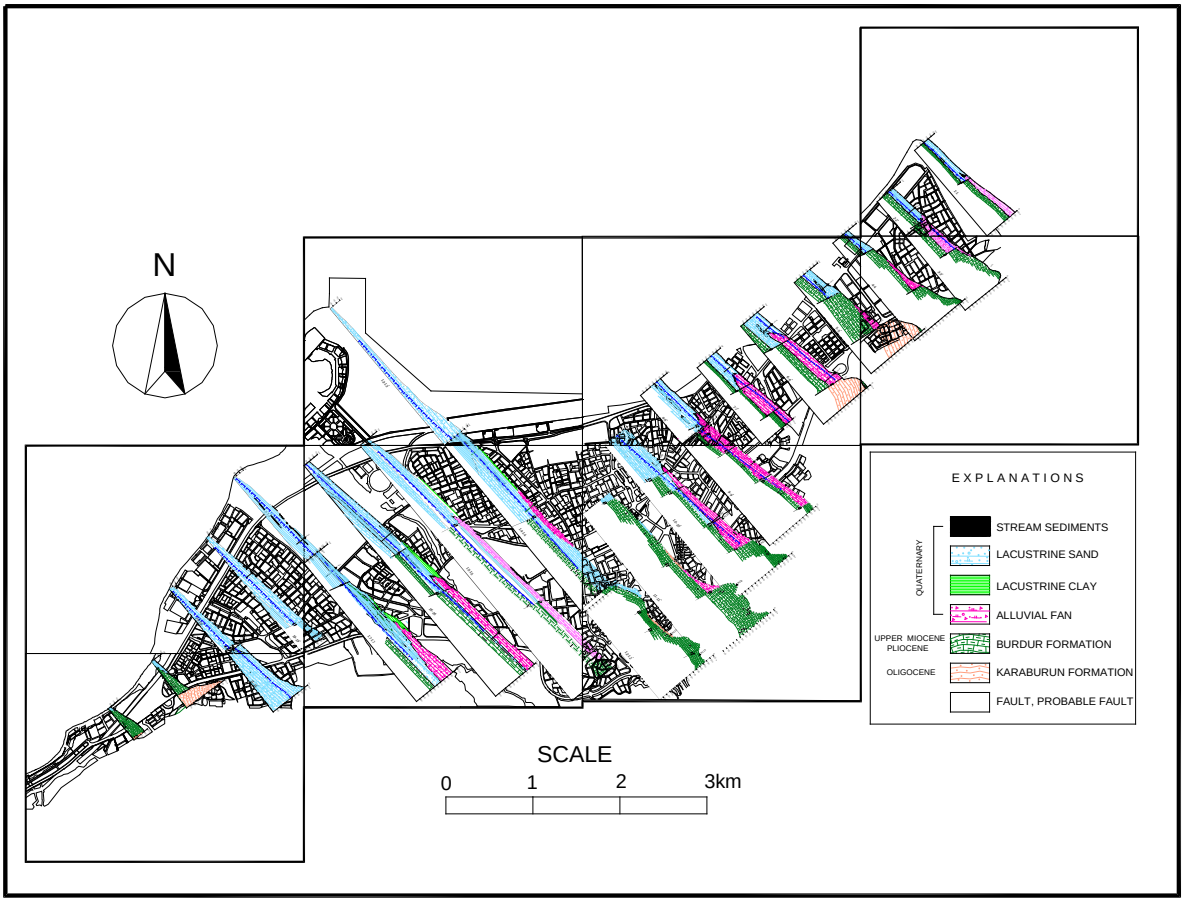

Figure 6. Dimentional (3D) Engineering Geological Section Map of the Burdur Urban Area

The basic geological map at the area was prepared and the lithological units were determined. Geotechnical, hydrogeological and geophysical studies were carried out in the area where the basic geological investigations were made and 24 boreholes were drilled at different locations at Burdur city centre. Cored boreholes were drilled at 24 locations in order to determine the geotechnical properties of the geological profile of the area to carry out in-situ tests. The engineering geological map was prepared.

In engineering geological studies, ground classification or grading is generally expressed on an engineering geological map. The extent and variation of each is predicted from borehole records, field observations, geotechnical data, and when these maps are backed up by laboratory test results, they become very useful. Engineering geological maps for 1-3 m, 3-7 m, 7-13 m, 13-20 m and > 20 m depths were prepared separately for different engineering purposes. As a result of the evaluation of data obtained from the examination of cores, together with field studies, engineering geological maps were prepared.

5. REFERENCES

Anon. 1972, The preparation of maps and plans in terms of engineering geology. *Quaterly Journal of Engineering Geology*, 5, pp. 293-381.

Anon. 1976, *Engineering geological maps:. A guide to their preparation.* The UNESCO Press, Paris, p. 79

Anon. 1981, BS 5930:1981: Code of practice for site investigation (formerly CP 2001). British Standarts Institutions, London, p. 147

Anon. 1996a, Geotechnics in civil engineering: Identification and classification of soil (ISO/DIS 14688). International Orgnization for Standardization, p. 28

Anon. 1996b, Geotechnics in civil engineering: Identification and classification of soil (ISO/DIS 14688). International Orgnization for Standardization, p. 27

Culshaw, M.G. 1998, Reports from commissions. Commission No. 1 Engineering Geology maps. *IAEG Newsletter*, 25, pp. 21-24.

Dearman, W.R. 1991, Engineering Geological mapping. Butterworth-Heinemann, Oxford, p. 387

Ertunç, A., Karagüzel, R., Yağmurlu, F., Türker, E., Keskin, N., 2001, Report of investigation of Burdur municipality and nearby surrounding in reference to earthquake and residential comnities. Suleyman Demirel University, Isparta (in Türkish)

Eurocode 7, Geotechnical design. Part 1: general rules. *CEN European Committee for Standardization.* Bruxelles, 1997.

IAEG 1981a, Rock and soil description and classification for engineering geological mapping. *Report by the IAEG Commission on Engineering Geological Mapping Bull.* IAEG, 24 pp. 235-274.

IAEG 1981b, Recommended symbols for engineering geological mapping. *Report by the IAEG Commission on Engineering Geological Mapping. Bull*. IAEG, 24 pp. 227-234.

Şenel, M. 1997, Türkiye Jeoloji haritaları Isparta J10 paftası, MTA Genel Müdürlüğü Jeoloji Etüdleri Dairesi, Ankara.

Varnes, D.J. 1974. The logic of Geological Maps with reference to their Interpretation and Use, U.S *Geological Survey Professional Paper,* 837, Washington.

Varnes, D.J. 1984: Landslides hazard zonation: a review of principles and practice. *Natural Hazards*, 3, UNESCO, Paris.

(This page is left blank intentionally.)

AFTERSHOCK BEHAVIOURS OF THE EARTHQUAKES IN AKŞEHİR-AFYON AND GÖKOVA GRABENS, TURKEY

Özer N.[1], Altınok Y.[1], Ceylan S.[1], Kurt H.[2] and Kolçak D.[1]

[1] Istanbul University, Engineering Faculty, Department of Geophysical Engineering, 34320 Avcılar, Istanbul, (naside@istanbul.edu.tr),

[2] Istanbul Technical University, Mining Faculty, Department of Geophysics, 34390 Maslak, Istanbul.

Abstract: The correlation between b and p-values is important to construct a model for interpretation of aftershock behaviours. In this paper, the variations of b-value, p-value and their relations are examined in order to see how these parameters change according to time and space for the earthquakes of Aksehir-Afyon Graben (AAG) in west-central Anatolia and Gokova Graben in southwestern Anatolia.

Hellenic and Cyprus arcs are two main dynamic elements in the eastern Mediterranean. NW-SE directed AAG is located in the north of Isparta Angle where Hellenic and Cyprus arcs intersect and E-W directed Gokova Graben is located on the back arc of Hellenic Arc. The aftershock behaviours of 15 December 2000 Sultandagi-Aksehir (Mw=6.0), 03 February 2002 Cay-Eber (Mw=6.5) and Cobanlar (Mw=5.8) earthquakes in AAG and 04 December 2004 Gulf of Gokova (Mw=5.5), 20 December 2004 Ula (Mw=5.3) and 10 January 2005 Oren (Mw=5.4) earthquakes in Gokova Graben are investigated by means of the b-value of Gutenberg-Richter, the p-value of modified Omori formula and their correlations, using aftershocks larger than or equal to 2.5. The calculated b and p-values vary between 0.34-2.85 and 0.58-1.77 for earthquakes in AAG and 0.56-1.78, 0.51-3.7 for earthquakes in Gökova Graben, respectively.

Key words: b-value, p-value, aftershock behaviour, western Anatolia

INTRODUCTION

The 2000 and 2002 earthquakes occurred on the northern part of the Sultandagi-Aksehir Fault (SAF), which is the border fault of the Aksehir-Afyon Graben (AAG), in west-central Anatolia. The AAG is the NE flank of the Isparta Angle (IA) and it separates the extensional regime of western Anatolia from the relatively stable Central Anatolian Plateau. The 2004 and 2005 earthquakes occurred in the Gulf of Gokova, under an N-S extensional tectonic regime of western Anatolia-Aegean region. The gulf was mainly opened by a buried major listric normal fault called Datca Fault (Figure 1). The north-dipping and E-W trending Datca Fault is located at the southern part of the Gulf associated by anthithetic faults located at the north (Kurt et al., 1999).

DATA AND THEIR ANALYSIS

The b-value is the slope of Gutenberg-Richter law which describes an exponential relationship between the ocurrence number of earthquakes and their magnitudes (Gutenberg and Richter, 1944). It varies from region to region, time to time in the same region, and also from depth to depth (Ogata and Katsura, 1993). The p-value of the modified Omori law (Utsu, 1957) describes the decay of aftershock frequencies with time and it was initially described by Omori (1894). The variability of p-value may be related to structural heterogeneity, stress and temperature in the crust (Utsu et al., 1995).

The aftershock sequences of 15 December 2000 Sultandagi-Aksehir (Mw=6.0, 16:44:47.6 UTC), 03 February 2002 Çay-Eber (Mw=6.5, 07:11:28 UTC) and 03 February 2002 Cobanlar (Mw=5.8, 9:26:43 UTC) earthquakes in AAG system and 04 August 2004 Gokova (Mw=5.5), 20 December 2004 Ula (Mw=5.3) and 10 January 2005 Oren (Mw=5.4) earthquakes in the Gulf of Gokova are analyzed to estimate p- and b-values.

The obtained b-values are found in the ranges of $0.56 \leq b \leq 1.12$, $0.96 \leq b \leq 1.78$,

0.77≤b≤1.50 for Gokova (2004), Ula (2004), Oren (2005) earthquakes in the Gokova Graben and 1≤b≤1.33, 0.34≤b≤1.77 and 0.94≤b≤2.85 for Sultandagi-Aksehir (2000), Cay-Eber and Cobanlar (2002) earthquakes in the AAG, respectively. Since only three aftershocks occurred in the first hour of the Cobanlar earthquake, the obtained b-value by the regression analysis is quite high with the value of 4.77, and it is neglected. The calculated p-values are in the range of 0.64≤p≤2.26, 0.51≤p≤1.71, 0.62≤p≤3.7 and ≤p≤0.77, 0.58≤p≤1.30, 0.44≤p≤1.07 (Figure 2).

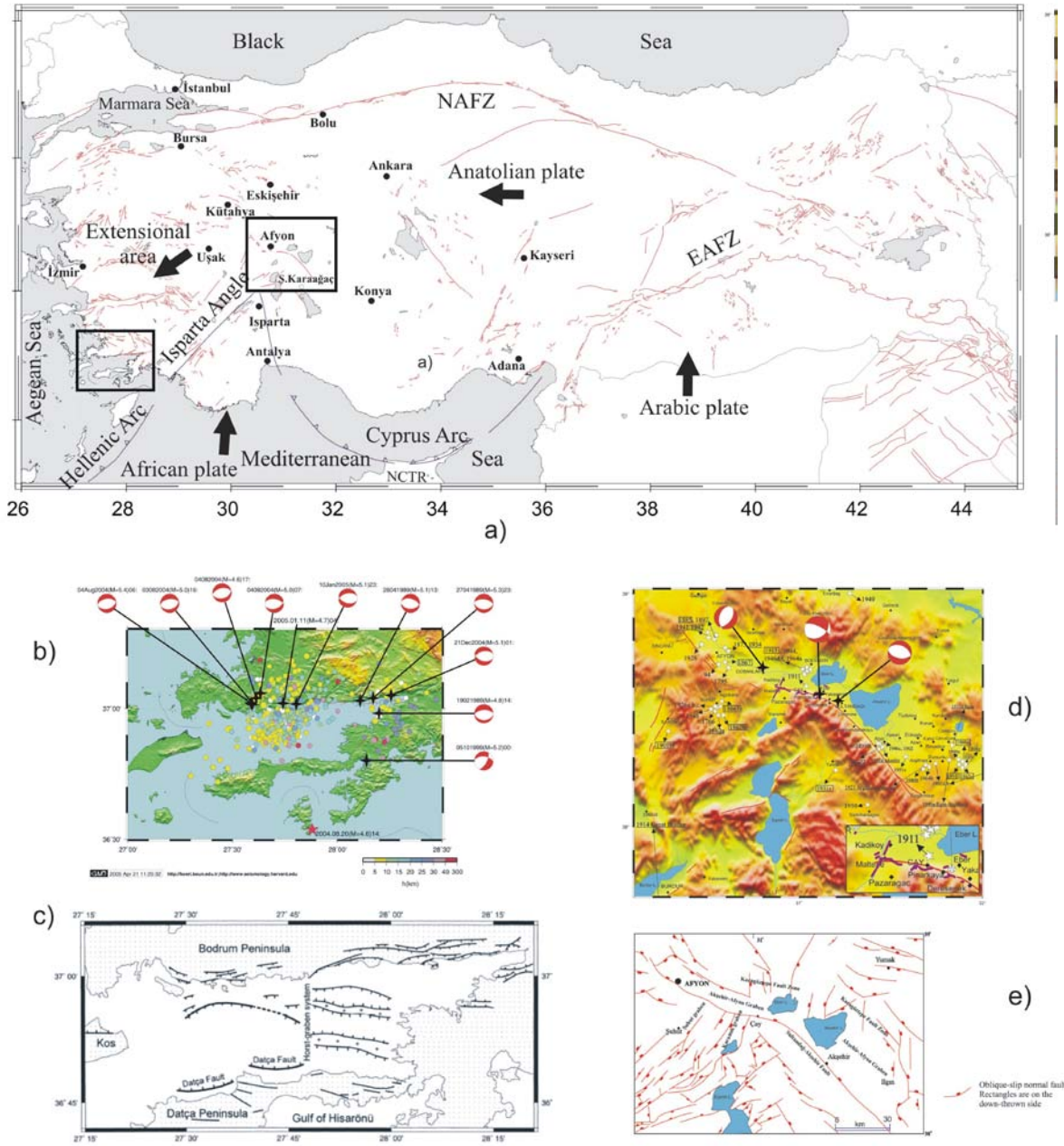

Figure 1. a) Locations of the investigated areas; b) The earthquakes with the focal mechanism solutions and aftershock distributions for the Gulf of Gokova. Stars and circles denote epicenters of the main shock and the aftershocks, respectively; c) Active faults in the Gulf of Gokova by Kurt et al. (1999); d) Historical seicmicity and the earthquakes with the focal mechanism for Aksehir-Afyon Graben System by Ozer and Altinok (2005); e) Active faults in AAG by Koçyiğit (2002)

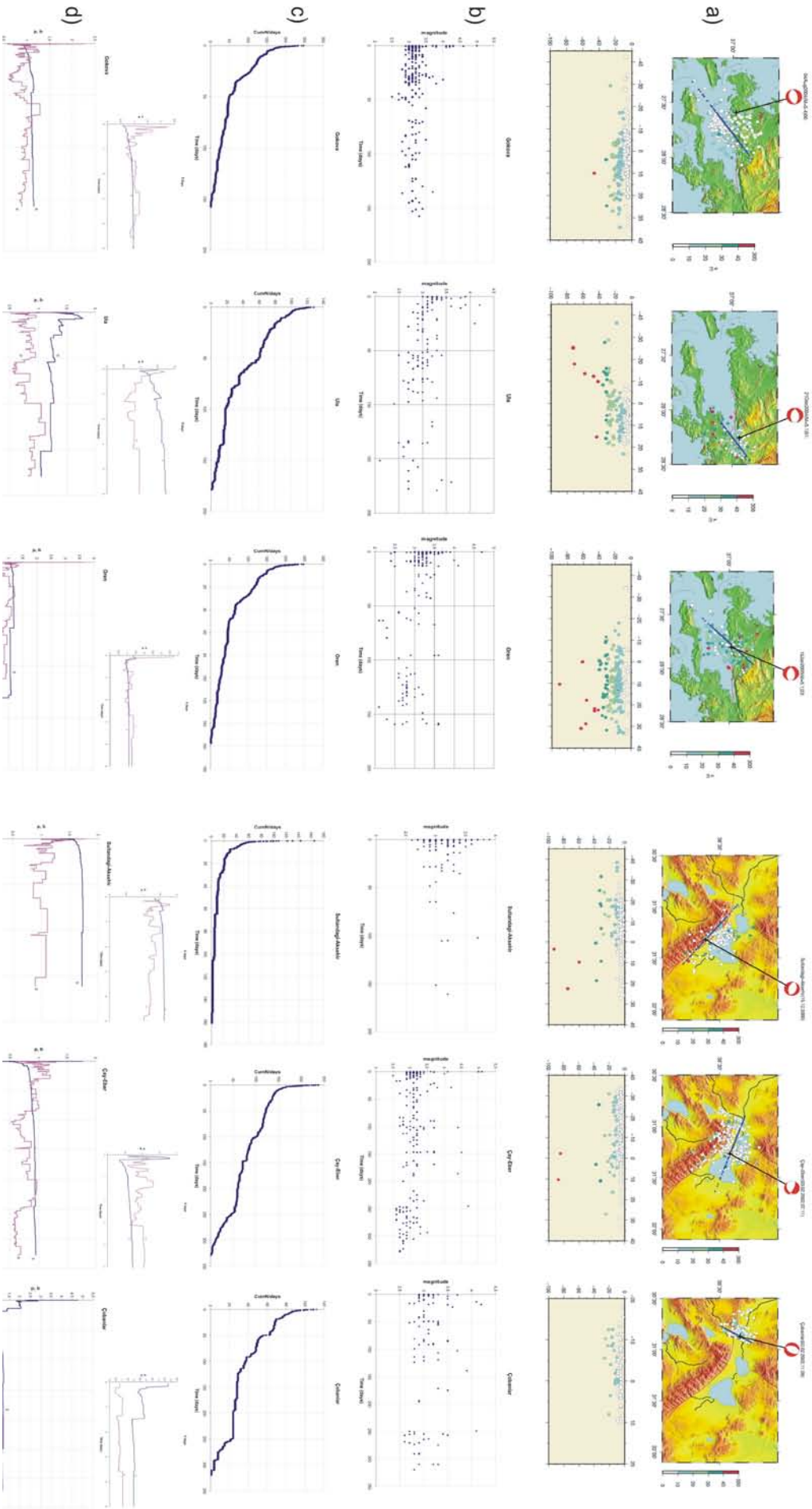
a)
b)
c)
d)
Gediz
Ula
Ören
Bahadıroğlu Akarsuları
Çine Çayı
Çubuklar

Figure 2. a) The focal mechanism solutions of 04 December 2004 Gulf of Gokova, 20 December 2004 Ula and 10 January 2005 Oren earthquakes in Gokova Graben and 15 December 2000 Sultandağı-Aksehir, 03 February 2002 Çay-Eber, and 03 February 2002 Çobanlar earthquakes in Afyon Akşehir Graben; with aftershocks and depth sections of the aftershock sequences; b) The size of the aftershocks against time in days with time increment of an hour; c) Cumulative number of aftershocks; d) The deduced p- and b-values against time in days. The small charts on the upper right corners of the graphs show the b- and p-value changes in the first 5 days.

CONCLUSION AND DISCUSSION

Considerably high p-values, which indicate an aftershock activity with a fast decay, are found in Gokova, Oren and Sultandagi-Aksehir aftershock sequences, while Ula, Cay-Eber and Cobanlar earthquakes have a relatively slower decay with lower p-values. Gokova and Cay-Eber earthquakes have larger aftershocks in the first day, so that they have the lowest b-values of all other sequences in this period. Afterwards, a systematic increase is observed with b<1.0 (Figure 2d).

Wang (1994) reported that if larger aftershocks occur earlier in the earthquake sequence, the b-value should be smaller for the earlier-occurring events than the late-occurring events. Aftershock behaviours of Gokova and Cay-Eber earthquakes verify his suggestion. Ula, Sultandagi-Aksehir and Cobanlar sequences have higher b-values which indicate low stress drops. On the other hand, Gokova, Oren and Cay-Eber earthquakes have relatively lower b-values in general. Hence, it can be assumed that the released strain energy by Gokova, Oren and Cay-Eber earthquakes was higher compared to the others.

ACKNOWLEDGEMENTS

This work is partly supported by the Research Fund of the Istanbul University; Projects: 145/20082003, BYP-456/02082004, UDP-402/21102004. Some figures used in this paper are prepared by using the Generic Mapping Tools software of Wessel and Smith (1998).

REFERENCES

Gutenberg, R., and Richter, C. F., 1944. Frequency of earthquakes in California, *Bull. Seism. Soc. Am.*, 34, 185-188.

Koçyiğit, A., 2002. Nature of neotectonic regime within the Isparta angle: Origin of Egridir Lake, *Aktif Araştırma grubu Altıncı Toplantısı (ATAG-6) Bildiri Özleri,* MTA Genel Müdürlüğü, 21-22 Kasım 2002, Ankara, 29-33.

Kurt, H., Demirbağ, E. and Kuşçu, İ., 1999. Investigation of the submarine active tectonism in the Gulf of Gökova, southwest Anatolia-southeast Aegean Sea, by multi-channel seismic reflection data, *Tectonophysics*, 305, 477-496.

Ogata, Y., and Katsura, K., 1993. Analysis of temporal and spatial heterogeneity of magnitude frequency distribution inferred from earthquake catalogues, *Geophys. J. Int.*,113, 727-738.

Omori, F., 1894. On the aftershocks, *Rep. Imp. Earthq. Invest. Comm.*, 2, 103-139.

Özer, N. and Altınok, Y., 2005. Akşehir-Afyon Grabeni; Sultandağı Yöresinin Depremselliği, *İ.Ü. Araştırma Fonu Proje Raporu*, No: 145/20082003, 2003-2005.

Utsu, T., 1957. Magnitude of earthquakes and occurrence of their aftershocks, *J. Seism. Soc. Japan,* II, 10, 35-45 (in Japanese).

Utsu, T., Y. Ogata, and R. S. Matsu'ura, 1995. The centenary of the Omori formula for a decay law of aftershock activity, *T. Phys. Earth*, 43, 1-33.

Wang, J. H., 1994. On the correlation of observed Gutenberg-Richter's b-value and Omori's p value for aftershocks, *Bull. Seism. Soc. Amer.*, 84, 2008-2011.

Wessel, P. and Smith, W. H. F., 1998. New improved version of Generic Mapping Tools Released, *EOS*, 79, 579.

(This page is left blank intentionally.)

GROUNDWATER POTENTIAL OF SENİRKENT-ULUBORLU (ISPARTA) BASIN

Seyman F. and Karagüzel R.

Süleyman Demirel University, Department of Geological Engineering, 32260, Isparta
Email: fatma@mmf.sdu.edu.tr, kguzel@mmf.sdu.edu.tr

Abstract: In this study, it is aimed to determine the groundwater potential of Senirkent-Uluborlu basin, which covers an area of 753 km^2, and the groundwater discharge from the basin to Eğirdir Lake. Because water pollution has been observed in the basin, the discharge into the lake has a growing importance. According to the estimated water budget, the differences between total recharge ($465x10^6$ m^3/yr) and discharge ($377x10^6$ m^3/yr) of the basin is $86x10^6$ m^3/yr. Taking into consideration the probable errors made in calculations and measurements, the reliable water storage of the Senirkent-Uluborlu basin was determined approximately as $52x10^6$ m^3/yr, which is equal to 60 % of the differences between total recharge and discharge. Surface discharge to Eğirdir Lake was found as $26x10^6$ m^3/yr and underground discharge as $38x10^6$ m^3/yr.

Key words : Senirkent-Uluborlu basin, hydrogeology, groundwater potential

INTRODUCTION

While the average global annual rainfall, which is the source of both ground and surface water, is approximately 1000 mm, the amount Turkey receives is 643 mm (State Hydraulic Works-SHW,1997). This situation shows that Turkey is poor in water sources. For this reason, water use in Turkey has to be sustained without over exploiting water resources and deteriorating the water quality. Due to the growing population, the amount of water per capita decreases every year. The potential of water resources is sufficient for now. But, it is necessary to determine whether there will be enough good quality water resources or not for the future. Therefore, it is necessary to carry out hydrogeological investigations of the basin.

Eğirdir Lake, with its 4 billion m^3 water potential, is one of the most important freshwater Lakes in Turkey (Karagüzel et al., 1995). One of the problems of this lake is that groundwater flow from neighboring basins is not known. In this study, it is aimed to determine the groundwater potential of Senirket-Uluborlu basin located in Eğirdir Lake water shed (Figure 1), and the groundwater discharge from Senirkent-Uluborlu basin into Eğirdir Lake. For this purpose, geology, hydrogeology and groundwater dynamics of the region were investigated in detail.

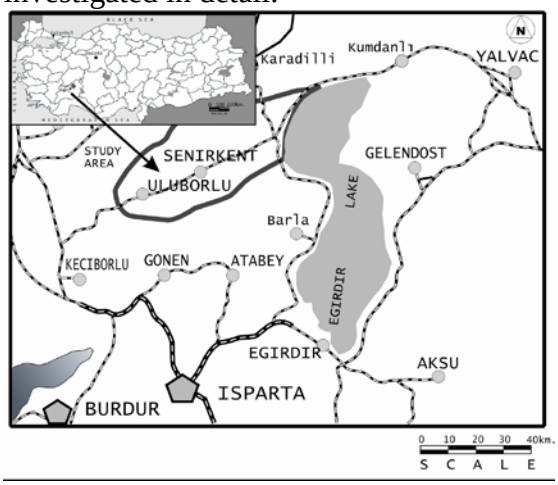

Figure 1. Location map of the investigation area

GEOLOGY-HYDROGEOLOGY

The basement of the study area consists of Mesozoic carbonate rocks (Mc). Medium-thick bedded and brittle dolomitic limestones of Triassic age are the oldest rock units in the region (Özgül et al., 1991). Medium-thick bedded Jurassic-Cretaceous limestones interbedded with clayey limestones are underlain comformably by the basement rocks and are overlain conformably by Paleogene flysch (TPf) composed of thin-medium-thick bedded sandstone, claystone, siltstone and conglomerates (Özgül et al., 1991). All these lithologies

are overlain discomformably by Miocene volcanics consisting of tuff, aglomerate and lavas (TNv) (Koçyiğit, A., 1983). Neogene conglomerates (TNc) consisting mainly of loosely cemented claystone, sandstone, and poligenic pebblies rest conformably on the underlying units. All units are covered by the alluvial (Qal) sediments (Figure 2).

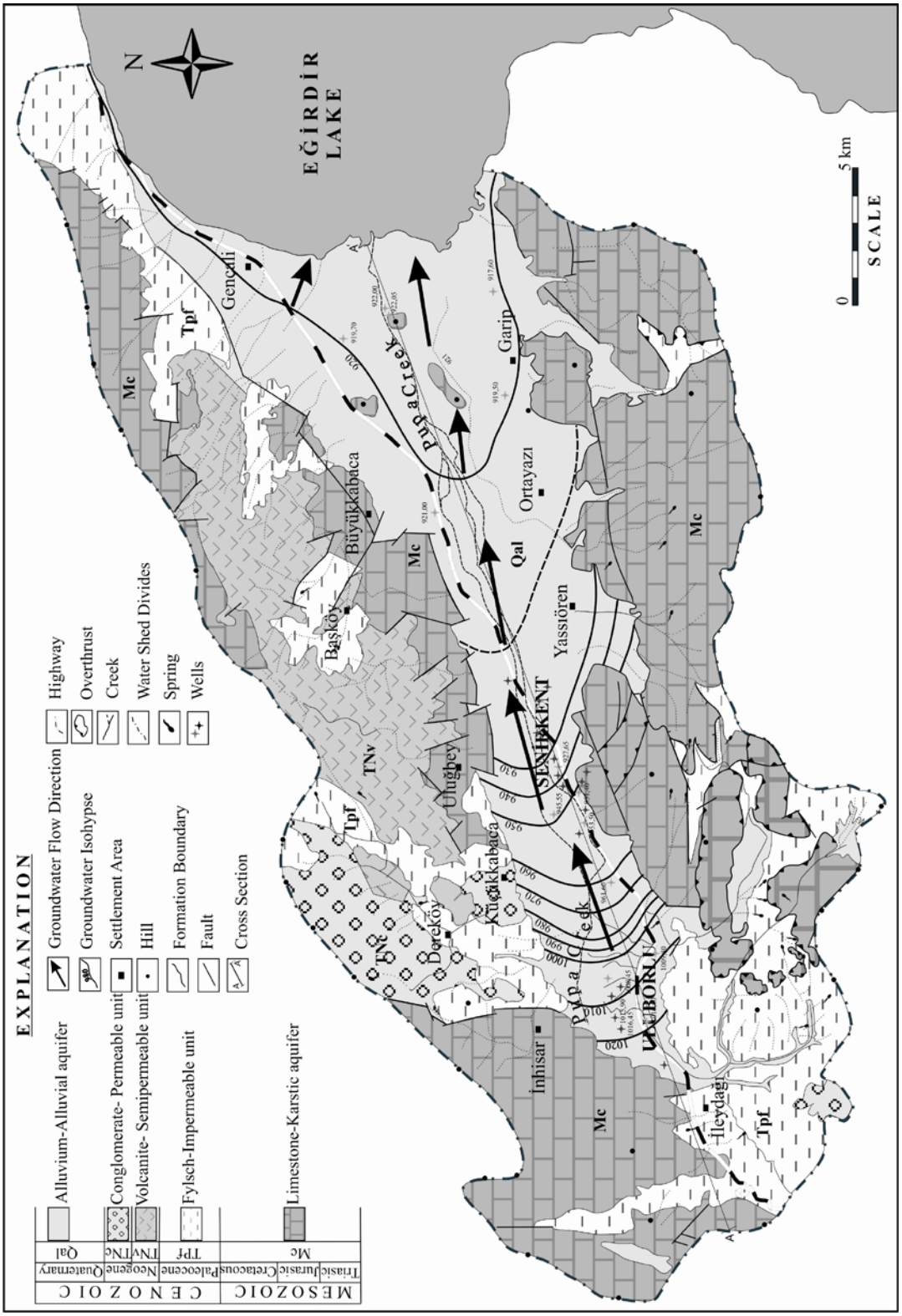

Figure 2. Geological and hydrogeological map (Modified from Gutnic et al. 1979, Dumont et al. 1975, Tay, 2005, Seyman 2005)

Aquifers

When the physical and hydrogeological features of the geological units in the study area are taken into consideration, Mesozoic carbonates having high amount of fractures and solution cavities display good karstic aquifer features. When the setting of these porous structures is considered, the hydrologic relation between carbonate rocks and Eğirdir Lake is clearly seen (Figure 3). Alluvial sediments consisting mainly of unconsolidated clay, silt, sand and pebble size material outcropping in an area of 140 km^2 were defined as alluvial aquifer. When the geological cross section and the contours of groundwater levels shown in Figure 3 are inspected, a hydraulic relation between karstic aquifer and Eğirdir Lake in vertical direction is clearly seen.

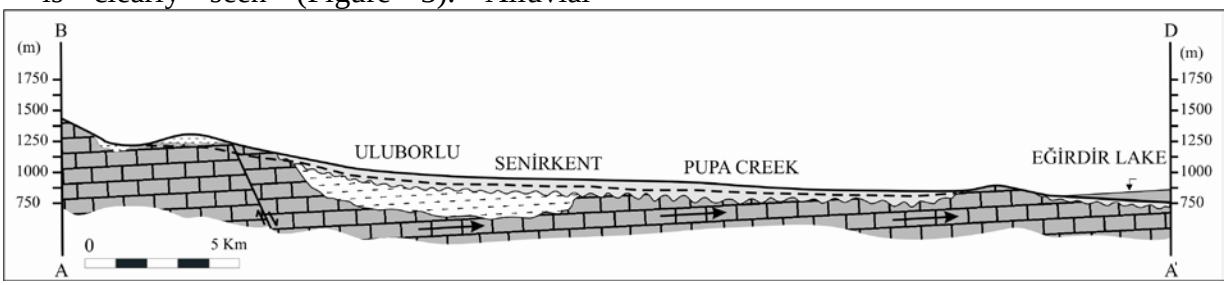

Figure 3. Geological cross section of the investigation area

Carbonate cemented Neogene conglomerates with their fractures and karstic cavities display features of an aquifer. However, this permeable unit occurring in the western side of the study area is important in terms of recharging to neighboring aquifers. Miocene volcanics were identified as semi-permeable units due to their fracture. Paleogene flysch composed of claystone, siltstone, sandstone, and marl is classified as an impermeable unit.

HYDROLOGY

The results of rainfall measurements of 38 years were taken from State Meteorological Service (State Meteorological Service-SMS, 2004) to carry out hydrological investigation of the study area.

The average annual rainfall of the basin is calculated as 558 mm by using the Isohyet method (Figure 4). Water supply for irrigation by pumping from Eğirdir Lake was taken from SHW.

Meteorological water budget was prepared. The amount of evaporation which is the most important discharge of the study area is calculated by the Thornthwaite method (Table 1). Average potential evaporation and real evaporation were calculated as Etp= 701 mm/yr and Etr= 379 mm/yr, respectively (Table 1).

Table 1. Meteorologic water budget calculated by Thornthwaite method

SENİRKENT ULUBORLU	January	February	March	April	May	June	July	August	September	October	November	December	Total
Monthly Temperature oC	1.10	2.30	6.20	10.90	15.80	20.20	23.40	23.20	18.80	12.90	7.00	3.00	
Monthly Index (i)	0.10	0.31	1.38	3.25	5.71	8.28	10.35	10.08	7.43	4.20	1.66	0.46	53.21
Etp (mm)	1.71	4.44	20.16	45.35	82.11	114.50	141.28	130.75	87.20	49.95	19.53	6.23	701.21
Rainfall (mm)	73.50	68.40	69.30	67.40	58.00	34.00	19.90	13.00	14.30	42.30	67.30	94.60	622.00
Groundwater Storage	100	100	100	100	74.30	0	0	0	0	0	47.90	100	
Etr (mm)	1.71	4.44	20.16	45.35	82.11	109.89	19.90	13.00	14.30	42.30	19.53	6.23	378.92
Change of Groundwater Storage	0	0	0	0	-24.11	-75.89	0	0	0	0	47.77	52.23	
Water Deficient (mm)	0	0	0	0	0	4.61	121.38	117.75	72.90	7.65	0.00	0.00	324.29
Excess Water (mm)	71.79	63.96	49.14	22.05	0	0	0	0	0	0	0	36.14	243.08
Correction Coefficient of Latitude	0.86	0.84	1.03	1.10	1.22	1.23	1.25	1.17	1.03	0.97	0.85	0.83	

The Pupa creek, which drains the surface runoff through the basin, is flowing from west to east, Eğirdir Lake. Groundwater flows through alluvial and karstic aquifers. Groundwater discharges from limestone and alluvium were calculated by using pumping data and available groundwater level maps.

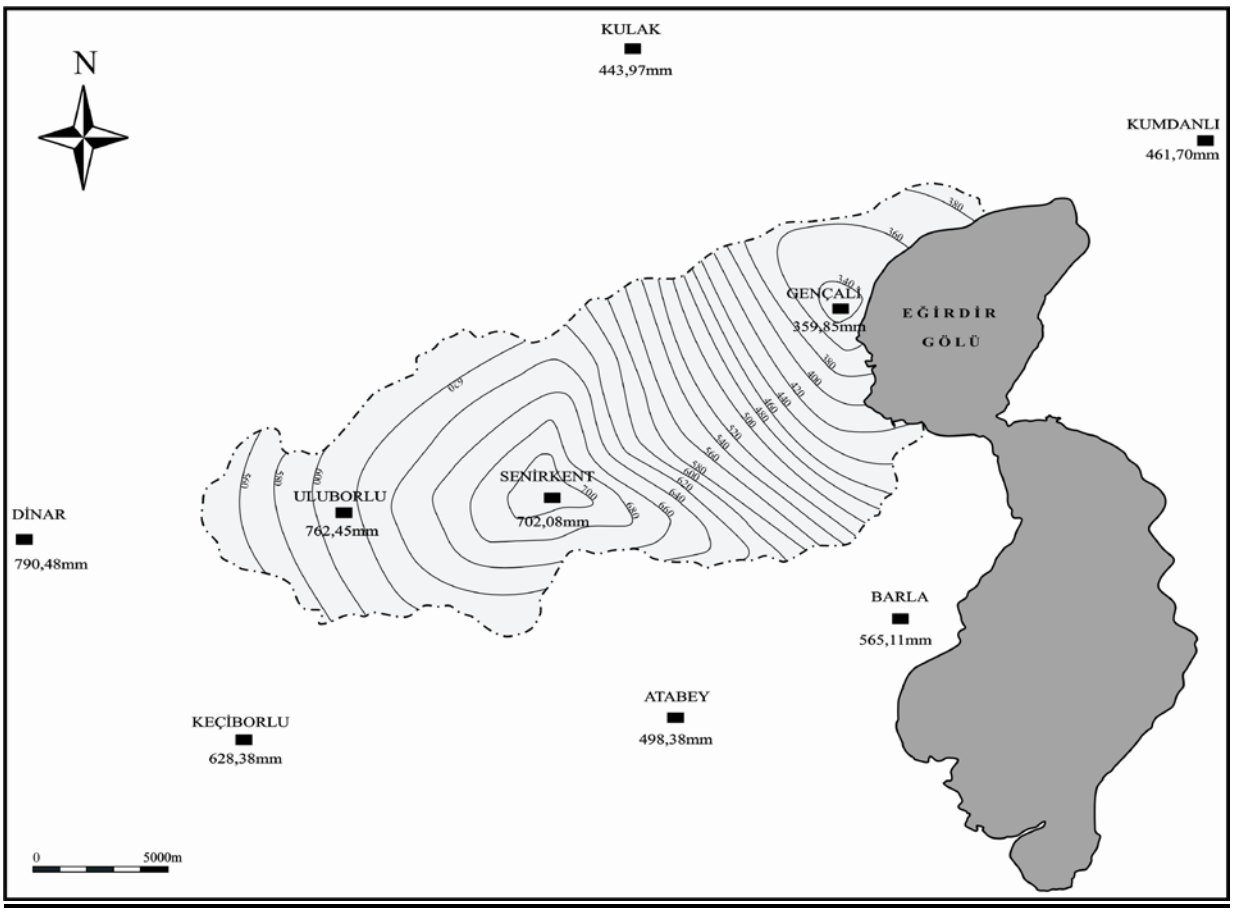

Figure 4. Isohyet map of the investigation area

WATER BUDGET

-Groundwater recharge

Senirkent-Uluborlu basin covers an area of 753 km^2, and annual average precipitation is 558 mm ($420x10^6$ m^3/yr). Another source of recharge in the basin is the irrigation water taken from Eğirdir Lake. Quantity of the average water taken from Eğirdir Lake is $45x10^6$ m^3/yr. Because of the geological structure of the basin, springs originating in the basin and discharging into the basin are not taken into consideration as a source of recharge (Table 2).

-Groundwater discharge

The most important discharge component of the investigation area is evapo-transpiration. Discharge from 753 km^2 investigation area occurs with the average real evapo-transpiration value of 379 mm/yr, which is equivalent to average evapo-transpiration $285x10^6$ m^3/yr. Sixty wells belonging to the public organizations and private sector with/without a permission are found in the basin. The total amount of the water pumped from these wells within the basin was calculated as $7x10^6$ m^3/yr. The surface flow towards Pupa creek and Eğirdir Lake was measured as $13x10^6$ m^3/yr in the middle of the basin. When the whole drainage basin system considered, the discharge through surface flow to the Eğirdir Lake was estimated as $26x10^6$ m^3/yr. Quantity of the water taken from Uluborlu Dam and İleydağı Pond for irrigation is $13 x10^6$ m^3/yr. The amount of the irrigation water used by plants is $6x10^6$ m^3/yr (which is equivalent to the 46

% of total irrigation water). $15x10^6$ m^3/yr water, which is 33% of the total irrigation water ($45x10^6$ m^3/yr) taken from Eğirdir Lake, is considered as discharge, $2x10^6$ m^3/yr annual discharge of the Kayaağzı spring, whose flow rate is 45 l/s, directly discharges to Eğirdir Lake and is taken into account for the water budget calculations (Table 2).

Groundwater discharge was calculated by the equation (1); Q=T.I.G, where T is transmisivity coefficient (m^2/day), I is hydraulic gradient, G is width of the discharge area (m^2).

Table 2. Water budget

RECHARGE	($x10^6$) m^3/yr	DISCHARGE	($x10^6$) m^3/yr
Rainfall	420	Evaporation	285
Irrigation from Eğirdir lake	45	Pumping from wells	7
		Discharge of Pupa creek	26
		To use for plant, irrigation water taken from ponds	6
		To use for plant, irrigation water taken from Eğirdir lake	15
		Discharge from Kayaağzı spring Eğirdir lake	2
		Groundwater discharge Eğirdir lake	38
TOTAL	**465**	**TOTAL**	**379**

Transmisivity coefficient was calculated as 346 m^3/day by using pumping tests of the alluvial aquifer, and its hydraulic gradient (I) is determined as 0,003 (Seyman, 2005). The distance between the discharge area and Eğirdir Lake is about 10 km. According to these data groundwater discharge from basin to Eğirdir Lake is calculated as $38x10^6$ m^3/yr (Table 2).

The difference between total recharge ($465x10^6$ m^3/yr) and discharge ($379x10^6$ m^3/yr) of the basin is determined as $86x10^6$ m^3/yr (Table 2).

When possible errors to be made are taken into account, the reliable amount of water that can be used was determined as 60 % of the budget difference. The dynamic water storage in Senirkent-Uluborlu basin is also found approximately as $52x10^6$ m^3/yr (Table 2).

In the chemical and pollution analyses of the water samples collected from representative wells, nitrate, nitrite, and pollution by heavy metals such as Mn, Cu, Zn, Pb, Hg, Cd, Se, As, Fe, Cr were detected (Seyman, 2005).

CONCLUSIONS

In the present study, it is aimed to determine groundwater potential of Senirkent-Uluborlu basin (which has an area of 753 km^2) and the groundwater discharge from this basin to Eğirdir Lake. Consequently, a geologic map of the region is prepared and the aquifer features of lithological units are discussed. It is shown that the discharge of the alluvial and karstic aquifers in the basin is towards Eğirdir Lake. Primary source of recharge of Senirkent-Uluborlu basin is rainfall. The amount of average annual rainfall was determined as $420x10^6$ m^3/yr in the water shed. Another source of recharge in the basin is $45x10^6$ m^3/yr irrigation water taken from Eğirdir Lake. In the study area the most important discharge is evapo-transpiration and is calculated using Thornthwaite method and annual average evapo-transpiration was found to be $285x10^6$ m^3/yr. Total water production obtained from wells in the basin was calculated as $7x10^6$ m^3/yr. Surface runoff from the basin to Eğirdir Lake through Pupa creek is $26x10^6$ m^3/yr. Part of the water used for irrigation consumed by

plants was considered as discharge. Taking into account of the irrigation productivity of SHW this amount was calculated as $21x10^6$ m^3/yr. Because springs originated in the basin discharges into the same basin were not taken into account in the water budget. However, for more reliable budgets, a detailed hydrogeologic study of the springs is necessary. The discharge from Kayaağzı spring located on the Eğirdir Lake coast to Eğirdir Lake is $2x10^6$ m^3/yr and is assumed as a direct discharge. As indicated by geological and hydrogeological studies, the discharge from the alluvium of the plains and limestone in the basement of the Eğirdir Lake is an groundwater discharge and is calculated as $38x10^6$ m^3/yr. According to the budget calculations made from existing data, water storage was found as $52x10^6$ m^3/yr in Senirkent-Uluborlu basin. For a more reliable water budget; i) to construct flow observation stations on the drainage network, especially along Pupa creek near the lake, should be constructed; and ii) observation wells should be established between Senirkent and Eğirdir Lake in order to have a more representative ground water level measurement and aquifer characteristics. Groundwater pollution in the study area is thought to be caused by solid and liquid waste disposal sites located within the basin.

AKNOWLEDGEMENTS

This work was supported by the Research Fund of The Suleyman Demirel University. Project number: 03 YL 654. The authors would like to express their thanks to Ömer Tezcan Akıncı and Ömer Elitok for their valuable contribution.

REFERENCE

SHW, 1969, Senirkent-Uluborlu havzası hidrojeolojik etüd raporu, SHW 18. Bölge Müdürlüğü, Isparta

SHW, 1997, Devlet Su İşleri (State Hydraulic Work) Haritalı İstatistik Bülteni, TC Enerji ve Tabii Kaynaklar Bakanlığı, SHW Genel Müdürlüğü, Apk Daire Başkanlığı, Ankara

SMS, 2004, Devlet Meteoroloji İşleri (State Meteorological Service) Genel Müdürlüğü, 1968-2002 yılları arası meteoroloji elemanları ölçüm değerleri, Ankara

Dumont, J,F, Kerey, E., 1975. Eğirdir Gölü güneyinin (Isparta ili) temel jeolojik etüdü, *TJK Bülteni*, Cilt:18, Sayı:2, 1-10.

Gutnic, M., Monod, O., Poisson, A., ve Dumont, F., D., 1979. Geology des Taurides occidentales (Turquie): *Mem-Soc. Geol. Fr.*, N.S., S8, S: 112.

Karagüzel., R., Taşdelen, S., Akyol E., 1995. An analysis of the level fluctuations of Eğirdir Lake SW Turkey, *International Earth Sciences Colloquium on the Aegean Region* 701-710, Izmir-Güllük, Turkey.

Koçyiğit, A., 1983. Hoyran Gölü (Isparta Büklümü) dolayının tektoniği, *Türkiye Jeoloji Kurumu Bülteni*, C:26, 1-10.

Özgül, N., Bölükbaşı, S., Alkan, H., Öztaş, Y., Korucu, M., 1991. Göller bölgesinin tektono-stratigrafik birlikleri, *Ozan Sungurlu Sempozyumu Bildiriler Kitabı,* s.213-237, Ankara

Seyman, F., 2005, Senirkent Uluborlu Havzasının Hidrojeoloji İncelemesi, *S.D.Ü. Fen Bilimleri Enstitüsü, Yüksek Lisans Tezi*, Isparta (unpublished)

Tay, Ş., 2005, Senirkent – Uluborlu (Isparta) Havzasının Katı Atık Düzenli Depolama Yeri Seçimine Yönelik Jeolojik – Jeoteknik İncelemesi, *SDÜ, Fen Bilimleri Enstitüsü, Yüksek Lisans Tezi*, Isparta (unpublished)

ASSESSMENT OF LIGNITE-DERIVED CONTAMINATION DEGREE OF ALFEIOS RIVER SEDIMENTS, CENTRAL PELOPONNESE, GREECE

Siavalas G., Kalaitzidis S., Chatziapostolou A. and Christanis K.

Department of Geology, University of Patras, GR-26500 Rio-Patras, Greece, e-mail: christan@upatras.gr

Abstract: The organic matter of modern sediments deposited by the Alfeios River in central Peloponnese, Greece, is examined under the microscope. The aim is to estimate the degree of contamination that originates from the nearby Megalopolis Lignite Centre.

Proximate and ultimate analyses, as well as mineralogical determinations using X-ray diffraction were carried out on the feed lignite and on bottom and fly ash samples. Density separations using heavy liquids ($ZnCl_2$) were applied in order to concentrate the organic matter dispersed within the river sediments. The concentrated organic matter, as well as feed lignite samples from the Megalopolis power plants were microscopically examined using standard coal-petrography techniques.

The organic contamination of the Alfeios sediments occurs in the form of unburned lignite particles, which constitute ~64 vol.-% of the contained organic matter, carbonized and semi-carbonized particles (14.5% vol.-%) and inorganic fly-ash particles. The fresh organic matter that derives from modern plant residues comprises 21.6 vol.-% of the organic matter present in these sediments.

Key words: environment, lignite, organic petrography, Megalopolis, Greece

1 INTRODUCTION

Megalopolis Lignite Centre (MLC) is located in Peloponnese (Southern Greece, see Figure 1) and is the second most important energy centre of Greece, hosting four power units with total installed capacity of 850 MW. The lignite deposits of the Megalopolis Basin have been exploited since 1969 with open cast mining and nowadays, the annual production of lignite reaches 15 Mt. Megalopolis Basin is physically drained by Alfeios River and its tributaries (Figure 1).

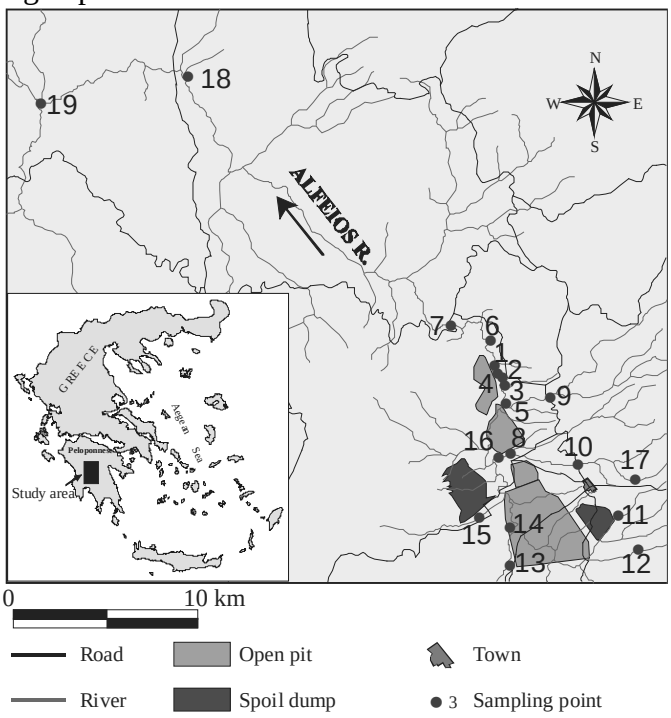

Figure 1. Sketch map of the study area and the sampling points

A series of processes related with mining, transportation and – above all – combustion of lignite are considered to be significant sources for the emission of hazardous pollutants and contaminants in the environment. The combustion by-products are gaseous emissions (CO_2, CO, CH_4, SO_x, NO_x) and solid residues. The latter, generally known with the term ash, can be distinguished into two categories, i) bottom ash or slag, which remains in the combustion chamber, and ii) fly ash that includes fine grained solid particles, transported by the flu gases (Thomas, 2002). Although the existing technology reduces the emissions into the environment, a part of them escapes and is transported through air and surface water, until certain solid compounds fall down and deposit in soils and sediments.

Although fly ash is mainly composed of inorganic constituents, residues of organic origin may also contribute significantly. They derive from the incomplete combustion of organic particles and are generally called with the term "char" (Taylor *et al*., 1998). The level of unburnt char in fly ash varies widely and in some power stations exceeds 5 wt.-%, which is the upper level for the optimum function of power stations (Nandi *et al*., 1977).

Over the past few years many researchers have used various methods in order to estimate coal-derived organic particles in soils and sediments. These methods include field and stratigraphic observation (French, 1998), geochemical analyses (Ellenson *et al*., 1997; Rumpell *et al*., 1998) and microscopic observation (Kleineidam *et al*., 1999; Mastalerz *et al*., 2001; Cornelissen *et al*., 2004). The microscopic observation of the organic matter present in sediments is based on the different optical features, which the organic particles reveal in dependence on their origin. Thus, microscopic observation can be a useful tool for the distinction between fresh and fossil organic matter or its combustion derivatives (char) in surface sediments. In this study, fossil fuel particles and chars are named anthropogenic particles. The application of techniques used in Organic Petrography can lead to a quantitative approach for the presence of these particles in soils and sediments (Mastalerz *et al*., 2001; Kalaitzidis *et al*., 2005).

This study is an attempt to characterize the organic matter present in Alfeios River sediments using standard organic petrography techniques in order to distinguish the anthropogenic from the naturally derived particles, as well as to assess the contamination degree caused by the lignite exploitation.

2 GEOLOGICAL SETTING

The Megalopolis Basin occupies a 180-km^2 large area in central Peloponnese. The basement and the margins of the basin consist of limestones, dolomites, cherts, and flysch, which formed from Upper Eocene to Upper Oligocene (Vinken, 1965).

The sedimentary sequence filling the basin deposited in a tectonic graben from Upper Pliocene until today and reflects a variety of terrestrial, fluvial, limnic, and limnotelmatic environments. The coal-bearing formation deposited in Lower Pleistocene and is composed of alternations of clays, clayey marls and marls with thin lignite layers.

3 MATERIALS AND METHODS

Twenty eight (28) sediment samples were collected from 19 points along Alfeios River (Figure 1) according to the procedures described in Rees *et al*. (1998), Swennen and van der Sluys (1998) and Kralik (1999). Twenty three (23) samples represent channel deposits, whereas five (5) samples represent overbank deposits. All samples were transported to the laboratory and stored at +4 °C. They were dried at 60 °C, sieved to pass 2 mm mesh and ground to Ø<500 μm.

Organic matter content was determined as the loss of weight after the oxidation of

the sample in 440 °C for 16h (Nelson and Sommers, 1996).

A heavy-media density separation technique using a $ZnCl_2$ solution was applied in order to concentrate the low content of the organic matter and facilitate its microscopic observation (Cornelissen *et al.*, 2004). Polished blocks were prepared according to ASTM D2797 (1990). On each block, maceral analysis was carried out using standard coal-petrography techniques and applying the nomenclature adopted by the International Committee for Coal and Organic Petrology (ICCP, 1993; 1998; 2001; Taylor *et al.*, 1998; Sýkorová *et al.*, 2005), a char classification scheme (Bailey *et al.*, 1990) and a classification scheme for fresh plant remnants (Kalaitzidis and Christanis, 2000).

Additionally, three feed lignite samples, three fly ash, three bottom ash and four dump ash samples were picked up in order to characterize Megalopolis lignite and its solid combustion by-products. Proximate analysis including total moisture, ash, volatile matter and fixed carbon content determinations were performed according to ASTM D3302 (1989), D3174 (1989), D3175 (1989), respectively. Ultimate analysis (i.e. determination of C, H, N, S contents) was performed using a Carlo Erba automatic analyzer. On the lignite samples, maceral analysis was also performed as described above.

Mineralogical determinations were performed using a Philips® PW1050 diffractometer in lignite and respective ashes (750 °C), fly ash, bottom ash, dump ash samples and selected sediment samples with a step of 0.02°/0.5s covering a 2θ interval from 3-65°.

4 RESULTS

4.1 Proximate and Ultimate Analyses

The results of proximate and ultimate analyses for lignite and ash samples are summarized in Table 1. Interesting characteristics are the relatively high ash content of the Megalopolis lignite and the high sulphur content, which has a negative impact from environmental point of view; thus, a desulphurization unit is installed in order to minimize the SO_x emissions. Carbon, hydrogen and nitrogen contents display moderate values, which are generally accepted for energy production (Thomas, 2002).

Table 1. Results of proximate and ultimate analyses (moisture is expressed in wt.-%, all other data in wt.-% on dry basis)

Sample No		Moisture	Ash	Volatile matter	Fixed carbon	C	H	N	S	O
Lignite	BLM1	65.0	27.0	51.1	21.9	44.7	2.9	1.7	2.4	21.3
	BLM2	66.2	24.7	49.5	25.8	45.3	3.0	1.6	2.3	23.1
	BLM3	63.8	34.6	46.5	18.9	39.0	3.7	1.6	3.0	18.1
Dump ash	AM1	30.7	89.1	9.8	1.1	4.9	0.8	0.2	0.4	4.6
	AM2	29.2	89.5	9.2	1.3	5.3	0.5	0.1	0.3	4.3
	AM3	29.3	88.8	10.9	0.3	5.1	0.7	0.1	0.4	4.9
	AM4	29.7	91.9	7.3	0.8	2.4	0.4	0.1	0.9	4.3
Fly ash	FAM1	0.2	95.5	3.8	0.7	1.9	0.1	0.1	0.6	1.8
	FAM2	0.2	95.7	3.5	0.8	1.7	0.1	0.1	0.7	1.7
	FAM3	0.5	95.5	3.6	0.9	2.9	0.1	0.3	0.5	0.7
Bottom ash	BAM1	48.5	78.7	18.4	2.9	10.7	1.4	0.3	0.3	8.6
	BAM2	53.1	69.4	23.9	6.7	10.7	1.4	0.6	0.3	17.6
	BAM3	45.5	79.3	17.7	3.0	10.3	1.2	0.3	0.4	8.5

Organic matter of the Alfeios River sediments ranges from 0.9-43.4 wt.-%, revealing intense scattering of the values (Table 2).

Table 2. Maceral composition of the Megalopolis lignite and the Alfeios River sediments; (OM: organic matter content, coal: lignite and bituminous coal particles, H: Huminite, I: Inertinite, L: Liptinite, Ch: char particles, F.T.: fresh tissues, A.P.: ash particles, MIN, minerals)

Sample		OM[a]	Coal[b]	H[b]	I[b]	L[b]	Ch[b]	F.T.[b]	A.P.[c]	MIN[c]
Lignite	BLM1	73.0		94.0	2.0	4.0				15.5
	BLM2	75.3		93.2	1.6	5.2				14.0
	BLM3	65.4		90.2	3.0	6.8				16.0
Sediments	ALF1a	13.5	68.5	59.3	1.2	8.0	6.3	25.2	7.0	17.1
	ALF1b	43.4	94.0	87.4	2.0	4.6	6.0			4.9
	ALF1c	1.9	36.8	36.2		0.6	3.2	60.0	2.5	2.7
	ALF2a	3.3	90.8	87.2	0.4	3.2	7.2	2.0	10.0	3.4
	ALF2b	4.9	79.8	77.8	0.4	1.6	11.8	8.4	10.4	4.1
	ALF3	9.0	92.8	89.2	0.8	2.8	6.0	1.2	2.2	4.7
	ALF4a	1.8	57.2	54.6	0.1	2.5	33.6	9.2	23.0	59.7
	ALF4b	5.9	83.9	78.5	1.7	3.7	11.3	4.8	12.8	28.2
	ALF5	3.6	69.7	66.1	1.1	2.5	13.6	16.7	18.0	10.4
	ALF6a	5.7	70.2	61.4	0.8	8.0	10.1	19.7	11.0	19.3
	ALF6b	3.3	75.3	67.6	2.3	5.4	19.4	5.3	3.2	47.6
	ALF7a	6.0	81.4	77.5	0.3	3.6	14.7	3.9	6.4	39.2
	ALF7b	3.8	83.6	83.2	0.2	0.2	13.2	3.2	0.4	50.1
	ALF8	7.8	83.0	77.6	1.5	3.9	8.8	8.2	5.5	11.3
	ALF9	1.2	41.7	39.3		2.4	35.8	22.5	0.3	72.2
	ALF10	1.2	39.3	38.0	0.1	1.2	23.9	36.8	3.3	19.4
	ALF11	2.8	40.9	39.7	0.1	1.1	12.9	46.2	0.2	67.0
	ALF12	2.9	13.6	12.5	0.4	0.7	8.2	78.2	1.4	32.7
	ALF13a	2.6	45.2	45.0		0.2	28.1	26.7	1.7	87.2
	ALF13b	1.5	31.6	31.5			15.8	52.7	4.5	25.0
	ALF14	27.7	91.3	82.1	0.6	8.6	6.8	1.8		1.4
	ALF15a	1.6	56.3	56.3			19.2	24.5	21.3	4.5
	ALF15b	1.6	33.0	33.0			10.7	56.3	0.6	84.1
	ALF16a	2.8	67.3	62.9	0.6	3.8	25.7	7.0	8.8	17.1
	ALF16b	10.3	86.4	83.6	0.4	2.4	12.8	0.8	3.2	7.5
	ALF17	1.1	46.5	46.5			12.3	41.2	1.6	76.3
	ALF18	1.3	82.0	79.4	0.3	2.3	5.3	12.7	0.3	42.4
	ALF19	0.9	48.4	47.4		1.0	23.4	28.2	9.9	56.9

[a]: wt.-% on dry basis, [b]: vol.-% on mineral matter free basis, [c]: vol.-% in bulk sample

4.2 Mineralogical determinations

The dominant minerals contained in Megalopolis lignite are clays, quartz and feldspars, which indicate clastic sedimentation, authigenic pyrite, as well as calcite, which may be of clastic or authigenic origin. Micas, dolomite and bassanite, the latter probably formed from partly dehydrated gypsum (Ward *et al*., 2001), occur subordinately.

All ash samples reveal a similar mineralogical composition with variations in the mineral concentrations. Quartz, feldspars, anhydrite, ghelenite and mullite are the major minerals. Ghelenite and mullite are high-temperature phases often reported in fly and bottom ash from all over the world (e.g. Vassilev and Vassileva, 1996; Spears, 2000; Karayigit and Gayer, 2001; Hower and Robertson, 2004; Vassilev *et al*., 2005). Ghelenite is

usually formed during the combustion of low rank coals from the reaction of fine-grained CaO, bound to carboxylic groups, with clay minerals (Chen *et al*., 2004), whereas mullite derives from the thermal breakdown of clay minerals and especially kaolinite (Spears, 2000).

The main minerals identified in Alfeios River sediments are quartz, clay minerals, chlorite and feldspars. Calcite, micas and pyrite are also present in lesser amounts. No minerals contained in fly ash (ghelenite, mullite) were identified with this method, possibly due to their low concentrations in the sediments. Pyrite may be the only mineral, which is related to lignite particles, as quartz and clays are very common in soils and sediments. In general, it is difficult to extract a solid differentiation between minerals, which originate from natural processes and those that derive from the lignite utilization.

4.3 Organic petrography of Megalopolis lignite and Alfeios River sediments

Huminite is the dominant maceral group in Megalopolis lignite reaching 92.5 vol.-% on a mineral-matter free basis, with attrinite being the most common maceral (28.2 vol.-%). Liptinite and inertinite maceral groups are less common (4-7 vol.-% and <3 vol.-%, respectively; see Table 2). Mineral matter displays an average of 15.2 vol.-% in the bulk sample, mainly composed of clays, carbonates and pyrite.

The organic matter contained in the Alfeios River sediments is composed of lignite and char particles, deriving from incomplete combustion processes, and fresh tissues originating from modern plant remnants.

Lignite particles constitute up to 63.9 vol.-% on average of the sediments, organic matter being the most common group. Char particles participate with an average of 14.5 vol.-%, while fresh tissues represent only the 1/5 on average (21.6 vol.-%) of the organic matter present in Alfeios River sediments (Table 2).

The coal-petrographic composition of the lignite particles found in the sediments is similar to this of Megalopolis lignite, indicating that these particles derive obviously from mining and transportation processes. Nevertheless an origin due to erosion processes on natural outcrops is possible for a small portion of these particles.

An interesting aspect, which turned up during the microscopic study, was the presence of more reflectant macerals than those of huminite group. These macerals belong to the vitrinite group and derived from the use of small amounts of bituminous coal during 1993-1996 in order to improve the performance of power generation (*personal communication with MLC*). The presence of these particles is very important as it provides a measure for the period represented by the collected samples.

Char particles, which mainly participate in fly ash, are mainly composed of fragments (Ø<10 μm), although solid particles occur frequently too. Cenospheres are less common, possibly due to fragmentation processes during their transportation through air and water. Mixed char particles (mixed dense and mixed porous) are also present mainly deriving from bituminous coal particles.

Fresh organic matter is mainly composed of structured macerals (pre-textinite, textinite A), although pre-attrinite is also present in high concentrations (21.2 vol.-% of the fresh tissues).

5 DISCUSSION

The lateral distribution of the different phases of organic matter along Alfeios River (Figure 2) can lead to conclusions about the depositional processes and transportation means of anthropogenic particles. The term “anthropogenic particles” is referred to lignite and char particles together, although some part of the lignite particles may have derived from natural processes (erosion).

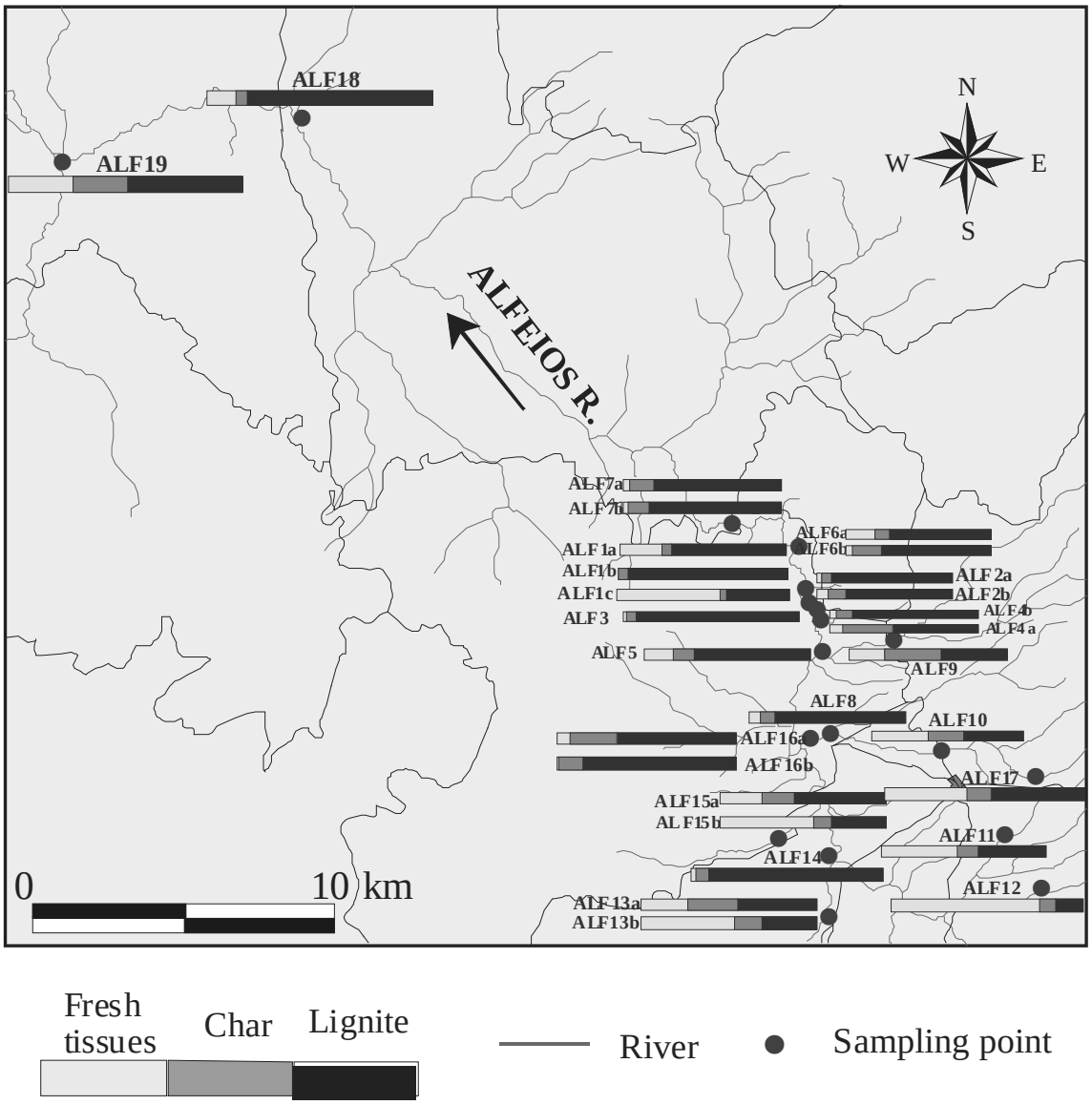

Figure 2. Lateral distribution of the natural and anthropogenic organic particle contents in the sediments of the study area

In samples obtained from the MLC area (1a, 1b, 2a, 2b, 3, 4a, 4b, 5, 6a, 6b, 8, 14, 16a and 16b), the anthropogenic particles constitute more than 75 vol.-% of the total organic matter for all samples reaching 100% at some sites (1b). This general rule excludes sample 1c, which contains 60% of fresh tissues, possibly due to the rich vegetation remnants, both herbaceous and arboreal, of the sampling site.

Samples upstream of the MLC (9, 10, 11, 12, 13a, 13b, 15a, 15b and 17) display low concentrations of anthropogenic particles, which have been wind-transported and deposited. The concentration of anthropogenic particles gradually increases northwards pointing out the main wind direction.

Samples 7a, 7b, 18 and 19 represent sites downstream of the MLC and display relatively low concentrations of organic matter. Nevertheless, it mainly comprises of anthropogenic particles. This trend shows that lignite and char particles can be transported through air and water and deposited in distances more than 30 km from the emission source.

The general aspect of the coal-petrographic study of the organic matter contained in Alfeios River sediments is the intense variation on maceral

concentrations, due to the organic matter heterogeneity and alterations caused during transport and depositional processes.

Further investigation is needed in order to extract safe conclusions about the distribution of both lignite and char particles in surface sediments and the related transportation and depositional processes. Also the formation of char particles must be investigated with respect to the maceral composition of the feeding lignite and the distribution of them between combustion by-products.

6 CONCLUSIONS

The utilization of Megalopolis lignite for energy generation obviously affects the nature of the organic matter present in Alfeios River sediments and disturbs their carbon budget, in a broad area around the MLC. The transportation of lignite and char particles is accomplished through air and surface water towards all directions around MLC.

There is no specific relationship between the distribution of organic matter and the distance from the power plants. This indicates that the concentration of the anthropogenic particles in the sediments seems to be more or less independent of the distance from the emission source, for distances less than 30 km.

Organic petrography can be a useful tool for a quantitative approach of coal contaminated sites, providing evidence for the origin and distribution of different phases of organic matter in surface sediments.

ACKNOWLEDGEMENTS

The authors would like to thank Dr. Antonis Bouzinos for his contribution in the field work and Mr. Dimitris Vachliotis for technical support of the ultimate analysis. George Siavalas thanks the National Grand Foundation of Greece for financial support.

REFERENCES

American Society for Testing and Materials (ASTM), D3174-1989. Ash in the analysis sample of coal and coke from coal. In *Annual Book of ASTM Standards*, Gaseous fuels: coal and coke, Philadelphia, Part 26: 291-294.

American Society for Testing and Materials (ASTM), D3175-1989. Volatile matter in the analysis sample of coal and coke. In *Annual Book of ASTM Standards*, Part 26: 392-395.

American Society for Testing and Materials (ASTM), D3302-1989. Total moisture in coal. In *Annual Book of ASTM Standards*, Gaseous fuels: coal and coke, Philadelphia, Part 26: 326-332.

American Society for Testing and Materials (ASTM), D2797-1990. Preparing coal samples for microscopical analysis by reflected light. In *Annual Book of ASTM Standards*, Gaseous Fuels: coal and coke, Philadelphia, Part 26: 270-273.

Bailey, J.G., Tate, A., Diessel, C.F.K. and Wall, T.F., 1990. A char morphology system with applications to coal combustion. *Fuel*, 69, 225-239.

Chen, Y., Shah, N., Huggins, F.E., Huffman, G.P., Linak, W.P. and Miller, C.A., 2004. Investigation of primary fine particulate matter from coal combustion by computer controlled scanning electron microscopy. *Fuel Processing Technology*, 85, 743-761.

Cornelissen, G., Kukulska, Z., Kalaitzidis, S., Christanis, K. and Gustafsson, Ö., 2004. Relations between environmental black carbon sorption and geochemical sorbent characteristics. *Environmental Science & Technology*, 38, 3632-3640.

Ellenson, W.D., Mukerjee, S., Stevens, R.K., Willis, R.D., Shadwick, D.S., Sommerville, M.C. and Lewis, R.G., 1997. An environmental scooping study in the lower Rio Grande Valley

of Texas-II. Assessment of transboundary pollution transport and other activities by air quality monitoring. *Environment International*, 23, 643-655.

French, P.W., 1998. The impact of coal production on the sediment record of the Severn Estuary. *Environmental Pollution*, 103, 37-43.

Hower, J.C. and Robertson, J.D., 2004. Chemistry and petrology of fly ash derived from the co-combustion of western United States coal and tire-derived fuel. *Fuel Processing Technology*, 85, 359-377.

International Committee for Coal Petrology (I.C.C.P.), 1993. International Hanbook of Coal Petrography 3rd supplement to the 2nd edition. *Centre National de la Recherche Scientifique*, Paris, France.

International Committee for Coal Petrology (I.C.C.P.), 1998. The new vitrinite classification (ICCP System 1994). *Fuel*, 77, 349-358.

International Committee for Coal Petrology (I.C.C.P.), 2001. The new inertinite classification (I.C.C.P. System 1994). *Fuel*, 80, 459-471.

Kalaitzidis, S., and Christanis, K., 2000. Petrography, mineralogy and geochemistry of the Holocene peat of the Philippi peatland, Hellas: Preliminary results. *Sustaining our Peatlands, 11th International Peat Congress*, Quebeck, Canada, 2, 593-603.

Kalaitzidis, S., Christanis, K., Cornelissen, G. and Gustafsson, Ö., 2005. Tracing dispersed coaly-derived particles in modern sediments: an environmental application of organic petrography. *9th International Conference on Environmental Science & Technology (CEST)*, Rhodes, Greece, A, 626-631.

Karayigit, A.I. and Gayer, R.A., 2001. Characterization of fly ash from the Kangal Power Plant, Eastern Turkey. *International Ash Utilization Symposium*, University of Kentucky, paper #4, 8 pp.

Kleineidam, S.E., Rogner, K.N., Ligouis, B.D. and Grathwohl, P., 1999. Organic matter facies and equilibrium sorption of phenanthrene. *Environmental Science & Technology*, 33, 1637-1644.

Kralik, M., 1999. A rapid procedure for environmental sampling and evaluation of polluted sediments. *Applied Geochemistry*, 14, 807-816.

Mastalerz, M., Souch, C., Filippeli, G.M., Dollar, N.L. and Perkins, S.M., 2001. Anthropogenic organic matter in the Great Marsh of the Indiana Dunes National Lakeshore and its implications. *International Journal of Coal Geology*, 46, 157-177.

Nandi, B.N., Brown, T.D. and Lee, G.K., 1977. Inert coal macerals in combustion. *Fuel*, 56, 125-130.

Nelson, D.W. and Sommers, L.E., 1996. Total Carbon, Organic Carbon and Organic Matter. In: Methods of Soil Analysis (Part 3: Chemical Methods). *Soil Science Society of America Inc., American Society of Agronomy Inc.*, Madison Wisconsin, USA.

Rees, J.G., Ridgway, J., Knox, R.W.O.B., Wiggans, G. and Breward, N., 1998. Sediment-borne contaminants in rivers discharging into the Humber estuary, UK. *Marine Pollution Bulletin*, 37, 316-329.

Rumpell, C., Knicker, H., Kögell-Knabner, I. and Hüttl, R.F., 1998. Airborne contamination of immature soil (Lusatian mine district) by lignite-derived materials: its detection and contribution to the soil organic matter budget. *Water Air and Soil Pollution*, 105, 481-492.

Spears, D.A., 2000. Role of clay minerals in UK coal combustion. *Applied Clay Science*, 16, 87-95.

Sýkorová, I., Pickel, W., Christanis, K., Wolf, M., Taylor, G.H. and Flores, D., 2005. Classification of huminite-ICCP System 1994. *International Journal of Coal Geology*, 62, 85-106.

Swennen, R. and van der Sluys, J., 1998. Zn, Pb, Cu, and As distribution patterns in overbank and medium-order stream sediments samples: their use in exploration and environmental geochemistry. *Journal of Geochemical Exploration*, 65, 27-45.

Taylor, G.H., Teichmüller, M., Davis, A., Diessel, C.F.K., Littke, R. and Robert, P., 1998. Organic Petrology. *Gebrüder Borntraeger*, Berlin, Germany.

Thomas, L., 2002. Coal Geology. *John Wiley & Sons Ltd*, West Sussex, UK.

Vassilev, S.V. and Vassileva, C.G., 1996. Mineralogy of combustion wastes from coal-fired power stations. *Fuel Processing Technology*, 47, 261-280.

Vassilev, S.V., Vassileva, C.G., Karayigit, A.I., Bulut, Y., Alastuey, A. and Querol, X., 2005. Phase-mineral and chemical composition of composite samples from feed coals, bottom ashes and fly ashes at the Soma power station, Turkey. *International Journal of Coal Geology*, 61, 35-63.

von Vinken, R., 1965. Stratigraphie und tektonik des beckens von Megalopolis (Peloponnes, Griechenland). *Geologisches Jahrbuch*, 83, 97-148.

Ward, C.R., Taylor, J.C., Matulis, C.E. and Dale, L.S., 2001. Quantification of mineral matter in the Argonne Premium Coals using interacting Rietveld-based X-ray diffraction. *International Journal of Coal Geology*, 46, 67-82.

(This page is left blank intentionally.)

DOMESTIC SOLID WASTE LANDFILL SITE SELECTION IN SENİRKENT-ULUBORLU (ISPARTA) BASIN

Şener (Tay) Ş. , Karagüzel R. and Mutlutürk M.

Süleyman Demirel University, Department of Geological Engineering, 32260, Isparta
(✉)*sehnaz@mmf.sdu.edu.tr*, *kquzel@mmf.sdu.edu.tr*, *mutlu@mmf.sdu.edu.tr*

Abstract: Senirkent-Uluborlu Basin is located in the Eğirdir Lake water catchment basin. In the basin, the disposal of solid waste must be regulated. The first and most important step in planning solid waste landfill site is to find a proper location. Detailed investigations which are already completed on geology, hydrology, hydrogeology, land use, transport and special environmental protection areas are the fundamental criteria for site selection. The thematic maps prepared according to the results of these investigations and suitable regions for solid waste landfill were determined.

In the suitable regions, three alternative locations were determined which are topographically suitable to construct a landfill. These locations are evaluated in terms of site suitability, location factors and public acceptance by using the method developed by Mutlutürk and Karagüzel (2003, 2005). As a result, one area having the highest rank in this evaluation was selected as the most suitable landfill–site.

Keywords: Landfill, Senirkent- Uluborlu Basin, site selection, solid waste.

1. INTRODUCTION

Solid wastes, generated from industrial organisations and urban areas is a serious problem having the first priority of the environmental problems (Chaulya, S, K. 2003, Wycisk, P. et al., 2002, Mikkelsen, P., S., et al., 1998). Out of 3215, only 11 municipalities have secure landfills of solid waste in our country (www.cevreorman.gov.tr).

Senirkent-Uluborlu Basin, chosen as the working area, is located in the Eğirdir Lake water collecting basin which is 768 km^2 (Figure 1). An important increase in the amount of domestic and industrial solid waste is expected because of the increase in population and developments in agricultural industry existing in settlement areas in the basin. There is no secure solid waste landfill site in the Eğirdir Lake basin (Mutlutürk, et al., 1991). However, Eğirdir Lake is the source of drinking water of Isparta and neighboring residential areas. Soil, air, surface and groundwater pollution of the basin is expected because of the unregulated solid waste sites of residential areas. Secure landfill has to be built in order to protect the groundwater and the water quality of Eğirdir Lake by law. The first and most important step in planning solid waste landfill is to choose a proper site (Waele, J., De et al., 2004, Mummolo, G., 1996).

2. METHODOLOGY

Investigation methods to be applied for solid waste landfill site selection in the Senirkent-Uluborlu Basin are shown in Table 1 in the following order; 1- Population projection and expected solid waste volume were calculated. 2- There have been detailed investigations made on geology, hydrology, hydrogeology, land use, settlement areas, routs and special environmental protection areas, which are the fundamental criteria for site selection. The thematic maps were prepared according to the results of these investigations, and suitable places for solid waste landfill were determined by superposing two maps by means of a computer.

3. RESULTS AND DISCUSSION

3.1 Waste Inventory

A future population projection of the residential area was calculated according to the method of Iller Bank (1985). According to the calculation the expected solid waste volume was found to be 954

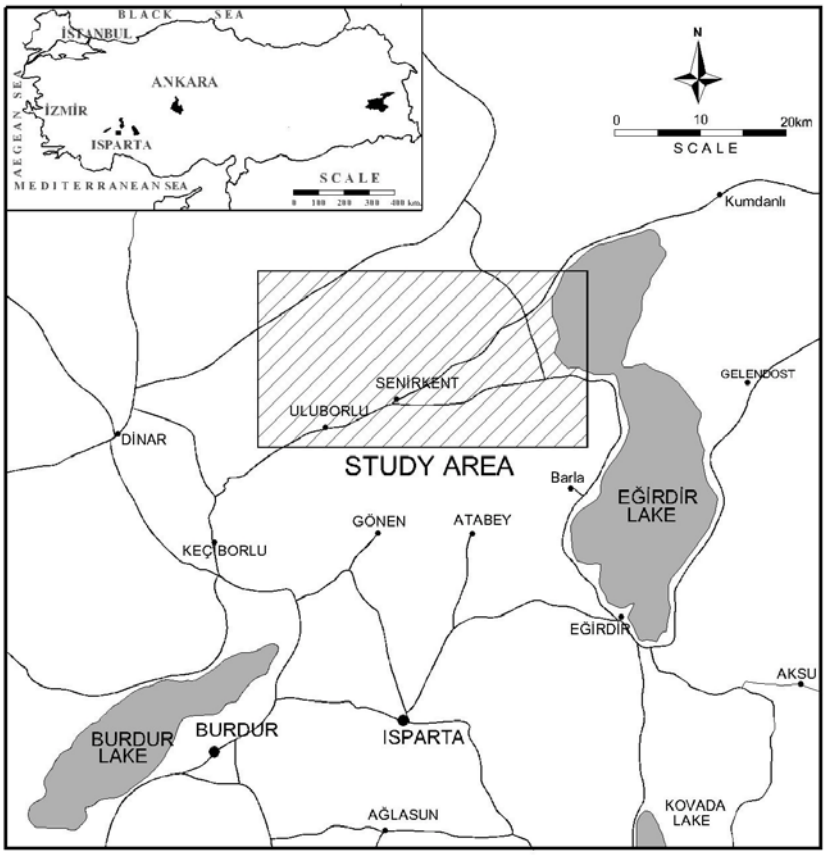

Figure 1. Location map of the investigation area

Table 1. Investigation method and steps

Step		Investigation Method
I.	Waste Inventory	- Projection of Population - Amount of waste to be stored
II.	Determination of alternative regions	- Geology - Hydrology - Hydrogeology - Settlement Areas and Transport - Special Environmental Protection areas - Land use The thematic maps are prepared according to the results of these investigations and to determine suitable regions
III.	Determination of alternative locations and selection of the most suitable landfill site.	

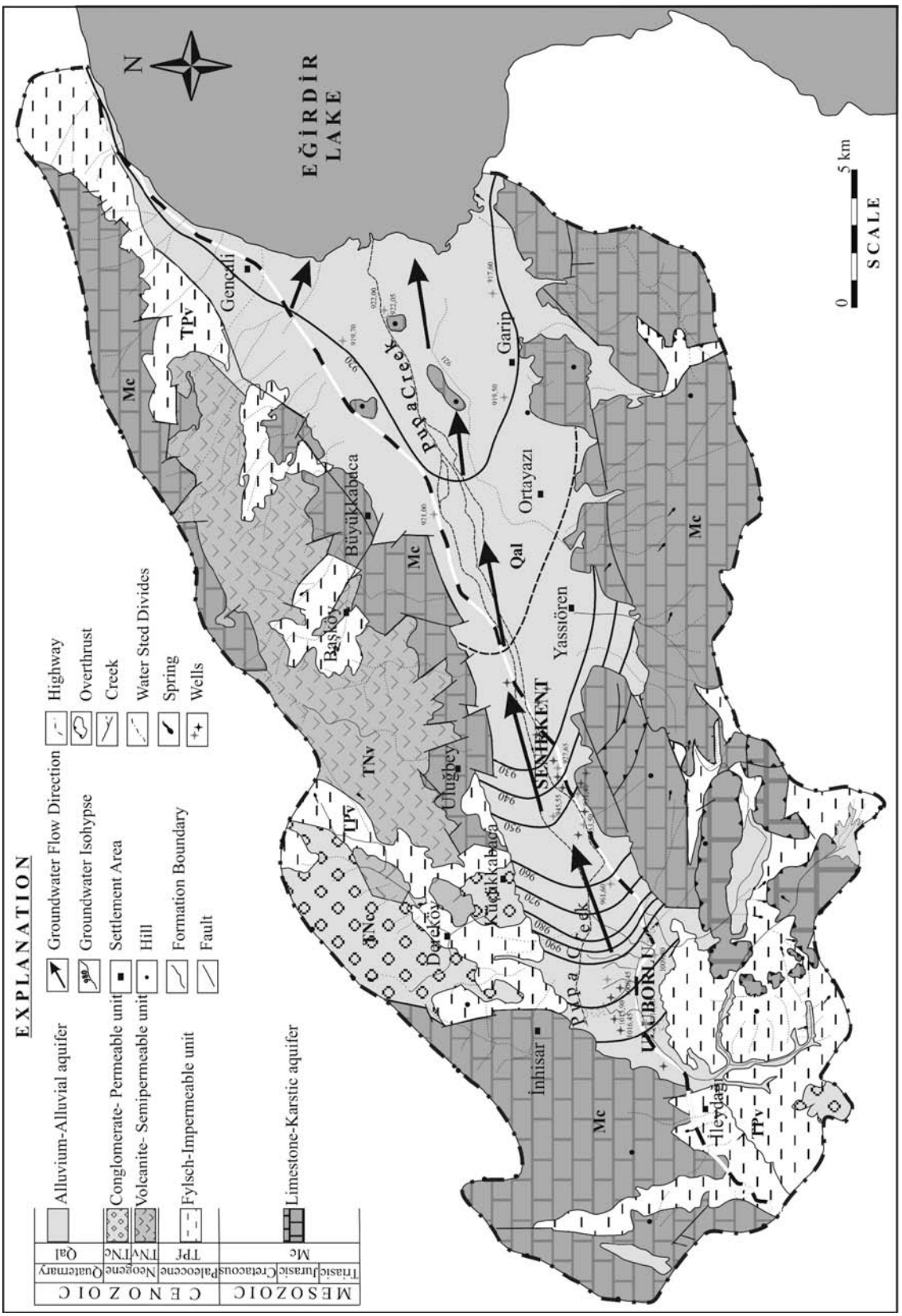

Figure 2. Geological and hydrogeological map of the investigation area

128 m^3. The landfill waste ratio comprises 27.72 % of the total garbage volume at the investigation area. Under these circumstances, the volume of total garbage must not exceed 264 484 m^3 for 50 year. If the stored garbage height is asumed to be 15 m at the landfill site, approximately a 1.76 ha area is needed as a landfill site. Therefore, the criterion of a 1.76 ha area is to be taken into account in landfill site selection.

3.2 Geology

Geological units in different age and lithologies outcrop are in the study area. The units are from bottom to top as follows; Mesozoic aged carbonate rocks, Cenozoic aged clastic and volcanics. Cenozoic units unconformably overlie the Mesozoic carbonates. Clastic rocks consist of Paleocene –Eocene aged Uluborlu flysch, Pliocene aged terrestrial sediments and loosely cemented Quaternary aged cover sediments. Volcanic units are known as Zendevi volcanics. Pliocene aged terrestrial sediments are clay, silt, sand, and gravel. Alluvuim comprises materials such as clay, silt, sand, and gravel covering unconformably the whole of the other units (Figure 2).

Based on the geological properties of the region, natural impermeable areas suitable for solid waste landfill site selection are determined. According to the geological map with a scale of 1/ 100 000, claystone and mudstone levels of Paleocene flysch, Zendevi volcanics and terrestrial sediments are defined as suitable sites and limestones, conglomerate and alluvial sediments in the area defined as unsuitable sites for solid waste landfill (Figure 2).

3.3 Hydrology & Hydrogeology

According to the Solid Waste Control Regulation (1991) prepared by Ministry of Environment and Forestry, the entire water collecting basin of Eğirdir Lake, which is being used for drinking water, is classified as unsuitable areas for landfill site.

In the basin, a neigbouring area of springs (approximately in 50 m distance) is classified as unsuitable. In addition, flooding area of streams and water collecting basin of Uluborlu Dam and Ileydag pond is classifed as unsuitable areas as well.

Based on the findings related to groundwater flow directed towards Eğirdir Lake and physical properties of the lithological units existing in the area (Figure 2), the karstic and alluvial aquifers and the permeable units were classified as unsuitable areas, the semi permeable units and the impermeable units were accepted as suitable areas for landfill site selection.

3.4 Land Uses & Settlement Locations

In the land use map prepared by Rural Services of Isparta Municipality, the first grade agricultural area is defined as unsuitable for solid waste landfill. According to the solid waste regulations prepared by the Ministry of Environment and Forestry, the solid waste landfill site must be 1 km away from a settlement area. According to these criteria all the suitable and unsuitable regions were determined.

3.5 Determination of Alternative Locations for Waste Landfill Site

The thematic maps prepared using the results of the above mentioned investigations, the suitable places for solid waste landfill were prepared by superposing the maps by means of a computer (Figure 3).

Three alternative areas suitable for landfill construct were determined topographically (Figure 3). These places are Ortabatak (Alternative Location I), Çatma (Alternative Location II) and Birgüney (Alternative Location III). These places are evaluated according to the format developed by Mutlutürk and Karagüzel (2005) for site suitability, location factors and public acceptance considerations (Tables 2, 3, 4).

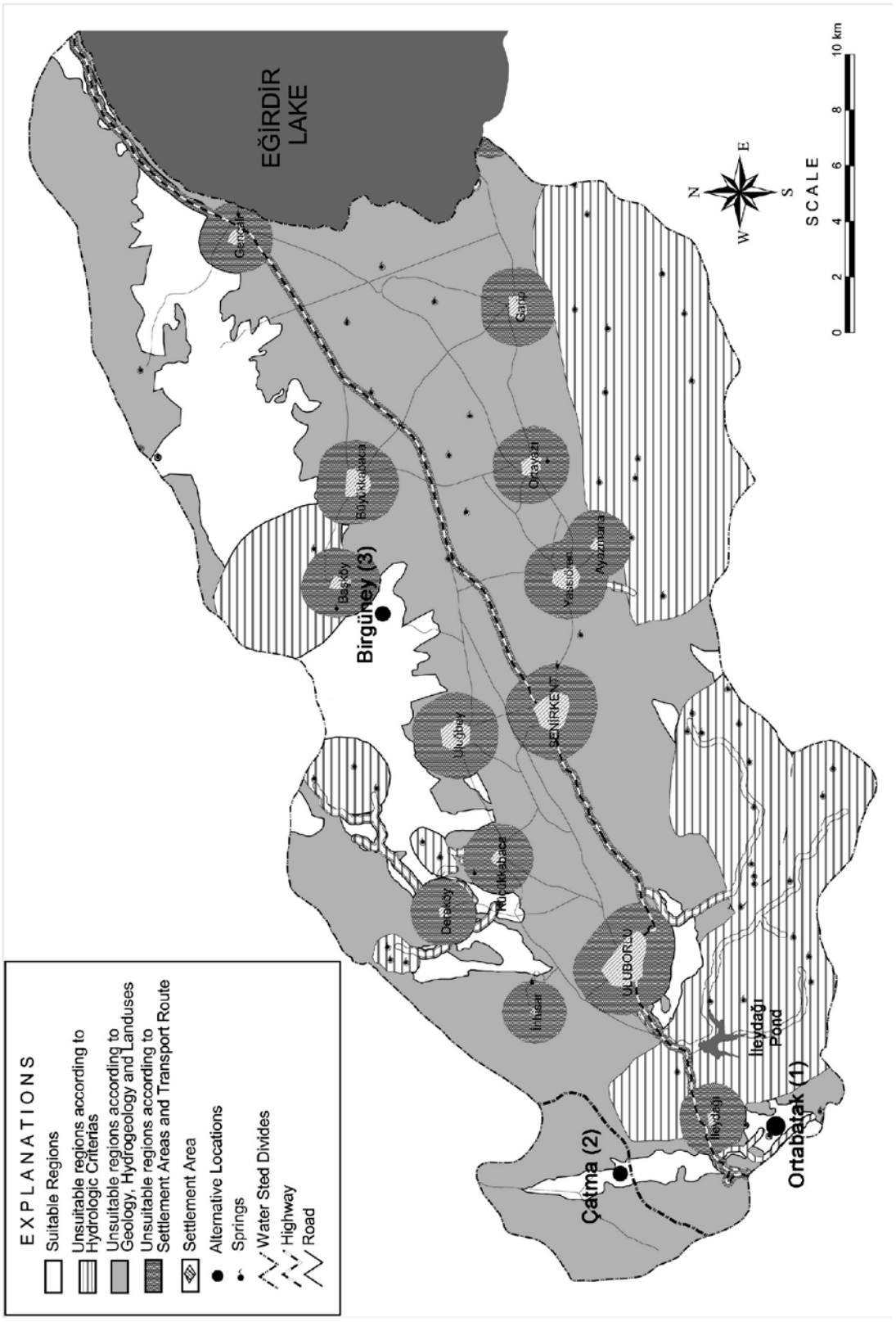

Figure 3. Thematic map of the investigation area

Table 2. Site suitability Parameters for evaluation (Mutlutürk and Karagüzel, 2003)

GEOLOGY	Point	Alternative Location I	Alternative Location II	Alternative Location IIII
	60	**(Ortabatak)**	**(Çatma)**	**(Birgüney)**
Lithology	**36**			
Clay sediments	36			
Sandy clay, gravelly clay sediments	27	√	√	
Flysch, metamorphics, ophiolites	18			
Massive and bedded rocks	9			
Fractured, crushed, karstic rocks and sandy-gravely sediments	0			√
Geological Structure	**24**			
Horizontally bedded	24	√	√	√
Vertical bedded	12			
Folded bedded	6			
Folded and fractured	3			
Faulty	0			
Total		**51**	**51**	**24**
Hydrogeology	**Point**			
	60			
Permeability Characteristics	**20**			
High	0			
Medium	5			
Low	10	√		√
Very Low	15			
Practically impermeable	20		√	
Groundwater Depth	**20**			
<3m	0			
3≤ <5 m	1			
5≤ <10 m	5			
10≤ ≤ 20m	10			
> 20m	20	√	√	√
Groundwater pollution risk	**20**			
Yes	5			√
No	20	√	√	
Total		**50**	**60**	**35**
Hydrology-Meteorology	**60**			
Surface water	**36**			
No	36	√	√	√
Spring	12			
Stream	4			
Spring and stream or lake	0			
Correlation of main wind and	**24**			
Effective	6			√
No effective	24	√	√	
TOTAL		**161**	**171**	**101**

Table 3. Location Factors for evaluation

GEOGRAPHY	Point	Alternative Location I (Ortabatak)	Alternative Location II (Çatma)	Alternative Location III (Birgüney)
	24			
Distance from waste collection center	**9**			
< 3 km	9			
3≤ < 5 km	7			
10≤ < 15 km	3	√	√	√
> 15 km	1			
Transport	**6**			
Very good	6		√	
Good	4	√		
Medium	2			√
Bad	1			
Very bad	0			
Landuse	**9**			
Empty	9			
Grassland	6			
Arid cultivation	2	√	√	√
Wet cultivation	0			
Total		**9**	**11**	**7**
FILLING MATERIAL	**Point 24**			
Distance to impermeable material	**8**			
< 3 km	8		√	
3≤ < 5 km	6	√		
5 ≤ < 10 km	4			
10≤ < 20 km	2			√
> 20 km	0			
Distance to drainage material	**8**			
< 3 km	8			
3≤ < 5 km	6			
5 ≤ < 10 km	4			√
10≤ < 20 km	2	√	√	
> 20 km	0			
Distance to filling material	**8**			
< 3 km	8			
3≤ < 5 km	6			
5≤ < 10 km	4			√
10≤ < 20 km	2	√	√	
> 20 km	0			
Total		**10**	**12**	**10**

Table 3: (continued)

GEOTECHNICAL	Point	24	Alternative Location I (Ortabatak)	Alternative Location II (Çatma)	Alternative Location III (Birgüney)
Rock Properties	**8**				
Massive and high strength	8				
Large space, low persistence, medium strength	5				√
One-two joint set, low strength	3				
Three or more joint set, crushed	0				
Soil classes	**8**				
CL-CH	8			√	
GC-SC	5		√		
SW-GW, SP-GP	3				
OL-OH	0				
Mass movement	**6**				
No	6		√	√	√
Potential	4				
Dangerous	2				
Yes	0				
Cut and Fill	**4**				
Low	4		√	√	
Medium	2				√
High	0				
Flood risk	**6**				
Yes	0				
No	6		√	√	√
Landfill Capasity	**Point**				
	18				
< 20 year	0				
20≤ ≤30 year	6				
30≤ ≤40 year	12				
> 40 year	18		√	√	√
Total			**39**	**42**	**37**
TOTAL			**58**	**65**	**54**

As a result of these evaluations, Çatma area (Location II) has got the highest rank of the site suitability criteria with 171 points, which is very good (A), location factors of 65 points, which is good (B), public acceptance of 18 points, which is good (B). Consequently, this site was selected as the most suitable landfill area (see Tables 5, 6).

CONCLUSIONS

Senirkent-Uluborlu Basin is located in the Eğirdir Lake catchment basin. It is expected that amount of domestic and industrial solid waste will increase because of increasing population and developments in agricultural industry located around the residential areas in the basin. If necessary precautions are not taken to stop the pollution, the water quality of Eğirdir Lake will be affected negatively.

In this study, at the chosen water basin, single solid waste landfill site selection has been planned for the whole settlement locations. There have been detailed investigations made on geology, hydrology, hydrogeology, land use and

private protection areas, which are the fundamental criteria for site selection. The thematic maps were prepared according to the results of these investigations, and suitable regions for solid waste landfill were determined by superposing the maps by means of a computer.

Table 4. Public Acceptability for evaluation

SOCIAL	Point 30	Alternative Location I (Ortabatak)	Alternative Location II (Çatma)	Alternative Location III (Birgüney)
Distance from nearest settlement	**12**			
< 3 km	4			√
3≤ < 5 km	6	√	√	
5 ≤ < 10 km	8			
10≤ < 15 km	10			
> 15 km	12			
Morphology	**6**			
Valley	0			
Flat	1			
One – two side closed	3	√		√
Three – four side closed	6		√	
Esthetic	**6**			
It can be seen everywhere	0			
It can be seen only nearest site	2			√
It can be seen only nearest waste site	4	√	√	
It can not be seen anywhere	6			
Psychological	**6**			
Waste vehicles moving on main highways	0			
Waste vehicles moving through 3-4 settlements	2	√	√	√
Waste vehicles moving through 1-2settlements	6			
Total		**15**	**18**	**11**
GENERAL TOTAL		**234**	**254**	**166**

Table 5. Ratings and corresponding classification (Mutlutürk and Karagüzel, 2003)

Invertal Designation	E (Very Poor)	D (Poor)	C (Fair)	B (Good)	A (Very Good)
Site Suitability	SS < 35	35≤SS≤ 62	62≤SS≤110	110≤SS≤150	SS ≥ 150
Location Factors	LF < 15	15 ≤LF≤ 34	34≤LF≤ 60	60≤ LF≤ 70	LF ≥ 70
Public Acceptability	PA < 7	7 ≤PA≤ 13	13 ≤PA≤ 17	17≤PA≤ 26	PA ≥ 26

Table 6. Suitability evaluation of alternative locations

Alternative Locations	I Ortabatak	II Çatma	III Birgüney
Site Suitability	A	A	C
Location Factors	C	B	C
Public Acceptability	C	B	D

In suitable regions three alternative sites, topographically suitable to construct landfill, were determined. These places are evaluated for site suitability, location factors and public acceptance considerations according to the format developed by Mutlutürk and Karagüzel, (2003, 2005). As a result of these evaluations the Çatma area, which has got the highest point, was selected as the most suitable landfill area. Çatma area is not located in Eğirdir Lake basin. This property is another reason for selecting this site as the solid waste landfill site. However, if a solid waste landfill site is decided to be built in the Çatma site, further detailed geotechnical investigations must also be carried out in the area.

ACKNOWLEDGEMENTS;

This work was supported by the Research Fund of The Suleyman Demirel University. Project number: 03 YL 794. The authors would like to express their thanks to Ömer Tezcan Akıncı and Ahmet Doğan for their valuable contributions.

REFERENCE

Çevre ve Orman Bakanlığı, 1991, Katı Atıkların Kontrolü Yönetmeliği, 14.03.1991 tarih ve 20814 sayılı *Resmi Gazete*.

Çevre ve Orman Bakanlığı web sitesi, 2004, http://www. cevreorman.gov.tr, 18 October 2004

Chaulya, S. K., 2003, Water Resource Development Study for a Mining Region, *Water Resources Management* 17 : pp. 297-316, , Netherlands.

Gutnic, M., 1977, Geologie du Taurus Pisidien au nord d'Isparta, Turquie: Principaux résultats exraits des notes de M. Gutnic entre 1964 et 1971 par O. Monod, Universite du Paris-Sud Orsay, p. 130.

Gutnic, M., Monod, O., Poisson, A., ve Dumont, F., D., 1979. Geology des Taurides occidotales (Turquie): *Mem-Soc. Geol. Fr.,* N.S., S8, p. 112.

İller Bankası İçme Suyu Projesine ait Şehir ve Kasaba İçmesuyu Projelerinin hazırlanmasına Ait Yönetmelik, 22 Nisan 1985 tarih, 19733 sayılı *Resmi Gazete*.

Mikkelsen, P.S., Häfliger, M., Ochs, M., Jacobsen, P., Tjell J.C. and Boller, M., 1998, Pollution of Soil and Groundwater from Infiltration of Highly Contaminated Stormwater - A Case Study, *Water Science and Technology,* Volume 36, Issues 8-9, 1997, pp. 325-330

Mutlutürk, M., Karagüzel, R., Köseoğlu, M., Oran, S., Oğlakçı, M. ve Taşdelen, S.,1991, Eğirdir Gölü ve Havzası Kirletici Faktörlerin Araştırılması, , *Göller Bölgesi Tatlı Su Kaynaklarının Korunması ve Çevre Sorunları Sempozyumu*, pp. 479-489, Isparta

Karagüzel, R., Özçelik, H., Mutlutürk, M., Gülgal, V., Tokgözlü, A., Beyhan, M., Türk, G., Tay, Ş., Seyman, F., 2003, MATAB Katı Atık Düzenli Depolama, Kompost ve Geri Kazanım Tesisi ÇED Raporu (Göğü-Manavgat), SDÜ Mühendislik Mimarlık Fakültesi Döner Sermaye İşletmesi, Isparta. (unpublished)

Mutlutürk, M., Karagüzel, R., 2003, Katı Atık Depolama Yer Seçimi için Yeni Bir Öneri , LAQ, 57. *Türkiye Jeoloji Kurultayı Bildiri Özleri Kitabı,* s. 182, 8-12 Mart, Ankara

Mutlutürk, M., Karagüzel, R., 2005, Determination of The Landfill Area Quality (LAQ), *III.International Symposium, Prognostication, prevention and liquidation of disastrous and te place of the terrorism in extreme situations*, pp. 23-25 November, Bakü

Mummolo, G., 1996, An Analytic Hierarchy Process Model for Landfill

Site Selection, *J. Environmental Systems*, Vol. 24 (4) p. 445-465

Seyman, F., 2005, Isparta (Senirkent - Uluborlu) Havzası Hidrojeoloji İncelemesi, *SDÜ, Fen Bilimleri Enstitüsü, Yüksek Lisans Tezi*, Isparta. (unpublished)

Tay, Ş., 2005, Senirkent – Uluborlu (Isparta) Havzasının Katı Atık Düzenli Depolama Yeri Seçimine Yönelik Jeolojik – Jeoteknik İncelemesi, *SDÜ, Fen Bilimleri Enstitüsü, Yüksek Lisans Tezi*, Isparta. (unpublished)

Waele, J. De., Nyambe, I.A., Gregorio, A.Di., Gregorio, F.Di., Simasiku, S., Follesa, R., and Nkemba, S., 2004, Urban waste lanfill planning and karstic groundwater resources in developing countries: The example of Lusaka (Zambia), *Journal of African Earth Sciences*, Volume 39, Issues 3-5, pp. 501-508

Wysick, P., Weiss, H., Kaschl, A., Heisrich, S. and Sommerwerk K., 2003, Groundwater Pollution and Remediation Options for Multisource Contaminated Aquifers (Bitterfeld/Wolfen, Germany), *Toxicology Letters*, pp. 140-141, 343-351, Elsevier.

(This page is left blank intentionally.)

THE HYDROGEOLOGICAL AND GEOLOGICAL ASSESSMENTS OF THE TORBALI AND SELÇUK WASTE SITES AND ITS ENVIRONMENTAL EFFECTS

Şimşek C.

Department of Torbalı Technical Vocational School of Higher Education, Dokuz Eylül University, (35860) Izmir/Turkey
e- mail: celalettin@deu.edu.tr

Abstract: Torbalı and Selçuk plains are situated on a unconfined alluvial aquifer which is an important part of Küçük Menderes Basin, containing high productive alluvium aquifer. Torbalı and Selçuk and surrounding communities with a population of 100,000 are storing 150.000 m^3/yr of solid wastes (residential and industrial) in trenches dug into permeable, granular material along Fetrek and Küçük Menderes Rivers, without taking any precautionary measures.

Both solid waste disposal areas are located on unfavorable sites overlying surfacial aquifers that have significant groundwater potential. As no state of the art site selection procedure is implemented, both sites have significant environmental impacts. A total of 10 hydrogeological parameters are selected to assess the suitability of the two disposal sites of the districts of Torbalı and Selçuk, which are important industrial and touristic resorts. The results of the hydrogeological and geological assesment reveal the fact that both sites are not suitable for sanitary disposal of solid wastes. Also, the usage of the regular depositional area of the old clay mines was researched. Old clay pits are found to be suitable for deposition of the solid waste of Torbalı based on the geological and hydrogeological properties of the basement rock and the requirements stated in the "section 24 of the solid waste control regulation".

Key words: Solid waste sites, site selection, environmental effects, Torbalı, Selçuk

1. INTRODUCTION

The solid waste sites constitute hazardous pollutants for the environment. In general solid wastes are composed of domestic and industrial composition. The different compositon of pollutans in the solid waste dumped from the domectic and industrial developments are causing serious environmental problems (Appleyard, 2001).

Turkey has failed to develope a good strategy for the storage of solid waste. Especially, waste areas that are used before and those that are still used, pollute the environment. In recent years to choose the right location for waste storage, aquifer pollution and other index studies are commonly used. In some areas applications are done according to geological, hydrogeological and environmental parameters (Karagüzel and Mutlutürk,1997; Dörhöfer and Siebert, 1998; Şimşek and Filiz, 2005; Şimşek *et al*., 2006).

Generally, locations like closed or abandoned mines which have low water potential and impermeable layers should be preferred, but unfortunately in Turkey, as it is easier and more economical, municipalities prefer level lands where there are water drainage canals. And this application unfortunately causes environmental pollution.

In this study, Torbalı and Selçuk locations are evaluated by choosing the geological and hydrogeological parameters that are essential for waste storage areas. In addition to this, two alternative storage areas are recommended.

2. MATERIAL AND METHODS

A total of 3 boreholes were utilized in the study areas. The holes were drilled using a rotary system with a 90 mm diameter. From these boreholes, whose depths varied between 12 and 25 m, undisturbed and disturbed samples were

taken from various beds, and soil classification was done according to the Unified Soil Clasification System (USCS) (ASTM D2488-93, 1999).

Table 1. The selection parameters of a waste disposal site (modified by Şimşek and Filiz, 2005)

	Parameters	Range	Suitability	Torbali site	Selçuk site	Saibler site	Ahmetli Site
Aquifer Lithology	**Frac tured rocks**	1					
	Unconsolidated sediments	3		3	3		
	Consolidated sediments	6	6			6	6
		10					
Aquifer Potential	Regional aquifer	1		1	1		
	Local aquifer	3					3
	Poor aquifer	6	6			6	
		10					
Aquifer Type	Unconfined Aquifer Semi-Confined Aquifer Unconfined Aquifer Aquitard	1 2 3 4	 4	1	1	 4	 3
		10					
Depth to Groundwater	<5m	1			1		
	5-15m	3					3
	>15m	6	6	6		6	
		10					
Distance of River and water well	<150 m 150-300 m >300 m	1 3 6	 6	1	1	 6	 6
		10					
Dreinage Potential	Dense Medium Seldom	1 3 6	 6	1	1	 6	 3
		10					
Effects on water sources	Both groundwater and surfacewater Only groundwater Only Surface	1 3 6	 6	1	1	 6	 6
		10					
Permeability of basement	Permeable (>10^{-4} m/s) Medium permeable (10^{-4}> k<10^{-7} m/s) Impermeable (< 10^{-7} m/s)	1 3 6	 6	1	 3	 6	 6
		10					
Impermeable barrier thickness	<3m 3-10m >10m	1 3 6	 6	1	1	 6	 3
		10					
Bottom leakage Potential (Lp)	Lp >24 High 24< Lp> 12 Medium 12<Lp> 6 Low Lp<6 Very Low	1 2 3 4	 4	1	 2	 4	 4
		10					
		100	**58**	**17**	**15**	**52**	**43**

In these boreholes, permeability experiments were performed in situ in ground above the water table (Daniel, 1989). First permeability coefficients were obtained from the various intersected lithologies, then total permeability

coefficients were obtained from the products of their thicknesses; these then were divided by total metrage, thus yielding a total vertical permeability coefficient for the entire depth of the borehole.

On the basis of actual hydrogeological and geological data, parameters of the site sensitivity index are given weight (Şimşek *et al*., 2006). The value of sensitivity index is accumulated to the corresponding weight. A total of 10 hydrogeological parameters are selected to assess the suitability of the disposal sites. Each one of the parameters discussed previously are given a weighing coefficient (Table 1) from 1 to 6 such that the most and the least important factors in solid waste disposal site selection are given the highest (6) and lowest (1) points. The total score for proposed disposal sites are varying from 10 to 50. On the basis of the results obtained from the site suitability index the lowest score is 10, which has minimal parameters and must be avoided when the site selection decision is made.

In the grading system that is used, convenience of waste storage areas is evaluated in four categories. In the first category, areas that are graded 10 points or less, show the inappropriate areas for waste storage. When we look at the general characteristics of these areas, we see that they are permeable on regional scale, they have high leakage potential, have water in their structure and lack impermeable layers consisting of essential aquifers. These areas are usually used as drinking and potable water sources. For this reason it is important that these locations not used as waste storage areas. Otherwise they may cause rapid ground and surface water pollution.

The second category areas graded between 11-31 points are the areas which have partially fractured essential aquifers on regional or local scale, or have permeable sandy and pebbly soils, or have very thin or no impermeable layers with high leakage potential, or where mid and ground water is close to surface. Also in these areas surface drainage and usage of ground water is very high. For this reason these areas should also be protected from the waste activities. They should be away from waste storage areas or strict precautions should be taken (impermeable cover and ground barrier system, gas evacuation chimneys etc.)

Table 2. The clasification of waste disposal site suitability

Site Suitability	Range
Not suitable site	<10
Low suitable site	11-31
Medium suitable site	31-51
Suitable site	>51

The third category areas graded between 31-51 points are medium suitable areas (Table 2). These areas should have low permeable alluvium or clay formations, ground water should be at mid depth (>25m), should have impermeable layers with semi or low leakage potential, and with limited water zones. But in these areas you may find aquifers or impermeable zones on local scale, these features should be well examined. Some important precautions must be taken for environmental welfare. Some of which are; impermeable soil and cover layers. These areas should be used as alternative storage areas where there is no ideal location.

The fourth category areas graded 51 or higher points are the suitable sites. These areas have the parameters, which minimize the environmental effects of waste storage. The most important parameters are; impermeable layers, very little ground water which is deep beneath

the surface, having low leakage potential and having aquifer lithology consisting of impermeable rocks or soils like claystone, shale, massive rocks, silt stones, clays and silts etc. In addition to this, as these areas have no water potential, water zones are very rare. The cost of constructing waste storage in these areas are considerably low and their impacts on the environment are less than the other areas.

2.1. Selected Parameters

A total of 10 hydrogeological parameters are selected to assess the suitability of the two disposal sites of the districts of Torbalı and Selçuk. The aquifer lithology refers to consolidated, unconsolidated or fractured rocks, and also the aquifer types are defined as unconfined, semi-confined and confined aquifers. The aquifer most vulnerable to contamination is determined to be unconfined unconsolidated and fractured rocks. Depth to groundwater is a very important parameter for groundwater vulnerability. The depth to groundwater is determined to the distance from the surface to the water table. Aquifer potential is related to regional water capasity and potable water quality. The aquifer potential is determined as three catagories, and a regional aquifer is important for water suply, other local and poor aquifers are less important water supplies. The permeability of the unsaturated zone and the thicknes of the impermable zone are important, because these control the rate of contaminant movement in the aquifer (Bagch, 1994).

The leakage potantial is the tendency for precipitation entering the landfill through cover soil to cary deposited waste in suspension since an absolutely impermeable medium does not exist in nature (Frempong, 1999).

$$Lp = \frac{300\ (k)^{1/3}}{t_b}$$

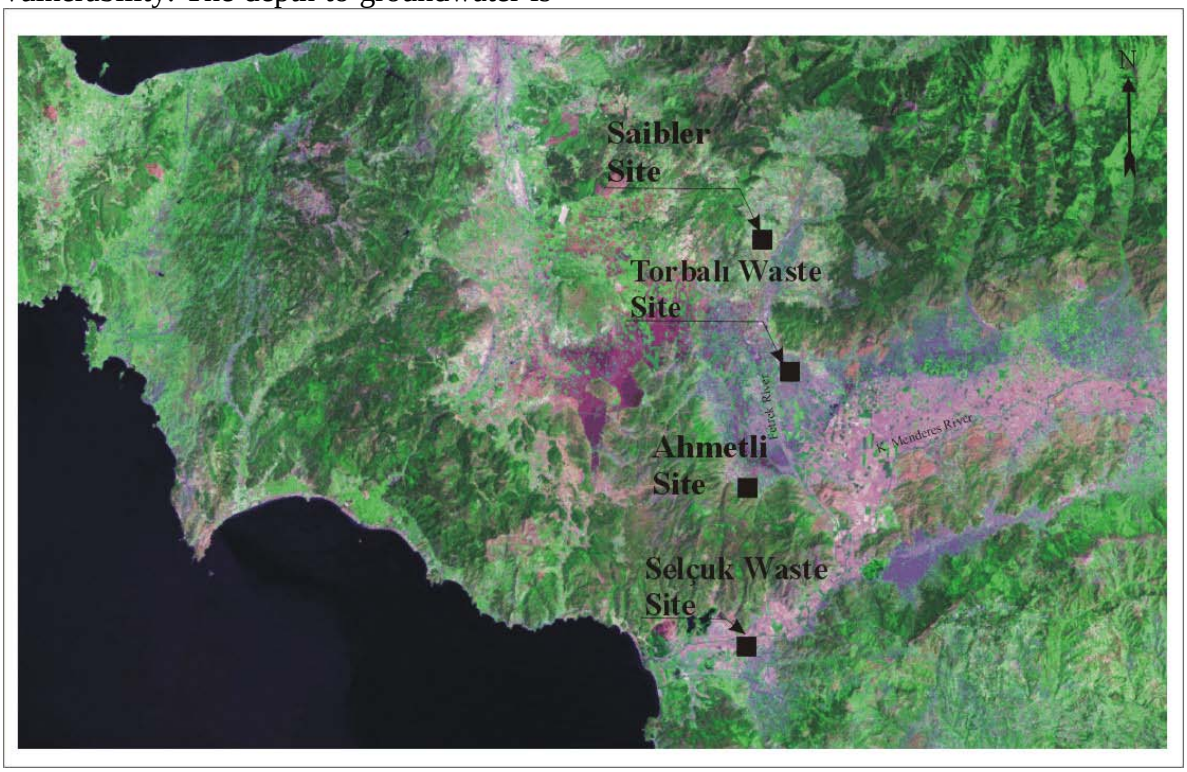

Figure 1. Location map of the waste sites

Where k is soil permeability (cm/s), tb bottom soil thickness (cm) and Lp is potantial leakage of leachate materials from the base of landfill through the substrata in to the groundwater body. The other factor of landfill consruction is

waterways. No landfill should be constructed within 300 m of a waterway (i.e. lake, pond, river, well, dense drainage way).

2.2. Study Area

In the western part of Turkey, Küçük Menderes Basin, located in the south of Izmir, a center of industry and tourism, is situated on an alluvial aquifer having high water potential (Figure 1). In the region, water needs of industrial and residential areas and for irrigation are met entirely from Quaternary alluvium. Groundwater potantial of Küçük Menderes Basin has 0.6% of the groundwater potantial of Turkey.

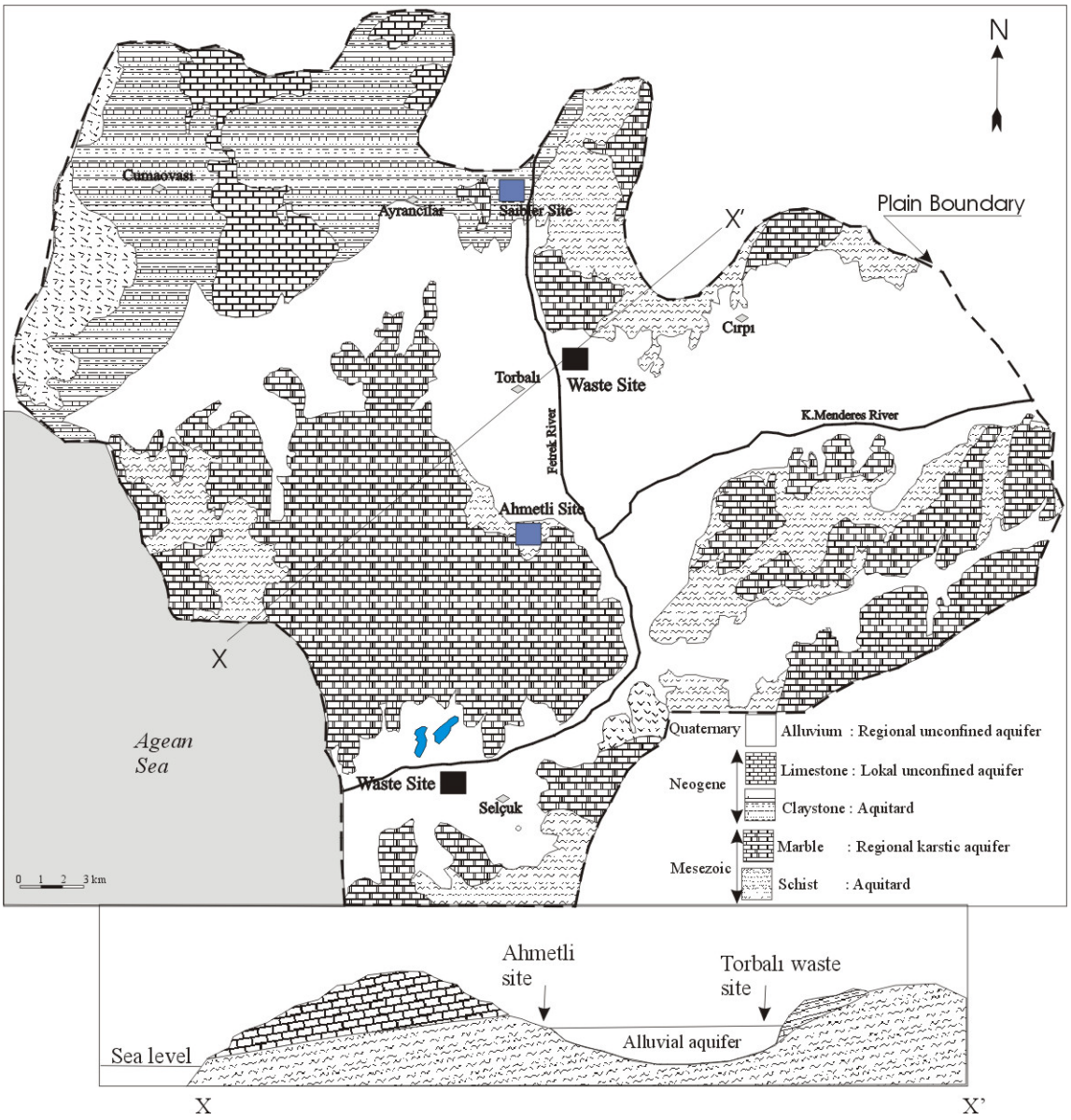

Figure 2. Aquifer map of the study area (modified by Elçi et al., 2001;Şimşek 2002; Şakıyan and Yazıcıgil, 2004)

The Torbalı and Selçuk towns are located nearly 50 km to the south of Izmir in the western region of Turkey (Figure 1). The study area is a Mediterranean climate zone. The region has much rainfall during the months of November, December, January and February. According to 20 years of meteorological data, the average rainfall in Küçük Menderes Basin and the surrounding area is 718 mm/year. The rainfall is the highest during the months of November and December with values of 90-153 mm/month. The lowest rainfall occurs

during July and August, at 1.5-4 mm/month. 55% of the rainfall occurs during the winter months. The average temperature is 17 °C (Şimşek, 2002).

The Torbalı and Selçuk Plains, which form a part of the Küçük Menderes River Basin, are located in a wide alluvial plain (Figure 1). The Mesozoic Menderes Massive rocks are the basement of the study area and located in the eastern and western parts of the plain. The Menderes Metamorphic Massive contains mica and chlorite schists in the lower levels and continues with dolomitic limestone in the upper sections. The schists are nearly impermeable and it is very difficult to lift the ground water in the area. The marble is a karstic aquifer that has a big potantial groundwater in the region. The Neogen aged (Miocene-Pliocene) Visneli Formation, which is formed of limestone and claystone, overlie the Menderes Massive (Erdoğan and Güngör, 1992). The claystone, which is located under the alluvium, has characteristics of impermeable rock and form the lower boundary for the alluvium aquifer (Figure 2).

2.3. Site Evaluation

Both Torbalı and Selçuk waste sites are located on the Quaternary alluvium unit. On the basis of drilling, it was determined that the coarse-grained lithologies containing 10-35% clay and silt exceed 40 m in thickness. Coarse-grained pebbly sands were intersected near Torbalı Fetrek River in particular, in drilled wells (Simsek, 2002). In permeability tests done in coarse-grained materials, it was determined that permeability coefficients vary between 10^{-3} m/s and 10^{-4} m/s. In soil classification done in the laboratory, it was determined that there are two predominant types of material in the areas: coarse-grained (granuler) and fine-grained (cohesive) materials. The coarse-grained material comprises gray, moderately to well-graded, tight silty and pebbly sands.

In boreholes done in the Selçuk waste site, black, indurated to semi-indurated, low plasticity lensoidal sand-bearing sands and silts were intersected. The thickness of the materials in this area was found to be greater than the depth of the deepest borehole, that is >12 m. In laboratory tests of the permeability of cohesive materials, values varying between 10^{-5} m/s and 10^{-7} m/s were obtained. In permeability classification on the basis of material types proposed by Terzaghi and Pect (1996), areas where Torbalı waste site is were deemed "well-drained and permeable aquifer" areas, and areas where Selçuk waste site resides were deemed "well-moderately drained and moderately permeable aquifer" areas.

The Torbalı waste site is situated on granular, "well-drained and permeable aquifer" materials, whereas the Selçuk waste site is situated on cohesive, "moderately drained and moderately permeable aquifer" materials.

Although the level of ground water is 30-35m deep in Torbalı and its environment, it is 25-30 cm deep in Selçuk plain in the wet season. In Selçuk, ground water and waste leakage water are in direct contact, whereas the groundwater level in Torbalı plain is very deep. Near the Torbalı waste site, no silt and argillaceous layers are found in pebbly and sandy soils to block the surface pollutants. As there is no impermeable layer beneath the waste site, surface pollutants can easily affect soil and ground water quality.

Both waste storage areas are on alluvium aquifers, which are essential in regional sense. Küçük Menderes river basin, an important center of agriculture, industry and tourism in Aegean Region, has important ground water sources. Especially most of the drinking, potable and irrigation water is obtained from alluvium aquifers. Although waste storage areas should be away from these aquifers, both areas are located on them. Küçük Menderes river basin has Turkey's 0,6% water potential. Locations with such high

water potential should be protected from waste storage areas.

The alluvium unit under the waste storage areas has high leakage potential. Also above the alluvium there are two large rivers running in N-S and W-E directions, which form the main drainage net. Both of the rivers feed the aquifers and the two waste storage areas are located close to these rivers. As waste leakage waters have a connection with the rivers, it fastens the transfer of the pollutants further. If used as irrigation water it harms the plants and the environment.

According to the geological and hydrogeological studies, these areas fall into low suitability category. Negative effects on the environment are inevitable if necessary precautions are not taken. Environmental effects are discussed below. In the river basin where Torbalı and Selçuk waste storage areas are located; Saibler and Ahmetli are recommended as alternative locations. Results of the evaluations show that Saibler is a suitable location for waste storage areas, whereas Ahmetli is a medium suitability site for waste disposal. Both alternative locations can be used as waste storage areas if necessary precautions are taken.

3. ENVIRONMENTAL EFFECTS

Torbalı and Selçuk waste storage areas are located on alluvium aquifers. No precautions are taken at these waste areas where there are aquifers under high risk of pollution. Especially, environmental studies done at Torbali waste area show chemical and heavy metal pollution, originating from waste water (Simsek, 2002). The leakage water constitutes the salt-water characteristics with Na-Cl water type. Also electirical conductivities of leakage water of both these locations, vary between 3750 – 4575 µS/cm. Similarly, Fe, Mn, Li concentrations in leakage samples exceed the limits of drinking water quality standard. It shows that if no precautionary measures are taken, this leakage water will pollute the aquifer. As they have no cover systems, on the other hand, waste sites are also causing air and landscape pollution near these areas. Especially in summer, bad odour and flying waste particles disturb the public living nearby. During rainy periods, rainfall water carries the pollutants from the waste storage areas rapidly to unprotected alluvium aquifers. Although the groundwater level beneath is 25-30 m in Torbalı plain, some pollutants may reach the ground water rapidly. When it is considered that ground water level in Selçuk is 50cm deep, pollutants will reach much faster than they do in Torbalı.

Torbalı and Selçuk waste sites are located on very important aquifers, constructed without any precautions, and are expected to have negative effects on the environment. This pollution of drinking and irrigation water not only threatens public health, but also effects the agricultural land negatively.

4. CONCLUSIONS AND DISCUSSION

Torbali and Selçuk waste storage areas are located on unprotected, permeable aquifers, which are important on a regional scale. This aquifer is in the river basin that shelters 0,6% of Turkey's water potential. According to the geological and hydrogeological parameters chosen to find out the convenience of these waste storage areas, both locations were graded between 15–17. And this reflects that Torbali and Selçuk waste storage areas are not suitable sites for waste facilities. Mainly suitable areas should be graded 50 points or over. Gradings in the study areas show that both locations lack the important parameters for waste storage like impermeable soil, deep ground water, low leakage potential, local or impermeable layer. Alternative locations are recommended for Selçuk and Torbali waste storage areas, which are determined as Ahmetbeyli and Saible sites in respect of their hydrogeological conditions. The recommended locations

are medium suitable and suitable area for waste disposal fasilities according to the grading system. If low-cost precautions are taken, these locations could become ideal waste storage areas.

Ten parameters are chosen to facilitate the preliminary studies to locate the right waste storage areas. In the areas chosen according to these parameters, detailed final studies should also be added. Borders of the storage areas should be determined by detailed land studies by way of drillings and geophysical examinations.

REFERENCES

ASTM, D2488-93., 1999. Practice for Description and Identification of Soils(Visual-Manual Procesudure), ASTM Standarts on Groundwater and Vadose Zone Investigations, *Drilling, Sampling, Geophysical Logging, Well Installation and Decommissioning*, 2nd edition.

Appleyard, S.J., 2001. Impact of Liquid Waste Disposal on Potable Groundwater Resources Near Perth, *Environmental Geology*, 28(2): 106-110, Springer-Verlag.

Bagch A., 1994. Design, construction and monitoring of landfills, 2nd edition, John Wiley and Sons Inc., New York, NY

Daniel D.E., 1989. In situ Hidraulic Conductivity Tests for Compacted Clay, *J. Geotech. Eng. Div. Am. Soc. Civ. Eng*., Vol. 115, no 9: 1205-1226.

Dorhofer, G. and Siebert ,H., 1998. The search for landfill sites – requirements and implementation in Lower Saxony, Germany. *Environmental Geology* 35: 55-65 DOI 10.1007/s002540050292

Elçi, H., Şimşek C., Koca, Y., 2001. Selçuk ve Çevresinin Mühendislik Jeolojisi, *İzmir ve Çevresinin Deprem – Jeoteknik Sorunları Sempozyumu,* 12-14 Kasım, İzmir

Erdoğan, B. and Güngör, T., 1992. Menderes Masifinin Kuzey Kanadının Stratiğrafisi ve Tektonik Evrimi, *TPJD Bülteni*, C.4/1-Aralık.

Frempong, E.M., 1999. Engineering geological assessment of a proposed waste disposal site in coastal southwestern Ghana, *Environmental Geology*, 37(3);255-260.

Karagüzel, R. and Mutlutürk, M., 1997. Katı atık depolanmasında yer seçimi ve Isparta örneği, *II Izmir ve Çevresinin Deprem Jeoteknik Sorunları Sempozyumu*, 22-24 Ekim, Izmir

Sakiyan, J., Yazicigil, H. 2004. Sustainable development and management of an aquifer system in western Turkey. *Hydrogeol. J. 12:66–80*

Şimşek, C., 2002. The hydrogeological investigations for the site selection of the landfill area of the Torbalı Plain. PhD Thesis, *The Graduate School of Natural and Applied Science, Dokuz Eylul University*, Izmir

Şimşek, A., Kincal., C. and Gündüz, O., 2006. A Solid Waste Disposal Site Selection Procedure Based on Groundwater Vulnerability Mapping; *Environmental Geology*, 49; 620-633

Şimşek, C., Filiz, Ş. 2005. Torbalı (İzmir) katı atık depolama sahasının jeolojik ve hidrojeolojik özelliklerinin incelenmesi, *DEÜ Mühendislik Fakültesi Fen ve Mühendislik Dergisi*, 7-2;39-56.

Terzaghi, K., Peck, R.B. and Mesri, G., 1996. Soil Mechanics in Engineering Practice, 3rd edition, John Wiley and Sons Inc., New York, NY

PANORMOS BAY AU-AG-TE EPITHERMAL MINERALIZATION, TINOS ISLAND, HELLAS: MULTIPLE MECHANISMS OF DEPOSITION FOR AN UNUSUAL CALC-ALKALINE GRANITE RELATED SYSTEM

Tombros S. F.[1], St. Seymour K.[1,2], Spry P. G.[3], Williams-Jones A. E.[4] and Zouzias D.[1]

[1]Department of Geology, Laboratory of Economic Geology, University of Patras, Rion, 26500, Patras, Hellas

[2]Department of Chemistry, Geography, Concordia University, Montreal, Canada.

[3]Department of Geological and Atmospheric Sciences, 253 Science I, Iowa State University, Ames, Iowa 50011-3212

[4]Department of Earth and Planetary Sciences, 3450 University Street, Montreal, Quebec H3A 2A7, Canada

[1]Corresponding author: e-mail, tompros@mailbox.gr; noisis2001@yahoo.com

Abstract: Gold-silver telluride mineralization at Panormos Bay is uncommon in its occurrence in Miocene marbles, and in its overall spatial and temporal association to the leucogranitic phase of the Tinos calc-alkaline pluton. The mineralization is associated with a stockwork of early milky and late clear quartz syntaxial veins, filling a conjugate system of strike-slip faults, in the marbles. Modeling the genesis of the Panormos Bay mineralization, must take into consideration its diverse set of sulfides, sulfosalts, tellurides and native metals related to multiple metal sources and the distance over which the corrosive (pH=3.3) F-Cl-CO_2-H_2S-B-bearing hydrothermal fluids traveled to the site of deposition.

The high permeability of the marble host permitted inflow of cooler, meteoric waters and subsequent mixing and cooling of the ore fluids, as indicated by stable isotope and fluid inclusion studies. This resulted in condensation of tellurium and gold ligands from the metalliferous vapours into the aqueous phase. The high reactivity of the marble provided an important mechanism that controlled ore precipitation. Carbon dioxide effervescence, which caused a pH shift towards neutral, resulted in the destabilization of bisulfide complexes, the release of H_2S and the precipitation of precious metal as tellurides. Carbofracturing and hydraulic fracturing allowed the conduits to remain open, permitting fluid flow and volatile to escape.

Key words: Au-Ag-Te ores, Panormos, fluid evolution.

INTRODUCTION

Low sulfidation epithermal Au-Ag-Te ores constitute important sources of precious metals. Studies of Au-Ag-Te deposits provide information on the mechanisms of hydrothermal ore deposition in general and of telluride ores in particular (i.e. Casadevall and Ohmoto, 1977; Ahmad *et al.*, 1987; Zhang and Spry, 1994; Choi *et al.*, 1996; Cooke and McPhail, 2001; Kovalenker *et al.*, 1997; Kelley *et al.*, 1998; Alderton and Fallick, 2000). Previous studies of Panormos hydrothermal system include the evolution of the alteration zones (Tombros and St. Seymour, 2003); the conditions of formation of new unnamed sulfotellurides (Tombros *et al.*, 2004) and the formation of zincian greenockite (Tombros *et al.*, 2005). In this study, we attempt to constrain the major mechanisms of deposition which resulted in precious metal telluride ore formation.

GEOLOGICAL SETTING

Tinos Island is a part of the Attico-Cycladic Massif in the Cyclades Blueschist Belt. Tinos consists of a package of Alpine nappes, which are stacked on top of an igneous basement of Hercynian age (Okrusch and Bröcker, 1990) (Figure 1). The lowest nappe, or "Basal unit", represents a Late -Triassic to -Cretaceous platform of neritic limestones tectonically overlain by the "Blueschist

unit" (Figure 1), which was initially a Mesozoic continental margin of neritic sediments and basic to acid volcanic rocks (Avigad and Garfunkel, 1989; Matthews *et al.*, 1999; Bröcker and Franz, 2000). High pressure-low temperature metamorphism occurred during the Eocene and exhumation in the Oligocene-Miocene, and was accompanied by a Barrovian overprint (Avigad and Garfunkel, 1989; Bröcker *et al.*, 1993). The Blueschist unit is overlain tectonically by ophiolites of the "Upper unit" (Figure 1) (Okrusch and Bröcker, 1990; Boronkay and Doutsos, 1994; Katzir *et al.*, 1996; Boronkay, 1995). Emplacement of the Miocene granodiorite-leucogranite Tinos pluton postdated overthrusting of the Upper unit (Faure *et al.*, 1991; Mastrakas and St. Seymour, 2000). The Tinos pluton appears to have intruded along syn-magmatic ductile faults (Famin *et al.*, 2004). The contact with the country rocks was used as a conduit for a boron and fluorine-rich, peraluminous tourmaline-allanite-apatite-garnet-bearing leucogranite, which formed peripherally to a metaluminous granodiorite (Mastrakas, 2006). K-Ar ages of ca. 18 to 15 Ma were obtained for the Tinos granodiorite and the leucogranite has been dated at 14 ± 0.1 Ma (Altherr *et al.*, 1982).

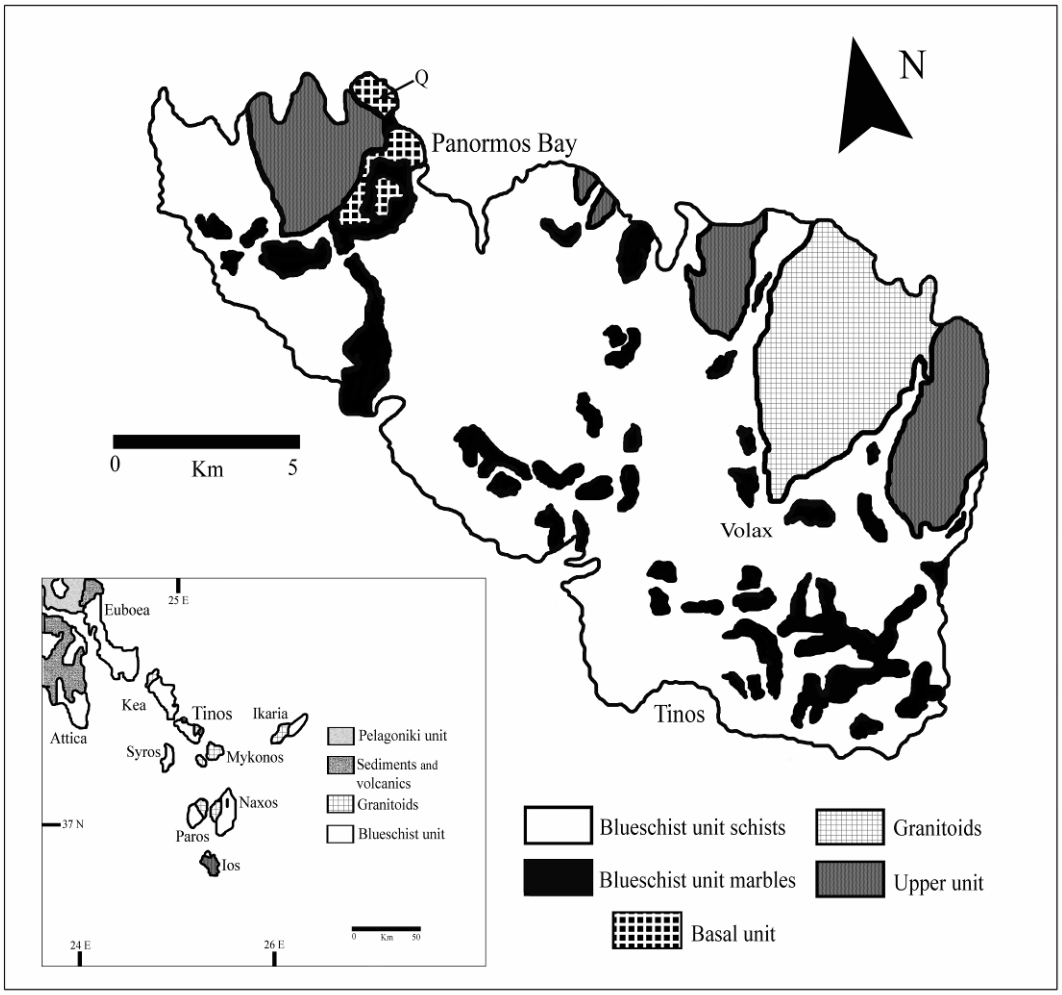

Figure 1. Map showing generalized geology of Tinos Island and the location of the Panormos Bay Au-Ag-Te mineralization (modified after Mastrakas and St. Seymour, 2000; Tombros *et al.*, 2005)

THE PANORMOS BAY VEIN SYSTEM

A tectonic window in the area exposes Triassic dolomitic marbles of the Basal unit through the marbles of the Blueschist unit, and hosts the Panormos Bay vein system, approximately 15 km from the western border of the Tinos pluton (Melidonis, 1980; Tombros, 2001). The Panormos vein system consists of 30 subparallel high-angle quartz veins that extend vertically for at least 500 m, filling a conjugate system of NE-trending sinistral and NW dextral strike-slip faults. These syntaxial veins form a stockwork that cuts both marble units and is filled with two generations of quartz: an older northeasterly trending set of milky quartz and a younger northwesterly set of clear quartz veins. Milky quartz veins (with widths up to 2m) contain tetrahedrite, chalcopyrite and bornite, whereas the clear quartz veins of 50 cm to 2 m wide, display well-developed "open space filling" textures, and galena and sphalerite as the main ore. Crustification is apparent, as four different zones, types A to D (with widths up to 50 cm) (Tombros *et al.*, 2005).

HYDROTHERMAL ALTERATION AND ORE PETROGRAPHY

Zones of alteration develop around barren milky and clear quartz veins. The zones are widest around the thickest veins, at vein intersections, along fault planes, and where marble is dolomitic and brecciated. Alteration haloes consist of two zones: an inner talc zone and an outer chlorite zone. Eight paragenetic stages of hypogene mineralization (I to VIII) followed by a supergene stage (IX) (Tombros, 2001) have been identified. Stage I is characterized by pyrite and minor arsenopyrite-pyrrhotite intergrowths. Stage II is dominated by massive aggregates of tetrahedrite, minor tennantite and rare goldfieldite. These minerals are replaced by Stage III chalcopyrite and bornite. Stage IV sulfosalts and arsenides, such as mawsonite, stannite, boulangerite, bournonite, luzonite, famatinite, niccolite, laggisite and gersdorffite; occur as replacement rims on stage III ore. Stage V is characterized by precipitation of tellurides in early-, middle- and late-substages and consists of altaite, hessite, sylvanite, native tellurium, stützite, unnamed Ag-Cu sulfotelluride; melonite, rickardite, vulcanite, weissite; kostovite, petzite, calaverite, krennerite and unnamed Ag-Au-Cu sulfotelluride. Stage VI galena, betekhtinite and argentite replaced minerals of all earlier stages. In Stage VII, disseminations of wurtzite, greenockite, magnetite, siderite, and smithsonite were deposited (Tombros *et al.,* 2005). The central parts of stage VIII veins are characterized by native gold, silver, copper, arsenic, as well as, stromeyerite and pyrargyrite. Lastly, stage IX consists of a variety of supergene oxides (i.e. tenorite, delafossite, lepidocrocite, goethite, and hematite), carbonates (malachite, azurite, cerussite), copper sulfides (chalcocite, digenite, covellite, and idaite), and a sulfate (anglesite).

FLUID INCLUSION AND STABLE ISOTOPES STUDIES

Analytical Methods

Microthermometric determinations were performed on doubly polished wafers 50-100 μm thick using a modified USGS-type stage, in the Laboratory of High Temperature Processes at the Department of Earth and Planetary Sciences of McGill University. Temperatures were measured with an alumel-chromel thermocouple, and the readings were calibrated with synthetic inclusions. Measurements are accurate to within ± 0.5^{o}C for temperatures <31^{o}C and to ± 1^{o}C for temperatures >31^{o}C. Material for stable isotope studies was obtained from vein and alteration minerals, host marbles and smoky quartz phenocrystals from the Tinos leucogranite. Isotopic compositions of

oxygen, hydrogen and carbon were analyzed on a VGSIRA12 triple collector mass spectrometer and those of sulfur with a VGMM602E double collector mass spectrometer. The analyses were performed at Geochron Laboratory, Massachusetts, U.S.A. The isotopic ratios are reported in standard δ notation per mil relative to SMOW for oxygen and hydrogen, Pee Dee belemnite for carbon, and Cañon Diablo troilite for sulfur. Analytical precision was better than ± 0.2 per mil for $\delta^{18}O$ and $\delta^{13}C$, ± 1 per mil for δD, and ±0.3 per mil for $\delta^{34}S$.

Fluid inclusions

Fluid inclusion data were obtained from milky and clear quartz occurring as vein fill in the talc and chlorite zones, smoky quartz in the leucogranite miarolitic cavities, fine- and coarse-grained calcite, and stage VII-sphalerite and siderite (Tombros, 2001). At room temperature, two types of fluid inclusion were identified: Type L-V inclusions consisting of aqueous liquid + vapor and type L-L-V inclusions of aqueous liquid + carbonic liquid + carbonic vapor. The temperatures of initial ice melting (T_e) of the L-V and L-L-V inclusions range from -48° to -30°C and -40° to -34°C, respectively, suggesting the presence of appreciable $CaCl_2$ and $MgCl_2$ in addition to NaCl (Kotel'nikov and Kotel'nikova, 1990). Temperatures of last melting of ice for the clathrate-bearing and clathrate-free L-V inclusions range from -10.3° to -1.4°C, which correspond to salinities of 0.63 to 13.3 wt percent NaCl equivalent. The decomposition temperatures of clathrate are between 7.5° and 9.7°C. These values indicate salinities of 0.8 to 4.9 wt percent NaCl equivalent (Figure 2). In L-L-V inclusions ice was nearly pure CO_2. All the inclusions can be described in the H_2O-CO_2-NaCl±$CaCl_2$±$MgCl_2$ ternary system (Kotel'nikov and Kotel'nikova, 1990). The L-V fluid inclusions homogenize to liquid at temperatures of 198° to 290°C, except in smoky quartz, for which the range is from 281° to 321°C. The L-L-V fluid inclusions homogenize to liquid between 266° and 294°C. The X_{CO2} values in milky quartz inclusions range from 4.1 at 251° to 8.9 at 290 °C (Figure 2).

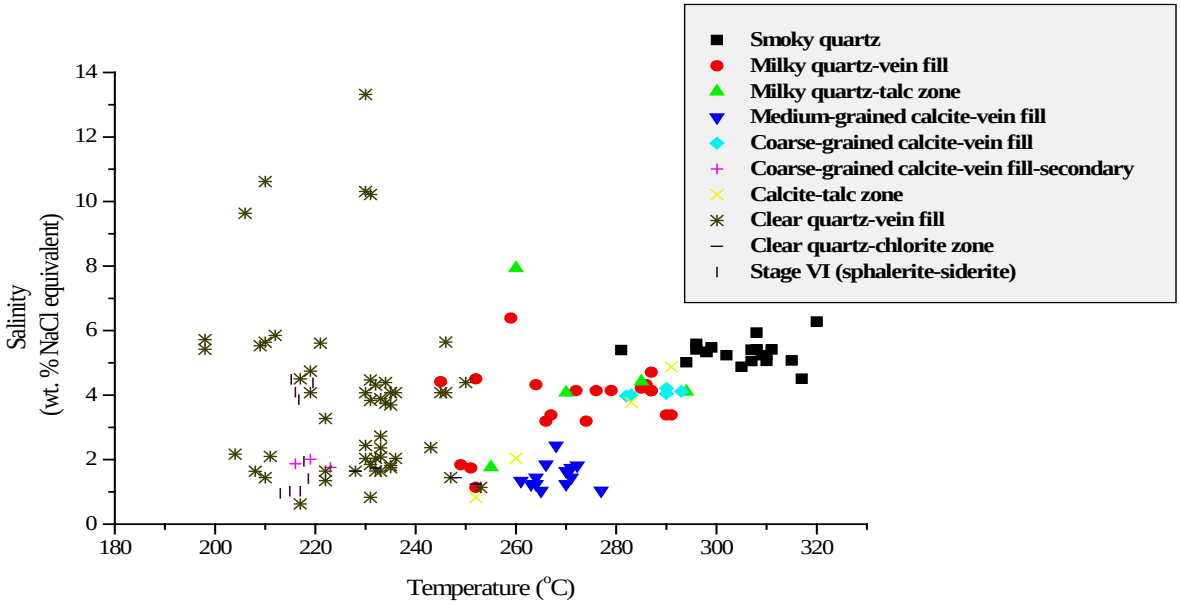

Figure 2. Liquid-vapor homogenization temperature vs. salinity plot in the CO_2-NaCl-H_2O system, from fluid inclusions (Tombros *et al.*, 2005)

Stable isotopes

Oxygen and *hydrogen* isotope compositions were obtained from fluids released from vein muscovite. The $\delta^{18}O$ and δD values of muscovite from milky quartz and clear quartz veins range from 12.4 to 14.3 and 15.9 to 16.2 per mil and from -59 to -76 and -98 to -99 per mil respectively. The calculated $\delta^{18}O$ and δD values of the fluid in equilibrium with muscovite are 3.7 to 5.1 and -1.3 to -1.8 per mil and -62 to -73 and -100 to -103 per mil, respectively. Values of $\delta^{18}O$ of milky quartz and clear quartz in veins and in the talc and chlorite zones are 12.6 to 14.2 and 16.0 to 17.9 per mil and 6.6 to 6.8 and 16.0 per mil, respectively. The calculated $\delta^{18}O$ values of water in equilibrium with milky and clear quartz range from 2.6 to 3.0 and 3.9 to 4.3 per mil and -3.3 to -3.2 and 3.8 per mil, respectively. A value of $\delta^{18}O$ of 11.2 per mil was obtained for a sample of smoky quartz taken from a miarolitic cavity in the leucogranite, and yielded a calculated $\delta^{18}O$ value for the water of 2.6 per mil (Tombros *et al.*, 2005b).

Carbon and *oxygen* isotope compositions were obtained from fine- to medium- and coarse-grained calcite coexisting with vein milky quartz and from the talc alteration zone. For these minerals $\delta^{18}O$ and $\delta^{13}C$ values are between 13.3 and 18.8 per mil and -0.3 to 1.2 per mil, respectively. The calculated $\delta^{18}O$ values of the fluids in equilibrium with calcite range from 7.3 to 12.2 per mil, whereas the $\delta^{13}Cco_2$ values range from -0.3 to -2.0 per mil, respectively.

Sulfur isotope compositions were obtained on samples of pyrite, tetrahedrite, chalcopyrite and bornite, galena and sphalerite (from Stages I, II, III, VI and VII). The $\delta^{34}S$ values range from -12.9 to 1.9 per mil and the calculated $\delta^{34}S_{H2S}$ values for the fluid were from 0.8 to -10.5 per mil (Tombros, 2001).

DISCUSSION

Several mechanisms have been proposed for epithermal ore deposition that include cooling, mixing with oxygenated meteoric waters, boiling, condensation, throttling, and wall rock interaction (Cooke and McPhail, 2001). The studies by McPhail (1995), Cooke and McPhail (2001) and Ronacher et al., (2004) reveal that several mechanisms are responsible for ore deposition in most epithermal deposits. In Panormos Bay mineralization there is an overall decrease in temperatures from type A to D crustification bands. This decrease in temperature was likely caused by mixing of the precious metal laden fluid with meteoric and modified meteoric waters as it entered the highly permeable carbonate host (Tombros 2001). Cooling resulted in the condensation of tellurium from the metalliferous vapours into the aqueous phase and reaction with Au-Ag bisulfide ligands, via reactions (1), (2), (3) and (4).

$$H^+_{(aq)} + HTe^-_{(aq)} = H_2Te_{(aq)} \quad (1)$$

$$H_2Te_{(g)} = H_2Te_{(aq)} \quad (2)$$

$$4HS^-_{(aq)} + Ag_2Te_{(s)} + H^+_{(aq)} = 2Ag(HS)^-_2 + HTe^-_{(aq)} \quad (3)$$

$$2HS^-_{(aq)} + AuTe_{2(s)} + 1.5H_2O_{(l)} = Au(HS)^-_{2(aq)} + 2HTe^-_{(aq)} + 0.75O_{2(g)} + H^+_{(aq)} \quad (4)$$

$$CaMg(CO_3)_{2(s)} + 5SiO_{2(aq)} + 3Mg^{+2} + 5H_2O_{(l)} =$$

$$Mg_3Si_4O_{10}(OH)_{2(s)} + Mg(OH)_{2(s)} + CaCO_{3(s)} + CO_{2(g)} + SiO_{2(s)} + 6H^+ \quad (5)$$

$$H_2S_{(g)} = H_2S_{(aq)} \quad (6)$$

$$H_2S_{(aq)} = H^+_{(aq)} + HS^-_{(aq)} \quad (7)$$

$$0.5H_2O_{(l)} + Au(HS)^-_{2(aq)} = Au_{(s)} + 2HS^-_{(aq)} + H^+_{(aq)} + 0.25O_{2(g)} \quad (8)$$

$$Ag_{(s)} + H_2S_{(aq)} + HS^-_{(aq)} + 0.25O_{2(g)} = Ag(HS)^-_{2(aq)} + 0.5H_2O_{(l)} \quad (9)$$

At Panormos Bay mineralization fluid inclusion data, as well as the presence of subangular vein breccias and the open, layered, banded, and comb-textured nature of veins constitute compelling evidence for phase separation associated with precious metal deposition. Evidence of CO_2 effervescence in the Panormos fluids was observed in fluid inclusions that homogenize over 200°C. Carbon dioxide released from carbonates (reaction 5) would have assisted H_2S escape (Lowenstern, 2001), and increase the pH from 3.3 to 6.7 (reactions 6, 7). This mechanism may have extracted tellurium and subsequently promoted the precipitation of precious metal tellurides from the hydrothermal fluid. As CO_2 effervescence promotes escape of volatiles, wall-rock interaction would have caused destabilization of the bisulfide ligand. Loss of $H_2S(g)$ and pH neutralization would have allowed subsequently the precious metals to react with HTe^- and promote their precipitation as Au-Ag tellurides. Continuous escape of all hydrogen gases (i.e. H_2S, HF and H_3BO_4), and O_2 assisted by CO_2 effervescence drove reactions (3) and (4) to the left until all HTe^- was depleted and thus, in principle, lowered the activity of HS^- and H^+ in the residual liquid.

An increase in the f_{Te2} preceded Stage V but reached a maximum with tellurides precipitation. Values of f_{Te2} subsequently declined after stage V and reached to very low values during stage VIII, where native gold, silver, copper, and arsenic formed. Deposition of native metals coincided with a decrease in f_{O2} assisted by effervescence, and pH from values of $10^{-35.9}$ and 5.7 at 250°C, to 10^{-41} and 6.7 at 200°C, respectively. While the values of these parameters decreased the f_{H2S} content remained almost constant ($10^{-3.7}$ at 300°C and $10^{-3.5}$ at 200°C). Such physicochemical conditions also facilitated the precipitation of native metals via reactions (8) and (9).

The Panormos Bay epithermal precious metal telluride system contains a diverse array of elements that were likely derived from the Tinos leucogranite and leached from the meta-igneous package (Tombros, 2001). The diverse set of Au-Ag-Te ores is related to the multiple metal sources, the distance over which the hydrothermal fluid traveled to the site of deposition, and the corrosive nature of the low pH fluids that carried fluorine, chlorine, CO_2, H_2S, and boron. The Panormos Bay area served as the site of precious metal tellurides because the high permeability of the marble host permitted mixing of magmatic fluids with modified meteoric waters. Wall-rock interaction of the hydrothermal fluids with the host marbles produced talc-brucite alteration and caused carbofracturing. Effervescence of CO_2 was a crucial factor in the precipitation of tellurides, because it shifted the pH of the hydrothermal fluid from acid to neutral, destabilizing gold bisulfide complexes. The effervescence of CO_2 facilitated the creation of a density gradient that allowed the influx of denser oxygenated waters. Low sulfidation gold-telluride systems related to plutonic rocks are rare in Hellas (Greece), however this is an open question as our recent exploration includes other parts of the Attico-Cycladic Massif, which hosts granitic intrusions with leucogranitic phases such as Laurium, Mykonos, Paros, Naxos, Ikaria, and Serifos.

ACKNOWLEDGEMENTS

The late Professor Nickolaus Melidonis geologically mapped Tinos and first reported the polymetallic mineralization at Panormos. Research funds for this work were obtained from government grants to KStS, and a "Pythagoras II" grant and post-doctoral fellowship to KStS and S. Tombros, respectively. We thank the European Social Fund (ESF), Operational Program for Educational and Vocational Training II (EPEAEK II), and particularly the Program PYTHAGORAS II, for funding the above work.

REFERENCES

Ahmad, M., Solomon, M., and Walshe, J.L. 1987. Mineralogical and geochemical studies of the Emperor gold-telluride deposit, Fiji. *Economic Geology*, 87, 345-370.

Alderton, D.H.M. and Fallick, A. E., 2000. The nature and genesis of gold-silver-tellurium mineralization in the Metaliferi Mountains of western Romania. *Economic Geology*, 95, 495-516.

Altherr, R., Kreuzer, H., Wendt, I., Lenz, H., Wagner, G.A., Keller, J., Harre, W. and Hohndorf, A., 1982. A late Oligocene/Early Miocene high temperature belt in the Attico-Cycladic crystalline complex (SE Pelagonia, Greece). *Geologisches Jahrbuch*, 23, 971-164.

Avigad, D. and Garfunkel, Z., 1989. Low angle faults underneath and above a Blueschist Belt-Tinos Island, Cyclades, Greece. *Terra Nova*, 2, 182-187.

Boronkay, K., 1995. Geotectonic evolution of the Cyclades. PhD thesis, *University of Patras*, Hellas (unpublished).

Boronkay, K. and Doutsos, T., 1994. Transpression and transtension within different structural levels in the central Aegean region. *Journal of Structural Geology*, 16, 1555-1573.

Bröcker, M., Kreuzer, H., Matthews, A. and Okrusch, M., 1993. $^{40}Ar/^{39}Ar$ and oxygen isotope studies of polymetamorphism from Tinos island, Cycladic Blueschist Belt, Greece. *Journal of Metamorphic Geology*, 11, 223-240.

Bröcker, M. and Franz, L., 2000. The contact aureole of Tinos, Cyclades, Greece: tourmaline-biotite geothermometry and Rb-Sr geochronology. *Mineralogy and Petrology*, 70, 257-283.

Casadevall, T. and Ohmoto, H., 1977. Sunnyside mine, Eureka Mining District, San Juan Country, Colorado: Geochemistry of gold and base metal ore deposition in a volcanic environment. *Economic Geology*, 72, 1285-1320.

Choi, S.H., Yun, S.T. and So, C.S., 1996. Fluid inclusion and stable isotope studies of gold- and silver-bearing vein deposits, South Korea: Geochemistry of a Te-bearing Au-Ag mineralization of the Imcheon mine. *Neues Jahrbuch Mineralogie Abhandlungen*, 171, 33-59.

Cooke, D.R. and McPhail, D., 2001. Epithermal Au-Ag-Te mineralization, Acupan, Baguio district, Philippines: Numeral simulations of mineral deposition. *Economic Geology*, 96, 109-132.

Famin, V., Philippot, P., Jolivet, L. and Agard, P., 2004. Evolution of hydrothermal regime along a crustal shear zone, Tinos Island, Greece. *Tectonics*, 23, 1-23.

Faure, M., Bonneau, M. and Pons, J., 1991. Ductile deformation and syntectonic granite emplacement during the Late Miocene extension of the Aegean (Greece). *Bulletin Société Géologique France*, 162, 455-477.

Katzir, Y., Matthews, A., Garfunkel, Z. and Schliestedt, M., 1996. The tectono-

metamorphic evolution of a dismemebered ophiolite (Tinos, Cyclades, Greece). *Geological Magazine*, 133, 237-254.

Kelley, K.D., Romberger, S.B., Beaty, D.W., Pontius, J.A., Snee, L.W., Stein, H.J. and Thompson, T.B., 1998. Geochemical and geochronological constraints on the genesis of Au-Te deposits at Cripple Creek, Colorado. *Economic Geology*, 93, 981-1012.

Kotel'nikov, A.R. and Kotel'nikova, Z.A., 1990. The phase state of the H_2O-CO_2-NaCl system, examined from synthetic fluid inclusions in quartz. *Geokhimiya*, 4, p. 526-537.

Kovalenker, V.A., Safonov, Y.G., Naumov, V.B. and Rusinov, V.L., 1997. The epithermal gold-telluride Kochbulak deposit (Uzbekistan). *Geology of Ore Deposits*, 39, 107-128.

Lowenstern, J.B., 2001. Carbon dioxide in magmas and implications for hydrothermal systems. *Mineralium Deposita*, 36, 490-502.

Mastrakas, N., 2006. Tinos granite and the associated skarn deposits. PhD thesis, *University of Patras*, Hellas (unpublished).

Mastrakas, N. and St. Seymour, K., 2000. Geochemistry of Tinos granite: A window to the Miocene microplate tectonics of the Aegean region: *Neues Jarhbuch Mineralogie Abhandlungen*, 175, 295-315.

Matthews, A., Lieberman, J., Avigad, D. and Garfunkel, Z., 1999. Fluid-rock interaction and thermal evolution during thrusting of an Alpine metamorphic complex (Tinos Island, Greece). *Contributions in Mineralogy and Petrology*, p. 135, pp. 212-224.

McPhail, C.D., 1995. Thermodynamic properties of aqueous tellurium species between 250 and 300 °C. *Geochemica et Cosmochimica Acta*, 59, 851 -866.

Melidonis, N.G., 1980. The geological structure and mineral deposits of Tinos Island (Cyclades, Greece): A preliminary study. *Institute of Geology and Mineral Exploration*, 13 (in Greek).

Okrusch, M. and Bröcker, M., 1990. Eclogites associated with high-grade Blueschists Cyclades Archipelago, Greece. *European Journal of Mineralogy*, 2, 451-478.

Ronacher, E., Richards, J.P., Reed, M.H., Bray, C.J., Spooner, E.T.C. and Adams, P.D., 2004. Characteristics and evolution of the hydrothermal fluid in the North Zone high-grade area, Porgera gold deposit, Papua New Guinea. *Economic Geology*, 99, 843-867.

Tombros, S., 2001. The Au-Ag-Te polymetallic mineralization of Tinos island, Cyclades, Aegean sea, Hellas. PhD thesis, *University of Patras*, Hellas (unpublished).

Tombros, S. and St. Seymour, K., 2003. Evolution of alteration zones accompany the Panormos Bay Au-Ag-Te mineralization. An approach based on the a_{K^+}/a_{H^+}, a_{Na^+}/a_{H^+}, $a_{Ca^{++}}/(a_{H^+})^2$ και $a_{Mg^{++}}/(a_{H^+})^2$ ratios. *Mineral Wealth*, 129, 9-24.

Tombros, S., St. Seymour, K. and Spry, P.G., 2004. Description and conditions of formation of new unnamed Ag-Cu and Ag-Cu-Au sulfotellurides in epithermal polymetallic Ag-Au-Te mineralization, Tinos Island, Hellas. *Neues Jahrbuch Mineralogie Abhandlungen*, 179, 295-391.

Tombros, S., St. Seymour, K., Spry, P.G., and Williams-Jones, A., 2005. Description and conditions of formation of new unnamed Zn-rich greenockite in epithermal polymetallic Ag-Au-Te mineralization, Tinos Island, Hellas. *Neues Jahrbuch für Mineralogie, Monastshefte*, 182, 1-9.

Zhang, X. and Spry, P.G., 1994. Petrological, mineralogical, fluid inclusions and stable isotopes studies of the Gies gold-silver telluride deposit, Judith Mountains, Montana. . *Economic Geology*, 89, 602-627.

(This page is left blank intentionally.)

NEW INDEXES FOR COAL GENETIC TYPE DETERMINATION

Turchanina O.N.[1], Butuzova L.F.[1], Bechtel A.[2], Safin V.A.[3], Isaeva L.N.[3] and Butuzov G.N.[1]

[1]Donetsk National Technical University, Artema str. 58, Donetsk 83000, Ukraine. E-mail: ksyu_t@mail.ru
[2]University Bonn, Mineralogisch-Petrologisches Institut, Poppelsdorfer Schloss, D-53115 Bonn, Germany
[3]National Academy of Science of the Ukraine, L.M. Litvinenko Institute of Physical Organic and Coal Chemistry, 70 R. Luxemburg str., Donetsk 83114, Ukraine

Abstract: The research of the molecular structure, supermolecular organization of the coals and the products of their thermal destruction permit to suggest the new indexes for determination of different genetic types by reductivity. DRIFT-spectroscopy, X-ray analyses and gas chromatography-mass spectrometry show are different in the structure of these low-rank coals.

Keywords: genetic type by reductivity, molecular structure of coal

INTRODUCTION

It is well known that the properties of coals depend on its genetic types, rank level, and petrographic composition. One of the most important genetic features of coal is its susceptibility to vitrinite reduction. This property has rarely been investigated and consequently has not been adequately described. Formerly was shown that content of heteroatom, mostly oxygen and sulphure, is a basic indicator of coal quality. Van Krevelen and Shuyer (1957) considerate the values of the atomic ratio O/C as a primary indicator of coal rank. There is no evidence for a straight forward relationship between nitrogen and sulphur content and coal rank. However, it was found that the elemental composition, coking ability, geochemical and thermochemical characteristics of low- and high-sulphur coals of similar rank are different (Jurovsky, 1960; Lifshits, 1954; Murchison and Pearson, 2000; Butuzova et al., 2001; Bechtel et al., 2002). Formation of these coals during early diagenesis (the peat-formation period) proceeded under marine transgressions and regressions involving variations in marine and terrestrial input (Ammosov, 1963). High sulphur content in coals results from the increased availability of sulphate ions in sea water (as opposed to fresh water) coupled with the activity anaerobic bacteria. Typical marine-influenced coals that formed under reduction conditions (RC) are characterized by the extensive primary decomposition of the plant matter as a consequence of high pH values. The great abundance of bacterial biomasses in these conditions is evinced by the high concentration of bacterial biomarker hopanes derived from bacterial membranes. The pH value and the quantity of bacteria are lower in a freshwater swamp than in a salt marsh. Coals that formed under less reductive conditions (LRC) are distinguished by a lower content of general and pyrite sulphur and hydrogen compared to RC of any rank. Their volatile yields are lower than would be expected from their degree of coalification (Taylor et al., 1998). Variations of the sulphur content in coal seams are determined by the paleogeographical conditions during ancient peat accumulation and are independent of the rank (Stach et al., 1975).

The sulphur content in the organic mass of coals (OMC) is one of the most important indicator of its quality, because sulfur compounds exert a favorable influence upon the processes of thermal processing, which causes technological and ecological problems (poisoning of catalizator, corrosion of the equipment, environment pollution, etc.).

Sulfur content in coal attracts the attention of the researchers because of many reasons:

1. *Sulfur accumulation in coals is one of the structural elements of the geological history of the coal layer, which is connected with the formation of coals of different genetic types by reductivity (GTR). Its concentration in coal depends upon geochemistry and geomorphology of the landscape. However, many of the fundamental questions on biochemistry of sulfur remain unclear.*
2. *In the structure of the organic mass of coals (OMC) sulphur containing components, as well as oxygen containing groups, represent reaction-ability centres, where transformations directed at thermal and chemical influence mainly take place. These transformations serve the base for practically all solid fuels processes treatment. However, because of the difficulties of the direct quantitative definition of all the variety of sulfur containing compounds in coals, these processes are studied insufficiently.*
3. *High content of sulphur limits the usage of coals in energy production, coking and other technological processes.*
4. *Mine layers with sulphur content from 3.0 to 4.5 % are characterised by high self-ignition ability. The average quantity of self-ignition cases is nearly 20 times higher for sulfur coals.*

Also a very important aspect is that indexes of coal genetic type by reductivity do not affect the International Coal Classification.

Thus, study of structures of coals with different GTR, the general rules of their transformations under the influence of different technological and chemical factors, the influence of sulfur containing groups upon the character of structural transformations of the organic mass of coal are the actual problems for the modern coal chemistry, geochemistry, and technology of the processing of coals. The aim of the present scientific work is the research into the molecular structure, supermolecular organization of the coals of different genetic type by reductivity.

MATERIALS AND METHODS

Main methods of study of reduced (RC) and low-reduced (LRC) coals and their thermal destruction products include ultimate and proximate analyses, petrographyc analyses, DRIFT-spectroscopy (FT-IR "Bio-Red" FTS-7 spectrometer with a DRIFT technique), X-ray (apparatus "Kristalloflex Siemens" using filtered cuprum radiation), extraction (Dionex ASE 200), gas chromatography-mass spectroscopy (Finnigan MAT GCQ), differential thermal analyses (Paulic-Paulic-Erdei Q-1500D), classic Fisher and Sapozhnikov methods. Chemical treatment of coals carried out directly before the thermal destruction by the introduction of 1-% solutions of the radical polymerization initiator (acrylic acid dinitrile $C_8H_{12}N_4$ – AAD) and products of coal-tar distillation (absorber oil).

Investigated coals are petrographically homogeneous, since the content of the vitrinite reaches 80-89 %. Samples of reduced coals (RC) are distinguished by lower value of vitrinite reflectance ($R_{o,r}$), higher content of inertinite and lithotype with finely crystalline pyrite.

Proximate and ultimate analyses showed distinction in the structure of the coals of different genetic type: samples of reduced coals (RC) are distinguished from low-reduced coals corresponding to the same degree of coalification by higher H/C ratio and yields of volatile matter and by higher S_o^d, S_p^d and total sulphur contents. Organic sulphur S^d_o for studied coals is the main form of sulphur (Turchanina et al., 2005).

RESULT AND DISCUSSION

Earlier we have showed that one of the most important indexes of genetic type by reductivity of Donetsk basin coals is the

content of organic sulphure or atomic S^{daf}_o/C^{daf} ratio as an atomic O^{daf}/C^{daf} ratio is important indexes of rank level of coals.

On the base of reference and experimental information was obtained from the correlation connect between the content of organic sulphure S^{daf}_o and volatile matter of yield V^{daf} for low-rank coals with correlation coefficient r=0.95. Its size grows to 0.98 at more precise of rank level (Butuzova et al., 2005).

Infrared spectroscopy with DRIFT techniques were applied to the semi-quantitative evaluation of the origin of structural peculiarities in coals of different genetic types (Butuzova et al., 2005). The LRC and RC spectra contain a set of absorption bands due to the following functional groups: H-bonded hydroxyl (≈3300 cm^{-1}); aliphatic CH_3, CH_2 and CH group (2970, 2920, 1440, 1380 cm^{-1}); C_{ar}-H bonds (≈3050 cm^{-1} and 900-700 cm^{-1}); aromatic C=C bonds (1600 cm^{-1}); carbonyl functional group (1725, 1700, 1650 cm^{-1}), including quinines (1653-1663 cm^{-1}); -C-O- groups (≈1280 cm^{-1}). The band at 1100 cm^{-1} is assigned to -S-groups because it correlated with the elemental composition of coals. Figure 1 compared the relative intensities (areas) of the absorption bands of individual components. As can be seen from the figure, the RC samples are distinguished by their greater proportion of -S- ($S_{1100-1000}$), -O- (ether groups, 1280 sm^{-1}), and C_{ar}-H ($S_{900-700}$) bonds.

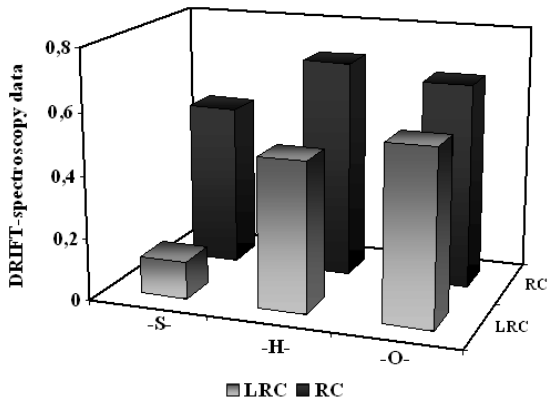

Figure 1. The sulphur- (-S-), hydrogen- (-H-), and oxygen-containing (-O-) group in the structure LRC and RC coals

The change of relative intensity of these bands (Figure 1) successfully correlates with ultimate analyses as well as in semi-coking (Table 1, Turchanina et al., 2005), namely:

1) relative intensity of -S- band is 4 times higher for RC coals and for their thermal destruction products in comparison with LRC;

2) -S-bridges and C_{ar}-H group (Figure 1) have an important role in the structure of the reduced coals, which corresponds to their coking ability and formation of the fritted semi-coking (Table 1). This could be due to high rates of aromatization and lasing processes.

3) the RC contains a greater proportion of -S- and -O- bonds, which facilitate their destruction. These bonds also promote reactions with high values of effective activation energy, and encourage the removal of active functional sulphur- and oxygen-content and aliphatic groups. Several periods of consumption and accumulation of bridge bonds differing in thermal stability are observed during heating (Butuzova and Krzton, 2003). They act as cross-bonding agents that prevent the tight arrangement of structural units and provide microporosity, compactness, and microstructure in semi-cokes and cokes.

The gas chromatography-mass spectrometry (GC-MS) analysis of the aliphatic and aromatic fractions revealed a marked quantitative difference in compounds extracted from the LRC and RC coals (Table 2). Particularly pronounced differences are in content of the sulphur-bearing compounds. The RC coals indeed possess considerably higher absolute concentrations of dibenzothiophene (17.9-20.3 μg/g C^{daf}) as compared with the LRC coals (6.8-9.1 μg/g C^{daf}). Also the overall content of aromatic hydrocarbons is nearly twofold higher in the RC, which is in accord with their good coking properties, even for lower rank coals. Lower values of pristane/phytane ratio for respective RC counterparts can be explained by their formation under more reductive

conditions during early diagenesis. The following correlations were determined (Butuzova et al., 2005):

1) *between the yield of extractable (soluble) organic matter (SOM) and atomic H^{daf}/C^{daf} ratio;*
2) *between atomic $S_o{}^{daf}/C^{daf}$ ratio versus content of hopanes;*
3) *between atomic $S_o{}^{daf}/C^{daf}$ ratio versus content of steranes/hopanes ratio;*
4) *the $\delta^{13}C$ values of the total organic carbon of the coals;*
5) *content dibenzothiophene and the dibenzothiophene/phenanthrene ratio.*

Table 1. The characteristic initial coals and semi-coke, wt. %

№	Coal, semi-coke	Type	A^d	V^{daf}	S^d_t	C^{daf}	H^{daf}	Characteristic by semi-coke
1	coal semi-coke	***LRC***	2.42 3.40	35.6 13.8	2.17 1.40	79.30 87.81	4.94 3.61	powder-like
2	coal semi-coke	***LRC***	1.60 2.86	37.3 13.0	1.05 1.03	78.40 88.83	4.95 3.19	powder-like
3	coal semi-coke	***LRC***	5.30 13.4	37.2 18.9	1.04 1.00	79.30 85.01	5.07 3.18	powder-like
1'	coal semi-coke	***RC***	9.95 12.6	41.8 12.9	2.87 2.40	77.90 86.78	5.30 3.67	fritted
2'	coal semi-coke	***RC***	4.64 7.30	46.2 12.6	5.85 2.90	76.10 85.28	5.43 3.36	fritted
3'	coal semi-coke	***RC***	8.60 9.10	43.0 15.0	5.60 1.40	76.10 87.71	5.22 3.21	fritted

Table 2. The results of the extraction for coals of different genetic types by reductivity

№	Type	C^{daf}, wt. %	Yield of soluble organic matter (CH_2Cl_2), mg/g C^{daf}	Relative content asphaltens, %	Relative content aromatic hydrocarbons, %	Relative content aliphatic hydrocarbons, %	(N+S+O), %
1	***LRC***	76,70	10,80	59	15	5	21
2	***LRC***	76,30	10,54	53	17	4	26
1'	***RC***	71,90	13,54	36	30	5	30
2'	***RC***	69,00	15,77	37	25	6	31

The elevated microbial activity was associated with sulphate reduction and hence leading to the positive correlation between atomic $S_o{}^{daf}/C^{daf}$ ratio and hopanes concentration. The higher concentration of steranes relative to hopanes is a characteristic feature of marine influence. Therefore, the higher steranes/hopanes ratio found for the RC indicates the increased abundance of marine photosynthetic organisms relative to aerobic bacteria and is interpreted to reflect enhanced inflow of seawater.

X-Ray characteristics have shown that supermolecular organization of reduced coals and low-reduced coals are different by heights of "crystallite" (L_c), the lattices extent (L_a), degree of order (h/l) and proportion of "crystalline" phase and amorphous phases (I_{cr}), (Table 3). For RC the parameters L_c and I_{cr} are higher and parameters L_a and h/l are lower in comparison with LRC, i.e. their structures

have a higher ability of deformation and lower degree of order.

Table 3. X-Ray result for initial coals and semi-coke.

№	2. Type	Chemical treatment	T, ^{0}C	L_c	L_a	L_a/L_c	d_{002}	h/l	I_{cr}
1	***LRC***	-	20	1.27	1.54	1.05	0.356	1.42	0.79
		-	520	1.45	2.03	1.40	0.356	2.32	1.59
		AAD	520	1.70	2.37	1.39	0.356	2.83	1.48
		oil	520	1.63	2.58	1.58	0.356	2.44	1.13
2	***LRC***	-	20	1.16	1.99	1.72	0.356	1.46	0.82
		-	520	1.57	2.50	1.59	0.356	3.46	1.77
1'	***RC***	-	20	1.31	1.48	1.25	0.356	0.59	0.69
		-	520	1.36	2.65	1.95	0.356	1.43	1.79
		AAD	520	1.36	2.73	2.01	0.356	1.67	1.25
		oil	520	1.57	2.36	1.50	0.356	1.89	1.23
2'	***RC***	-	20	1.20	1.71	1.43	0.356	0.68	0.42
		-	520	1.31	2.92	2.23	0.356	1.97	1.85

During semi-coking processes the indexes h/l increase for low-reduced coals in 1.6-2.4 times and for reduced coals in 2.4-2.9 times. Semi-coking of reduced coals in the presence of AAD results in a 1.8-2.0 fold acceleration of the lattices extent (L_a) and in a 2.3-4.4 fold - the proportion of "crystalline" phase which indicates the network lacing, improvement of the cross-linking processes in the coal carbonization products and desulphurization effect. X-Ray characteristics have shown that under the action of additives the stack sizes and degree of order (h/1) increases: for low-reduced coals in 1.6 – 2.4 times, and for reduced coals in 2.4 – 2.9 times (Table 3). Chemical pretreatment has a considerable influence on the coal reactivity, yield and composition of semi-coking products. It results in changing of the sulphur distribution and structural parameters of solid products. After the chemical pretreatment of the coals changes in supermolecular organization parameters are observed for the semi-coke. As a consequence we observe an increase of heights of "crystallite" (L_c) and of parameter h/l in 3.2 times for reduced coals and in 1.7 times for low-reduced coals. This confirms the influence of chemical reagents on the sewing process in the solid products and the formation of strong fritted semi-cokes from high-sulphur coals (RC).

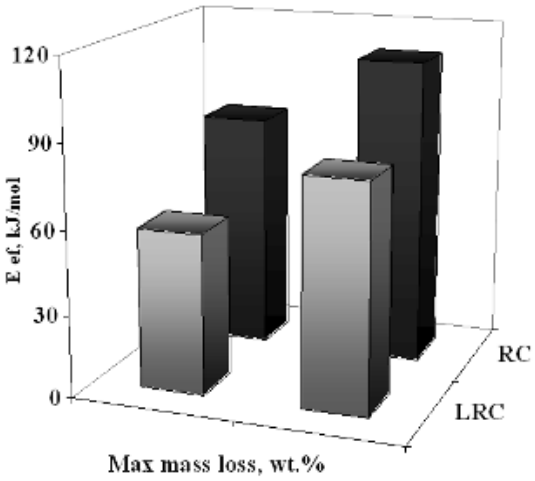

Figure 2. Dependence of mass loss variations on the effective energy of activation of the thermodestruction process of coals

As is seen in Figure 2, the effectively energy of activation (E) value changes considerably with the change of coal genetic type. The maximal E values are observed for reduced coals, which agree with the higher value of mass loss at 850ºC. Decreasing the thermodestruction process E for LRC results in the stepwise decrease of the mass loss value. An inversely proportional linear relation

between the parameters E and the mass loss at 850ºC has been observed. Figure 3 presents comparative data on the composition of gaseous products (for example, H_2S, H_2, CH_4) obtained from the semi-coking of coals of various genetic types by reductivity. The main component of the semi-coking gas is methane (CH_4), the content of which reaches 56% for low-reduced coals and 38% for reduced coals. The gas from reduced coals differs from that of low-reduced coals by having higher contents of hydrogen (H_2), hydrogen sulphide (H_2S), and carbon dioxide (CO_2) (Turchanina et al., 2005). The heat of combustion of the semi-coking gas is higher for low-reduced coals. This is connected to the large methane content. All research on the low-reduced and reduced coals permit to suggest the new indexes for determination of different genetic types by reductivity.

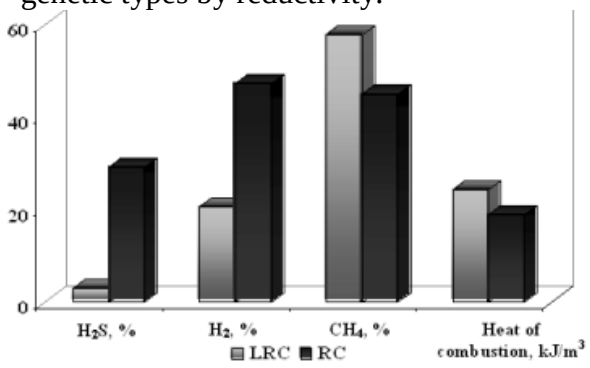

Figure 3. Composition and heat of combustion of the semi-coking gas

CONCLUSIONS

In the present work new structural indexes were discovered for the first time, which characterize the genetic type by reductivity of coal and are correlated with the content of organic sulphure S^{daf}:

1) *A relative content of aromatic hydrogen carbons and oxygen-content group (by data of DRIFT-spectroscopy).*
2) *Content of dibenzothiophene, hopanes, steranes, the $\delta^{13}C$ values of the total organic carbon of the coals, and dibenzothiophene/phenanthrene ratio (by data of GC-MS).*
3) *The yield of extractable (soluble) organic matter (SOM) (by data of extraction).*
4) *The proportion of "crystalline" phase and amorphous phases (by data of X-ray).*
5) *Content of H_2, H_2S, CH_4 in semi-coking gas.*
6) *Maximum of mass loss during pyrolysis (by data of DTA).*

REFERENCES

Ammosov I. I. 1963: Geology of coal and oil deposits in the USSR. Gos. *NTI literatury po geologii I okhrane nedr*, Moskow.

Bechtel A., Butuzova L., Turchanina O. 2002: Thermochemical and geochemical characteristics of sulphur coals. *Fuel Proces. Technol.* 77-78, 45-52.

Butuzova L, Krzston A. 2003: About the mechanism of soft coal pyrolisys. *Acta Univ. Carol. – Geol.* 45, 2 – 4, 23 – 26.

Butuzova L., Bechtel A., Turchanina O., Safin V., Butuzov G., Isajeva L. 2005: Organic sulphur as a main indexes for determining the genetic type of low-rank coals. *Bulletin of Geosciences.* Volume 80, №1, 3-8.

Butuzova L., Bechtel A., Turchanina O., Isajeva L., Matsenko G. 2001: Effect of the coal genetic type on the pyrolysis products composition and structure. *Acta Univ. Carol., Geol.* 45, 17-22.

Jurovskij A. Z. 1960: Sulphur of black coals. Academy of Science of USSR, Moscow.

Lifshits M.M. 1954: Genetic classification of coals / Geological – geochemical map of the Donetsk Basin. *Ugletekhizdat*, Moskow.

Murchison D., Pearson J. 2000: The anomalous behavior of properties of seams at the Plessey (M) horizon of the Northumberland and Durham coalfields. *Fuel*, 79, 865-871.

Stach E., Mackowsky M., Teichmuller M., Taylor G. H., Chandra D., Teichmuller R. 1975: Coal Petrology. Gebrueder Borntraeger, Berlin.

Taylor G. H., Teichmuller M., Davis A., Diessel C. F. K., Littke R., Robert P. 1998: Organic petrology. *Gebrueder Borntraeger,* Berlin.

Turchanina O., Butuzova L., Safin V., Isajeva L. 2005: The possibility of sulphur redistribution in the semi-coking products of low-reduced and reduced coals. *Bulletin of Geosciences.* Volume 80, №1, 99-103.

Van Krevelen D. W. and Schuyer J. 1957: Coal Science. Elsevier, Amsterdam.

(This page is left blank intentionally.)

SOME CEMENT BASED GROUT MIX APPLICATIONS IN TERRACE UNITS PLACED THROUGH DALAMAN RIVER

Üşenmez K.[1], Kıncal C.[2] and Koca M.Y.[2]

[1]Spektra Jeotek AS, Kumkapı sokak no. 20/2, Cankaya, Ankara
[2]Dokuz Eylül University, Department of Geological Engineering, Bornova, Izmir

Abstract: Dalaman – Akköprü is a clay core – rock fill dam and is under construction for irrigation, flood control and electrical power. The seepage in base rock is controlled by grout curtain applications in dam constructions. Different ratios of mixes should be used for different rock types. To minimize the seepage, grouting should be done under suitable mixes with suitable timing. In this work, four different types of cement mixes are compared for the Terrace unit. Different grout mix intakes examined with test holes, first time in Terrace unit, will offer a solution for further work.

Key words: Grout, ratio of mixture, fill, Lugeon.

1. INTRODUCTION

Dalaman - Akkopru Dam is located on the Dalaman River, 24km east of Koycegiz, Mugla, (Figure 1). The dam is being built for irrigation, flood control and electrical power. Its purpose is to protect the Dalaman plain from the damage of flood. Also with the 115MW hydro electrical power plant to be built, the dam will produce 343 GWh of electric power (DSI, 1993). The characteristics of the Dalaman Akkopru Dam are presented in Table 1.

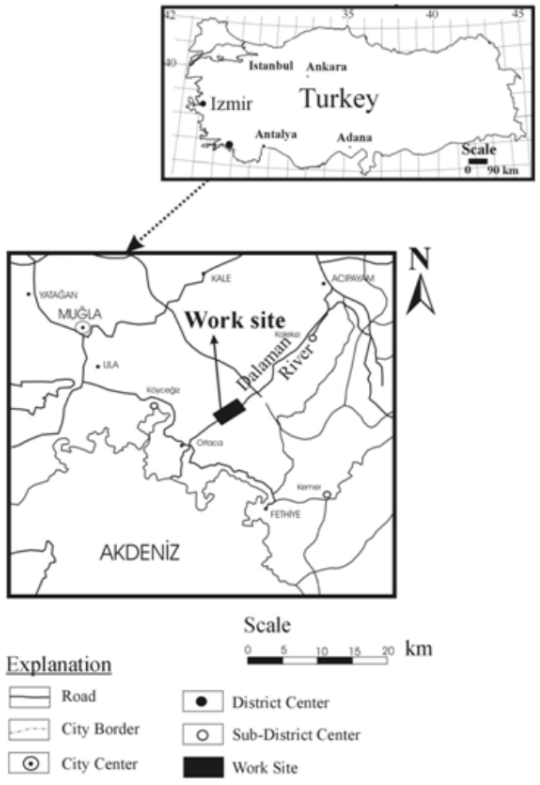

Figure 1. Work site location map

In dam constructions, some measures are taken to stabilize and seal the base rock under the dam body (Pettersson, Moulin, 1999). To determine a need for grouting is a major concern in dam foundation treatment. Grouting the base rock through the dam axis is the most common one among these measures. Grouting is defined as filling the liquid material under pressure into the space between the structure and ground or the fractures in the ground, generally inside from drill holes (Kutzner, 1996). The liquid material pumped into the ground becomes gelly or hard after a period of time. The main goal of grouting is to create a kind of ground or rock mass which is more stable and less permeable (Tosun, 2000). Different types of grout mixes may be needed for less stable and less permeable rock types, different than generally used. Stabilizing these kinds of rock types will be economic where the cost of excavating is very high. Under these conditions, the mix types and ratios will be very important.

Test grouting is applied into the Terrace unit located at the downstream right bank of Dalaman-Akkopru Dam, which is under construction on the Dalaman River. Four different types of grouts are applied for four different rows located at the same area. The grouting is processed under the same conditions with different types of grouts to find the best

type of grout mix with the best ratio among these four.

Table 1. The Characteristics of Dalaman - Akkopru Dam.

Type	: Clay core rockfill
Height from the basement	: 162m
Height from the talweg	: 112m
Total volume of the embankment	: 12hm^3
Crest length	: 689m
Crest width	: 12m
Crest elevation	: 207m
Minimum water elevation	: 173m
Maximum water elevation	: 204m
Dead storage capacity	: 196hm^3
Maximum capacity	: 419hm^3

Inclined check holes are drilled with applying Water Pressure Tests (WPT) through the echelons which have the higher values of grout intakes. The check holes were drilled after a period of time after the grouting finished in the row. During drilling the check holes, water pressure tests were applied. The grouting was made after the last WPT, from bottom to the collar, as the procedure of grout holes. In the meantime, the permeability of the test row is evaluated by the Lugeon values.

This work is aimed to check the success of grouting application with classical grout mixes and pressures in Terrace units located throughout the Dalaman River. Under the conditions of high costs of excavation like in dam constructions, to stabilize and seal the Terrace unit by grouting can be planned. In some projects, significant structures like the dam body or power plant can be designed over the Terrace unit. However, it will be important to choose the technique of grouting with the correct ratios and pressures. The Terrace unit is made of flow materials of the rivers. The cement is generally silt, sand, clay or even carbonate. This affects the permeability of the unit. On the other hand, Terrace unit never shows a homogenic structure because of irregular flow conditions. It's also easy for talweg to be affected by tectonics and to create secondary porosity.

The performances of four different types of cement mixes for the Terrace unit are examined in this work. An attempt has been made to choose the best one as regards permeability.

2. GEOLOGY

The base rock at the Dalaman–Akkopru Dam site and reservoir area is autochthon which is comprised mainly of Aktas Limestone (Paleocene) and Gokseki Formation. Allochton Paleozoic–Mesosoic group is composed of Cehennem Limestone, and Demirli Melange and the Peridotite–Serpantine unit overlay autochthon units with a tectonic contact. All these units are overlain by young sedimentary units.

All Paleozoic and Mesosoic series which are represented by highlands have been thrusted over the autochthon units which are represented by limestone and flysch series. According to Graciansky (1972), this thrust zone is very interesting as three different structural groups overlay each other with unconformity. The successions of these groups are as follows: At the base autochthon limestone series of Senomanian age and marly and sandy units of Burdigalien age can be observed. Interim series represented by allochton complex and peridotite – serpantine nappe overlay these all.

2.1. Allochton Sedimentary Units

Cehennem Limestone: This unit represents the oldest one in the study area. The outcrops of this unit can be observed along the right abutment of Dalaman River and eastern part of left abutment. It has a massive structure and the bottom parts are white although some grey outcrops can be observed. This unit has a heavily jointed structure and some parts have karstification.

2.2. Autochton Sedimentary Units

Aktas Limestone: The outcrops are observed at upstream of the dam site. It has massive appearance and looks crystalline in texture. It also has a rough structure. In some parts platy limestone

levels are observed. Although it is generally white, some dark colored bituminious intercalations are also distinguished. The total thickness is around 400 meters (Sekercioglu, 1999). It has a jointed and karstic structure.

Gokseki Formation: The outcrops are observed at the left abutment. The thickness is around 300 meters. Claystone, marl, sandstone and limestone intercalations are dominant.

2.3. Quaternary Units

Terrace: The outcrops are observed along the Dalaman River. It is tightly cemented by carbonate. The gravels from the units of upstream form the unit Terrace components. Components are gathered from peridotite, serpantine, limestone and chert gravels. The gravels are well rounded. Because of carbonate cement, karstification effect can be distinguished in some parts. Vertical thickness is about 40 meters (Figure 5). This work has been applied to the Terrace unit placed at the right abutment of Dalaman River, downstream of Dalaman – Akkopru Dam (Figure 2).

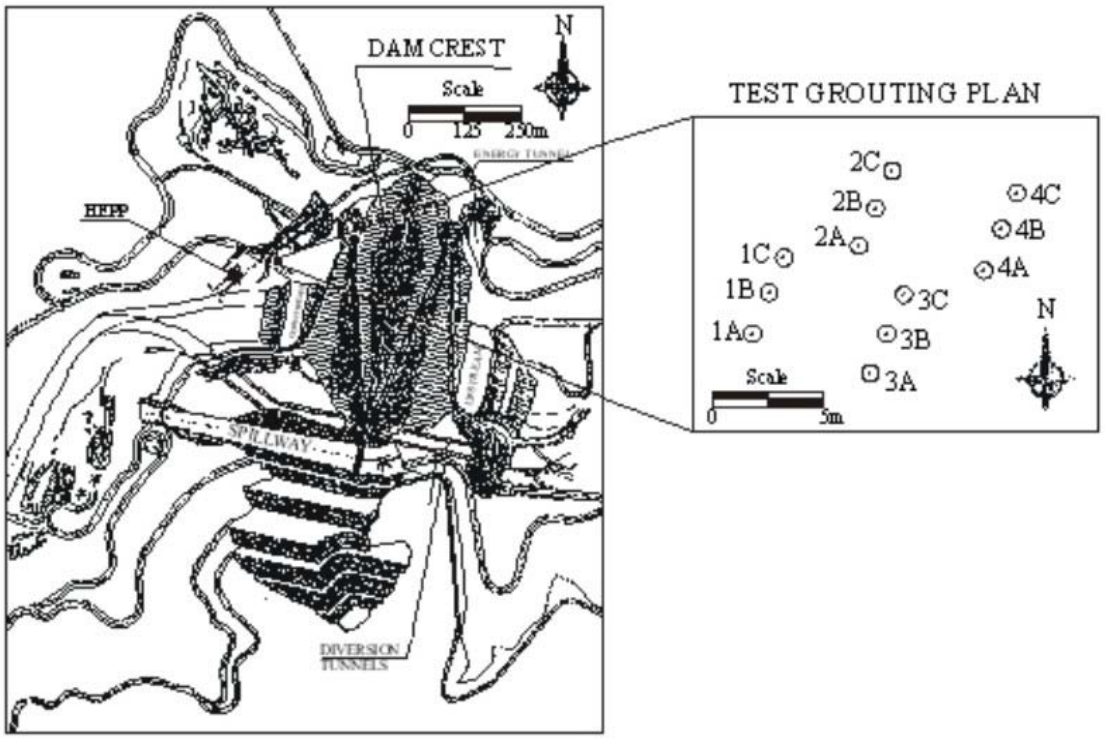

Figure 2. Test grouting plan

According to Sekercioglu (1999), the permeability coefficient of this terrace unit is generally $K=10^{-4}$-10^{-5} cm/sec. and is classified as 'moderately permeable rock' according to the classification of permeability grades of rocks suggested by IAEG (Anon. 1979a).

Alluvium: The thickness at the dam site is maximum 38 meters. Generally it has coarse, tabular, rounded limestone and ultrabasic gravels. Coarse material has no sorting but sorting for fine material is good

2.4. Magmatic Units

Peridotite – Serpantine: This unit has wide outcrops around the study area. The thickness is around 700 meters (Sekercioglu, 1999) and the contacts with adjacent units are faulted but at these contact zones, metamorphism cannot be observed. Ultrabasic unit is generally made of peridotite and harzburjite. The harzburjites and dunites are mostly serpantinized (Figure 3).

Demirli Melange: The outcrops are observed along both abutments of the Dalaman River. It is constituted by a

complex of serpantine, radiolarite, diabase and limestone. It is observed between the allochton peridotite – serpantine unit and the allochton Cehennem limestone unit as an intercalation. The evidence of this unit along the thrust zones proved that this unit has occurred as a result of tectonics (Sekercioglu, 1999).

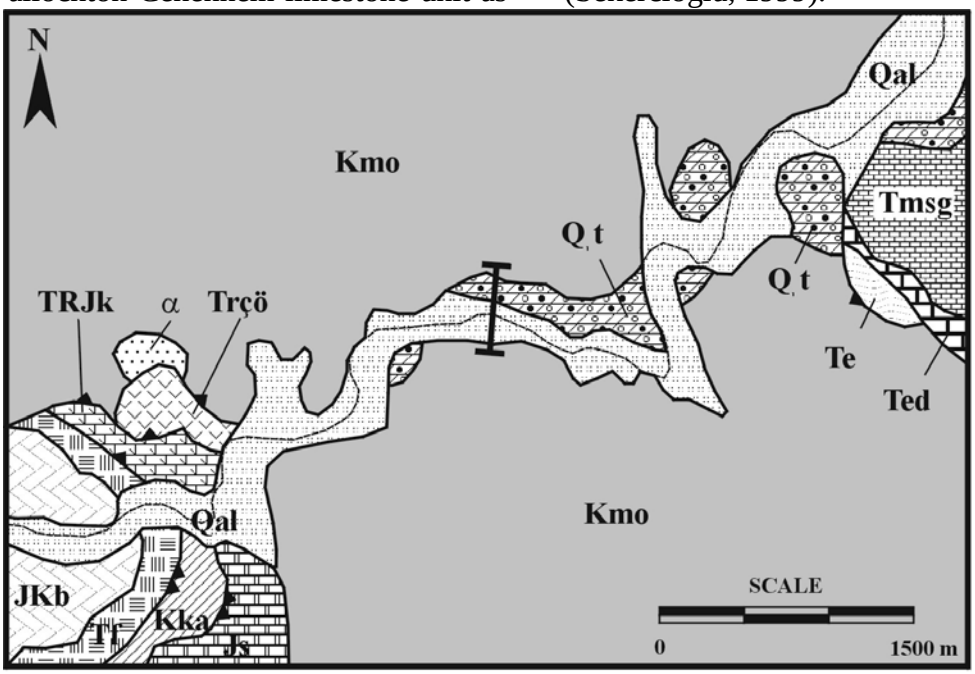

Explanation

- Qal — Alluvium
- Q t — Fluvial (old) Terrace Fills
- Kmo — Marmaris Peridotite (Harzburgite, dunite, serpantinite, serpentinized harzburgite, etc.)
- Trçö — Covenliyayla Volcanite (Basalt, spilitic basalt, chert, shale and cherty limestone)
- Kka — Karabogurtlen Formation (Sandstone, claystone, cherty limestone, conglomerate)
- Js — Sandak Formation (Limestone, dolomite, dolomitic limestone, cherty micrite)
- CONTACT
- CREST
- TALWEG
- Tf — Faralya Formation (Red micrite, breccia, spilite, basalt, sandstone, claystone)
- TRJk — Karakoy Dolomite (dolomite, dolomitic limestone)
- Jkb — Babadag Formation (Micrite, cherty micrite, calciturbidite)
- Te — Elmali Formation (Sandstone, claystone, siltstone)
- Tmsg — Gomuce Member (Algal limestone)
- Ted — Disitastepe Formation (Micrite, cherty micrite)
- OVERTHRUST EARLY LANGHIAN AGE
- OVERTHRUST LATE EOCENE AGE

Figure 3. Geological Map of the Study Area and its vicinity (modified from Sekercioğlu and Ozguler, 1999)

3. METHOD

At the right bank of the Dalaman River, downstream of Akköprü Dam, on the slope path located at the elevation of 122m, grouting is applied to four rows with three holes each (Figure 2). The holes are drilled in 20 meters deep, as deep as the average depth of the terrace unit for this area. Grouting was applied from the bottom to the collar of the holes. Prior to grouting, the holes were cleaned with clean water after the drilling process. The holes at the two ends of each test row were drilled and grouted firstly, then the middle holes were drilled after the grouting of the tip holes were completed. In every echelon, water pressure tests have been done to determine the water loss elevations. The inclined holes were drilled to check which parts have most intake values for each test row. Check holes were drilled as WPT's. Grouting followed WPT's as the procedure of test holes, from the bottom to the collar. These data also check the success of the test grouting like WPT's. All the check holes and the first hole (1A) of the first test row were drilled coring.

Four different types of mixes were tested to find an appropriate mix to use for making an impermeable curtain in the terrace unit. Those mixes were composed as below:

MIX – I: Cement+Water+Bentonite

MIX – II: Cement+Water +Bentonite+Additive

MIX – III: Cement+Water + Additive

MIX – IV: Cement+Water

Generally, the need of grouting is determined by the results of WPT's. Houlsby (1985) expresses the Lugeon criteria according to cement grouting as shown in Table 2.

Table 2: The relation between grouting necessity and Lugeon values.

Type of the structure	Lugeon values 1 $min^{-1}.m^{-1}$ (at 1 MPa)
Concrete dam – one row curtain	3 – 5
Clay core earth-fill dam – More than one row curtain	7 – 15
Erosable material at the base	3 – 4
When water leakage is dangerous	1 – 3

There are some doubts as to whether the results of water pressure tests are sufficient to evaluate the need for grouting. Such doubts are supported by the facts that up to now there has been no clear relationship between water and grout absorption, and that the differences of this relationship are related to the rock anisotropy. For instance Lombardi (1985) concludes that there's no relationship because of the different rheological properties of water and grout. If no continuous joint system is found in the rock, the amount of water which is pumped by water pressure tests prior to grouting might be captured. This stable water would affect grouting negatively. The pumped water could not get out of the hole and the ground. The location where it is captured is usually unknown. The pressure applied during water pressure tests could create new cracks, also. Kutzner (1996), as opposed to Lombardi (1985), says that a relationship is expected to exist and to be found since the water pressure test is still the main tool for the design of grouting work.

The connection between permeability and grout consumption is expected, but the form and the strength of this relationship is still debated (Nonveiller, 1989). Lombardi (1985) denies such a possibility by pointing out the different flow characteristics of water and injected cement. By classifying the water loss and grout consumption into low and high categories, Heitfeld (1965) showed that all possible combinations of water loss and grout consumption were found in the applications. Similar results were obtained

by Ewert (1992), Karagüzel (1989) and Karagüzel & Kılıç (2000).

Table 3 shows the revised grouting criteria after some experiments. In contrast to other criteria, the requirement of cement based grouting is shown to depend on the type of structure, on the type of rock in terms of isotropy and anisotropy (Kutzner, 1991). The permissible Lugeon values depend on the isotropy and anisotropy properties of the rock and joint aparture and the rock properties to be base rock, are shown in Table 3.

Table 3. Permissible values of water absorption in the rock foundations of dams ($1\ min^{-1}.m^{-1}$ at 1 MPa)

Permeability Conditions of Rock	Quasi – Isotropic Rock		Extremely Anisotropic Rock			
Flow of seepage	Free[1]		Free[1]		Partly blocked[2]	
Absorption Test WPT	Laminar	Turbulent	Laminar	Turbulent	Laminar	Turbulent
Seepage Investigation	-	-	-	-	Not Made	Favorable
	Narrow aparture	Open joint	Narrow aparture	Open joint		
Homogeneous embankment (long seepage path)	10 to15	8 to12	10 to15	8 to12	<20	<40
Rockfill dam/Earth core (medium seepage path)	8 to12	5 to 8	8 to12	5 to 8	<15	<30
Rockfill dam/membrane sealing (short seepage path)	5 to 8	3 to 5	5 to 8	3 to 5	<12	<20
Concrete dam (uplift reduction by drainage)	5 to 8	3 to 5	5 to 8	3 to 5	<12	<20
Special cases: Risk of erosion Risk of solution Risk of environmental defects Risk of unacceptable loss of water	3 to 5	1 to 3	3 to 5	1 to 3	<5	<10
Lower limit of groutability by use of cement /kg/m)	30	30	30	30	30	30

[1]Free: Strike of permeable layers is parallel to valley

[2]Partly blocked: Strike of layers of low permeability is accross the valley

Laminar flow conditions with the absorption test allow for slightly higher permissible values than turbulent flow (Table 3). This is because turbulent flow conditions reflect open joints which again reflect increased permeability and groutability. As indicated in Table 3, the lowest permissible values apply to projects of special risks.

Low (H<10m) and high (H>15m) dams and the indicated Lugeon values are applied for different types of dams and upper and bottom parts of the grout curtain as indicated (Table 3). The bottom line of the Table 3 gives a lower limit of rock groutability by cement. A take of 30 kg/m corresponds to about 5 – 10 times the borehole filling.

Grouting is applied under greater pressures than the pressures applied during water pressure tests. Higher pressures can create new cracks and may result in more grout intake values. This indicates that fractures have been opened up due to excess pressure. Graphed WPT results can say much about rock grout intake character.

Under laminer flow conditions, water loss during WPT increases while the pressure increases. When the pressure decreases the water loss value gets back to the first value. The grout intake values in these kinds of grounds are very low (Figure 4a) (Çatal, 1993). If the water loss value increases suddenly while the pressure is increasing, and gets back after pressure decreases, it is called 'Turbulent Flow'. Under these conditions, the grout intakes are quite higher (Figure 4b, where 'P' represents pressure and 'Q' represents water loss values).

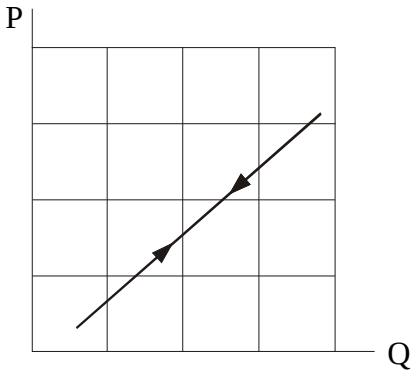

Figure 4a. Laminar flow

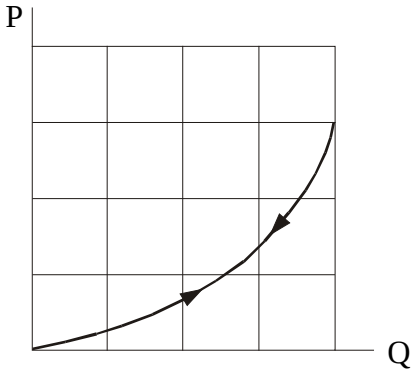

Figure 4b. Turbulent flow

If increase in pressure results with low increasing values in water and can't get to the first value when the pressure decreases, there's 'Plugging' (Figure 4c). A sudden increase in water loss with pressure together with a failure to return to the first value with the decreasing of the pressure show washing out of the gouge material from the fractures (Figure 4d). Normal increasing values occur with the increase in pressure.

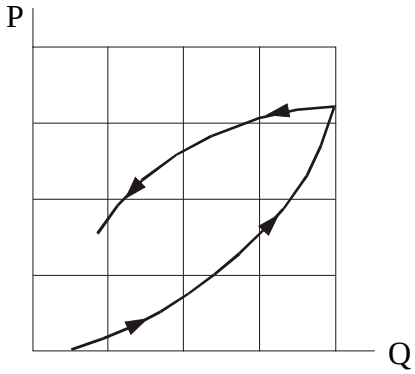

Figure 4c. Plugging of fissures

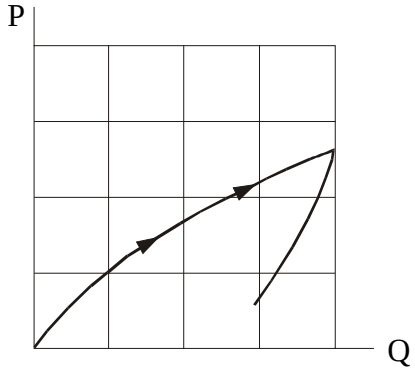

Figure 4d. Erosion of fracture fill

According to the intakes of formations, grout changed from thin to thicker mix in density during injecting. First of all, grouting started with injecting ratio of 1/3 cement to water in weight, and continued in order with the cement to water ratios of 2/3, 1/1 and 7/5. After intake of 500 liters, the next mix is used. Grouting started with 1/3 ratio in the application of classical cement–bentonite-water mix (Mix – I), for the other mixes grouting started with 2/3 ratio. Because of being unstable and easily settling, 1/6 ratio has never been used. Viscosity, stability and density values were designated frequently. Settling values and other characteristics were indicated. Bentonite had always been hydrated as 1/10 ratio of bentonite to

clean water in weight, minimum 24 hours before being used to increase the stability (TS 977, 1971). Portland cement with specific surface more than 4000cm^2/gr is used in all grouting applications (TSE 19, 1985). The most important property for the selection of the cement is its fineness, which should be as high as possible when granular soil or fissured rock with narrow fissures is to be grouted (Nonveiller, 1989).

The fineness of cement is controlled by Blaine Value. Portland cement is mostly fine grained and it can be used for grouting without any restriction. In cement grouting, cement with high Blaine Value (>3500 cm^2/gr) is significant to grout fine fissured rock. Hydratation will be faster when fine cement is used, also the time of solidification will be shorter.

All the grouting pressures for consolidation holes are calculated from the equation – 1 in Dalaman - Akkopru Dam construction (DSI, 1993, Figure 5).

P_t=0,23H Equation 1

On the other hand, all the curtain grouting pressures are calculated from the equation – 2.

Pt=0,33H Equation 2

Where P_t represents echelon total effective pressure; H, height between the collar and the middle point of echelon in meters. To convert the effective pressure to the pressure seen on the manometer, equation – 3 is used.

Pm=Pt+(W/L)cosα Equation 3

Where 'W' represents grout density, 'L' represents the height between the manometer and the middle point of echelon, and 'α' represents the angle from the vertical. The consolidation grouting pressures are used in this work. The pressures converted to be seen in manometer for each echelon are shown in Table 4.

Table 4. Grouting pressures in manometer used in Dalaman - Akköprü Dam.

Echelon (m) (From the collar to bottom)	Pressure (kgf / cm²) Consolidation Grouing
0 – 2.5	0.5
2.5 – 5	1
5 – 10	2
10 – 15	3
15 – 20	4

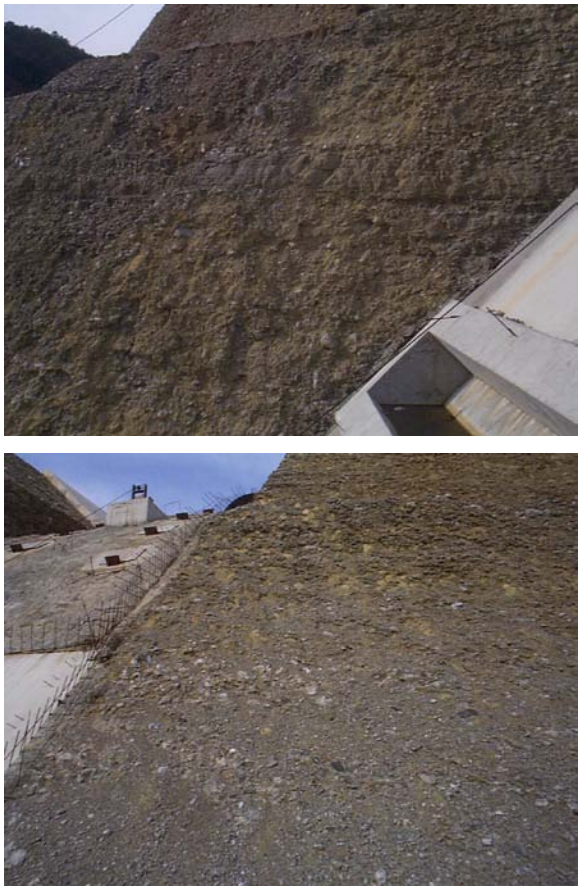

Figure 5: View from the work area slope, Terrace Unit, right bank of Dalaman – Akkopru Dam downstream.

After getting up to the required pressure value during injecting, when there was no intake, 1/3 ratio mix was pumped for twenty minutes. During this period, the intake of 0,6L/m/min or less was considered an acceptable value.

4. MATERIALS USED IN MIXES

Materials combined in grout mixes are cement, water, bentonite and sodium phosphate as an additive.

Cement: Normal Portland Cement was used because there was no risk of sulphate in the water. In case of 600mg/L or more SO_4 ions found in water, cement enduring sulphate should have been used. Cement with a specific surface more than 4000cm^2/gr is used to grout fine fissures and pores easily. The characteristics of cement are shown in Table 5.

Table 5. Characteristics of cement used (Batı Söke, 2002).

Properties	Unit	Laboratory Results	Required Values	
			Minimum	Maximum
Chemical Properties				
Sulfur Trioxide (SO_3)	%	2.44	-	3.50
Chlorine (Cl)	%	0.0084	-	0.1000
Total Additives	%	16.96	6.00	20.00
Physical Properties				
7 days compressive strength	MPa	31.50	16.00	-
28 days compressive strength	MPa	40.30	32.50	-
Initial setting time	Min	175	60	-
Soundness (Le Chatelier)	Mm	2.00	-	10.00
Specific surface	cm^2/g	4453	2800	-

Table 6 Characteristics of bentonite used (Karakaya Bentonite, 2002).

Properties	Unit	Laboratory Results	Required Values	
			Minimum	Maximum
Physical Properties				
Value over the no. 200 sieve (Wet sieve analyze)	%	1.32	-	2.00
Value under no. 100 sieve (Dry sieve analyze)	%	99.50	98.00	-
Liquid limit (W_L%)	%	412.00	400.00	-
Humidity Ratio	%	9.25	-	10.00
Viscosity	sec	33	32	45

Bentonite: Unadulterated bentonite with liquid limit value more than 400% is used. The characteristics of bentonite are shown in Table 6.

Water: Free of chemicals such as oil and acid, clean ground water is used for preparing the grout mixes.

Additive: Sodium phosphate is used as thinner in the mixes.

5. APPLICATION

In this research, the sedimentation times of the mixes were determined by testing the viscosity, stability and density of each grout mix. The ratios of the mixes used and the volumes of these mixes are shown in detail in Table 7.

Table 7. Grout mix ratios used in Dalaman - Akkopru Dam.

MIX – 1

Type (c/w)	Cement (kg)	Water (lt)	Bentonite (kg)	Volume (lt)	Bentonite %	Density (gr/cm^3)	Viscosity (sec)
1/3	50	150	2,5	167	5		
2/3	100	150	3	184	3	1,268	56
1/1	150	150	3	200	2	1,432	68
7/5	200	142	2	208	1	1,510	98

MIX - 2

Type (c/w)	Cement (kg)	Water (lt)	Bentonite (kg)	Additive (kg)	Volume (lt)	Additive %	Bentonite %	Density (gr/cm^3)	Viscosity (sec)
2/3	100	150	2	1	184	1	2	1,238	38
1/1	150	150	1,5	1,5	201	1	1	1,384	50
7/5	200	142	0,5	2	210	1	0,5	1,480	58

MIX - 3

Type (c/w)	Cement (kg)	Water (lt)	Additive (kg)	Volume (lt)	Additive %	Density (gr/cm^3)	Viscosity (sec)
2/3	100	150	1	183	1	1,305	32
1/1	150	150	1,5	200	1	1,408	36
7/5	200	142	2	210	1	1,545	40

MIX - 4

Type (c/w)	Cement (kg)	Water (lt)	Volume (lt)	Density (gr/cm^3)	Viscosity (sec)
2/3	100	150	183	1,326	33
1/1	150	150	199	1,470	35
7/5	200	142	208	1,542	42

Explanation: c: cement, w: water, Additive %: sodium phosphate % of cement weight.

In Figures 6 and 7, density – viscosity and stability test results are shown in order. According to the density – viscosity graph shown in Figure 6, in Mix – I which represents the classical cement based grout mix, sudden increase in viscosity occurs (becoming gel) with the increase in the density. Thus, both local clog occurs and pumping gets harder.

In Figure 6, Mix - 3 and Mix – 4 contain small amounts of additives so they show similar characteristics with Mix – 1 in low densities. While Mix - 3 shows laminar increase in viscosity by the

increase in density, Mix - 4 shows a sudden increase. In Mix – 4, cement can't stay in the water for a long time, which causes a heterogeneous liquid structure and obstructs the grout to be injected into the ground. In Mix – 3, viscosity is lower then it is in Mix – 2; which may cause grout to move far and inject into the pores and cracks distant from the hole. According to Figure 6, settling properties being dependent on time, Mix – 2 has lower settling values then the others. Although settling for lenthier periods of time makes grout setting last longer, this property is not designative. Mix which sets in for longer time periods can keep its properties and may stay homogeneous while traveling far. These laboratory results show that the best mix among these four is Mix – 2.

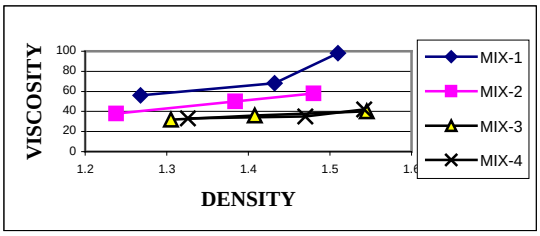

Figure 6. Density - viscosity dispersions of the mixes used.

Control of the application

Inclined check holes were drilled coring to intersect the echelons which have the highest grout intake values. Water pressure tests were applied for every echelon during drilling. Grouting followed drilling after cleaning the hole properly. The Lugeon values (1 Lugeon: water loss occurs in 1m of echelon in 1 minute under 10 bars of pressure), determined the impermeability of related row, and the values were below the limits (DSI, 1993). In Table 8, solid material intake values according to the mixes and grouting holes with check holes are shown.

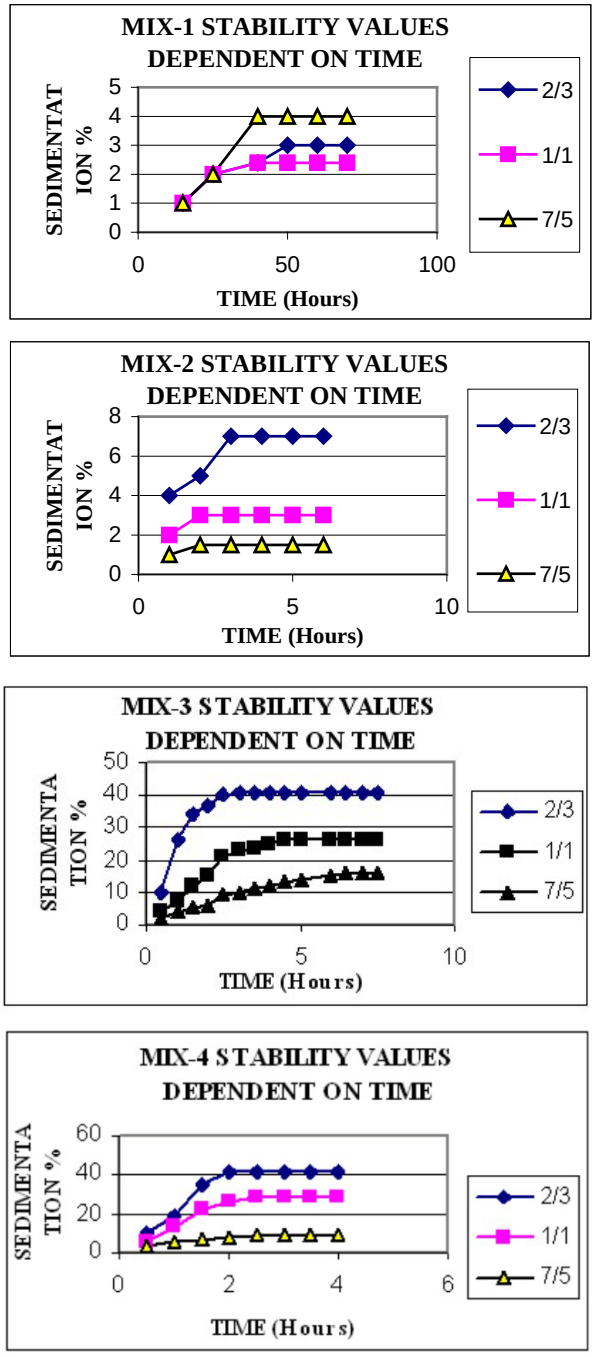

Figure 7. Stability values for the Mix-1, Mix-2, Mix-3 and Mix-4 dependent on time (Explanation: Mix - I, cement-water-bentonite; Mix - 2, cement-water-bentonite-additive; Mix - 3, cement-water- additive; Mix - 4, cement-water)

Table 8. Correlation of the intake values of the grout and solid materials used in grout holes and check holes in rows.

Row of Mix-1

Echelon	Grout Intake (Lt)				Grout Solid Material Intake kg/m			
	A	B	C	**Check Hole**	A	B	C	**Check Hole**
0-2,5	582	15	373	**15**	130	3	84	**3**
2,5-5	3.252	20	15	**105**	1.120	4	3	**24**
5-10	3.039	1.365	962	**135**	519	194	124	**15**
10-15	383	10	55	**30**	43	1	6	**3**
15-20	772	209	110	**962**	95	23	62	**124**
TOTAL	**8.028**	**1.619**	**1.515**	**1.247**	**1.907**	**225**	**279**	**169**

Row of Mix-2

Echelon	Grout Intake (Lt)				Grout Solid Material Intake kg/m			
	A	B	C	**Check Hole**	A	B	C	**Check Hole**
0-2,5	189	15	15	**10**	42	3	9	**2**
2,5-5	2.840	378	1.375	**373**	956	85	390	**84**
5-10	1.585	189	194	**20**	236	22	22	**2**
10-15	60	30	30	**15**	7	9	3	**2**
15-20	100	1.795	40	**40**	11	276	4	**5**
TOTAL	**4.774**	**2.407**	**1.654**	**458**	**1.252**	**395**	**428**	**95**

Row of Mix-3

Echelon	Grout Intake (Lt)				Grout Solid Material Intake kg/m			
	A	B	C	**Check Hole**	A	B	C	**Check Hole**
0-2,5	371	10	15	**10**	82	2	3	**2**
2,5-5	188	376	20	**188**	42	83	4	**42**
5-10	1.999	20	1.164	**193**	314	2	153	**21**
10-15	737	10	105	**35**	81	12	12	**4**
15-20	193	140	80	**30**	21	4	9	**3**
TOTAL	**3.488**	**556**	**1.384**	**456**	**540**	**103**	**181**	**72**

Row of Mix-4

Echelon	Grout Intake (Lt)				Grout Solid Material Intake kg/m			
	A	B	C	**Check Hole**	A	B	C	**Check Hole**
0-2,5	10	193	188	**10**	2	21	20	**2**
2,5-5	3.028	188		**25**	1.022	21		**5**
5-10	1.780	2.815	193	**377**	271	471	21	**41**
10-15	85	1.775	85	**35**	9	21	9	**4**
15-20	376	371	1.780	**193**	41	21	271	**21**
TOTAL	**5.279**	**5.342**	**2.246**	**640**	**1.345**	**555**	**321**	**73**

6. CONCLUSIONS

In the terrace unit located at the right bank of Dalaman – Akkopru Dam downstream test grouting was applied under the procedure of consolidation grouting. Without stating the practical application procedure, the grout formed is detailed as one, and the laboratory test results of the mixes are determined and the technical application procedure was designated. The validity of the application was controlled by check holes. It's shown that the values were under the limits of requirements of DSI. The intakes and the success values have been determined according to different types of mixes. However, it is hard to say which one of the mixes is appropriate for the terrace unit located through Dalaman River. This paper may be helpful for future studies and works designed near Dalaman River. These data will constitute a reference for future studies and work related to the same unit.

As for the materials and mixes used in this study, for the terrace unit which has outcrops through Dalaman River, it's been determined that Mix – 2 has the best stability and viscosity values among those four for grouting. In the test grouting, Mix – 2 has the appropriate values of grout intake. On the other hand, Mix – 3 has appropriate intake of solid material per meters. For this selection; hole grout intakes and water loss values with check holes grout intakes and water loss values have been compared. The difference at the value of grout intake at the beginning and the value of grout intake at check hole is biggest at the Mix – 2 row. This proves that the best mix is Mix – 2 among the four mixes compared in this work, under the conditions detailed.

7. REFERENCES

Anon. 1979a, 'Classification of rocks and soils for engineering geological mapping, Part I – Rocks and Soil Materials, *Bull. Int. Ass. Eng. Geol.*, 19, 364 –371.

Batı Söke Çimento T.A.Ş. (2002), Cement Analysis Report, Report Number: 201.

Çatal, A. (1993), Geotechnical Applications During Atatürk Dam Construction; Atak Ofset, Ankara.

DSI State Hydrolic Works (1983), Lower Dalaman Project Master Plan Report, Ankara. (unpublished)

DSI State Hydrolic Works (1999), Application Projects, Aydın, unreleased. (unpublished)

DSI State Hydrolic Works (1993), Technical Contract of Drilling – Grouting Works, Ankara. (unpublished)

Ewert, F.K., 1992, Rock Grouting : With Emphasis on Dam Sites, Springer Verlag.

Graciansky, P.C. (1972), Geological Researches in the Western Lycean Taurus (South Western Turkey), *PhD Thesis*, MTA, Ankara. (unpublished)

Heitfeld, K.H., 1965, Hydro- und baugeologische Untersuchungen über die Durchlässigkeit des Baugrundes an Talsperren des Sauerlandes. *Geologische Mitteilungen, RWTH,* Aachen, Heft 1.

Houlsby, A.C. (1985), Design and Construction of Cement Grouted Curtains. *15th ICOLD Congress*, Lausanne, III: 995-1015;

Karagüzel, R., 1989, Über Gebirgsdurchlässigkeit und Untergrundinjektionen an der Grossen Dhünn Talsperre und ihren Vorsperren, *Mitteilungen zur Ingenieur- und Hydrogeologie der RWTH,* Heft 31, 226 S, Aachen.

Karagüzel, R., Kılıç, R., 2000, The Effect of the alteration degree of the ophiolitic melange on permeability and grouting, *Engineering Geology,* Elsevier Science, 57 (2000), 1-12.

Karakaya Bentonite (2002), Laboratory Test Results, December;

Kutzner, C. (1991), New Criteria for Rock Grouting in Dam Engineering. *17th ICOLD Congress*, Vienna, III: 307-317;

Kutzner, C. (1996), Grouting of Rock and Soil, A.A. Balkema, Rotterdam, Netherlands;

Lombardi, G. (1985), The Role of Cohesion in Cement Grouting of Rock. *15th ICOLD Congress*, Lausanne, III: 235-261;

MTA (1997). Geological Map of the Fethiye – L7 Quadrangle, Ankara;

Nonveiller, E. (1989). Grouting Theory and Practice. Developments in Geotechnical Engineering, 57, Elsevier, p.21-83;

NTF Construction (2000), Advertisement Brochure, Muğla (unreleased).

Pettersson, S., Moulin, H. (1999), Grouting & Drilling for Grouting, *Atlas Copco Craelius AB*, Sweden;

Sekercioğlu, E., Ozguler, E. (1999), Geotechnical Investigations on Leakage Problem of Akkopru Dam, *ICOLD*, Antalya, Turkey;

Tosun, H. (2000), Principals of Grout Curtain Design for Embankment Dams and A Practice in Turkey, *8th National Congress on Soil Mechanics and Basement Engineering*, Istanbul;

Unal, S.M. (2001), Impermeability Curtains for Embankment Dam Foundations and Applications on Akköprü Dam, *Osmangazi University Institute of Science, M.Sc. Thesis*, Eskişehir. (unpublished)

TS 19 (1985), Portland Cements UDK 669.94, Institute of Turkish Standarts, Ankara.

TS 977 (1971), Bentonite as a Drilling additive UDK 622.36, Institute of Turkish Standarts, Ankara.

EVALUATION OF PHYSICAL PROPERTIES OF MORTAR MATERIALS USED IN PSIDIA ANTIOCHEIA AT ANATOLIA

Yücel K. T.[1], Gülmez S.[2] and Eroğlu Ö.[3]

[1]Süleyman Demirel University, Faculty of Architectural & Engineering, Civil Engineering Department, Division of Structure, 32260 Isparta/TURKIYE, kyucel@mmf.sdu.edu.tr

[2]Süleyman Demirel University, The Institute of Sciences Civil Engineering Department Division of Structural Engineering , 32260 Isparta /TURKIYE, sgulmez07@hotmail.com

[3]Süleyman Demirel University, The Institute of Sciences Geology Engineering Department Division of Geology Engineering , 32260 Isparta /TURKIYE, ozeroglu@hotmail.com

Abstract: In this study, physical properties like unit weight, specific weight, water absorption ratio and porosity of mortar specimens collected from the structures at Psidia Antiocheia Antique City in Anatolia are investigated. These specimens are from Roman and Byzantine Periods. For the determination of specific weight, a He-picnometer having a sensitivity of ± % 0.1 – 0.2 is used. For other analyses, calculations and measurements are performed by taking into consideration the Archimedes Principal. Data obtained from physical analyses helped to reveal data on the porosity, quality and physical properties of the specimens. Thus, information about technological behavior and production techniques of historical nations is gained. From the results of these experiments, an attempt was made to understand how these structural members survived till today. These experimental results are compared with the experimental results of modern materials technology.

Key words: unit weight, specific weight, water absorption, ratio, porosity, Psidia Antiocheia

1. INTRODUCTION

Mortars are one of the oldest building materials which have been used for centuries. Historical mortar is the common name given to the mortars used at structures before invention and use of the Portland cement. Historical mortars were prepared from a binder (hydraulic or aerial lime), silicate, carbonate, or dolomite sand and some additives (finely ground bricks, volcanic pozzolans, etc.) for improving workability, adhesion, strength or durability. The use of hydraulic lime mortars, first using volcanic powder and later also ceramic fragments, was already known to Greeks in the sixth and fifth centuries BC. and became more widespread during the fourth century BC. (Yücel and Gülmez, 2005).

Antiocheia is a city in Psidia established on the fertile land lying along the southern slopes of Sultan Mountains at approximately 1 km north of Yalvaç District of Isparta Province (Demirer, 2002; Taşlıalan, 1997). It is located in the western section of the Mediterranean lake district land between Agean, Middle Anatolian and Mediterranean zone (Demirer,2002; Taşlıalan,1997). This city was established by Seleukos I or his son Antiokhos. It was constructed at a date between the years 39 and 36 BC. (Anonim, 1983). The history of Antiocheia dates back to late Neolithic period (6000 BC.

1.1. Nymphaeum

The monumental fountain is at the northern end of the south - north street. The base ruins can be seen today (Figure 1.) (Taşlıalan, 1999). As the result of the excavations, presence of a developed water system in Antiokheia has been brought into light. Nymphaeum may have been constructed towards the end of 1st century (http://www.kultur.gov.tr/portal/arkeoloji_en.).

1.2. Augustus Temple

The temple is constructed in the holy area at the highest location of the city after the death of Emperor Augustus. The base of the building is formed by cutting the natural rock (Figure 2.). It is alleged to be

constructed at AD 1st century (Demirer, 2002).

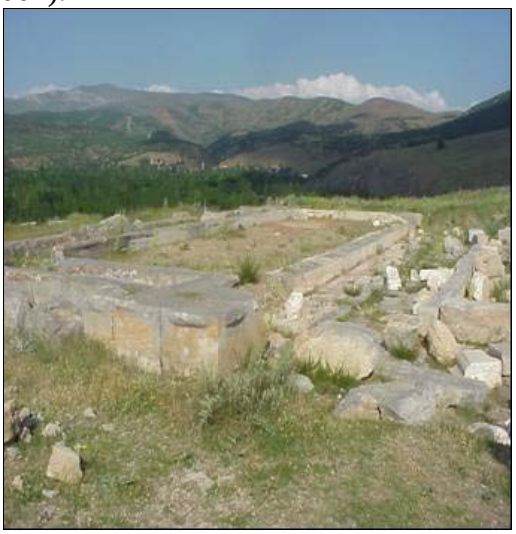

Figure 1. Antiocheia - Nymphaeum

Figure 2. Antiocheia - Augustus Temple

1.3. Roman Bath

It is one of the largest and strongest roman bath examples like the roman bath of Sagalassos and is dated to the early 1st century AD. (Figure 3) (Demirer, 2002). It was built as a bath and a palaestra. The palaestra is located at the east of the bath. Sizes are 37 m and 29 m. The Bath is 69 m in length and 54 m in width. It was made from stone and mortar (Kaya et al., 1997).

1.4. Small Church

Excavation director Robinson said that "after cleaning trancept walls, we have successfully obtained a plan of the church in the shape of a crucifix" in July 1924. Also Woodbridge made a simple plan of the church. In terms of structure, plan and material, this church may have been constructed in the 5th century AD. (Figure 4.) (Demirer, 2002).

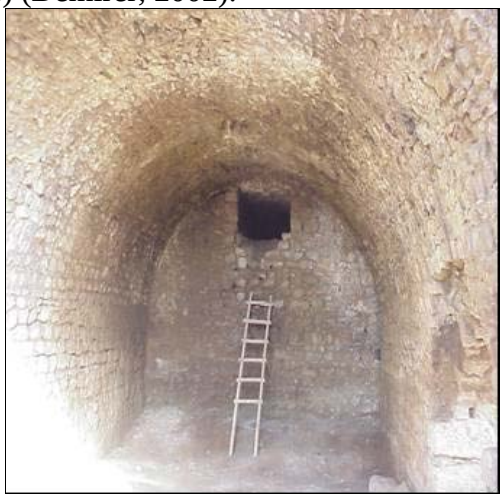

Figure 3. Antiocheia – Roma Bath

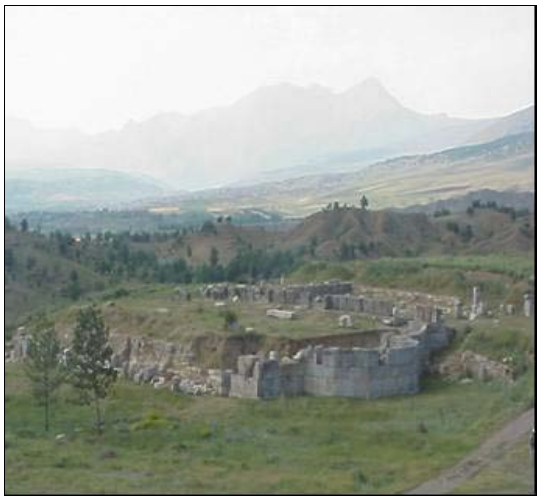

Figure 4. Antiocheia – Small Church

2. MATERIAL AND METHODS

Unit weight, water absorption, specific weight, porosity and compacity tests were made on brick materials which were obtained from Psidia Antiocheia.

2.1. Unit Weight and Water Absorption

The mortar specimens may be in any regular form with the smallest dimension being not less than 50 mm. At least five specimens were prepared from each sample. The weight of samples is at least 350 gr. The specimens were dried for 48 h in a ventilated oven at a temperature of 60 ± 2 ^{o}C. After drying, the specimens were cooled in the room for 30 min and weighed. The specimens were weighed immediately after cooling and stored in a

desiccator. The weights were determined to the nearest 0.01 g by using Gec Avery type scale (G_k). The specimens were immersed completely in filtered or distilled water at 22 ± 2 ^oC for 48 h. Following this period, the specimens were taken out of the water. The specimens were then rolled in a large absorbent cloth until all the visible films of water were removed. Then specimens were weighted (G_{dh}). The sample was soaked in water and taken out and the saturated weight of the sample was found to the nearest 0.1 g by using Sortorius type scale (G_{ds}). Unit weight and water absorption were defined as follows:

$$\Delta_h = \frac{G_k}{G_{dh} - G_{ds}} \qquad (3.1.)$$

$$S_k = \frac{G_{dh} - G_k}{G_k} x100 \qquad (3.2.)$$

$$S_h = \frac{G_{dh} - G_k}{G_{dh} - G_{ds}} x100 \qquad (3.3.)$$

Here;

Δ_h = Unit weight of specimen (gr/cm^3),

S_k = Massed water absorption ratio of specimen (m/m, %),

S_h = Bulk water absorption ratio of specimen (v/v, %),

G_k = Weight of the sample in oven-dry state (gr),

G_{dh} = Weight of the sample in saturated and surface dry condition (gr),

G_{ds} = Weight of the saturated sample in water (gr) (BS EN 12808 – 5, 2001; ASTM C 67 - 03a, 2003; ASTM C 97).

2.2. Specific Weight

The samples which were obtained from various fragments by crushing were pulvarized and drained. Thus, samples can pass from 0.2 mm sieve. He-picnometre which was filled by water at the room temperature was rolled in an absorbent cloth until all the visible films of water were removed. Then picnometre was weighed (G_{ps}) .The water in picnometre was taken out and dried in an oven and weighed in oven-dry state (G_p). 250 ± 5 g pulvarized sample was placed in picnometre and weighed by using Gec Avery type scale (G_{pn}). Picnometre with sample was filled 1/4 volume water and air between grains was taken out by using a vacuum pump. Then the picnometre was filled with water completely. Visible films of water were removed by means of absorbent cloth and picnometre was weighted (G_{pns}). Specific weight was determined as follows:

$$d_o = \frac{G_{pn} - G_p}{\left(G_{pn} - G_p\right) - \left(G_{pns} - G_{ps}\right)} \qquad (3.4.)$$

Here;

d_o = Specific gravity of sample (g/cm^3),

G_{pn} = Picnometre + sample weight (gram),

G_p = Picnometre weight (gram),

G_{pns} = Picnometre + sample + water weight (gram),

G_{ps} = Water filled Picnometre weight (gram) (TS 699, 1987).

2.3. Compacity

By using unit weight and specific weight, the compacity was determined as follows:

$$k = \frac{\Delta_h}{d_o} x100 \qquad (3.5.)$$

Here;

k = Compacity ratio of the sample (m/m, %),

Δ_h = Unit weight of the sample (gr/cm^3),

d_o = Specific weight of the sample (g/cm^3) (TS699, 1987).

2.4. Porosity

By using unit weight and specific weight, porosity was determined as follows.

$$P = \left(1 - \frac{\Delta_h}{d_o}\right) x100 \qquad (3.6.)$$

$$P = (1-k)x100 \qquad (3.7.)$$

Here;

P = Sample Porosity (v/v, %),

Δ_h = Unit weight of sample (gr/cm^3),

d_o = Specific weight of sample (g/cm^3)

k = Sample compacity (m/m, %) (TS 699, 1987).

3. RESULTS AND DISCUSSIONS

In this study, firstly physical properties of mortar samples were classified as seen in Table 1.

When we examined physical analysis of mortar samples (Table 2), unit weight values of brick samples were found to be between (Δ_h), 1.85 - 1.89 gr/cm^3, specific weight values between (d_o), 2.64 - 2.74 gr/cm^3.

Table 1. Chronology of mortar samples

Number	Sample Number	Name Of The Antique City	Name Of The Building	Construction Date
1	M1	Psidia Antiocheia	Augustus Temple	Middle of 1st century AD.
2	M2	Psidia Antiocheia	Monumental Fountains	Last quarter of 1st century
3	M3	Psidia Antiocheia	Roman Bath	1st century AD.
4	M4	Psidia Antiocheia	Small church	5th century AD.

Table 2. Physical analysis results of mortar samples

Number	Sample number	Δ_h Unit Weight gr/cm^3	S_k Water absorption in mass %	S_h Water absorption in volume %	d_o Specific Weight gr/cm^3	K Composity %	P Porosity %
1	M1	1.87	13.58	25.34	2.74	68.2	31.8
2	M2	1.85	10.78	19.93	2.64	70.1	29.9
3	M3	1.89	12.44	23.53	2.73	69.2	30.8
4	M4	1.88	13.91	26.19	2.71	69.4	30.6

Table 2 shows that unit weight of M1 sample was higher. Hence, void ratio has a smaller value in these materials, and they have high compressive strength values.

4. CONCLUSION

Data obtained from these experiments provide information about ancient production techniques and material technology. This information will be useful in material choice in restoration and rehabilitation studies. The investigation of material properties which are used in historical buildings will form a bridge between the past and the near future. The importance of an engineering point of view can easily been seen in these studies.

REFERENCES

Anonim, 1983. Isparta Valiliği (in Turkish). Isparta, Turkey.

ASTM C67 - 3a, 2003. Standard Test Methods for Sampling and Testing Brick and Structural Clay Tile. *American Society for Testing and Materials,* United States.

ASTM C97 – 02. Standard Test Methods for Absorption and Bulk Specific Gravity of Dimension Stone. *American Society for Testing and Materials.* United States.

BS EN 12808-5, 2001. Grouts for tiles - Determination of water absorption. *British Standard,* Brussels.

Demirer, Ü., 2002. Pisidia Antiokheia'sı (in Turkish), Isparta, Turkey.

Republic of Turkey Ministry of Culture and Tourism, 2005. http://www.kultur.gov.tr/portal/arkeoloji_en.asp?belgeno=669

Kaya M.A., Keçeli D.A., Özyalın Ş., Uyanık O., Çınar K., Kalyoncuoğlu Y., 1997. Pisidia Antiocheia'sı Roma Hamamı, *I. Uluslararası Pisidia Antiocheia Sempozyumu Bildiriler Kitabı* (in Turkish). Kocaeli Ofset Matbaacılık, 51-67, Isparta, Turkey.

Taşlıalan, M., 1997. Pisidia Antiocheia'sının Tarihçesi, *I. Uluslararası Pisidia Antiocheia Sempozyumu Bildiriler Kitabı* (in Turkish), Kocaeli Ofset Matbaacılık, 5-20, Isparta, Turkey.

Taşlıalan, M., 1999. Pisidia Antiocheia'sı 1997 yılı Çalışmaları, *IX. Müze Kurtarma Kazıları Semineri* (in Turkish), Kültür Bakanlığı Milli Kütüphane Basımevi, 21-39, Ankara, Turkey.

TSE 699, 1987. Tabii Yapı Taşları Muayene ve Deney Metotları. *Türk Standardları Enstitüsü* (in Turkish), 1-70, Ankara, Turkey.

Yücel K.T. and Gülmez S., 2005. "Chemical, Mineralogical and Petrographical Analyzes of Historical Building Materials of Hellenistic, Roman, Byzantine and Seljuk's Period of Anatolia". *10th Euroseminar on Microscopy Applied to Building Materials,* 2005, Historic Masonry Group University of Paisley. Paisley, Scotland. CD Paper Name. Yucel_Gulmez.

(This page is left blank intentionally.)

REVIVING THE DREAM: A PILOT PROJECT ON THE SUSTAINABLE DEVELOPMENT OF NISYROS VOLCANO

Zouzias D.[1] and St. Seymour K. [1], [2]

[1]Department of Geology, University of Patras, 26500 Rion, Patras, Hellas (GR) dizouzias@upatras.gr
[2]Departments of Geography, Chemistry, Concordia University, Montreal, Canada H4B1R6 (CA)
kstseymr@upatras.gr

Abstract: Nisyros is an entirely volcanic island southeast of Kos. Quaternary volcanism in Nisyros occurred in two cycles: one andesitic stratovolcano-building and a second intensely explosive period which resulted in caldera formation. Several phreatic craters and fumaroles are situated on the caldera floor and hot springs are located mainly on the southern and northern coasts. In 1973 a project was launched generating electricity from geothermal energy. For Nisyros to develop in a sustainable direction, it has to overcome the challenges of adequate quantities of quality water and easily accessible cheap energy. Our plan for water and energy management of Nisyros would include additional desalination capacity by taking advantage of geothermal and other "soft" energy sources (R.E.S., Renewable Energy Sources) and management of desalination and physical water sources such as rainfall, runoff and underground water reservoirs. The Nisyros of the past was a renown city for its baths. The development of the hot springs into Spa Centers would re-establish Nisyros to its ancient status and as an important attraction pole for ecotourism. Finally, we propose the establishment of an institute to monitor the RES applications, act as a volcanological observatory, and as a museum of physical history and volcanological education.

Key words: Nisyros, volcano, sustainable development, R.E.S., Volcanological Observatory.

1 INTRODUCTION

Nisyros is a high enthalpy geothermal field and a rare natural monument for volcanological education of the public. Sustainable development of an island such as Nisyros has to be accomplished in accord with the socioeconomic needs of its inhabitants, its volcanic and semi-arid nature and the application of environment-friendly solutions. Nisyros is a small island with a permanent population of nearly 900. Its economy depends on daytime tourism during summer months and on the exploitation of a pumice quarry north of Nisyros on the volcanic islet of Yali. Livestock feeding is unrestricted, destroying any attempt to promote agricultural activities on the island. Lack of fresh water resources is a crucial factor with immediate adverse consequences on the economy (tourism, agriculture etc). This pilot project proposes a sustainable development plan, which aspires to solve the problems of water management and cheap energy and to promote the progress of the volcano in an environment-friendly way. The sustainable development plan (Figure 1a): is three-pronged: its first objective is the redirection of the economy towards 'alternative tourism' with the development of the thermal springs into Spa Centers, and ecotourism with the development of the volcano into a National Park. Alternative tourism, and tourism in general, requires quality water, which in turn requires a rigorous plan of water management, taking advantage of any groundwater, rainfall, runoff and desalination waters. A sound water management plan for Nisyros will require the construction of a second desalination plant. Both desalination units should take advantage of the cheap R.E.S. in the form of geothermal, wind and solar energy. The establishment of an institute monitoring RES applications, acting as a Volcanological Observatory and as a Museum of Physical History, and volcanological education is a final but crucial factor for the effective application of a sustainable development plan on a volcanic environment such as Nisyros.

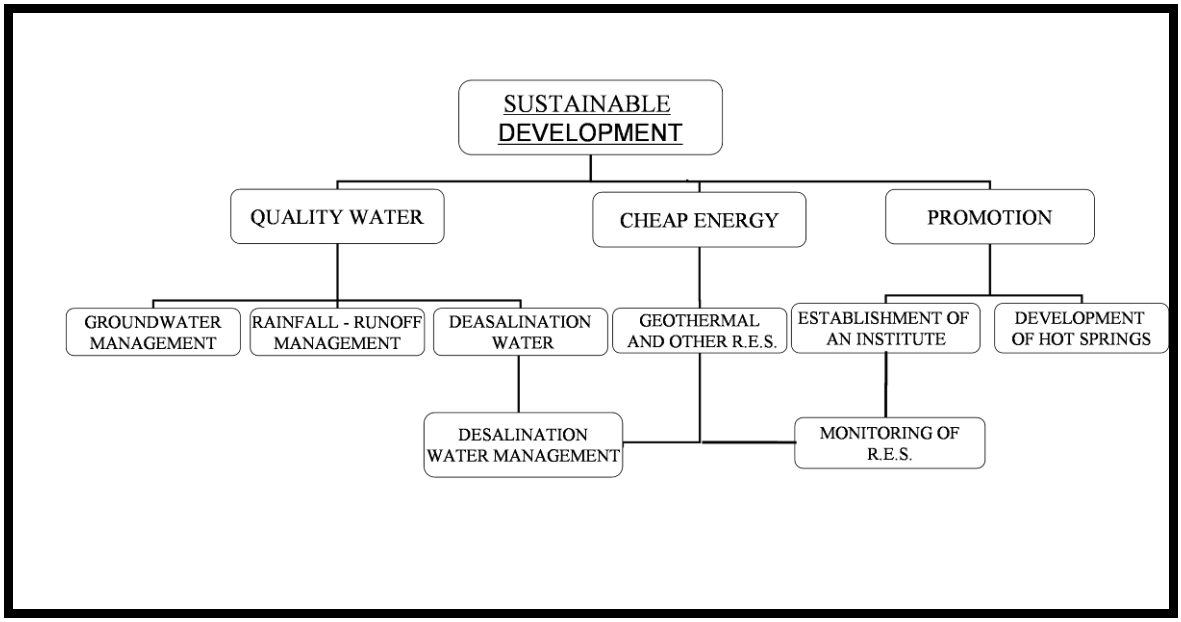

Figure 1a. Proposed sustainable development plan for Nisyros Volcano

2. VOLCANO-TECTONIC SETTING

Nisyros is an entirely volcanic island located in the easternmost corner edge of the Quaternary volcanic arc of the Aegean Sea (Figure 2a) (at 36o35' latitude and at 27o10' longitude), 10 miles south of the island of Kos (Figure 2a, inset). Other volcanic centers in the arc clockwise are: Sousaki, Methana, Aigina, Poros, Milos and Thera. Nisyros is characterized by a calcalkaline sequence as a result of subduction of the African plate under an Aegean microplate, which started c.a. 5 Ma, at the beginning of Pliocene (McKenzie, 1972; Le Pichon and Angelier, 1979; Jackson, 1994). Recent phreatomagmatic activity has been reported in Nisyros from 1422 to 1888A.D. (Georgalas, 1962). Seismological studies suggest a magma chamber at a depth of 2-8 km (Papadopoulos, 1984; Papadopoulos et al., 1998). One possible interpretation for the ground deformation of Nisyros during the period 1995-2002 has been variable degrees of inflation of such a magma chamber (Lagios et al., 2005).

Nisyros has a diameter of 8 km and a surface of 42 km^2. It is characterized by a rough relief with a mean elevation ~ 400 m and a maximum elevation of 698 m (Prophet Helias dome). The caldera of Nisyros has a diameter of 4 km and a depth of 300 m (Figure 1b). Several phreatic craters are situated on the caldera floor, such as the renown 'Stefanos', with a diameter of 300 m and a depth of 25 m (Figure 2b). One of the oldest volcanic exposures on Nisyros gave a K/Ar age of 0.2 m.y. B.P. and the volcanic submarine activity is thought to have been initiated in the period between 3.0 to 0.2 m.y. B.P. (Di Paola, 1974). The volcanic evolution of Nisyros can be divided into two cycles: one stratovolcano-building with basic andesitic-andesitic to dacitic-rhyodacitic flows, domes and pyroclastics products, and a second cycle which was intensely explosive and resulted in the formation of a caldera and extrusion of post-caldera dacitic domes along a northeasterly trending fault system (Figure 1b). The petrochemistry, petrogenetic evolution and volcanic hazard potential of Nisyros and Yali have been studied by Martelli (1917), Georgalas (1962), Davis (1967), Di Paola (1974), Bohla and Keller (1987), Lodice (1987), Vougioukalakis (1989), St. Seymour and Vlassopoulos (1989), Wyers and Barton (1989), Limburg and Varekamp (1990), St. Seymour and Lalonde (1990), Papanikolaou et al. (1991), Gansecki (1991), Vougioukalakis

(1993), Marini et al. (1993), Francalanci et al. (1995), St Seymour (1996), Parcharidis and Lagios (2001), Sachpazi et al. (2002), Chiodini et al. (2002), Buettner et al. (2005) and Lagios et al. (2005).

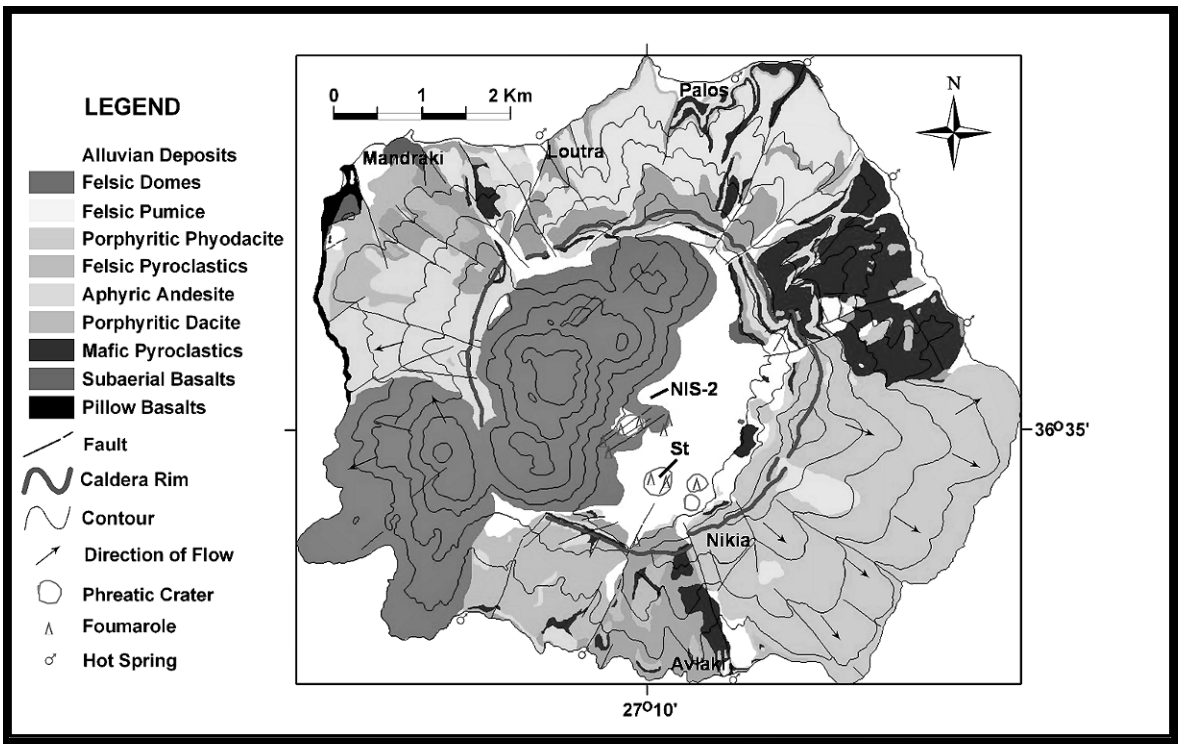

Figure 1b. Simplified geological map of Nisyros volcano (Modified after Vougioukalakis 1989, IGME) with positions of phreatic craters, fumaroles, hot springs, main villages and of the geothermal well

Five major fault systems (Figure 1b) have been identified (Papanikolaou et al., 1991; Vougioukalakis, 1993; Papanikolaou and Nomikou, 2001). Two major fault systems trending NE-SW and NW-SE dipping 70o-80o cause vertical displacements of 120 to 150 m visible on the caldera wall (Vougioukalakis, 1993). Another fault system trending E-W is possibly the result of an in-depth joining of a system of conjugate NE-SW and NW-SE faults (Lagios et al., 2005). North-South and ESE-WNW fault systems appear to be present also in Kos and actually characterize the entire vicinity (Lagios et al., 2005).

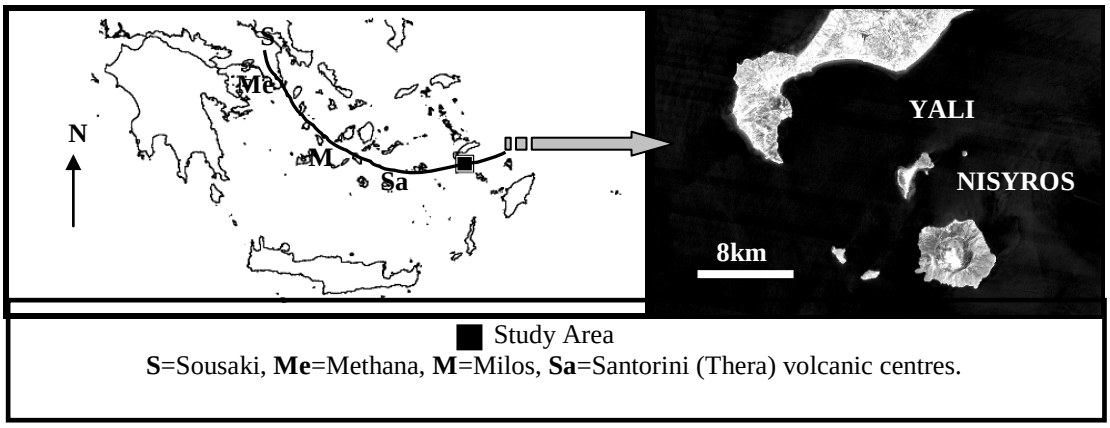

Figure 2a. Hellenic volcanic arc and volcanic centres. (Inset; Nisyros and adjacent islands, Landsat satellite image)

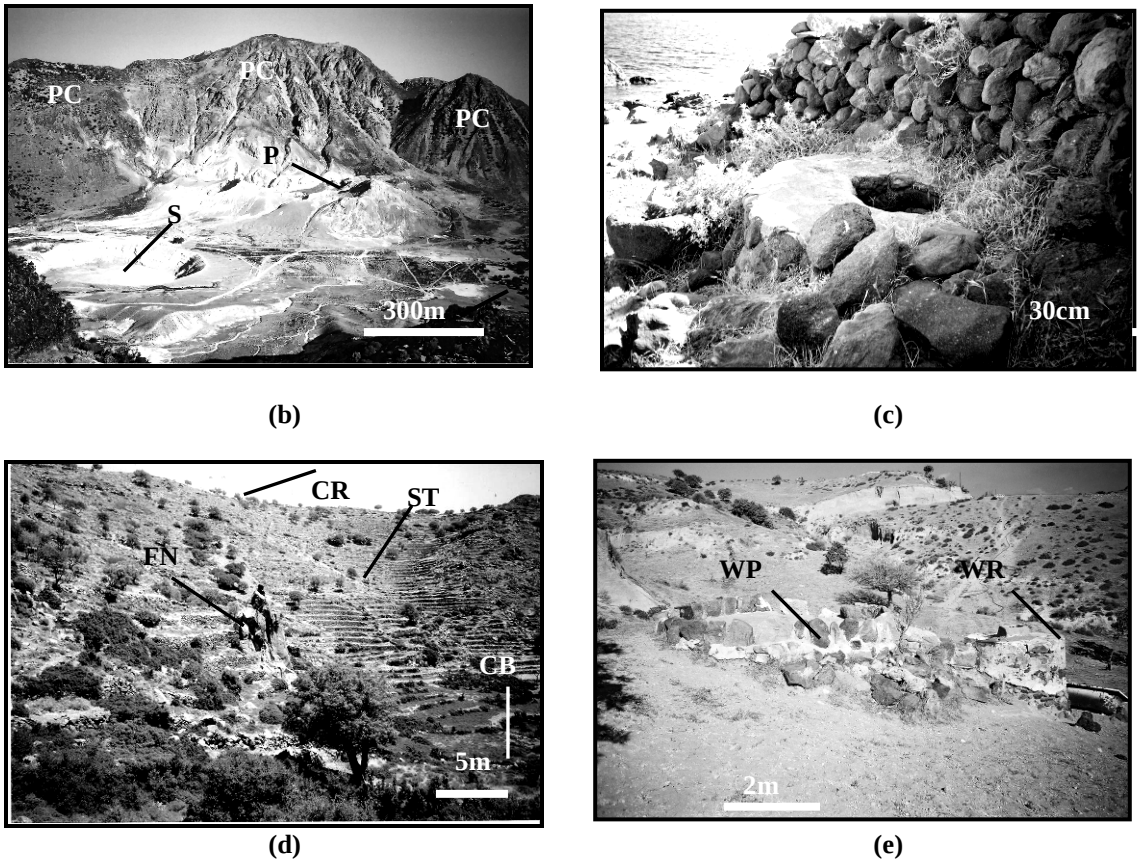

Figure 2. (b) View of the caldera floor of Nisyros volcano where phreatic craters, Stefanos (S, on the left) and Polyvotis (P, in the middle) and post-caldera domes (PC, on the back) are situated

(c) Abandoned well in the vicinity of Hellinika used for watering animals

(d) A series of steps (ST) from the caldera bottom (CB) to the caldera rim (CR) were constructed in the past to increase the ground surface and retain rainfall and soil for agricultural purposes. It can be distinguished a feeder neck of andesitic lava (FN) in the middle of the picture

(e) Old-built water reservoir in the vicinity of Hellinika where it can be distinguished the rainfall collector platform (WP) which fulfils the water reservoir (WR)

3. PRESENT CONDITIONS

Sustainable development is a process of developing (land, cities, businesses, communities, etc.) that "meets the needs of the present without compromising the ability of future generations to meet their own needs" (Brundtland Report, 1987). The sustainable development of Nisyros volcano requires quality water in sufficient quantities. The efforts of the inhabitants to explore for water have been abandoned, as it appears from the lack of wells around the island. Forty wells exist in the vicinity of the main village Mandraki that are used for gardening. Only three abandoned wells have been observed in the rest of the island (Figure 2c). A series of steps from the caldera bottom to the caldera rim have been created in historical times by the inhabitants of Nisyros, to increase the ground surface and retain rainfall and soil for agricultural purposes, but this effort has been presently abandoned (Figure 2d). Two natural springs located at Loutra and east of Nikia (Panagia Kyra) were abandoned due to mixing with hydrothermal water and overdrawing of waters respectively. However, numerous old- and newly-built water reservoirs exist all around the island (Figure 2e), which are used to retain rainfall for the irrigation of vegetable, grapevine and citrus tree plots. Many of the newly-built reservoirs are mainly filled with desalinated water

from a desalination unit which has a capacity of 350 m^3 per day (Figure 3a). The technical standards of this water reservoir are low, adulterating the quality of the desalinated water. The desalination unit supplies Mandraki, Palos, Nikia and Emporios villages, in this order of priority, with water weekly through a network or with tankers, which further damage the quality of the desalinated water. A recent major water reservoir built for collecting rainfall, in the vicinity of Hellinika east of Palos, has been abandoned since the very beginning due to technical problems with its construction (Figure 3b). Mixing of hot geothermal waters with meteoric and sea water results in numerous thermal springs (30-60^o C), which issue around the coasts of the island. Nisyros was selected by the Father of Medicine, Hippocrates, for its baths and was a renown Loutropolis during Roman times and even later during the late 1800's. Presently, the hot springs have not been developed, except for local use of the Loutra baths by the inhabitants of the island (Figure 3c).

From the viewpoint of energy, Nisyros is more than endowed with, as any other island in the Dodecanese (Figure 2a), cheap energy, because in addition to high winds and solar energy it possesses a high enthalpy geothermal field. However, no serious effort has been made to develop R.E.S. on the island. In 1973 a project to generate electricity from geothermal energy was launched. On the eastern portion of the caldera floor the sealed geothermal well NIS-2 (Figure 3d) is still closely monitored by PPC (Public Power Corporation). The geothermal project was abandoned at its inception due to inadequate information given by PPC at the time.

Presently, the economy of the island depends on daytime and sparse permanent tourism during summer months and on the exploitation of pumice from the quarry of Yali (Figure 3e). Daytime visiting tourist groups from nearby Kos attend lectures given by travel bureau guides, on the volcanology of Nisyros. Yali sustains the permanent population of Nisyros due to pumice and more recently to perlite extraction via leasing of the grounds and creation of employment. Ships are loading pumice, which is used for construction (Figure 3f) (e.g. new port of Patras). Part of the profits of the mining company adds to the economy of the municipality of Nisyros due to the leasing of the grounds arrangements.

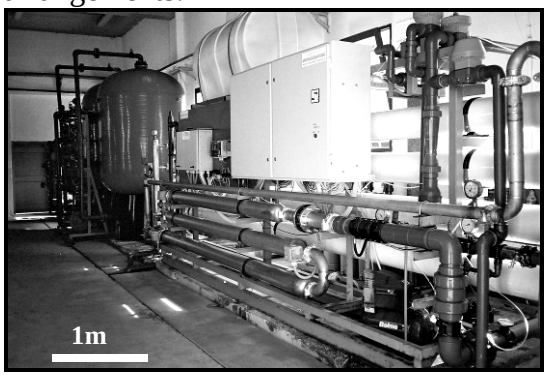

Figure 3(a): Desalination unit situated in the vicinity of Loutra. The picture shows the sea water filters in the back and the tubes of high pressure in the right cleansing the filtered water.

Figure 3(b):Abandoned water reservoir of municipality of Nisyros in the vicinity of Hellinika

Figure 3(c): View of the building of the Palos baths

Figure 3(d): View of the sealed geothermal well NIS–2 on the caldera floor

Figure 3(e): View of the Lava Co. pumice quarry on the volcanic islet of Yali

Figure 3(f): Loading of Yali pumice with Nisyros volcano in the background

4 DISCUSSION AND CONCLUSIONS

4.1 Sustainable Orbit

To take its place on the orbit of sustainable development, Nisyros has to overcome the challenges of providing quality water and cheap energy. Water management presupposes initially a thorough investigation of underground water resources by hydrogeological and geophysical research methods. The hydrogeological research will lead to conclusions to be applied in the making of a plan for underground water management, mainly for local irrigation purposes. The processing of rainfall and structural (tectonic) data will be useful to develop and propose the repair of the water reservoir in the vicinity of Hellinika. Last but not least, monitoring of the water needs of Nisyros for the periods from April to October and November to March will specify the capacity for a second desalination plant which will provide for the full coverage of needs for quality water for the island. This second desalination plant will operate solely on R.E.S. and the supply of the already existing desalination unit on Nisyros will be evaluated for the possibility of conversion to R.E.S. The hot springs and the fresh water springs should be water-drilled for a better use and development in a sustainable way.

Nisyros is an island where R.E.S. can be applied successfully, due to its high enthalpy geothermal field and the high wind and solar energy potential it shares with the rest of the islands in the Aegean Sea. Renewable energy sources have multiple applications that could promote the society of Nisyros to a better standard of living. Such applications could be the heating of houses, hotels, public buildings and greenhouses. They can provide a sustainable source for cheap electricity for Nisyros and the nearby islands and for the production of desalinated water. Presently R.E.S. is promoted worldwide for island communities, due to their high potential of wind, solar, wave energy and due to low cost of R.E.S. compared to energy provided by fuel and coal. Nisyros has the additional advantage of a high enthalpy geothermal field. Application of R.E.S. in Nisyros could represent a cheap solution for energy, a source of income by selling to or exchanging electrical power with the municipalities of the nearby islands, some of which have economies heavily leaning on tourism (e.g. Kos, Rhodes). As such R.E.S. represents a major factor for environment-friendly sustainable development.

4.2 Proposed Plan

We propose the initial investigation of underground water and processing of rainfall data, as well as monitoring the Nisyros community's water needs, with the purpose to evaluate what percentage of these needs can be met by natural waters and for what type of use (e.g. irrigation). To succeed full coverage of the needs in water we propose also the repair and the development of the water reservoir in the vicinity of Hellinika and the construction of an additional desalination unit in the vicinity of Nikia. The additional desalination unit should be constructed near Nikia to revive this traditional village and to promote it as a pole of tourist attraction due to the unique view it has of the Nisyros caldera. Also a new network for supplying water should be constructed, fulfilling better standards of safety and daily supply. The development of hot springs into Spa Centers would promote Nisyros to its ancient status of Loutropolis and it would be a great pole of attraction for tourists due to a high standard of living in a sustainable Nisyros.

Provision of cheap energy in Nisyros is attainable without great difficulty due to its high potential of wind, solar and geothermal energy. Wind and solar energy are to be used for generating electricity for the desalination units, providing in turn cheap 'quality-water'. Geothermal energy is the application that would solve most of the problems of the island. Electricity generated by geothermal energy, would be adequate for Nisyros and the adjacent touristy islands, providing additional income. Other applications of geothermal energy on the island would be the heating of the houses, spas, hotels, public buildings and greenhouses for local agricultural production.

Pumice and perlite quarries are located on the partly submerged volcano of Yali, north of Nisyros. The municipality of Nisyros has leased the pumice quarry to the company Lava Co. More employment positions will decidedly be created for the inhabitants of Nisyros if the expansion of perlite will be held in situ.

Finally, we propose the establishment of an institute in the Nikia village. The institute would be responsible for monitoring and preserving the R.E.S. applications, act as a Volcanological Observatory with plans for volcanic hazards and evacuation, and as a Museum of Physical History and volcanological education for school, university and tourist visits. With the proper water and energy management, the extreme natural beauty of volcanological sites, the great variety of ornithological species and rare fauna could promote the island to the status of a National Park.

ACKNOWLEDGEMENT

We would like to thank C. Katagas for the contribution of ideas for the sustainable development plan and the scientific discussions and also S. Tombros for his technical contribution in making of the poster presentation for this work.

REFERENCES

Bohla, M. and Keller, J., 1987. Petrology and Plinian eruptions of Nisyros volcano, Hellenic arc. *Terra Cognita*, 7, 171.

Brundtland Report, 1987. http://en.wikipedia.org/wiki/Sustainable_development 11 January 2006.

Buettner, A., Kleinhanns, I.C., Rufer, D., Hunziker, J.C. and Villa, I.M., 2005. Magma generation at the easternmost section of the Hellenic arc: Hf, Nd, Pb and Sr isotope geochemistry of Nisyros and Yali volcanoes (Greece). *Lithos*, 83, 29-46.

Chiodini, G., Brombach, T., Caliro, S., Cardellini, C., Marini, L. and Dietrich, V., 2002. Geochemical indicators of possible ongoing volcanic unrest at Nisyros island (Greece). *Geophys. Res. Lett.*, 29.

Davis, E., 1967. Zur geologie und petrologie der inseln Nisyros und Jali

(Dodecanes). *Proceeding of University of Athens*, 42, 235-252.

Di Paola, G.M., 1974. Volcanology and petrology of Nisyros island (Dodecanese, Greece). *Bulletin of Volcanology*, 38, 944-987.

Francalanci, L., Varekamp, J.C., Vougioukalakis, G., Defant, M.J., Innocenti, F. and Manetti, P., 1995. Crystal retention, fractionation and crustal assimilation in a convecting magma chamber, Nisyros volcano, Greece. *Bull. Volcanol.*, 56, 601-620.

Gansecki, C., 1991. Petrology of the domes and inclusions of Nisyros volcano, Dodecanese islands, Greece. *B.A. thesis*, Wesleyan Un., Middletown, CT, 97.

Georgalas, G.C., 1962. Catalogue of the active volcanoes of the world including solfatara fields. Part: 12, Greece. *International Association of Volcanology*, Rome, 29-36.

Jackson, J., 1994. Active tectonics of the Aegean region. *Ann. Rev. Earth Planet Sci*., 22, 239-271.

Lagios, E., Sakkas, V., Parcharidis, I. and Deitrich, V., 2005. Ground deformation of Nisyros volcano (Greece) for the period 1995-2002: Results from DInSAR and DGPS observations. *Bulletin of Volcanology*, 68, 201-214.

Le Pichon, X. and Angelier, J., 1979. The Hellenic arc and trench system: a key to the evolution of the eastern Mediterranean. *Tectonophysics*, 60, 1-42.

Limburg, E.M. and Varekamp, J.C., 1990. Young pumice deposits on Nisyros, Greece. *Bulletin of Volcanology*, 54, 68-77.

Lodice, L., 1987. Petrology and geochemistry of Nisyros volcano (Dodecanese, Greece). *Ms. Thesis*, Wesleyan Un., Middletown, CT, 245.

Marini, L., Principe, C., Chiodini, G., Cioni, R., Fytikas, M. and Marinelli, G., 1993. Hydrothermal eruptions of Nisyros (Dodecanese, Greece). Past events and present hazards. *J. Volcanol. Geotherm. Res.*, 56, 71-95.

Martelli, A., 1917. Il gruppo eruttivo di Nisyros nel mare Egeo. *Mem. Soc. Geol. Ital. Sc*. (detta dei XL), Serie 3a, vol. XX.

McKenzie, D.P., 1972. Active tectonics of the Mediterranean region. *Geophys. J. R. Astron. Soc*., 30, 109-185.

Papadopoulos, G.A., 1984. Seismic properties in the eastern part of the south Aegean volcanic arc. *Bull. Volcanol.*, 47, 143-152.

Papadolpoulos, G.A., Sachpazi, M., Panopoulou, G. and Stavrakakis, G., 1998. The volcano-seismic crisi of 1996-97 in Nisyros, SE Aegean Sea, Greece. *Terra Nova*, 10, 151-154.

Papanikolaou, D., Lekkas, E. and Sakelariou, D.T., 1991. Geological structure and evolution of Nisyros volcano. *Bulletin of Geological Society of Greece*, 25, 405-419.

Papanikolaou, D. and Nomikou, P., 2001. Tectonic structure and volcanic centres at the eastern edge of the Aegean volcanic arc around Nisyros Island. *Bull. Geolog. Soc. Greece* XXXIV: 1289-1296, *Proc. 9th Int. Congress*, Athens, Sept. 2001.

Parcharidis, I. and Lagios, E., 2001. Deformation in Nisyros volcano (Greece) using Differential Radar Interferometry. *Bull. Geol. Soc. Greece*, 34, 1587-1594.

Sachpazi, M., Kontoes, C., Voulgaris, N., Laigle, M., Vougioukalakis, G., Sykioti, O., Stavrakakis, G., Baskoutas, J., Kalogeras, J. and Lepine, J.C., 2002. Seismological and SAR signature of unrest at Nisyros caldera, Greece. *J. Volcan. Geoth. Res.*, 116, 19-33.

St. Seymour, K. and Vlassopoulos, D., 1989. The potential for future explosive volcanism associated with dome growth at Nisyros, Aegean volcanic arc, Greece. *J. Volcanol. Geother. Res.*, 37, 351-364.

St. Seymour, K. and Lalonde, A.E., 1990. Monitoring oxygen fugacity conditions in pre-, syn- and postcaldera magma chamber of Nisyros volcano, Aegean island arc, Greece. *J. Volcanol. Geotherm. Res.*, 46, 231-240.

St. Seymour, K., 1996. Geochemistry of the Yali volcano rhyolites and their relationship to the volcanic products of Nisyros, Aegean volcanic arc. *N. Jb. Miner. Mh.*, H.2, 57-72.

Vougioukalakis, G., 1989. Geologic map of Nisyros island, 1:25,000, *IGME*.

Vougioukalakis, G., 1993. Volcanic stratigraphy and evolution of Nisyros island. *Bull. of Geol. Soc. Greece*, XXVIII/2: 239-258, Athens, 1993.

Wyers, P.G. and Barton, M., 1989. Polybaric evolution of calc-alkaline magmas from Nisyros, southeastern Hellenic arc, Greece. *J. Petrol.*, 30, 1-37.

(This page is left blank intentionally.)

INDEX OF AUTHORS

Author **Page Number**

A

Akbulut M., ... 1, 7
Akyol N., ... 9
Altınok Y., ... 283
Aydan Ö., ... 15, 231

B

Baykal A., ... 261
Baysal G., ... 31
Bechtel A., ... 335
Bulyga O. S., ... 43
Butuzov G.N., ... 335
Butuzova L.F., ... 43, 335

C

Çakıcı S., ... 181
Caldarola F., ... 51
Ceylan S., ... 59, 283
Chatziapostolou A., ... 295
Christanis K., ... 295
Çoban F., ... 65, 213
Coşar Y.Z., ... 117

D

Danışman M. A., ... 9
Diamantopoulos A., ... 71, 81

E

Ercan A. Ö., ... 91
Eroğlu Ö., ... 357
Ertunç A., ... 273
Esmaeily D., ... 143, 153

G

Galant Y., ... 111
Grippo A., ... 51
Guario I. M., ... 51
Gülmez S., ... 357

I

İnaner H., ... 117, 125
Isaeva L.N., ... 335
Isayeva L.N., ... 43

K

Kalaitzidis S., ... 295
Karagüzel R., ... 289, 305
Karayiğit A. İ., ... 1, 205
Khalaji A. A., ... 143, 153
Kıncal C., ... 31, 163, 173, 181, 193, 343
Kırdım Ö., ... 205
Koca M. Y., ... 163, 173
Koca M.Y., ... 343
Kocabaş C., ... 65, 213
Kolçak D., ... 283
Kozłowska A., ... 221
Küçükuysal (İpekgil) C., ... 137
Kumsar H., ... 15, 231
Kurt H., ... 283
Kuruoğlu M., ... 243

Author **Page Number**

L

Laviano R., ... 51
Lünel A. T., ... 137

M

Melinte M. C., ... 251
Menlikli G. F., ... 261
Milella M., ... 51
Mitchell B. J., ... 9
Mutlutürk M., ... 305

N

Nakoman E., ... 117

O

Özçelik M., ... 273
Özden G., ... 243
Özer N., ... 59, 283
Özyalın Ş., ... 193

P

Pişkin Ö., ... 1, 7

Q

Querol X., ... 205

S

Safin V.A., ... 335
Scandale E., ... 51
Şener (Tay) Ş., ... 305
Şener E., ... 273
Seyman F., ... 289
Siavalas G., ... 295
Şimşek C., ... 317
Sözbilir H., ... 9
Spry P. G., ... 325
St. Seymour K., ... 325, 363

T

Tabatabaee S.H., ... 91
Tecim V., ... 31
Tombros S. F., ... 325
Turchanina O.N., ... 43, 335
Türk N., ... 15

U

Üşenmez K., ... 343

V

Valizadeh M.V., ... 143, 153

W

Williams-Jones A. E., ... 325

Y

Yücel K. T., ... 357

Z

Zarif H., ... 193
Zhu L., ... 9
Zouzias D., ... 325, 363
Zubkova V.V., ... 43